JOURNAL OF CHEMICAL PHYSICS

BOARD OF EDITORS

CLYDE A. HUTCHISON, JR., *Editor*

JOSEPH E. MAYER, *Acting Editor*

Associate Editors

Term ending December 31, 1953	*Term ending December 31, 1954*	*Term ending December 31, 1955*
HOWARD M. BADGER	BRYCE L. CRAWFORD, JR.	JAMES R. ARNOLD
DAVID M. DENNISON	H. S. GUTOWSKY	JACOB BIGELEISEN
JOHN G. KIRKWOOD	WILLIAM M. LIPSCOMB	WALTER GORDY
E. BRIGHT WILSON, JR.	ELLIOTT W. MONTROLL	ALVIN H. NIELSEN
W. WEST WYCKOFF	GEORGE SCATCHARD	EARLE K. PLYLER
	J. W. STOUT	WAYNE H. SHAFFER
	GREGORY H. WANNIER	T. F. YOUNG

This Journal of Chemical Physics is published [illegible] American Institute of Physics. Its purpose is to bridge a gap between journals of physics and journals of chemistry. The artificial boundary between physics and chemistry has now been in actual fact completely eliminated, and a large and active group is engaged in research which is as much the one as the other. It is to this group that the Journal is rendering its principal service and makes its greatest appeal, both as a prestige and efficient medium for publication of research and as a convenient and carefully edited assemblage of pertinent information.

Information for Contributors

Send manuscripts to Clyde A. Hutchison, Jr., Editor, *The Journal of Chemical Physics*, Institute for Nuclear Studies, University of Chicago, Chicago 37, Illinois. Under the terms stated submission of a manuscript is a representation that it has been neither copyrighted, published, nor submitted for publication elsewhere. Textual material (abstract, body of the paper, tabular material, references, and figure captions) must be in English, typewritten (including mathematical expressions) double spaced with wide margins on a durable, white paper, preferably bond size. The original copy, not the carbon, should be submitted. For general style, spellings, abbreviations, and [illegible] consult recent issues of this Journal. The authors' institutions are requested to pay a publication charge of $25.00 per page which, if honored, entitles them to 100 free reprints. Contributions will be sent both galley proofs.

An abstract must accompany each article. It should be adequate as an index and as a summary.

All but the simplest mathematical expressions should be carefully printed in by hand. Be sure to distinguish between capital and small letters. Indicate clearly superscripts and subscripts by inverted carets and carets respectively. Avoid complicated superscripts and subscripts. Avoid repetition of complicated expressions by representing it by a symbol. Identify in the margin Greek letters and unusual symbols. Use fractional exponents instead of root signs. Use the solidus (/) for fractions wherever [illegible] will save vertical space.

References should appear as footnotes, numbered consecutively. Abbreviations of technical journals should be [illegible] as listed in the Style Manual of the American Institute of Physics and Chemical Abstracts (Chem. Abstracts 45, 1-CCLV (1951)).

Tables may be typewritten on sheets separate from the running text. Each table must have a caption which will make the data in the table intelligible without reference to the text. Avoid complicated column headings.

Wherever possible figures should be planned for the width of a column (3 in.). A convenient reduction ratio is about 2:1 or 3:1. Lettering should be large enough on the original that when reduced it shall not be less than about $\frac{1}{16}$ in. (~1.5 mm). Line drawings must be in *india ink* on white paper or tracing cloth. Coordinate paper is not desirable but if used must be blue lined and the coordinate lines which are to show must be inked over. Pictures of apparatus, etc., should be glossy prints and should have maximum black and white contrast. Identify each original drawing or photograph on the back with the author's name and the figure number. Figures should be numbered consecutively. Captions should be typed on a separate sheet of paper.

A limited number of alterations in proof are unavoidable, but the cost of making extensive alterations after the article has been set in type will be charged to the author.

Proof and all correspondence concerning papers in the process of publication should be addressed to the Publication Manager, American Institute of Physics, 57 East 55 Street, New York 22, New York.

Subscription Price

	U. S. and Canada	Elsewhere
To members of the American Institute of Physics and Affiliated Societies	$12.00	$13.00
To all others	15.00	17.00

Back Number Prices

Yearly rate when complete year is available: $18.00.
Single copies: $1.75 each.

Subscriptions, renewals, and orders for single copies should be addressed to the American Institute of Physics, 57 East 55 Street, New York 22, New York.

Changes of address should be sent to the American Institute of Physics.

[illegible] at Prince and Lemon Streets, Lancaster, Pennsylvania.

[illegible] Post Office at Lancaster, Pa., under the Act of August 24, 1912. [illegible] Sec. 34.40, P. L. & R. of 1938, authorized February 5, 1933

THE JOURNAL
OF
CHEMICAL PHYSICS

VOLUME 23, NUMBER 11 NOVEMBER, 1955

π-Electronic Structure of the HCN Molecule

KAORU IGUCHI
Electrical Communication Laboratory, Musashino-shi, Tokyo, Japan
(Received January 10, 1955)

The HCN molecule is treated as a system of four π electrons moving in a suitable potential field. Its lower excited states are calculated, using both the molecular orbital method with configuration interaction and the Heitler-London method including ionic-homopolar resonance.

Slater atomic orbitals with effective charges $2\delta=3.18$ for the C atom and 3.85 for the N atom are employed.

The calculated energy levels with the $^1\Sigma^+$ ground state as zero are 3.53 ev ($^3\Sigma^+$), 5.60 ev ($^1\Sigma^-$), 7.71 ev ($^3\Delta$), etc. The effect of configuration interaction is remarkable, amounting to several electron volts, and ionic terms have almost the same weight as homopolar terms.

I. INTRODUCTION

π-electronic structures of C—C double bonds have been extensively investigated by many authors using atomic or molecular orbital methods. The C—C triple bond structure of the acetylene molecule has been recently studied by Nakamura and others,[1] but the C—N triple bond structure seems not to have been studied yet because of the difficulty of evaluation of heteronuclear integrals.

We will calculate here the π-electronic structure of the HCN molecule, utilizing methods recently developed by several authors for heteronuclear integrals.[2–4]

We treat this molecule as a system of four π electrons, and the effects of other electrons are replaced by a suitable potential field. This Hueckel[5] approximation simplifies the situation a great deal and has been used by many authors with much success.[5,6]

We take Slater functions as the atomic orbitals, and for the atomic energy values when required in the calculation of configuration interaction, we use experimental values. This scheme, recommended by Moffit,[7] makes the numerical calculation not too formidable and yields good results in spite of its simplicity.

The necessity for inclusion of configuration interaction in MO (molecular orbital) calculations has been discussed by Craig,[8] Coulson,[6] and others, and a good example has been given by Nakamura and others[1] in a calculation on the acetylene molecule.

In HL (Heitler-London) theory, this requires the inclusion of the resonance among various homopolar and ionic structures, or ionic-homopolar resonance.

The full inclusion of CI (configuration interaction) or IHR (ionic-homopolar resonance) demands almost unpracticable calculation in complicated molecules. So, we have selected the HCN molecule as the simplest one containing the C—N triple bond.

Results of MO method and HL method are different in general, but, if CI or IHR are included fully, they must perfectly coincide. We prefer to express final results in the HL scheme, because this is more convenient in discussion of the nature of chemical bonding in a molecule.

II. ORBITALS AND HAMILTONIAN

We take Slater functions for the $2p\pi$ orbitals. Thus for the carbon atom, we have

$$\phi_c^{\pm}(j)=(\delta^5/2\pi)^{\frac{1}{2}}r_{cj}\exp(-\delta r_{cj})\sin\theta_{cj}\exp(\pm i\varphi_j), \quad \delta=1.590 \quad (1)$$

and for the nitrogen atom,

$$\phi_N^{\pm}(j)=(\delta^5/2\pi)^{\frac{1}{2}}r_{Nj}\exp(-\delta r_{Nj})\sin\theta_{Nj}\exp(\pm i\varphi_j). \quad \delta=1.925 \quad (1)'$$

[1] Nakamura, Ohno, Kotani, and Hijikata, Progr. Theoret. Phys. (Japan) **8**, 387 (1952).
[2] C. C. J. Roothaan, J. Chem. Phys. **19**, 1445 (1951).
[3] K. Ruedenberg, J. Chem. Phys. **19**, 1459 (1951).
[4] M. P. Barnett and C. A. Coulson, Trans. Roy. Soc. (London) **243**, 221 (1951).
[5] E. Hueckel, Z. Physik **70**, 204 (1931).
[6] Coulson, Craig, and Jacobs, Proc. Roy. Soc. (London) **A206**, 297 (1951).
[7] W. Moffit, Proc. Roy. Soc. (London) **A210**, 223 (1951).
[8] D. P. Craig, Proc. Roy. Soc. (London) **A200**, 474 (1950).

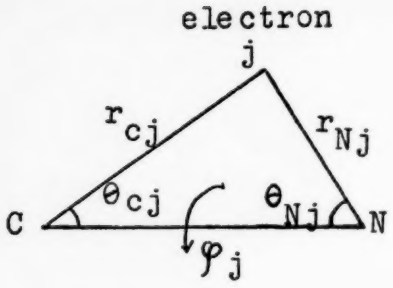

FIG. 1. Polar coordinates.

The polar coordinates r, θ, and φ are defined as shown in Fig. 1.

The Hamiltonian of the system may be written in the following form:

$$H=-\tfrac{1}{2}\sum_{j=1}^{4}\Delta_j+\sum_{j=1}^{4}U_j+\sum_{j>k=1}^{4}\frac{1}{r_{jk}}; \tag{2}$$

here U_j denotes the potential acting on the jth electron, and we use the atomic units 27.204 ev and 0.5292 A for energy and length.

We may put, for the $\phi_c^{\pm}$ orbital,

$$U_j=U_c(j)+U_N(j),$$

$U_c(j)=u_c(j)\cdots$potential due to $2p\sigma$ electron and inner core.

$$U_N(j)=-\frac{5}{r_{Nj}}+\int\frac{1}{r_{jk}}\rho_N(k)d\tau_k-\int\frac{1}{r_{jk}}[|\phi_N^{+}(k)|^2+|\phi_N^{-}(k)|^2]d\tau_k, \tag{3}$$

$$\rho_N(k)=|\phi_N^{+}(k)|^2+|\phi_N^{-}(k)|^2+2|\phi_{2sN}(k)|^2+|\phi_{2pN}(k)|^2,$$

and for the ϕ_N orbital,

$$U_j=U_c(j)+U_N(j),$$

$U_N(j)=u_N(j)\cdots$potential due to $2p\sigma$ electron and inner core,

$$U_c(j)=-\frac{4}{r_{cj}}+\int\frac{1}{r_{jk}}\rho_c(k)d\tau_k-\int\frac{1}{r_{jk}}[|\phi_c^{+}(k)|^2+|\phi_c^{-}(k)|^2]d\tau_k,$$

$$\rho_c(k)=|\phi_c^{+}(k)|^2+|\phi_c^{-}(k)|^2+|\phi_{2sc}(k)|^2+|\phi_{2pc}(k)|^2. \tag{3'}$$

The carbon-nitrogen distance is taken to be 1.15 A.[9,10]

[9] F. A. Miller, J. Chem. Phys. **21**, 110 (1953).
[10] Wilcox, Goldstein, and Simmons, J. Chem. Phys. **22**, 516 (1954).

III. MOLECULAR ORBITAL CALCULATION

The molecule has the symmetry $C_{\infty v}$, and we compose zero-approximation wave functions spanning the irreducible representations of the group as follows:

$$\begin{aligned}&\pi_1:\psi_1^{\pm}=(2N_1)^{-\frac{1}{2}}(\phi_c^{\pm}+\phi_N^{\pm}),\quad N_1=1+S,\\&\pi_2:\psi_2^{\pm}=(2N_2)^{-\frac{1}{2}}(\phi_c^{\pm}-\phi_N^{\pm}),\quad N_2=1-S,\end{aligned} \tag{4}$$

where

$$S=\int\phi_c^{-}(j)\phi_N^{+}(j)d\tau_j\ \text{(overlap integral)}^{11}=0.3126. \tag{5}$$

The one-electron orbital energies e_1 and e_2 are given by

$$\begin{aligned}2N_1e_1&=2N_1\int\psi_1^{-}(j)[-\tfrac{1}{2}\Delta_j+U_j]\psi_1^{+}(j)d\tau_j\\&=I_c+I_N+F_{cN}+F_{Nc},\\2N_2e_2&=2N_2\int\psi_2^{-}(j)[-\tfrac{1}{2}\Delta_j+U_j]\psi_2^{+}(j)d\tau_j\\&=I_c+I_N-F_{cN}-F_{Nc},\end{aligned} \tag{6}$$

where

$$\begin{aligned}I_c&=\int\phi_c^{-}(j)[-\tfrac{1}{2}\Delta_j+U_j]\phi_c^{+}(j)d\tau_j=E_c^{2p}-A_c-K_c-2D,\\I_N&=\int\phi_N^{-}(j)[-\tfrac{1}{2}\Delta_j+U_j]\phi_N^{+}(j)d\tau_j=E_N^{2p}-A_N-K_N-2D.\end{aligned} \tag{7}$$

Also,

$$\begin{aligned}F_{CN}&=\int\phi_c^{-}(j)[-\tfrac{1}{2}\Delta_j+U_j]\phi_N^{+}(j)d\tau_j=E_c^{2p}S-L_c-2L_N-J_c,\\F_{NC}&=\int\phi_N^{-}(j)[-\tfrac{1}{2}\Delta_j+U_j]\phi_c^{+}(j)d\tau_j=E_N^{2p}S-L_N-2L_c-J_N.\end{aligned} \tag{8}$$

For E_c^{2p} and E_N^{2p}, we have relations such as

$$\begin{aligned}\left[-\tfrac{1}{2}\Delta_j+u_c(j)+\int\frac{1}{r_{jk}}|\phi_c^{-}(k)|^2d\tau_k\right]\phi_c^{+}(j)&=E_c^{2p}\phi_c^{+}(j),\\\left[-\tfrac{1}{2}\Delta_j+u_N(j)+\int\frac{1}{r_{jk}}|\phi_N^{-}(k)|^2d\tau_k\right]\phi_N^{+}(j)&=E_N^{2p}\phi_N^{+}(j).\end{aligned} \tag{9}$$

[11] Mulliken, Rieke, Orloff, and Orloff, J. Chem. Phys. **17**, 1248 (1949).

Then we have

$$2e_1 = E_c^{2p} + E_N^{2p} + (1+S)^{-1}[-A_c - K_c - A_N - K_N - 4D - 3L_c - 3L_N - J_c - J_N], \quad (10)$$

$$2e_2 = E_c^{2p} + E_N^{2p} + (1-S)^{-1}[-A_c - K_c - A_N - K_N - 4D + 3L_c + 3L_N + J_c + J_N],$$

and

$$e_2 - e_1 = -S(1-S^2)^{-1}[A_c + K_c + A_N + K_N + 4D] + (1-S^2)^{-1}[3L_c + 3L_N + J_c + J_N] = 9.0085 \text{ ev}. \quad (11)$$

The meanings and values of A_c, K_c, etc., are given in Table I. Values of K, J are calculated according to the scheme of Parr and Crawford[12] and using Coulson's formulae.[13]

The symmetry of the molecule is $C_{\infty v}$, and we have thirty-six antisymmetrized MO functions spanning the irreducible representations. These are listed in Table II.

TABLE I. Two-electron integrals.

$$(ab;cd) = \int \frac{a(1)b(1)c(2)d(2)}{r_{12}} d\tau_1 d\tau_2$$

$A_c = (\phi_c^+\phi_c^-;\ \phi_c^+\phi_c^-) = 16.0176$ ev	$A_c' = (\phi_c^+\phi_c^+;\ \phi_c^-\phi_c^-) = 1.8248$ ev
$A_N = (\phi_N^+\phi_N^-;\ \phi_N^+\phi_N^-) = 19.3924$	$A_N' = (\phi_N^+\phi_N^+;\ \phi_N^-\phi_N^-) = 2.2093$
$C = (\phi_c^+\phi_N^-;\ \phi_c^+\phi_N^-) = 1.3881$	$C' = (\phi_c^+\phi_N^+;\ \phi_c^-\phi_N^-) = 0.1632$
$D = (\phi_c^+\phi_c^-;\ \phi_N^+\phi_N^-) = 10.5154$	$D' = (\phi_c^+\phi_c^+;\ \phi_N^-\phi_N^-) = 0.4244$
$L_c = (\phi_N^+\phi_c^-;\ \phi_c^+\phi_c^-) = 4.2657$	$L_c' = (\phi_N^+\phi_c^+;\ \phi_c^-\phi_c^-) = 0.4174$
$L_N = (\phi_c^+\phi_N^-;\ \phi_N^+\phi_N^-) = 4.6806$	$L_N' = (\phi_c^+\phi_N^+;\ \phi_N^-\phi_N^-) = 0.4021$

$$J_c = -\int \phi_N^-(j)\Big[-\frac{5}{r_{Nj}} + \int \frac{1}{r_{jk}}\cdot\rho_N(k)d\tau_k\Big]\phi_c^+(j)d\tau_j = 3.9934 \text{ ev}$$

$$J_N = -\int \phi_c^-(j)\Big[-\frac{4}{r_{cj}} + \int \frac{1}{r_{jk}}\cdot\rho_c(k)d\tau_k\Big]\phi_N^+(j)d\tau_j = 3.0597$$

$$K_c = -\int \phi_c^-(j)\Big[-\frac{5}{r_{Nj}} + \int \frac{1}{r_{jk}}\cdot\rho_N(k)d\tau_k\Big]\phi_c^+(j)d\tau_j = 0.6726$$

$$K_N = -\int \phi_N^-(j)\Big[-\frac{4}{r_{cj}} + \int \frac{1}{r_{jk}}\cdot\rho_c(k)d\tau_k\Big]\phi_N^+(j)d\tau_j = 1.4575$$

Here the following abbreviation is used:

$$(abcd;\chi_i) = (4!)^{-\frac{1}{2}}\sum_p (-1)^p Pa(1) \times b(2)c(3)d(4)\chi_i(1,2,3,4). \quad (12)$$

The spin functions χ_i are the same as those in reference 1 and are given in the Appendix.

For these ASMO functions X_ν, we can evaluate the energy levels by the formula

$$E_\nu = \int X_\nu^* H X_\nu d\tau. \quad (13$$

The Coulomb-type integrals are evaluated by the method of Roothaan,[7] the exchange type by that of Ruedenberg,[3,14] and the hybrid type by that of Barnett and Coulson.[4] The energy levels calculated are listed in the right column of Table II. One might set the zero of energy at the lowest of the $^1\Sigma^+$ state in this list, but we will see later that by CI the $^1\Sigma^+$ ground state is lowered by 3.44 ev and we have taken this as the zero.

TABLE II. Single configuration MO functions.

Symmetry	MO function	Energy in ev
$^1\Sigma^+$	$A_1 = (\psi_1^+\psi_1^+\psi_1^-\psi_1^-;\ \chi_1)$	3.44
	$A_2 = (\psi_1^+\psi_1^-\psi_2^+\psi_2^-;\ \chi_3)$	20.97
	$A_3 = (\psi_1^+\psi_1^-\psi_2^+\psi_2^-;\ \chi_4)$	25.21
	$A_4 = (2)^{-\frac{1}{2}}[(\psi_1^+\psi_1^+\psi_2^-\psi_2^-;\ \chi_1) + (\psi_1^-\psi_1^-\psi_2^+\psi_2^+;\ \chi_1)]$	21.58
	$A_5 = (\psi_2^+\psi_2^+\psi_2^-\psi_2^-;\ \chi_1)$	37.70
	$A_6 = (2)^{-\frac{1}{2}}[(\psi_1^+\psi_1^+\psi_1^-\psi_2^-;\ \chi_2) + (\psi_1^-\psi_1^-\psi_1^+\psi_2^+;\ \chi_2)]$	23.18
	$A_7 = (2)^{-\frac{1}{2}}[(\psi_2^+\psi_2^+\psi_2^-\psi_1^-;\ \chi_2) + (\psi_2^-\psi_2^-\psi_2^+\psi_1^+;\ \chi_2)]$	40.31
$^1\Sigma^-$	$B_1 = -i(2)^{-\frac{1}{2}}[(\psi_1^+\psi_1^+\psi_2^-\psi_2^-;\ \chi_1) - (\psi_1^-\psi_1^-\psi_2^+\psi_2^+;\ \chi_1)]$	21.58
	$B_2 = -i(2)^{-\frac{1}{2}}[(\psi_1^+\psi_1^+\psi_1^-\psi_2^-;\ \chi_2) - (\psi_1^-\psi_1^-\psi_1^+\psi_2^+;\ \chi_2)]$	9.95
	$B_3 = -i(2)^{-\frac{1}{2}}[(\psi_2^+\psi_2^+\psi_2^-\psi_1^-;\ \chi_2) - (\psi_2^-\psi_2^-\psi_2^+\psi_1^+;\ \chi_2)]$	27.08
$^1\Delta$	$E_1 = (\psi_1^+\psi_1^+\psi_2^+\psi_2^-;\ \chi_2)$	19.69
	$E_1^* = (\psi_1^-\psi_1^-\psi_2^-\psi_2^+;\ \chi_2)$	
	$E_2 = (\psi_2^+\psi_2^+\psi_1^+\psi_1^+;\ \chi_2)$	19.69
	$E_2^* = (\psi_2^-\psi_2^-\psi_1^-\psi_1^+;\ \chi_2)$	
	$E_3 = (\psi_1^+\psi_1^+\psi_1^-\psi_2^+;\ \chi_2)$	10.37
	$E_3^* = (\psi_1^-\psi_1^-\psi_1^+\psi_2^-;\ \chi_2)$	
	$E_4 = (\psi_2^+\psi_2^+\psi_2^-\psi_1^+;\ \chi_2)$	27.49
	$E_4^* = (\psi_2^-\psi_2^-\psi_2^+\psi_1^-;\ \chi_2)$	
$^1\Gamma$	$G_1 = (\psi_1^+\psi_1^+\psi_2^+\psi_2^+;\ \chi_1)$	15.38
	$G_1^* = (\psi_1^-\psi_1^-\psi_2^-\psi_2^-;\ \chi_1)$	
$^3\Sigma^+$	$H_1 = (\psi_1^+\psi_1^-\psi_2^+\psi_2^-;\ \chi_5)$	20.86
	$H_2 = (2)^{-\frac{1}{2}}[(\psi_1^+\psi_1^+\psi_1^-\psi_2^-;\ \chi_5) + (\psi_1^-\psi_1^-\psi_1^+\psi_2^+;\ \chi_5)]$	7.25
	$H_3 = (2)^{-\frac{1}{2}}[(\psi_2^+\psi_2^+\psi_2^-\psi_1^-;\ \chi_5) + (\psi_2^-\psi_2^-\psi_2^+\psi_1^+;\ \chi_5)]$	24.38
$^3\Sigma^-$	$I_1 = (\psi_1^+\psi_1^-\psi_2^+\psi_2^-;\ \chi_6)$	18.56
	$I_2 = (\psi_1^+\psi_1^-\psi_2^+\psi_2^-;\ \chi_7)$	18.56
	$I_3 = -i(2)^{-\frac{1}{2}}[(\psi_1^+\psi_1^+\psi_1^-\psi_2^-;\ \chi_6) - (\psi_1^-\psi_1^-\psi_1^+\psi_2^+;\ \chi_6)]$	9.95
	$I_4 = -i(2)^{-\frac{1}{2}}[(\psi_2^+\psi_2^+\psi_2^-\psi_1^-;\ \chi_6) - (\psi_2^-\psi_2^-\psi_2^+\psi_1^+;\ \chi_6)]$	27.08
$^3\Delta$	$L_1 = (\psi_1^+\psi_1^+\psi_2^+\psi_2^-;\ \chi_5)$	17.28
	$L_1^* = (\psi_1^-\psi_1^-\psi_2^-\psi_2^+;\ \chi_5)$	
	$L_2 = (\psi_2^+\psi_2^+\psi_1^+\psi_1^-;\ \chi_5)$	17.20
	$L_2^* = (\psi_2^-\psi_2^-\psi_1^-\psi_1^+;\ \chi_5)$	
	$L_3 = (\psi_1^+\psi_1^+\psi_1^-\psi_2^+;\ \chi_5)$	8.60
	$L_3^* = (\psi_1^-\psi_1^-\psi_1^+\psi_2^-;\ \chi_5)$	
	$L_4 = (\psi_2^+\psi_2^+\psi_2^-\psi_1^+;\ \chi_5)$	25.73
	$L_4^* = (\psi_2^-\psi_2^-\psi_2^+\psi_1^-;\ \chi_5)$	
$^5\Sigma^+$	$N_1 = (\psi_1^+\psi_1^-\psi_2^+\psi_2^-;\ \chi_9)$	11.13

TABLE III. Results of CI.

Symmetry	Energy in ev	Depression by CI	MO function	HL function
$^1\Sigma^+$	0.00	3.44	$0.934A_1 + 0.143A_2 + 0.199A_3 - 0.150A_4 + 0.064A_5 - 0.093A_6 + 0.067A_7$	$-0.534A_a + 0.151A_b + 0.335A_c + 0.451A_d - 0.091A_e - 0.125A_f + 0.020A_g$
$^1\Sigma^-$	5.60	4.35	$-0.390B_1 + 0.897B_2 - 0.208B_3$	$0.390B_a + 0.730B_b + 0.282B_c$
$^1\Delta$	10.08	0.29	$0.039E_1 - 0.018E_2 + 0.990E_3 + 0.130E_4$	$-0.015E_a + 0.040E_b + 0.698E_c + 0.418E_d$
$^3\Sigma^+$	3.53	3.72	$-0.137H_1 + 0.900H_2 + 0.073H_3$	$-0.137H_a + 0.586H_b - 0.429H_c$
$^3\Sigma^-$	9.41	0.54	$0.035I_1 + 0.026I_2 + 0.968I_3 - 0.171I_4$	$0.043I_a + 0.006I_b - 0.730I_c + 0.362I_d$
$^3\Delta$	7.71	0.89	$-0.002L_1 + 0.002L_2 + 0.976L_3 + 0.217L_4$	$-0.003L_b + 0.784L_c - 0.317L_d$
$^1\Gamma$	15.38	0.00	G_1	G_a
$^5\Sigma^+$	11.13	0.00	N_1	N_a

[12] R. G. Parr and B. L. Crawford, J. Chem. Phys. **16**, 1049 (1948).

[13] C. A. Coulson, Proc. Cambridge Phil. Soc. **38**, part 2, 210 (1942).

[14] Kotani, Amemiya, and Shimose, Proc. Phys.-Math. Soc. Japan **20**, extra No. 1, (1938).

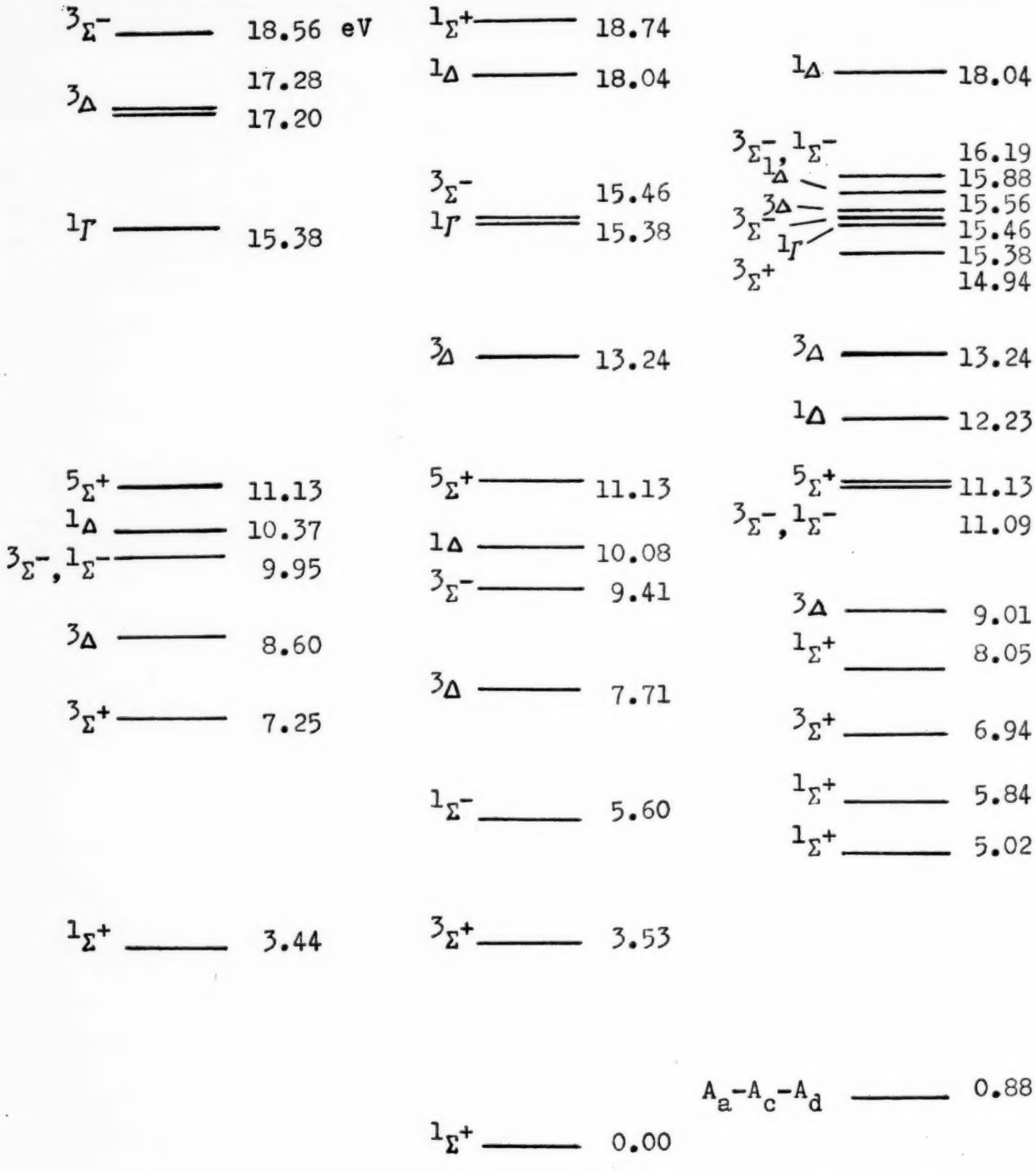

FIG. 2. Energy levels.

Next we proceed to the CI calculation. The new energy levels and wave functions are given by solving the following secular equation in each symmetry space:

$$\mathrm{Det}|H_{ij}-ES_{ij}|=0, \tag{14}$$

where

$$H_{ij}=\int X_i^* H X_j d\tau, \quad S_{ij}=\int X_i^* X_j d\tau. \tag{15}$$

In this step, terms including $E_c^{2p}-E_N^{2p}$ appear in the

TABLE IV. HL functions without IHR.

Symmetry	HL function	Structure	Energy in ev
$^1\Sigma^+$	$A_a=(1+S^2)^{-1}(\phi_c^+\phi_c^-\phi_N^+\phi_N^-;\chi_4)$	$\phi_c^+\phi_N^+)\phi_c^-\phi_N^-)$	5.02
	$A_b=(1-S^2+S^4)^{-\frac{1}{2}}(\phi_c^+\phi_c^-\phi_N^+\phi_N^-;\chi_3)$	$\phi_c^+\phi_c^-)^+\phi_N^+\phi_N^-)$	21.66
	$A_c=(2+2S^4)^{-\frac{1}{2}}[(\phi_c^+\phi_c^+\phi_N^-\phi_N^-;\chi_1)+(\phi_c^-\phi_c^-\phi_N^+\phi_N^+;\chi_1)]$	$\phi_c^+)^2\phi_N^-)^2$	8.05
	$A_d=2^{-1}(1+6S^2+S^4)^{-\frac{1}{2}}[(I)+(II)+(III)+(IV)]$	$\phi_c^+)^2\phi_c^-\phi_N^-)$	5.84
	$A_e=(2+2S^4)^{-\frac{1}{2}}[(\phi_c^+\phi_c^+\phi_c^-\phi_c^-;\chi_1)+(\phi_N^+\phi_N^+\phi_N^-\phi_N^-;\chi_1)]$	$\phi_c^+)^2\phi_c^-)^2$	32.92
	$A_f=2^{-1}(1-S^4)^{-\frac{1}{2}}[(I)-(II)+(III)-(IV)]$	$\phi_c^+)^2\phi_c^-\phi_N^-)$	23.48
	$A_g=(2-2S^4)^{-\frac{1}{2}}[(\phi_c^+\phi_c^+\phi_c^-\phi_c^-;\chi_1)-(\phi_N^+\phi_N^+\phi_N^-\phi_N^-;\chi_1)]$	$\phi_c^+)^2\phi_c^-)^2$	30.25
$^1\Sigma^-$	$B_a=-i(2-2S^2)^{-1}[(I)+(II)-(III)-(IV)]$	$\phi_c^+)^2\phi_c^-\phi_N^-)$	21.58
	$B_b=-i(2-2S^4)^{-\frac{1}{2}}[(\phi_c^+\phi_c^+\phi_N^-\phi_N^-;\chi_1)-(\phi_c^-\phi_c^-\phi_N^+\phi_N^+;\chi_1)]$	$\phi_c^+)^2\phi_N^-)^2$	11.09
	$B_c=-i(4-4S^4)^{-\frac{1}{2}}[(I)-(II)-(III)+(IV)]$	$\phi_c^+)^2\phi_c^-\phi_N^-)$	16.19
$^1\Delta$	$E_a=2^{-\frac{1}{2}}(1-S^2)^{-1}[(\phi_c^+\phi_c^+\phi_N^+\phi_N^-;\chi_2)+(\phi_N^+\phi_N^+\phi_c^+\phi_c^-;\chi_2)]$	$\phi_c^+)^2\phi_N^+\phi_N^-)$	18.04
	$E_a^*=2^{-\frac{1}{2}}(1-S^2)^{-1}[(\phi_c^-\phi_c^-\phi_N^-\phi_N^+;\chi_2)+(\phi_N^-\phi_N^-\phi_c^-\phi_c^+;\chi_2)]$		
	$E_b=2^{-\frac{1}{2}}(1-S^2)^{-1}[(\phi_c^+\phi_c^+\phi_c^-\phi_N^+;\chi_2)+(\phi_N^+\phi_N^+\phi_N^-\phi_c^+;\chi_2)]$	$\phi_c^+)^2\phi_c^-\phi_N^+)$	21.34
	$E_b^*=2^{-\frac{1}{2}}(1-S^2)^{-1}[(\phi_c^-\phi_c^-\phi_c^+\phi_N^-;\chi_2)+(\phi_N^-\phi_N^-\phi_N^+\phi_c^-;\chi_2)]$		
	$E_c=2^{-\frac{1}{2}}(1-S^4)^{-\frac{1}{2}}[(\phi_c^+\phi_c^+\phi_N^+\phi_N^-;\chi_2)-(\phi_N^+\phi_N^+\phi_c^+\phi_c^-;\chi_2)]$	$\phi_c^+)^2\phi_N^+\phi_N^-)$	12.23
	$E_c^*=2^{-\frac{1}{2}}(1-S^4)^{-\frac{1}{2}}[(\phi_c^-\phi_c^-\phi_N^-\phi_N^+;\chi_2)-(\phi_N^-\phi_N^-\phi_c^-\phi_c^+;\chi_2)]$		
	$E_d=2^{-\frac{1}{2}}(1-S^4)^{-\frac{1}{2}}[(\phi_c^+\phi_c^+\phi_c^-\phi_N^+;\chi_2)-(\phi_N^+\phi_N^+\phi_N^-\phi_c^+;\chi_2)]$	$\phi_c^+)^2\phi_c^-\phi_N^+)$	15.88
	$E_d^*=2^{-\frac{1}{2}}(1-S^4)^{-\frac{1}{2}}[(\phi_c^-\phi_c^-\phi_c^+\phi_N^-;\chi_2)-(\phi_N^-\phi_N^-\phi_N^+\phi_c^-;\chi_2)]$		
$^1\Gamma$	$G_a=(1-S^2)^{-1}(\phi_c^+\phi_c^+\phi_N^+\phi_N^+;\chi_1)$	$\phi_c^+)^2\phi_N^+)^2$	15.38
	$G_a^*=(1-S^2)^{-1}(\phi_c^-\phi_c^-\phi_N^-\phi_N^-;\chi_1)$		
$^3\Sigma^+$	$H_a=(2-2S^2)^{-1}[(i)+(ii)+(iii)+(iv)]$	$\phi_c^+)^2\phi_c^-)\phi_N^-)$	20.86
	$H_b=(1-S^4)^{-\frac{1}{2}}(\phi_c^+\phi_c^-\phi_N^+\phi_N^-;\chi_8)$	$\phi_c^+\phi_N^+)\phi_c^-)\phi_N^-)$	6.94
	$H_c=(4-4S^4)^{-\frac{1}{2}}[(i)-(ii)+(iii)-(iv)]$	$\phi_c^+)^2\phi_c^-)\phi_N^-)$	14.94
$^3\Sigma^-$	$I_a=2^{-\frac{1}{2}}(1-S^2)^{-1}[(\phi_c^+\phi_c^-\phi_N^+\phi_N^-;\chi_6)+(\phi_c^+\phi_c^-\phi_N^+\phi_N^-;\chi_7)]$	$\phi_c^+\phi_c^-)\phi_N^+)\phi_N^-)$	15.46
	$I_b=(2-2S^2)^{-1}[(i)+(ii)-(iii)-(iv)]$	$\phi_c^+)^2\phi_c^-)\phi_N^-)$	21.66
	$I_c=(2-2S^4)^{-\frac{1}{2}}[(\phi_c^+\phi_c^-\phi_N^+\phi_N^-;\chi_6)-(\phi_c^+\phi_c^-\phi_N^+\phi_N^-;\chi_7)]$	$\phi_c^+\phi_c^-)\phi_N^+)\phi_N^-)$	11.09
	$I_d=(4-4S^4)^{-\frac{1}{2}}[(i)-(ii)-(iii)+(iv)]$	$\phi_c^+)^2\phi_c^-)\phi_N^-)$	16.19
$^3\Delta$	$L_a=2^{-\frac{1}{2}}(1-S^2)^{-1}[(\phi_c^+\phi_c^+\phi_N^+\phi_N^-;\chi_5)+(\phi_N^+\phi_N^+\phi_c^+\phi_c^-;\chi_5)]$	$\phi_c^+)^2\phi_N^+)\phi_N^-)$	13.24
	$L_a^*=2^{-\frac{1}{2}}(1-S^2)^{-1}[(\phi_c^-\phi_c^-\phi_N^-\phi_N^+;\chi_5)+(\phi_N^-\phi_N^-\phi_c^-\phi_c^+;\chi_5)]$		
	$L_b=2^{-\frac{1}{2}}(1-S^2)^{-1}[(\phi_c^+\phi_c^+\phi_c^-\phi_N^+;\chi_5)+(\phi_N^+\phi_N^+\phi_N^-\phi_c^+;\chi_5)]$	$\phi_c^+)^2\phi_c^-)\phi_N^+)$	21.22
	$L_b^*=2^{-\frac{1}{2}}(1-S^2)^{-1}[(\phi_c^-\phi_c^-\phi_c^+\phi_N^-;\chi_5)+(\phi_N^-\phi_N^-\phi_N^+\phi_c^-;\chi_5)]$		
	$L_c=(2-2S^4)^{-\frac{1}{2}}[(\phi_c^+\phi_c^+\phi_N^+\phi_N^-;\chi_5)-(\phi_N^+\phi_N^+\phi_c^+\phi_c^-;\chi_5)]$	$\phi_c^+)^2\phi_N^+)\phi_N^-)$	9.01
	$L_c^*=(2-2S^4)^{-\frac{1}{2}}[(\phi_c^-\phi_c^-\phi_N^-\phi_N^+;\chi_5)-(\phi_N^-\phi_N^-\phi_c^-\phi_c^+;\chi_5)]$		
	$L_d=(2-2S^4)^{-\frac{1}{2}}[(\phi_c^+\phi_c^+\phi_c^-\phi_N^+;\chi_5)-(\phi_N^+\phi_N^+\phi_N^-\phi_c^+;\chi_5)]$	$\phi_c^+)^2\phi_c^-)\phi_N^+)$	15.56
	$L_d^*=(2-2S^4)^{-\frac{1}{2}}[(\phi_c^-\phi_c^-\phi_c^+\phi_N^-;\chi_5)-(\phi_N^-\phi_N^-\phi_N^+\phi_c^-;\chi_5)]$		
$^5\Sigma^+$	$N_a=(1-S^2)^{-1}(\phi_c^+\phi_c^-\phi_N^+\phi_N^-;\chi_9)$	$\phi_c^+)\phi_c^-)\phi_N^+)\phi_N^-)$	11.13

$(I)=(\phi_c^+\phi_c^+\phi_c^-\phi_N^-;\chi_2)$, $(II)=(\phi_N^+\phi_N^+\phi_N^-\phi_c^-;\chi_2)$, $(III)=(\phi_c^-\phi_c^-\phi_c^+\phi_N^+;\chi_2)$, $(IV)=(\phi_N^-\phi_N^-\phi_N^+\phi_c^+;\chi_2)$,

$(i)=(\phi_c^+\phi_c^+\phi_c^-\phi_N^-;\chi_5)$, $(ii)=(\phi_N^+\phi_N^+\phi_N^-\phi_c^-;\chi_5)$, $(iii)=(\phi_c^-\phi_c^-\phi_c^+\phi_N^+;\chi_5)$, $(iv)=(\phi_N^-\phi_N^-\phi_N^+\phi_c^+;\chi_5)$.

expression of H_{ij}. Here we utilize the experimental values of the first ionization potentials of C and N in their valence states, -11.17 ev and -13.81 ev, respectively.[15] The results are given in Table III and Fig. 2. We see a remarkable similarity between HCN and C_2H_2 molecules, although there is a slight difference in the result of CI. The effect of CI is much larger in HCN because of the reduction of symmetry of the molecule and consequent combination of more wave functions than in C_2H_2.

IV. HEITLER-LONDON CALCULATION

We construct HL wave functions X_i from the Slater $2p\pi$ orbitals as seen in Table IV. Here we use Mulliken's symbolism.[16] The dot connection of orbitals such as $\phi_c^+\cdot\phi_N^+)$ means an electron pair bond, and $\phi_c^+)^2$ shows a lone pair in the ϕ_c^+ orbital. The energy levels of the HL functions are given for MO functions by the formula,

$$E_i=\int X_i^* H X_i d\tau,$$

[15] R. S. Mulliken, J. Chem. Phys. **2**, 782 (1934).

[16] R. S. Mulliken, J. Chem. Phys. **19**, 900 (1951).

and they can be evaluated in terms of the integrals S, A_c, K_c, etc., in Table I. On the other hand, we know the linear transformation between MO functions and HL functions, so we can evaluate HL energy levels directly from MO levels. Both results coincide, giving the right column of Table IV.

V. CONCLUSION

In Fig. 2 we show the energy levels calculated by the MO method and by the HL method, and the results of CI or IHR.

We observe that the effect of CI or IHR is remarkable, amounting to several electron volts. Moreover, there appears to be no distinct regularity due to term symmetry or spin multiplicity in the amount of energy depression or the selection of configuration. We may only say that the effect is larger in Σ states than in Δ states. In spite of Coulson's statement,[6] the depression of the $^3\Delta$ state is larger than that of the $^1\Delta$ state. In terms of HL functions, we can express the lowest $^1\Sigma^+$ state as (see Table III):

$$^1\Sigma^+ = -0.534A_a + 0.151A_b + 0.335A_c + 0.451A_d - 0.091A_e - 0.125A_f + 0.020A_g. \quad (16)$$

Here the ionic term A_d is contained in a large amount nearly equal to that of the homopolar term A_a, and we may attain a good approximation with only A_a, A_c, and A_d. We have tried this with the crude function

$$X = A_a - A_c - A_d \text{ (to be normalized)} \quad (17)$$

and attained the energy level 0.88 ev, which is also shown in Fig. 2.

The only theoretically allowed transition from the ground state $^1\Sigma^+$ is to the upper $^1\Sigma^+$ state, for which the computed energy difference is about 19 ev or 650 A. This would be difficult to observe. The transition from the lowest $^3\Delta$ state to the upper $^3\Delta$ state gives an energy difference 5.53 ev or 2245 A, and that from the lowest $^3\Sigma^-$ state to the upper $^3\Sigma^-$ state gives 6.05 ev or 2058 A. Exact experimental data are not available now.

The author wishes to express sincere thanks to the members of the Kotani Laboratory for valuable discussions and advice.

APPENDIX

For the system of four particles, each of spin $\frac{1}{2}$, we can construct four singlet, four triplet, and one quintet spin functions, as follows:

singlet state functions:

$$\chi_1 = \alpha(1)\beta(2)\alpha(3)\beta(4),$$
$$\chi_2 = 2^{-\frac{1}{2}}\alpha(1)\beta(2)[\alpha(3)\beta(4) - \beta(3)\alpha(4)],$$
$$\chi_3 = 2^{-1}[\alpha(1)\beta(2) - \beta(1)\alpha(2)][\alpha(3)\beta(4) - \beta(3)\alpha(4)],$$
$$\chi_4 = 2^{-1}[\alpha(1)\beta(3) - \beta(1)\alpha(3)][\alpha(2)\beta(4) - \beta(2)\alpha(4)];$$

triplet state functions:

$$\chi_5 = \alpha(1)\beta(2)\alpha(3)\alpha(4),$$
$$\chi_6 = 2^{-\frac{1}{2}}\alpha(3)\alpha(4)[\alpha(1)\beta(2) - \beta(1)\alpha(2)],$$
$$\chi_7 = 2^{-\frac{1}{2}}\alpha(1)\alpha(2)[\alpha(3)\beta(4) - \beta(3)\alpha(4)],$$
$$\chi_8 = 2^{-1}\alpha(1)\alpha(2)[\alpha(3)\beta(4) + \beta(3)\alpha(4)] - 2^{-1}\alpha(3)\alpha(4)[\alpha(1)\beta(2) + \beta(1)\alpha(2)];$$

quintet state function:

$$\chi_9 = \alpha(1)\alpha(2)\alpha(3)\alpha(4).$$

Vibrational Spectrum of Fluorotrichloroethylene*

D. E. Mann and Earle K. Plyler
National Bureau of Standards, Washington, D. C.
(Received May 7, 1954)

The infrared spectrum of gaseous fluorotrichloroethylene, FClC:CCl_2, has been obtained in the range 3–50 microns. The Raman spectrum of a liquid sample has also been determined. Earlier data and new force constant calculations for some other fluorochloroethylenes are reviewed and used to establish a satisfactory vibrational assignment for FClC:CCl_2. The planar fundamentals appear at 1645, 1181, 988, 857, 520, 407, 358, 250, and 174 cm^{-1}; the out-of-plane vibrations occur at 537, 313, and probably near 130 cm^{-1}. A necessary revision in the existing assignment for F_2C:CCl_2 is indicated. A table of the thermodynamic functions is given for FClC:CCl_2 in the ideal gaseous state.

INTRODUCTION

THE vibrational spectra of several members of the fluorochloroethylene family have been investigated recently, and complete assignments are now available for F_2C:CF_2,[1–4] F_2C:CFCl,[5] F_2C:CCl_2,[6–7] and Cl_2C:CCl_2.[4] In connection with the normal coordinate analyses of some fluorinated ethylenes, and referred to in some detail later in this paper, it was considered desirable to study the infrared and Raman spectra of FClC:CCl_2.

EXPERIMENTAL

A sample of FClC:CCl_2 was made available to us by Dr. D. R. Stull of the Dow Chemical Company, and was further purified by distillation through a Piros-Glover column.

The equipment and methods used for the measurement of the infrared spectrum have been previously described.[5] Prisms of LiF, NaCl, KBr, CsBr, and CsI were employed in appropriate spectral regions to ensure adequate resolution over the range 3–50 microns. The infrared spectrum of gaseous FClC:CCl_2 is shown in Fig. 1, where for convenience a scale linear in wave number has been used. The measured values of all observed bands are given in Table I.

The Raman spectrum of the liquid sample was photographed on Eastman Kodak 103a–0 plates with a Hilger E-612 glass 2-prism spectrograph. The camera has an aperture of $f/5.7$. The reciprocal dispersion near 4358 A is 18 A/mm, and 32 A/mm at 5000 A. Filters of Rhodamine 5 GDN extra and Wratten 2A were employed to remove, as far as practicable, incident radiation other than the mercury triplet at 4358 A. The standard Hilger irradiation apparatus and Raman tubes were used. Exposures times ranged up to 8 hours. Dense background made longer exposures impractical. Iron arc reference spectra were photographed on every Raman plate. Wavelength shifts were measured with an optical comparator. Polarization data were not obtained. The frequency shifts and approximate relative intensities of all observed Raman lines, including those whose reality may be doubted, are given in the first two columns of Table I. Several of the lines reported were found on only one plate for the longest exposure taken and will later be shown to be spurious.

Interpretation

Preliminary Discussion of Spectra

No structural data are available for FClC:CCl_2. Bond lengths and angles were estimated with the aid of the results obtained by Karle and Karle for F_2C:CF_2[8] and Cl_2C:CCl_2.[9] For the calculation of the moments of inertia it was assumed that the molecule has C_s symmetry, CC, CF, and CCl distances of 1.31 A, 1.31 A, and 1.72 A, respectively; and CCF and CCCl angles equal to 123°. The principal moments of inertia are then 340.070, 568.884, and 908.954×10^{-40} gcm.^{2}

Nine of the 12 fundamental vibrations are planar modes and belong to the species a' of the point group C_s. The three remaining motions are nonplanar and belong to the a'' species. All the fundamentals are permitted to appear in both infrared and Raman spectra. Those in a' should have hybrid or mixed type A–type B infrared band envelopes and polarized Raman lines. The a'' modes should give rise to characteristic type C band contours having quite prominent Q branches, and to depolarized Raman lines.

It should be possible to predict rather closely the regions in which the fundamentals of FClC:CCl_2 may be expected to occur from the spectral data and vibrational assignments available for F_2C:CF_2,[1–4] F_2C:CFCl,[5] F_2C:CCl_2,[6,7] and Cl_2C:CCl_2.[4] The essential results given most recently in the literature for the last four molecules are summarized in Table II. In addition, the calculated fundamentals taken from very recently completed and as yet unpublished force constant

* This work has been supported in part by the Office of Naval Research.
[1] Nielsen, Claassen, and Smith, J. Chem. Phys. **18**, 812 (1950).
[2] A. Monfils and J. Duchesne, J. Chem. Phys. **18**, 1415 (1950).
[3] A. Monfils and J. Duchesne, Compt. rend. **236**, 685 (1953).
[4] Mann, Acquista, and Plyler, J. Research Natl. Bur. Standards **52**, 67 (1954).
[5] Mann, Acquista, and Plyler, J. Chem. Phys. **21**, 1949 (1953).
[6] Nielsen, Claassen, and Smith, J. Chem. Phys. **18**, 485 (1950).
[7] P. Torkington and H. W. Thompson, Trans. Faraday Soc. **41**, 236 (1945).
[8] I. L. Karle and J. Karle, J. Chem. Phys. **18**, 963 (1950).
[9] I. L. Karle and J. Karle, J. Chem. Phys. **20**, 63 (1952).

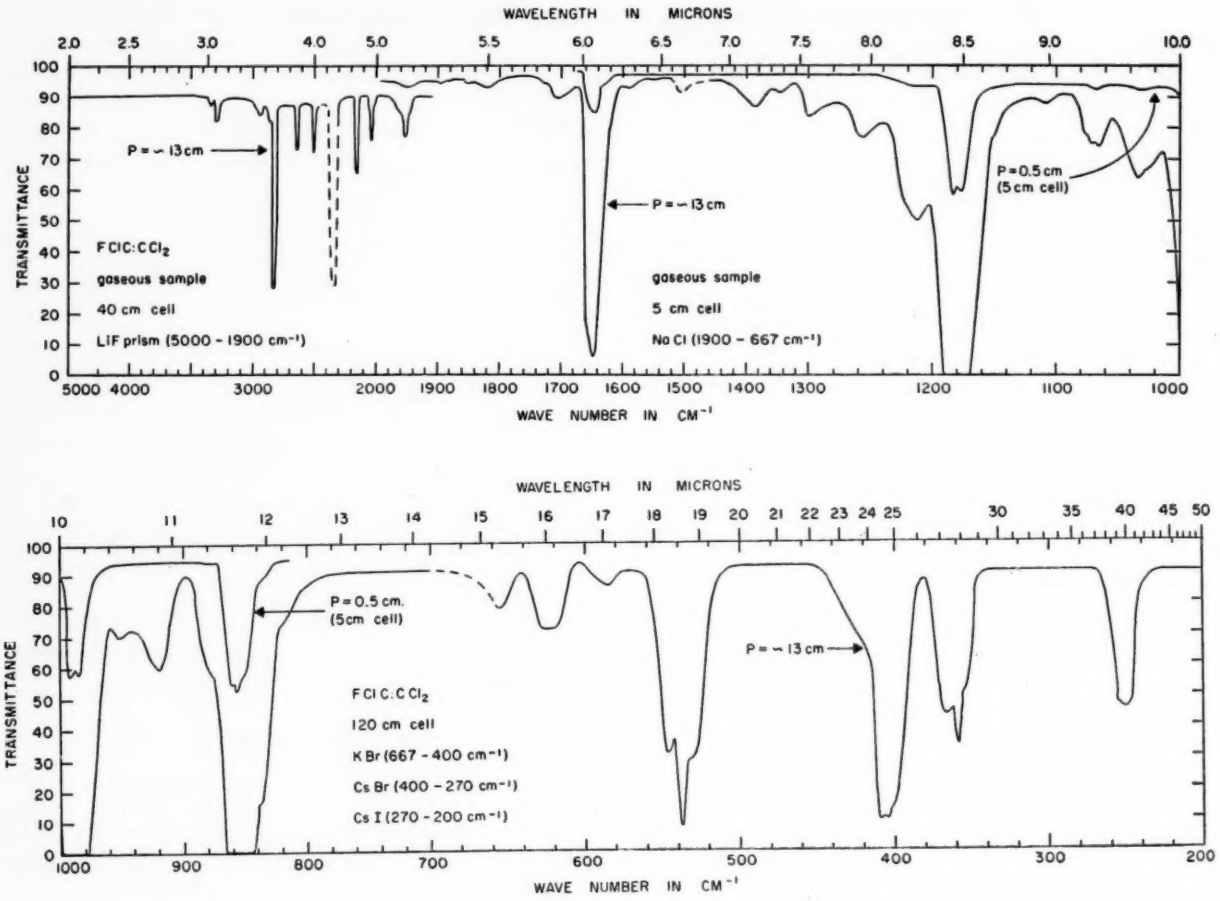

FIG. 1.

studies made by Mann, *et al.*† are given for all five ethylenes referred to above.

Examination of Table II reveals several interesting and useful facts about the agreement between the calculated and observed frequencies, and the correlation of fundamentals among the various ethylenes. Disregarding for the moment the present results for $FClC:CCl_2$ we notice that for $F_2C:CF_2$, $F_2C:CFCl$, $Cl_2C:CCl_2$, and about half of the planar fundamentals of a-$F_2C:CCl_2$ the agreement between calculated and observed frequencies is quite good. From the nature of the assumptions made by Mann, *et al.* in their force constant treatment of the fluorochloroethylenes,‡ it is not surprising to find fairly smooth and clear cut trends in the fundamentals as one proceeds from the completely fluorinated member of the series to tetrachloroethylene. On this basis it would be a simple matter indeed to assign the fundamentals in the observed spectra of $FClC:CCl_2$ were it not for the discordantly poor agreement between several of the fundamentals in the existing assignments for a-$F_2C:CCl_2$[6,7] and the predicted values. It was considered worthwhile, therefore, to re-examine the spectrum of the asymmetric compound. Its infrared spectrum between 25 and 53 microns, in conjunction with the results of the force constant calculation, indicates a revised assignment which seems more nearly in accord with the facts than earlier interpretations. It is necessary to reassign the strong and apparently depolarized Raman line at 258 cm^{-1} to the totally symmetric species a_1§ This is in accord with the observation that in the infrared spectrum the band at 258 cm^{-1} does not appear to have a type C envelope. We also find a weak band at 323 cm^{-1} and ascribe it to the lower b_2 out-of-plane wagging fundamental. This would explain the infrared band at 640 and the polarized Raman line at 646 cm^{-1} as 2×323. Certain other features of the earlier assignment that were unsatisfactory are also improved as a result of the present revision. The complete new list of fundamentals is given in Table III.

† Mann, Meal, Shimanouchi, and Fano (unpublished results).

‡ In the force constant calculations carried out by Mann *et al.* for the fluorochloroethylenes a slightly modified Urey-Bradley function was fitted as well as possible by the criterion of least squares to the planar fundamentals of $F_2C:CF_2$ and $Cl_2C:CCl_2$. The maximum number of force constants used was seven. For the intermediate fluorochloroethylenes the necessary force constants were either transferred intact from, or simply interpolated between, the corresponding results for $F_2C:CF_2$ and $Cl_2C:CCl_2$. No least-squares adjustments were made for the intermediate cases.

§ This assignment was adopted earlier by Torkington and Thompson. See reference 7.

The good agreement between the calculated values and the observed fundamentals of the new assignment for *a*-F_2C:CCl_2 lends additional support to the expectation that the fundamentals of FClC:CCl_2 are not far from the predicted values given in Table II. Unfortunately, however, these calculations did not become available until after a provisional assignment for fluorotrichloroethylene had been suggested. The results of the force constant treatment made it quite clear that certain features of the provisional assignment were not correct. Very shortly thereafter Professor J. Rud Nielsen very kindly made known to us the results of his investigation of the infrared and Raman spectra of the same molecule|| and confirmed the essential correctness of the revised assignment based on that predicted by the force constant analysis.

As remarked earlier, the three out-of-plane modes may be expected to give rise to type *C* infrared bands and depolarized Raman lines. The lowest of these, which may be construed as arising from what is essentially a torsional mode, occurs in a region inaccessible to our present infrared instruments. Inspection of Fig. 1 reveals two bands, at 537 and 358 cm^{-1}, with prominent *Q* branches and apparent type *C* envelopes. In the absence of depolarization data the earlier, provisional assignment was made on this basis. Three subsequent developments showed unequivocally that whereas the 537 cm^{-1} band does in fact belong to species a'', that at 358 cm^{-1} does not, despite its apparent a'' envelope. Reference to Table II will show that the predicted frequencies are clear on this point: the 358 cm^{-1} band arises from a planar mode. Professor Nielsen's observation of the polarized character of the corresponding Raman line leaves no room for doubt that 358 cm^{-1} is a fundamental belonging to a'. Professor Nielsen also reported a faint, diffuse Raman line at 313 cm^{-1} and ascribed it to the intermediate a'' fundamental. We have also been able to find an ex-

TABLE I. Infrared and Raman spectra of FClC:CCl_2.

Raman (liquid) $\Delta\nu$ (cm^{-1})	*I*	Infrared (gas) ν (cm^{-1})	*I*		Interpretation
123	vw				spurious[a]
144	vw				spurious
174	w				$\nu_9(a')$
253	vs	250	~m[b]	*Q*	$\nu_8(a')$
		~255, sh	~m	*R*	
		313[c]	vvw		$\nu_{11}(a'')$
		355, sh	m	*P*	
365	s	358	m	*Q*	$\nu_7(a')$
		365	m	*R*	
		404	m	*P*	
403	w, d	407	m	*Q*	$\nu_6(a')$
		409	m	*R*	
		~425, sh	m		174+250=424
520	s	~520, sh	vvw		$\nu_5(a')$[d]
		532, sh	m	*P*	
532	m	537	m	*Q*	$\nu_{10}(a'')$
		546	m	*R*	
		585	vw		174+407=581
		624, b	vw		2×313=626
		655	vw		250+407=657
		~815, sh	vw		2×407=814
		~837, sh	w		313+520=833(A'')
		~853, sh	vs	*P*	
		857	vs	*Q*	$\nu_4(a')$
		861	vs	*R*	
		~880, sh	w		358+520=878(A'')
		920	w		407+520=927
		952	w		407+537=944(A'')
		985	vs	*P*	
986	s, sharp	(988)$_e$[e]			$\nu_3(a')$
		993	vs	*R*	
		1027, sh	w	*P*	
		1033	w	*Q*	2×520=1040; 174+857=1031
		1065	w	*P*	
(~1060)	?	1071	w	*Q*	2×537=1074
		1078	w	*R*	
		1107	vw		250+857=1107
		~1152, sh	vw		174+988=1162
		1176	vs	*P*	
~1171	vw, d	(1181)$_e$			$\nu_2(a')$
		1183	vs	*R*	

|| Private communication from Professor J. Rud Nielsen.

TABLE I—*Continued.*

Raman (liquid) $\Delta\nu$ (cm^{-1})	I	Infrared (gas) ν (cm^{-1})	I		Interpretation
(~1219)	?	1212	m		358+857=1215
		~1224, sh	m		3×407=1221
		1255	m		407+857=1264
		1299	w		313+988=1301(A'')
		1346	w		358+988=1346
		1385	w		520+857=1377; 537+857=1394(A''); 407+988=1395
		1504	w		520+988=1508
		1587	w		407+1181=1588
		~1625, sh	m		358+407+857=1622; 250+520+857=1627
1644	s, d	1645	s		$\nu_1(a')$
		~1660, sh	m		313+358+988=1659(A'')
		1709	w		2×857=1714; 520+1181=1701
		1730	vw		358+520+857=1736
		1818	vw		174+1645=1819
		1852	vw		857+988=1845
		1898	vw		250+1645=1895
		~1947, sh	vw	P	
		1954	vw	Q	313+1645=1958(A'')
		~1958, sh	vw	R	
		~2020, sh	vw		2×520+988=2028
		2034	vw		857+1181=2038
		~2051, sh	vw		407+1645=2052
		2165	vw		520+1645=2165
		~2172, sh	vw		988+1181=2169
		~2347[f]	w		2×1181=2362
		2502	vw		857+1645=2502
		2637	vw		988+1645=2633
		2828	w		1181+1645=2826
		2867	vw		358+857+1645=2860; 520+2×1181=2882
		2941	vw		313+988+1645=2946(A'')
		3292	vw		2×1645=3290
		3338	vw		988+2×1181=3350; 520+1181+1645=3346

[a] As mentioned in the text, the lines corresponding to 123 and 144 cm^{-1} Raman shifts are almost certainly spurious. Nielsen and his co-workers, while finding more than twice as many lines in their study of the Raman spectrum of liquid FClC:CCl$_2$, did not observe these two lines.

[b] The intensities of the bands observed in the cesium iodide region are somewhat uncertain relative to the remainder of the spectrum since the partial pressure of the absorbing gas, which was contained in the monochromator housing, was not determined.

[c] Found in spectrum of liquid.

[d] The species of the combination or overtone is understood to be A' unless A'' is given explicitly.

[e] A wave number given in the form $(\cdots)_e$ is the measured value of the trough between P and R branches. The designation 'sh' means shoulder, 'b' stands for broad, and 'd' for diffuse. The tilde (~) is used to indicate that the measured quantity may be more than normally uncertain, and applies in particular to very weak lines or bands, shoulders, and broad or diffuse lines or bands.

[f] This band is overlapped by atmospheric CO$_2$ absorption. The wave number listed is taken from the dashed curve, corrected for background and CO$_2$ interference, given in Fig. 1.

TABLE II. Summary of existing assignments for F$_2$C:CF$_2$,[a] F$_2$C:CFCl,[b] *a*-F$_2$C:CCl$_2$,[c] FClC:CCl$_2$,[d] and Cl$_2$C:CCl$_2$.[a,n] Values for the fundamentals calculated by Mann, *et al.* are also given.

F$_2$C:CF$_2$			F$_2$C:CFCl			*a*-F$_2$C:CCl$_2$			FClC:CCl$_2$			Cl$_2$C:CCl$_2$		
Species	Obs'd (cm^{-1})	Calc'd (cm^{-1})	Species	Obs'd (cm^{-1})	Calc'd (cm^{-1})	Species	Obs'd (cm^{-1})	Calc'd (cm^{-1})	Species	Obs'd (cm^{-1})	Calc'd (cm^{-1})	Species	Obs'd (cm^{-1})	Calc'd (cm^{-1})
a_g	1872[e]	1871	a'	1792[f]	1804	a_1	1749	1731	a'	1645	1656	a_g	1571[g]	1571
b_{1g}	1340[e]	1349	a'	1336	1332	b_1	1327	1327	a'	1181	1206	b_{1g}	1000[g]	1009
b_{2u}	1337	1294	a'	1215	1235	a_1	1032	1065	a'	988	970	b_{2u}	908[h]	881
b_{3u}	1186	1211	a'	1058	1062	b_1	993	957	a'	857	856	b_{3u}	777[h]	801
a_g	778[e]	783	a'	689	691	a_1	640	(a_1)611	a'	520[g]	525	a_g	447[g]	453
b_{3u}	558	553	a'	512	515	a_1	622	(b_1)443	a'	407	398	b_{1g}	347[g]	341
b_{1g}	551[g]	547	a'	463	453	b_1	459	(a_1)433	a'	358	365	b_{3u}	310[h]	308
a_g	394[e]	395	a'	338	349	a_1	434[g,i]	(a_1)260	a'	250	253	a_g	235[g]	234
b_{2u}	218	216	a'	194	200	b_1	192[i]	192	a'	174[g]	180	b_{2u}	176[h]	176
b_{2g}	508[g]	508	a''	538	516	b_2	564	523	a''	537	517	b_{2g}	512[g]	512
b_{1u}	406	406	a''	369	377	b_2	258[g,i]	337	a''	313	318	b_{1u}	288[h]	288
a_u	190	190	a''	158[j]	169	a_2	(167)[k]	157	a''	(130)[l]	129	a_u	110[m]	110

[a] Taken from reference 4.

[b] Taken from reference 5.

[c] Taken from reference 6, but see reference 7 also.

[d] Results of present investigation.

[e] From Raman spectrum of gas.

[f] Except where otherwise noted all experimental entries are taken from infrared spectra of substances in gaseous state.

[g] From Raman spectrum of liquid.

[h] From infrared spectrum of liquid.

[i] Also found by Mann and Plyler in infrared spectrum of vapor.

[j] Deduced from combination tones and third-law entropy data.

[k] Based on uncertain and very weak Raman line found in spectrum of liquid.

[l] Estimated value; see text.

[m] From overtone found in Raman spectrum of liquid.

[n] Added in proof: Assignment of reference 4 for angular modes of b_{1u} and b_{3u} species revised to accord with more recent results.

TABLE III. Fundamental vibrational assignments for a-$F_2C{:}CCl_2$ and $FClC{:}CCl_2$.

a-$F_2C{:}CCl_2$ Species	Wave number (cm^{-1})	$FClC{:}CCl_2$ Species	Wave number (cm^{-1})
a_1	1749[a]	a'	1645[a]
b_1	1327	a'	1181
a_1	1032	a'	988
b_1	993	a'	857
a_1	622	a'	520[b]
b_1	459	a'	407
a_1	434	a'	358
a_1	258	a'	250
b_1	192	a'	174[b]
b_2	564	a''	537
b_2	323	a''	313
a_2	(167)[c]	a''	(130)[d]

[a] Except where otherwise noted values are taken from infrared spectrum of vapor.
[b] From Raman spectrum of liquid.
[c] See footnote *k* to Table II.
[d] See footnote 1 to Table II.

tremely weak infrared band having about the same wave-number value, but its low intensity and the strong background due to atmospheric water vapor make it difficult to obtain a reliable indication of its contour. Nevertheless, it seems established as the intermediate a'' fundamental.

With the exception of the lowest a'' fundamental, the remainder of the assignment is easily established. The strong infrared band at 1645 cm^{-1}, and the intense Raman line at 1644 cm^{-1}, may be ascribed without hesitation to the CC stretching fundamental. Next in order, the bands at 1181, 988, and 857 cm^{-1} may be assigned to three of the four carbon-halogen stretching modes. The fourth does not appear at all in our infrared spectra of the vapor of $FClC{:}CCl_2$, but shows up quite strongly at 520 cm^{-1} in the Raman spectrum of the liquid. Of the four planar angular modes, the one at 358 cm^{-1} has already been discussed. The infrared bands at 407 and 250 cm^{-1}, and the corresponding Raman lines at 403 and 253 cm^{-1}, are to be ascribed to two of the three remaining planar modes. The force constant calculations show clearly that the Raman line at 174 cm^{-1} arises from the lowest planar mode, which has the character of a rocking motion.

Only the lowest a'' fundamental remains to be determined. Either the 123 or 144 cm^{-1} Raman lines could be used for this purpose. Professor Nielsen has informed us that although he has observed more than twice as many Raman lines as we have, he found no lines at near 123 or 144 cm^{-1}. We must conclude, therefore, that these lines are spurious and should be disregarded. Nevertheless, it is clear from Table II that the torsion fundamental of $FClC{:}CCl_2$ may quite reasonably be expected to lie near 130 cm^{-1}, and is probably not more than five, or at most ten, wave numbers from this estimated central value.

TABLE IV. Thermodynamic functions for $FClC{:}CCl_2$ in dimensionless units.

$T°K$	$C_p°/R$	$(H°-E_0°)/RT$	$-(F°-E_0°)/RT$	$S°/R$
200	9.162	6.300	30.87	37.17
273.16	10.56	7.264	32.98	40.24
298.16	10.95	7.557	33.62	41.19
300	10.98	7.578	33.68	41.26
400	12.21	8.592	36.00	44.59
500	13.09	9.408	38.01	47.42
600	13.72	10.08	39.79	49.86
700	14.18	10.63	41.38	52.01
800	14.52	11.10	42.83	53.93
900	14.78	11.49	44.16	55.66
1000	14.98	11.83	45.39	57.22
1100	15.14	12.13	46.53	58.66
1200	15.26	12.38	47.60	59.98
1300	15.36	12.61	48.60	61.21
1400	15.44	12.81	49.54	62.35
1500	15.51	12.99	50.43	63.42

The vibrational assignment for fluorotrichloroethylene is now essentially complete. It is in accord with that determined by Professor Nielsen and with that predicted by Mann, *et al.* The final assignments for both a-$F_2C{:}CCl_2$ and $FClC{:}CCl_2$ are summarized in Table III.

Thermodynamic Functions

The necessary molecular constants and the vibrational assignment given in Table III were used in the calculation of the ideal-gas thermodynamic functions for $FClC{:}CCl_2$ by the usual statistical methods. The conventional rigid-rotator, harmonic-oscillator approximation was made. The contribution of translation and rotation to the entropy is, in dimensionless units, $[S°/R]_{T,R}=12.3674+9.2103\log T$.

The actual computations were carried out by the National Bureau of Standard's electronic digital computer, the SEAC. The results given in Table IV are taken from the more extensive and finely spaced tabulation available.

ACKNOWLEDGMENTS

The authors are grateful to Dr. D. R. Stull of the Dow Chemical Company for providing them with a generous sample of $FClC{:}CCl_2$. Thanks are also due Mr. N. Acquista and Mr. T. Bagg for their assistance with the experimental work, and to Professor J. Rud Nielsen for making his results available in advance of publication.

Note added in proof.—Recent work on the vibrational spectrum of C_2Br_4 [Mann, Meal, and Plyler, J. Chem. Phys. (to be published)] has necessitated some revision of the assignment given for C_2Cl_4 in reference 4. The angular modes of species b_{1u} and b_{2u} are now taken to be 288 and 310 cm^{-1}, respectively. The arguments and conclusions of the present paper are unaffected by these new results and remain unchanged. It is to be noted that the calculated frequencies of Table II were obtained from force constants based on the new assignment for C_2Cl_4.

Infrared and Raman Spectra of Fluorinated Ethylenes. VI. Fluorotrichloroethylene*

J. Rud Nielsen, C. W. Gullikson, and A. H. Woollett
Department of Physics, University of Oklahoma, Norman, Oklahoma

(Received February 7, 1955)

The infrared spectrum of gaseous CCl_2:CClF has been observed from 2 to 22μ with NaCl and KBr prisms. The Raman spectrum of the liquid has been photographed with a three-prism glass spectrograph of linear dispersion 15 A/mm at 4358 A, and the depolarization ratios of the stronger Raman bands have been measured. All but one of the fundamental vibration frequencies have been assigned, and the spectra have been interpreted in detail.

INTRODUCTION

THE spectral data reported here for CCl_2:ClF were obtained nearly two years ago, but publication was deferred until infrared data could be obtained in the region 22 to 38μ. Recently, D. E. Mann and E. K. Plyler of the National Bureau of Standards have kindly sent us the results of their work on this molecule, which includes infrared data out to 50μ, and Raman data without polarization measurements.[1] In the present paper our spectral data are presented and an assignment of 11 of the 12 fundamentals is given which agrees with that of Mann and Plyler.

EXPERIMENTAL RESULTS AND DISCUSSION

The sample was obtained from Halogen Chemicals, Inc. No information was available about its purity. The infrared absorption spectrum, obtained with a spectrometer similar to one described by Wright,[2] is shown in Fig. 1. The wave numbers of the observed absorption maxima are listed in Table I. The Raman data, obtained with a three-prism glass spectrograph of linear dispersion 15 A/mm, are listed in Table II.

Mann and Plyler, using CsBr and CsI prisms, observed infrared absorption maxima at 250, 358, 365, 404, and 409 cm^{-1}, which lie outside the spectral region covered in the present work. In addition, they found 18 very weak absorption maxima, or shoulders on stronger bands, not observed here. On the other hand, Table I contains eight maxima or shoulders not listed by Mann and Plyler. Some of these, in particular the very weak maxima at 456, 470, and 500 cm^{-1}, may possibly be caused by impurities. Apart from one band, found by Mann and Plyler at 585 and here at 609 cm^{-1}, the agreement with our somewhat less accurate data is within the experimental error.

More than twice as many Raman bands were observed here as at the Bureau of Standards. Nevertheless, no indication was found of the very weak bands observed by Mann and Plyler at 123 and 144 cm^{-1}. This can hardly be attributed to the background surrounding the 435 A mercury line; hence, the reality of these bands is open to doubt. The agreement between the Raman shifts measured both at the Bureau of Standards and here is satisfactory.

ASSIGNMENT OF FUNDAMENTALS

The CCl_2:CClF molecule has the symmetry C_s and hence nine normal vibrations of species a' and three of

Table I. Infrared spectrum of fluorotrichloroethylene (gas).

Wave number	Description[a]	Interpretation
~456	w	858−407=451 A′?
470	vw	174+313=487 A″?
~500	vw	2×250=500 A′
~528	w	
536	m	a'' fundamental
543	m	
609	vw	250+364=614 A′
626	vw	2×313=626 A′
~662	vw	250+407=657 A′
769	w	364+407=771 A′
820	m	2×407=814 A′
836	s	313+520=833 A″
853	vs	
858	vs	a' fundamental
863	vs	
878	s	364+520=884 A′
921	s	407+520=927 A′
954	m	407+536=943 A″
968	vw	250+313+407=970 A″
986	vs	a' fundamental (990)
995	vs	
1025	w	174+858=1032 A′
1035	m	2×520=1040 A′
1048	w	520+536=1056 A″
1066	w	
1072	w	2×536=1072 A′
1077	w	
1110	vw	250+858=1108 A′
1152	m	174+990=1164 A′
1180	vs	a' fundamental (1183)
1187	vs	
1215	s	364+858=1222 A′
1245	m	250+990=1240 A′
1262	m	407+858=1265 A′
1299	m	313+990=1303 A″
~1343	w	364+990=1354 A′
1393	m	407+990=1397 A′
1510	m	520+990=1510 A′
1649	s	a' fundamental
1704	w	520+1183=1703 A′
1808	w	174+1649=1823 A′
1945	vw	313+1649=1962 A′
2029	vw	858+1183=2041 A′
2157	vw	520+1649=2169 A′
2800	w	1183+1649=2832 A′

[a] The following abbreviations have been used: vs, very strong; s, strong; m, medium; w, weak; vw, very weak.

* This work has been supported by the U. S. Atomic Energy Commission under contract.

[1] Private communication from D. E. Mann.

[2] N. Wright, Ind. Eng. Chem., Anal. Ed. **13**, 1 (1941).

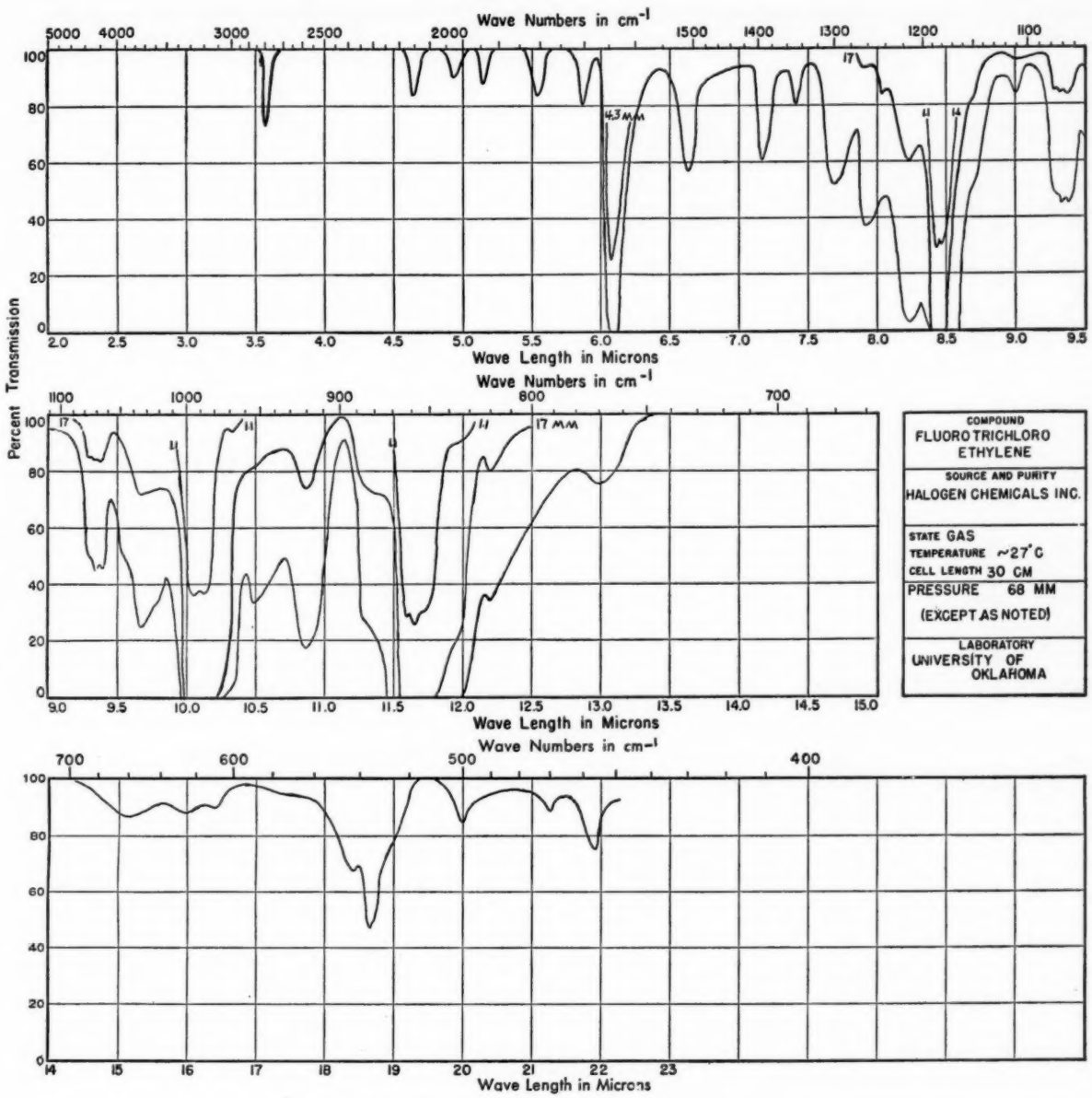
Wave Numbers in cm⁻¹
5000 4000 3000 2500 2000 1500 1400 1300 1200 1100
Percent Transmission
4.3 MM
17
11
14
2.0 2.5 3.0 3.5 4.0 4.5 5.0 5.5 6.0 6.5 7.0 7.5 8.0 8.5 9.0 9.5
Wave Length in Microns
Wave Numbers in cm⁻¹
1100 1000 900 800 700
17 MM
9.0 9.5 10.0 10.5 11.0 11.5 12.0 12.5 13.0 13.5 14.0 14.5 15.0
Wave Length in Microns
COMPOUND
FLUORO TRICHLORO ETHYLENE
SOURCE AND PURITY
HALOGEN CHEMICALS INC.
STATE GAS
TEMPERATURE ~27°C
CELL LENGTH 30 CM
PRESSURE 68 MM
(EXCEPT AS NOTED)
LABORATORY
UNIVERSITY OF OKLAHOMA
Wave Numbers in cm⁻¹
700 600 500 400
14 15 16 17 18 19 20 21 22 23
Wave Length in Microns

FIG. 1. Infrared spectrum of fluorotrichloroethylene gas.

species a''. The latter should be depolarized in the Raman spectrum and be of type C in the infrared. The a' fundamentals should be polarized in the Raman spectrum and have the infrared contours of bands that are hybrids of types A and B. The wave numbers of the a'' fundamentals, which correspond to out-of-plane wagging and twisting motions, may be expected to lie below 550 cm^{-1}.

The intense infrared bands at 1649, 1183, 990, and 858 cm^{-1}, and their counterparts in the Raman spectrum, must all be interpreted as a' fundamentals, as must the very strong polarized Raman band at 520.5 cm^{-1}. The highest of these can be characterized fairly accurately as arising from C=C stretching; the others involve C−F and C−Cl stretching. It is interesting to note that the a' fundamental at 851 cm^{-1} is very weak in the Raman spectrum but very strong in the infrared, whereas the opposite is true for the a' fundamental at 520.5 cm^{-1}. This is in accord with the fact that, of the corresponding fundamentals in C_2Cl_4, one is infrared-active and the other Raman-active.

The strong Raman band at 364.2 cm^{-1} is definitely polarized and is therefore interpreted as an a' fundamental. If it is assumed that it is associated with CCl_2 deformation, the presence of a sharp Raman band at 360.1 cm^{-1}, of about one-third the intensity, can readily be explained as caused by molecules containing an atom of Cl^{37} in the CCl_2 group.

The strong Raman band at 174.4 cm^{-1} appears to be polarized and is interpreted as an a' fundamental as-

TABLE II. Raman spectrum of fluorotrichloroethylene (liquid).

Wave number	Description[a]	Depolarization ratio	Exciting Hg lines[a]	Interpretation
174.4	s, sh	0.75	±e	a' fundamental
253	vs	0.85	±ek s	a' fundamental
313	vw, d		e	a'' fundamental
360.1	m, sh		±e	a' fundamental Cl^{37}
364.2	s, sh	0.40	±ek	a' fundamental Cl^{35}
405	m	0.85	±e	a' fundamental
520.5	vs	0.60	±efk	a' fundamental
531	s	0.8	±efk	a'' fundamental
~580	vvw		e	174+405=579 A′
628	w, d		e	2×313=626 A′
691	vvw		e	174+520=694 A′
717	vvw		e	313+405=718 A″
800	vvw		e	2×405=810 A′
851	vvw		e	a' fundamental
983	w	0.9	e	a' fundamental
1062.2	w, sh		e	2×531=1062 A′
1173	m	0.70	e	a' fundamental
~1210	vvvw		e	364+851=1215 A′
1341	vvw		e	174+1173=1347 A′; 364+983=1347 A′
1390	vvw		e	405+983=1388 A′
1505	vvw		e	520+983=1503 A′
1643.7	vvs, sh	p	efg	a' fundamental
1694	w		e	520+1173=1693 A′
1824	vvw		e	174+1644=1818 A′
1892	vvw		e	253+1644=1897 A′
1961	vw		e	2×983=1966 A′
2002	vvw		e	364+1644=2008 A′
2160	vvw		e	520+1644=2164 A′
2335	vvw		e	2×1173=2346 A′

[a] The following abbreviations and symbols have been used: vs, very strong; s, strong; m, medium; w, weak; vw, very weak; vvw, very very weak; sh sharp; d, diffuse; e, Hg 4358 A; f, Hg 4348 A; g, Hg 4339 A; k, 4046 A; ±e means that the Raman frequency has been measured both as Stokes and anti-Stokes shift from Hg 4358 A.

sociated with rocking. Of the remaining two a' fundamentals one, involving CClF deformation, may be expected to lie in the range 400–550 cm^{-1}. In addition to the band at 520 cm^{-1}, already assigned as an a' fundamental, there are two bands in this region, at 405 and at 531.0 cm^{-1} (in liquid CCl_2:CClF). The Raman data do not provide any conclusive evidence as to the species of these bands. However, the infrared contour indicates definitely that the latter band is associated with an out-of-plane motion. Moreover, it would be rather improbable for bands of the same species to lie as close as 521 and 531 cm^{-1}. Hence, the band at 405 cm^{-1} is assigned as an a' fundamental and that at 531 cm^{-1} as the highest a'' fundamental.

The last a' fundamental, associated roughly with a rocking motion in which the carbon atoms move out of phase, should lie between 200 and 350 cm^{-1}. The intermediate a'' fundamental, involving CCl_2 wagging, may be expected to lie in the same region. Two Raman bands are observed, a strong depolarized band at 253 cm^{-1} and a very weak diffuse band at 313 cm^{-1}. Since the high rocking frequency in C_2Cl_4 is Raman-active, it does not seem reasonable to assign the weak Raman band at 313 cm^{-1} to this mode. Moreover, the infrared band observed by Mann and Plyer at 250 cm^{-1} does not seem to have type C contour. This band is therefore interpreted as an a' fundamental.

TABLE III. Fundamental vibrational frequencies for fluorotrichloroethylene.

Symmetry species	Infrared (gas) Wave number	Infrared (gas) Description[b]	Raman (liquid) Wave number	Raman (liquid) Description[b]	Raman (liquid) Depolarization ratio
a'	1649	s	1643.7	vvs, sh	p
a'	1183	vs	1173	m	0.70
a'	990	vs	983	w	0.9
a'	858	vs	851	vvw	...
a'	...	...	520.5	vs	0.60
a'	407[a]	w	405	m	0.85
a'	365[a]	w	364.2	s, sh	0.40
a'	250[a]	w	253	vs	0.85
a'	...	...	174.4	s, sh	0.75
a''	536	m	531	s	0.8
a''	...	...	313	vw, d	...
a''	...	...	...	...	...

[a] Observed by Mann and Plyler (reference 1).
[b] The following abbreviations have been used: vs, very strong; s strong; m, medium; w, weak; vw, very weak; vvw, very very weak; sh, sharp; d, diffuse.

The faint diffuse Raman band at 313 cm^{-1} is assigned as the intermediate a'' fundamental. Its low intensity is in accord with the fact that the corresponding fundamental in C_2Cl_4 is inactive in the Raman effect. Although one would expect it to be fairly strong in the infrared, Mann and Plyler found only a very faint band at 313 cm^{-1} in liquid CCl_2:CClF and no absorption in the gas. The assignment of this fundamental must therefore be regarded as tentative.

No sufficient evidence was found for assigning the lowest a'' fundamental, which is associated with a twisting motion of the CCl_2:CClF molecule. The assumption that it has the value 184 cm^{-1}, and is masked by the lowest a' fundamental at 174 cm^{-1}, would explain the rather strong zero branch found by Mann and Plyler at 358 cm^{-1} as resulting from the combination 174+184=358 A″. However, this assignment does not explain any other infrared or Raman bands that are not interpreted satisfactorily otherwise, and 184 cm^{-1} appears rather high for this fundamental. The value 130 cm^{-1} assumed by Mann and Plyler, lies in the wave number region where one would expect the torsional fundamental for this molecule.

The assigned fundamental vibration frequencies are listed in Table III. In terms of these fundamentals it has been possible to interpret all of the remaining Raman bands, and all but one of the infrared bands, as first overtones or binary combinations. The very weak infrared band at 968 cm^{-1} is interpreted in two different ways as a ternary sum band. The interpretations are listed in the last columns of Tables I and II. Except for the two weak infrared bands at 456 and 470 cm^{-1}, which were not observed by Mann and Plyler, the interpretations given seem satisfactory.

ACKNOWLEDGMENT

The writers are indebted to Dr. D. E. Mann and Dr. E. K. Plyler for making their results available before publication.

Report on Notation for the Spectra of Polyatomic Molecules*

(Received February 28, 1955)

1. INTRODUCTION AND SUMMARY

A SATISFACTORY standardization of notation for diatomic molecules and their spectra already exists.[1] The problem of standardization for polyatomic molecules is much more complicated, because of the greater number of degrees of freedom for rotation and vibration, and because of the considerable variety of types of symmetry, or *symmetry groups*, to which polyatomic molecules belong, as contrasted with only two types ($C_{\infty v}$ and $D_{\infty h}$) for diatomic molecules. Fortunately, the system used in Herzberg's well-known book on infrared and Raman spectra[2] is already very generally accepted, and forms a suitable basis for the standard notation proposed here. However, when one considers the entire range of polyatomic spectroscopy, from ultraviolet to microwave and magnetic resonance spectra, there are several points of notation which need clarification, revision, supplementation, or simply codification and affirmation in a form to which spectroscopists of all wavelengths can conveniently refer. The principal need for supplementation, as compared with Herzberg's book, arises from the consideration of molecules in nontotally-symmetric electronic states, a matter which is especially essential for electronic spectra.

In some points the problem of notation for polyatomic spectra overlaps that for other related areas; in particular, valence theory, and the states of atoms in crystals. Some consideration has been given in this report to the needs of these areas, and a few recommendations have been made.

The problems are rather different for small molecules, the high symmetry of which is often very important for the classification of vibration modes and quantized states, and large molecules, where rigorous symmetry is often nonexistent or unimportant (though approximate or local symmetry is often important). Some consideration has been given in this report to large molecules, but the major emphasis is on the smaller or more symmetrical molecules.

This report in draft form has been sent to some 150 molecular spectroscopists and persons in allied fields for their criticism, comments, and suggestions, and the replies (from some 65 persons) have been very helpful in arriving at an end result which is believed to be acceptable in nearly all respects to almost all those who were consulted.

The conclusions reached are summarized in Table I, while the background for these conclusions, and certain further considerations, are presented in the subsequent text.

Where it is believed that existing practice is sufficiently well established, fairly unanimous, and ripe for current standardization, the conclusions are embodied in *Recommendations*. In a few cases where standardization would be premature or where the need for it is less definite, *Suggestions* have been made.

In some cases, more than one alternative notation has been included in a Recommendation, or it has been recommended that a particular notation be usually used, but that alternatives be not excluded under special circumstances. However, the acceptance of more than one alternative standard notation has never been recommended unless the alternatives are so different in form that there is no danger of their leading to confusion.

In this Report, pending a final decision by the Joint Commission,[3] the symbol cm^{-1} rather than K, and ν rather than σ for wave number, have been used. Further, as a matter of convenience to microwave spectroscopists, the symbol ν as well as related term symbols and molecular constants are permitted to signify quantities which may be expressed either in the usual cm^{-1} units, or in frequency (Mc/sec) units.

At all stages in the preparation of this Report, the writer has consulted extensively with Dr. G. Herzberg, whose cooperation and criticism have been of extremely great value, and who is in essential agreement with all the Recommendations, including those few which involve departures from notation of reference 2.

II. VIBRATIONAL AND ELECTRONIC STATES

1. Classification According to Symmetry Species

(a) *General Considerations*

The notation problem is in many respects very similar for vibrational and for electronic motions in molecules, hence it is convenient to treat these together. The major problem is to select definitions and symbols for the various symmetry-characterized types or "species" of classical normal modes of vibration and of

* This report was prepared at the request of the Joint Commission for Spectroscopy of the International Astronomical Union and the International Union of Pure and Applied Physics, and was officially adopted by the Commission at its meeting in Lund in July, 1954. In order to make the Report readily available to the maximum number of interested scientists, publication in the *Journal of Chemical Physics* seemed very desirable. However, unlike research papers, it seemed proper that the *entire cost* of publication be covered. This cost is being met with the financial assistance of UNESCO, through the International Council of Scientific Unions.

[1] F. A. Jenkins, J. Opt. Soc. Am. **43**, 425 (1953).

[2] G. Herzberg, *Infrared and Raman Spectra of Polyatomic Molecules* (D. Van Nostrand Company, Inc., New York, 1945). Other authors have given tables differing slightly in a few of the species symbols or definitions from those in Herzberg's book.

[3] See Minutes of Lund meeting, J. Opt. Soc. Am.

TABLE I. Summary and index of symbols and definitions.

Symbols or other items	Explanation	Reference
	(1) Quantum Numbers	
$\lambda, \sigma, \omega, \Lambda, \Sigma, \Omega; S$	Electronic quantum numbers for linear molecules, the same as for diatomic molecules (reference 1); resultant angular momentum of electron spins.	Rec. 2b
$v_i (i=1, 2, \cdots)$	Vibrational quantum numbers.	Rec. 8
v_2^+, v_2^- (e.g. $0^+, 0^-, 1^+, \cdots$)	Vibrational quantum numbers with superscripts to indicate inversion doubling components.	Rec. 11
$l_i, v_i l_i, l$	Absolute value of vibrational angular momentum for degenerate vibrations of linear molecules; l_i for vibration with quantum number v_i, l for resultant angular momentum from all vibrations.	Recs. 9, 10
l_i	Angular momentum index for degenerate vibrations of symmetric-rotor molecules.	Rec. 9
J	Resultant angular momentum excluding nuclear spins.	Recs. 20, 25, 26
N	Resultant angular momentum excluding electron and nuclear spins, for the case that electron spin is present but loosely coupled.	Rec. 25
M, M_N, M_S	Projection of vector J, N, or S, respectively, on axis of axially symmetrical external electric or magnetic field.	Rec. 27
K	Absolute value of total angular momentum along axis of symmetric (or quasi-symmetric) rotor, exclusive of electron spin if present. For linear molecules, K is absolute value of vibronic (i.e., electronic×vibrational state) angular momentum for the case of electron spin zero or loosely coupled.	Rec. 21; Secs. III 2(b), (c), (d)
Σ	Component of vector S along axis of linear molecule or symmetric or quasi-symmetric rotor, if tightly coupled to vector K. The sign of Σ is positive or negative according as the component of vector S has the same or the opposite direction to K.	Rec. 26
P	Absolute value of total angular momentum along symmetry axis when vector S is tightly coupled to the latter. For linear molecules, $P=\lvert\pm\Lambda\pm l\rvert$. For symmetric (or quasi-symmetric) rotors, $P=\lvert K+\Sigma\rvert$.	Recs. 18, 26
(J,K)	Symbol for quantized rotational levels of symmetric-rotor molecules.	Rec. 21
$J_{K_a K_c}$ or J_τ	Symbols for quantized rotational levels of asymmetric-rotor molecules.	Rec. 22
I (or I_i)	Angular momentum of nuclear spin for one nucleus.	Rec. 28
T (or T_i)	Resultant angular momentum of nuclear spins for a set of like nuclei.	Rec. 28
F	Resultant angular momentum including everything.	Rec. 28
M_F, M_I, M_J	Projection of F, I, or J, respectively, on axis of axially symmetrical external electric or magnetic field.	Rec. 28
	(2) Electronic and Vibronic States	
General Considerations on Electronic States		Recs. 1, 14; Secs. II 1(a), II 3(a), (c)
General Considerations on Vibronic States		Sec. II 1(a), II 4
T_e	Electronic term (in cm^{-1} or Mc/sec).	Rec. 29
e, ev, v (as left superscript)	To distinguish electronic (^{e}) and vibronic (^{ev}), and vibrational (^{v}) states, *if necessary*.	Sug. 1
g, u (as subscripts)	Parity species symbols for orbitals and electronic and vibronic states of molecules *having a symmetry center* (g, u, denote symmetric or antisymmetric, respectively, on inversion at the center).	Recs. 2, 3
${}^m\Sigma^+$, ${}^m\Sigma^-$, ${}^m\Pi$, ${}^m\Delta$, $\cdots$	Species symbols for electronic or vibronic states of unsymmetrical linear molecules ($m=2S+1=$spin multiplicity), the same as for diatomic molecules (reference 1).	Rec. 2, Table II, and Sec. II 1(b)
${}^m\Sigma_g^+$, ${}^m\Sigma_u^+$, ${}^m\Sigma_g^-$, ${}^3\Pi_u$, etc.	Species symbols for electronic or vibronic states of symmetrical linear molecules, the same as for diatomic molecules (reference 1).	Rec. 2, Table II, and Sec. II 1(b)
${}^3\Pi_1$, ${}^2\Delta_{5/2}$, ${}^2\Pi_{(3/2)u}$, etc.	Linear-molecule electronic state symbols including subscripts for multiplet components, needed if spin is strongly coupled to molecular axis; the numerical subscript is the value of $\Lambda+\Sigma$, the same as for diatomic molecules (reference 1).	Rec. 2, and Sec. II 1(b)
${}^mA$, ${}^mB$, ${}^mE$, ${}^mF$ or ${}^mT$, usually with right subscripts or superscripts of one or more kinds	Species symbols for electronic or vibronic states of nonlinear molecules ($m=2S+1$); also for *atoms in crystals*. See SPECIAL RULES for B_i species (below).	Recs. 1, 3; Rec. 16

TABLE I.—*Continued.*

Symbols or other items	Explanation	Reference
B_i, often with further subscripts or superscripts	SPECIAL RULES are being recommended for labelling axes or planes in PLANAR and some other molecules in order to fix the uncertain meaning of the numerical subscript i in B_i and b_i species labels.	Recs. 4, 5a–d, Fig. 1
N, T, V, Q, V_i, ${}^3Q_u$, ${}^3L_a$, ${}^1L_b$, etc.	Informal symbols for special electronic states.	Rec. 15
	(3) Orbitals and Electron Configurations	
General Considerations		Sec. II 3(b), (c)
g, u (as subscripts)	See under "(2) Electronic and Vibronic States."	
orbital	One-electron orbital wave function.	Rec. 12
spinorbital	One-electron wave function.	Rec. 12
AO, MO	Atomic orbital, molecular orbital.	Rec. 12
GO, SO, ASO, MSO	Group orbital, spin orbital, atomic spin orbital, molecular spin orbital.	Sug. 5
LCAO or LCAO-MO	MO approximated by a linear combination of AO*s*.	Sug. 5
σ, π, δ, $\cdots$	Species symbols for MO*s* in linear molecules; also, for bond AO*s* of atoms in molecules; also, for bond MO*s*.	Recs. 2, 2a, Table I; Sug. 5
a, b, e, f or t, usually with subscripts or superscripts	Species symbols for MO*s* or GO*s* of nonlinear molecules; also, for AO*s* of atoms in crystals or molecules. For b_i species, see B_i above, under "(2) Electronic and Vibronic States," for SPECIAL RULES.	Recs. 3, 16
Electron Configurations and Numbering of MO*s*		Rec. 13, and what follows it
	(4) Vibrational States	
General Considerations		Rec. 1
v (as left superscript)	To distinguish vibrational from electronic or vibronic states, *if necessary*.	Sug. 1
ζ_i	Coefficient of l_i in vibrational angular momentum of ith degenerate vibration.	Rec. 19a.
$G(v_1,v_2,\cdots)$	Vibrational term (in cm^{-1} or Mc/sec).	Recs. 29, 30
$\Delta_i G(v_i)$, $\Delta_m G(v_i)$	Vibrational term differences, in particular $\Delta G(v_i) = G(v_1v_2,\cdots v_i+1,\cdots v_n) - G(v_1v_2\cdots v_i\cdots v_n)$.	Rec. 33
ω_i, x_{ik}, $\cdots$	Coefficients in power series expression for vibrational term: $G=\Sigma_i \omega_i(v_i+\frac{1}{2}d_i) + \Sigma_i \Sigma_{k\geq i} x_{ik}(v_i+\frac{1}{2}d_i)\times(v_k+\frac{1}{2}d_k)+\cdots$. Note that the definitions of ω and x here are different than for diatomic molecules,[1] where $G=\omega_e(v+\frac{1}{2}) - x\omega_e(v+\frac{1}{2})^2+\cdots$.	Rec. 30
ν_i	Symbol for ith vibration mode, also for wave number of corresponding fundamental band; for *numbering* of modes, see Rec. 6.	Rec. 6
σ, π, a, b, e, f, usually with subscripts or superscripts	Species symbols for vibration modes. For b_i species, see B_i under "(2) Electronic and Vibronic States," for SPECIAL RULES.	Recs. 1, 2a, Table II; Rec. 3
$\nu_3 b_{1u}$, $\nu_{16} e_g$, etc.	Combined numbering and species labeling of vibration modes.	Rec. 7
$\nu_1(\nu CH)a_g$, $\nu_3(\delta CH_2)a_g$, $\nu_4(\tau CH_2)a_u$, etc., $\nu(CCl)$, $\nu(\rho CCl)$	Examples of descriptive symbols for vibration modes which are fairly well localized.	Sugs. 2, 3
Σ^+, Σ^-, Π, Δ, $\cdots$ (or also with g, u subscripts)	Species symbols for vibrational states of linear molecules.	Recs. 1, 2, Table II, and Sec. II 1(b)
A, B, E, F, usually with subscripts or superscripts	Species symbols for vibrational states of nonlinear molecules. For B_i species, see B_i under "(2) Electronic and Vibronic States," for SPECIAL RULES.	Rec. 3
$(\nu_1 a_{1g})^2(\nu_6 b_{1u})^2$ $(\nu_{16} e_{2g})^2$, B_{1u} or $(\nu_1\sigma_g)^2(\nu_2\pi_u)^2$ $(\nu_3\sigma_u)$, Δ_u	Examples of vibrational configuration and state symbols.	Sug. 4
	(5) Rotational and Over-all States	
General Considerations; Fine Structure		Secs. III 2(a), III 1
Eulerian Angles		Sec. III 1(a)
I_A, I_B, I_C or I^a, I^b, I^c, often with subscripts e, 0, or v_1, $v_2\cdots$	Principal moments of inertia, always with $I^c \geq I^b \geq I^a$. Subscript e denotes a true *equilibrium* value, subscripts v_1, v_2, $\cdots$ or 0 (for $v_1=v_2=\cdots=0$) indicate effective moments of inertia.	Rec. 19
A, B, C, usually with subscript e, 0, or v_1, $v_2\cdots$	Rotational constants (in cm^{-1} or Mc/sec), with e.g. (in cm^{-1}) $A_e=h/8\pi^2cI_e^a$. Always $A \geq B \geq C$.	Rec. 19
$F(J)$, $F(J,K)$, $F(J_\tau)$, etc.	Rotational term (in cm^{-1} or Mc/sec) for linear or spherical-rotor molecule, symmetric-rotor, or asymmetric rotor, respectively.	Recs. 29, 31

TABLE I.—*Continued.*

Symbols or other items	Explanation	Reference
$F_1(J)$, $F_2(J)$, $\cdots$ $F_1(J,K)$, $\cdots$	Term designations for components of fine structure levels due to loosely coupled electron spin. F_1, F_2, $\cdots$ refer to levels with $J=N+S$, $N+S-1$, $\cdots$.	Rec. 31, Part (2)
$F_a(J)$, $F_b(J)$, $F_{1a}(J)$, etc.	Components of l-doublets or similar doublets; F_a and F_b are respectively the components of lower and higher energy.	Rec. 32
$F^{(+)}(J)$, $F^{(0)}(J)$, $F^{(-)}(J)$	Term designations for Coriolis fine structure levels in 3-fold degenerate (F) vibrational states of spherical rotor molecules.	Rec. 32
$\Delta_1F(J)$, $\Delta_2F(J)$, $\Delta_2F(J,K)$, $\Delta_2{}^KF(J,K)$, $\Delta_2F_{1a}(J)$, etc.	Rotational term differences, e.g. $\Delta_1F(J)=F(J+1)-F(J)$, $\Delta_2F(J,K)=F(J+1,K)-F(J-1,K)$, $\Delta_2{}^KF(J,K)=F(J,K+1)-F(J,K-1)$.	Rec. 33
$A_{[v]}$, $B_{[v]}$, $C_{[v]}$, $-D_{[v]}{}^J$, $-D_{[v]}{}^{JK}$ or $-D_{[v]}{}^{NK}$, $-D_{[v]}{}^K$ or $-D_{[v]}{}^N$	Rotational constants in power series expressions for $F(J,K)$ or $F_i(J,K)$ for linear or symmetric rotor molecule.	Rec. 31, parts (1)–(3)
$-\alpha_i$, $-\alpha_i{}^B$, $-\alpha_i{}^A$, $-\alpha_i{}^C$	Coefficients in power series expressions $B_{[v]}=B_e-\Sigma_i\alpha_i(v_i+\frac{1}{2}d_i)+\cdots$, etc.	Rec. 31, part (5)
A, A_1, A_2, B_1, B_2, B_3, E, F	Species symbols for rovibrational or rovibronic levels (i.e. over-all levels exclusive of hyperfine structure) of nonlinear molecules classified under rotational subgroup of vibrational symmetry group.	Rec. 23
s, a	Species symbols for classification of rovibrational or rovibronic levels of symmetrical linear molecules with respect to exchange of sets of identical nuclei.	Rec. 23
$+$, $-$	Parity species symbols for rovibronic levels (especially for linear and planar molecules).	Rec. 24
l- (or Λ-, Ω-, K-, or P-) doubling	Splitting of rovibronic levels into parity doublets.	Rec. 24 and the following
$++$, $+-$, $-+$, $--$; or A, B_c, B_a, B_b	Symbols for the four asymmetric-rotor rotational species.	Rec. 22

Symbols or other items	Explanation	Reference
	(6) Spectroscopic Transitions	
$'$ $''$ (prime and double prime)	Used to distinguish the upper ($'$) and lower ($''$) levels in a spectroscopic transition. Examples: F', $G(v_1',v_2',\cdots)$, J'', $B_{[v]}''$.	Rec. 34, Sec. IV 2(a)
ΔJ, ΔK, Δv_i, etc.	ΔJ means $J'-J''$, $\Delta v_i=v_i'-v_i''$, etc.	Rec. 35
$-$ (minus sign or dash)	Placed between symbols of upper state (*always first*) and lower state, as symbol for a spectroscopic transition. Examples: $^3B_2-{}^1A_1$ electronic transition; (3,2)$-$(2,1) rotational line of symmetric rotor molecule.	Rec. 36
$\leftarrow$, $\rightarrow$	Used instead of $-$ sign if it is desired to indicate specifically an absorption transition ($T'\leftarrow T''$) or an emission transition ($T'\rightarrow T''$).	Rec. 36
$\nu_1+2\nu_2-\nu_3$, or the like	To indicate a band in the vibrational spectrum.	Rec. 37
ν_e	Electronic "frequency" or origin of a band system (in cm^{-1}); $\nu_e=T_e'-T_e''$.	Rec. 38
ν_0	Origin of a band (in cm^{-1}): $\nu_0=\nu_e+(G'-G'')$.	Rec. 38
band; (electronic) transition; band system		Rec. 39
O, P, Q, R, S	To denote band branches with ΔJ (or ΔK)$=-2$, -1, 0, $+1$, $+2$ respectively.	Rec. 40
$^RQ(J)$, etc.	Band line with $\Delta K=1$, $\Delta J=0$, and a value of J'' equal to the J value given in parentheses; etc.	Rec. 40
$^RQ_{12}(J)$, etc.	Like $^RQ(J)$, etc. but with loosely coupled electron spin S whose orientation is implicitly given by the numerical subscripts (first subscript for upper state, second for lower state); $J'=N'+S=J''=N''+S-1$ in example given.	Rec. 41
Use of R, S in rotational Raman spectra		Rec. 42

quantum-mechanical eigenfunctions. These species are best characterized by group-theoretical methods. For any molecule of given symmetry, each symmetry species is defined, and its species label assigned, to correspond to a characteristic behavior under each of the various "classes" of symmetry operations of the symmetry group.

The classification according to symmetry species is most important for small molecules of high symmetry. For molecules lacking any symmetry, no rigorous classification is possible, but partial or approximate classifications based on local or approximate symmetry are often useful.

The things which require classification fall into the five categories given just below. **It is recommended (REC. 1)** that, *for any given symmetry group*, identically the same set of species symbols be used for all five categories, except that *lower case letters* be used for

categories (a) and (c), *capital letters* for (b), (d), and (e).

(a) *Normal vibration modes:* lower case letters.
(b) *Vibrational state wave functions:* capital letters.
(c) *Orbitals* (i.e., one-electron orbital electronic wavefunctions): lower case letters.
(d) *Electronic state wave functions:* capital letters.
(e) *Vibronic state* (i.e., combined electronic × vibrational state) *wave functions:* capital letters.

The use of the same capital-letter species symbols for categories (b), (d), and (e) will seldom cause confusion. The context will usually make clear which category is involved. However, **it is suggested** (**SUG. 1**) that, *if necessary* for clarity, the species symbols be prefixed by a left superscript ^{v}, ^{e}, or ^{ev} for a vibrational, electronic, or vibronic state respectively; for example, $^{v}E_{2g}$, $^{e3}B_1$, $^{ev2}A'$.

(b) *Linear Molecules*

Two systems of species symbols are in common use. One, using Greek letters, was first developed for orbitals and electronic states of diatomic molecules. Diatomic, and also *linear polyatomic*, molecules belong to symmetry groups $C_{\infty v}$ for unsymmetrical, $D_{\infty h}$ for centrosymmetric, molecules. Hence **it is recommended** (**REC. 2**), in agreement with general practice, that use of the diatomic electronic species symbols be extended to all of the five classification categories given above, for all *linear molecules*.

Table II and the subsequent discussion indicate the species symbols for molecules of symmetry $C_{\infty v}$. In categories (d) and (e), a left superscript to denote the spin multiplicity m is usually included, e.g., $^1\Sigma^+$, $^3\Pi$, and so on. Right subscripts to indicate multiplet components are also added if the spin if sufficiently strongly coupled to the symmetry axis (Hund's diatomic case *a*) e.g., $^3\Pi_1$, $^2\Delta_{5/2}$.[1] If the spin-orbit coupling is very strong (Mulliken's case *c*), other species symbols (0^+,0^-,1,2,$\cdots$) related to the multiplet component subscripts of Hund's case *a* are used.[1]

In categories (a) and (c), not all of the species which otherwise exist are possible. The only σ species are σ^+, never σ^-. Hence **it is recommended** (**REC. 2a**) that the species symbol σ^+ be abbreviated to σ, as in Table II, in agreement with diatomic practice.[1]

For molecules of symmetry $D_{\infty h}$, there are *two* species corresponding to each *one* of Table II. These are distinguished by a right subscript g or u. For example, there are σ_g, σ_u, π_g, and π_u vibration modes, Σ_g^+, Σ_g^-, Σ_u^+, Σ_u^-, $\cdots$ vibrational states, electronic states such as $^2\Sigma_g^+$, $^2\Sigma_u^+$, $^4\Sigma_g^-$, $^3\Pi_{1u}$, $^2\Delta_{(5/2)g}$, and so on.

TABLE II. Species symbols for symmetry $C_{\infty v}$.

(a) Vibration modes:	σ,	π					
(b) Vibrational states:	Σ^+,	Σ^-,	Π,	Δ,	Φ,	Γ,	$\cdots$
(c) Orbitals:	σ,	π,	δ,	ϕ,	γ,	$\cdots$	
(d) Electronic states:	$^m\Sigma^+$,	$^m\Sigma^-$,	$^m\Pi$,	$^m\Delta$,	$^m\Phi$,	$^m\Gamma$,	$\cdots$
(e) Vibronic states:	$^m\Sigma^+$,	$^m\Sigma^-$,	$^m\Pi$,	$^m\Delta$,	$^m\Phi$,	$^m\Gamma$,	$\cdots$

In addition to species symbols, quantum number symbols are needed. For categories (c) and (d), **it is recommended** (**REC. 2b**) that the same angular momentum quantum number symbols (in particular, λ_i, S, Λ, Σ, Ω) be used for *all linear molecules* as for diatomic molecules.[1] For categories (a) and (b), however, distinctive symbols (l_i and l instead of the analogous diatomic λ_i and Λ; also v_i) are recommended [see Sec. II2 (b), Recommendations 8–10]. Likewise for category (e), distinctive symbols for angular momentum quantum numbers are recommended (see Sec. II 4).

(c) *Nonlinear Molecules*

A second system of species symbols, using italic letters with subscripts and superscripts, was developed by Placzek for nonlinear molecules.[4] This was first used for vibrational modes and states, but was soon applied also to orbitals and electronic and vibronic states.[5] The most complete tabulations of the symbols and the group-theoretical specifications of the possible symmetry species, for all important molecular symmetry groups, are those given by Herzberg.[2] Herzberg uses the diatomic symbols for linear molecules, and the Placzek symbols with minor changes for nonlinear molecules.

It is recommended (**REC. 3**) that species symbols and their definitions precisely as given by Herzberg in Chapter II, Sec. 3, of his book[2] *be adopted as standard for nonlinear molecules*, for all the five categories of vibrational and electronic classification given above, with capital or lower case letters in accordance with Recommendation 1, and left superscripts to indicate multiplicity (in the same way as for linear molecules, see Table I) for electronic and vibronic states; but leaving open the possibility of using alternative symbols when particularly desirable in special situations; in particular, the symbols[5] T and t should be used instead of F and f for triply-degenerate states or orbitals of atoms in crystals [see Sec. II 3(d)].

Recommendations 1–3 still leave unsolved one troublesome problem which arises for symmetry species bearing labels B_i or b_i ($i=1$, 2, and sometimes also 3), or B_{ip} or b_{ip} ($p=g$ or u), for the symmetry groups C_{2v}, C_{4v}, C_{6v}, D_2, D_4, D_6, D_{2h}, D_{4h}, and D_{6h}. (No such difficulty arises for B species of other groups, nor for A, E, or F species of any group.) The difficulty is that the distinctions between B or b species differing in numerical subscript depend on their behavior toward certain pairs of classes of symmetry operations which, while group-theoretically distinct, cannot be distinguished by any general specification for the particular symmetry group, but only by a specification for a particular molecule or type of molecule. As a result, confusing divergences exist: for

[4] G. Placzek, in Marx's *Handbuch der Radiologie* (Akademische Verlagsgesellschaft, Leipzig, Germany, 1934), Vol. VI, 2, p. 205; article on Raman spectra.
[5] R. S. Mulliken, Phys. Rev. **43**, 279 (1933).

example, one author calls B_1 the same species which another calls B_2, and vice versa. There seems to be no *general* solution for this problem. Hence **it is recommended** (**REC. 4**) that in general every author, in referring to B_i or B_{ip} (or b_i or b_{ip}) species of the symmetry groups mentioned above, shall define these species clearly *in each paper* in terms of the specific geometry of the molecules he is discussing and in so doing, that he shall make an effort to follow previous usage if such exists and there is no strong reason to change.

However, for the very large and important class of *planar* molecules of symmetry groups C_{2v}, D_{2h}, D_{4h}, and D_{6h}, the need for an immediate standardization of B_i or b_i species labels is urgent. In defining the problem, it should be noted that *not all* molecules of the groups mentioned are planar; but also that planar molecules exist belonging to other symmetry groups (C_s,C_{ph},D_{3h},D_{5h}) for which no B_i problem exists either because there are no B species or (C_{ph}) because only B_g and B_u species occur.

The group-theoretical species table for C_{2v} is given in Table III. The species B_1 and B_2 are distinguished by their behavior for reflection in the two planes $\sigma_v(xz)$ and $\sigma_v(yz)$. The z-axis is the axis of symmetry, but the choice of the x- and y-axes, hence the identification of the two planes, is arbitrary, with two choices possible. To resolve the resulting ambiguity in the meaning of the B species labels, **it is recommended** (**REC. 5a**) that, for *planar* C_{2v} molecules, the x-axis always be chosen perpendicular to the plane of the molecule unless there are very exceptionally strong reasons for a different choice; and that the choice of axes used also be explicitly stated, as per REC. 4, even if it is the standard choice. Application of this rule to some typical examples is illustrated in the followlng Fig. 1.

The group-theoretical species table for D_{2h} is given in Table IV.[2] The species B_{1p}, B_{2p} and B_{3p} ($p=g$ or u) can most conveniently be characterized by their respective behaviors for 180° rotations around the three mutually perpendicular 2-fold principal axes of symmetry z, y, and x. However, the assignment of the labels z, y, and x to the three axes in a particular molecule is arbitrary, with six choices possible. To resolve the resulting ambiguity in assigning B species labels, **it is recommended** (**REC. 5b**) that, for *planar* D_{2h} molecules, the x axis be chosen perpendicular to the plane of the molecule and the z-axis so that it passes through the greatest number of atoms or, if this rule is not decisive, so that it cuts the greatest number of bonds; these rules are to be followed unless there are very exceptionally strong reasons for a different choice; and that the choice of axes used also be explicitly stated, as per REC. 4, even if it is the standard choice. Application of REC. 5b to some typical examples is illustrated in Fig. 1.

TABLE III. Species table for symmetry C_{2v}.

C_{2v}	I	$C_2(z)$	$\sigma_v(xz)$	$\sigma_v(yz)$
A_1	+1	+1	+1	+1
A_2	+1	+1	−1	−1
B_1	+1	−1	+1	−1
B_2	+1	−1	−1	+1

TABLE IV. Species table for symmetry D_{2h}.

D_{2h}	I	$\sigma(xy)$	$\sigma(xz)$	$\sigma(yz)$	i	$C_2(z)$	$C_2(y)$	$C_2(x)$
A_g	+1	+1	+1	+1	+1	+1	+1	+1
A_u	+1	−1	−1	−1	−1	+1	+1	+1
B_{1g}	+1	+1	−1	−1	+1	+1	−1	−1
B_{1u}	+1	−1	+1	+1	−1	+1	−1	−1
B_{2g}	+1	−1	+1	−1	+1	−1	+1	−1
B_{2u}	+1	+1	−1	+1	−1	−1	+1	−1
B_{3g}	+1	−1	−1	+1	+1	−1	−1	+1
B_{3u}	+1	+1	+1	−1	−1	−1	−1	+1

The group-theoretical tables for D_{4h} and D_{6h} molecules (Herzberg[2]) read in part as in Tables V and VI. (It may

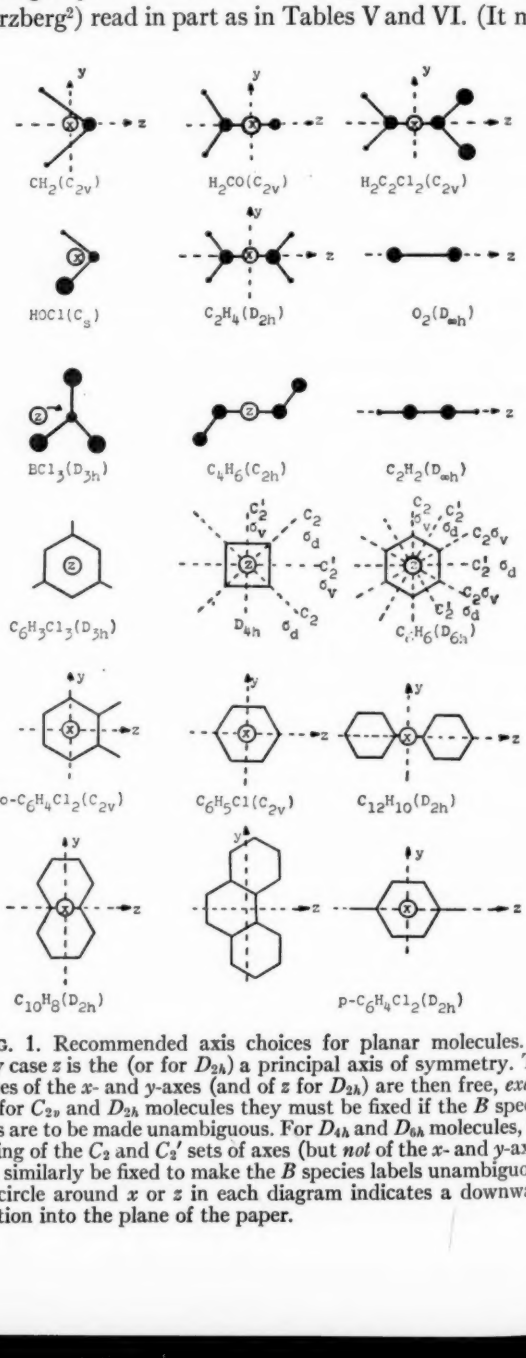

FIG. 1. Recommended axis choices for planar molecules. In every case z is the (or for D_{2h}) a principal axis of symmetry. The choices of the x- and y-axes (and of z for D_{2h}) are then free, *except* that for C_{2v} and D_{2h} molecules they must be fixed if the B species labels are to be made unambiguous. For D_{4h} and D_{6h} molecules, the labeling of the C_2 and C_2' sets of axes (but *not* of the x- and y-axes) must similarly be fixed to make the B species labels unambiguous. The circle around x or z in each diagram indicates a downward direction into the plane of the paper.

TABLE V.

D_{4h}	I	⋯	$2C_2$	$2C_2'$	$2\sigma_v$	$2\sigma_d$
B_{1g}	+1	⋯	+1	−1	+1	−1
B_{1u}	+1		+1	−1	−1	+1
B_{2g}	+1		−1	+1	−1	+1
B_{2u}	+1		−1	+1	+1	−1

TABLE VI.

D_{6h}	I	⋯	$3C_2$	$3C_2'$	$3\sigma_v$	$3\sigma_d$
B_{1g}	+1	⋯	+1	−1	−1	+1
B_{1u}	+1		+1	−1	+1	−1
B_{2g}	+1		−1	+1	+1	−1
B_{2u}	+1		−1	+1	−1	+1

be noted that the tables contain implicit definitions of the operations σ_v and σ_d in terms of C_2 and C_2', as follows: for D_{4h}, $\sigma_v = iC_2'$, $\sigma_d = iC_2$; for D_{6h}, $\sigma_v = iC_2$, $\sigma_d = iC_2'$ (i is the inversion operation). **It is recommended** (**REC. 5c**) that the following rule, which in the most important cases is in agreement with the current practice of most authors, be adopted for *planar* D_{4h} and D_{6h} molecules in order to make the designations of their B_{1p} and B_{2p} species unambiguous: the C_2 and C_2' classes of operations in the tables shall be distinguished by specifying that, (a), the C_2 axes shall pass through the greater numbers of atoms or, (b), in case specification (a) is not decisive, shall intersect the greater numbers of bonds. Application of this rule to some examples is illustrated in Fig. 1.

A similar standardization of B species labels appears desirable for those C_{4v} and C_{6v} molecules which, while not planar, nonetheless contain a square or hexagonal planar arrangement of atoms. The group-theoretical tables[2] here read in part as follows:

C_{4v}	⋯	$2\sigma_v$	$2\sigma_d$	C_{6v}	⋯	$3\sigma_v$	$3\sigma_d$
B_1		+1	−1	B_1		+1	−1
B_2		−1	+1	B_2		−1	+1

Here **it is recommended** (**REC. 5d**) that the σ_v and σ_d classes of operations be distinguished by the specification that, (a), the σ_v planes shall pass through the greater number of those atoms which are in the square or hexagonal (or similar) array, or, (b), in case specification (a) is not decisive, shall intersect the greater number of bonds among such atoms. The locations of the σ_v planes are thus similar to those of the C_2 axes in the D_{4h} and D_{6h} cases in Fig. 1.

It will be noted that the foregoing recommendations 5a–5d do not resolve ambiguities as to B species labels for molecules of groups D_2, D_4, or D_6, nor for *nonplanar* molecules of groups C_{2v}, D_{2h}, D_{4h}, or D_{6h}. For these cases, it appears best merely to follow REC. 4.

A few comments are needed on the changes required in current practice by RECS. 5a and 5b. At the present time, most workers on electronic structure and spectra[5] are already in accord with these recommendations; but most workers on infrared and Raman spectra[2] use a notation corresponding to an interchange of the x and y axes as compared with REC. 5a for C_{2v} molecules and of the x- and z-axes as compared with REC. 5b for D_{2h} molecules. The infrared workers must then interchange their x- and y-axis labels and their B_1 and B_2 species labels if they are to follow REC. 5a. They may also have to change the present numbering of some of the vibration modes of some C_{2v} molecules (not, however, for a B_2 molecules) if they also follow REC. 6 below. For D_{2h} molecules they must interchange their present x and z axis labels and consequently (see Table IV) their B_{1p} and B_{3p} species labels ($p = g$ or u) if they are to follow REC. 5b.

RECS. 5a and 5b have the advantage that planar molecules of symmetries C_{2v} and D_{2h}, and related linear molecules, usually have the z axis in a convenient and natural direction (see Fig. 1), and the x-axis perpendicular to the molecule plane (and/or to the principal axis). It may be noted that **RECS. 5a** and **5b** have the endorsement of Dr. G. Herzberg.

2. Normal Vibration Modes and Vibrational State Wave Functions

(a) *Vibration Modes*

The *labeling* of *normal modes of vibration* according to group-theoretical species has been covered in RECS. 1–5d (also, see Table II and Fig. 1). Further, **it is recommended** (**REC. 6**) that the vibration modes of any molecule be labeled and *numbered* in the way described at the top of p. 272 of Herzberg's book,[2] beginning the numbering with ν_1 for the highest frequency totally symmetric mode; but following Herzberg also in designating the perpendicular vibration of linear XY_2 and XYZ molecules, as a single exception to the usual rule, always by ν_2; it is to be understood that these symbols are not only labels for vibration modes but also symbols for the wave number values, of the corresponding fundamental bands (see Sec. IV); further, the parallel use for special purposes (for example, comparisons between isotopic molecules) of other modes of numbering normal modes of vibration should not be entirely excluded.

For a more complete description of any vibration mode, **it is recommended** (**REC. 7**) that the species symbol be added, for example $\nu_{16}e_{2g}$.

In case it is known that the motion in a particular mode is largely localized in a particular bond or a particular group or groups of atoms, **it is suggested** (**SUG. 2**) that further descriptive symbols be included, for example $\nu_1(\nu CH)a_g$; $\nu_2(\nu C{=}C)a_g$; $\nu_3(\delta CH_2)a_g$; $\nu_4(\tau CH_2)a_u$; $\nu_5(\nu CH)b_{1g}$; $\nu_6(\rho CH_2)b_{1g}$; $\nu_7(\omega CH_2)b_{3u}$; $\nu_8(\omega CH_2)b_{2g}$ for some of the normal modes of C_2H_4 (ν = stretching, δ = deformation or spreading, τ = twisting, ω = wagging, ρ = rocking). The use of symbols such as ν, δ, ρ, τ, ω should be avoided except when it is known that they represent reasonable approximations to the actual motions. For semilocalized vibrations of

large molecules or molecules of *low symmetry* where the vibration modes have not been identified and numbered in terms of symmetry species, **it is suggested (SUG. 3)** that, when warranted, symbols such as $\nu(CCl)$, $\nu(\rho CCl)$, $\nu(\omega CCl)$ be used.

(b) *Quantum Numbers and Vibrational State Wave Functions*

It is recommended (REC. 8) that the vibrational quantum number for the ith vibrational mode be designated by v_i.

In the special case of degenerate vibrations of linear and symmetric-rotor molecules, a second quantum number or index besides v_i is needed; **it is recommended (REC. 9)** that this be designated l_i and that particular values of the pair v_i, l_i be written in the form $v_i^{l_i}$ for example $v_2^{l_2}=2^2$ or 3^1; in linear molecules, l_i is vibrational angular momentum around the molecular axis in units of $h/2\pi$. In symmetric-rotor molecules, l_i gains significance only for rovibrational states where there is rotation ($K>0$) around the molecular axis; for each degenerate vibration there is then a vibrational angular momentum $(\pm\zeta_i l_i)h/2\pi$, the sign depending on whether l_i is parallel ("$+l_i$") or antiparallel ("$-l_i$") to K; the use of the symbol ζ_i **is recommended (REC. 9a)** for the purpose indicated here. There is an energy splitting between the $+l_i$ and $-l_i$ states: see Sec. IV, REC. 31, part (1), also Sec. III 2(b).

The labeling of over-all vibrational state wave functions has been covered in RECS. 1–5d. In the case of linear molecules, a quantum number label for the resultant vibrational angular momentum quantum number (vector Σl_i) around the figure axis is also needed, and **it is recommended (REC. 10)** that l be used for this purpose [$l=0, 1, 2, \cdots$ for Σ^+ or Σ^-, Π, Δ, $\cdots$ states (see Table II)].

For more detailed characterization of vibrational states, **it is suggested (SUG. 4)** that *vibrational configuration symbols* be combined with state symbols as in the following examples:

$(\nu_1)^2\nu_6(\nu_{16})^2$, B_{1u} or $(\nu_1 a_{1g})^2(\nu_6 b_{1u})(\nu_{16}e_{2g})^2$, B_{1u}
$(\nu_1)^2(\nu_2)^2\nu_3$, Δ_u or $(\nu_1\sigma_g)^2(\nu_2\pi_u)^2(\nu_3\sigma_u)$, Δ_u

for a nonlinear and a linear molecule, respectively.

In cases, such as NH_3, where *inversion doubling* of vibrational levels occurs, designations for the two sublevels are needed. Herzberg (reference 2, pp. 222, 295), uses superscripts + and − (e.g., 0^+, 0^-, 1^+, 1^-, $\cdots$ for $v_2=0, 1, \cdots$ in the case of NH_3). **It is recommended (REC. 11)** that these be used.

3. Electron Configurations and Electronic States

(a) *General Considerations on the Classification of Electronic Wave Functions*

(1) It is important to keep in mind that the group-theoretical species classification of electronic wave functions of molecules is based on the symmetry of the geometrical configuration of the nuclear framework, ordinarily for an idealized situation in which the nuclei are thought of as held fixed in positions corresponding to equilibrium for the particular electronic state under consideration. Unlike the symmetry for vibrational modes and states, the equilibrium molecular symmetry for an electronic state is practically unaffected by isotopic substitution; hence the appropriate electronic state species classification is the same for all isotopic molecules. For example, the ground state of CO_2 is classified as $^1\Sigma_g^+$ ($D_{\infty h}$ symmetry) equally for $O^{16}C^{12}O^{16}$, $O^{16}C^{12}O^{18}$, and other isotopes. The spectroscopic properties of an electronic state (i.e., the selection rules and over-all intensities of transitions to other electronic states) are to a good approximation governed by this fact. However, in a higher order of approximation, the classification can also be given in terms of that lower symmetry which is appropriate in classifying the vibrational states; for example the ground state of $O^{16}C^{12}O^{18}$ may be classified as $^1\Sigma^+$ (symmetry $C_{\infty v}$).

(2) When substituent groups are introduced into a molecule, the major spectroscopic properties, at least for some electronic transitions, are often little affected, in spite of the fact that the rigorous symmetry classifications of the states involved may be changed. For example, all unconjugated aldehydes RCHO and ketones R_2CO show a characteristic weak ultraviolet absorption band system near $\lambda 2900$, indicating that all have a very similar excited electronic state, and that to a rather good approximation all behave as if they had symmetry C_{2v} like H_2CO. The situation is similar to that for isotopic substitution, although the effects of substitution are in general greater. For this reason, classification according to approximate or local symmetry is more frequently useful for electronic than for vibrational states.

(3) Different electronic states of a molecule in general differ in their nuclear equilibrium configurations, in respect to (a) interatomic distances; (b) often also symmetry. When situation (b) occurs, the species classification must be made in terms of different symmetry groups for different states. Nevertheless, because of the operation of the Franck-Condon principle, the electronic selection rules and the over-all intensity of the system of bands (and/or continuum) associated with an electronic transition always correspond in first approximation to those for a transition without change of symmetry, in other words to those for a transition keeping the symmetry of the *initial state* (whether in absorption or in emission). Hence classification of the final state wave function according to the initial state symmetry is often desirable.

For a detailed consideration of individual bands and band-lines, however, one must use electronic (and/or vibronic) selection rules corresponding to a sort of *greatest common denominator* of the symmetries of the initial and final equilibrium configurations.

In assessing the likelihood that situation (b) may occur, it is important to keep in mind the Jahn-Teller

theorem,[6] which states that orbitally-degenerate (i.e., *E* or *F*) states of *nonlinear* molecules are configurationally unstable. However, no quantitative studies of the Jahn-Teller effect have been made, and it is possible that in many cases only a small or moderate departure from a geometrical configuration of the original symmetry may occur. On the other hand, changes of symmetry on going to excited states are frequent even for orbitally nondegenerate states and for linear molecules.

(4) Among large aromatic molecules there are often extensive close analogies between the ultraviolet spectra of molecules which would not on any obvious grounds be expected to be spectroscopically related.[7] Here an empirical classification of electronic states becomes more useful than one based on symmetry species.

(b) *General Considerations on the Labeling of Orbitals in Molecules and Crystals*

The labeling of one-electron wave functions of molecules,[8,9] and of atoms in crystals, is a problem common to valence theory and to spectroscopy. As a preliminary to the discussion, **it is recommended (REC. 12)** that the word "orbital" be used only to mean "one-electron orbital wave function;"[9(a)] further, that the words "*atomic orbital*" (which may be abbreviated AO) and "*molecular orbital*" (which may be abbreviated MO) be used to refer to one-center and two-or-more center orbitals, respectively; further, that "spin orbital" be used to mean a one-electron wave function which is a product of an "orbital" times a one-electron spin function.[9b] Further, **it is suggested (SUG. 5)** that, in polyatomic molecules, MO*s* belonging to a pair of linked atoms, and to the molecule as a whole, be respectively called *bond* MO*s* (or BMO*s*), *group* orbitals (or GO*s*), and *nonlocalized* or *whole-molecule* MO*s*; BMO*s* and GO*s* are respectively localized and semilocalized MO*s*; when MO*s* of any kind are approximated as linear combinations of atomic orbitals, they may be called LCAO-MO*s*, or LCAO*s*; spinorbitals (or SO*s*) include "atomic spinorbitals" (ASO*s*) and "molecular spinorbitals" (MSO*s*).

In molecular spectroscopy, whole-molecule MO*s* are usually the most convenient orbitals to use. It should be noted, however, that automatic localization often occurs so that some whole-molecule MO*s* take the form, to a more or less good approximation, of GO*s* or even AO*s*. In valence theory, whole-molecule MO*s*, GO*s*, BO*s*, and variously-selected AO*s* (including both proper AO*s* and "hybrid" AO*s*), are all useful for various purposes. For atoms in crystals, variously-selected AO*s* are used.

When AO*s* are used for atoms in molecules, the viewpoint is essentially the same as for atoms in crystals, namely that the AO*s* used are selected and classified to conform to the symmetry of the *local field* set up by the action of neighboring atoms. In both cases, one may often classify the AO*s* according to a *dominant* but approximate symmetry, corresponding, perhaps, to the local fields of next-neighbor atoms only, or according to an (often lower) *rigorous* symmetry corresponding to the fields of all sufficiently near atoms. Classifications according to both dominant and rigorous symmetry are important for the spectroscopy of atoms in crystals. Molecules or molecular ions in crystals are subject to similar considerations.

(c) *Electron Configurations and Electronic States of Molecules Using Whole-Molecule Orbitals*

The labeling of MO*s* and of electronic state wave functions according to group-theoretical species has already been dealt with in RECS. 1–5d (see also Table II and Fig. 1).

For the designation of electron configurations together with electronic states in spectroscopy, **it is recommended (REC. 13)** that, ordinarily, whole-molecule MO*s* be used and that, *within each group-theoretical species*, these be numbered consecutively, beginning with 1 for the most firmly bound MO of the given species; however, when more convenient, inner-shell orbitals may be assigned to AO*s* of the separate atoms, and the numbering of the MO*s* begun with the valence-shell MO*s*. Following are some examples, for the ground states of several molecules.

CO_2: $(1\sigma_g)^2\ (1\sigma_u)^2\ (2\sigma_g)^2\ (3\sigma_g)^2\ (2\sigma_u)^2\ (4\sigma_g)^2\ (3\sigma_u)^2\ (1\pi_u)^4\ (1\pi_g)^4,\ {}^1\Sigma_g^+\ (D_{\infty h})$;

or

$(1s_O)^2\ (1s_O)^2\ (1s_C)^2\ (1\sigma_g)^2\ (1\sigma_u)^2\ (2\sigma_g)^2\ (2\sigma_u)^2\ (1\pi_u)^4\ (1\pi_g)^4,\ {}^1\Sigma_g^+\ (D_{\infty h})$.

CH_4: $(1a_1)^2\ (2a_1)^2\ (1f_2)^6,\ {}^1A_1\ (T_d)$.

H_2CO: $(1a_1)^2\ (2a_1)^2\ (3a_1)^2\ (4a_1)^2\ (1b_2)^2\ (5a_1)^2\ (1b_1)^2\ (2b_2)^2,\ {}^1A_1\ (C_{2v})$.

$CrO_4^{=}$: $(1a_1)^2\ (1f_2)^6\ (1e)^4\ (2f_2)^6\ (2a_1)^2\ (3f_2)^6\ (1f_1)^6,\ {}^1A_1\ (T_d)$.

The electron configurations of molecules are formally (but only formally) closely similar to vibrational configurations [see Sec. II 2(b)]. Just as in the case of vibrational modes [see Sec. II 2(a)], the standard brief orbital symbols in an electron configuration may, *when warranted*, be supplemented by the addition of further symbols giving approximate descriptions of the detailed forms of the MO*s*; symbols more or less similar to those used for this purpose for diatomic molecules[1] are appropriate.

In case there can be any doubt [see Sec. IV 3(a), item (3)] as to the symmetry which is being assumed for a molecule in a particular electronic state, **it is recommended (REC. 14)** that the symbol for the sym-

[6] See, for example, H. Sponer and E. Teller, Revs. Modern Phys. **13**, 75 (1941).
[7] See J. R. Platt, J. Chem. Phys. **17**, 484 (1949); **19**, 101, 1418 (1951).
[8] F. Hund, Z. Physik **73**, 1 (1932).
[9] R. S. Mulliken, (a) Phys. Rev. **41**, 50 (1932); (b) J. chim. phys. **46**, 502 (1949).

metry group be added in parentheses after the state species symbol, as in the examples given above. This procedure is especially useful when there is a change of symmetry upon electronic excitation. For example, CO_2 is linear in its ground state, but nonlinear in its first singlet excited state. It has been suggested that the latter corresponds to a $^1\Pi_g$ state of a linear molecule,[10] but that this is split into a $^1A_2(C_{2v})$ and a $^1B_2(C_{2v})$ state, with the observed absorption bands going to the $^1B_2$ state. The electronic transition might then be described as

$$^1B_2(C_{2v})-^1\Sigma_g^+(D_{\infty h}).$$

For brief reference, **it is recommended (REC. 15)** that, in agreement with common practice, various simple letter symbols be used (with or without species symbol) to identify particular electronic states. For example, N may be used for the ground state, E, T, V, Q, ^3Q_u, V_i, ^3L_a, ^1L_a, ^3L_b, for various types of excited states, but a definite standardization of these letter symbols does not seem necessary at present.

(d) *Orbitals and States of Atoms in Crystals*

For atoms in crystals, if the crystalline fields are strong enough to break down the original spin-orbit couplings, exactly the same electronic state species symbols as for molecules are suitable, and **it is recommended (REC. 16)** that they be used, except that the molecular symbols F and f be replaced by T and t (see REC. 3), in order to avoid confusion with the atomic species symbols F and f. For example, an atom in a $^3D^\circ$ state, when subjected to a strong enough crystalline field of symmetry O_h, gives rise to a ^3E_u and a $^3T_{2u}$ state; if to a strong enough field of symmetry C_{2v}, to one $^3A_1$, two $^3A_2$, one $^3B_1$, and one $^3B_2$ states.[5]

This nomenclature, however, does not provide for the classification of weak-field states, or of multiplet components, except in the unlikely case of a perturbing field with symmetry $C_{\infty v}$ or $D_{\infty h}$, where the diatomic nomenclature surveyed in Sec. II 1(b) is appropriate. In other cases, resort must be had, for the time being, to the relatively uninformative notation introduced by Bethe.[11] A suitable extension of the Placzek notation is needed here.

In very strong crystalline fields, a classification not only of the states, but also of the AO*s* of the outer electrons according to crystalline-field species is needed. For example, in a strong enough O_h field a $3d$ AO gives rise to an e_g (twofold degenerate) and a t_{2g} (threefold degenerate) AO; or in a C_{2v} field to an a_1, two a_2, a b_1, and a b_2 AO. For a complete description, one may speak here of $3de_g$ and $3dt_{2g}$, or of $3da_1$, $3da_2$, $3db_1$, and $3db_2$ AO*s*. Perhaps these crystalline-field AO*s* might be designated as CAO*s*.

[10] See R. S. Mulliken, Revs. Modern Phys. **14**, 204 (1942); but also see A. D. Walsh, J. Chem. Soc. **1953**, 2266.
[11] H. Bethe, Ann. Physik [5], **3**, 133 (1929).

4. Vibronic States

The labeling of vibronic (i.e., electronic × vibrational) state wave functions has been covered in RECS. 1–5d. One special point should be noted: the species classification for any vibronic state is to be based on the symmetry group appropriate for the vibrational and not for the electronic state involved, in case these differ, as for example because of isotopic substitution [see Sec. II 3(a)].

For the vibronic states of *linear molecules*,[12,13] certain special angular momentum quantum numbers are sometimes needed. In general, one may have an electronic resultant orbital angular momentum quantum number Λ ($\Lambda=|\text{sum of } \pm\lambda_i\text{'s}|$), just as for diatomic molecules,[1] and a vibrational resultant orbital angular momentum quantum number l ($l=|\text{sum of } \pm l_i\text{'s}|$), see REC. 10.

There are now two cases, depending on how strongly the electronic spin S is coupled to the molecular axis by the magnetic field corresponding to Λ (and/or, possibly, to l). If $S=0$, or if with $S>0$ the spin is loosely coupled, Λ and l form a resultant, and **it is recommended (REC. 17)** that this be called K; $|\pm\Lambda\pm l|=K$; if $\Lambda=0$ (the usual case for infrared and Raman spectra), $l\equiv K$, but the notation l is usually to be preferred, while if $l=0$, $\Lambda\equiv K$, but the notation Λ is usually to be preferred; however, in comparisons with nonlinear molecules,[12] or in comparisons between different electronic states not all having $\Lambda=0$ or $l=0$, K should be used.

In the case of tight spin coupling, one has the electronic quantum number Ω (usually $\Omega=|\Lambda+\Sigma|$), as in diatomic molecules.[1] Ω and l then form a resultant, and **it is recommended (REC. 18)** that this be called P:

$$|\pm\Omega\pm l|=P;$$

if $l=0$, $\Omega\equiv P$, but the notation Ω is usually to be preferred.

III. ROTATIONAL AND OVER-ALL STATES

1. Pure Rotational States

Although the rotational motion of a molecule is never completely independent of its electronic and vibrational motions, nevertheless if the electronic and vibrational state wave functions are *both* totally symmetrical, or at least *nondegenerate*, the molecule may usually be treated as a quasi-rigid rotor in the description of its major rotational properties. This viewpoint will be followed in the present subsection.

(a) *Eulerian Angles*

It has been suggested by several people that it would be desirable, in the theoretical discussion of rigid rotor functions, to agree on a single standard way of choosing Eulerian angles. However, since any such standardization should have the agreement of other groups in

[12] R. S. Mulliken, Phys. Rev. **60**, 506 (1941).
[13] H. Sponer and E. Teller, Revs. Modern Phys. **13**, 75 (1941).

addition to the spectroscopists, it is proposed that such a cooperative agreement be sought at a later date.

(b) *Rotational Constants*

For the three moments of inertia of any molecule and the corresponding spectroscopic constants, **it is recommended (REC. 19)** that the symbols I_A, I_B, I_C (or I^a, I^b, I^c if preferred) and A, B, C be respectively used, in such a way that $I_C \geq I_B \geq I_A$ and $A \geq B \geq C$ *in all cases* ($A = h/8\pi^2 c I_A$, and so on, in cm^{-1}; or in Mc/sec); with added subscripts e (for equilibrium), 0 (for $v_1 = v_2 = \cdots = 0$), or $v_1 v_2 \cdots$ to indicate vibrational quantum numbers, when needed. In general theoretical discussions of symmetric rotor energies, it is convenient to have a single symbol for the *unique* moment of inertia, whether this be I_C (oblate case) or I_A (prolate case). At present I_A is commonly used in both cases; REC. 19 is intended to do away with this confusing practice, which is especially bad when one has to make comparisons with quasi-symmetric asymmetric rotor molecules. However, REC. 19 creates a new, though it is believed minor problem in that, for general discussions of symmetric rotors, symbols are needed for the moments of inertia parallel and perpendicular to the symmetry axis, and for the corresponding rotational constants. No formal recommendation or suggestion is made here to solve this problem, but it is informally suggested that symbols such as $I^{\parallel}$ and $I^{\perp}$, $B^{\parallel}$ and $B^{\perp}$ might be used.

(c) *Pure Rotational State Symbols*

It is recommended (REC. 20) that the symbol J always be used for the quantum number of total angular momentum exclusive of nuclear spin.

It is recommended (REC. 21) that for symmetric rotors, the symbol K be used for the quantum number of axial angular momentum, and that rotational levels be designated by (J,K), e.g. (3,2); and that the same symbol K be used also for asymmetric rotor level-pairs which approximate to levels of symmetric rotors.

For asymmetric rotor levels, **it is recommended (REC. 22)** that either of the two following notations be used according to convenience: (1) $J_{K_a K_c}$, e.g. $5_{1,4}$ or $12_{11,2}$, where K_a (prolate K value) is the K value of the given level if the molecule were distorted to a prolate symmetric rotor ($I^c = I^b > I^a$) and K_c is the oblate K value, corresponding to distortion to $I^c > I^b = I^a$; or (2) J_τ, e.g. 12_9, where the "rank" τ runs from $-J$ to $+J$ in order of increasing energy.[14] Notation (1) contains implicitly a classification of the level according to one of the four group-theoretical asymmetric-rotor species, $(++, +-, -+$, and $--$, or, respectively, A, B_c, B_a, B_b, where, e.g., $+-$ or B_c corresponds to K_c even and K_a odd, and so on); further, $\tau = K_a - K_c$.[14]

[14] King, Hainer, and Cross, J. Chem. Phys. **11**, 27 (1943), have used K_{-1}, K_{+1} with the same respective meanings as K_a, K_c [R. S. Mulliken, Phys. Rev. **59**, 873 (1941)].

2. Fine Structure Levels

(a) *General Remarks*

For molecular states in which either the electronic state is degenerate, or degenerate vibrations are excited, or both, there is usually so much interaction between the electronic and/or vibrational and the rotational motion that it is better to emphasize a classification of the combined or "*rovibronic*" (or rovibrational in case the electronic state is totally symmetrical) wave functions and energy levels rather than of purely rotational states. Rovibronic levels often group themselves in such a way that they may be regarded as *fine structures* of rotational levels. The terms rovibronic and rovibrational are not necessarily being recommended here, but, for want of better terms, are being used in this explanatory text to fill an evident need.

Even without rotational motion, fine structures can arise from splittings of degeneracy, usually (1), in harmonics of degenerate vibrations; or (2), in the interaction of degenerate electronic and vibrational states (in linear molecules). Fine structures can also arise (3), in Coriolis interactions between degenerate vibronic states and symmetric-rotor or spherical-rotor angular momentum; or (4), in the interaction of electron spin with rotational motion. In situations (1) and (2), the resulting vibrational or vibronic states are in part nondegenerate and in part degenerate. Each such state which is *nondegenerate* gives rise to a set of rotational levels which may be classified as in Subsection 1; for each such state which is *degenerate*, situation (3) exists. It should be noted that situations (1)–(3) do not arise for asymmetric-rotor molecules, but nevertheless a classification of the rotational levels according to rovibronic as well as rotational species is often useful for these too.

(b) *Rovibronic States for Zero Electron Spin*

The quantum numbers J (REC. 20) and K (REC. 17 for linear molecules, REC. 21 for symmetric rotors) are in general really *rovibronic* rather than pure rotational quantum numbers. In general, K corresponds to *total axial* angular momentum. For linear molecules it consists exclusively of vibronic (i.e., electronic and/or vibrational) angular momentum. For symmetric rotors in degenerate vibrational states, it includes in general some vibrational angular momentum, proportional to an index number $\pm l_i$ for each degenerate vibration v_i (see discussion following REC. 9).

Besides the J and (when appropriate) K and vibrational $\pm l_i$ classification, the species classification of rovibrational states according to their behavior under the rotational subgroup of the vibrational symmetry group of the molecule is important. This is true especially because for nonlinear molecules this same classification determines the behavior of the rovibrational wave function with respect to exchanges of identical nuclei, and so (when nuclear spin functions are also

considered) governs the statistical weights of rovibrational levels for molecules containing sets of identical nuclei.[15] **It is recommended (REC. 23)** that for nonlinear molecules the usual Placzek symbols be used for this rovibrational species classification[15]; and that for symmetrical linear molecules the symbols s and a (symmetric and antisymmetric, respectively, for exchanges of identical sets of nuclei) be used, the same as for diatomic molecules.[1] Following are some examples[15]; it should be recalled that the label E always refers to a twofold degenerate state.

(1) For a molecule of symmetry C_{3v} (rotational subgroup C_3), e.g., the prolate rotor CH_3I, the possible rovibrational species are A and E. For a (7,2) rotational level (see REC. 21) of an E vibrational state, there is a fine structure consisting of one E and two A rovibrational sublevels. And if, for example, the E vibrational state is due to excitation of a single degenerate vibration ν_i with angular momentum index l_i, the E rovibrational sublevel corresponds to $+l_i$ and the two A sublevels to $-l_i$ (see discussion following REC. 9, and see reference 2, Figs. 117–118).

(2) For symmetry D_{3h} (rotational subgroup D_3), e.g., the planar oblate rotor BCl_3, the possible rovibrational species are A_1, A_2, and E. For a (7,2) rovibrational level of an E'' vibrational state, there are one A_1, one A_2, and one E rovibrational sublevels.

(3) For the nonplanar oblate rotor NH_3 (symmetry C_{3v}), the vibrational states are doubled by inversion and the resulting sub-states can be classified according to symmetry D_{3h}; the rovibrational states are then classified under D_3. For a (7,2) rotational level of an E vibrational state, there are one A_1, one A_2, and one E rovibrational sublevels for each of the two sub-states of the inversion doubling.

(4) For an asymmetric rotor of symmetry D_{2h}, e.g. the planar molecule C_2H_4, the rovibrational species are A, B_1, B_2, B_3. For the 3_{+1} rotational level (using the J_τ notation, see REC. 22) of a B_{1u} or B_{1g} vibrational state, the rovibrational species is B_2; for the 3_{+1} level of an A_g or A_u vibrational state, the rovibrational species is B_3.

(5) For a spherical rotor molecule of symmetry T_d, e.g., CH_4, the rovibrational species are A, E, and F. For the $J=6$ rotational level of an E vibrational state, there are two A, three E, and six F sub-levels. In the case of threefold degenerate (F) vibrational states of spherical rotor molecules, Coriolis interaction with rotation causes a primary splitting of the otherwise $3(2J+1)$-fold degenerate rovibrational levels into three components called $F^+(J)$, $F^{(0)}(J)$, and $F^-(J)$; on each of these is superposed a much finer splitting into A, E, and F rovibrational sub-levels.

In addition to the foregoing classification by J and K and by rovibrational species, each rovibrational level of a *linear* or *planar* molecule can be further usefully characterized by its *parity species* (based on its behavior under inversion). **It is recommended (REC. 24)** that rovibrational levels be called positive (+) or negative (−), respectively, just as for diatomic molecules, according as their wave functions are symmetric or antisymmetric to inversion.[1] The parity species classification is particularly useful for labeling the two components of l-doublets (or Λ doublets, K-doublets, or Ω doublets: see RECS. 17, 18) of linear molecules.

For nonplanar molecules, each rovibrational level is usually an unresolved doublet (parity degeneracy), so that the parity species classification is useless. In exceptional cases (notably NH_3), these doublets are appreciably split (inversion doubling), one of the two resulting components being +, the other −.

(c) *Rovibronic States for Electron Spin Loosely Coupled*

If a nonzero electron spin is present, but loosely coupled, a second quantum number of total angular momentum is needed in addition to J. **It is recommended (REC. 25)** in agreement with recently revised diatomic nomenclature,[1] that this be called N, where, for linear or symmetric-rotor molecules,

$$|\mathbf{K}+\mathbf{rotation}| = N,$$

with N replacing J in REC. 21 so that symmetric-rotor levels are indexed by (N,K); and with N similarly taking the place of J in REC. 22 for asymmetric-rotor molecules so that rotational levels are indexed by $N_{K_aK_c}$ or N_τ; further, in all cases,

$$|\mathbf{N}+\mathbf{S}| = J;$$

if $S=0$, N becomes identical with J, but the symbol J is to be preferred. Rovibronic sublevels with different J for a given N constitute spin fine structure. In general, this is superposed on a fine structure associated with N, the same as described in Subsections III 2(a) and III 2(b) except that in these subsections J (expressed or implied) is everywhere to be replaced by N.

(d) *Rovibronic States for Electron Spin Tightly Coupled to Molecular Axis*

A tightly-coupled electron spin is most likely to occur for linear molecules; this case is covered by REC. 18. It can, however, also occur for symmetric-rotor molecules (e.g., in degenerate excited electronic states of CH_3I)[16] in which a rovibronic axial angular momentum contains a large electronic component. It can occur even in quasi-symmetric asymmetric-rotor states, e.g., for nontotally-symmetrical electronic states of ClO_2.[17] In the latter case, the spin is axis-quantized in the magnetic field of K. **It is recommended (REC. 26)** that the total resultant axial angular momentum quantum number including electron spin be called P in general, just as in the case of linear molecules (see REC. 18):

$$|K+\Sigma| = P,$$

[15] See reference 2, Chap. IV.

[16] See R. S. Mulliken and E. Teller, Phys. Rev. **61**, 283 (1942).

[17] See J. B. Coon, J. Chem. Phys. **14**, 665 (1946).

Σ being the quantum number giving the component of the spin S along K, and being essentially the same as the diatomic quantum number Σ. In all cases with tightly-coupled electron spin,

$$|\mathbf{P}+\text{rotation}| = J,$$

in agreement with REC. 20.

3. Stark and Zeeman Effect Levels

In the case of "weak-field" spectra (electron spin zero or tightly coupled, or external field very weak), **it is recommended** (**REC. 27**) that M_N and M_S be used for the rotational and electron spin magnetic quantum numbers. (It is assumed here that the applied field is axially symmetrical.) These quantum numbers are needed especially for radio-frequency spectra, also for the Zeeman and Stark effects in electronic spectra.

4. Nuclear Hyperfine Structure Levels

It is recommended (**REC. 28**) that I be used for the quantum number of the spin of any one nucleus (I_1, I_2, $\cdots$ if there are several nuclear species); T (or T_1, T_2, $\cdots$) for the resultant spin (or spins) of one (or several) sets of identical nuclei in case such resultants are significant; F for the over-all resultant of J and the I's (or T's); M_F for weak-field electric or magnetic quantum number; M_J and a set of M_I's (or perhaps an M_T or M_T's) for strong-field magnetic or electric quantum numbers. In microwave spectra in which only nuclear-quadrupole hyperfine structure is resolved, nuclei having $I<1$ may be ignored and treated as if not contributing to F. In nuclear magnetic resonance all nuclei having $I>0$ must in general be considered as contributing to F.

IV. SPECTRAL TERMS, LINES, AND BANDS

1. Term Formulas and Coefficients

Spectroscopic "terms" (conventionally, in energy/hc, i.e., in cm^{-1} units; or in microwave spectra in Mc/sec frequency units) for polyatomic molecules are conveniently expressed, just as for diatomic molecules,[1] by term formulas in which the total term is written as a sum of parts. **It is recommended** (**REC. 29**) that term formulas be expressed in the general form

$$T=T_e+G(v_1,v_2,\cdots)+F(J,\text{ etc.})+\cdots+(\text{fine structure}),$$

using the symbols T for the total, T_e for the "electronic," G for the "vibrational," and F for the "rotational" term, with G and F defined, somewhat arbitrarily, according to RECS. 30 and 31 below.

It is recommended (**REC. 30**) that coefficients ω_i and x_{ij} be defined as indicated in expressions of the following type for vibrational terms;

$$G(v_1,v_2,\cdots)=\sum_i \omega_i(v_i+\tfrac{1}{2}d_i)+\sum_i\sum_{k\geq i} x_{ik}(v_i+\tfrac{1}{2}d_i)(v_k+\tfrac{1}{2}d_k)+\cdots+(\text{fine structure arising from splitting of any vibrational degeneracy})$$

[d_i=degree of degeneracy in ith vibration mode].

It is recommended (**REC. 31**) that F and the coefficients $A_{[v]}$, $B_{[v]}$, $C_{[v]}$, $D_{[v]}{}^J$ or $D_{[v]}{}^N$, $D_{[v]}{}^{JK}$ or $D_{[v]}{}^{NK}$, $D_{[v]}{}^K$, ζ_i, and α_i be defined as indicated in the following expressions (subscript $[v]$ indicates the ensemble v_1, v_2, $\cdots$).

(1) Linear Molecules with Electron Spin S Zero or Tightly Coupled (see REC. 9)

$$F(J)=B_{[v]}[J(J+1)-K^2]-D_{[v]}J^2(J+1)^2+\cdots+(fs,hfs).$$

[Instead of K read Ω or P (see REC. 18) if $S>0$, and for $S=0$ read Λ if $l=0$, or l if $\Lambda=0$ (see REC. 17). In the above, *fs* refers to fine structure exclusive of any arising from nuclear degeneracy, *hfs* to hyperfine structure; these are given only to indicate that the rotational term F is defined to include *fs* and *hfs*.]

(2) Linear Molecules with Electron Spin Loosely Coupled (see REC. 25)

$$F_i(J)=B_{[v]}[N(N+1)-K^2]-D_{[v]}N^2(N+1)^2+\cdots+f_i(N,K)+(fs,hfs).$$

[For K, read Λ if $l=0$, or l if $\Lambda=0$. Use F_1 for $J=N+S$, F_2 for $J=N+S-1$, $\cdots$, just as for diatomic molecules.[1]]

(3) Symmetric-Rotor Molecules (See Subsections III 2(b), (d), also RECS. 9 and 19)

$$F(J,K)=B_{[v]}{}^{\perp}[J(J+1)-K^2]+B_{[v]}{}^{\parallel}[K^2-2K\Sigma_i(\pm\xi_i l_i)]-D_v{}^J J^2(J+1)^2-D_{[v]}{}^{JK}J(J+1)K^2-D_{[v]}{}^K K^4+\cdots+(fs,hfs).$$

[Instead of K read P (see REC. 26) if $S>0$ and tightly coupled. For $S>0$ and loosely coupled, replace J by N, and add a term $f_i(N,K)$, as in the linear molecule case (2).]

(4) Asymmetric Rotor Molecules

$F(J_\tau)$ or $F(J_{K_a,K_c})$ = complicated expressions[18]; or, if loosely coupled electron spin is present,

$F_i(J,N_\tau)$ or $F_i(J,N_{K_aK_c})$ = complicated expressions $+f_i(N_\tau)$.

[18] See Reference 2, pp. 210, 370–371, 400, 447, 460, etc.

(5) *B Expressions*

$B_{[v]}=B_e-\Sigma_i\alpha_i^B(v_i+\frac{1}{2}d_i)+\cdots$, with similar expressions for $A_{[v]}$ and $C_{[v]}$; in linear molecules, α_i^B is written simply α_i.

It is recommended (**REC. 32**) that fine structure components be indicated when convenient by subscripts or superscripts attached to F; in particular, by $F_i(J)$ for electron spin fine structure [see (2) above]; or as in $F_a(J)$, $F_b(J)$, $F_{ia}(J)$, etc., using $_a$ and $_b$ respectively (as for diatomic molecules)[1] to denote the lower and upper components in l-doublets and the like (see REC. 24); in the case of threefold degenerate vibrational states of spherical rotor molecules (see Sec. III 2(b), the symbols $F^{(+)}(J)$, $F^{(0)}(J)$, and $F^{(-)}(J)$ are recommended for the three (groups of) rovibrational substates resulting from Coriolis splitting.

It is recommended (**REC. 33**) that symbols for *differences* of vibrational and of rotational term values be used with definitions as illustrated in the following examples[19]:

$$\Delta_1G(v_i)=G(v_1v_2\cdots v_i+1\cdots v_n)-G(v_1v_2\cdots v_i\cdots v_n),$$
$$\Delta_mG(v_i)=G(v_1v_2\cdots v_i+m\cdots v_n)-G(v_1v_2\cdots v_i\cdots v_n),$$
$$\Delta_1F(J)=F(J+1)-F(J),$$
$$\Delta_2F(J,K)=F(J+1,K)-F(J-1,K),$$
$$\Delta_2{}^KF(J,K)=F(J,K+1)-F(J,K-1),$$
$$\Delta_2F_{ia}(J)=F_{ia}(J+1)-F_{ia}(J-1).$$

2. Spectral Lines and Bands

(a) *General*

In some branches of spectroscopy, absorption spectra are studied; in others, both emission and absorption spectra. To avoid misunderstandings between workers in absorption and emission spectroscopy, it is advisable to avoid words and symbols related to the ideas of "initial" and "final" levels, but to emphasize the "upper" and "lower" states or levels involved in any spectroscopic transition. For this purpose, **it is recommended** (**REC. 34**) that symbols belonging to the upper level of a transition be labeled with a prime, e.g., J', v_3' (for quantum numbers), T', G', F' (for spectroscopic terms); and those belonging to the lower level with a double prime, e.g., J'', v_3'', T'', G'', or F''. For the *difference* in any quantum number between an upper and a lower level, **it is recommended** (**REC. 35**) that symbols such as ΔJ, meaning $J'-J''$, or Δv_3, meaning $v_3'-v_3''$, or ΔK, or ΔN, be used. RECS. 34 and 35 are in agreement with those for diatomic spectra.[1]

To designate any spectroscopic transition, **it is recommended** (**REC. 36**) that suitable upper state term symbols or quantum numbers be written first, corresponding lower state symbols second, separated by a minus sign or dash[1] to indicate subtraction; for example,

$$T'-T'';$$
$$G(v_1'v_2'\cdots)-G(v_1''v_2''\cdots);$$
$$F(J',K')-F(J'',K'');$$
$$(J_{K_aK_b})'-(J_{K_aK_b})'';$$

or instead of a minus sign an arrow to left or right may be used if one wishes to designate the emission or absorption character of the transition, as for example

$$J_{\tau'}\leftarrow J_{\tau''} \quad \text{or} \quad 10_5\leftarrow 9_4,$$
$$F_1(J+1,K)\leftarrow F_1(J,K),$$

for certain absorption transitions, and

$$J_{\tau'}\rightarrow J_{\tau''} \quad \text{or} \quad 10_5\rightarrow 9_4,$$
$$F_1(J+1,K)\rightarrow F_1(J,K),$$

for corresponding emission transitions.

The wave number (cm^{-1}) or frequency (in Mc/sec) of any transition is usually given by

$$\nu=T'-T'',$$

with appropriate specialization of T' and T'' to correspond to the particular case. But in the special case of Raman spectra, the wave number which is directly observed is given by

$$\nu=\nu_{\text{exc.}}\mp(T'-T''),$$

for "Stokes" and "anti-Stokes" lines or bands, respectively.

(b) *Bands and Electronic Transitions*

For bands in vibrational spectra, **it is recommended** (**REC. 37**) that designations such as

$$\nu_1+2\nu_2-\nu_3$$

for a certain combination band, or

$$2\nu_2-\nu_2$$

for a "hot" fundamental, be used when convenient. Similar designations might also be used for bands in electronic spectra, but the attribution to upper or lower electronic states must then be indicated, as for example by

$$\nu_1'+2\nu_2'-\nu_3''.$$

It is recommended (**REC. 38**) that the wave number or frequency of any spectroscopic transition be expressed (corresponding to RECS. 29–31 for term symbols and formulas) in the general form

$$\nu=\nu_e+\nu_v+\nu_r,$$

where

$$\nu_e=T_e'-T_e''; \quad \nu_v=G'-G''; \quad \nu_r=F'-F'',$$

and that for the *origin* of any vibrational or electronic

[19] In reference 1, the definitions $\Delta_1F(J+\frac{1}{2})=F(J+1)-F(J)$ and $\Delta_1G(v+\frac{1}{2})=G(v+1)-G(v)$ are recommended for diatomic molecules, but the often used simpler form recommended here seems preferable. The present definition of $\Delta_1F(J)$ is used in reference 2.

band, the symbol ν_0 be used:

$$\nu_0=\nu_e+\nu_v;$$

ν_e denotes the *origin of a band system*. REC. 38 corresponds to the same notation as for diatomic spectra.[1]

In diatomic spectra, one distinguishes between individual "bands," each corresponding to a definite pair of quantum numbers v', v'', and "band systems," each composed of an ensemble of bands associated with a particular electronic transition. In polyatomic spectra, often (a), the individual bands of an electronic transition are so numerous and strongly overlapping that it is difficult or impossible to distinguish them individually, or (b), the electronic transition gives rise only to continuous absorption; in both these situations, the entire spectrum of the electronic transition is commonly called a band. **It is recommended** (**REC. 39**) that the word "band" be reserved for definite individual bands, and that "electronic transition" or "transition" be used for the entire spectrum, whether discrete, pseudo-continuous, or strictly continuous, associated with an electronic transition; or "band system" if the spectrum consists of discrete bands.

(c) *Band structures*

In vibrational (infrared and Raman) and electronic bands, long series of lines (*branches*) occur for which it is convenient to have standard designations. **It is recommended** (**REC. 40**) that the letters O, P, Q, R, S be used to designate band branches with $\Delta J=-2$, -1, 0, $+1$, $+2$ respectively (see REC. 35); with corresponding left superscript O, P, Q, R, or S (e.g., ${}^{Q}P$ to denote $\Delta K=0$, $\Delta J=-1$) to denote ΔK in the case of symmetric-rotor and quasi-symmetric asymmetric-rotor molecules; and in general that band branches, subbranches, and fine structures be designated as in Herzberg's book.[20]

[20] See reference 2, Chap. IV.

In case a *loosely-coupled* electron spin S is present, **it is recommended** (**REC. 41**) that numerical subscripts be added to indicate spin fine structure, for example ${}^{P}R_{12}(J)$ for $\Delta K=-1$, $\Delta J=1$, and an F_1 upper and an F_2 lower state [hence $\Delta N=0$ if $S=\frac{1}{2}$; see REC. 31(b)]; but for linear molecules, the left superscript is to be omitted, since K is then a vibrational or electronic rather than a proper rotational quantum number (see REC. 17).[21]

Branch symbols are needed in vibrational and in rotational Raman spectra as well as in vibrational and electronic bands. For vibrational Raman bands,

$$\nu=\nu_{\text{exc.}}\mp[(G'-G'')+(F'-F'')],$$

with the $-$ or $+$ sign for Stokes and anti-Stokes bands respectively. REC. 40 is applicable here, for both Stokes and anti-Stokes bands; the definitions $\Delta J=J'-J''$, $\Delta K=K'-K''$ should be kept in mind. A corresponding recommendation has been made[1] for diatomic Raman spectra.

For pure *rotational* Raman bands,

$$\nu=\nu_{\text{exc.}}\mp(F'-F'').$$

At least in the case that F depends only on J, ΔJ is necessarily positive (since $F'>F''$ by definition); therefore **it is recommended** (**REC. 42**) that the symbols R, S be used for $\Delta J=+1$ and $+2$ for *both* Stokes and anti-Stokes branches, even though the Stokes branches with $\Delta J=+1$ and $+2$ simulate P and O branches.[22] A corresponding recommendation has been made[1] for diatomic Raman spectra.

[21] For diatomic band branches (see reference 1) a left superscript O, P, Q, R, or S is used to designate ΔN when a loosely coupled electron spin is present. However, this practice, though convenient, is not really necessary, since when ΔJ and the spin subscripts are given, the value of ΔN is determined. To avoid confusion between ΔK and ΔN, it seems best in polyatomic spectra to use the left superscript only to denote ΔK of nonlinear molecules.

[22] See reference 5, page 35 and footnote 17 there.

Concerning the Temperature Coefficient of the emf of Reversible Galvanic Cells Operated at Variable Concentration. II

JAMES C. M. LI*
Department of Chemistry and Chemical Engineering, University of California, Berkeley, California
(Received October 11, 1954)

The general expression including concentration coefficients of the emf of the cell is derived for an open system. The limitation in the application of the Gibbs-Helmholtz equation is further discussed in general with additional examples.

THE application of the Gibbs-Helmholtz equation, namely,

$$d\Delta F/dT=-\Delta S \tag{1}$$

to reversible galvanic cells with both temperature and concentration variables has been discussed by several papers.[1-5] A general expression including the concentration coefficients of the emf has been presented, namely,

$$\frac{d\Delta F}{dT}=-\Delta S+\sum_i\left(\frac{\partial\Delta F}{\partial c_i}\right)_{T,c'}\frac{dc_i}{dT}. \tag{2}$$

A derivation of Eq. (1) for closed systems (materially isolated) has been given by Barieau.[4] It is the purpose of this communication to derive Eq. (2) for an open system and to discuss the applicability of Eq. (1) in general.

Consider the thermodynamic system of a galvanic cell taking in n_j moles of species j during reversible discharge under constant external conditions, the free energy change of the system is

$$\Delta F_s=\sum_j n_j\bar{F}_j-N\mathcal{E}\mathfrak{F}, \tag{3}$$

where N is the number of faradays, $\mathcal{E}$ is the emf of the cell, and $\mathfrak{F}$ is the faraday. In order words, the free energy change of the reaction corresponding to the emf of the cell is

$$\Delta F=\Delta F_s-\sum_j n_j\bar{F}_j. \tag{4}$$

Differentiate Eq. (4) with respect to temperature and remember that

$$\Delta S=\Delta S_s-\sum_j n_j\bar{S}_j, \tag{5}$$

Eq. (2) is obtained.

Equations (1) and (2) are identical for systems where concentrations are not variables. This includes closed systems since their properties are only functions of external conditions. However, as pointed out by Barieau,[2] on applying Eq. (1) a correct reaction has to be used which can be obtained by his principle or by a mathematical method.[3] This correct reaction has simple forms of the coefficients for many cases where the system has two-component phases. The coefficients may become complicated as shown[3] for systems having multicomponent phases. The information required to evaluate the correct reaction is then equivalent to or more than what is needed in Eq. (2) when the system is considered open. On the other hand, if the system is actually open, Eq. (1) cannot be applied unless it can be considered closed in some manner. This can be illustrated with the following examples.

The example given by Stout[4] as suggested by Barieau is actually an open system because the amount of water or hydrogen in the gaseous phase has to be changed when temperature changes in order to keep equilibrium with the solution such that the concentration of HCl remains constant. It can be closed since it is equivalent to a closed system where the volume of the gaseous phase is negligibly small compared to the volume of solution. Barieau's method can then be used to this closed system to obtain the correct reaction to which Eq. (1) can be applied.

However, if the NaCl in that cell is replaced by a hydrate such as[6] $MgCl_2\cdot 12H_2O$, the cell is equivalent to a closed system where the ratio of the volume of hydrogen to that of solution is such that the concentration of HCl remains constant when temperature changes. This volume ratio is a function of temperature. If the temperature is in the range where the solubility of $MgCl_2\cdot 12H_2O$ decreases with the increase of temperature, the ratio is negative. In that case, the cell can no longer be considered closed and therefore Eq. (1) cannot be applied.

Cells can be so defined that they are open and cannot be considered closed in any manner such as the following[6]

$$Zn(s)\,|\,ZnCl_2(m)\;MgCl_2(\text{sat.})\,|\,MgCl_2\cdot 6H_2O(s),\;AgCl(s),\;Ag(s) \tag{6}$$

where m is the concentration of $ZnCl_2$ in mole ratio with respect to water and is kept unchanged with temperature. The cell presented before by the author[3] is of the same nature except that the irreversible reaction between cupric ion and hydrogen may be too fast to

* Present address: Department of Chemistry, Carnegie Institute of Technology, Pittsburgh, Pennsylvania.

[1] F. G. Brickwedde and L. H. Brickwedde, Phys. Rev. **II 60**, 172 (1941).
[2] R. E. Barieau, J. Am. Chem. Soc. **72**, 4023 (1950).
[3] J. C. M. Li, J. Chem. Phys. **19**, 1059 (1951).
[4] R. E. Barieau, J. Chem. Phys. **21**, 1827 (1953).
[5] J. W. Stout, J. Chem. Phys. **21**, 1829 (1953).

[6] Suggested by Professor George Scatchard at the Massachusetts Institute of Technology, Cambridge, Massachusetts.

be considered reversible when the concentration of sulfuric acid is small. But this is certainly not the reason why Barieau's method cannot be applied. The reason is simply that the cell is open since the amount of sulfuric acid has to be changed when the temperature changes in order to keep the constant molality with respect to water and therefore Eq. (2) should be used.

It is of interest to notice, as pointed out before,[3] that Eq. (1) can be applied to any cell such as (6) provided that the reaction is evaluated mathematically to allow the second term on the right hand side of Eq. (2) to vanish. The reaction for cell (6) is,

$$\mathrm{Zn}(s)+2\mathrm{AgCl}(s)+q\mathrm{MgCl_2}(\mathrm{soln})+6q\mathrm{H_2O}(\mathrm{soln}) \rightarrow \mathrm{ZnCl_2}(\mathrm{soln})+2\mathrm{Ag}(s)+q\mathrm{MgCl_2}\cdot 6\mathrm{H_2O}(s), \quad (7)$$

in which

$$q=[(6c-1)(\partial m/\partial c)_{F,T}-6m]^{-1}, \quad (8)$$

where c is the concentration of $MgCl_2$ in solution in mole ratio with respect to water and F is the partial molal free energy of $MgCl_2$ (not hydrate) in solution. The ΔS of reaction (7) corresponds to the temperature coefficient of the emf of the cell (6). But this is not the actual reaction in the isothermal discharge of cell (6). The actual reaction which can be obtained by Barieau's principle is otherwise the same as reaction (7) except that in the q expression the F is replaced by F_0, the free energy of solid $MgCl_2\cdot 6H_2O$. As shown by Stout,[4] the two reactions are identical when the system is closed. They are different as shown here for open systems and have different significance.

In conclusion, although Barieau's method is very useful in many cases where the thermodynamic system of the cell can be considered closed, to avoid the misuse of Eq. (1), Eq. (2) would be more safe to apply, with which any correct reaction can be used. There is no great advantage to restrict consideration to the actual reaction for the purpose of the examination of temperature coefficient, and as shown it may be misleading when the cell is not closed as temperature changes even though it is closed at any specified temperature.

ACKNOWLEDGMENTS

The author is indebted to Professor K. S. Pitzer at the University of California for some discussions.

THE JOURNAL OF CHEMICAL PHYSICS VOLUME 23, NUMBER 11 NOVEMBER, 1955

Heat Capacity of Zinc Fluoride from 11 to 300°K. Thermodynamic Functions of Zinc Fluoride. Entropy and Heat Capacity Associated with the Antiferromagnetic Ordering of Manganous Fluoride, Ferrous Fluoride, Cobaltous Fluoride, and Nickelous Fluoride

J. W. Stout and Edward Catalano*
Institute for the Study of Metals and Department of Chemistry, University of Chicago, Chicago, Illinois
(Received February 21, 1955)

The heat capacity of ZnF_2 has been measured calorimetrically between 11 and 300°K. In addition to the direct experimental data, values of heat capacity, entropy, enthalpy, and free energy are tabulated at selected temperatures. The values of entropy, and enthalpy at 298.16°K are $S^0=17.61\pm0.03$ cal deg^{-1} mole^{-1} and $H^0-H_0^0=2827\pm5$ cal mole^{-1}. The heat capacity of ZnF_2 has been used, with a corresponding states argument, to estimate the lattice contributions to the entropy and heat capacity of the isomorphous fluorides MnF_2, FeF_2, CoF_2, and NiF_2 which exhibit heat capacity maxima associated with antiferromagnetic ordering at 66.5, 78.35, 37.70, and 73.22°K, respectively. The values of electronic entropy at the maximum in heat capacity are: MnF_2, $0.85R\ln 6$; FeF_2, $0.87R\ln 5$; CoF_2, $0.80R\ln 2$; NiF_2, $0.71R\ln 3$. The electronic entropies and heat capacities are compared with molecular field and spin wave theories of antiferromagnetism. At very low temperatures the electronic heat capacity on NiF_2 is varying approximately as T^3 whereas that of the other antiferromagnetic fluorides depends much more strongly on temperature. This behavior of the electronic heat capacity of NiF_2 is believed to be associated with the small ferromagnetic moment found in magnetic anisotropy measurements on this salt.

IN earlier papers the results of low temperature heat capacity measurements on MnF_2,[1] FeF_2,[2] CoF_2,[2] and NiF_2[3] have been presented. Each of these compounds exhibits a lamdba-shaped anomaly in heat capacity associated with the antiferromagnetic ordering of the atomic magnetic moments. These four antiferromagnetic compounds, together with diamagnetic ZnF_2, form an isomorphous series of compounds of the rutile structure.[4] The heat capacity of ZnF_2 may therefore be used as a guide in the estimation of the contributions of the lattice vibrations to the heat capacities of MnF_2, FeF_2, CoF_2, and NiF_2 and by

* Eastman Kodak Company Fellow 1951–1952; Allied Chemical and Dye Corporation Fellow 1952–1953.

[1] J. W. Stout and H. E. Adams, J. Am. Chem. Soc. **64**, 1535 (1942).

[2] E. Catalano and J. W. Stout, J. Chem. Phys. **23**, (to be published) (1955).

[3] E. Catalano and J. W. Stout, J. Chem. Phys. **23**, 1284 (1955).

[4] For precise lattice parameters see J. W. Stout and S. A. Reed, J. Am. Chem. Soc. **76**, 5279 (1954).

TABLE I. The heat capacity of ZnF_2. 0°C=273.16°K. Molecular weight 103.38.

T_{Av} °K	Approx. ΔT	$\Delta H/\Delta T$ cal deg^{-1} mole^{-1}	T_{Av} K	Approx. ΔT	$\Delta H/\Delta T$ cal deg^{-1} mole^{-1}
59.18	4.23	3.598	21.47	2.51	0.298
54.53	2.64	3.110	23.94	2.58	0.420
58.80	5.91	3.554	26.82	2.93	0.594
65.25	7.01	4.226	29.72	2.83	0.796
72.14	6.77	4.916	32.72	3.22	1.027
78.81	6.56	5.583	35.93	3.38	1.293
85.27	6.36	6.221	39.25	3.25	1.593
91.62	6.39	6.805	43.10	4.40	1.954
98.14	6.65	7.389	47.56	4.52	2.393
104.09	5.91	7.891	52.10	4.61	2.849
110.31	6.49	8.393	56.98	5.14	3.364
117.03	6.97	8.930	188.59	6.90	12.93
124.09	7.20	9.459	195.71	7.14	13.21
131.60	7.82	9.969	203.00	7.03	13.46
139.40	7.78	10.47	210.03	6.72	13.69
147.63	8.53	10.96	217.10	7.07	13.90
155.00	7.90	11.39	224.10	6.78	14.11
162.90	7.75	11.79	233.54	6.43	14.37
170.80	7.95	12.17	240.41	6.85	14.53
178.91	8.11	12.53	247.27	6.61	14.69
11.03	0.42	0.033	253.92	6.39	14.84
11.89	0.92	0.040	260.57	6.19	14.98
12.96	1.40	0.053	267.49	5.99	15.11
14.68	1.23	0.080	272.66	5.85	15.24
16.19	1.56	0.112	279.50	6.80	15.35
17.87	1.49	0.159	286.36	6.59	15.50
19.48	1.75	0.216	292.97	6.42	15.59
			299.42	6.24	15.73

subtracting the estimated contributions of the lattice from the experimentally measured totals a detailed picture of the entropy changes and heat capacities associated with the antiferromagnetic ordering may be obtained.

In this paper the data on the heat capacity of ZnF_2 are given. By use of a corresponding states argument the lattice contributions to the entropy and heat capacity of the antiferromagnetic compounds are estimated. The electronic heat capacities and entropies are calculated and compared with theoretical predictions.

ZINC FLUORIDE

Preparation of Sample

Zinc carbonate was precipitated by the addition of solid NH_4HCO_3 to a concentrated aqueous solution of $Zn(NO_3)_2 \cdot 6H_2O$. The washed zinc carbonate was added to a 40% HF solution. $ZnF_2 \cdot 4H_2O$, crystallized from this solution, was dried in air at 120°C to remove most of the water of hydration and then converted completely to anhydrous ZnF_2 by heating at 900°C in a stream of anhydrous HF. During this treatment the material was contained in a graphite boat and the nickel furnace tube was equipped with a carbon liner to prevent the introduction of metallic impurities into the sample. Although Haendler, Patterson, and Bernard[5] report a melting point for ZnF_2 of 875°C in a nitrogen atmosphere we found that to melt our material in an atmosphere of HF a temperature greater than 950°C was required. The sintered material from the dehydration in HF at 900°C was transferred to a large graphite crucible which was heated, in an atmosphere of HF, to 980°C, and then slowly cooled. The ZnF_2 melted and the boule contained large, colorless crystals of the order of one centimeter in size. The sample used was material from the inside of the boule, crushed to a particle size ranging from 0.5 to 4 mm.

A spectrochemical analysis of the sample used for the heat capacity measurements showed the presence, in weight percent, of: Mg, 0.001; Al, 0.006; Ni, 0.002; Fe, 0.005; Cu, 0.002; Na, 0.003; K, 0.001. Mn, V, Co, Si, and Ca were not detected. The sample was analyzed for zinc gravimetrically by dissolving the ZnF_2 in aqua regia, precipitating the sulfide, and weighing as $ZnSO_4$.[6] The results of four determinations were, in weight percent zinc: 63.21, 63.50, 63.10, 63.10; that calculated for ZnF_2 is 63.24.

The Heat Capacity of ZnF_2

The calorimeter and the methods of measurement were the same as those described previously.[3,2] The defined calorie equal to 4.1840 absolute joules is used. The ice point temperature was taken as 273.16°K. The calorimeter contained 269.44 g *in vacuo* (2.6063 moles) of ZnF_2. The experimental heat capacities, listed in Table I, are the ratios of the increase in enthalpy, ΔH, to the rise in temperature, ΔT, and are equal to the differential heat capacity, C_p, only when the correction for curvature is negligible. Also listed in Table I are T_{Av}, the arithmetic mean of the initial and final temperature of each measurement and the approximate temperature rise, ΔT. As was expected there are no anomalies in the heat capacity of ZnF_2.

Thermodynamic Properties of ZnF_2

Values of the heat capacity, entropy, enthalpy, and the free energy function for ZnF_2 are given in Table II.

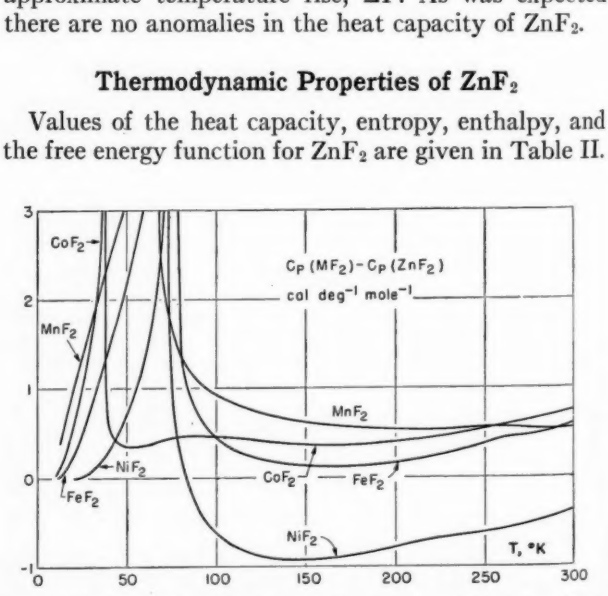

FIG. 1. Heat capacity of MnF_2, FeF_2, CoF_2, and NiF_2 less heat capacity of ZnF_2 *versus* temperature.

[5] Haendler, Patterson, and Bernard, J. Am. Chem. Soc. 74, 3167 (1952).

[6] H. A. Fales and G. M. Ware, J. Am. Chem. Soc. 41, 487 (1919).

TABLE II. Thermodynamic properties of ZnF_2.

T °K	C_p^0 cal deg^{-1} mole^{-1}	S^0 cal deg^{-1} mole^{-1}	$H^0-H_0^0$ cal deg^{-1}	$-\frac{F^0-H_0^0}{T}$ cal deg^{-1} mole^{-1}
15	0.086	0.027	0.31	0.007
20	0.235	0.070	1.07	0.017
25	0.479	0.147	2.81	0.034
30	0.816	0.262	6.02	0.062
35	1.213	0.417	11.07	0.101
40	1.660	0.608	18.24	0.152
45	2.139	0.831	27.72	0.215
50	2.637	1.082	39.65	0.289
55	3.158	1.358	54.14	0.374
60	3.682	1.655	71.24	0.468
65	4.200	1.970	90.95	0.571
70	4.701	2.300	113.2	0.683
80	5.703	2.993	165.2	0.928
90	6.662	3.721	227.1	1.198
100	7.547	4.469	298.2	1.487
110	8.374	5.228	377.9	1.793
120	9.157	5.990	465.6	2.111
130	9.863	6.751	560.7	2.438
140	10.51	7.506	662.6	2.773
150	11.10	8.252	770.7	3.114
160	11.65	8.986	884.5	3.458
170	12.14	9.707	1003.4	3.804
180	12.58	10.413	1127.0	4.152
190	12.99	11.104	1254.9	4.500
200	13.35	11.780	1386.6	4.847
210	13.69	12.440	1521.9	5.193
220	13.99	13.084	1660.3	5.537
230	14.27	13.712	1801.7	5.879
240	14.53	14.325	1945.7	6.218
250	14.76	14.923	2092.2	6.554
260	14.97	15.506	2240.8	6.887
270	15.18	16.075	2391.6	7.217
280	15.38	16.631	2544.4	7.543
290	15.56	17.173	2699.1	7.866
300	15.72	17.704	2855.4	8.185
273.16	15.24	16.25	2440	7.32
298.16	15.69	17.61	2827	8.13
		±0.03	±5	±0.02

The C_p listed is the differential heat capacity corrected for curvature. The extrapolation to 0°K was made on a plot of C_p/T^3 *versus* T. The extrapolated contribution to the entropy below 10°K was 0.008 cal deg^{-1} mole^{-1}. The accuracy of the smoothed heat capacity data is estimated as 3% at 15°K, 1% at 20°K and 0.2% between 40 and 200°K. Above 200°K, because of the increased heat leak, the uncertainty increases, reaching about 0.5% at 300°K. The accuracy of the functions S^0, $H^0-H_0^0$ and $-(F^0-H_0^0)/T$ is about 0.2% above 60°K but for internal consistency the entries in Table II are given to a higher precision than this. The values of entropy and free energy in Table II do not include the contributions from nuclear spin randomness or isotopic mixing and are therefore the conventional ones to be used in calculations of chemical equilibria.

ELECTRONIC ENTROPY AND HEAT CAPACITY OF MnF_2, FeF_2, CoF_2, AND NiF_2

Estimation of the Lattice Contributions

In order to calculate the entropy changes and heat capacity associated with the antiferromagnetic ordering in MnF_2, FeF_2, CoF_2, and NiF_2 it is necessary to subtract from the experimentally measured quantities the contributions arising from the lattice vibrations. A comparison of the experimental heat capacities is shown in Fig. 1. In this figure the difference between the heat capacity of each of the four antiferromagnetic fluorides and that of zinc fluoride is plotted *versus* temperature. It is evident from an examination of Fig. 1 that there are electronic contributions to the heat capacity of the antiferromagnetic fluorides over a wide range of temperature and that an attempt to estimate the vibrational heat capacity by drawing a smooth curve connecting the experimental data above and below the region of clearly anomalous heat capacity, as was done for MnF_2 by Stout and Adams,[1] will overestimate the vibrational heat capacity, particularly on the low temperature side of the anomaly. Osborne and Westrum[7,8] have assumed that the lattice contribution to the heat capacities of UO_2 and NpO_2 equals the heat capacity of the isomorphous diamagnetic ThO_2 and that the heat capacity of ThF_4 represents the lattice contribution in UF_4. It is clear from Fig. 1 that such an assumption is not tenable for the iron group fluorides since at high temperatures the observed heat capacity of NiF_2 is considerably less than that of the isomorphous diamagnetic ZnF_2.

In Table III are listed the formula weights, the lattice constants a and c, the axial ratio c/a, the volume per unit cell (containing two molecules), and the approximate melting point for each of the five fluorides. Also included is the temperature of the maximum in heat capacity associated with the antiferromagnetic ordering for the four magnetic fluorides. The variation in structural parameters is not large, although evidently great enough so that the thermal properties of the lattice are not identical for all five compounds. As the next approximation we shall use an assumption that the vibrational contributions to the entropy and heat capacity of MnF_2, FeF_2, CoF_2, NiF_2, and ZnF_2 obey a law of corresponding states. Then the lattice entropy,

TABLE III. Some properties of the iron group fluorides.

Substance	Formula weight	a, A[a]	c, A[a]	c/a	Vol unit cell, A^3	Approx mp, °C	T, °K of C_p(max)
MnF_2	92.93	4.8734	3.3099	0.6792	78.61	929.5[e]	66.5[f]
FeF_2	93.85	4.6966	3.3091	0.7046	72.99	1020[b]	78.35[g]
CoF_2	96.94	4.6951	3.1796	0.6772	70.09	1250[b]	37.70[g]
NiF_2	96.69	4.6506	3.0836	0.6631	66.69	1450[b]	73.22[h]
ZnF_2	103.38	4.7034	3.1335	0.6662	69.32	875[d] 950[e]	...

[a] J. W. Stout and S. A. Reed, J. Am. Chem. Soc. **76**, 5279 (1954).
[b] L. M. Matarrese, thesis, University of Chicago (1954).
[c] M. Griffel and J. W. Stout, J. Am. Chem. Soc. **72**, 4351 (1950).
[d] Haendler, Patterson, and Bernard, J. Am. Chem. Soc. **74**, 3167 (1952).
[e] See text under "Preparation of Sample."
[f] J. W. Stout and H. E. Adams, J. Am. Chem. Soc. **64**, 1535 (1942).
[g] E. Catalano and J. W. Stout, J. Chem. Phys. (to be published).
[h] E. Catalano and J. W. Stout, J. Chem. Phys. **23**, 1284 (1955).

[7] D. W. Osborne and E. F. Westrum, Jr., J. Chem. Phys. **21**, 1884 (1953).
[8] Lohr, Osborne, and Westrum, J. Am. Chem. Soc. **76**, 3837 (1954).

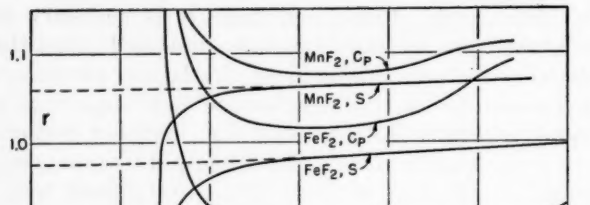

FIG. 2. Corresponding states ratios, $r(MF_2, S)$ and $r(MF_2, C_p)$ (see text) *versus* temperature for MnF_2, FeF_2, and NiF_2. Solid lines are experimental curves. Dashed lines are extrapolations to low temperatures of $r(MF_2, S)$ for estimation of lattice contributions to entropy and heat capacity.

$S(\text{lat})=\Phi(T/\theta)$, and the lattice heat capacity, $C_p(\text{lat}) = (T/\theta)\Phi'(T/\theta)$, where Φ is the same function for all five compounds and θ is a characteristic temperature different for each compound.

In the case of MnF_2, FeF_2 and NiF_2 our knowledge of the magnetic properties permits the evaluation, at temperatures well above the maximum in heat capacity, of the electronic contributions to the entropy and heat capacity. The high temperature magnetic susceptibilities of MnF_2,[9,10] FeF_2,[11] and NiF_2 [10] are consistent with the "spin-only" model.[12] On this picture the splitting of the orbital states by the electrostatic crystalline fields is large compared to kT at room temperature, which in turn is large compared to the splitting of the 2S+1 spin states. S is the spin quantum number which has the values: Mn^{++}, 5/2; Fe^{++}, 2; Ni^{++}, 1. From some temperature sufficiently above the maximum in heat capacity so that there is essentially an equal distribution among the spin states, up to room temperature, one would anticipate a negligible contribution of the electronic system to the heat capacity and a constant electronic contribution to the entropy of $R\ln(2S+1)$. One can then check the validity of the corresponding states approximation. If $S(MF_2, T)$ represents the entropy of an antiferromagnetic fluoride, denoted generally by MF_2, at temperature T, then $S^*(MF_2, T)=S(MF_2, T)-R\ln(2S+1)$ is equal to the lattice contribution to the entropy of MF_2 provided the electronic entropy is fully excited. When the electronic entropy is less than $R\ln(2S+1)$ then $S^*(MF_2, T)$ is less than the true lattice entropy of MF_2. From Table II one finds the temperature T' where $S(ZnF_2, T')$ is equal to $S^*(MF_2, T)$. The ratio $T'/T=\theta(ZnF_2)/\theta(MF_2)$ is denoted by $r(MF_2, S)$. Similarly one finds a temperature T'' where ZnF_2 has the same heat capacity as does MF_2 at temperature T and denotes the ratio T''/T by $r(MF_2, C_p)$. If the principle of corresponding states were exactly followed one would expect to find that at the higher temperatures $r(MF_2, S)$ and $r(MF_2, C_p)$ were equal to one another and were both temperature independent. As one goes to lower temperatures the electronic entropy will begin to drop below $R\ln(2S+1)$. When this happens the temperature T' will be too small, since one has subtracted too much electronic entropy to obtain the lattice entropy. Even though the corresponding states principle is exact the $r(MF_2, S)$ as described above will drop rapidly as the electronic entropy of MF_2 is lost. Associated with the loss of electronic entropy is an electronic heat capacity. The temperature T'' is therefore too large and the ratio $r(MF_2, C_p)$ will rise as the electronic heat capacity increases.

The curves of $r(MF_2, S)$ and $r(MF_2, C_p)$, calculated as described above from the experimental entropies and heat capacities,[1-3] are shown for MnF_2, FeF_2, and NiF_2 in Fig. 2. At temperatures below 150°K the values of $r(MF_2, C_p)$ rise as expected because of the appearance of electronic heat capacity, and those of $r(MF_2, S)$ drop. The experimental values of $r(MF_2, C_p)$ go through a minimum between 150 and 200°K, and above 200°K the values of $r(MF_2, S)$ rise slowly with temperature instead of remaining constant. In MnF_2 and NiF_2 there are certainly no electronic states contributing to the heat capacity other than the 2S+1 low-lying ones and one therefore would expect that above the low-temperature maximum the electronic heat capacity would decrease monotonically with increasing temperature. The rise in $r(MF_2, C_p)$ above 200°K and the nonequality of $r(MF_2, C_p)$ and $r(MF_2, S)$ must therefore be ascribed to a failure of the principle of corresponding states. In FeF_2 we believe that the failure of corresponding states is the principal reason for the rise in $r(FeF_2, C_p)$ above 170°K although here the excitation to other orbital levels[13] may possibly contribute an electronic term to the heat capacity.

It is not surprising that the principle of corresponding states is less accurate at the higher temperatures and that the deviations from this principle are more pronounced in $r(MF_2, C_p)$ than in $r(MF_2, S)$. As a rough approximation one may consider the heat capacity of ZnF_2, and the vibrational heat capacity of the other fluorides, to consist of a Debye-like component, rising to a maximum of $3R$, and corresponding to the motions of the heavy atoms (or MF_2 molecules), plus internal vibrations, with maximum contribution $6R$, involving principally the fluorine atoms and contributing Einstein functions to the heat capacity. If the ratio of the frequencies of the fluorine vibrations in MnF_2, FeF_2, and NiF_2 to those in ZnF_2 is less than the corresponding ratios of the heavy

[9] H. Bizette and B. Tsai, Compt. rend. **209**, 205 (1939).
[10] de Haas, Schultz, and Koolhaas, Physica **7**, 57 (1940).
[11] H. Bizette and B. Tsai, Compt. rend. **212**, 119 (1941).
[12] J. H. Van Vleck, *Electric and Magnetic Susceptibilities* (Oxford University Press, London, 1932), p. 286.
[13] See K. Niira and T. Oguchi, Progr. Theoret. Phys. **11**, 425 (1954).

metal frequencies, then one would expect $r(MF_2, C_p)$ to be larger than $r(MF_2, S)$ since the fluorine vibrations will contribute more to the heat capacity than to the entropy. One would also, in this case, expect both $r(MF_2, S)$ and $r(MF_2, C_p)$ to increase with increasing temperature.

The expected error in $r(MF_2, C_p)$, arising from the experimental error in the heat capacity measurements, increases considerably at higher temperatures. This is partly because the heat capacity measurements themselves are less precise in the neighborhood of 300°K than at lower temperatures, but also because, since dC_p/dT decreases at the higher temperatures, a given fractional error in C_p produces a larger error in $r(MF_2, C_p)$. The accuracy of the smoothed values of heat capacity of MF_2 and of ZnF_2 has been estimated as 0.2% at 200°K and below, and 0.5% at 300°K. The corresponding errors in $r(MF_2, C_p)$ would be 0.25% at 100°K, 0.55% at 200°K, and 2.2% at 300°K. The expected error in $r(MF_2, S)$ is much less. If the individual smooth values of the entropy are in error by 0.2%, the error in $r(MF_2, S)$ would be about 0.2% from 100 to 200°K, and 0.3% at 300°K.

We conclude, therefore, that the principle of corresponding states may be used to obtain reliable values of the electronic contributions to the entropy and heat capacity of MnF_2, FeF_2, and NiF_2 in the neighborhood of the experimental maxima in heat capacity and at lower temperatures where the lattice contributions are comparatively small. At temperatures much above those of the maxima, however, the electronic heat capacity becomes small relative to that of the lattice and this, together with the increased uncertainty in the corresponding states assumption and the increased error in the values of r arising from the experimental errors in the heat capacity measurements, makes the values of the electronic heat capacity increasingly unreliable as the temperature increases

Since the function $r(MF_2, S)$ is more dependent than $r(MF_2, C_p)$ on the heavy metal frequencies, which will be of principal importance at low temperatures, we have made use of extrapolated values of this function in order to estimate the vibrational contributions to the entropy of MnF_2, FeF_2, and NiF_2. The dashed curves in Fig. 2 are the extrapolated values of $r(MF_2, S)$. In the neighborhood of the minimum in the $r(MF_2, C_p)$ curves the electronic heat capacity has become small and the extrapolated curves of $r(MF_2, S)$ are drawn as smooth continuations of the observed curves at higher temperatures, beginning to depart from the observed curves in the neighborhood of the temperatures of the minima in $r(MF_2, C_p)$ and becoming temperature independent at low temperatures. We have assumed that the contributions of the lattice and of the electronic system are independent of one another and that there is no interaction between them. Such an interaction is reflected in the anomalies in coefficient of expansion[14] and x-ray structure[15–17] found in MnO, FeO, CoO, and NiO. No such measurements have yet been made on the anhydrous fluorides but since the dimensional changes found in the oxides were small, and would be expected to be still less important in the fluorides where the antiferromagnetic ordering occurs at lower temperatures than in the oxides, we do not believe that lattice changes associated with the antiferromagnetic ordering will introduce serious errors in the estimation of the lattice entropy by the extrapolation from high temperatures of the curves of $r(MF_2, S)$.

The Electronic Entropy and Heat Capacity of MnF_2, FeF_2, and NiF_2

Having the extrapolated curves of $r(MF_2, S)$ one may readily calculate the electronic contributions to the entropy and heat capacity. From the tables compiled from the experimental heat capacity data[1–3] one finds the total entropy $S(MF_2, T)$ at a temperature T. The lattice contribution to the entropy, $S(\text{lat}, T) = S(ZnF_2, rT)$, is found in Table II of this paper and is subtracted from $S(MF_2, T)$ to give the electronic entropy of MF_2 at temperature T. The lattice contribution to the heat capacity is obtained from the thermodynamic relation

$$\begin{aligned} C_p(\text{lat}, T) &= T dS(\text{lat}, T)/dT \\ &= T\{d[S(ZnF_2, rT)]/d(rT)\}[d(rT)/dT] \\ &= C_p(ZnF_2, rT)[1+(d\ln r)/(d\ln T)]. \end{aligned} \quad (1)$$

The electronic entropy and heat capacity so calculated are given in Table IV for MnF_2, FeF_2, and NiF_2. For comparison the vibrational contributions to the entropy and heat capacity are included in this table.

The accuracy of the values of the electronic entropy and heat capacity in Table IV at temperatures of the observed heat capacity maxima and below depends mainly on the possible error in the extrapolation of the curves of $r(MF_2, S)$ used to calculate the vibrational contributions. We estimate that the error in the extrapolated values of $r(MF_2, S)$ is about 1%. At the temperatures of the observed maxima in heat capacity an error of 1% in $r(MF_2, S)$ leads to errors in the calculated magnetic entropy of: MnF_2, 1.6%; FeF_2, 1.9%; NiF_2, 2.5%. The errors in the electronic entropy at other temperatures may be estimated from Table IV and the fact that a 1% error in r produces an error in $S(\text{lat})$ of 3% below $rT=40$, 2.4% at $rT=50$, 2% at $rT=70$, and 1.5% at $rT=120$. The uncertainties in the electronic heat capacity are somewhat greater since the calculation of the vibrational heat capacity involves the slope of the $r(MF_2, S)$ *versus* T curve as well as the magnitude of $r(MF_2, S)$. We estimate the errors in the vibrational heat capacity in Table IV are about

[14] M. Foëx, Compt. rend. **227**, 193 (1948).
[15] H. P. Rooksby, Acta Cryst. **1**, 226 (1948).
[16] N. C. Tombs and H. P. Rooksby, Nature **165**, 442 (1950).
[17] S. Greenwald and J. S. Smart, Nature **166**, 523 (1950).

TABLE IV. Electronic entropy and heat capacity of MnF_2, FeF_2, and NiF_2.

T, °K	Extrap. $r(MF_2, S)$	S(lat)	S(elec)	C_p(lat)	C_p(elec)	$\frac{S(\text{elec})}{R\ln(2S+1)}$
			cal deg^{-1} mole^{-1}			
			MnF_2			
15	1.060	0.033	0.189	0.11	0.53	0.053
20	1.060	0.085	0.393	0.29	0.90	0.110
25	1.060	0.178	0.633	0.57	1.26	0.178
30	1.060	0.314	0.893	0.95	1.60	0.251
35	1.060	0.494	1.163	1.40	1.90	0.327
40	1.060	0.712	1.435	1.89	2.18	0.403
45	1.061	0.964	1.709	2.41	2.49	0.480
50	1.061	1.25	1.99	2.95	2.84	0.559
55	1.061	1.57	2.26	3.53	3.24	0.636
60	1.061	1.89	2.58	4.07	3.83	0.726
65	1.061	2.23	2.93	4.60	4.85	0.822
66.5	1.061	2.34	3.04	4.77	5.2	0.854
70	1.061	2.59	3.19	5.14	1.84	0.895
75	1.061	2.96	3.29	5.67	1.23	0.924
80	1.061	3.35	3.36	6.20	0.88	0.943
90	1.062	4.13	3.44	7.18	0.55	0.966
100	1.062	4.94	3.49	8.09	0.38	0.979
110	1.062	5.75	3.52	8.95	0.26	0.988
120	1.063	6.56	3.54	9.74	0.17	0.993
			FeF_2			
15	0.977	0.025	0.014	0.080	0.075	0.004
20	0.977	0.065	0.059	0.217	0.262	0.019
25	0.977	0.136	0.145	0.45	0.53	0.045
30	0.977	0.244	0.267	0.77	0.83	0.084
35	0.977	0.390	0.421	1.13	1.18	0.132
40	0.977	0.571	0.599	1.58	1.51	0.187
45	0.977	0.783	0.799	2.04	1.88	0.250
50	0.978	1.024	1.017	2.53	2.28	0.318
55	0.978	1.29	1.25	3.03	2.72	0.392
60	0.978	1.58	1.51	3.55	3.21	0.473
65	0.978	1.88	1.79	4.06	3.82	0.560
70	0.978	2.20	2.10	4.56	4.62	0.658
75	0.978	2.53	2.46	5.06	6.00	0.770
78.35	0.979	2.76	2.79	5.39	12.4	0.871
80	0.979	2.87	2.84	5.56	1.89	0.889
85	0.979	3.22	2.93	6.05	1.10	0.916
90	0.979	3.58	2.98	6.52	0.84	0.933
100	0.980	4.32	3.06	7.42	0.57	0.956
110	0.981	5.07	3.10	8.27	0.42	0.970
120	0.981	5.82	3.13	9.07	0.31	0.980
130	0.982	6.57	3.16	9.81	0.24	0.987
140	0.983	7.33	3.17	10.48	0.19	0.992
150	0.984	8.07	3.18	11.11	0.14	0.996
			NiF_2			
15	0.843	0.016	0.034	0.050	0.044	0.015
20	0.843	0.040	0.053	0.129	0.103	0.025
25	0.843	0.083	0.088	0.281	0.219	0.040
30	0.843	0.152	0.143	0.50	0.39	0.065
35	0.843	0.260	0.209	0.78	0.61	0.096
40	0.843	0.375	0.317	1.11	0.86	0.145
45	0.844	0.526	0.435	1.48	1.15	0.199
50	0.844	0.702	0.573	1.87	1.48	0.262
55	0.844	0.901	0.730	2.29	1.84	0.334
60	0.845	1.12	0.91	2.72	2.29	0.416
65	0.845	1.35	1.11	3.17	2.86	0.510
70	0.845	1.60	1.35	3.62	3.74	0.620
73.22	0.846	1.77	1.55	3.91	5.32	0.708
75	0.846	1.87	1.62	4.07	2.21	0.741
80	0.846	2.15	1.73	4.51	1.43	0.793
85	0.847	2.43	1.81	4.95	1.13	0.828
90	0.847	2.73	1.87	5.38	0.94	0.855
100	0.848	3.34	1.95	6.25	0.68	0.984
110	0.849	3.97	2.01	7.06	0.54	0.920
120	0.850	4.62	2.05	7.83	0.46	0.940
130	0.851	5.27	2.09	8.56	0.39	0.956
140	0.852	5.94	2.11	9.26	0.33	0.968
150	0.853	6.60	2.13	9.91	0.29	0.977

5% at $rT=20$ and below, 3% at $rT=50$, 2% at $rT=80$, and 1.5% at $rT=120$.

The Electronic Entropy and Heat Capacity of CoF_2

The magnetic susceptibility[18,19] of CoF_2 between the temperature of liquid nitrogen and room temperature does not agree with that expected from the spin-only formula. We cannot, therefore, assume as we did for MnF_2, FeF_2, and NiF_2 that at high temperatures the electronic entropy approaches the value $R\ln(2S+1)$. In magnetically dilute cobalt salts the magnetic susceptibility data also deviate markedly from the spin-only formula. Theoretical calculations[20,21] of the splittings produced by the electrostatic crystalline fields lead to the expectation that there will be separations of electronic states of the order of a few hundred cm^{-1}. In free Co^{++} ion the ground level is $3d^7\ ^4F$. In an electrostatic crystalline field of cubic symmetry this level, together with some admixture of the excited level $3d^7\ ^4P$, gives rise to a twelve-fold degenerate ground level and excited levels which are of the order of 10 000 cm^{-1} or more higher in energy and will therefore contribute nothing to the entropy at room temperature. The ground level is further split by the combined action of crystalline electrostatic fields of symmetry lower than cubic and by the spin-orbit coupling into six levels whose energy spacings are of the order of 100 to 1000 cm^{-1}. Each of these six levels has the twofold Kramers[22] degeneracy.

The magnetic anisotropy[23] of CoF_2 changes spectacularly between 37.70°K, the temperature of the maximum in heat capacity, and 200°K. This unusual behavior of the magnetic anisotropy is evidence of an excited electronic level in the crystal whose separation from the ground level is larger than kT at 37.70°K but smaller than kT at room temperature. The behavior of the magnetic anisotropy has been interpreted by Nakamura and Taketa[24] on a model where the crystalline field splitting of the twelve-fold degenerate ground level is assumed large compared to the perturbation by the spin-orbit coupling. There are then two doubly degenerate lowest levels with an energy separation of $129.5k$ needed to fit the anisotropy measurements.

Regardless of the details of the energy level pattern produced by the electrostatic crystalline fields and the spin orbit coupling, each level will, in the absence of exchange or other atomic interactions, have the twofold Kramers[22] degeneracy characteristic of systems with

[18] W. J. de Haas and B. H. Schultz, Physica **6**, 481 (1939).
[19] P. Henkel and W. Klemm, Z. anorg. u. allgem. Chem. **222**, 73 (1935).
[20] R. Schlapp and W. G. Penny, Phys. Rev. **42**, 666 (1932).
[21] A. Abragam and M. H. L. Pryce, Proc. Roy. Soc. (London) **A206**, 173 (1951).
[22] H. A. Kramers, Proc. Koninkl. Akad. Wetenschap. Amsterdam **33**, 959 (1930).
[23] J. W. Stout and L. M. Matarrese, Revs. Modern Phys. **25**, 338 (1953).
[24] T. Nakamura and H. Taketa, Progr. Theoret. Phys. **13**, 129 (1955). We are indebted to Dr. Nakamura and Dr. Taketa for sending us their manuscript prior to publication.

an odd number of electrons. The entropy change associated with the antiferromagnetic ordering which produces the maximum in heat capacity at 37.70°K would therefore be an integral multiple of $R\ln 2$. In Fig. 3 are plotted values of $r(C_p, CoF_2)$ and of $r(S=R\ln 2, CoF_2)$ and $r(S=R\ln 4, CoF_2)$, calculated as described previously, and corresponding to assumptions that the electronic entropy is $R\ln 2$ and $R\ln 4$, respectively. It is apparent from these curves that the entropy change associated with the antiferromagnetic ordering is $R\ln 2$ rather than $R\ln 4$. Indeed, the total entropy of CoF_2, including that of the lattice, does not become equal to $R\ln 4 = 2.75$ cal deg^{-1} mole^{-1} until a temperature of 57.5°K is reached.

The existence, in CoF_2, of low-lying electronic energy states above the doubly degenerate ground state principally involved in the antiferromagnetic ordering makes it impossible to obtain a value of $r(CoF_2, S)$ by extrapolation from higher temperatures as was done for MnF_2, FeF_2 and NiF_2. At 100°K one would expect $r(CoF_2, C_p)$ to be too high since the excitation to higher electronic states will contribute to the electronic heat capacity. The electronic entropy will also become greater than $R\ln 2$ and so $r(CoF_2, S=R\ln 2)$ becomes too large. By trial we have found that the value 0.96 for $r(CoF_2, S)$ and $r(CoF_2, C_p)$ yields reasonable values for the electronic heat capacity in the range 50–100°K, and we have used this value to calculate the electronic entropy and heat capacity of CoF_2 given in Table V. Because of the existence of appreciable electronic heat capacity at temperatures well above the maximum in heat capacity at 37.70°K the choice of an r value is less certain for CoF_2 than for the other antiferromagnetic fluorides. We estimate that the value of r chosen may be in error by 5%. An error of this magnitude corresponds to an error of 6 to 7% in the calculated electronic entropy and of 4 to 6% in the calculated electronic heat capacity at temperatures of 37.70°K and below. At 100°K, however, a 5% change in the value of r corresponds to a 50% change in the electronic heat capacity.

The electronic heat capacity of CoF_2 calculated with the value $r=0.96$ passes through a minimum near 50°K and then increases to a maximum of 0.80 cal deg^{-1} mole^{-1} near 100°K. This behavior is what one would expect if, superimposed on the high-temperature tail of the heat capacity arising from the antiferromagnetic ordering, there is an electronic excitation to a doubly degenerate level lying at an energy about $240k$ above the two ground states. The electronic heat capacity calculated from a Schottky function with two states, each doubly degenerate, and separated in energy by $240k$ is 0.56 cal deg^{-1} mole^{-1} at 60°K, has a maximum of 0.87 cal deg^{-1} mole^{-1} at 100°K and drops to 0.71 cal deg^{-1} mole^{-1} at 150°K. This is in essential agreement with that calculated for CoF_2 assuming $r=0.96$. The magnitude of the high-temperature electronic heat capacity of CoF_2, although not the position of the maximum near 100°K, is very sensitive to the choice of

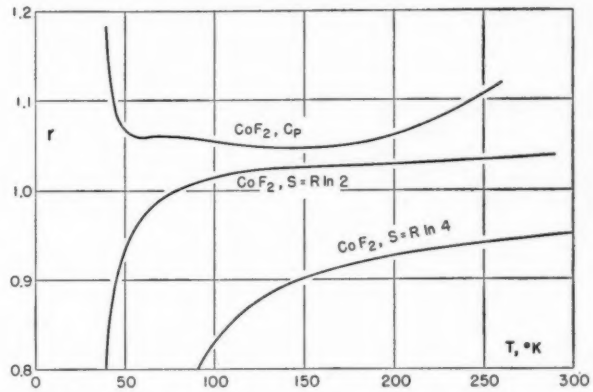

FIG. 3. Corresponding states ratios (see text), $r(CoF_2, C_p)$, $r(CoF_2, S=R\ln 2)$ and $r(CoF_2, S=R\ln 4)$ *versus* temperature.

r and our choice of $r=0.96$ was based partly on the agreement of the electronic heat capacity with that calculated from a Schottky function. Although the estimate of $240k$ as the separation of the two doubly degenerate lowest levels in CoF_2 is rather uncertain, it is clear from the heat capacity measurements that the separation of these levels of $129.5k$ estimated by Nakamura and Taketa[24] from the magnetic anisotropy data is too small. With such a level separation there is too much electronic entropy in the temperature range between 70° and 150°K and the vibrational entropies obtained by subtracting from the observed values those calculated from this level separation decrease much more rapidly with decreasing temperature than could reasonably be expected from the principle of corresponding states and the known vibrational entropy of ZnF_2.

Comparison with Molecular Field Theories

The cooperative ordering in an antiferromagnetic substance has been treated theoretically by Néel[25]

TABLE V. Electronic entropy and heat capacity of CoF_2 vibrational contributions calculated, assuming $r=0.96$.

T, °K	S(lat)	S(elec)	C_p(lat)	C_p(elec)
15	0.02	0.05	0.08	0.23
20	0.06	0.16	0.20	0.58
25	0.15	0.32	0.42	1.03
30	0.23	0.57	0.73	1.59
35	0.37	0.87	1.10	2.46
37.70	0.46	1.10	1.32	4.32
40	0.54	1.18	1.51	0.74
45	0.75	1.25	1.96	0.56
50	0.98	1.31	2.43	0.55
60	1.51	1.41	3.43	0.61
70	2.11	1.51	4.42	0.70
80	2.77	1.61	5.38	0.78
90	3.45	1.71	6.33	0.80
100	4.17	1.79	7.20	0.80
120	5.62	1.94	8.79	0.78
150	7.81	2.10	10.75	0.74

[25] L. Néel, Ann. phys. **5**, 232 (1936); Compt. rend. **202**, 304 (1936).

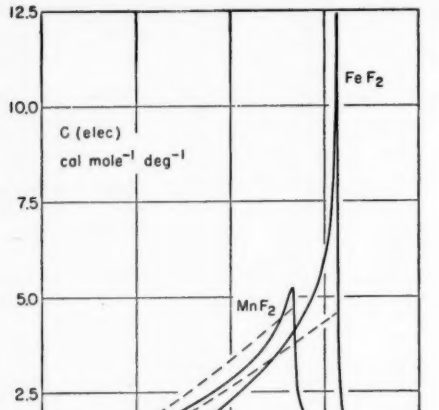

FIG. 4. Electronic heat capacity of MnF_2 and FeF_2 *versus* temperature. Solid lines are experimental curves corrected for lattice contributions. Dashed lines are calculated from Van Vleck theory.

and by Van Vleck.[26] These theories are equivalent in their quantum-mechanical and statistical approximations to the Weiss-Heisenberg theory of ferromagnetism. The interatomic potentials are assumed to be isotropic exchange interactions of the form $V_{ij} = -2J\mathbf{S}_i \cdot \mathbf{S}_j$ where $\mathbf{S}_i$ and $\mathbf{S}_j$ are spin angular momentum vectors on atoms i and j, and J is the exchange integral. J is positive in a ferromagnetic substance and negative in an antiferromagnetic one. In the antiferromagnetic case it is necessary to divide the lattice into two sublattices corresponding to the two different directions of spin orientation in an ordered antiferromagnetic substance at the absolute zero. The interactions are approximated statistically by a molecular field, formally equivalent to an internal magnetic field, on each sublattice proportional to the magnetization on the other sublattice.

The neutron diffraction measurements of Erikson[27] have shown that in MnF_2, FeF_2, and CoF_2 the atomic moments are ordered into two sublattices with spins parallel and antiparallel to the c-axis of the tetragonal crystal, and that NiF_2 has a similar structure with a slight cocking of spins indicated both by the neutron diffraction experiments and by magnetic anisotropy measurements.[28] The magnetic anisotropy of MnF_2[29] is in qualitative agreement with that calculated on the Van Vleck theory provided that one assumes an anisotropy energy to prevent the rotation of the entire spin system relative to the crystal axes when an external magnetic field is applied along the axis of spin alignment.

It appears, therefore, that the two-sublattice model is a reasonable description of the antiferromagnetic ordering in MnF_2, FeF_2, CoF_2, and, NiF_2 and it is of interest to compare the electronic heat capacities of these substances calculated earlier in this paper with the predictions of the Van Vleck theory. The electronic heat capacities, calculated by subtracting from the observed total heat capacities the vibrational contributions estimated, as described previously, from a corresponding states approximation are shown by the solid lines in Fig. 4 for MnF_2 and FeF_2, and in Fig. 5 for CoF_2 and the NiF_2. The curves shown as dashed lines in the figures are electronic heat capacities calculated on the Van Vleck[26] theory taking spin quantum numbers $S=5/2$, 2, $\frac{1}{2}$, and $\frac{3}{2}$ for MnF_2, FeF_2, CoF_2, and NiF_2, respectively. On this model the thermodynamic quantities are calculable in terms of a parameter $x \equiv g\beta H_i S/kT$, where g is the Lande splitting factor, β the Bohr magneton, H_i the equivalent internal magnetic field on either sublattice and k the Boltzmann constant. The temperature is related to x by

$$\frac{T}{T_c} = \frac{3S}{S+1} \frac{B_S(x)}{x} \tag{2}$$

and the electronic heat capacity is given by

$$\frac{C(\text{elec})}{R} = -x^2 B_S'(x) \frac{d \ln x}{d \ln (T/T_c)}. \tag{3}$$

Here T_c is the critical temperature, which we took as the temperature of the observed maximum in heat capacity, $B_S(x)$ is the Brillouin function, $B_S'(x)$ is the first derivative of the Brillouin function and R is the gas constant. The tables of Schmid and Smart[30] which list the Brillouin function and its first derivative facilitated the calculations.

It is apparent from Figs. 4 and 5 that in general the observed electronic heat capacity at low temperatures is lower than that calculated on the Van Vleck theory. In the neighborhood of the maximum the observed heat capacity is larger than the calculated. There appears to be a correlation between the height of the observed maximum and the magnetic anisotropy[23,28,29] observed at high temperatures in the disordered state. In MnF_2, where the room temperature magnetic anisotropy is only 0.1% of the susceptibility, the observed heat capacity maximum is only 11% higher than that calculated on the Van Vleck theory, whereas in FeF_2, whose room temperature anisotropy is 20% of the powder susceptibility, the observed peak is very narrow and is 2.7 times as high as that calculated. Because of the statistical approximations involved in the Van Vleck theory the calculated heat capacity is zero above the critical temperature and the complete electronic entropy of $R \ln(2S+1)$ is acquired at this temperature. In the actual substances the fraction of the complete electronic entropy acquired at the temperature of the

[26] J. H. Van Vleck, J. Chem. Phys. **9**, 85 (1941).
[27] R. A. Erikson, Phys. Rev. **90**, 779 (1953).
[28] L. M. Matarrese and J. W. Stout, Phys. Rev. **94**, 1792 (1954).
[29] M. Griffel and J. W. Stout, J. Chem. Phys. **18**, 1455 (1950).
[30] L. P. Schmid and J. S. Smart, Navord Report 3640, U. S. Naval Ordnance Laboratory, White Oak, Maryland (1954).

maximum in heat capacity ranges from 0.71 in NiF_2 to 0.87 in FeF_2. A better statistical approximation is the Bethe[31] theory which has been applied to the case of antiferromagnetism by Firgau.[32] On this theory there is some heat capacity associated with short-range order above the critical temperature but the corresponding loss in entropy at this temperature is considerably smaller than that observed in the antiferromagnetic fluorides. In the ordered antiferromagnetic structure[27] each magnetic ion is surrounded by two nearest neighbors, in the [001] directions, with spins parallel to the central ion, and by eight next nearest neighbors, in the [111] directions, with spins antiparallel to the central ion. If the antiparallel arrangement is energetically favorable for both nearest and next nearest neighbors, then the ordered state is raised in energy, because of the unfavorable orientation of the two nearest neighbors, above what it would be if only the eight next nearest neighbor interactions were considered. Consequently the temperature of ordering is lowered and the short-range order and the decrease of entropy below the completely disordered value is larger then one calculates on the Bethe theory with eight neighbors all of which become antiferromagnetically arranged in the ordered state. A similar proposal has been made by Anderson[33] and by Smart[34] to account for discrepancies between the observed critical temperature and the Curie-Weiss Θ in various antiferromagnetic substances. Preliminary calculations indicate that by proper choice of the magnitude of the nearest and next-nearest neighbor interactions it is possible to depress the critical temperature sufficiently to obtain on the Bethe theory a decrease in electronic entropy below the disordered value comparable to those listed in Tables IV and V.

Comparison with the Spin-Wave Theory

Recently various authors[35–39] have used the Bloch spin wave method to calculate the properties of antiferromagnetic substances. This theory is valid only at low temperatures where the deviations from the completely ordered antiferromagnetic state, described as spin waves, are small. Kubo[36] pointed out that when the microscopic anisotropy energy is very small compared to the exchange energy the macroscopic anisotropy of the magnetic susceptibility at low temperatures should vary as T^2, in agreement with the measurements[29] on MnF_2. Under such conditions the electronic heat capacity varies as T^3 and there is a simple relation between the magnetic susceptibility parallel to the axis of spin alignment, $\chi_{\parallel}$, and the electronic heat capacity,

$$\frac{C(\text{elec})}{R}=\frac{4\pi^2}{5}\frac{kT}{Ng^2\beta^2}\chi_{\parallel}. \tag{4}$$

Here N is Avogadro's number and the other symbols have been defined previously. This relation is independent of the lattice type. In the first approximation the magnetic susceptibility perpendicular to the axis of alignment, $\chi_{\perp}$, is independent of temperature so one may write $\chi_{\parallel}$ in terms of the temperature coefficient of the measured magnetic susceptibility anisotropy, namely

$$\chi_{\parallel}=T^2 d(\chi_{\parallel}-\chi_{\perp})/d(T^2). \tag{5}$$

From the measurements of Griffel and Stout[29] on MnF_2 between 11.9 and 20.37°K one finds that $d(\chi_{\parallel}-\chi_{\perp})/d(T^2)$ is constant within the accuracy of measurement over this temperature range and equal to 0.98×10^{-5} cm^3 mole^{-1} deg^{-2}. Substituting in Eqs. (4) and (5) one obtains

$$C(\text{elec})=1.02\times10^{-4}T^3 \text{ cal deg}^{-1}\text{ mole}^{-1} \tag{6}$$

as the heat capacity predicted from the first approximation in spin wave theory and the observed magnetic anisotropy data.

In Fig. 6 are plotted on a doubly logarithmic scale the experimental points for the electronic heat capacity of MnF_2, FeF_2, CoF_2, and NiF_2 between 10 and 30°K. For comparison, slopes corresponding to the variation

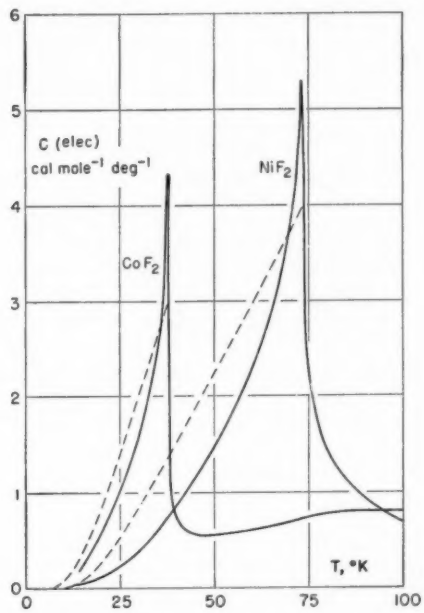

FIG. 5. Electronic heat capacity of CoF_2 and NiF_2 *versus* temperature. Solid lines are experimental curves corrected for lattice contributions. Dashed lines are calculated from Van Vleck theory.

[31] H. Bethe, Proc. Roy. Soc. (London) **A150**, 552 (1935).
[32] U. Firgau, Ann. phys. **40**, 295 (1941).
[33] P. W. Anderson, Phys. Rev. **79**, 705 (1950).
[34] J. S. Smart, Phys. Rev. **86**, 968 (1952).
[35] P. W. Anderson, Phys. Rev. **86**, 694 (1952).
[36] R. Kubo, Phys. Rev. **87**, 568 (1952); Revs. Modern Phys. **25**, 344 (1953).
[37] J. M. Ziman, Proc. Phys. Soc. (London) **A65**, 540, 548 (1952); **A66**, 89 (1953).
[38] J. R. Tessman, Phys. Rev. **88**, 1132 (1952).
[39] J. A. Eisele and F. Keffer, Phys. Rev. **96**, 929 (1954).

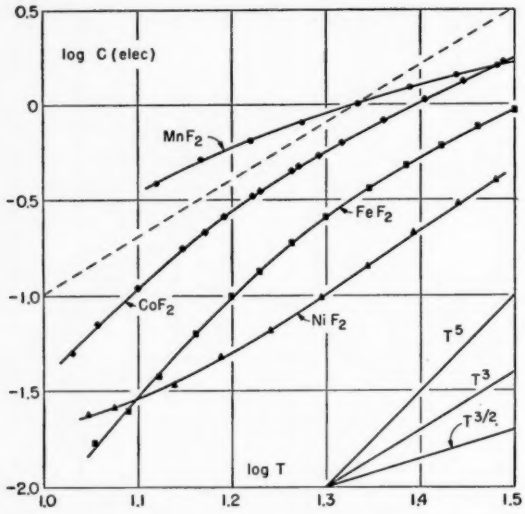

FIG. 6. Logarithm of the electronic heat capacity (cal deg^{-1} mole^{-1}) *versus* logarithm of temperature (°K). Points are experimental values corrected for lattice contributions to the heat capacity. Dashed line is electronic heat capacity of MnF_2 calculated from observed temperature variation of magnetic anisotropy and spin wave theory. Solid straight lines in lower right corner indicate slopes corresponding to variation of electronic heat capacity as T^5, T^3, and $T^{\frac{3}{2}}$.

of the electronic heat capacity as T^5, as T^3 and as $T^{\frac{3}{2}}$ are drawn in the lower right corner of the figure. The electronic heat capacities are obtained by subtracting from the measured values the vibrational contribution calculated as described above from a corresponding states assumption. The dashed line in Fig. 6 is a plot of the heat capacity of MnF_2 given by Eq. (6). Although there is qualitative agreement in the magnitude of the heat capacity of MnF_2 observed and given by Eq. (6), the temperature variation of the observed heat capacity between 13 and 20°K is considerably less than the predicted T^3 law. At the lowest temperatures the experimental points seem to be approaching a T^3 law but with a heat capacity about 70% larger than that calculated from Eq. (6). Kubo[36] points out that in a higher approximation $\chi_\perp$ drops with increasing temperature, varying as $1-bT^2$, where b is a constant. The effect of this correction is to lower the calculated electronic heat capacity by 20%, worsening the agreement with experiment. From the experimental point of view it should be pointed out that the measurements on MnF_2, unlike those on the other fluorides, were made on a finely divided powdered sample, of particle size estimated to be between 10^{-5} and 10^{-6} cm, and there is a possibility that at low temperatures both the lattice and electronic heat capacities might be somewhat higher for this finely divided sample than for one containing only large crystals.

When the microscopic anisotropy energy is large, as the high temperature measurements[23,28] of the anisotropy of the magnetic susceptibility indicate to be the case in FeF_2, CoF_2, and NiF_2, both the heat capacity and the parallel magnetic susceptibility are less than when the microscopic anisotropy energy is small. Eisele and Keffer[39] have calculated curves showing the effect of the microscopic anisotropy energy on the electronic heat capacity and the parallel susceptibility. No simple relation exists between these two quantities and a quantitative calculation involves a knowledge of the anisotropy constant. At very low temperatures both the heat capacity and the parallel susceptibility approach zero in an exponential fashion. In the liquid hydrogen range the experimental anisotropies of the magnetic susceptibility[23] of FeF_2 and CoF_2 follow a T^4 law rather than the T^2 law found for MnF_2. Qualitatively the electronic heat capacities of FeF_2 and CoF_2 shown in Fig. 6 are what would be expected on the spin-wave theory if the anisotropy field is playing an important role. The heat capacities at the lowest temperatures are smaller than would be calculated in the absence of an appreciable microscopic anisotropy and the slope of log$C$(elec) *versus* log$T$ is increasing rapidly as the temperature decreases, reaching at 12° the value 5.6 for FeF_2 and 4.6 for CoF_2. In contrast to this behavior the corresponding slope of the NiF_2 curve decreases with decreasing temperature and at 12° is equal to 1.7. The curve for NiF_2 is not of the shape expected on the spin-wave theory for an antiferromagnetic material. It is of interest to note that Matarrese and Stout[28] found in magnetic anisotropy measurements on a single crystal of NiF_2 that below 73.2°K there was evidence of the appearance of a small ferromagnetic moment. At low temperatures the electronic heat capacity of a ferromagnetic material, calculated by the spin-wave theory,[40] varies as $T^{\frac{3}{2}}$. It appears that the anomalous temperature variation of the electronic heat capacity of NiF_2 is associated with the presence of a ferromagnetic moment in this salt.

We thank Miss Myrtle Bachelder for the chemical analysis, Mrs. Althea Tompkins for the spectrochemical analysis, and Mr. Stanley Reed for assistance with the calculations. The preparation of material in this paper for publication was supported in part by the Office of Naval Research (Contract N6ori-02051).

[40] N. F. Mott and H. Jones, *Theory of the Properties of Metals and Alloys* (Oxford University Press, London, 1936), p. 237.

THE JOURNAL OF CHEMICAL PHYSICS VOLUME 23, NUMBER 11 NOVEMBER, 1955

Thermodynamics of a Fluid Substance in the Electrostatic Field

HENRY S. FRANK
Department of Chemistry, University of Pittsburgh, Pittsburgh, Pennsylvania
(Received December 23, 1954)

An "apparatus" is described in which, in a thought experiment, the whole of a sample of fluid may be subjected to a uniform electrostatic field under controlled conditions. The work done in such a process can be written into fundamental thermodynamic equations so as to enable the field strength E to be a variable of state in a way which is essentially symmetrical with the way in which P and T are variables of state. This enables a variety of differential coefficients to be obtained, some of which appear to be new. A discussion is given of the relationship between "electrostriction pressure" (as derived in electrostatics) and thermodynamic pressure. Application of the formalism to systems of more than one component is illustrated by discussion of the change in composition produced by charging the plates of a small condenser immersed in a large volume of binary fluid mixture. The customary representation of the "energy density" in a field as equal to $E^2K/8\pi$ is discussed, and found to be limited in formal validity when the field is nonuniform, when the charging process takes place under conditions which do not hold the volume constant, or when dielectric saturation is taken into account.

1. INTRODUCTION

THE methods currently employed in treating the thermodynamics of the electrostatic field are exemplified in discussions of electrostriction pressure,[1] and of changes of entropy[2–4] and volume[4] when a fluid is placed in an electric field, which are to be found in several recent books. None of them suffices to enable the field strength E to be written as a variable of state of the fluid in as general a sense as that in which the pressure P and the temperature T are variables of state. For example, Stratton's treatment[1] of electrostriction pressure derives a difference in pressure between different regions in the fluid. Again, both Fröhlich[2] and Böttcher[3] restrict their discussions to conditions of constant volume, while such treatments as those given by Guggenheim[4] and Rossini[5] make use of an "apparatus" consisting of a (small) condenser immersed in a (large) vessel full of fluid, which has as a consequence that the amount of matter between the plates changes as E changes. For some purposes this is not a serious drawback, but for others it is. For example, as Guggenheim remarks, it excludes pressure from explicit discussion.

Described below is a different kind of apparatus, designed to overcome these limitations. Using it in a thought experiment makes possible the application of Gibbsian thermodynamics in such a manner that E enters the formalism in a way which is essentially symmetrical with the ways in which P and T enter. This, in turn, leads to a number of differential relations, of which some are well known, but some seem to be new. These make possible, among other things, a clarification of the relation which electrostriction pressure bears to thermodynamic pressure. They also point up the importance of fastening attention not only upon the field but also upon the dielectric fluid as a chemical substance, or mixture of substances.

2. METHOD

It is desired to evaluate the work done on a fluid when it is subjected to changes in an electric field under such conditions that (a) the field strength may be made a truly independent variable, (b) the whole of the fluid sample under discussion is subject to the same (instantaneous) field strength, temperature, and pressure, whatever changes the sample may undergo during any charging process, and (c) portions of fluid, or of any component of it, if it is a mixture, may be added to or withdrawn from the sample in a controllable and reversible manner.

For this purpose we wish to consider experiments which may be carried out in the apparatus sketched in Fig. 1, which consists of two parallel condenser plates of area A, separated by a distance l, and held apart by

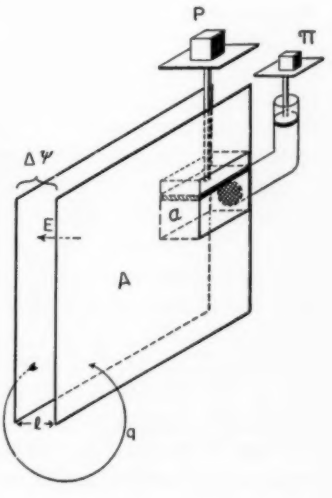

FIG. 1. Condenser containing cell in which test fluid is studied. A = total area of condenser plates; a = area of the portion of the condenser plates in contact with fluid. P represents the pressure on the fluid in the field E. π represents the pressure on the portion of the fluid which is outside the field.

[1] J. A. Stratton, *Electromagnetic Theory* (McGraw-Hill Book Company, Inc., New York, 1941), pp. 149–151.
[2] H. Fröhlich, *Theory of Dielectrics* (Clarendon Press, Oxford, England, 1949), pp. 9–13.
[3] C. J. F. Böttcher, *Theory of Electric Polarization* (Elsevier Amsterdam, 1952), pp. 116–118.
[4] E. A. Guggenheim, *Thermodynamics* (Interscience Publishers, Inc., New York, 1949), pp. 361–366.
[5] F. D. Rossini, *Chemical Thermodynamics* (John Wiley and Sons, Inc., New York, 1950), pp. 420–421.

three strips of insulating material which form two side walls and the bottom of a cell within the condenser. The other two side walls of the cell are portions (of area a) of the condenser plates. This cell is so placed that one of its vertical insulating walls lies along a condenser edge, and is closed at the top by a nonconducting piston which fits tightly but moves without friction. The cell contains the fluid under consideration, which is thus under a pressure P determined by the weight carried on the platform which the piston supports. The plate area in contact with fluid is a and the volume v of the fluid is thus al. The condenser is assumed located in a vacuum, and all changes in pressure, volume, charge, potential, etc., are assumed to be made so slowly that the temperature is always equal (to the first order) to that of the walls of the Hohlraum, with which the condenser is in radiative equilibrium. This temperature can be held constant, for isothermal processes, or kept equal to that of the sample for adiabatic ones. The conductor of which the condenser plates are made, and the solid nonconductors which bound the cell, are alike assumed to have zero coefficient of thermal expansion, and zero coefficient of compressibility. Their heat capacities can also be assumed zero or negligibly small. In the "outer" wall of the cell is a membrane permeable to the fluid, communicating on the outside with a cylinder containing additional fluid which can be varied in chemical potential, μ, by the pressure (π) on the auxiliary piston, which may or may not be the same as that (P) upon the fluid within the cell. This outside liquid is not in the electric field but is a sample of the same chemical substance as is in the field. When it is desired to consider the fluid under discussion as subject to variations in composition, a separate membrane and outside reservoir may be provided for each component, each membrane permeable only to the single pure substance to which it corresponds. The fluid is, of course, assumed to be a "good" dielectric—i.e., electrically nonconducting, and chemically inert toward all materials with which it is in contact.

If a pure chemical substance, the fluid is characterized thermodynamically by its density ρ, and its chemical potential μ, which may be considered to be functions of P, T, E (electric field strength) or, in general, of any 3 of the usual interlocking quantities. Three independent variables are required in this discussion because of the inclusion in it of electrical energy. If variations in composition are to be considered, there will, of course, be a separate chemical potential for each component, and these, along with ρ, will be functions of the variables specifying the composition (one mole ratio for each component beyond the first) as well as of P, T, and E.

The inductive capacity of the fluid, ϵ, its dielectric constant K, and its susceptibility χ are often taken to be, in the first instance, functions of P and T, or of ρ and T only (and of composition, where this is variable), and not of E explicitly. There is, in general, no need to impose this restriction, however, and, except where the contrary is stated, the results reported below do not presuppose it. ϵ, K, χ are defined by the electrostatic equations which are here assumed as given, namely,

D (=dielectric displacement)$=\epsilon E$ (ϵ=permittivity).
$D=\epsilon_0 E$ *in vacuo*. $K=\epsilon/\epsilon_0$=dielectric constant.
$D=E+4\pi\mathcal{P}$, in general, where $\mathcal{P}$ is the polarization of the fluid, and equals $E\epsilon_0\chi$. This makes $\chi=(K-1)/4\pi$. χ is the susceptibility.

The quantity ϵ_0, the permittivity of free space, appears in these definitions for dimensional reasons but can be assigned the value unity. In what follows we adopt this convention, writing for brevity, $K=\epsilon$, $D=KE$, and $\mathcal{P}=\chi E$. The important relation $4\pi\chi=K-1$ is not affected by this simplification.

Now when a charge q is carried from one plate to another, there is set up an electric field E, and a difference in potential $\Delta\psi$ between the plates such that $\Delta\psi=El$. Since the plates are conductors, q is distributed over the surfaces. Its surface density will be called σ_A outside of the cell, and σ_a in the cell. It is assumed that a and A are of such size and shape that l is small compared to any other linear dimension, so that edge effects may be neglected. Then

$$q=(A-a)\sigma_A+a\sigma_a=A\sigma_A+a(\sigma_a-\sigma_A).$$

Also, to increase the charge on the condenser by an amount dq will require doing work w_e on the system such that

$$\begin{aligned} w_e&=\Delta\psi dq=Eld[A\sigma_A+a(\sigma_a-\sigma_A)] \\ &=EVd\sigma_A+Ed[v(\sigma_a-\sigma_A)]. \end{aligned}$$

Here V=the (constant) volume between the whole spread of the condenser plates, and v=the (variable) volume of the fluid enclosed in the cell. Since the piston can move up or down, v is variable.

Now, again from electrostatics, $D=4\pi\sigma$ in general, so that

$$w_e=\frac{EV}{4\pi}dD_A+\frac{E}{4\pi}d[v(D_a-D_A)].$$

But $D_A=E$, and $D_a=E+4\pi\mathcal{P}$ so that

$$w_e=V\cdot\frac{EdE}{4\pi}+Ed(v\mathcal{P}). \tag{1}$$

By electrostatics, also, $v\mathcal{P}=M$, the dipole moment of the matter in the cell. Both E and M are vectors. Here, however, since the working substance is a fluid, and therefore isotropic, these vectors are parallel to each other, and the product $Ed(M)$ which appears in w_e is equivalent to $\mathbf{E}\cdot\mathbf{dM}$, the increment of work done on the system in producing an increment of moment $\mathbf{dM}$ in the fluid sample when the field equals $\mathbf{E}$.

In Eq. (1), the first term is the work that would be done in charging the condenser *in vacuo*—i.e., if there were no fluid present. We therefore reject this, and

retain only the second term, writing it

$$w_e' = EdM = Ed(v\mathcal{P}) \tag{2}$$

as the electrical work done *on the fluid* in the condenser during any infinitesimal and reversible change to which the fluid may be subjected.

We may now apply the first law of thermodynamics and write, for an infinitesimal reversible process involving changes in P, v, and E,

$$dU = Q - w = Q - Pdv + Ed(v\mathcal{P}). \tag{3}$$

Here, as usual, dU is the increment in internal energy of the sample of fluid, w is the total work done by the sample, and Q is the heat it absorbs in the process. By the second law we may write $Q = TdS$, since the process is reversible. Also, to make possible the treatment of changes in the quantity of matter in the sample, we follow the method of Gibbs, and write

$$dU = TdS - Pdv + Ed(v\mathcal{P}) + \sum_i \mu_i dn_i \tag{4}$$

as the fundamental equation for the thermodynamics of a fluid in the field. The chemical potential of the ith substance in the cell is μ_i, expressed per unit quantity, in the same unit in which n measures the quantity itself (mass, number of moles, etc.). In what follows the mole will be employed.

Fundamental equations in terms of other variables can now be set up in the customary manner. Thus a function H^*, an analog of enthalpy, may be defined

$$H^* = U + Pv - E(v\mathcal{P})$$

$$dH^* = TdS + vdP - (v\mathcal{P})dE + \sum_i \mu_i dn_i. \tag{5}$$

Also, for the Helmholtz free energy, we obtain

$$F = U - TS$$

$$dF = -SdT - Pdv + Ed(v\mathcal{P}) + \sum_i \mu_i dn_i. \tag{6}$$

The analog Gibbs free energy becomes

$$G^* = H^* - TS$$

$$dG^* = -SdT + vdP - (v\mathcal{P})dE + \sum_i \mu_i dn_i. \tag{7}$$

These fundamental equations make possible the derivation of differential relationships in the customary way. As a first illustration we may consider some of these which relate to volume changes, restricting ourselves (until Sec. 6) to systems in which the fluid is a "pure" substance, permitting the use of only one μ and one n.*

* The fundamental Eqs. (4) to (7) are written as is customary for fluids, namely, on the assumption that the working substance can be depended upon to exert the same pressure in all directions—i.e., it has been assumed that a single pressure P gives a product Pdv which is the same regardless of the direction of the expansion or contraction which produces dv. It may be queried whether this is true in general when the fluid is in an electrostatic field, since the field is known to make the fluid optically anisotropic (electro-optic Kerr effect). Certainly the cube faces bounding a fluid in a field will be subject to different forces depending on whether they are parallel or perpendicular to the field vector. There seems to be no reason to believe, however, that the fluid itself would "resist" the change in shape which this influence would tend to produce, and in our apparatus it would appear that all forces of this kind are sustained by the rigid framework of the condenser. Of course, v cannot change without a motion of the piston, which will cause the interface between fluid and wall to change in area, and it may be argued that the energetics of this surface change would be different according to whether the area in question was oriented along or across the field. Such differences, on the other hand, seem to be in the same category as the absolute surface effects which are neglected in defining the bulk pressure in the absence of a field. We therefore proceed on the assumption that the fluid in the field can be treated as mechanically isotropic—i.e., that it continues to obey Pascal's principle. Alternatively, we could choose to define this as one of the properties of the model fluid to which our treatment refers. The writer is indebted to Professor J. E. Mayer for correspondence on this point.

3. ELECTROSTRICTION

From Eq. (7),

$$\frac{\partial^2 G^*}{\partial P \partial E} = \left(\frac{\partial v}{\partial E}\right)_{P,T,n} = -\left(\frac{\partial (v\mathcal{P})}{\partial P}\right)_{E,T,n}.$$

But $v\mathcal{P} = vE\chi$, whence

$$\left(\frac{\partial (v\mathcal{P})}{\partial P}\right)_{E,T,n} = vE\chi\left[\left(\frac{\partial \ln \chi}{\partial P}\right)_{E,T,n} + \left(\frac{\partial \ln v}{\partial P}\right)_{E,T,n}\right],$$

so that

$$\left(\frac{\partial v}{\partial E}\right)_{P,T,n} = -vE\left[\left(\frac{\partial \chi}{\partial P}\right)_{E,T} - \chi\beta\right]$$

$$= -\frac{vE}{4\pi}\left[\left(\frac{\partial K}{\partial P}\right)_{E,T} - (K-1)\beta\right], \tag{8}$$

where $\beta = -1/v(\partial v/\partial P)_T$, the coefficient of isothermal compressibility of the fluid substance.

It follows from Eq. (8) that, in general, when the weight on the piston which closes the cell is not allowed to change, and no matter is allowed to pass through the diaphragm, then as a field is applied isothermally between the plates the volume of the fluid will change and the piston will move. Qualitatively this is a well-known result, but Eq. (8) differs in several respects from previous quantitative expressions with which it might be compared.[4,5]

The most important difference is that v is now the same on both sides of the equation, which makes it possible to write

$$\frac{1}{v}\left(\frac{\partial v}{\partial E}\right)_{P,T} = -\frac{1}{\rho}\left(\frac{\partial \rho}{\partial E}\right)_{P,T}$$

$$= -\frac{E}{4\pi}\left[\left(\frac{\partial K}{\partial P}\right)_{E,T} - (K-1)\beta\right]. \tag{9}$$

This defines a specific property of the fluid, and by a

slight rearrangement, we may write

$$\frac{1}{\rho}\left(\frac{\partial\rho}{\partial E^2}\right)_{P,T}=-\frac{1}{v}\left(\frac{\partial v}{\partial E^2}\right)_{P,T}$$
$$=\frac{1}{8\pi}\left[\left(\frac{\partial K}{\partial P}\right)_{E,T}-(K-1)\beta\right] \quad (10)$$

and call this quantity the coefficient of (isothermal and isobaric) electrostriction, in full analogy with the coefficient of (isothermal) compressibility β.

Another difference between Eq. (8) and earlier analogs is in the appearance of the second term in the brackets on the right-hand side. Physically this corresponds to the fact that the tendency which Eq. (8) represents, namely, to increase the total polarization which exists between the plates (i.e., to increase the extent to which the charge on the condenser is "neutralized" by bound charge), could be satisfied in either of two separate ways, namely, by increasing the polarizability of the fluid (this tendency is represented by the first term) or by increasing the plate area covered by it (represented by the second term). In this experiment these two possibilities work against each other, and the net result is a sum which is smaller than the absolute value of either term. We shall discuss these two tendencies in more detail below, noting in the meantime that if one could conceive of a hypothetical fluid of which the dielectric susceptibility were weakly enough dependent on its density, it would be possible to imagine this substance to *expand* in the electric field and display a negative coefficient of electrostriction. This can be seen by noting that

$$\left(\frac{\partial K}{\partial P}\right)_{E,T}=\left(\frac{\partial K}{\partial\rho}\right)_{E,T}\left(\frac{\partial\rho}{\partial P}\right)_{E,T}=\beta\rho\left(\frac{\partial K}{\partial\rho}\right)_{E,T}.$$

This converts Eq. (10) to

$$\frac{1}{\rho}\left(\frac{\partial\rho}{\partial E^2}\right)_{P,T}=-\frac{1}{v}\left(\frac{\partial v}{\partial E^2}\right)_{P,T}$$
$$=\frac{\beta}{8\pi}\left[\rho\left(\frac{\partial K}{\partial\rho}\right)_{E,T}-(K-1)\right]. \quad (11)$$

Still another feature which differentiates Eq. (8) from previous expressions is that here, in the first instance, the equations contain (and the fluid is characterized by) χ rather than K. This corresponds to the fact that the dielectric permittivity of space is, so to speak, the same whether the space is "free" of or is full of matter, so that K represents the simple additive response to the field of the space itself plus whatever matter happens to be present in it. It is characteristic of the present treatment that fastening attention upon the matter means subtracting out the things which would happen if the matter were absent.

An interesting corollary of Eq. (11) is that since K is a function of ρ and ρ changes with E at constant pressure and temperature, K is not a constant *vis-a-vis* changes in E under these conditions. That is, the ordinary assumption that (at constant temperature, and in the absence of saturation effects) K is independent of field strength is, for a fluid substance, correct only when the charging takes place at constant volume, and incorrect for laboratory experiments in which pressure (or any other property than volume) is held constant. The numerical values of $\partial K/\partial P$ or $\partial K/\partial\rho$ found for ordinary liquids, however, give exceedingly small changes in K when E is not enormously large.

Some of the other differential relations which can be derived from Eqs. (4) through (7) require, in addition to simple cross-differentiation, the application of other customary methods, as may be exemplified by the following sequence:

$$\left(\frac{\partial\mu}{\partial E}\right)_{P,T,N}=-\left(\frac{\partial(v\mathcal{P})}{\partial n}\right)_{P,T,E}=-E\chi V, \quad (12)$$

where V is the molal volume, v/n or $\partial v/\partial n$ of the substance. Also, $(\partial\mu/\partial P)_{E,T}=V$, as is conventional. Then

$$\left(\frac{\partial P}{\partial E}\right)_{\mu,T}=\frac{-(\partial\mu/\partial E)_{P,T}}{(\partial\mu/\partial P)_{E,T}}=E\chi=\frac{E}{4\pi}(K-1). \quad (13)$$

Equation (13) tells how P must be changed when E changes at constant temperature if there is to be no tendency for fluid to enter or leave the cell through the membrane which communicates with the reservoir of liquid outside of the field. P must increase to compensate for the fact that, by itself, the field tends to "suck in" liquid, as shown by the lowering of μ described in Eq. (12). Continuing,

$$\left(\frac{\partial v}{\partial E}\right)_{\mu,T,n}=\left(\frac{\partial v}{\partial E}\right)_{P,T,n}+\left(\frac{\partial v}{\partial P}\right)_{E,T,n}\left(\frac{\partial P}{\partial E}\right)_{\mu,T,n}$$
$$=-vE\left[\left(\frac{\partial\chi}{\partial P}\right)_{E,T}+\chi\left(\frac{\partial\ln v}{\partial P}\right)_{E,T}\right]$$
$$+\left(\frac{\partial v}{\partial P}\right)_{E,T}\cdot E\chi$$
$$=-vE\left(\frac{\partial\chi}{\partial P}\right)_{E,T}=-\frac{vE}{4\pi}\left(\frac{\partial K}{\partial P}\right)_{E,T}. \quad (14)$$

This gives a different coefficient of electrostriction,

$$\frac{1}{\rho}\left(\frac{\partial\rho}{\partial E^2}\right)_{\mu,T}=-\frac{1}{v}\left(\frac{\partial v}{\partial E^2}\right)_{\mu,T}$$
$$=\frac{1}{8\pi}\left(\frac{\partial K}{\partial P}\right)_{E,T}=\frac{\beta}{8\pi}\rho\left(\frac{\partial K}{\partial\rho}\right)_{E,T}, \quad (15)$$

the coefficient of electrostriction at constant temperature and activity. Since constant μ means constant escaping tendency or "vapor tension," a suitable name for this coefficient might be the coefficient of isotonic electrostriction. This, it may be noted, is the coefficient applicable to the matter between the plates of a condenser dipping into an open reservoir of fluid which extends far enough beyond the condenser to insure that some of the fluid is outside of the field. Under these circumstances, the activity, or the vapor tension, or the chemical potential, of the fluid between the plates, must be the same as that outside; a condition which will be created by a crowding of liquid into the space between the plates until the thermodynamic pressure there is that given by Eq. (13). The sum of the action of this pressure, and of the "direct" action of the field, produces the volume change given by Eq. (15). This, in turn, produces a change in dielectric constant,

$$\left(\frac{\partial K}{\partial E^2}\right)_{T,\mu}=\left(\frac{\partial K}{\partial \rho}\right)_T\left(\frac{\partial \rho}{\partial E^2}\right)_{T,\mu}.$$

By Eq. (15) this becomes

$$\left(\frac{\partial K}{\partial E^2}\right)_{T,\mu}=\frac{\beta}{8\pi}\left[\rho\left(\frac{\partial K}{\partial \rho}\right)_T\right]^2. \tag{16}$$

This is over and above any direct change in K which a change in E may produce by dielectric saturation or the like.

Still another coefficient of electrostriction can be defined, and an expression for it obtained, if an adiabatic process is considered instead of an isothermal one. This involves more algebra, including the obtaining of

$$\left(\frac{\partial S}{\partial E}\right)_{P,T,n}=vE\left[\left(\frac{\partial \chi}{\partial T}\right)_{P,E}+\alpha\chi\right], \tag{17}$$

where $\alpha(\equiv 1/v(\partial v/\partial T)_P)$ is the coefficient of thermal expansibility, and of

$$\left(\frac{\partial T}{\partial E}\right)_{S,P,n}=\frac{-(\partial S/\partial E)_{P,T,n}}{(\partial S/\partial T)_{E,P,n}}$$

$$=-\frac{T}{C_P}vE\left[\left(\frac{\partial \chi}{\partial T}\right)_{P,E}+\alpha\chi\right]. \tag{18}$$

The end result simplifies down to the same form as before, namely,

$$\frac{1}{\rho}\left(\frac{\partial \rho}{\partial E^2}\right)_{S,P}=-\frac{1}{v}\left(\frac{\partial v}{\partial E^2}\right)_{S,P}$$

$$=\frac{1}{8\pi}\left[\left(\frac{\partial K}{\partial P}\right)_{S,E}-(K-1)\beta_s\right], \tag{19}$$

where β_s is the *adiabatic* compressibility coefficient.

4. ELECTROSTRICTION PRESSURE

Returning to Eq. (13), it will be noted that this is an expression for one kind of electrostriction pressure, namely, the difference between the pressure on the fluid between the condenser plates and that in a field-free region if fluid has been permitted to flow between the two regions during the charging process.

Another kind of electrostriction pressure is represented by the expression, which is easily derived,

$$\left(\frac{\partial P}{\partial E^2}\right)_{v,T,n}=-\frac{1}{2}\left[\rho\left(\frac{\partial \chi}{\partial \rho}\right)_{E,T}-\chi\right]$$

$$=\frac{-1}{8\pi}\left[\rho\left(\frac{\partial K}{\partial \rho}\right)_{E,T}-(K-1)\right]. \tag{20}$$

This tells how the external pressure must be decreased as field increases if the volume of a homogeneous portion of the fluid is not to decrease, and, so to speak, measures the suction which the fluid exerts on the piston when field is applied under these conditions.

Still another electrostriction pressure is evaluated as follows: A simple derivation shows that

$$\left(\frac{\partial \mu}{\partial E}\right)_{v,T,n}=-VE\rho\left(\frac{\partial \chi}{\partial \rho}\right)_{E,T}. \tag{21}$$

[Note the difference between (21) and (12).] This tells how the chemical potential of the fluid is changed when the condenser is charged, the volume of the fluid sample being kept constant. Now, if equilibrium through the membrane is to be maintained, then, as E changes, the pressure π on the fluid in the outside reservoir must be changed in such a way that $d\mu_{\text{inside}}=d\mu_{\text{outside}}$. Then

$$\left[\left(\frac{\partial \mu}{\partial E}\right)_{v,T,n}dE\right]_{\text{inside}}=\left[\left(\frac{\partial \mu}{\partial \pi}\right)_T d\pi\right]_{\text{outside}},$$

or

$$-VE\rho\left(\frac{\partial \chi}{\partial \rho}\right)_{E,T}dE=Vd\pi,$$

$$\frac{d\pi}{dE}=-E\rho\left(\frac{\partial \chi}{\partial \rho}\right)_T=-\frac{E}{4\pi}\rho\left(\frac{\partial K}{\partial \rho}\right)_T. \tag{22}$$

This measures the suction which the field produces upon the piston closing the outer cylinder—i.e., the amount by which the pressure upon fluid outside the field must be lowered to keep it from being drawn into the field, if the fluid in the field is maintained at constant density.

It is of interest that the result obtained from integration by Eq. (22) (virtual, as if ρ and $\partial K/\partial\rho$ were constant), namely,

$$\pi_0-\pi=\frac{E^2}{8\pi}\rho\left(\frac{\partial K}{\partial \rho}\right)_T \tag{23}$$

is the same (except for the factor 4π arising out of the difference in electrostatic units employed) as that given by Stratton[1] for the "difference in pressure" between portions of a fluid inside of and outside a field. Our derivation does not sustain this interpretation, since the fluid in the field, by our equations, is under a pressure given by Eq. (20), namely (again, as if ρ were constant)

$$P_0-P=\frac{E^2}{8\pi}\left[\rho\left(\frac{\partial K}{\partial \rho}\right)_T-(K-1)\right]. \tag{24}$$

Since π_0 and P_0 were the same before the charging started, we get

$$P-\pi=\frac{E^2}{8\pi}(K-1) \tag{25}$$

for the difference to which Stratton's wording refers. [Equation (25) could have been obtained directly from Eq. (13).] The relation between electrostriction pressure as discussed in electrostatics and the thermodynamic pressures defined in terms of experiments imagined to be performed on our apparatus therefore requires further discussion.

In order to clarify this relationship it is necessary to distinguish between total or resultant pressure, as used in the thermodynamic sense, and the components of pressure which mechanistic analysis gives us. An example of such a distinction is found in the interpretation often offered[6] for the "thermodynamic equation of state"

$$P=T\left(\frac{\partial P}{\partial T}\right)_v-\left(\frac{\partial U}{\partial v}\right)_T$$

which represents the external or thermodynamic pressure P as the balance which must be applied to make up the difference between the "thermal (distending) pressure" $T(\partial P/\partial T)_v$, and the "internal (cohesive) pressure," $(\partial U/\partial v)_T$. In the electrostatic case we shall also have to consider more closely the two "pressure components" represented by the two terms on the right-hand side of Eq. (20). These are obviously related to the two tendencies, previously discussed, which are represented by the two terms in, say, Eq. (10) for isothermal and isobaric electrostriction. These two tendencies are physically quite distinct. The first, represented by the term $\rho(\partial K/\partial \rho)$ in Eq. (20), is "contractive" and is directed toward changing the density of the fluid. The second, which we may call "tractive," is represented by the term $(K-1)$ and is directed toward pulling fluid into the field, i.e., changing its location.

When the mechanical circumstances of the charging process are such as to permit the density to change "as much as it wants," as in charging at a constant activity, Eq. (15) tells how much it will change. Taken the other way, Eq. (15) states that, in the field, the density increases by $(\beta/8\pi)\rho^2(\partial K/\partial \rho)dE^2$ without changing the chemical potential of the fluid. This is clearly because, for this change in density, an additional internal repulsive pressure is evoked which raises the chemical potential just enough to balance the "primary" lowering of chemical potential betokened by the cohesive pressure set up by the field. If this is true, however, then, if the fluid is allowed to change density in this way, no external, nor sensible, pressure need, nor can, appear to correspond to this *cohesive component of electrostriction pressure*, which will, instead, be internally compensated.

In full agreement with this, the external, or sensible, pressure which Eq. (13) tells us will appear in this experiment (charging at constant μ) consists only of the *tractive component of electrostriction pressure*. This produces the apparently paradoxial situation in this experiment that, whereas both pressure and density change, these changes are, in a significant sense, unrelated to each other, since the former is proportional to $K-1$ and the latter to $\rho(\partial K/\partial \rho)$.

Paraphrasing and recapitulating the last two paragraphs, it appears that when the fluid in the field stands in "free" communication with fluid outside of the field, only the *tractive* component of pressure will show up as sensible, or observable pressure, and only the *contractive* component will "get its hooks in" on the balance between attractive and repulsive forces which determines the density of the fluid. It is possible, however, to devise experiments with our apparatus which will combine the contractive and tractive components into a "mixed" observable pressure [Eq. (20)], or even to isolate the contractive pressure as a separately observable entity [Eq. (23)].

This analysis makes it appear that what Stratton has derived from electrostatic considerations of virtual work is what we have called the cohesive pressure, and that the wording of his statement about it should be amended to read that the pressure given by Eq. (23) is the difference between the values of the *cohesive component of pressure* in regions of fluid situated inside and outside of the field. The same interpretation presumably applies to the other electrostatic electrostriction pressures (e.g., that of Zwicky)[7] to be found in the literature. If this is true it means that such pressures must not be looked for as mechanical pressures observed between the plates of a small condenser dipping into a large vessel of fluid, nor in the field surrounding a charged sphere immersed in an infinite fluid. Rather, the mechanical pressure in such cases will be that given by Eq. (13).

On the other hand, if it is preferred to say that a pressure may be "observed" by observing the effects which it can be imagined to have produced, then Eq. (15) does indeed correspond to an observation of

[6] See, for example, J. H. Hildebrand and R. L. Scott, *The Solubility of Nonelectrolytes* (Reinhold Publishing Corporation, New York, 1950), third edition, p. 98.

[7] F. Zwicky, Physik. Z. **27**, 271 (1926).

Stratton's pressure. To show this we note that the pressure which, in the absence of the field, would produce the volume change which the field produces may be obtained by use of the identity:

$$dv=-\beta v dP.$$

Inserting dv from Eq. (15)

$$dv=-\frac{v\beta}{8\pi}\rho\left(\frac{\partial K}{\partial \rho}\right)_{T,E}dE^2$$

$$dP=\frac{1}{8\pi}\rho\left(\frac{\partial K}{\partial \rho}\right)_{T,E}dE^2$$

where dP is the *virtual* increment in pressure which would, acting alone, produce the volume change actually produced by dE^2. This, again is the electrostatically derived pressure.

5. ENTROPY EXPRESSIONS

No attempt will be made to derive all of the differential expressions to which this formalism could lead. Three expressions for changes in entropy are of special interest, however. These are

$$\left(\frac{\partial S}{\partial E}\right)_{P,T}=\frac{vE}{4\pi}\left[\left(\frac{\partial K}{\partial T}\right)_{P,E}+(K-1)\alpha\right], \quad (26)$$

$$\left(\frac{\partial S}{\partial E}\right)_{v,T}=\frac{vE}{4\pi}\left(\frac{\partial K}{\partial T}\right)_{v,E}, \quad (27)$$

$$\left(\frac{\partial S}{\partial E}\right)_{\mu,T}=\frac{vE}{4\pi}\left(\frac{\partial K}{\partial T}\right)_{P,E}. \quad (28)$$

Equation (27) is the well-known equation given in the standard references cited in the introduction.[2-4] It is of interest, however, that laboratory experiments are more likely to be performed under the conditions specified for Eqs. (26) and (28), particularly the latter. It is also of interest to note that $(\partial K/\partial T)_v-(\partial K/\partial T)_P$ is equal to $\alpha\rho(\partial K/\partial\rho)$, a quantity which, for water, amounts to some 7% of the value of the temperature coefficient at constant pressure, the one usually measured and quoted.

6. CHANGES IN COMPOSITION

The generalization of the method to apply it to a fluid which is a mixture of two or more components presents no difficulties of principle but in practice requires some care in the manipulation of the number of variables which must now be taken account of. As an example we may obtain an expression for the change in local composition which will be produced when a field is applied, by means of a small dipping condenser, to a small portion of a very large body of a binary mixture. In this small region the field will tend to produce changes in the chemical potentials of the components, and these changes will, in general, have to be offset by changes in both composition and density in order that each chemical potential may continue to fulfill the requirement of uniformity from point to point throughout the whole mass of fluid. For bookkeeping reasons the composition change in the field must evoke a compensating change in composition outside of the field. The fractional change outside the field may be made as small as desired, however, by choosing a large enough total volume of fluid. In the limit, therefore, the change in composition in the small region between the plates of the dipping condenser may be considered to take place with the chemical potentials of both components remaining constant. This change will be represented by $(\partial N_1/\partial E)_{\mu_1,\mu_2}$. Here $N_1(\equiv n_1/n_1+n_2)$ is the mole fraction of component 1. Its change completely describes the change in composition, since $N_1+N_2=1$.

Rewriting Eq. (7) for two components

$$dG^*=-SdT+vdP-(v\mathcal{P})dE+\mu_1 dn_1+\mu_2 dn_2. \quad (29)$$

From this,

$$\left(\frac{\partial \mu_1}{\partial E}\right)_{P,T,n_1,n_2}=-\left(\frac{\partial (v\mathcal{P})}{\partial n_1}\right)_{P,T,E,n_2}$$

$$=-\bar{V}_1 E\chi-vE\left(\frac{\partial \chi}{\partial n_1}\right)_{P,T,E,n_2}$$

$$=-\bar{V}_1 E\chi-VEN_2\left(\frac{\partial \chi}{\partial N_1}\right)_{P,T,E}. \quad (30)$$

($\bar{V}_1$ is the partial molal volume of component 1.) In rearranging Eq. (30), account was taken of the fact that χ, as an intensive property of the solution, can depend on n_1 only through N_1 or N_2. The fact that μ_1 is also intensive means that it, also, depends on n_1 and n_2 only through their ratio. This, since the simultaneous constancy of n_1 and n_2 means constant N_1, makes it possible to rewrite Eq. (30)

$$\left(\frac{\partial \mu_1}{\partial E}\right)_{P,T,N_1}=-\bar{V}_1 E\chi-VEN_2\left(\frac{\partial \chi}{\partial N_1}\right)_{P,T,E}. \quad (31)$$

Using Eq. (31) we may write, for one kind of change in composition,

$$\left(\frac{\partial N_1}{\partial E}\right)_{\mu_1,P,T}=\frac{-(\partial \mu_1/\partial E)_{P,T,N_1}}{(\partial \mu_1/\partial N_1)_{P,T,E}}$$

$$=\frac{1}{(\partial \mu_1/\partial N_1)_{P,T,E}}\left[\bar{V}_1 E\chi+VEN_2\left(\frac{\partial \chi}{\partial N_1}\right)_{P,T,E}\right]. \quad (32)$$

Now, at constant T (we shall omit T as a subscript in what follows) N_1, E, P, and μ_1 may be taken as a

mutually dependent set of quantities, so that

$$dN_1=\left(\frac{\partial N_1}{\partial E}\right)_{\mu_1,P}dE+\left(\frac{\partial N_1}{\partial P}\right)_{\mu_1,E}dP+\left(\frac{\partial N_1}{\partial \mu_1}\right)_{P,E}d\mu_1. \quad (33)$$

For a change taking place while both μ_1 and μ_2 are held constant, therefore,

$$\left(\frac{\partial N_1}{\partial E}\right)_{\mu_1,\mu_2}=\left(\frac{\partial N_1}{\partial E}\right)_{\mu_1,P}+\left(\frac{\partial N_1}{\partial P}\right)_{\mu_1,E}\left(\frac{\partial P}{\partial E}\right)_{\mu_1,\mu_2}. \quad (34)$$

Now

$$\left(\frac{\partial N_1}{\partial P}\right)_{\mu_1,E}=\frac{-(\partial\mu_1/\partial P)_{E,N_1}}{(\partial\mu_1/\partial N_1)_{P,E}}=\frac{-\bar{V}_1}{(\partial\mu_1/\partial N_1)_{P,E}}. \quad (35)$$

Also, making use of the Gibbs-Duhem relation

$$N_1\frac{\partial\mu_1}{\partial N_1}+N_2\frac{\partial\mu_2}{\partial N_1}=0;$$

$$\frac{N_2}{N_1}=-\frac{(\partial\mu_1/\partial N_1)_{P,E}}{(\partial\mu_2/\partial N_1)_{P,E}}=+\frac{(\partial\mu_1/\partial N_1)_{P,E}}{(\partial\mu_2/\partial N_2)_{P,E}}, \quad (36)$$

it can be shown that

$$\left(\frac{\partial P}{\partial E}\right)_{\mu_1,\mu_2}=E\chi \quad (37)$$

as was to be expected by analogy with Eq. (13). Insertion of Eqs. (35) and (37) in Eq. (34) yields

$$\left(\frac{\partial N_1}{\partial E}\right)_{\mu_1,\mu_2}=\frac{EVN_2}{(\partial\mu_1/\partial N_1)_{P,E}}\left(\frac{\partial\chi}{\partial N_1}\right)_{P,E}=\frac{EVN_2}{4\pi(\partial\mu_1/\partial N_1)_{P,E}}\left(\frac{\partial K}{\partial N_1}\right)_{P,E} \quad (38)$$

for the quantity it was desired to obtain.

Equation (38) can be subjected to a test since the sum $(\partial N_1/\partial E)_{\mu_1,\mu_2}+(\partial N_2/\partial E)_{\mu_1,\mu_2}$ should equal zero. Use of Eq. (38) twice with appropriate changes in subscripts, and application of Eq. (36), gives

$$\left(\frac{\partial N_1}{\partial E}\right)_{\mu_1,\mu_2}+\left(\frac{\partial N_2}{\partial E}\right)_{\mu_1,\mu_2}=\frac{EVN_2}{(\partial\mu_1/\partial N_1)_{P,E}}\left[\left(\frac{\partial\chi}{\partial N_1}\right)_{P,E}+\left(\frac{\partial\chi}{\partial N_2}\right)_{P,E}\right]$$

which vanishes as required.

For the special case of an ideal solution, $\mu_1=\mu_1^0+RT\ln N_1$. This gives

$$\left(\frac{\partial N_1}{\partial E}\right)_{\mu_1,\mu_2}=\frac{EV}{4\pi RT}N_1N_2\left(\frac{\partial K}{\partial N_1}\right)_{P,T,E}. \quad (39)$$

In the hypothetical case where V and $(\partial K/\partial N_1)$ remain constant as E changes, this integrates to

$$\ln\frac{N_1}{N_2}-\ln\frac{N_1^0}{N_2^0}=\frac{VE^2}{8\pi RT}\left(\frac{\partial K}{\partial N_1}\right)_{P,T,E}, \quad (40)$$

where N_1^0 and N_2^0 are the unchanged values of N_1 and N_2 at points in the fluid distant enough to be out of the field—i.e., where $E=0$.

7. SALTING OUT

The relation Eq. (40) may be compared with a similar one derived in 1927 by Debye[8] as a basis for the calculation of the salting out effect of strong electrolytes in solvents containing nonpolar, or weakly polar, admixtures. Debye's expression is

$$V_1\ln\frac{N_1}{N_1^0}-V_2\ln\frac{N_2}{N_2^0}=\frac{Z^2e^2}{8\pi kTK^2r^4}\left[V_1\frac{\partial K}{\partial n_1}-V_2\frac{\partial K}{\partial n_2}\right], \quad (41)$$

where Z is the valence of an ion, e the electronic charge, and r the distance from the ion to the site where composition is considered. n_1 and n_2 here represent numbers of molecules per cc of the two substances making up the solvent, and V_1 and V_2 are molecular volumes satisfying the identity

$$n_1V_1+n_2V_2=1.$$

Equation (41) is seen to be essentially the same in content as Eq. (40) if account is taken of the fact that in Debye's derivation the total volume of solvent is held constant with respect to changes in field strength or in composition, and E is required to have the form Ze/Kr^2, restrictions which were not necessary in the derivation of Eq. (40). The derivation of Eq. (41) involves the minimization, subject to the restrictive condition of constant total volume, of the volume integral of free-energy density, the latter being the sum of $n_1(\mu_1^0{}_{\text{molecule}}+kT\ln N_1)+n_2(\mu_2^0{}_{\text{molecule}}+kT\ln N_2)$ and the electrostatic free-energy density (discussed later in Sec. 8) written as $Z^2e^2/8\pi Kr^4$. Because of the need for the restrictive condition upon volume, and of the approximate nature of the free-energy density assumption for this system (see following) Eq. (41) seems to be less general than Eq. (40).

For several reasons, however, neither of these equations can be expected to give an exact account of salting-out in solutions of finite salt concentration. For one thing, there are questions involving the validity of a continuous-medium treatment for the coarse-grained

[8] P. Debye, Z. physik. Chem. **130**, 56 (1927).

situation near the ion. For another, there is uncertainty in the value of K and in the form of E arising from electrostriction, dielectric saturation, and alteration in composition. Finally, a fundamental condition on which both derivations rest is violated in salt solutions which are not infinitely dilute. This is because μ_1 and μ_2, while of course remaining the same at all points in the system, do not, in the salt solution, have the values they would have in a field-free sample of the solvent liquid. That is, during a charging process (of initially "uncharged ions"; the Debye charging process of the Debye-Hückel theory) what is wanted for a proper salting-out discussion is not $(\partial N_1/\partial E)_{\mu_1,\mu_2}$, but $(\partial N_1/\partial E)_{X_1,X_2}$, where X has been written as a symbol for the condition that μ is independent of r, but not of E. How greatly such a coefficient would differ from that of Eq. (40) cannot be stated off-hand.

Even though not exact in any numerical application, Eq. (40) can presumably be used to obtain a qualitative idea of the amount of sorting an ion can be expected to produce in a mixed solvent. At 25°C it may be rewritten, in practical units,

$$\log\frac{N_1}{N_2}-\log\frac{N_1^0}{N_2^0}=7.75\times10^{-18}VE^2\left(\frac{\partial K}{\partial N_1}\right)_{P,T,E}, \quad (42)$$

where V is in cc per mole, and E in v/cm. In a water solution of dioxane or ethanol, V, will be between 18 and 50 or 80 cc. $\partial K/\partial N_1$ will be in the neighborhood of 75 or 50, as an average. At R A from a singly charged ion $E=(144\times10^7/KR^2)$ v/cm if a simple "continuous medium" calculation is to be employed (and changes in the form of E, arising from variations in K, are to be ignored). This suggests that in the immediate neighborhood of an ion N_1/N_2 could change by several powers of 10—a rather complete sorting.

The razor blade and coaxial wire condenser experiments of P. Debye and his colleagues[9] also present experimental situations to which Eqs. (38) or (39) should be applicable.

8. ENERGY DENSITY

It has been common practice[10] to write the quantity $E^2K/8\pi$ as the *free-energy density* or free energy residing in a unit volume of the dielectric medium in a system which has been brought under the influence of an electric field. This form of representation can be justified, and its limitations made clear, by writing, as in Eq. (6)

$$dF=-SdT-Pdv+Ed(v\mathcal{P})+\sum\mu_i dn_i \quad (6)$$

which shows that the (infinitesimal) electrical work increment is an increment in the ordinary Helmholtz free energy. Now, in general,

$$w_e'=Ed(v\mathcal{P})=Ed(vE\chi)$$
$$=E\left[v\chi+E\chi\frac{\partial v}{\partial E}+Ev\frac{\partial\chi}{\partial E}\right]dE. \quad (43)$$

Here $\partial v/\partial E$ and $\partial\chi/\partial E$ will have different forms (given in the foregoing Sec. 3 for constant composition) corresponding to the different conditions under which the charging process has been carried out. (In a mixed fluid, they may also have to contain terms $(\partial v/\partial N)(\partial N/\partial E)$ and $(\partial\chi/\partial N)(\partial N/\partial E)$, to reflect the sorting action which the field may have on the components of the mixture. We shall omit consideration of such effects, as also of direct changes which E may impose upon K through dielectric saturation.)

For the special case of a uniform field and constant volume, w_e becomes simply $Ev\chi dE$, of which the integral, $W_e'=\frac{1}{2}E^2v\chi$, is seen to be the finite increment in F produces by a finite field E. From this $(E^2\chi)/2$ is the straightforward density of free energy residing in the matter of which the dielectric is composed. The space which the matter is filling has also reacted to the field, however, requiring work to be done equal to $E^2v/8\pi$. The total work done per unit volume, therefore, is

$$\frac{W_e}{v}=\frac{E^2\chi}{2}+\frac{E^2}{8\pi}=\frac{E^2(4\pi\chi+1)}{8\pi}=\frac{E^2K}{8\pi}. \quad (44)$$

This, by Eq. (6), is correctly called the electrostatic free-energy density [in the space (including matter)] in the field.

When pressure, instead of volume, is held constant during the charging process and the field is still uniform, it is useful to consider the conventional Gibbs free energy, $F+Pv$, [quite different from the analog defined in Eq. (7)], for which $dG=-SdT+vdP+Ed(v\mathcal{P})+\sum\mu_i dn_i$. Here again, w_e' will be the increase in free energy produced by the charging process (at constant pressure). Here, however, v will not be constant during the charging process, and this makes a somewhat different development desirable. We write

$$w_e'=Ed(v\mathcal{P})=Ed(vE\chi)=Ev\chi dE+E^2d(v\chi)$$
$$=\tfrac{1}{2}v\chi dE^2+E^2d(v\chi). \quad (45)$$

Thus,

$$W_e'=\int_0^E w_e'=\tfrac{1}{2}\int_0^E v\chi dE^2+\int_0^E E^2d(v\chi)$$
$$=\tfrac{1}{2}E^2v\chi+\tfrac{1}{2}\int_0^E E^2d(v\chi). \quad (46)$$

In the case under consideration, namely, constant pressure, the integral of Eq. (46) may be developed by writing

$$d(v\chi)=\left[\chi\left(\frac{\partial v}{\partial E^2}\right)_{P,T}+v\left(\frac{\partial\chi}{\partial E^2}\right)_{P,T}\right]dE^2. \quad (47)$$

[9] Debye, Debye, Eckstein, Barber, and Arquette, J. Chem. Phys. 22, 152 (1954).
[10] See, for example, reference 8.

But

$$\left(\frac{\partial v}{\partial E^2}\right)_{P,T} = -v\cdot\frac{1}{\rho}\left(\frac{\partial \rho}{\partial E^2}\right)_{P,T},$$

and

$$\left(\frac{\partial \chi}{\partial E^2}\right) = \frac{\partial \chi}{\partial \rho}\left(\frac{\partial \rho}{\partial E^2}\right)_{P,T}, \tag{48}$$

whence

$$d(v\chi) = v\left[\left(\frac{\partial \chi}{\partial \rho}\right)_T - \frac{\chi}{\rho}\right]\left(\frac{\partial \rho}{\partial E^2}\right)_{P,T} dE^2. \tag{49}$$

Also, by Eq. (11)

$$\frac{1}{\rho}\left(\frac{\partial \rho}{\partial E^2}\right)_{P,T} = \tfrac{1}{2}\beta\left[\rho\left(\frac{\partial \chi}{\partial \rho}\right)_T - \chi\right],$$

so that

$$d(v\chi)_{P,T} = \tfrac{1}{2}\beta v\left[\rho\left(\frac{\partial \chi}{\partial \rho}\right)_T - \chi\right]^2 dE^2. \tag{50}$$

This gives, finally, for the Gibbs free-energy density for this case,

$$\frac{W_e'}{v} = \tfrac{1}{2}E^2\chi + \tfrac{1}{4}\cdot\frac{1}{v}\int_0^E E^2 v\beta\left[\rho\frac{\partial \chi}{\partial \rho} - \chi\right]^2 dE^2. \tag{51}$$

It follows from Eq. (51) that when charging takes place at constant pressure, the Gibbs total electrostatic free-energy density will be $E^2K/8\pi$ when, and only when, the integral on the right-hand side is zero or may be neglected. It would be zero if χ were directly proportional to ρ, since then $\rho(\partial\chi/\partial\rho)$ would be equal to χ. This is the case in dilute gases, but not in liquids. (For water at room temperature, $\rho(\partial\chi/\partial\rho)-\chi$ has a value of about 1.85.) The integral would also be zero if β were zero, and the free-energy density expression is therefore appropriate to the discussion of artificial models in which the medium is considered incompressible. It is also not bad, however, when E is small or moderate in magnitude. Equation (51) can be integrated formally to give

$$\frac{W_e'}{v} = \tfrac{1}{2}E^2\chi\left(1 + \tfrac{1}{4}\left\langle\frac{\beta}{\chi}\left[\rho\frac{\partial \chi}{\partial \rho} - \chi\right]^2\right\rangle_{Av} E^2\right), \tag{52}$$

where the indicated expression is an appropriate average, presumably not entirely different numerically from what is obtained by inserting the values the quantities have for $E=0$. When this is done, for water at 25°C the coefficient of the E^2 term in parentheses comes out to be 5×10^{-11}, where E is in v/cm. This term would therefore presumably not come into practical account except in fields strong enough to produce other effects on K.

This raises the question of the applicability of the expression $E^2K/8\pi$ to the regions about an ion in an electrolytic solution. Here the discussion is complicated by the fact that, while the external pressure on the solution may be held constant during a charging process, the pressure that any volume element of solvent "feels" is altered by electrostriction. In the general expression for w_e', however, we may, for a dilute enough (see preceding section) solution, insert $(\partial v/\partial E)_\mu$ and $(\partial\chi/\partial E)_\mu$ in Eq. (47) to get a correct representation. The result, analogous to Eq. (52), reads

$$\frac{W_e'}{v} = \tfrac{1}{2}E^2\chi\left[1 + \tfrac{1}{4}\left\langle\frac{\beta}{\chi}\rho\frac{\partial \chi}{\partial \rho}\left(\rho\frac{\partial \chi}{\partial \rho} - \chi\right)\right\rangle_{Av} E^2\right]. \tag{53}$$

Here again, the coefficient of E^2 is expected to be small (of the order of 10^{-10}), so that for a brass ball in a bathtub, the free-energy density is sensibly $E^2K/8\pi$ as before. The fields near ions, however, may presumably be strong enough to make the E^2 term in the parentheses of Eq. (53) non-negligible in comparison to unity.

Attention may also be called to the fact that the value of χ to be used in the integrated expression (52) and (53) is the value corresponding to the final field strength, and in the cases where electrostriction comes seriously into account this will make $E^2K/8\pi$ differ from $E^2K_0/8\pi$ by amounts comparable to the other corrections which Eqs. (52) and (53) contain. Also, in real cases, $d(vE\chi)$ will, at very high fields, contain a term $vE(\partial\chi/\partial E)$ arising from the progressive effect of E in "saturating" the dielectric. This will add another correction, which, unlike the ones discussed above, will be present even at constant v. Current theory[11] makes it seem likely that this will also be proportional to E^2, with a coefficient which may well be in the neighborhood of 10^{-12} (cm/volt)^2.

We are therefore led to the conclusion that in real systems the expression $E^2K/8\pi$ is never a *formally* correct representation of free energy density, since αE^2 is never identically zero no matter how small α may be. It is *practically* correct, however, whenever saturation and electrostriction effects can be ignored. When it is desired to discuss ionic solutions it seems likely that neither saturation nor electrostriction can in fact be left out of account except in artificial models, where they may be excluded by hypothesis. In the latter case, and for all weak-field applications, the energy density representation is permissible and useful.

[11] D. C. Grahame, J. Chem. Phys. 18, 903 (1950).

THE JOURNAL OF CHEMICAL PHYSICS VOLUME 23, NUMBER 11 NOVEMBER, 1955

Dispersion and Absorption of Sound in Imperfect Gases in General Chemical Equilibrium and Its Application to Chemical Kinetics

DAISAKU TABUCHI
Institute of Scientific and Industrial Research, Osaka University, Hirakata, Osaka, Japan
(Received April 8, 1954)

Previously, it was shown that there occur the dispersion and the absorption of sound owing to the chemical reaction in the gas in general chemical equilibrium such as $aA+bB+\cdots\rightleftarrows qQ+rR+\cdots$. As the velocity and the absorption coefficient of sound are affected predominantly by the imperfection of the gas over other factors, the case of imperfect gases is considered. The velocity and the absorption coefficient are derived from the complex velocity of sound, and the characteristic of the dispersion and absorption curves are examined. The velocity and the absorption coefficient of sound are formulated in terms of the pressure, the density, the virial coefficients, the equilibrium constant, namely, the composition, the reaction heat at a constant volume, the molar heat at a constant volume, and the rate constant of the chemical reaction. By measuring the velocity and the absorption coefficient of sound, it is possible to calculate the rate constant of the chemical reaction and the reaction heat. As special cases, the formulas for the perfect gas and for a mixture of imperfect gases in which no chemical reactions occur, are derived. As an example of the calculation, the case of the dissociation equilibrium $A\rightleftarrows B+B$ was treated.

1. INTRODUCTION

THE velocity of sound in a perfect gas is constant, being independent of the pressure of the gas. However, the velocity of sound in actual gases changes with the pressure of the gas. This is attributed to the forces acting between the molecules, and the effect of these forces on the velocity of sound is predominant over other effects. As to the velocity in an imperfect gas, various considerations[1] have been reported. It has been shown that there occurred the dispersion of the velocity of sound due to the finite rate of the chemical reaction in gases in general chemical equilibrium, as well as the absorption of sound due also to the chemical reaction in the dispersive region.[2] Further, it was pointed out that we could derive the rate constant of chemical reaction and the heat of reaction from the measurements of the velocity and absorption coefficient of sound. As the chemical reaction is apt to occur, if the molecule is apart from the perfect state, we consider the dispersion and the absorption of sound due to the chemical reaction, when the gas is imperfect, and they are in general chemical equilibrium.

It is widely known nowadays that there occur the dispersion and the absorption of sound by the vibration or the rotation of the molecules.[3] But the molecular acoustics which deal with these problems started rather with the consideration of the dispersion of the velocity due to the dissociation equilibrium.[4] As for the absorption of sound in a liquid by chemical reaction, several authors[5] discussed this problem. Besides the above considerations Damköhler[6] treated the problem of determing the rate of very rapid reactions by acoustics method. His method is complicated and different from the present author's.

In this paper, the calculation will be made under the following three assumptions: (1) The gas obeys the state equation of the form of virial expansion. (2) The rate of the transition between the quantum states of the vibration or the rotation of the molecule through the molecular collisions are fast enough to give rise to no dispersion and absorption by this cause. That is, the specific heat is constant being independent of the frequency of the sound. (3) In an imperfect gas, there is the classical absorption of sound due to viscosity, heat conduction, and heat radiation, but we consider the problem without these effects. When we compare the formulas with the experimental results, it is necessary to subtract the absorption due to the above effect from the experimental data.

2. COMPLEX VELOCITY OF SOUND IN IMPERFECT GAS IN GENERAL CHEMICAL EQUILIBRIUM

Let the molecules of the type $A, B, \cdots, Q, R, \cdots$ be contained in the gas, whose pressure and volume are respectively P and v. The gas is assumed to be in the chemical equilibrium such as

$$aA+bB+\cdots\rightleftarrows qQ+rR+\cdots. \tag{2.1}$$

The molecular species are denoted by $i, j, k\cdots$ and the number of moles of molecule i is denoted by n_i, the molecular weight m_i, and the molar heat at a constant

[1] L. Bergmann, *Der Ultrashall* (1948), p. 355; A. Eucken and R. Becker, Z. Physik. Chem. **B27**, 219 (1934); R. Schulze, Ann. Phys. **34**, 41 (1939); A. van Itterbeck, and O. van Paemel, Physica **5**, 593, 845 (1938); Hardy, Telfair, and Pielemeier, J. Acoust. Soc. Am. **13**, 226 (1942).

[2] D. Tabuchi, J. Chem. Soc. Japan, Pure Chem. Sect. **71**, 329 (1950).

[3] Markam, Beyer, and Lindsay, Revs. Modern Phys. **23**, 353 (1951).

[4] F. Keutel, Inaug. Diss. Berlin (1910); A. Einstein, Sitzber. preuss. Akad. Wiss. 380 (1920); D. G. C. Luck, Phys. Rev. **40**, 440 (1932); W. T. Richards and J. A. Reid, J. Chem. Phys. **1**, 114, 737 (1933); C. E. Teeter, J. Chem. Phys. **1**, 251 (1933); H. O. Kneser and O. Gauler, Physik. Z. **37**, 667 (1936).

[5] H. O. Kneser, Ann. Phys. **32**, 277 (1938); L. Hall, Phys. Rev. **73**, 775 (1948); L. Liebermann, Phys. Rev. **76**, 1520 (1949); R. Barthel, J. Acoust. Soc. Am. **24**, 313 (1952); M. Manes, J. Chem. Phys. **20**, 1658 (1952); **21**, 1791 (1953); E. Freedman, J. Chem. Phys. **19**, 1316 (1951); **21**, 1784 (1953).

[6] G. Damköhler, Z. Elektrochem. **48**, 62, 116 (1942).

volume c_i. The total number of moles in the gas is n and the density is ρ.

As the state equation of an imperfect gas, the following one which is expanded in virial coefficients is taken:

$$Pv=nRT[1+(n/v)\sum_i\sum_j B_{ij}x_ix_j + (n/v)^2\sum_i\sum_j\sum_k C_{ijk}x_ix_jx_k+\cdots], \quad (2.2)$$

where R is the gas constant, T the absolute temperature and B_{ij}, C_{ijk}, etc. $\cdots$ the second, the third, etc. $\cdots$ virial coefficient respectively. x_i is the mole fraction of molecule i.

When sound wave passes through the gas, the number of moles of each species changes periodically with time depending on the sound frequency.

$$n_Q=\bar{n}_Q+\Delta n_Q=\bar{n}_Q+(\Delta n_Q)_0e^{i\omega t}, \quad (2.3)$$

where $\bar{n}_Q$ is the number of moles of molecule Q at the equilibrium state, and Δn_Q its small change, and ω the circular frequency of sound. The same relation holds for other molecules.

Let r be the net reaction rate, and r_f and r_b be the forward and the backward reaction rates, respectively.

$$r=r_f-r_b, \quad (2.4)$$

r_f and r_b may be expressed by:

$$r_f=k_fa_A^{a'}a_B^{b'}\cdots a_Q^{q'}a_R^{r'}\cdots, \quad (2.5)$$

and

$$r_b=k_ba_Q^{q''}a_R^{r''}\cdots a_A^{a''}a_B^{b''}\cdots, \quad (2.6)$$

where k_f and k_b are the rate constants of the forward and the backward reaction. a_A is the activity of the species of A. In the case in which the equilibrium Eq. (2.1) expresses just what is occurring, $a', b', \cdots q', r'\cdots$ coincide with the stoichiometric coefficients $a, b, \cdots q, r\cdots$. On the other hand, if the reaction proceeds through any intermediate stage, these sets of values may be different from each other, and the factors concerning a_Q, $a_R\cdots$ may appear in r_f and a_A, $a_B\cdots$ in r_b. The activity of each species A is denoted by

$$a_A=\gamma_An_A/v. \quad (2.7)$$

γ_A is the activity coefficient, and has the following content when the state equation is expressed by (2.2)[7]:

$$\gamma_A=1+(n/v)2\sum_i B_{Ai}x_i+(n/v)^2\times[(3/2)\sum_i\sum_j C_{Aij}x_ix_j-2(\sum_i B_{Ai}x_i)^2]+\cdots. \quad (2.8)$$

Considering (2.2), (2.4), and the energy relation, we have the following equation for the square of the complex velocity of sound $\Delta P/\Delta\rho$:

$$\frac{\Delta P}{\Delta\rho}=\frac{P}{\rho}\left(1+\frac{k_fX+i\omega Z}{k_fY+i\omega C_v}\right), \quad (2.9)$$

$$X=v\prod_f(a_A)_0^{a'}(W+\chi Z), \quad (2.10)$$

$$Y=v\prod_f(a_A)_0^{a'}(E^2/RT^2+\chi C_v), \quad (2.11)$$

$$W=\frac{E^2}{RT^2}\frac{\mu-\vartheta}{\vartheta}+\frac{E}{T}\frac{1}{\vartheta}\left[\vartheta+T\left(\frac{\partial\vartheta}{\partial T}\right)_v\right]\times(\sigma-\zeta)+C_v\frac{\sigma\zeta}{n\vartheta}, \quad (2.12)$$

$$Z=\frac{nR}{\vartheta}\left[\vartheta+T\left(\frac{\partial\vartheta}{\partial T}\right)_v\right]^2+C_v\frac{\mu-\vartheta}{\vartheta}, \quad (2.13)$$

$$\chi=\sum_A a^2/n_A+\sum_Q q^2/n_Q, \quad (2.14)$$

$$\vartheta=1+(n/v)\sum_i\sum_j B_{ij}x_ix_j+(n/v)^2\sum_i\sum_j\sum_k C_{ijk}x_ix_jx_k+\cdots, \quad (2.15)$$

$$\mu=1+2(n/v)\sum_i\sum_j B_{ij}x_ix_j+3(n/v)^2\sum_i\sum_j\sum_k C_{ijk}x_ix_jx_k+\cdots, \quad (2.16)$$

$$\sigma=(\sum_Q q-\sum_A a)+2(n/v)\times(\sum_Q\sum_j qB_{Qj}x_j-\sum_A\sum_j aB_{Aj}x_j)+3(n/v)^2\times(\sum_Q\sum_j\sum_k qC_{Qjk}x_jx_k-\sum_A\sum_j\sum_k aC_{Ajk}x_jx_k)+\cdots. \quad (2.17)$$

$$\zeta=\sum_Q q-\sum_A a. \quad (2.18)$$

$\sum_A$ means the sum over the molecular species on the left-hand side in (2.1) and $\sum_Q$ on the right-hand side. The subscript 0 represents the value at the equilibrium state. C_v is the heat capacity at a constant volume, and E the reaction heat at a constant volume.

$$C_v=\sum_i C_i-nRT[2\xi+T(\partial\xi/\partial T)_v], \quad (2.19)$$

$$\xi=(n/v)\sum_i\sum_j(dB_{ij}/dT)x_ix_j+\tfrac{1}{2}(n/v)^2\sum_i\sum_j\sum_k(dC_{ijk}/dT)x_ix_jx_k+\cdots. \quad (2.20)$$

[7] J. E. Mayer and M. G. Mayer, *Statistical Mechanics* (John Wiley and Sons, Inc., 1940), p. 290.

In (2.17) and (2.18),

$$\sum_Q q-\sum_A a=(q+r+\cdots)-(a+b+\cdots), \tag{2.21}$$

$$\sum_Q\sum_j qB_{Qj}x_j-\sum_A\sum_j aB_{Aj}x_j$$
$$=(\sum_j qB_{Qj}x_j+\sum_j rB_{Rj}x_j+\cdots)$$
$$-(\sum_j aB_{Aj}x_j+\sum_j bB_{Bj}x_j+\cdots). \tag{2.22}$$

For the third term of the right-hand side in (2.17), the similar notation has been used. We shall show the example of these later.

If we insert the relaxation time of the chemical reaction τ,

$$1/\tau=(r_f)_0v\chi, \tag{2.23}$$

or

$$1/\tau=(r_f)_0v\sum_f a'a/n_A+(r_b)_0v\sum_b q''q/n_Q, \tag{2.24}$$

the complex velocity of sound is

$$\Delta P/\Delta\rho=\gamma P/\rho, \tag{2.25}$$

$$\gamma=(C_P+C_P{}^r)/(C_v+C_v{}^r), \tag{2.26}$$

where

$$C_P=C_v+Z, \tag{2.27}$$

$$C_P{}^r=(E^2/RT^2+W)/\chi(1+i\omega\tau), \tag{2.28}$$

$$C_v{}^r=E^2/RT^2\chi(1+i\omega\tau). \tag{2.29}$$

3. VELOCITY AND ABSORPTION COEFFICIENT OF SOUND

The velocity and the absorption coefficient of sound is calculated from the complex velocity of sound. The plane wave of sound may be written as follows:

$$\Delta P=\Delta P_0\exp[i\{\omega(t-x/V)+\varphi\}-\alpha x], \tag{3.1}$$

$$\Delta\rho=\Delta\rho_0\exp[i\omega(t-x/V)-\alpha x], \tag{3.2}$$

where α is the absorption coefficient of the amplitude of sound per unit length of the path, V the phase velocity, φ the phase angle between the pressure wave and the density wave. If λ be the wavelength of sound, and α_λ be the absorption coefficient of the amplitude per wavelength,

$$\alpha_\lambda=\alpha\lambda. \tag{3.3}$$

From (3.1), (3.2), and (3.3), we have

$$\theta=\alpha_\lambda/2\pi=[1+(\tan\varphi)^{-2}]^{\frac{1}{2}}-(\tan\varphi)^{-1}$$
$$=\tfrac{1}{2}\tan\varphi(1-\tfrac{1}{4}\tan^2\varphi+\tfrac{1}{8}\tan^4\varphi\mp\cdots), \tag{3.4}$$

$$V^2=[(1+\theta^2)^2/(1-\theta^2)]Re(\Delta P/\Delta\rho)$$
$$=Re(\Delta P/\Delta\rho)(1+\tfrac{3}{4}\tan^2\varphi-\tfrac{1}{8}\tan^4\varphi\pm\cdots), \tag{3.5}$$

$$\tan\varphi=Im(\Delta P/\Delta\rho)/Re(\Delta P/\Delta\rho), \tag{3.6}$$

where $\Delta P/\Delta\rho$ is the square of the complex velocity of sound, $Re(\Delta P/\Delta\rho)$, and $Im(\Delta P/\Delta\rho)$ are its real and imaginary part, respectively. When the phase angle is small and $\tan\varphi\ll1$, then approximately

$$\alpha_\lambda=\pi\tan\varphi, \tag{3.7}$$

$$V^2=Re(\Delta P/\Delta\rho). \tag{3.8}$$

From the complex velocity of sound (2.9), we have

$$\tan\varphi=\frac{\omega k_f(YZ-XC_v)}{k_f{}^2Y(X+Y)+\omega^2C_v(Z+C_v)}, \tag{3.9}$$

$$Re(\Delta P/\Delta\rho)=\frac{P}{\rho}\left(1+\frac{k_f{}^2XY+\omega^2ZC_v}{k_f{}^2Y^2+\omega^2C_v{}^2}\right). \tag{3.10}$$

Now, we shall examine the characteristic of the dispersion curve and the absorption curve of sound. If we plot V^2 against $\ln\omega$, we obtain a dispersion curve of the type —⁀—. The velocity of sound at low frequency V_0 and at the high frequency V_∞ are

$$V_0{}^2=(P/\rho)(1+X/Y), \tag{3.11}$$

$$V_\infty{}^2=(P/\rho)(1+Z/C_v). \tag{3.12}$$

The frequency ω_{inf} and the velocity of sound V_{inf} at the inflection point of the dispersion curve are given as follows:

$$\omega_{\text{inf}}=k_fY/C_v, \tag{3.13}$$

$$V_{\text{inf}}{}^2=\tfrac{1}{2}(V_0{}^2+V_\infty{}^2). \tag{3.14}$$

If we plot α_λ against $\ln\omega$, we get a bell-shaped absorption curve. The frequency $\omega_{\max}$ and the value of the absorption coefficient $(\alpha_\lambda)_{\max}$ of sound at the maximum of the absorption curve are

$$\omega_{\max}=k_f[Y(X+Y)/C_v(Z+C_v)]^{\frac{1}{2}}, \tag{3.15}$$

$$(\alpha_\lambda)_{\max}=\frac{\pi}{2}\frac{YZ-XC_v}{[Y(X+Y)C_v(Z+C_v)]^{\frac{1}{2}}}. \tag{3.16}$$

From (3.13) and (3.15), the following relation is derived:

$$\omega_{\text{inf}}/\omega_{\max}=V_\infty/V_0=Q; \tag{3.17}$$

that is, the frequency of the maximum absorption is slightly lower than the frequency of the inflection point of the velocity of sound. From (3.11), (3.12), and (3.16), we have

$$\Delta V^2=V_\infty{}^2-V_0{}^2, \tag{3.18}$$

$$(\alpha_\lambda)_{\max}=(\pi/2)\Delta V^2/V_0V_\infty. \tag{3.19}$$

If we denote the velocity and the absorption coefficient of sound by ω_{inf}, $\omega_{\max}$, V_0, V_∞, and ΔV, we get

$$V^2=V_0{}^2+\Delta V^2(\omega/\omega_{\text{inf}})^2/[1+(\omega/\omega_{\text{inf}})^2], \tag{3.20}$$

$$\alpha_\lambda=2(\alpha_\lambda)_{\max}(\omega/\omega_{\max})/[1+(\omega/\omega_{\max})^2]. \tag{3.21}$$

(3.19), (3.20), and (3.21) can be written in various forms by using Q. Let f be the frequency of sound,

then we have the following formula:

$$\frac{\alpha}{f^2}=\frac{2}{V}\frac{(\alpha_\lambda)_{\max}}{f_{\max}}\frac{1}{1+(f/f_{\max})^2}. \tag{3.22}$$

By using above relations, we can calculate the rate constant of the chemical reaction from the experimental results.

4. PERFECT GAS AND MIXTURE OF IMPERFECT GASES

As a special case of the general calculation considered above, we consider a case where the gas is perfect.[2] In this case, B_{ij}, $C_{ijk}\cdots$ are zero, and we have

$$\frac{\Delta P}{\Delta\rho}=\frac{P}{\rho}\left(1+\frac{k_fX_0+i\omega nR}{k_fY_0+i\omega C_v^0}\right), \tag{4.1}$$

$$X_0=v\prod_A\left(\frac{n_A}{v}\right)_0^{a'}\Big[(\sum_Q q-\sum_A a)\times\left\{2\frac{E}{T}+\frac{C_v^0}{n}(\sum_A a-\sum_Q q)\right\}+\left(\sum_A\frac{a^2}{n_A}+\sum_Q\frac{q^2}{n_Q}\right)nR\Big], \tag{4.2}$$

$$Y_0=v\prod_A\left(\frac{n_A}{v}\right)_0^{a'}\left[\frac{E^2}{RT^2}+\left(\sum_A\frac{a^2}{n_A}+\sum_Q\frac{q^2}{n_Q}\right)C_v^0\right]. \tag{4.3}$$

If there occurs no chemical reaction, the gas is merely the mixture of imperfect gases. Then, k_f and k_b are zero. The complex velocity of sound becomes as follows:

$$\Delta P/\Delta\rho=(P/\rho)[\mu/\vartheta+(nR/\vartheta C_v)\times\{\vartheta+T(\partial\vartheta/\partial T)_v\}^2]. \tag{4.4}$$

That is, the phase angle between the pressure wave and the density wave is reduced to zero, and, therefore, there is no absorption of sound.

$$\tan\varphi=\alpha_\lambda=\theta=0. \tag{4.5}$$

It is verified that the velocity derived in the foregoing coincides with the exact equation of Hardy, Telfair, and Pielemeier.[1]

5. EXAMPLE

As it may be hard to understand the contents of the general formulas derived in the preceding sections, an example will be shown in order to make them clear.

We consider the dissociation reaction $A\rightleftarrows B+B$, which was treated by Einstein, Luck, Richards, Reid, Teeter, Kneser, and Gauler.[4] In this case, the general formulas is reduced to the following ones:

$$\frac{\Delta P}{\Delta\rho}=\frac{P}{\rho}\left(1+\frac{k_fX+i\omega Z}{k_fY+i\omega C_v}\right), \tag{5.1}$$

$$X=v(\gamma_An_A/v)[W+(1/n_A+4/n_B)Z], \tag{5.2}$$

$$Y=v(\gamma_An_A/v)[E^2/RT^2+(1/n_A+4/n_B)C_v], \tag{5.3}$$

$$W=\frac{E^2}{RT^2}\frac{\mu-\vartheta}{\vartheta}+\frac{E}{T}\frac{1}{\vartheta}\left[\vartheta+T\left(\frac{\partial\vartheta}{\partial T}\right)_v\right]\times(\sigma+1)-C_v\frac{\sigma}{n\vartheta}, \tag{5.4}$$

$$Z=\frac{nR}{\vartheta}\left[\vartheta+T\left(\frac{\partial\vartheta}{\partial T}\right)_v\right]^2+C_v\frac{\mu-\vartheta}{\vartheta}, \tag{5.5}$$

$$\gamma_A=1+(n/v)2(B_{AA}x_A+B_{AB}x_B)+(n/v)^2[(3/2)(C_{AAA}x_A^2+2C_{AAB}x_Ax_B+C_{ABB}x_B^2)-2(B_{AA}x_A+B_{AB}x_B)^2]+\cdots, \tag{5.6}$$

$$\vartheta=1+(n/v)(B_{AA}x_A^2+2B_{AB}x_Ax_B+B_{BB}x_B^2)+(n/v)^2(C_{AAA}x_A^3+3C_{AAB}x_A^2x_B+3C_{ABB}x_Ax_B^2+C_{BBB}x_B^3)+\cdots, \tag{5.7}$$

$$\mu=1+2(n/v)(B_{AA}x_A^2+2B_{AB}x_Ax_B+B_{BB}x_B^2)+3(n/v)^2(C_{AAA}x_A^3+3C_{AAB}x_A^2x_B+3C_{ABB}x_Ax_B^2+C_{BBB}x_B^3)+\cdots, \tag{5.8}$$

$$\sigma=1+2(n/v)[2(B_{BA}x_A+B_{BB}x_B)-(B_{AA}x_A+B_{AB}x_B)]+3(n/v)^2[2(C_{BAA}x_A^2+2C_{BAB}x_Ax_B+C_{BBB}x_B^2)-(C_{AAA}x_A^2+2C_{AAB}x_Ax_B+C_{ABB}x_B^2)]+\cdots, \tag{5.9}$$

$$\xi=(n/v)[(dB_{AA}/dT)x_A^2+2(dB_{AB}/dT)x_Ax_B+(dB_{BB}/dT)x_B^2]+\tfrac{1}{2}(n/v)^2[(dC_{AAA}/dT)x_A^3+3(dC_{AAB}/dT)x_A^2x_B+3(dC_{ABB}/dT)x_Ax_B^2+(dC_{BBB}/dT)x_B^3]+\cdots. \tag{5.10}$$

If the gas is perfect, the formulas become very simple. If we put $\bar{C}_v^0=C_v^0/n$, then we have

$$V^2=\frac{P}{\rho}\left(1+\frac{k_f^2X_0'Y_0'+\omega^2R\bar{C}_v^0}{k_f^2Y_0'^2+\omega^2\bar{C}_v^{02}}\right), \tag{5.11}$$

with

$$X_0'=(2E/T-\bar{C}_v^0)n_A/n+(1+4n_A/n_B)R, \tag{5.12}$$

and

$$Y_0'=(E^2/RT^2)n_A/n+(1+4n_A/n_B)\bar{C}_v^0. \tag{5.13}$$

These formulas coincide with the results of Einstein[4] derived in 1920.

6. CONCLUSION

The velocity and the absorption coefficient of sound in the imperfect gas in general chemical equilibrium were calculated, and the characteristic of the dispersion curve and the absorption curve of sound were examined. It was possible to derive the rate constant of chemical reaction and the reaction heat from the measurements of the velocity and the absorption coefficient of sound. As special cases, a perfect gas and a mixture of imperfect gases which has no chemical reaction were considered, and the calculated results about an example was shown. In the calculations made, the absorption of sound due to viscosity, heat conduction, and heat radiation which are accompanied with the imperfection of gas were considered separately. It is possible to calculate the velocity and the absorption coefficient by taking these effects into consideration, but the results would become very complicated. It is necessary to subtract these absorptions from the experimental data before one compares the formulas with experimental results.

THE JOURNAL OF CHEMICAL PHYSICS VOLUME 23, NUMBER 11 NOVEMBER, 1955

Microwave Spectrum and Molecular Structure of Methylchloroacetylene

C. C. COSTAIN
Division of Physics, National Research Council, Ottawa, Canada
(Received February 23, 1955)

The $J=6\leftarrow5$ rotational transitions have been observed for 10 isotopic species of CH_3CCCl, including four of the fully deuterated molecule. The values for D_J were calculated from the force constants of the molecule, and are tabulated with the resulting values for B_0. The structural parameters giving the best fit to the 10 moments of inertia I_B are: $r_0(C-Cl)=1.6371$ A, $r_0(C\equiv C)=1.2069$ A, $r_0(C-C)=1.4584$ A, $r_0(C-H)=1.117$ A, $\angle HCC=110°\,46'$, $r_0(C-D)=1.114$ A, and $\angle DCC=110°\,30'$. The quadrupole coupling constant eqQ was determined as -79.6 Mc/sec for Cl^{35} and -62.6 Mc/sec for Cl^{37}. For CH_3CCCl^{35}, CH_3CCCl^{37}, CD_3CCCl^{35}, and CD_3CCCl^{37} experimental values of D_{JK} and H_{JKK} were determined from the K structure. To fit the observed fine structure it was necessary to include the third-order term H_{JKK} in the expression for the rotational energy.

INTRODUCTION

THE microwave spectra of a number of acetylene derivatives have been measured,[1,2] and considerable information has been obtained on the bond distances in this group of molecules. In particular the structures of methylacetylene[2] and chloroacetylene[3] have been determined. A similar determination of the structure of the doubly substituted methylchloroacetylene is of interest for purposes of comparison. Recently samples of $CH_3C\equiv CCl$ and $CD_3C\equiv CCl$ were obtained through the kindness of Dr. L. C. Leitch,[4] which made it possible to investigate the microwave spectrum of this molecule.

In the investigation the $J=6\leftarrow5$ rotational transition was observed for 10 isotopic species of the molecule. From the measurement of 50 lines a number of the spectroscopic constants were obtained and the bond distances and angles were calculated. As will be shown below, the results are for the most part in close agreement with previous work on related molecules.

EXPERIMENTAL

A recording Stark spectrometer with 100 kc/sec square-wave modulation and phase-sensitive detection was used to obtain the methylchloroacetylene spectrum. The absorption cell consists of a 6.25-meter parallel plane waveguide, with plates 10 cm wide separated by 0.24 cm. The modulator could deliver a 100 kc/sec square wave with a maximum amplitude of 600 volts, giving a field of 2500 volts/cm between the plates. Two G.E. IN158 germanium diodes were used in series to hold the top of the square wave at zero voltage.

The frequencies of the lines were obtained by measuring their displacement from appropriate ammonia lines, which were displayed from a separate spectrometer employing source modulation. The direction of the sweeps of the two spectrometers could be reversed together to eliminate errors from circuit delays.

The uncertainty in the absolute values of the frequencies must include that of the ammonia lines and was taken to be ±0.04 Mc/sec. Frequency measurements relative to the same ammonia line were consistent to ±0.01 Mc/sec. Whenever possible the separation of adjacent ammonia lines was measured, and with one exception was found to agree with tabulated values[5]

[1] Gordy, Smith, and Trambarulo, *Microwave Spectroscopy* (John Wiley and Sons, Inc., New York, 1953), p. 371.
[2] Thomas, Sherrard, and Sheridan, Trans. Faraday Soc. **51**, 619 (1955).
[3] Westenberg, Goldstein, and Wilson, J. Chem. Phys. **17**, 1319 (1949).
[4] A. T. Morse and L. C. Leitch, Can. J. Chem. **32**, 500 (1954).
[5] P. Kesluik and C. H. Townes, Molecular Microwave Spectra Tables, Natl. Bur. Standards, Circular 518.

TABLE I. Observed and calculated frequencies of H_3CCCCl.

Molecule	K	F	Observed freq. Mc/sec	Calculated freq. Mc/sec
H_3CCCCl^{35}	5	9/2←7/2	26 790.76	26 790.77
	4	9/2←7/2	26 789.21	26 789.21
	3	9/2←7/2	26 787.99	26 788.01
	0	15/2←13/2 13/2←11/2	26 787.43	26 787.43
	0	11/2←9/2 9/2←7/2	26 786.53	26 786.52
	4	11/2←9/2	26 780.12	26 780.11
	4	13/2←11/2	26 777.41	26 777.41
	5	11/2←9/2	26 776.56	26 776.55
	5	13/2←11/2	26 771.84	26 771.83
H_3CCCCl^{37}	5	9/2←7/2	26 200.63	26 200.62
	4	9/2←7/2	26 199.74	26 199.75
	3	9/2←7/2	26 199.09	26 199.09
	0	15/2←13/2 13/2←11/2	26 199.01	26 199.01
	2	15/2←13/2 13/2←11/2	26 198.64	26 198.65
	0	11/2←9/2 9/2←7/2	26 198.31	26 198.30
	3	11/2←9/2	26 195.06	26 195.07
	3	13/2←11/2	26 194.19	26 194.19
	4	11/2←9/2	26 192.62	26 192.60
	4	13/2←11/2	26 190.49	26 190.48
	5	11/2←9/2	26 189.44	26 189.45
	5	13/2←11/2	26 185.73	26 185.74
D_3CCCCl^{35}	5	9/2←7/2	23 753.03	23 753.03
	4	9/2←7/2	23 750.78	23 750.79
	3	9/2←7/2	23 749.07	23 749.06
	0	15/2←13/2 13/2←11/2	23 747.77	23 747.77
	0	11/2←9/2 9/2←7/2	23 746.85	23 746.86
	1	11/2←9/2	23 746.52	23 746.54
	2	13/2←11/2 11/2←9/2	23 745.59	23 745.57
	3	11/2←9/2	23 743.97	23 743.95
	3	13/2←11/2	23 742.85	23 742.83
	4	11/2←9/2	23 741.70	23 741.69
	5	13/2←11/2	23 734.10	23 734.10
D_3CCCCl^{37}	5	9/2←7/2	23 217.02	23 217.02
	4	9/2←7/2	23 215.53	23 215.53
	3	9/2←7/2	23 214.38	23 214.38
	0	15/2←13/2 13/2←11/2	23 213.64	23 213.64
	3	11/2←9/2	23 210.33	23 210.35
	3	13/2←11/2	23 209.48	23 209.46
	4	11/2←9/2	23 208.34	23 208.35
	4	13/2←11/2	23 206.22	23 206.23
	5	13/2←11/2	23 202.09	23 202.09
$H_3CC^{13}CCl^{35}$	0	15/2←13/2 13/2←11/2	26 612.05	
	0	11/2←9/2 9/2←7/2	26 611.16	
$H_3C^{13}CCCl^{35}$	0	15/2←13/2 13/2←11/2	25 968.26	
	0	11/2←9/2 9/2←7/2	25 967.36	
$H_3CC^{13}CCl^{37}$	0	15/2←13/2 13/2←11/2	26 019.53	
$H_3C^{13}CCCl^{37}$	0	15/2←13/2 13/2←11/2	25 390.51	
$D_3CC^{13}CCl^{35}$	0	15/2←13/2 13/2←11/2	23 635.45	
$D_3C^{13}CCCl^{35}$	0	15/2←13/2 13/2←11/2	23 156.71	
	0	11/2←9/2 9/2←7/2	23 155.79	

to ±0.02 Mc/sec. The measurements show that the frequency listed for the $J=13$, $K=12$ line of NH_3 is 0.25 Mc/sec too high.

RESULTS

A. K Structure Analysis

The frequencies and identification of the lines that were measured are given in Table I. As can be seen from this table, for each of the molecules CH_3CCCl^{35}, CH_3CCCl^{37}, CD_3CCCl^{35}, and CD_3CCCl^{37} some ten lines resulting from the K splitting and the Cl quadrupole splitting of the $J=6\leftarrow5$ rotational transition were sufficiently well resolved to be measured. The quadrupole coupling constant eqQ for each of the above molecules was calculated from the separation of the $K=5$, $F=9/2\leftarrow7/2$ and $K=5$, $F=13/2\leftarrow11/2$ lines.

The lines with $K\neq0$ show a first-order Stark Effect and a field of 50 volts/cm was sufficient to remove the Stark components. The $K=0$ lines on the other hand show only a second-order Stark Effect and are barely resolved by a field of 2500 volts/cm. A dc field of 50 volts/cm could therefore be used to remove all lines with $K\neq0$, and it was possible to record the $K=0$ lines separately, even though they were not normally resolved from the other K structure. This was of great assistance in the analysis.

It was found that the value obtained for D_{JK} increased as K decreased, and it was therefore apparent that third-order terms should be included in the expression for the rotational energy of the nonrigid symmetric top. If the notation accepted for diatomic molecules[6] is extended to the symmetric top case then the rotational energy becomes

$$\begin{aligned}F(J,K)=&BJ(J+1)+(A-B)K^2-D_JJ^2(J+1)^2\\&-D_{JK}J(J+1)K^2-D_KK^4\\&+H_{JJJ}J^3(J+1)^3+H_{JJK}J^2(J+1)^2K^2\\&+H_{JKK}J(J+1)K^4+H_{KKK}K^6,\end{aligned}\quad(1)$$

and the pure rotation spectrum is given by

$$\begin{aligned}\nu=&2B(J+1)-4D_J(J+1)^3-2D_{JK}(J+1)K^2\\&+H_{JJJ}(J+1)^3[(J+2)^3-J^3]\\&+4H_{JJK}(J+1)^3K^2+2H_{JKK}(J+1)K^4.\end{aligned}\quad(2)$$

D_{JK} and H_{JKK} may be evaluated from the displacements of the unperturbed K lines from the $K=0$ line. With the H_{JKK} term included, it is possible to fit Eq. (2) to all of the K lines and, therefore, to improve the accuracy of the B_0 determination. In some published values of the K splitting, e.g., for CH_3CCH,[7] the same variation in D_{JK} found above is evident, and perhaps the data would justify the inclusion of third-order energy terms.

[6] G. Herzberg, *Spectra of Diatomic Molecules* (D. Van Nostrand Company, Inc., New York, 1950), p. 104.

[7] R. Trambarulo and W. Gordy, J. Chem. Phys. **18**, 1613 (1950).

The values of eqQ, D_{JK}, and H_{JKK} obtained for CH_3CCCl^{35}, CH_3CCCl^{37}, CD_3CCCl^{35}, and CD_3CCCl^{37} are listed in Table II. The constant D_{JK} still contains a third-order term $2H_{JJK}(J+1)^2$ which might be determined if D_{JK} was obtained for other J values, but which does not affect the evaluation of B_0.

B. Calculation of D_J

A comparison of the results for the $J=6\leftarrow5$ transition with some preliminary measurements on the $J=5\leftarrow4$ transition showed that D_J was too small to determine with sufficient accuracy. Since for $J=5$ the D_J term might still be a significant correction to B, it was decided to calculate D_J from the force constants of the molecule.

For a linear molecule with masses m_1, m_2, m_3, m_4, and m_5 and force constants between adjacent atoms k_1, k_2, k_3, and k_4, one finds

$$D_J=\frac{16\pi^2B^3}{I}\left[\frac{(m_1Z_1)^2}{k_1}+\frac{(m_1Z_1+m_2Z_2)^2}{k_2}+\frac{(m_1Z_1+m_2Z_2+m_3Z_3)^2}{k_3}+\frac{(m_5Z_5)^2}{k_4}\right], \quad (3)$$

where Z_i is the distance of m_i from the center of mass. If $m_1=m_2=m_3=0$, this reduces to $D_J=4B^3/\omega^2$ for a diatomic molecule.

The above expression must be modified for a symmetric top such as CH_3CCCl to include the effect of centrifugal forces on the H_3 group. In this molecule the contribution from the H_3 group is a small fraction of the total D_J so that simplifying approximations can be made which introduce little error. It was found that it was necessary to consider only the term which arises from the displacement of the H_3 group along the symmetry axis as a result of the change in the HCC angle, since the other terms are much smaller and very nearly cancel. For symmetrical distortions the bending-force constants for the HCH angle and the HCC angle may be added. Equation (3) may then be applied to this molecule with

$$m_1=3m_H,$$

$$I=I_B,$$

$$k_1=\frac{k_\delta}{r_0^2(\mathrm{C-H})\sin^2\alpha},$$

TABLE II. Spectroscopic constants derived from K structure.

Molecule	eqQ Mc/sec	D_{JK} kc/sec	H_{JKK} kc/sec
H_3CCCCl^{35}	-79.6 ± 0.1	21.5	1.9×10^{-2}
H_3CCCCl^{37}	-62.6	20.5	2.2×10^{-2}
D_3CCCCl^{35}	-79.6	15.0	1.3×10^{-2}
D_3CCCCl^{37}	-62.7	14.4	1.2×10^{-2}

TABLE III. Unperturbed frequencies for the $J=6\leftarrow5$ transition and B_0 values.

Molecule	Freq. in Mc/sec	$4(J+1)^3D_J$ Mc/sec	B_0 in Mc/sec
H_3CCCCl^{35}	26 787.12±0.04	0.136	2232.271
$H_3CC^{13}CCl^{35}$	26 611.74	0.134	2217.656
$H_3C^{13}CCCl^{35}$	25 967.96	0.127	2164.009
H_3CCCCl^{37}	26 198.77	0.130	2183.242
$H_3CC^{13}CCl^{37}$	26 019.29	0.128	2168.284
$H_3C^{13}CCCl^{37}$	25 390.27	0.121	2115.865
D_3CCCCl^{35}	23 747.47	0.117	1978.965
$D_3CC^{13}CCl^{35}$	23 635.14	0.115	1969.605
$D_3C^{13}CCCl^{35}$	23 156.40	0.110	1929.709
D_3CCCCl^{37}	23 213.40	0.112	1934.460

where α is the tetrahedral angle and k_δ is the sum of the two bending-force constants of the methyl group.

The force constants used in the calculations were obtained from Bernstein and Davidson.[8] To the accuracy required here the constants were the same as published by Meister.[9] The interaction force constants were assumed to be zero. The values obtained for D_J for the ten isotopic species are listed in Table III (multiplied by the factor $4(J+1)^3$), together with the unperturbed $J=6\leftarrow5$, $K=0$ frequencies and the resulting B_0 values. Since the contribution of the D_J term to B_0 is quite small, the accuracy of the calculations should be adequate.

C. Determination of the Structure of the Molecule

To obtain the five molecular parameters of CH_3CCCl, it is necessary to solve the simultaneous equations which can be set up using the moments of inertia I_B for five isotopic species of the molecule. A convenient method for the reduction of these equations has been given by Trambarulo and Gordy[7] in their paper on CH_3CCH, and in a more general treatment of the problem Kraitchman[10] has pointed out that to make the simultaneous equations independent, only one isotopic substitution may be made on a given atom.

The papers mentioned show that the distance of an atom on the symmetry axis from the center of mass can be determined by an isotopic substitution on the atom concerned. The equation is

$$Z^2=(I_B'-I_B)\mu^{-1}, \quad (4)$$

where $\mu=M\Delta m/(M+\Delta m)$ and $I_B'-I_B$ is the change in the moment of inertia resulting from a change in mass Δm of an atom at a distance Z from the original center of mass. M is the total mass of the original molecule. If it is assumed that the zero-point vibration does not change the effective positions of the atoms on isotopic substitution, Eq. (4) is exact.

The information which can be obtained from the experimental data directly by application of Eq. (4) is

[8] H. J. Bernstein and D. Davidson, Can. J. Chem. **33**, 1226 (1955).
[9] A. G. Meister, J. Chem. Phys. **16**, 950 (1948).
[10] J. Kraitchman, Am. J. Phys. **21**, 17 (1953).

TABLE IV. Distances from the center of mass in 10^{-8} cm.

Molecule	Z_2	Z_3	Z_5	Z_2-Z_3 $=r_0(C-C)$	Z_3-Z_5 $=r_0(C\equiv C-Cl)$
$Z_1Z_2Z_3Z_4Z_5$					
H_3CCCCl^{35}	2.6860	1.2277	−1.6165	1.4583	2.8442
H_3CCCCl^{37}	2.7282	1.2698	−1.5740	1.4584	2.8438
D_3CCCCl^{35}	2.5654	1.1070	−1.7368	1.4584	2.8438

given in Table IV. The distances from the center of mass along the symmetry axis, starting with the H_3 groups, are called Z_1, Z_2, Z_3, Z_4 up to Z_5 for the Cl atom. Z_2, Z_3, and Z_5 were determined for three "original" molecules, H_3CCCCl^{35}, H_3CCCCl^{37}, and D_3CCCCl^{35}. The data given in Table IV represent an intermediate step in the bond-distance calculations, but are included since they show which parameters are most accurately determined, namely the C−C single-bond distance and the sum of the C≡C and the C−Cl bond distances. Also, the differences of the Z's in a vertical column give experimental values for the shift of the center of mass in going from one isotopic species to another.

If it is assumed that the effective positions of the H and D atoms are the same, the data for CH_3CCCl and CD_3CCCl can be combined to solve explicitly for the remaining unknowns. Since this procedure leads to an impossible solution, namely an arrowhead configuration for the methyl group, it is apparent that the effective positions of the H and D atoms differ as a result of zero-point vibration.

For both CH_3CCCl and CD_3CCCl the moments of inertia of four independent isotopic species are available. Therefore, an alternative method of solution is to assume a value for one of the remaining parameters, for example, the C−Cl bond length, and to solve for the methyl parameters for both molecules. In Fig. 1 the distance of the H atoms from the symmetry axis, h, is plotted against the height of the methyl pyramid, Z_1', for various values of the C−Cl bond length in H_3CCCCl. On the same figure, h and Z_1' obtained for D_3CCCCl are plotted for the same C−Cl bond lengths. It can be seen that the position of the H and D atoms do not coincide for any value of the C−Cl bond. The solution taken is that for which there is a minimum displacement of the D atom from the position for H; that is, the value of the C−Cl bond length for which a perpendicular line can be drawn between the two curves.

This assumption of the minimum displacement does not necessarily give the correct solution, but it is the only possible choice, and should not be much in error. It is reasonable since for all other atoms it is assumed that the displacement on isotopic substitution is zero. If other values of the C−Cl bond length are assumed, and the methyl parameters taken from Fig. 1, there will be little change in the fit to the experimental moments of inertia. The assumption of a minimum displacement is therefore an additional criterion on which the solution is based.

The structural parameters obtained are the following:

$$r_0(C-Cl)=1.6371\text{ A}$$
$$r_0(C\equiv C)=1.2069\text{ A}$$
$$r_0(C-C)=1.4584\text{ A}$$
$$r_0(C-H)=1.1170\text{ A}\quad r_0(C-D)=1.1138\text{ A}$$
$$\angle HCC=110°46'\quad(\angle HCH=108°8')$$
$$\angle DCC=110°30'\quad(\angle DCD=108°25').$$

The moments of inertia I_B calculated from these parameters, and the observed moments of inertia, are given in Table V.

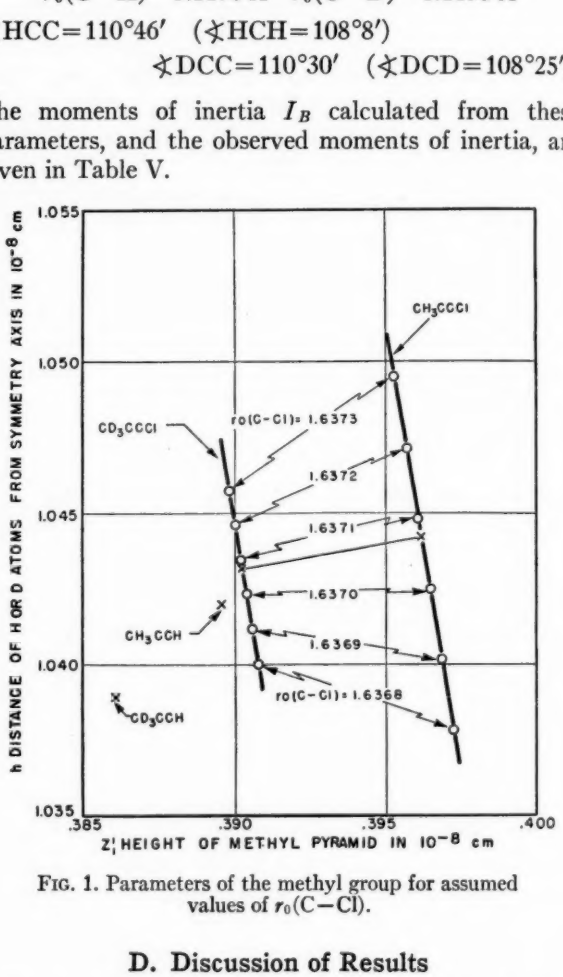

FIG. 1. Parameters of the methyl group for assumed values of $r_0(C-Cl)$.

D. Discussion of Results

The bond distances are given above to four decimal places (a further figure was required for the I_B calculations), but it is difficult to say with what accuracy these parameters are actually determined. The assumed accuracy of ±0.04 Mc/sec in the frequency measurements is equivalent to approximately ±0.0002 A in the bond distances between the heavier atoms, and while the data in Table IV tend to confirm this accuracy, it is probable that the three sets of values are all subject to a larger systematic error due to zero-point vibration. Apart from different values determined for H and D atoms, it has been assumed that the effective positions of the substituted atoms, and of all other atoms in the molecule, remain unchanged for the various isotopic substitutions. The errors arising from this neglect of the changes in the zero-point vibrations on isotopic substitution cannot be accurately estimated but may be expected to be larger than ±0.0002 A.

The agreement between the observed and the calculated values of I_B listed in Table V is surprisingly good, since the rms error in the fit for the ten isotopic species is the same as the experimental error. An estimate of the accuracy of the bond distances can be made by changing one bond length by a small amount and calculating the rms error when the other parameters are adjusted to give the best over-all fit. From a number of such trials it appears that the error in the bond distances between the heavier atoms is certainly less than ± 0.001 A, and probably not larger than ± 0.0005 A. The corresponding probable error in the location of the H atoms is about ± 0.005 A.

The relevant parameters of methylchloroacetylene, methylacetylene, and chloroacetylene are collected in Table VI, and it can be seen that the values of $r_0(C-C)$ and $r_0(C\equiv C)$ obtained for H_3CCCCl are in close agreement with those for H_3CCCH. To compare the methyl parameters for these two molecules the values for H_3CCCH have been included in Fig. 1. While there appears to be a real difference in these values, it is small enough to be accounted for by changes in the zero-point vibrations.

A comparison of the results for H_3CCCCl and $HCCCl$ shows a less satisfactory agreement. The sums of $r_0(C\equiv C)$ and $r_0(C-Cl)$ are almost the same for the two molecules, but $r_0(C\equiv C)$ increases by 0.004 A and $r_0(C-Cl)$ decreases by 0.005 A when the methyl group is replaced by an H atom. A change of this magnitude is outside the probable error of both determinations, and is surprisingly large since the acetylenic carbon triple bond is involved. In a recent paper Herzberg and Stoicheff[11] have pointed out that the length of the $r_0(C\equiv C)$ bond is little affected by its environment, and that the value of 1.207 A is normal for acetylene and acetylene derivatives.

If there is a real difference in $r_0(C-Cl)$ for these two molecules, it is to be expected that the chlorine quadrupole coupling constant eqQ would be different.[3] However, the values of eqQ for the first three isotopic species in Table II are, within the experimental error, the same as eqQ for the analogous HCCCl species. For the fourth species the value of -63.12 published for $DCCCl^{37}$ does not agree with the corresponding value of -62.7 in Table II. But since no significant change in eqQ was observed when H_3CCCCl^{35}, H_3CCCCl^{37}, and $HCCCl^{35}$ were deuterated, the value of -63.12 Mc/sec for $DCCCl^{37}$ appears to be too large when compared with the value of -62.75 Mc/sec published for $HCCCl^{37}$.

In view of the above disagreement with both the $r_0(C\equiv C)$ and $r_0(C-Cl)$ bond lengths published for HCCCl, it might be worthwhile to obtain the spectra of some of the C^{13} isotopic species of this molecule, particularly since the four species so far observed are not sufficient to determine the structure if different $r_0(C-H)$ and $r_0(C-D)$ bond lengths are assumed.

TABLE V. Observed and calculated moments of inertia I_B.

Molecule	I_B (10^{-40} g cm^2) observed	I_B (10^{-40} g cm^2) calculated
H_3CCCCl^{35}	375.8913±0.0006	375.8913
$H_3CC^{13}CCl^{35}$	378.3686	378.3678
$H_3C^{13}CCCl^{35}$	387.7489	387.7484
H_3CCCCl^{37}	384.3327	384.3328
$H_3CC^{13}CCl^{37}$	386.9840	386.9847
$H_3C^{13}CCCl^{37}$	396.5712	396.5724
D_3CCCCl^{35}	424.0051	424.0049
$D_3CC^{13}CCl^{35}$	426.0202	426.0207
$D_3C^{13}CCCl^{35}$	434.8280	434.8290
D_3CCCCl^{37}	433.7601	433.7603

TABLE VI. Comparison of bond lengths in acetylene derivatives.

	$r_0(C-C)$	$r_0(C\equiv C)$	$r_0(C-Cl)$
H_3CCCCl	1.4584	1.2069	1.6371
H_3CCCH	1.4577	1.2073	
$HCCCl$		1.211	1.632
C_2H_2		1.207	

ACKNOWLEDGMENTS

The author would like to express his thanks to Dr. L. C. Leitch and his colleagues, who, after the original preparation of the light and fully deuterated methylchloroacetylene, prepared further samples so that the microwave spectrum could be investigated.

[11] G. Herzberg and B. P. Stoicheff, Nature **175**, 80 (1955).

Equation of State of Gases by Shock Wave Measurements. I. Experimental Method and the Hugoniot of Argon*

RUSSELL H. CHRISTIAN† AND FREDERICK L. YARGER
University of California, Los Alamos Scientific Laboratory, Los Alamos, New Mexico

(Received February 11, 1955)

An experimental method is described for the simultaneous measurement of the velocity of a plane shock through a gas and the associated particle velocity. Shocks are generated by a plate driven by a high-explosive system. The velocities are recorded by a high-speed rotating-mirror smear camera with a precision of about $\pm\frac{1}{2}\%$. Data are presented defining the Hugoniot of argon between 200 and 1100 Los Alamos atmospheres. These data are compared with the theoretically predicted Hugoniot.

INTRODUCTION

THESE papers consider the behavior of gases shocked from near standard conditions to states of extreme pressure, temperature, and particle velocity associated with high-explosive detonation. This paper describes the experimental technique employed in the measurement of the equation of state parameters behind strong shock waves and presents data defining the argon Hugoniot. The substantial agreement of this experimental curve with the theoretical prediction confirms the validity of the experimental procedure. Further papers in this series will describe the application of these experimental methods to other gases.

The experimental method determines points on the Hugoniot by measuring the shock and particle velocity associated with shocks of constant strength generated in the gas being studied. The pressure and compression associated with these points follow from the laws conserving mass and momentum through the shock front.

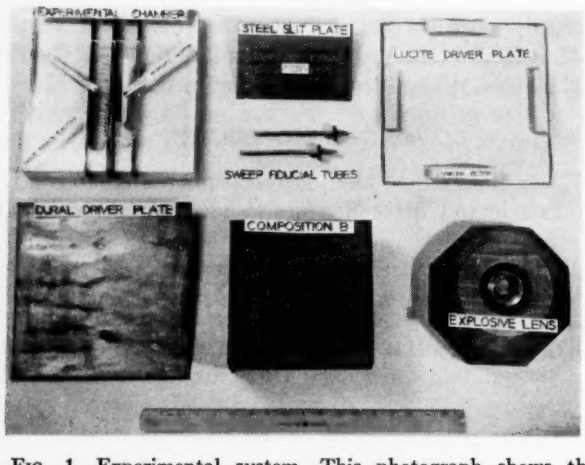

FIG. 1. Experimental system. This photograph shows the individual components of the experimental system. Masking tape has been placed over the wave trace grooves and the central cut in the free surface groove in order to make their locations more clear. The Lucite shim for the free surface groove is not shown.

EXPERIMENTATION

Data is obtained by using an experimental system, a field stand, and a rotating-mirror smear camera.

Figure 1 shows the individual components of the experimental system. The high explosive consists of a plane wave explosive lens which serves to detonate an 8 in. square 4 in. thick block of Composition B. The driver plate assembly consists of a 10 in.$\times$10 in. $\times\frac{1}{16}$ in. Dural plate in contact with the explosive, four spacer blocks $\frac{1}{2}$ in. thick, and a 10 in.$\times$10 in.$\times\frac{1}{8}$ in. Lucite plate. The experimental chamber is fabricated from a 10 in.$\times$10 in.$\times$1 in. Lucite block. The back, or driver plate, surface is machined with 3 wave trace grooves, a free surface wedge, and a step wedge. The 3 wave trace grooves are 10 mils deep, $\frac{1}{8}$ in. wide, and approximately 6 in. long. The 1 in. free surface wedge is cut into the block with a 1 in. end mill at an angle of approximately 10°, which is accurately measured later. A final 10 mil central cut is made with a $\frac{3}{8}$ in. end mill. A 5 mil thick, $\frac{1}{2}$ in. wide Lucite shim is placed in the bottom of the wedge. The stepped wedge is also milled with a 1 in. end mill and consists of 16 steps 1 mm deep and 1 cm wide. The step surfaces are polished; their depths are carefully measured. The experimental system is essentially completed with the addition of a $6\frac{1}{2}$ in. square, $\frac{1}{32}$ in. thick slit plate with five parallel slits 23 mils wide and $5\frac{1}{2}$ in. long. These slits are centered over the 3 wave trace grooves and the two wedges.

The experimental system mounted in its wooden field stand is shown in Fig. 2. The image of the setup in the film plane of the smear camera is shown in Fig. 3.

Briefly stated, the operation of the system is as follows: The explosive lens generates a plane detonation front in the high-explosive block. Ideally the explosive instantaneously accelerates the free surface of the metal driver plate to a constant velocity. Further discontinuous accelerations are received by this plate in traversing the gap defined by the spacers. Interaction with the Lucite driver plate ideally results in the instantaneous acceleration of the Lucite free surface

* Work done under the auspices of the U. S. Atomic Energy Commission. A version of this paper was presented at the Annual Meeting of the American Physical Society at New York in January, 1954.

† Now at the University of California Radiation Laboratory, Livermore, California.

to a constant velocity which is maintained throughout the interval of the experiment.

The 3 wave trace grooves are closed by the initial motion of the free surface of the Lucite driver plate in a time less than 10^{-7} second. In this operation the gas within the grooves becomes briefly (approximately 10^{-8} sec) and intensely luminous. This event is recorded on the camera record as three lines (see Fig. 3). The attitude of these lines serves to determine the shape of the "plane" free surface motion of the Lucite driver. The gas to be studied is contained in the stepped wedge. The free surface motion of the Lucite driver serves to generate a shock of constant strength in this gas. The velocity of this shock is determined by its arrival times at the steps. These times are recorded in the smear camera record by the increase in luminosity associated with the reflection of the shock from the

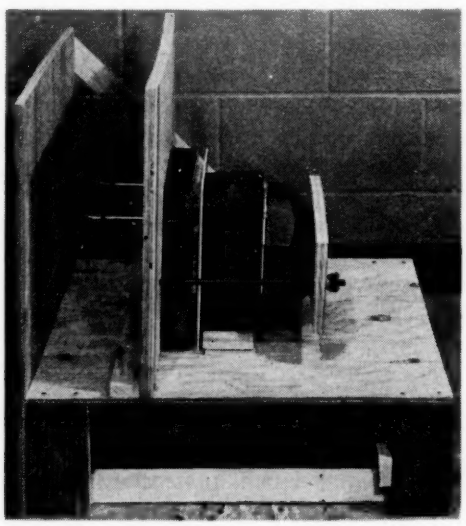

FIG. 2. A side view of the experimental system mounted in wooden field stand. A wooden brace has been omitted to better expose the system.

steps. Experiments have shown the luminosity to be sharply extinguished by the arrival of the Lucite driver free surface at the surface of the 16 steps. A measure of these times determines the Lucite driver free surface velocity, i.e., the gas particle velocity. This measurement is independently made by the light trace which records the closing of the gap in the free surface wedge by the Lucite driver. The independent measures of the particle velocity were required to agree within the 0.5% experimental error quoted for all velocities.

Several steps are taken to insure the correct interpretation of the film record. Marker tapes are placed on the slits to fix the space magnification on the film record. Two 6 in. long, $\frac{3}{16}$ in. i.d. aluminum sweep fiducial tubes are inserted in the front face of the experimental chamber. Luminous shocks generated in these tubes produce streaks on the film which accurately fix the camera sweep direction, i.e., time axis (see Figs. 1 and 3).

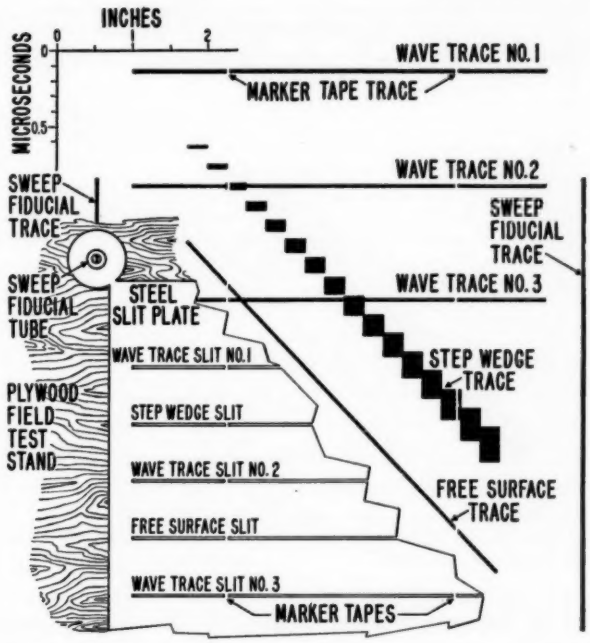

FIG. 3. Sweep camera image. In the lower left a cutaway section of a smear camera view of the experimental setup is shown. The corresponding record is constructed in the upper right. A cursory examination of the record gives a shock velocity of 8 mm/μsec, a free surface velocity of 7.2 mm/μsec.

The alignment of the experiment is not critical though some care is given to insure that the slit plate is perpendicular to the camera's line of sight, and that the slits are perpendicular to the direction of camera sweep.

With this system, particle velocities in the neighborhood of 8 mm/μsec are obtained. To attain lower velocities, the explosive or driver plate system is modified, e.g., the Lucite plate and spacer blocks can be removed, the dural driver plate thickened. Such changes are restricted by the requirement that free surface velocity must be constant for the initial 16 mm of motion.

It is of interest to consider whether or not a finite constant acceleration of the Lucite driver up to its measured final velocity could adversely affect the experiment. In this situation a compression wave would be generated in the gas which would develop into a shock front at a distance

$$x=\frac{C_0^2}{a}\left[\frac{2}{\gamma+1}\right]$$

from the initial position of the Lucite driver free surface. In this equation γ is the specific heat ratio, and C_0 is the sound speed in the undisturbed gas, and a is the acceleration of the surface. Realistic values of these constants for these experiments are $\gamma=1.67$, $C_0=0.330$ mm/μsec, and $a>1000$ mm/(μsec)^2; thus $x<10^{-4}$ mm. This result shows clearly that a possible finite accelera-

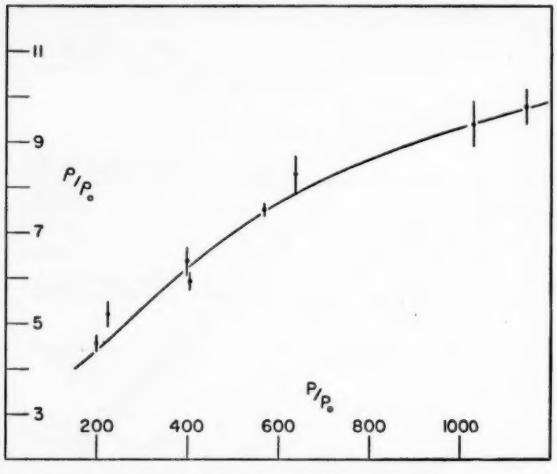

FIG. 4. This figure plots the experimental data along with a calculated Hugoniot. The initial conditions are $T_0=285°K$, $P_0=59.5$ cm Hg. The maximum error in ξ is $\pm 1\%$. The maximum error in η is as indicated.

tion of the free surface, instead of the discontinuous charge in velocity assumed, would not influence the experimental results.

THEORY

It is convenient to express both theoretical and experimental results in the pressure ratio, $\xi=p/p_0$, compression, $\eta=\rho/\rho_0$, plane. This transformation is made for measured values of the shock velocity U and the particle velocity u, through the equations conserving mass and momentum:

$$\eta=\frac{U}{U-u} \tag{1}$$

$$\xi=\frac{M}{RT_0}Uu+1 \tag{2}$$

where the 0 subscript denotes initial conditions.

In order to evaluate the experimental data it is desirable to refer all measurements to the same initial conditions, namely $T_0=285°K$ and $P_0=59.5$ cm Hg. Since this involves a small variation it is accomplished by an approximation which changes T_0 in Eq. (2) from the experimental temperature (see Table I) to 285°K. The correction for p_0 is small, of the second order, and is therefore neglected.

Unfortunately the $\pm 0.5\%$ maximum error in the velocities is sensitively exposed in the compression error. This result follows immediately from an error analysis of Eq. (1):

$$\frac{\delta\eta}{\eta}=(\eta-1)\left(-\frac{\delta U}{U}+\frac{\delta u}{u}\right). \tag{3}$$

Since the compressions caused by the strong shocks being considered are of the order of 10, the fractional error in the density ratio is an order of magnitude greater than that in the velocities. Fortunately, the uncertainty in the pressure ratio is of the same order as those in the velocities, as can easily be shown from Eq. (2).

$$\frac{\delta\xi}{\xi}=\frac{\delta U}{U}+\frac{\delta u}{u}. \tag{4}$$

TABLE I. Experimental data. The values of ξ and η are approximately corrected, as indicated in text, to an initial temperature of 285°K. The initial pressure and temperature at the time of each experiment are also listed.

Shock velocity U mm/μsec	Particle velocity U mm/μsec	Compression η	Pressure ratio ξ	p_0 (cm Hg)	T_0 (°K)
3.877	3.030	4.58±0.2	200	60.02	294
4.076	3.291	5.20±0.3	224	58.73	301
5.290	4.461	6.38±0.3	399	61.59	297
5.365	4.461	5.93±0.2	404	58.67	301
6.230	5.400	7.51±0.15	568	60.00	294
6.555	5.776	8.41±0.4	637	···	296
8.260	7.380	9.39±0.5	1029	59.92	288
8.700	7.810	9.78±0.4	1146	58.62	301

DISCUSSION

The experimental data is presented in Table I and Fig. 4. The theoretical Hugoniot shown in Fig. 4 was calculated by Bond[1] using the method employed by Bethe.[2] This calculation determines the equation of state for a plasma of argon atoms, singly charged argon ions, and electrons which is assumed to come to equilibrium at a negligible distance behind the shock front. The concentration of doubly charged ions is shown to be small and thus neglected. No consideration is given to the presence of electromagnetic radiation. The agreement between theory and experiment is within the accuracy of the experiment.

[1] J. W. Bond, Los Alamos Scientific Laboratory Publication LA-1693.
[2] H. A. Bethe, O.S.R.D. 469 (1942).

Equation of State of Gases by Shock Wave Measurements. II. The Dissociation Energy of Nitrogen*

R. H. CHRISTIAN,† R. E. DUFF, AND F. L. YARGER
University of California, Los Alamos Scientific Laboratory, Los Alamos, New Mexico

(Received February 11, 1955)

The results of equation of state measurements made behind strong shock waves in nitrogen are consistent only with the higher of the two spectroscopically acceptable values of the dissociation energy of nitrogen, 9.764 ev.

RECENT experimental results[1] indicate very strongly that the correct value of the dissociation energy for nitrogen is 9.764 ev and not 7.385 ev as was formerly assumed. In particular, the work of Hendrie practically proves the higher value to be the correct one. The first evidence not of spectroscopic origin that indicated that the higher of the two possible values of the dissociation energy was corrent was provided by Kistiakowsky, Knight, and Malin[1] in an investigation of the detonation velocity of cyanogen-oxygen mixtures. This work was criticized, however, because the conclusions drawn rested on the assumptions of the correctness of Chapman-Jouguet theory of the detonation process and the existence of thermodynamic equilibrium in a very complicated system of reacting gases. The present work was undertaken in an effort to circumvent these objections and to provide additional, independent evidence bearing on the question of the dissociation energy of nitrogen.

The experimental procedure whereby the pressure and density of a strongly shocked gas can be determined by measurements of shock and material velocity in the gas is described in detail in the first paper of this series.[2] Only a brief review of the method will be presented here.

The laws of conservation of mass and momentum applied to the flow through a shock wave lead to the following results:

$$\eta=\rho/\rho_0=\frac{U}{U-u} \tag{1}$$

$$\xi=\frac{p}{p_0}=1+\frac{1}{RT_0}uU \tag{2}$$

where ρ_0 and ρ are the initial and final values of density, p_0 and p are the initial and final values of pressure, T_0 is the initial temperature, R is the gas constant per gram, U is the shock velocity measured relative to the medium ahead of the shock, and u is the mass velocity change across the shock. It is clear that for a gas with given initial conditions, the simulanteous measurement of shock and material velocity is sufficient to determine the values of pressure and density attained behind the shock wave.

The experimental procedure consists of driving a metal plate at constant velocity by means of high explosive into a chamber of the gas under investigation. Shock velocity is determined by measuring the transit time of the shock over many known intervals. Material velocity is similarly determined by measuring the transit time of the metal plate over the same intervals.

SHOCK WAVE CALCULATIONS

In order to deduce information concerning the correct value of the dissociation energy of nitrogen from equation of state measurements, it was necessary to make calculations of the properties of shock waves in nitrogen over an extended range of shock strength for the two disputed values of the dissociation energy.

These calculations were made by a straightforward solution of the Hugoniot or conservation of energy equation written in the form

$$H-H_0=\tfrac{1}{2}(p-p_0)(v_0+v), \tag{3}$$

where p_0 and p, H_0 and H, and v_0 and v refer to initial and final values of the pressure, enthalpy, and volume, respectively. The fraction of the nitrogen originally present dissociated at a particular temperature and pressure is given by

$$\alpha=\left[\frac{K_p^2}{K_p^2+4p}\right]^{\frac{1}{2}}, \tag{4}$$

where K_p is the equilibrium constant for the reaction $\frac{1}{2}N_2\rightleftharpoons N$. The enthalpy of the mixture of atoms and molecules resulting from the partial dissociation of one mole of N_2 is

$$H=(1-\alpha)(H^0-H_0^0)_{N_2,T}+2\alpha(H^0-H_0^0)_{N,T}+2\alpha H_{0N}{}^0 \tag{5}$$

where $H^0-H_0^0$ is the enthalpy per mole of the component relative to an absolute zero reference state and

---

* Work done under the auspices of the U. S. Atomic Energy Commission.

† Now at the University of California Radiation Laboratory, Livermore, California.

[1] Kistiakowsky, Knight, and Malin, J. Am. Chem. Soc. **73**, 2972 (1951); J. Chem. Phys. **20**, 876 (1952); Thomas, Gaydon, and Brewer, J. Chem. Phys. **20**, 369 (1952); A. E. Douglas, Can. J. Phys. **30**, 302 (1952); J. M. Hendrie, J. Chem. Phys. **22**, 1503 (1954).

[2] R. H. Christian and F. L. Yarger, J. Chem. Phys. **23**, 2042 (1955), preceding paper.

TABLE I. Fit coefficients for thermodynamic functions for N_2 and N between 3000 and 12 000°K.

	a	b	c	d	k
N_2	2.51443	2.58314×10^{-4}	-2.84107×10^{-8}	1.24154×10^{-12}	2.74113
N	1.70375	-1.41798×10^{-4}	2.84705×10^{-8}	-1.17894×10^{-12}	3.06136

H_0^0 is the heat of formation per mole of the component at absolute zero, zero for nitrogen molecules and $\frac{1}{2}$ the dissociation energy for nitrogen atoms. The ideal gas equation of state is used to relate pressure, volume, and temperature.

$$pv=(1+\alpha)RT. \tag{6}$$

The calculational procedure was to assume a final temperature and iterate the Hugoniot equation until a value of pressure was found which satisfied all of the above equations. Shock velocity and material velocity behind the shock measured relative to a medium at rest were then calculated from the well-known relations.

$$U=v_0\left(\frac{p-p_0}{v_0-v}\right)^{\frac{1}{2}} \quad \text{and} \quad u=U\left(1-\frac{v}{v_0}\right). \tag{7}$$

These calculations were performed on an IBM card programmed calculator.

The thermodynamic functions for N_2 used were calculated by Fickett and Cowan,[3] those for N were calculated by one of the authors (R.E.D.) using the standard statistical mechanical procedure as outlined in Mayer and Mayer.[4] The four excited levels designated $^2D^0$ and $^2P^0$ were considered in this calculation. The values of $(E^0-E_0^0)/RT$ in the temperature range from 3000° to 12 000°K were fit by least-squares procedures to an expression of the form

$$(E^0-E_0^0)/RT=a+bT+cT^2+dT^3. \tag{8}$$

The entropy was obtained by integrating the second law of thermodynamics using the above expression to determine dE.

$$S^0/R=k+(a+1)\ln T+2bT+\tfrac{3}{2}cT^2+4/3dT^3, \tag{9}$$

where k is an integration constant chosen to give the best agreement with the statistical mechanical calculations. The equilibrium constant for the dissociation of nitrogen was calculated from the fundamental relation

$$RT\ln K_p=-\Delta F^0 \tag{10}$$

where F^0, the free energy, can be determined from the energy and entropy expressions given above.

$$(F-F_0^0)/RT=(a+1)(1-\ln T)-bT-\tfrac{1}{2}cT^2-\tfrac{1}{3}dT^3-k. \tag{11}$$

The values of the least-square constants used in these calculations are presented in Table I. The average deviation between the calculated value of energy and the value given by the least square cubic fit of the data is about 0.1%.

The results of the shock wave calculations are presented in Table II. Initial conditions are $T_0=25$°C and $p_0=58$ cm Hg (58 cm is used because this is approximately local atmospheric pressure). Since the thermodynamic fits are correct to 0.1%, the shock parameters are probably reliable to about the same degree. However, the partition function for diatomic molecules becomes slightly uncertain at high temperatures because the anharmonicity correction becomes large and also because there is uncertainty as to how to estimate the contribution from highly excited electronic levels. Any errors in the thermodynamic functions themselves arising from present limitations of the fundamental theory will of course cause corresponding errors in the shock wave parameters.

At 12 000°K the anharmonicity correction for N_2 contributes roughly 3% of the calculated value of the internal energy. The contribution from electronic excitation is about twice as large but the accuracy of the correction is certainly greater than for the anharmonicity. Therefore, if one can assume that these contributions are accurate to at least 25% the thermodynamic functions for nitrogen are good to about 1%. The shock wave parameters should be at least as accurate.

The calculations outlined above are correct at temperatures sufficiently low that no ionization occurs. However, at the highest temperatures assumed, a small amount of ionization should be expected. The effect of this ionization on the calculated equation of state point was estimated by using the Saha equation in the following form:

$$2\log\beta=5/2\log T-\frac{W}{2.303RT}-5.830-\log p_N, \tag{12}$$

where β is the fraction of the nitrogen atoms ionized and W is the ionization potential of nitrogen, and p_N is the pressure of nitrogen atoms. The statistical weight of the ground state of the atom was taken as 4 and that for the ion as 9. At 13 000°K $\beta=9.6\times10^{-3}$; thus slightly less than one percent of the nitrogen atoms are ionized. The ionization of nitrogen molecules was neglected because the ionization potential is higher and because the molecules constitute only 15% of the gas present at this temperature.

Under the assumption that the degree of dissociation would not be changed by this small amount of ioni-

[3] W. Fickett and R. D. Cowan, Los Alamos Scientific Laboratory Report, LA 1727.

[4] J. E. Mayer and M. G. Mayer, *Statistical Mechanics* (John Wiley & Sons, Inc., New York, 1940), p. 440.

TABLE II. Shock wave parameters in nitrogen for the two possible values of the dissociation energy of nitrogen. Initial conditions $T_0=25°C$ and $p_0=58$ cm.

	$D_{N_2}=9.764$ ev				$D_{N_2}=7.385$ ev			
$T°K$	p/p_0	ρ/ρ_0	α	U (mm/μsec)	p/p_0	ρ/ρ_0	α	U (mm/μsec)
3000	65.94	6.554	...	2.604	66.00	6.559	1×10^{-4}	2.605
4000	92.77	6.914	1×10^{-4}	3.081	94.58	7.027	3.2×10^{-3}	3.107
5000	121.3	7.219	1.7×10^{-3}	3.514	134.9	7.843	2.54×10^{-2}	3.685
6000	155.8	7.661	1.07×10^{-2}	3.969	202.9	9.218	9.35×10^{-2}	4.476
7000	205.7	8.435	3.88×10^{-2}	4.533	308.7	10.76	0.2223	5.478
8000	281.3	9.549	9.80×10^{-2}	5.263	448.4	11.93	0.4011	6.574
9000	389.1	10.79	0.1940	6.152	602.1	12.52	0.5934	7.603
10 000	528.2	11.90	0.3238	7.136	741.9	12.61	0.7542	8.438
11 000	688.2	12.66	0.4735	8.125	851.2	12.40	0.8614	9.046
12 000	849.7	13.02	0.6210	9.019	931.4	12.04	0.9226	9.475
13 000[a]	991.3	13.03	0.7449	9.742				
13 000[b]	1009.8	13.12	$\beta=9.6\times10^{-3}$	9.829				

[a] The thermodynamic fits are valid only to 12 000°K. This calculation was made by assuming the fits to be valid to 13 000°K. The answers are less reliable than those for lower temperatures.
[b] Ionization of nitrogen atoms considered. Degree of dissociation assumed unchanged by small amount of ionization.

zation, the pressure ratio behind the shock was determined from the Hugoniot equation.

$$\tfrac{1}{2}(p/p_0-1)\left[1+(1+\alpha+\beta)\frac{Tp_0}{T_0p}\right]$$
$$=\frac{H-H_0}{RT_0}+\beta\left(\frac{H^0-H_0^0}{RT_0}+\frac{W}{RT_0}\right)_{\text{electrons}}, \quad (13)$$

where $(H-H_0)/RT_0$ is the enthalpy difference for the atoms, ions, and molecules. The results of this calculation are presented in the last line of Table II. Clearly the correction for the small amount of ionization makes only a small change in the equation of state point at the highest temperature. The correction would decrease rapidly at lower temperature. (At 12 000°K only 0.5% of the nitrogen is ionized.)

EXPERIMENTAL RESULTS

The measured value of shock and material velocity for shock waves in nitrogen are presented in Table III. The corresponding values of pressure and density ratio calculated from Eqs. (1) and (2) are also included.

The experimental results are compared with the theoretical predictions in Fig. 1.

DISCUSSION

Before drawing the obvious conclusion from Fig. 1 that these results show conclusively the higher value of dissociation energy for nitrogen to be correct, the very important question of relaxation time for dissociation must be considered. The time duration of the experiments reported in this paper is very short. For instance, for a representative shock wave with a final temperature of 9000°K, the transit time of the shock wave across the shortest measuring interval is less than 0.2 μsec and across the longest interval it is only about 2.7 μsec. If thermodynamic equilibrium cannot be established in a time shorter than 0.2 μsec, then these results may be questioned.

Two kinetic mechanisms have been proposed which could lead to dissociation. The first considers dissociation to be the limit of vibrational excitation. If this proposal is correct, the theory of Landau and Teller[5] developed to explain the phenomenon of vibrational relaxation should be applicable. However, there are good reasons to believe this theory to be much too restrictive because the conditions existing behind a strong shock wave are quite different from those found in an ultrasonic wave. In particular, the energy of many of the collisions is very large compared to a vibrational quantum. Since the vibrational degree of freedom can be adequately approximated by a harmonic oscillator only for the lowest levels, imposition of the quantum mechanical restriction that the only allowed transitions are between neighboring states is unrealistic in this case. Furthermore, if the relaxation time is calculated on the basis of this theory, it is found to be so long that equilibrium could not be established in a time comparable to the time scale of these experiments. If dissociation comes about as the limit of a process of vibrational excitation, relaxation time effects should have been evident in this investigation.

TABLE III. Measured shock and material velocity and the corresponding density and pressure ratios, approximately corrected[a] to an initial temperature of 298°K. The maximum error in velocity measurement is ~0.5%. The initial pressure and temperature at the time of each experiment are also listed.

U (mm/μsec)	u (mm/μsec)	$\xi=p/p_0$	$\eta=\rho/\rho_0$	P_0 (cm Hg)	T_0 (°K)
4.34	3.80	187	8.0±0.2	60.81	305
5.02	4.46	254	9.0±0.1	59.69	293
5.55	4.97	313	9.6±0.4	60.91	292
5.96	5.39	364	10.5±0.3	59.41	293
6.10	5.51	381	10.3±0.4	60.94	297
7.18	6.55	533	11.4±0.6	60.91	297
7.57	6.97	598	12.6±0.6	61.09	283
9.61	8.90	968	13.5±0.5	60.91	288
9.71	8.98	987	13.3±0.8	60.66	298
9.74	8.99	991	13.0±0.3	60.94	300

[5] L. Landau and E. Teller, Physik. Z. Sowjetunion **10**, 34 (1936).

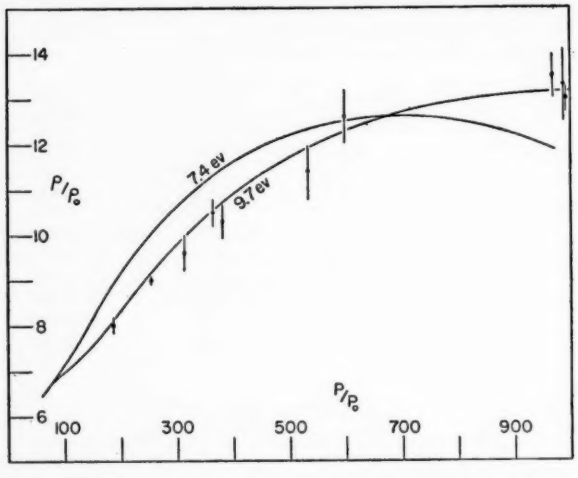

FIG. 1. This figure plots the experimental data along with the calculated Hugoniots. The initial conditions are $T_0=298°K$, $P_0=58$ cm Hg. The maximum error in ξ is $\pm 1\%$. The error in η is given for each experimental point.

An alternative and more realistic mechanism is one in which some large fraction of all molecular collisions with sufficient energy are assumed to cause dissociation. The number of collisions per unit volume and time with energy greater than E_0 is[6]

$$\omega=2n^2\sigma^2\left(\frac{\pi kT}{m}\right)^{\frac{1}{2}}(X_0^2+1)\exp(-X_0^2), \qquad (14)$$

where $X_0^2=(E_0/kT)$, n is the number of molecules per unit volume, σ is the molecular radius, and m is the molecular mass. An order of magnitude estimate of the time required to produce the degree of dissociation α calculated for a given final temperature is: $t=(\alpha n/\omega)$. This estimate assumes every collision with sufficient energy produces dissociation and it also neglects recombination. This latter assumption is reasonable because the three body collisions which can lead to recombination will be relatively rare until the equilibrium situation is approached. On the other hand the above expression also neglects the contribution to the dissociation rate from dissociations caused by multiple collisions.

Calculations using this relation based on a final shock wave temperature of 9000°K indicate that dissociative equilibrium should be attained in 1.4×10^{-7} second if the reaction proceeds isothermally at the equilibrium temperature and in 4.7×10^{-10} second if at the temperature of 18 000°K found behind the shock before dissociation occurs. Since the temperature behind the shock changes from 18 000°K to 9000°K as the reaction proceeds, a time intermediate between 1.4×10^{-7} second and 4.7×10^{-10} second should be required to produce dissociative equilibrium. Such a time would be short compared to the time scale of the experiments and no relaxation effects should have been observed.

The velocity of the metal plate used as a piston in these experiments is determined by its thickness and the amount and type of explosive used. It is not influenced appreciably by the atmosphere in front of it; and in particular it is not influenced by changes in shock pressure caused by the relaxation process. Therefore, the particle velocity behind the shock will be constant. As the relaxation process proceeds, temperature, density and pressure behind the shock change, and the change will be manifested by a change of shock velocity. As an example, for our representative 9000°K shock wave the initial shock velocity should be 6.69 mm/μsec. As equilibrium is approached the velocity will drop to its final value of 6.15 mm/μsec. This represents a change of almost 9% in shock velocity—a change which would have been easily observed if it had occurred. In no instance was any variation in shock velocity observed. Therefore, the relaxation time must have been small compared to the time scale of the experiment.

A weak argument can be made that all results at pressure ratios of less than 675 may be questionable since they could represent nonequilibrium final states. The idea is that the density ratio immediately behind the shock is slightly less than 6 (the value for shock waves of infinite strength in a gas with $\gamma=1.40$). As the relaxation process proceeds, the density ratio increases at almost constant pressure. However, the rate of increase decreases as equilibrium is approached. Therefore, the results which indicate final density ratios in agreement with predictions based on D_{N_2} of 9.764 ev are not conclusive since the equilibrium state could still correspond to values consistent with the $D_{N_2}=7.385$ ev curve. The observation of constant shock velocity is simply dismissed by saying that the reaction rate for the last part of the relaxation process is so slow that the velocity change is too small to be observed over the time interval in which the measurements are made.

This rather dubious argument fails completely to explain the results at pressure ratios in excess of 675. In fact these results are excellent evidence that the relaxation time is very short. This conclusion is based on the fact that the degree of dissociation is a monotone function along the Hugoniot curve. Therefore, all partial reaction Hugoniots corresponding to fixed degrees of dissociation must lie below the equilibrium Hugoniot; and it is impossible for a density ratio corresponding to incomplete reaction to exceed the equilibrium ratio. In other words the density change behind a shock wave caused by a relaxation process is monotone in time. Thus a final density ratio greater than that predicted by the 7.385 ev curve is very good evidence that the dissociation energy is greater than 7.385 ev.

[6] S. Chapman and T. G. Cowling, *The Mathematical Theory on Nonuniform Gases* (Cambridge University Press, London, 1952), p. 92.

CONCLUSIONS

The results of equation of state measurements behind strong shock waves in nitrogen show conclusively that the dissociation energy of nitrogen is the higher of the two spectroscopically acceptable values. Furthermore the kinetic mechanism leading to dissociation is probably not the step-by-step excitation of the vibrational degree of freedom. This investigation provides another illustration of how shock waves can be used to investigate physical chemical problems at very high temperatures.

ACKNOWLEDGMENTS

The authors are happy to acknowledge the encouragement and assistance of Professor G. B. Kistiakowsky and R. G. Shreffler in various phases of this work.

THE JOURNAL OF CHEMICAL PHYSICS VOLUME 23, NUMBER 11 NOVEMBER, 1955

The System Ozone-Oxygen*

A. C. JENKINS, F. S. DIPAOLO, AND C. M. BIRDSALL
Laboratory of Linde Air Products Company, A Division of Union Carbide and Carbon Corporation, Tonawanda, New York
(Received February 11, 1955)

At temperatures below −180°C liquid ozone and liquid oxygen are not miscible in all proportions. Two liquid phases occur over a definite range in composition which depends upon the temperature. The solubility diagram at saturation pressures has been determined experimentally by measuring vapor pressure *versus* composition isotherms at −183.0°C, −185.7°C, and −195.6°C. The upper or oxygen-rich liquid phase has been analyzed at −181.9°C, −182.9°C, −186.0°C, and −195.6°C. The critical solution temperature is −179.9°C±0.5°C. A liquid-vapor equilibrium diagram at one atmosphere total pressure has also been determined experimentally.

I. INTRODUCTION

A SURVEY of the literature reveals very few data on the physical properties of liquid ozone-oxygen mixtures. Many of the data which do appear are in error. For example, Schwab[1] reported the critical solution temperature for liquid ozone-oxygen mixtures as −158°C, while the correct value is about −180°C. Recently Schumacher[2] published a solubility diagram and a one-atmosphere temperature-composition diagram which were apparently both in error, as pointed out by Jenkins and Birdsall.[3]

At temperatures below −180°C, liquid ozone and liquid oxygen are not miscible in all proportions. Two liquid phases ("conjugate solutions"[4]) occur over a definite composition range which depends upon the temperature. The upper liquid phase is oxygen-rich and the lower phase is ozone-rich. The limits of solubility of ozone in liquid oxygen have now been accurately established experimentally by determining vapor pressure versus composition isotherms at −183.0°C, −185.7°C, and −195.6°C. Since the vapor pressure of the two-liquid-phase region is constant at constant temperature when there is equilibrium between the phases, regardless of how much of each phase is present, the breaks in these isotherms establish the limits of the two-liquid-phase region. In addition, the upper or oxygen-rich phase has been analyzed at −181.9, −182.9, −186.0, and −195.7°C by the iodometric method.[5] Once the limits of solubility had thus been established at several temperatures, the solubility diagram at saturation pressures could be constructed and the critical solution temperature and composition[6] determined.

The liquid-vapor equilibrium diagram for one atmosphere total pressure has also been determined experimentally.

II. PREPARATION AND PURIFICATION OF OZONE

The general method for the preparation and purification of liquid ozone has been described in a previous paper.[7] In the current work a specially redistilled supply of high purity (99.995%) oxygen was used to prepare ozone; this made the use of a purification train unnecessary. Stopcocks were lubricated with a mixture of "Fluorolube" LG, supplied by the Hooker Electrochemical Company, and colloidal silica.

III. VAPOR PRESSURE ISOTHERMS

The vapor pressure isotherms, Fig. 1, were determined by two methods, the "oxygen-removal" method and the "oxygen-addition" method. In the the oxygen-removal

* This work was performed under Contract NOa(s)-10945 for the Bureau of Aeronautics, United States Navy Department.
[1] G. M. Schwab, Z. Physik. Chem. **110**, 599–625 (1924).
[2] H. J. Schumacher, J. Chem. Phys. **21**, 1610–1611 (1953).
[3] A. C. Jenkins and C. M. Birdsall, J. Chem. Phys. **22**, 1779 (1954).
[4] Findlay, Campbell, and Smith, *The Phase Rule and Its Applications* (Dover Publications, New York, 1955), ninth edition, p. 93.
[5] Birdsall, Jenkins, and Spadinger, Anal. Chem. **24**, 662 (1952).
[6] See reference 4, p. 94.
[7] A. C. Jenkins and C. M. Birdsall, J. Chem. Phys. **20**, 1158–1161 (1952).

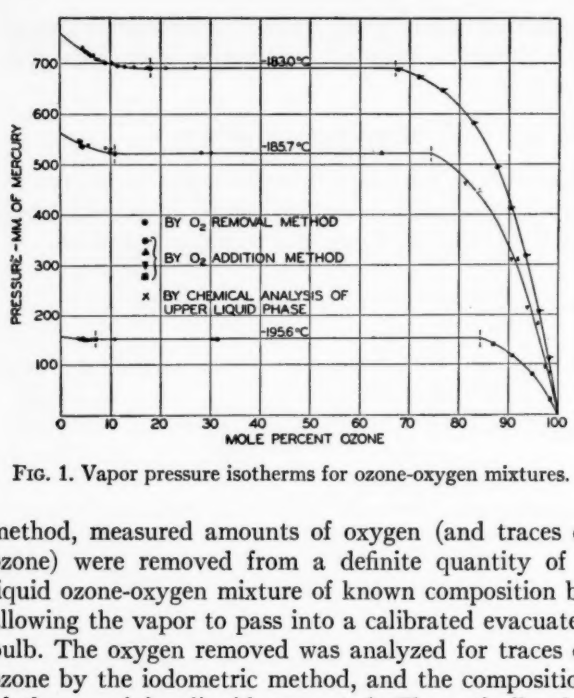

FIG. 1. Vapor pressure isotherms for ozone-oxygen mixtures.

method, measured amounts of oxygen (and traces of ozone) were removed from a definite quantity of a liquid ozone-oxygen mixture of known composition by allowing the vapor to pass into a calibrated evacuated bulb. The oxygen removed was analyzed for traces of ozone by the iodometric method, and the composition of the remaining liquid computed. Theoretically this method should give a perfect material balance, but in practice the material balance was usually in error by 1 or 2%. This had an appreciable effect only on the high-ozone portions of the curves; these were therefore determined by reversing the procedure and adding measured volumes of oxygen to the liquid, starting with a definite quantity of pure (100%) liquid ozone.

Description of Oxygen-Removal Method

Referring to the flow diagram, Fig. 2, the gaseous ozone-oxygen mixture containing 3 to 4 mole-% ozone was allowed to pass into the 12-liter calibrated bulb, which was enclosed in an insulated box, and out through a catalyst chamber in which all the ozone was decomposed. After an hour or more, the mixture leaving the bulb was analyzed. When two successive analyses showed a constant composition the flow was stopped, the pressure in the 12-liter bulb measured by means of

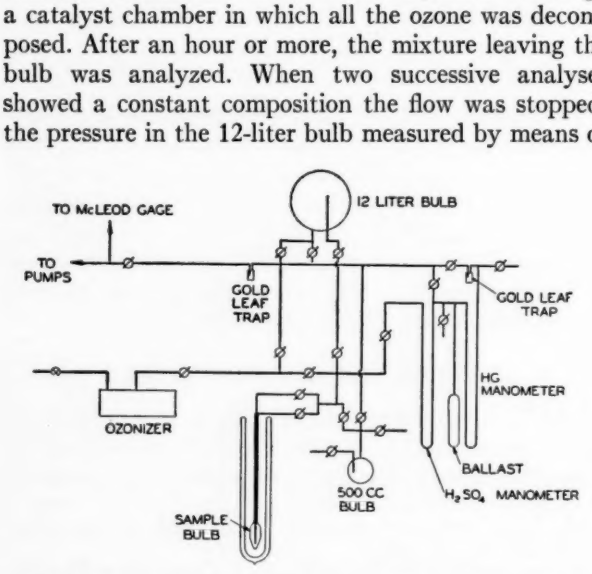

FIG. 2. Flow diagram of vapor pressure isotherm apparatus.

the sulfuric acid and mercury manometers, and the temperature of the bulb recorded. (Since ozone reacts with mercury, the pressure could not be measured directly with the mercury manometer.) The 12-liter bulb was then closed off and the rest of the system evacuated. Following this, a liquid nitrogen bath (for the −195.6°C isotherm) was placed around the sample bulb, the sample bulb was connected to the 12-liter bulb, and most of the ozone-oxygen mixture was allowed to condense into the sample bulb. The stopcocks leading to the sample bulb were then closed and the pressure, temperature, and ozone concentration of the gas left in the 12-liter bulb were measured. (The ozone concentration was determined by taking a sample in the evacuated 500-cc bulb, which was immersed in a water bath, measuring the pressure and temperature of the sample, and then purging it with oxygen through a spiral absorption vessel containing the KI solution.)

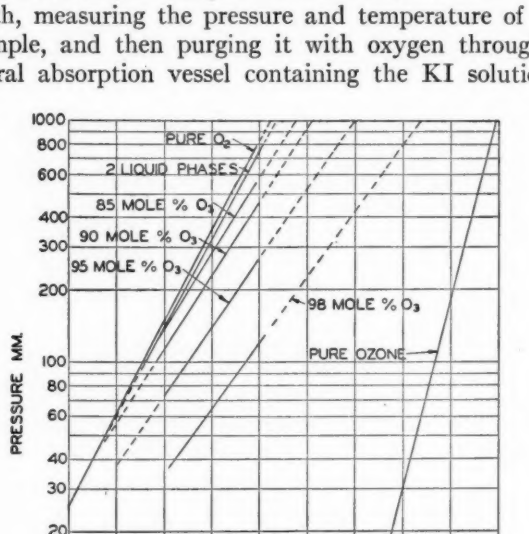

FIG. 3. Vapor pressures of ozone-oxygen mixtures.

The analyses of the residual gas showed an ozone concentration 0.1 mole-% less than that of the original gas mixture. On the assumption that this decrease was due to ozone decomposition, the mean value of the two analyses was used to compute the composition of the liquid. Corrections were made for gas left in the connecting tubing and for the vapor phase in the sample bulb.

After determining the ozone concentration in the starting liquid by the method described above, the vapor pressure above the sample was measured to give the first point on the isotherm. The sample bulb was then opened to the calibrated 500-cc bulb and the stepwise removal of oxygen begun. During each step the pressure in the calibrated bulb was allowed to approach the vapor pressure of the solution. The stopcock between the bulbs was then closed and the pressure, temperature, and ozone concentration of the gas in the

500-cc bulb determined. After equilibrium was established in the sample bulb, the vapor pressure of the remaining liquid, each time with a higher ozone content, was carefully measured on the manometers with a cathetometer. This step-wise removal of oxygen was repeated until the liquid reached a high-ozone concentration. Since the ozone content of the vapor was always very low and remained constant till near the end, it was not necessary to analyze each increment of vapor removed.

For the −183.0°C and −185.7°C isotherms the liquid nitrogen bath was replaced by liquid oxygen and liquid argon, respectively. In each case the bath was stirred by bubbling through it gas of the same composition as the liquid. Temperatures were measured with an accuracy of ±0.1°C using calibrated copper-constantan thermocouples.

Description of Oxygen-Addition Method

In the "oxygen-addition" method the quantity of the pure ozone to which oxygen was added was determined by following the same general procedure described above, except that in this case, as a matter of convenience, oxygen was removed from the starting mixture by means of the 12-liter bulb instead of the 500-cc bulb until pure 100% liquid ozone was left in the sample bulb. Oxygen was then added in increments from the 500-cc calibrated bulb. To insure equilibrium, the additions were made by bubbling the oxygen slowly through the liquid ozone by means of a small bore tube terminating at the bottom of the sample bulb beneath the surface of the liquid. Correction was made in each case for the oxygen in the vapor phase.

TABLE I. Total vapor pressure (O_2+O_3) over liquid ozone-oxygen mixtures at −183.0°C average temperature.

Point No.	Temp. °C	Pressure, mm of Hg	Mole-% ozone Liquid	Vapor
		Oxygen-removal method		
1	−183.1	731.2	4.68	...
2	−183.1	725.3	4.94	0.04
3	−183.1	722.5	5.21	0.03
4	−183.0	719.7	5.52	0.03
5	−183.0	718.2	5.85	0.02
6	−182.9	716.0	6.23	0.02
7	−183.0	714.9	6.65	0.02
8	−183.2	708.2	7.16	0.03
9	−183.1	707.1	7.74	0.01
10	−183.1	702.3	8.81	0.02
11	−183.1	700.6	9.21	0.01
12	−183.1	699.9	10.2	0.01
13	−183.1	694.1	11.4	0.02
14	−183.1	693.0	12.9	0.01
15	−183.1	692.6	14.8	0.03
16	−183.0	690.8	17.5	0.02
17	−182.8	690.1[a]	21.2[b]	0.02
18	−182.9	690.0[a]	27.1[b]	0.02
19	−182.8	687.5[a]	37.4[b]	0.02
20	−182.9	688.9[a]	60.1[b]	0.02
		Oxygen-addition method		
1	−182.9	0.1	100	
2	−182.9	111.8	98.2	
3	−182.9	206.0	96.2	
4	−182.9	318.5	93.6	
5	−182.9	413.0	90.4	
6	−182.9	494.0	87.7	
7	−182.9	582.0	82.8	
8	−182.9	647.2	76.6	
9	−182.9	671.0	71.8	
10	−182.9	688.0	67.7	

[a] Two-liquid-phase region.
[b] Over-all composition of the two liquid phases.

TABLE II. Total vapor pressure (O_2+O_3) over liquid ozone-oxygen mixtures at −185.7°C average temperature.

Point No.	Temp. °C	Pressure, mm of Hg	Mole-% ozone Liquid	Vapor
		Run I Oxygen-removal method		
1	−185.8	536.3	4.10	
2	−185.8	534.6	4.28	<0.01
3	−185.7	531.7	9.02	
4	−185.7	528.7	9.93	<0.01
5	−185.7	523.6[a]	28.2[b]	
		Oxygen-addition method		
1	−185.7	0.1	100	
2	−185.7	83.8	98.4	
3	−185.7	181.8	96.0	
4	−185.7	309.3	91.8	
5	−185.7	444.9	84.1	
6	−185.7	522.0[a]	64.4[b]	
		Run II Oxygen-removal method		
1	−185.7	547.6	3.82	<0.01
2	−185.7	547.0	4.00	
3	−185.7	539.5	5.61	
4	−185.8	523.2[a]	30.3[b]	
		Oxygen-addition method		
1	−185.7	0.1	100	
2	−185.7	94.2	97.6	
3	−185.7	215.0	94.0	
4	−185.7	310.8	90.7	
5	−185.7	463.0	81.4	

[a] Two-liquid-phase region.
[b] Over-all composition of the two liquid phases.

Discussion of the Two Methods

The oxygen-removal method is accurate for the low-ozone section of the curves, i.e., up to where the two-liquid-phase region starts, but it can lead to inaccuracies in the high-ozone part of the curve. Since the oxygen content of the high concentration liquid ozone sample is determined by the difference between the original oxygen present and the sum of the increments of oxygen removed, and since the quantity of oxygen removed is very large compared with the quantity of oxygen left in the high-concentration ozone, calculation of the composition of this ozone-rich solution depends upon a small difference between the two large volumes of oxygen, and undesirable situation. On the other hand,

TABLE III. Total vapor pressure (O_2+O_3) over liquid ozone-oxygen mixtures at −195.6°C average temperature.

Point No.	Temp. °C	Pressure, mm of Hg	Mole-% ozone Liquid	Vapor
		Oxygen-removal method		
1	−195.6	152.7	3.62	
2	−195.6	153.3	3.70	
3	−195.6	152.6	3.79	
4	−195.6	152.5	3.89	
5	−195.6	152.8	3.99	<0.01
6	−195.7	152.9	4.10	<0.01
7	−195.6	152.5	4.21	
8	−195.6	152.7	4.33	<0.01
9	−195.7	152.8	4.45	
10	−195.7	150.8	4.59	
11	−195.7	150.6	4.72	
12	−195.7	150.5	4.87	
13	−195.7	150.5	5.03	
14	−195.7	150.4	5.20	
15	−195.6	151.1	5.38	
16	−195.6	151.3	5.57	
17	−195.6	150.8	5.78	
18	−195.6	150.9	6.01	
19	−195.6	151.1	6.24	
20	−195.7	151.0[a]	10.8[b]	<0.01
21	−195.7	152.0[a]	30.6[b]	
		Oxygen-addition method		
1	−195.6	<0.1	100	
2	−195.6	32.1	98.4	
3	−195.6	80.1	94.8	
4	−195.6	116.8	90.8	
5	−195.6	140.9	86.9	
6	−195.6	151.9[a]	31.4[b]	

[a] Two-liquid-phase region.
[b] Over-all composition of the two liquid phases.

in the oxygen-addition method the small quantities of oxygen added can be determined accurately. A slight error in the quantity of ozone will produce only a negligible error in the calculated liquid composition. In the two-liquid-phase region, small errors in total composition are less important, since the vapor pressure of this region is constant at constant temperature. Two separate runs were made at −185.7°C. The agreement between the two sets of data indicates a precision of about ±0.5 mole-% in composition in the range of 75 to 100 mole-% ozone. The consistency of the data is indicated by the straight lines produced when the high-ozone range portions of the three curves are plotted on a $\log_{10}P$ *vs* $1/T$ basis for constant compositions, as shown in Fig. 3. The experimental data are given in Tables I, II, and III.

TABLE IV. Analyses of oxygen-rich phase of the two-liquid-phase system.

Temp. °C	Average composition[a] of O_2-rich phase, Mole-% O_3	Average pressure mm Hg	No. of analyses
−181.9	21.4±0.3	769	7
−182.9	17.9±1.5	692	9
−186.0	10.8±0.2	520	4
−195.7	6.9±0.2	151	7

[a] Deviations in compositions are the average deviations from the mean value.

IV. ANALYSES OF THE UPPER LIQUID PHASE

Each vapor pressure isotherm, Fig. 1, shows a sharp break at the ozone-rich end of the two-liquid-phase region. The composition at the point where the break occurs corresponds to the composition of the lower or ozone-rich phase of the two-liquid-phase system. Likewise the break at the oxygen-rich end of the isotherm gives the composition of the upper or oxygen-rich liquid phase. However, the breaks are less definite at the oxygen-rich end, and for this reason chemical analyses were made of the upper phase at several temperatures by the iodometric method.[5] The apparatus was essentially the same as that shown in Fig. 2. The sample bulb was attached by glass spirals so that it could be shaken to mix thoroughly the liquid ozone-oxygen mixture. (For the −181.9°C point a pressurized cryostat was used to obtain temperatures above the normal boiling point of liquid oxygen, and in this case the sample bulb was provided with a magnetic stirrer.)

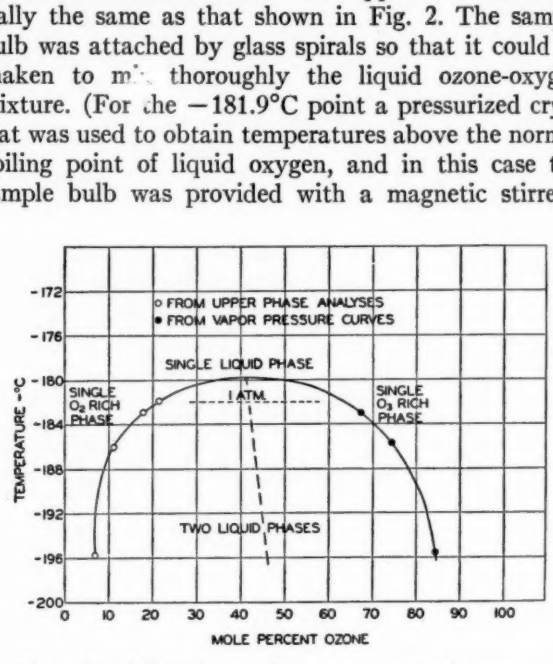

FIG. 4. Solubility diagram for ozone-oxygen mixtures at saturation pressures.

Following the mixing of the sample, the two liquid phases were allowed to separate and come to equilibrium. The two liquid phases were observed visually, and their presence was confirmed by vapor pressure measurements. Samples of the upper phase were withdrawn through a 0.5-mm diameter capillary and vaporized in a calibrated 500-cc bulb which had been previously evacuated. After the pressure and temperature of the sample were measured, the sample was diluted with oxygen and the bulb flushed with oxygen through a spiral absorption vessel containing the KI solution. The experimental data are given in Table IV. These data, together with the lower-liquid-phase compositions from the vapor pressure isotherms, were used to construct the solubility diagram at saturation pressures, Fig. 4. The critical solution temperature as shown by the diagram is −179.9°C. There is a possible uncertainty of ±0.5°C in this value, which depends upon the curvature of the top of the "dome." The boundaries of the two-liquid-phase region at various temperatures

are given in Table V. Application of the "law of the rectilinear diameter"[8] to the data leads to a "consolute"[6] ozone concentration of 41.2 mole-% at the critical solution temperature.

V. THE LIQUID-VAPOR COMPOSITION DIAGRAM FOR OZONE-OXYGEN MIXTURES AT ONE ATMOSPHERE TOTAL PRESSURE

The one-atmosphere diagram, shown in Fig. 5, was determined by essentially the same method as that used to determine the vapor pressure isotherms. The sample bulb in this case was enclosed in a 6-lb copper block, Fig. 6, which had four $\frac{3}{8}$-in. diameter copper rods attached to the bottom. These rods were immersed in liquid nitrogen to provide cooling by conduction. The temperature of the block was controlled by an external heating coil. The thermocouple was enclosed in a spiral glass well in the sample vessel, with its junction in the liquid. The block was controlled at the temperature which corresponded to a vapor pressure of one atmosphere. Samples of the vapor phase were withdrawn, their volumes were measured in a calibrated burette

TABLE V. Interpolated compositions at the boundary of the two-liquid-phase region in the liquid system ozone-oxygen.

Temperature (°C)	Mole-% ozone	
	Upper phase	Lower phase
−182 (1 atmos)	21.1	63.5
−183	17.6	67.2
−184	15.0	70.4
−186	10.8	75.0
−188	8.8	78.2
−190	7.7	80.6
−192	7.0	82.5
−194	6.8	83.7
−195.7	6.9	84.3

over distilled water (with suitable corrections for water vapor), and analyzed by the iodometric method. The composition of the liquid was computed for each point from the original volume and composition, and from the volumes and compositions of the sample removed. Corrections for the vapor phase were made from the vapor composition curve. One series of measurements was also made by the oxygen-addition method to obtain points on the liquid curve between 70 and 100 mole-% ozone. The experimental data are given in Table VI. It will be noted that the vapor phase analyses are somewhat erratic for points 1 to 14 inclusive. This is believed to be caused by the tendency of small quantities of more concentrated ozone to adhere to the walls of the vessel above the liquid surface. The correct vapor composition is 0.03 mole-% (Points 15 and 19) which is consistent with vapor pressure data at −183°C (Table I)).

The most difficult part of the diagram in Fig. 5 to establish accurately is the portion of the liquid 2 curve between 98 and 100 mole-% ozone, because of the large

[8] See reference 4, p. 95.

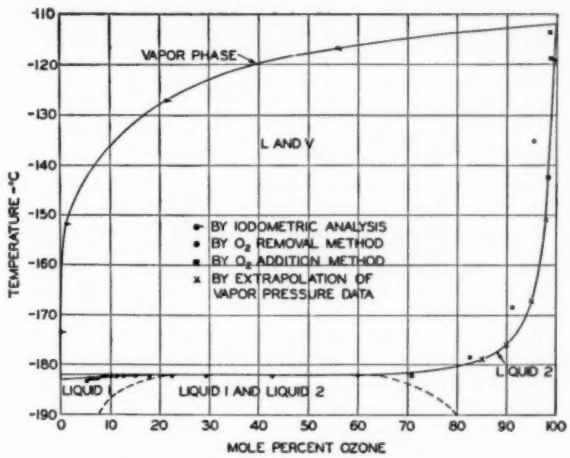

FIG. 5. Liquid-vapor composition diagram for ozone-oxygen mixtures at one atmosphere pressure.

correction for ozone in the vapor phase. It will be noted that the vapor composition is changing very rapidly in this region. Since the vapor composition curve was used to determine vapor phase corrections, the consistency of the liquid composition points in this range, determined by the oxygen-addition method, serves to confirm the accuracy of the vapor curve. Another means of establishing the liquid 2 curve is provided by the vapor pressure data (Fig. 3). Extrapolation of these data to 760-mm pressure (Table VII) is believed to be the most reliable method for determining this part of the diagram, particularly since the 98 mole-% curve is consistent with the data obtained by the oxygen-addition method.

The broken lines below the liquid line define the

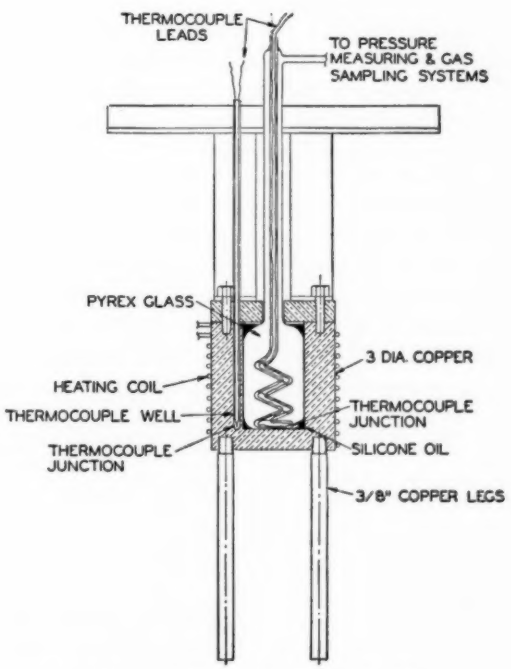

FIG. 6. Apparatus for determining liquid-vapor compositions at one atmosphere.

TABLE VI. Experimental data for liquid and vapor compositions of ozone-oxygen mixtures at one atmosphere total pressure. Oxygen-removal method.

Point No.	Vapor phase Mean temp. °C	Vapor phase Mole-% O_3	Liquid phase Temp. °C	Liquid phase Mole-% O_3
1	−183.1	0.08	−183.4	5.27
2	−183.2	0.21	−183.1	5.55
3	−183.0	0.39	−182.8	5.86
4	−182.9	0.19	−182.9	6.23
5	−182.9	0.12	−182.8	6.65
6	−182.9	0.16	−182.9	7.12
7	−182.9	0.15	−182.8	7.68
8	−182.7	0.11	−182.5	8.33
9	−182.5	0.07	−182.5	9.10
10	−182.5	0.07	−182.5	10.0
11	−182.5	0.07	−182.5	11.2
12	−182.5	0.13	−182.5	12.7
13	−182.5	0.08	−182.4	15.1
14	−182.4	0.12	−182.4	18.0
15	−182.4	0.03	−182.3	22.5[a]
16	−182.4	0.04	−182.4	29.5[a]
17	−182.3	0.04	−182.3	42.9[a]
18	−182.3	0.05	−182.2	59.9[a]
19	−178.5	0.03	−178.6	82.6
20	−173.5	0.12	−168.4	91.2
21	−151.8	1.09	−135.1	95.7
22	−127.2	21.44	−119.2	99.8
23	−116.8	55.94	−114.4	100.8
24			−112.0	

Point No.	Oxygen-addition method Temperature °C	Mole-% ozone Liquid phase
1	−111.9	100
2	−113.5	98.7
3	−118.8	98.9
4	−142.3	98.5
5	−182.2	71.0

[a] Over-all composition of the two liquid phases.

boundaries of the two-liquid phase region. Here the vapor pressure is less than one atmosphere. The intersections of these broken lines with the liquid line define the boundaries of the two-liquid-phase region at one atmosphere total vapor pressure.

The methods used in this work avoid the necessity of analyzing ozone-oxygen mixtures of high-ozone concentration, which can lead to errors because of decomposition. It is of interest to note that Schumacher's[9] data for the upper or oxygen-rich phase compositions are in good agreement with our data. (He obtained 18 mole-% ozone at −183°C where we obtained 17.6 mole-%.) His compositions of the lower or ozone-rich phase, however, are lower than ours by as much as 20 mole-% ozone, as are his data for the liquid curve in his one-atmosphere temperature-composition diagram. It may have been errors in his analysis of ozone-rich mixtures plus errors in temperature measurements which led him to assume that there was a maximum in the one-atmosphere diagram at −105.4°C, where both the liquid and vapor compositions were about 87 mole-% ozone.

[9] H. J. Schumacher, Anales asoc. quím. argentina **41**, 208–229 (1953).

TABLE VII. Vapor pressure data extrapolated to 760 mm.

Two liquid phases	− 182.0°C
85 mole-% O_3	− 179.1°C
90 mole-% O_3	− 176.0°C
95 mole-% O_3	− 167.1°C
98 mole-% O_3	− 150.9°C

Apparently Schumacher[2] made no measurements in the two-liquid-phase region at one atmosphere, but assumed that the liquid line was above the critical solution temperature. As a result, his one-atmosphere diagram is in error. The fact that there is no azeotropic maximum in the one-atmosphere diagram can be demonstrated by allowing an ozone-oxygen mixture to evaporate freely at atmospheric pressure, and recording its boiling temperature.[3] The boiling point remains constant in the two-liquid-phase region and then rises to −111.9°C, the boiling point of pure ozone.

Vapor pressures of pure oxygen used in this work were taken from the NBS–NACA Tables of the Thermal Properties of Gases.[10]

ACKNOWLEDGMENTS

This work was carried out under the general direction of Gerhard A. Cook, to whom the authors wish to extend thanks for guidance and helpful suggestions.

Consultations with Professor J. A. Beattie of the Massachusetts Institute of Technology during the course of the work are gratefully acknowledged.

Note added in proof.—After this paper was accepted for publication, an article entitled, "Phase Diagram of Liquid Ozone-Oxygen System," by Brown, Berger, and Hersh appeared [J. Chem. Phys. **23**, 1340 (1955)]. Qualitatively, the results given in the two papers are in good agreement. However, their vapor-composition curve at 1 atmos was calculated from vapor pressure data for pure O_3, and their liquid composition curve was based partly upon extrapolated vapor pressure data, whereas our diagram was constructed directly from experimental data.

[10] Harold J. Hoge, Table 9.50 "Vapor Pressure of Oxygen," in NBS–NACA Tables of Thermal Properties of Gases (1949).

THE JOURNAL OF CHEMICAL PHYSICS VOLUME 23, NUMBER 11 NOVEMBER, 1955

Regularities in the Absorption Spectra of Halides

LEONARD I. KATZIN
Argonne National Laboratory, Lemont, Illinois
(Received January 11, 1954)

Original absorption spectra of halides and a large body of literature absorption spectrum data are assembled. Certain characteristic features are pointed out which can be ascribed to transitions of electrons localized on the halide portion of a molecule or ion, such that their removal to an excited condition essentially leaves a neutral halogen atom as part of the excited state configuration. Recognition of this portion of the spectrum should assist understanding of halide spectra.

INTRODUCTION

THE basis for the modern understanding of the absorption spectra of gaseous metal halides was laid with the studies of James Franck and his students in the period 1925–1930, and this contribution is well reviewed in a paper by Rabinowitch.[1] An extension to aqueous solutions of ionized salts was made by Franck and Scheibe.[2] The crucial point in the analyses is the identification of the spectra as due to transfer of an electron from the halide to the companion metal atom or to water.[2,3] Only with the aqueous solution has there been apparent a practical basis for the estimation of the wavelength at which the absorption peak is to be expected.[2,3]

A very considerable body of empirical data on the absorption spectra of compounds containing halogen is now available. With the possible exception of molecular compounds between halogen and electron donor molecules, the spectra are generally treated on a whole-molecule basis. The author's interest in the general problem was aroused through observations of spectra in organic solvents[4,5] of what are generally considered to be ionic salts. It was found that in some cases the absorption spectrum of the anion group was very greatly modified. More specifically, the absorption spectrum of halide ions was shifted by cations such as Co(II) and Ni(II), so that even chloride peaks appeared at 40 or more millimicrons longer wavelengths, while at the same time the characteristically altered spectrum of the "complexed" metal ion was observed in the visible part of the spectrum. This suggested that one might often be able to distinguish portions of spectrum due to the halide and due to the companion groups in absorption spectra, and that the modifications found in the two portions of the spectrum could be used to learn more about the nature of the interaction between the component atoms of the molecule or radical. It is known that the modifications appearing in the absorption spectrum of a cation with complexing are often largely independent of the specific complexing group. The finding that the modifications induced in the iodide ion absorption spectrum were rather closely the same when the agents involved were, respectively, Co(II), Ni(II), and I_2, made further investigation promising. This investigation took the form of further spectral observations of our own, and to a larger extent, search of the literature on the spectra of halides for peaks which could with reasonable certainty be ascribed to the halide component.

HALIDE SPECTRA

The definitive basis for assigning a given portion of an absorption spectrum to a halide component is that used, for example, by Franck and Scheibe.[2] The halogen *atom* spectrum has a pair of levels, $^2P_{\frac{3}{2}}-{}^2P_{\frac{1}{2}}$ with a characteristic spacing: 7600 cm^{-1} for iodine, 3700 and 880 cm^{-1} for bromine and chlorine, respectively. The absorption spectrum of iodide ion shows two intense peaks with about this spacing, and the interpretation[2,3] is that an electron is removed from the ion, leaving the iodine atom in the ground ($^2P_{\frac{3}{2}}$) state, or in the excited ($^2P_{\frac{1}{2}}$) state. These absorptions are photochemically active both in solution and in the case of salt vapors. Therefore, when any iodide or bromide shows a pair of peaks with approximately the required spacing, the presumption is that one is seeing an absorption of that member of the compound, the transition being such that in the upper state an electron has been transferred from the halide to another member of the system.

The peak difference for the chloride is too small for resolution in most systems, and even with the bromide and iodide, one frequently finds apparent single peaks. With the bromide, in fact, this seems to be the more common form. In part this may be due to the lower-wavelength peak coming at wavelengths out of reach of the investigator's equipment, or because the investigator's observations were concentrated on the longer-wavelength peak. In some instances, one of the peaks is very much more intense than the second, making the latter hard or impossible to detect. Where the distinctive peak separation is not available as criterion, origination of intense new peaks where the companion atom does not normally show them is used as criterion, together with such cross-checks as can be made to eliminate peaks due to the companion atom. Support

[1] E. Rabinowitch, Revs. Modern Phys. **14**, 112 (1942).
[2] J. Franck and G. Scheibe, Z. physik. Chem. **A139**, 22 (1928).
[3] R. Platzman and J. Franck, *Z. Farkas Memorial Volume* (Research Council of Israel, Jerusalem, 1952), Special Publication No. 1.
[4] L. I. Katzin, J. Chem. Phys. **18**, 789 (1950).
[5] L. I. Katzin, J. Chem. Phys. **20**, 1165 (1952).

TABLE I. Halide absorption peaks of halogen-containing compounds.

Substance	Peak mμ	References	Peak separation cm⁻¹
A: Chlorides			
HCl (gas)	153.5	(2)	
NaCl (*c*)	158.1; <160	(32) (33)	
NaCl (vap.)	243	(34) (35)	
KCl (*c*)	161.6; 162.5	(32) (33)	
KCl (vap.)	248	(34)	
CsCl (*c*)	163	(33)	
CsCl (vap.)	247	(34) (36)	
RbCl (*c*)	167	(33)	
RbCl (vap.)	249	(34)	
LiCl (vap.)	243	(34)	
Cl^- (aq.)	181; <185; *ca* 188	(39) (5) (9)	
$CHCl_3$ (*t*-BuOH)	≷210	(1a)	
CCl_4 (*t*-BuOH)	≷210	(1a)	
$CdCl_2$ (aq. KCl)	187.5; <200	(46) (9)	
$HgCl_2$ (aq.)	200	(10)	
$HgCl_2$ (*t*-BuOH)	218	(1a)	
$HgCl_2$ (aq. KCl)	228.5	(10)	
AgCl (aq. K, NaCl)	216	(8)	
AgCl (subl. film)	250	(7)	
$NiCl_2$ (*t*-BuOH)	217	(1a)	
$SnCl_4$ (*t*-BuOH)	217	(1a)	
Cl_3^- (aq.)	227; 233	(1b) (9)	
ICl_2^- (acetonitril)	227	(31)	
$Co(NH_3)_5Cl^{++}$ (aq.)	274, 227	(4)	
$CoCl^+$ (*i*-PrOH)	228	(1b)	
$PbCl^+$ (aq.)	227	(9)	
$PbCl_2$ (aq. LiCl)	272	(9)	
$PbCl_2$ (vap.)	364, 325, 267	(22)	
TlCl (aq. Na, KCL)	242	(9)	
$SnCl_2$ (vap.)	243	(17)	
B: Bromides			
HBr (gas)	178.5	(2) (38)	
Br^- (alc.)	<186	(11)	
Br^- (aq.)	186	(11) (5)	
LiBr (*c*)	185, 172.5	(33)	4000
CsBr (*c*)	186.5, 174	(33)	3850
CsBr (vap.)	275, 254	(34) (36)	3020
KBr (*c*)	187.5, 173	(33)	4450
KBr (vap.)	276, 254	(34)	3160
NaBr (*c*)	190, 174	(33)	4850
NaBr (vap.)	274, 251; 272, 252	(34) (35)	3300; 2940
RbBr (*c*)	192, 178	(33)	4100
RbBr (vap.)	279, 258; 280, 257	(34) (35)	2950; 3200
CH_3CH_2Br (*t*-BuOH)	220(?), <210	(1a)	
H_3CBr (gas)	<205	(45)	
HCF_2Br (gas)	<205	(45)	
CF_3Br (gas)	208–9	(45)	
CF_2Br_2 (gas)	225–7	(45)	
$HCBr_3$ (*t*-BuOH)	224	(1a)	
CBr_4 (*t*-BuOH)	228	(1a)	
$CdBr_2$ (alc.)	211; 213, 192	(13) (11)	5000
$CdBr_2$ (aq. KBr)	217; 215.5	(9) (46)	
AgBr (aq. K, NaBr)	227	(8)	
$NiBr_2$ (*i*-PrOH)	227–8	(1b)	
$HgBr_2$ (aq.)	226; *ca* 232	(10) (13)	
$HgBr_2$ (vap.)	227, 210	(15)	3550
$HgBr_2$ (alc.)	234	(10)	
$HgBr_2$ (aq. K, NaBr)	249	(10)	
$PbBr^+$ (aq.)	235, *ca* 203	(9)	*ca* 6700
$PbBr_2$ (aq. K, NaBr)	304, 224	(9)	11 700
$PbBr_2$ (vap.)	414, 308, (247)	(22)	8350
$SnBr_4$ (hexane)	*ca* 235	(44)	
Br_3^- (alc.)	256–8	(12)	
Br_3^- (aq.)	265	(1b) (9) (12)	
$ClBr_2^-$ (aq. KBr)	260	(12)	
$ClBr_2^-$ (alc.)	266	(12)	
TlBr (aq. K, NaBr)	263	(9)	
$CoBr_2$ (*i*-PrOH)	266, 242	(1b)	3700
$BiBr_3$ (vap.)	(322.5), 266	(16)	
$TlBr_3$ (MeOH)	267	(37)	
FBr_2^- (?) (Br_2 on CaF_2(*c*))	267, 252	(43)	2230
α-$(CH_3)_2TeBr_2$ (alc.)	*ca* 270	(19)	
β-$(CH_3)_2TeBr_2$ (alc.)	*ca* 275	(19)	
$Co(NH_3)_5Br^{++}$ (aq.)	313, 253	(4)	7500
C: Iodides			
HI (gas)	215; 222	(2) (38)	
I^- (aq.)	225, 192; 227; 225, 192; 226, 193	(5) (6) (11) (13) (8)	7700
KI (*c*)	219, 187.5	(33)	7700
KI (alc.)	219; 217	(6) (11)	
KI (vap.)	324.2	(34)	
CsI (*c*)	219, (206) 185	(33)	8350
CsI (vap.)	324, 258	(36)	8000
LiI (*c*)	221, 185	(33)	8800
RbI (*c*)	222.5, 185.5	(33)	9000
RbI (vap.)	324.2, 258	(34) (36)	8000
NaI (*c*)	229.5, 187.5	(33)	9750
NaI (vap.)	324.2, 258	(34) (35) (36)	8000
ZnI_2 (alc.)	217, 189; 216	(11) (13)	7000
ZnI_2 (aq. KI)	238.5	(46)	
ZnI_2 (vap.)	238, 224.5	(22)	2500
CdI_2 (MeOH)	239	(13)	
CdI_2 (EtOH)	238, 192; 243, 192	(11) (13)	10 000–10 800
CdI_2 (PrOH, acetonitrile)	240–242	(13)	
CdI_2 (aq. KI)	256.5, 216; 240	(46) (9)	7300
CdI_2 (vap.)	261, 220	(15)	7200
HgI_2 (aq.)	265	(10)	
HgI_2 (vap.)	266, 224; 268, 224	(14) (15)	7200
HgI_2 (MeOH)	267	(3)	
HgI_2 (EtOH)	272; 270, 213; 274, 213	(10) (11) (13)	10 000–10 500
HgI_2 (*t*-BuOH; $CHCl_3$; CCl_4)	275	(1a)	
HgI_2 (aq. KI)	323–4, 267	(10)	6450
RH_2CI(EtOH)	255	(42) (11) (27) (28)	
RH_2CI (CCl_4)	257–260	(24)	
RH_2CI (pet. ether)	257.5	(42)	
RH_2CI (vap.)	257–8; 290	(42) (25)	
R_1R_2HCI (alc.)	260	(42)	
R_1R_2HCI (pet. ether)	260	(42)	
$(CH_3)_3CI$ (alc.)	268	(42)	
$(CH_3)_3CI$ (pet. ether)	270	(42)	
$EtMe_2CI$ (alc.)	265.5	(42)	
$EtMe_2CI$ (pet. ether)	267	(42)	
RHCFI (pet. ether)	261–3	(42)	
RCF_2I (vap, pet. ether)	269–70	(42)	
CF_3I (vap.)	267.5	(42)	
RHCCII (pet. ether)	277.5	(42)	
RCFCII (pet. ether)	283–292	(42)	
CCl_3I (pet. ether)	324	(42)	
CBr_3I (pet. ether)	346	(42)	
H_2CI_2 (alc.)	291, 247; 293; 288; 296	(42) (27) (28) (29)	6120

[1a] This paper.
[1b] L. I. Katzin, J. Chem. Phys. **20**, 1165 (1952).
[2] J. Romand and B. Vodar, Compt. rend. **226**, 238, 890 (1948).
[3] H. Ley, Z. angew. Chem. **41**, 845 (1928).
[4] M. Linhard and M. Weigel, Z. anorg. u. allgem. Chem. **266**, 49 (1951).
[5] J. Franck and G. Scheibe, Z. physik. Chem. **A139**, 22 (1928).
[6] Scheibe, Römer, and Rössler, Ber. deut. chem. Ges. **59**, 1321 (1926).
[7] K. V. Shalimova and A. V. Belkina, Zhur. Eksptl. i Teort. Fiz. **21**, 326 (1951).
[8] H. Fromherz and W. Menschick, Z. physik. Chem. **B3**, 1 (1929).
[9] H. Fromherz and Kun-Hou Lih, Z. physik. Chem. **153**, 321 (1931).
[10] H. Fromherz and Kun-Hou Lih, Z. physik. Chem. **167**, 103 (1933).
[11] G. Scheibe, Z. Elektrochem. **34**, 497 (1928).
[12] Gilbert, Goldstein, and Lowry, J. Chem. Soc. **1931**, 1092.
[13] E. Lederle, Z. physik. Chem. **B10**, 121 (1930).
[14] K. Wieland, Z. physik **76**, 801 (1932).
[15] K. Butkow, Z. physik **71**, 678 (1931).
[16] K. Butkow, Z. physik **90**, 810 (1934).
[17] K. Butkow, Physik. Z. Sowjetunion **5**, 906 (1934).
[18] K. V. Butkow, J. Exptl. Theoret. Phys. (U.S.S.R.) **9**, 561 (1939).
[19] Lowry, Goldstein, and Gilbert, J. Chem. Soc. **1928**, 307.
[20] J. Franck and H. Kuhn, Z. Physik **43**, 161 (1927).
[21] J. H. de Boer, Z. physik. Chem. **B14**, 149 (1931).
[22] K. Butkow, Physik. Z. Sowjetunion **4**, 577 (1933).
[23] J. H. de Boer and J. F. H. Custers, Z. physik. Chem. **B21**, 208 (1933).
[24] C. B. Alsopp, Proc. Roy. Soc. (London) **A158**, 167 (1937).
[25] T. Iredale, Z. physik. Chem. **B20**, 340 (1933).
[26] Durie, Iredale, and Jarvis, J. Chem. Soc. **1950**, 1181.
[27] Crymble, Stewart, and Wright, Ber. deut. Chem. Ges. **43**, 1183 (1910).
[28] Massol and Faucon, Compt. rend. **164**, 813 (1917).
[29] T. M. Lowry and R. R. Sass, J. Chem. Soc. **1926**, 622.
[30] A. D. Awtrey and R. E. Connick, J. Am. Chem. Soc. **73**, 1842 (1951).
[31] A. I. Popov and J. N. Jessup, J. Am. Chem. Soc. **74**, 6127 (1952).
[32] A. H. Pfund, Phys. Rev. **32**, 39 (1928).
[33] R. Hilsch and R. W. Pohl, Z. Physik **59**, 812 (1930).
[34] L. A. Müller, Ann. Physik (4) **82**, 39 (1927).
[35] Franck, Kuhn, and Rollefson, Z. Physik **43**, 155 (1927).
[36] H. D. Schmitt-Ott, Z. Physik **69**, 724 (1931).
[37] A. J. Berry and T. M. Lowry, J. Chem. Soc. **1928**, 1748.
[38] C. F. Goodeve and A. W. C. Taylor, Proc. Roy. Soc. (London) **A152**, 221 (1935); **A154**, 181 (1936).
[39] E. Rabinowitsch, Revs. Modern Phys. **14**, 112 (1942).
[40] F. L. Gilbert and T. M. Lowry, J. Chem. Soc. **1928**, 3179.
[41] F. L. Gilbert and T. M. Lowry, J. Chem. Soc. **1928**, 2658.
[42] R. N. Haszeldine, J. Chem. Soc. **1953**, 1764.
[43] J. F. H. Custers and J. H. de Boer, Physica **1**, 265 (1934).
[44] M. I. Grant, Trans. Faraday Soc. **31**, 433 (1935).
[45] N. Davidson, J. Amer. Chem. Soc. **73**, 467 (1951).
[46] E. Doehlemann and H. Fromherz, Z. physik. Chem. **171A**, 353 (1934).

TABLE I.—*Continued.*

Substance	Peak mμ	References	Peak separation cm^{-1}
C: Iodides—*Continued.*			
H_2CI_2 (pet. ether)	291.5, 248	(42)	6010
HCI_3 (vap.)	345, 294	(25)	5000
HCI_3 (alc.)	349, 296; 339, 290; 335, 288; 345, 294	(24) (27) (28) (19) (29)	5000
HCI_3 (CCl_4)	351, 306.5	(24)	4100
HCI_3 (CCl_4+1%CS_2)	349, 298.5	(24)	4950
CI_4 (alc.)	345, 238	(28)	5700
CI_4 (CCl_4)	386, 304	(24)	7000
ICH_2COO^- (aq.)	260, 224	(26)	6200
ICH_2COOH (aq., pH 1)	268	(26)	
ICH_2COOH (hexane)	271	(26)	
ICH_2COOH (alc.)	273, 224	(26)	8000
ICH_2COOH (pet. ether)	279	(42)	
ClI_2^- (aq. KCl)	247	(1b)	
BrI_2^- (aq. KBr)	260; 275	(1b) (12)	
I_3^- (aq. KI)	352, 288	(1, 30, 9, 12)	6300–6500
KI_3 (alc.)	355, 290	(19, 27, 29)	6300
I_3^- (alc., t-BuOH)	360, 290	(1a, 12)	6700
AgI (aq. KI)	252	(8)	
AgI (vap.)	317	(20)	
$Cr(NH_3)_5I^{++}$	291	(4)	
PbI^+ (aq.)	264	(9)	
PbI_2 (dil. KI)	308 (??), 272	(9)	
PbI_2 (aq. K, NaI)	364, 308(?), 272	(9)	
PbI_2 (vap.)	519, 400, 288, 238	(22)	
α-Et_2TeI_2 (*cyc*-hexane)	335, 270	(40)	7100
β-Et_2TeI_2 (*cyc*-hexane)	335, 267	(40)	7600
α-Et_2TeI_4 (*cyc*-hexane)	335, 263	(40)	8100
α-$MeTeI_2$ (*cyc*-hexane)	340, 268	(40)	7900
α-Me_2TeI_2 (alc.)	357, 284	(41)	7200
β-Me_2TeI_2 (*cyc*-hexane)	336, 264	(40)	8150
β-Me_2TeI_2 (alc.)	366, 290	(19)	7200
$C_5H_{10}TeI_2$ (alc.)	338, 270	(41)	7450
$C_5H_{10}TeI_4$ (alc.)	356, 288	(41)	6600
$(C_5H_{10})_3TeI_8$ (alc.)	356, 290	(41)	6400
α-Me_2TeI_4 (alc.)	361, 290	(19)	6800
SbI_3 (Et_2O)	342, 276	(18)	6950
SbI_3 (vap.)	343, 277	(16) (18)	6900
SbI_3 (alc.)	357, 292	(24) (18)	6200
SbI_3 (t-BuOH)	360, 290	(1a)	6500
SbI_3 ($CHCl_3$)	365, 285	(1a)	7700
SbI_3 (CCl_4+1%CS_2)	385, 315	(24)	5800
AsI_3 (alc.)	356, 294	(24)	5900
AsI_3 (vap.)	384, 276	(18)	10 200
BiI_3 (alc.)	356, 294	(24)	5900
BiI_3 (vap.)	415, (338.6) 281	(16)	
SnI_4 (t-BuOH)	360, 290	(1a)	6700
SnI_4 ($CHCl_3$)	365, 285	(1a)	7700
SnI_4 (hexane)	365, 285	(44)	7700
CH_3SnI_3 (alc.)	360, 291	(24)	6600
FI_2^-(?) (I_2 on CaF_2(c))	350, 285	(23)	6550
FI_2^-(?) (I_2 on BaF_2(c))	360, 280	(21)	7900
CoI^+ (i-PrOH)	350, 290	(1b)	6000
CoI_2 (i-PrOH)	360, 295	(1b)	6100
NiI^+ (i-PrOH)	360, 295	(1b)	6100
NiI_2 (i-PrOH)	358, 292	(1b)	6300
TlI (aq. KI)	357, 300	(9)	5300
TlI_3 (MeOH)	400, 255	(37)	14 200
$Co(NH_3)_5I^{++}$ (aq.)	383, 287	(4)	8800

for the assignments may be obtained when the several halides of the same companion atom can be compared. In the case of the mixed polyhalide anions, assignments may be made on the chemical criterion that the ions are considered formed of the interhalogen of the lightest and of the heaviest halogen atoms present, and the remaining halide ion.

The findings of measurements of our own (Fig. 1), and of a literature search for absorption spectra of halides (not claimed to be complete), are summarized in Table I, and in Fig. 2. The values tabulated are the longest-wavelength peak or pair of peaks ascribable to the halide. Only the former is plotted in Fig. 2. Data on the different spectra of a given compound are brought together, and in general, data on a given group of the

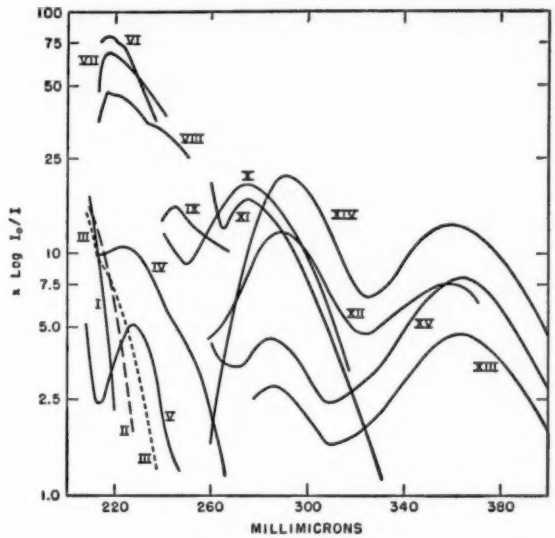

FIG. 1. Absorption spectra of halides ($\log I_0/I$ multiplied by arbitrary factor for plotting). Solvent is t-butyl alcohol unless otherwise noted. I—$CHCl_3$; II—CCl_4; III—CH_3CH_2Br; IV—$CHBr_3$; V—CBr_4; VI—$HgCl_2$; VII—$SnCl_4$; VIII—$NiCl_2$; IX—$SnBr_4$ in $CHCl_3$; X—HgI_2; XI—HgI_2 in $CHCl_3$, CCl_4; XII—SbI_3; XIII—SbI_3 in $CHCl_3$; XIV—SnI_4; XV—SnI_4 in $CHCl_3$.

periodic table are to be found together. The order within the groups and between groups has been based simply on the wavelength of the longest wavelength peaks. Intensity data are omitted. They are not available for a large fraction of the cases, and they are too often a function of conditions. For example, in our measurements with antimony triiodide and stannic tetraiodide, the relative peak heights varied with the solvent. In t-butyl alcohol, the intensity ratio of the approximately 360 and 290 millimicron peaks were about 1:1.6, whereas in chloroform or carbon tetrachloride the peaks approximated 365 and 285 millimicrons, with an intensity ratio 1.82:1, a reversal of the relative heights. Similar reports on SbI_3 in carbon disulfide, and iodoform, HCI_3, between ethanol and CCl_4+I%CS_2 (Table I, reference 24) can be found. In general, the value of logϵ for the more intense peak of a pair lies between 3.5 and 4.5. The value is somewhat less than this for complexes with Co(II) and Ni(II), and seems to be lowest for the monohalogenated organic compounds.

DISCUSSION

Coincidences in iodide absorption spectra similar to those that originally attracted our attention have been noticed by others (e.g., references 9, 24, 27, 29 of Table I) but have apparently not led to further work. The primary purpose of this paper is to bring to general attention the fact that there is a large body of absorption spectra showing characteristic features which can be ascribed to transitions of electrons localized on the halide portion of a molecule or ion, such that their removal to an excited condition essentially leaves a

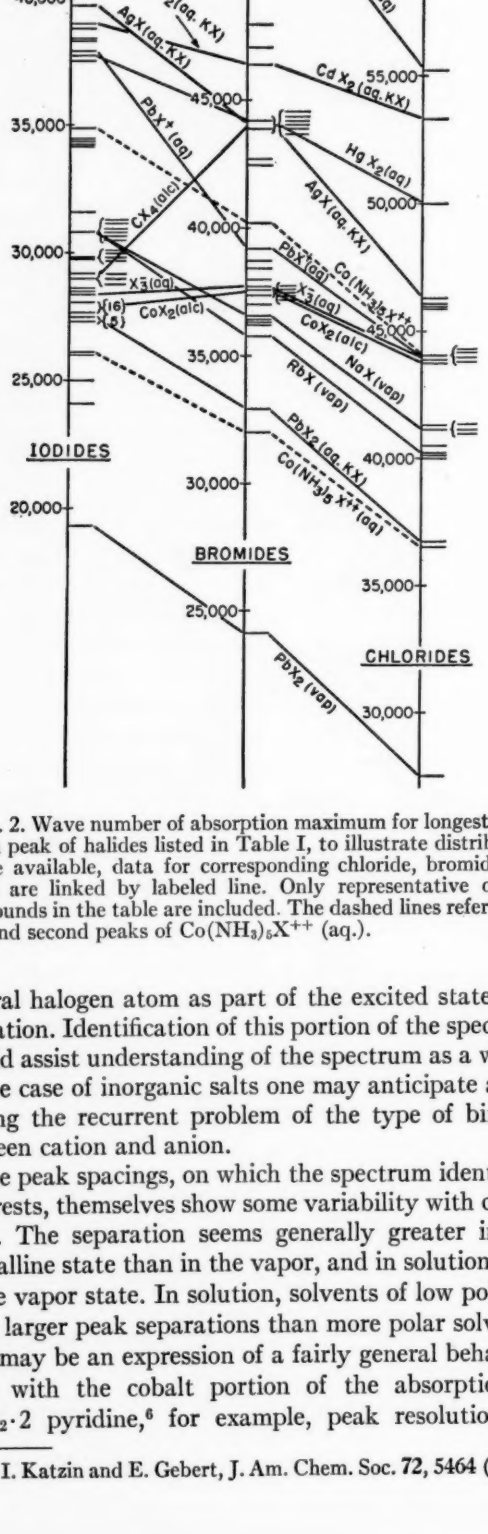

FIG. 2. Wave number of absorption maximum for longest wavelength peak of halides listed in Table I, to illustrate distribution. Where available, data for corresponding chloride, bromide, and iodide are linked by labeled line. Only representative organic compounds in the table are included. The dashed lines refer to the first and second peaks of $Co(NH_3)_5X^{++}$ (aq.).

neutral halogen atom as part of the excited state configuration. Identification of this portion of the spectrum should assist understanding of the spectrum as a whole. In the case of inorganic salts one may anticipate aid in solving the recurrent problem of the type of binding between cation and anion.

The peak spacings, on which the spectrum identification rests, themselves show some variability with conditions. The separation seems generally greater in the crystalline state than in the vapor, and in solution than in the vapor state. In solution, solvents of low polarity show larger peak separations than more polar solvents. This may be an expression of a fairly general behavior, since with the cobalt portion of the absorption of $CoCl_2 \cdot 2$ pyridine,[6] for example, peak resolution diminishes through the solvent series, benzene, chloroform, acetone, isopropanol. The wavelength relations of a given substance with medium seem to be closely dependent on the valence electron configuration—e.g., the behavior of the zinc-cadmium-mercury group as contrasted with the alkali metals. One regularity is that in all cases the lowest wavelength absorption is represented by the gaseous hydrogen halide, with the crystalline alkali metal halides close behind. Of significance would seem to be the fact that although the absorption peaks of aqueous iodide and aqueous bromide fall closely with those of the crystalline alkali halides, the absorption peak of aqueous chloride falls unmistakably at lower energy than that of the crystalline alkali chlorides. One also notices, in progressing from chloride through bromide to iodide spectra, that the apparent ease of production of the larger spectral alterations increases markedly. This suggests an important role of the polarizability of the halide ion in the shift.

The carbon iodides furnish a series of varied structures which might help throw some light on the influences determining the absorption properties of the carbon-halogen bond, and this might furnish some carry-over to the metal-halogen situations. The largest coherent body of data on these compounds is due to Haszeldine (Table reference 42). Primary alkyl iodides all absorb at about the same wavelength, 256 millimicrons (where the conditions are of relevance, reference is to petroleum ether solution). A secondary iodide such as isopropyl iodide shows its peak shifted a few millimicrons to longer wavelengths, and fluoroiodides, of the general formula RCHFI, show a similar shift. The suggestion of a fluoride-methyl equivalence seems to be borne out at the next step, since another shift to about 270 millimicrons is shown by $(CH_3)_3$ CI which is just matched by RCF_2I. A single chloro group has a much greater effect than two methyls or fluoros, as RCHClI absorbs at 279 mμ. Introduction of a fluoro group (RCFClI) makes the R—F—Cl combination equivalent to a single iodide (CH_2I_2 absorbs at the same wavelength). Three chloro groups (CCl_3I) move the absorption peak to 324 mμ, whereas three bromos (CBr_3I) give the same absorption peak wavelength as CHI_3 and CI_4. In the bromide series, the absorption peak of gaseous CHF_2Br, like CH_3Br, is below 205 mμ, CF_3Br absorbs at about 208 mμ, and CF_2Br_2 at 226 mμ. Alcoholic bromoform and carbon tetrabromide absorb at about the same wavelength as CF_2Br_2. For the chlorides there is information only on alcoholic $CHCl_3$ and CCl_4, which again seem to absorb at comparable wavelength, *ca* 200–210 mμ.

In correlating these relations with the theories of organic chemistry, one finds the relative effects of the several halides, and the essentially equal effects of fluorine and methyl groups, are in closest correspondence with the "inductomeric" effects tabulated by

[6] L. I. Katzin and E. Gebert, J. Am. Chem. Soc. **72**, 5464 (1950).

Ingold.[7] The implication is, therefore, that the principal effect of the substituents is on the excited state of the optical transition, which would correspond to modifying the radical resonance energy.[8–10] Confirmation that alterations of the ground state energy contribute in only a minor way can be found if one uses the carbon-halogen bond length as a criterion of ground-state energy level. Thus, a summary of the literature values for the carbon-halogen bond lengths[11–15] shows for the series H_3C-X, F_3C-X and $(CH_3)_3C-X$, agreement of $C-X$ distance to a few hundredths of an angstrom. Similar agreement is found in the four members of the series from CH_3Cl to CCl_4. One might therefore conclude, for the saturated organic halides, that the variations in absorption spectrum for a given halogen are primarily due to corresponding changes in the energy level of the excited state which in turn consists of the halogen atom and the organic free radical. [A similar conclusion was reached by Haszeldine (Table reference 42) on the basis of other evidence.] With more complex substitution on the carbon atom, the ground-state energy itself may of course undergo considerable alteration.

Since multiple compounds of the same metal atom and halogen generally involve different oxidation states of the metal, and since each metal-halogen pair presents a fresh ground state, carry-over of this analysis of the relations of the saturated aliphatic organic halides to the inorganic halides is not obvious. Some analogy may be found in successive stages of complexing of a given anion to a cation. This process, however, is replacement of one of a number of solvent groups by the anion, and the nature of the solvent groups concerned, the possible changes in the total coordination number, and manifold possibilities of changes of electronic configuration of the metal atom make the findings of regularities difficult. With the Co(II) and Ni(II) iodides,[5] for example, the effects of successive addition are changes in the halide absorption wavelength of only a few millimicrons—in the opposite directions for cobalt and for nickel. The mercuric halides illustrate another complication. Solid $HgCl_2$[16] and HgI_2 in the vapor state[17] approach linearity, as presumably does aqueous HgI_2. In solutions with excess alkali halides, complexes of the form HgX_3^- and HgX_4^{--} are formed,[18] with a probable alteration to a tetrahedral configuration, and there is seen a shift in spectrum to longer wavelengths. Solid HgI_2 is a deep brick red, compared to the straw yellow of its solution in water. As its structure shows tetrahedral iodines,[19] its absorption spectrum is probably related to that of the higher complexes rather than to the linear HgX_2, and the question of roles of coordination and geometry enters strongly into interpretations of the changes. Substitution of an iodine on SnI_4 by a methyl group seems not to affect the spectrum.

As can be seen in Fig. 2, there is a tendency for the relative positions of halides of a given pair of cations to remain fixed, evidenced by the rough parallelism of the corresponding lines. Superposed on this is a tendency for many iodide spectra to show the same peaks, illustrated by the behavior of the lines for CX_4(alc.), X_3^-(aq.) and CoX_2(alc.), which cut across the former group of lines as their iodides tend to peak at 27 000–28 000 cm^{-1}. A third tendency which the author believes may be significant is for wavelengths to "clump," most clearly visible in the chloride peaks plotted. This is not due solely to the groups being formed of elements from the same group of the periodic table, as $SnCl_2$ vapor and TlCl in excess alkali halide have peaks very close to that shown by NaCl vapor. A group at 217 millimicrons contains $HgCl_2$ in *t*-BuOH, AgCl in excess alkali halide, $NiCl_2$ in *t*-BuOH, and $SnCl_4$ in the same solvent. The clumping is also not due to the aforementioned tendency toward constancy of position, as the members of the 227 millimicron chloride group spread considerably as the bromides, and even more as the iodides. Further, though there is a large group of iodides absorbing at *ca* 27 000 cm^{-1} there are very few below this. Attention is called also to the dotted lines for $Co(NH_3)_5X^{++}$(aq.), which refer to the first and second peaks of the spectra, respectively. The peak separation for the bromide and iodide are too great for the characteristic doublet splitting, and there should be none for the chloride. Two sets of transitions seem to be involved.

The relative positions of different halides do not seem to follow any simple correlation, such as that of electronegativity differences.

Deep indebtedness is gratefully acknowledged to Dr. John R. Platt and Dr. L. Orgel for sympathetic and helpful discussion of the above material. The technical assistance of Miss Elizabeth Gebert in taking absorption spectra was most helpful. This work was performed under the auspices of the U. S. Atomic Energy Commission.

Measurements:—The Beckman Model DU spectrophotometer was used in making the spectral measure-

[7] C. K. Ingold, *Structure and Mechanism in Organic Chemistry* (Cornell University Press, Ithaca, 1953), Table 7–3.
[8] L. Pauling and G. W. Wheland, J. Chem. Phys. **1**, 362–374 (1933).
[9] G. W. Wheland, J. Chem. Phys. **2**, 474–482 (1934).
[10] E. T. Butler and M. Polanyi, Trans. Faraday Soc. **39**, 19–36 (1943).
[11] A. D. Walsh, Trans. Faraday Soc. **43**, 60–77 (1947).
[12] J. Duchesne, Nature **159**, 62–63 (1947).
[13] A. Gilchrist and L. E. Sutton, J. Phys. Chem. **56**, 319–321 (1952).
[14] S. H. Bauer, J. Phys. Chem. **56**, 343–351 (1952).
[15] R. C. Taylor, J. Chem. Phys. **22**, 714–716 (1954).
[16] H. Braekken and W. Scholten, Z. Krist. **89**, 448 (1934).
[17] H. Braune and S. Knoke, Naturwiss. **21**, 349 (1933); Gregg, Hampson, Jenkins, Jones, and Sutton, Trans. Faraday Soc. **33**, 852 (1937).
[18] L. G. Sillen, Acta Chem. Scand. **3**, 539 (1949) and earlier papers in series.
[19] M. L. Huggins and P. L. Magille, J. Am. Chem. Soc. **49**, 2357 (1927).

ments reported. Salts were commercial chemically pure product, except for SnI_4. This was prepared[20,21] by adding KI to a concentrated aqueous solution of $SnCl_4$. The sparingly soluble iodide was then either allowed to crystallize and separated, or simply solvent-extracted by shaking a portion of the red-orange aqueous solution with chloroform. The tertiary butyl alcohol used as solvent was the Shell synthetic product, containing in general less than 0.05% water.

[20] K. S. Pitzer and J. H. Hildebrand, J. Am. Chem. Soc. **63**, 2472 (1941).
[21] J. H. Hildebrand (private communication).

THE JOURNAL OF CHEMICAL PHYSICS VOLUME 23, NUMBER 11 NOVEMBER, 1955

Absorption Spectrum and Quantum States of the Praseodymium Ion. I. Single Crystals of Praseodymium Chloride*

EDWARD V. SAYRE, KENNETH M. SANCIER,† AND SIMON FREED
Department of Chemistry, Brookhaven National Laboratory, Upton, Long Island, New York
(Received February 7, 1955)

The structure of the polarization spectra exhibited by single crystals of anhydrous praseodymium chloride permitted the assignment of quantum states of the praseodymium ion because of the fact that the symmetry of the crystal fields had previously been determined by x-rays. The crystals which were diluted with isomorphic, colorless lanthanum chloride, were grown from melts.

Observations of transitions over the range from 2200 A to 18 000 A at the temperatures of liquid nitrogen and liquid helium led to the identification of seven upper states as well as the substates into which they were split by the crystal fields. The four lowest substates of the ground state also were characterized. The *F* triplet was found inverted.

All the transitions were forced electric dipole in nature.

A DETAILED understanding of the sharp line absorption spectra of the trivalent rare earth salts is gradually being realized. The well-substantiated assumption that spectra of ions of rare earths arise from the shielded $4f$ electrons of these ions led to Gibbs, Wilber, and White's[1] listing of the number of levels involved and their term designations for Russell-Saunders coupling. Hund's rules for the ground states have, of course, been well confirmed by many magnetic susceptibility measurements. The separate calculations of the energies of all of the $4f$ levels of praseodymium ions by Lange,[2] Mukherji,[3] Spedding,[4] and Trefftz[5]; and of terbium ions by Bethe and Spedding[6] and Gobrecht[7] have provided a quantitative framework with which to compare the observed spectra. However, these calculations have differed widely in the positioning of some of the levels. Most notably, the energies assigned to the $^1D_2$ and $^1G_4$ states of praseodymium have varied as much as 10 000 cm^{-1}. In the light of such disagreement it does not seem adequate to assign term designations to the observed states solely in terms of energy intervals. A simple qualitative knowledge of the absorption spectra is not adequate to lead to their complete understanding.

From detailed analyses of the polarization spectra of single crystals of rare earth salts, however, one can reliably assign J values to the observed states. This additional information combined with the energy calculations should be sufficient to make unambiguous the term assignments for the states. The theoretical apparatus needed for such an analysis is available either in Bethe's[8] or Hellwege's[9] treatment of the splitting of states due to the internal Stark effect within ionic crystal lattices. The two approaches are equivalent and differ fundamentally only in that Bethe used group theory and Hellwege, instead, a detailed analysis of the transformation properties of the zero-order wave functions. The use of single crystals is required so that one can determine the multipole character of the radiation, i.e., whether a group of lines results from an electric dipole, magnetic dipole, etc., transition. A knowledge of this is essential in order to interpret a group of lines correctly since the selection rules are different for transitions of different multipole character. The polarization properties also reveal the character and degeneracy of the individual split levels of the states involved in the transition.

In an important series of papers Hellwege and Hell-

* Research carried out under the auspices of the U. S. Atomic Energy Commission.
† Present address: Stanford Research Institute, Stanford, California.
[1] Gibbs, Wilber, and White, Phys. Rev. **29**, 790 (1929).
[2] H. Lange, Ann. Physik (5) **31**, 609 (1938).
[3] P. C. Mukherji, Indian J. Phys. **11**, 399 (1938).
[4] F. H. Spedding, Phys. Rev. **58**, 255 (1940).
[5] E. Trefftz, Z. Physik **130**, 561 (1951).
[6] H. A. Bethe and F. H. Spedding, Phys. Rev. **52**, 454 (1937).
[7] H. Gobrecht, Ann. Physik. **31**, 600 (1938).
[8] H. Bethe, Ann. Physik. **3**, 133 (1929).
[9] K. H. Hellwege, Nachr. Akad. Wiss. Göttingen, Math. Physik. Kl. 37–41 (1947), Ann. Physik (6) **4**, 95 (1948); (6) **4**, 127 (1948); (6) **4**, 136 (1948); (6) **4**, 143 (1948); (6) **4**, 357 (1949).

wege[10] have presented such an analysis of the visible portion of the polarization spectra of hydrated praseodymium-zinc nitrate and praseodymium-magnesium nitrate single crystals. They have worked, however, under the handicap of not knowing the structure of their crystals. On the basis of internal consistency of their results, they first deduced that the point symmetry of a praseodymium ion in their crystals was C_3. A more detailed study of the intensity relationships of their lines lead them to modify this to C_{3v}. On either basis, they could be reasonably certain that the lines in the blue region arise from the P triplet and those in the red from a $^1D_2$ upper state.

The crystal structure of anhydrous praseodymium chloride is known with an unusual degree of certainty. Its structure and that of more than twenty of its isotypes have been determined independently by Zachariasen[11] and Seitz.[12,13] It has a hexagonal lattice in which the metal ion occupies a site of C_{3h} symmetry.

We have, therefore, examined single crystals of anhydrous praseodymium chloride diluted with isomorphic colorless lanthanum chloride in order to achieve the desired density of absorption in a crystal of convenient size. The polarization absorption spectra of the crystals were taken at two temperatures, that of liquid nitrogen and of liquid helium. The spectra were examined from 2200 to 18 000 A. In addition to confirming Hellwege and Hellwege's results in the visible, term designations were assigned to three levels in the infrared. The interpretations of these observations were confirmed by examination of the absorption spectrum of a film of anhydrous praseodymium fluoride, another salt of known structure.[14]

PREPARATION OF SINGLE CRYSTALS

The chlorides were prepared from spectrographically pure praseodymium oxide and lanthanum oxide supplied by the Institute for Atomic Research of Iowa State College. Although other rare earth impurities could not be detected in these oxides by emission spectroscopy some neodymium lines at 5800 A did appear in the absorption spectra of the solid crystals. Additional specifically purified oxides were furnished by Professor Spedding which showed absence of neodymium even to this more sensitive test. All lines that were at all in doubt were checked for their appearance in the spectrum of a distilled pure praseodymium chloride film prepared from this new material. To obtain proper absorption densities, crystals containing 5, 2, and 0.1 mole percent praseodymium chloride were prepared. Dilution by lanthanum chloride did not affect the position of the absorption lines nor did it appear to affect their relative intensities from that observed in undiluted praseodymium chloride.

The oxides were dissolved in hydrochloric acid taken to near dryness, transferred into an open quartz boat, inclosed in a tube furnace, and dehydrated by being heated to slowly increasing temperatures in a stream of mixed hydrogen chloride and helium. The gas stream was predried by passing through two traps immersed in dry ice, one of which contained a fritted glass filter. After all evolved water had been swept out, the temperature was raised to melt the salt into a clear solid ball. The anhydrous chloride, after cooling, was transferred to a three-centimeter length of 8-mm quartz tubing, the bottom end of which had been drawn out to form a capillary tip about five centimeters long, in which crystal nucleation is initiated. This crystal holder was suspended in a vertical quartz tube through which the dried hydrogen chloride-helium gas could pass and around which a tube furnace could be raised. The chloride was once more carefully dehydrated, melted, and subjected briefly to a vacuum in order that the capillary end would be filled with melt. The tube furnace, which contained an internal temperature drop at its center of approximately 50° spanning the temperature necessary to melt the salt, was then slowly raised about the melt. The crystals always grew so that their crystallographic axes paralleled the axis of the tube in which they were held. Because the crystals were highly hygroscopic they were stored in a dried hydrocarbon oil and freshly cleaved under this oil immediately before use.

OBSERVATION OF THE SPECTRA

The spectra were measured with a Baird Eagle mounting grating spectrograph equipped with a four-inch, 15 000 lines per inch, concave grating of one meter focal length. Its dispersion is 15 A/mm in the first order, but its range, 2200 to 18 000 A, permitted all of the transitions in the visible to be observed in the third order at 5 A/mm.

The spectra were recorded on photographic plates to approximately 12 000 A. Beyond that in the infrared they were recorded by a scanner built in this laboratory, which used a lead sulfide cell as its light sensitive element. Light was sent through approximately one millimeter thickness of crystal in a direction parallel to the crystallographic axis to observe the isotropic "axial" spectrum and in a direction perpendicular to the crystallographic axis to observe the birefringent "transverse" spectrum. The transverse spectrum was separated into its two components by polarizing the entering light so that its electric vector was oriented parallel with or perpendicular to the crystallographic axis. Following established practice these will be called the π and σ spectra, respectively. The dichroism of

[10] A. M. Hellwege and K. H. Hellwege, Z. Physik **130**, 549 (1951); **133**, 174 (1952); **135**, 92 (1953).
[11] W. H. Zachariasen, J. Chem. Phys. **16**, 254 (1948); Acta. Cryst. **1**, 266 (1948).
[12] S. Schubert and A. Seitz, Z. Naturforsh. **1**, 321 (1946); Z. anorg. Chem. **254**, 116 (1947).
[13] R. Fricke and A. Seitz, Z. anorg. Chem. **254**, 109 (1947).
[14] E. V. Sayre and S. Freed, J. Chem. Phys. **23**, 2066 (1955), following paper.

μ	0	±1	±2	3
0			σ	π
±1		σ	π	σ
±2	σ	π	σ	
3	π	σ		

FIG. 1. Selection rules for electric dipole transitions of different polarization for praseodymium ions in sites of C_{3h} point symmetry.

praseodymium ions in C_{3h} symmetry is complete, i.e., no lines appear in both the π and σ spectra.

When measurements were made at liquid nitrogen temperatures, the crystals were imbedded in a glass of equal parts of methyl cyclopentane and methyl cyclohexane. When measurements were made at liquid helium temperatures, the crystals were mounted in a vacuum but in close thermal contact with the quartz windows of the cell in which they were held.

ANALYSIS OF THE SPECTRA

A comparison of the axial and transverse spectra of a uniaxial crystal differentiates between transitions of an electric dipole or magnetic dipole nature occurring within it. During the observation of the axial spectrum both the electric and magnetic vectors of the incident light are oriented perpendicular to the crystallographic axis. In the observation of the σ polarized transverse spectrum only the electric vector of the incident light is perpendicular to the crystallographic axis, and conversely during the observation of the π spectrum only the magnetic vector of the incident light is perpendicular to the axis. Therefore, if the axial and the σ spectra coincide the transition must be of an electric dipole nature. A magnetic dipole transition is indicated by coincidence of the π spectrum with the isotropic axial spectrum. Using this method it was determined directly that all of the lines observed in the photographic range, i.e., up to 12 000 A, arose from electric dipole transitions. No measurement of the axial spectrum of the crystal was made at longer wavelengths. The crystals cleaved very readily in planes parallel to the crystal axis, but it was very difficult to obtain good cross sections perpendicular to this direction. We were not successful in sending sufficient light through a crystal parallel to its axis to operate properly the less sensitive lead sulfide spectrum scanner. However, it was possible to determine, by methods described later, that the transitions observed at approximately 15 000 and 16 000 A were also of an electric dipole nature.

In accordance with Russel-Saunders coupling and the Pauli principle, the two $4f$ electrons of the trivalent praseodymium ion will give rise to the following states: $^1S_0$, $^3P_{0,1,2}$, $^1D_2$, $^3F_{2,3,4}$, $^1G_4$, $^3H_{4,5,6}$, and $^1I_6$. About these states there is essentially agreement that $^3H_4$ is the ground state and that the $^3P_{0,1,2}$ states give rise to the lines in the green-blue, 4500 to 4900 A. Also all the calculations have placed the transitions to the $^3F_{2,3,4}$ states in the region of 16 000 A. There is considerable disagreement about the placing of the remaining states, however.

THE TRANSITIONS TO THE $^3P_{0,1,2}$ STATES

Because of the previous knowledge of the states involved in these transitions, they offer a clear opportunity to determine the characters of the individual levels into which the ground state has been split by the Internal Stark effect. In the field of C_{3h} symmetry the $^3H_4$ ground state will be split into six levels characterized by μ, Hellwege's crystal quantum numbers, 0, ±1, ±2, ±2, 3, and 3. Those levels with a $\pm$ prefix are doubly degenerate, the remainder nondegenerate. The three upper states, $^3P_0$, $^3P_1$, and $^3P_2$, split into one, two, and three states, respectively, which are characterized 0; 0 and ±1; 0, ±1, and ±2. The absorption spectrum at liquid helium temperatures consists of one line at 4882.4 A, σ polarized, a pair of lines at 4738.7 and 4745.4 A with σ and π polarization, respectively, and three lines at 4493.5σ, 4497.6π, and 4501.5σ. Thus transitions are permitted from the lowest lying ground level to all of the levels within this upper triplet. The selection rules for electric dipole transitions between these levels, are for π transitions, $\Delta\mu=3 \bmod(6)$, for σ transitions, $\Delta\mu=\pm2 \bmod(6)$. Figure 1 presents a summary of the operation of these selection rules. It shows that transitions to all of the upper levels would be permitted only from a lower state characterized by $\mu=\pm2$. The observed polarization properties are also consistent with this assignment.

At the higher temperature, that of liquid nitrogen, additional lines appear to the red of the ones described indicating the presence of additional levels lying close to the lowest ground level. These new lines will be referred to as temperature induced lines, as distinguishable from the lines observed at liquid helium temperature which shall be called the base lines. Strong lines appeared 33 cm^{-1} to the red of all of the base lines except one in the $^3P_2$ group. In addition all of the temperature dependent lines offset 33 cm^{-1} were polarized oppositely with respect to the base lines to which they related. These lines and an analysis of them are shown in Fig. 2. On the basis of this evidence this new ground level must have a μ of 3.

Conversely, from this knowledge of the characters of the two lowest ground levels, the characters of the levels of the upper states can be determined. A σ polarized line accompanied at 33 cm^{-1} to the red by a temperature induced line of π polarization indicates an upper state level of $\mu=0$; a π polarized line accompanied by a σ one, an upper level of $\mu=\pm1$, and a σ polarized

base line not followed by a line 33 cm^{-1} to the red indicates an upper level of $\mu=\pm 2$. In this way the character of the states listed in Table I were determined. The energies of the upper states are, of course, by definition the energies of the transitions from the lowest ground level to them, and thus are given in Table I by the energies of the base lines.

In addition all of the base lines are repeated with their original polarization by a set of very weak lines at a distance of 97 cm^{-1}. Thus the second ground level characterized by $\mu=\pm 2$ must lie at 97 cm^{-1}. This level will be differentiated from the first by a prime, i.e., $\pm 2'$. These lines are so weak as to be just barely visible in Fig. 2. They appeared definitely, however, in the spectra of more concentrated crystals.

TABLE I. Positions and polarizations of transitions in anhydrous praseodymium chloride.

Final state Term	μ	Base lines A (in air)	Base lines cm^{-1} (in vac.)	Temperature induced lines A (in air)	Temperature induced lines cm^{-1} (in vac.)	Initial state Energy cm^{-1}	Initial state μ
$^3P_0$	0	4882.4	20 476σ			0	± 2
				4890.3	20 443π	33	3
				4905.6	20 379σ	97	$\pm 2'$
$^3P_1$	0	4738.7	21 097σ			0	± 2
				4745.4[a]	21 067π	30	3
				4760.4	21 001σ	96	$\pm 2'$
	± 1	4745.4[a]	21 067π			0	± 2
				4752.9	21 034σ	33	3
				4767.5	20 970π	97	$\pm 2'$
				4775.0	20 936σ	131	± 1
$^3P_2$	± 2	4493.5	22 248σ			0	± 2
				4513.2	22 151σ	97	$\pm 2'$
	± 1	4497.6	22 228π			0	± 2
				4504.4	22 194σ	34	3
				4517.3	22 131π	97	$\pm 2'$
				4524.3	22 097σ	131	± 1
	0	4501.5	22 209σ			0	± 2
				4508.2	22 176π	33	3
				4521.3	22 111σ	98	± 2
$^1D_2$	± 1	5957.9	16 780π			0	± 2
				5969.9	16 746σ	34	3
				5992.8	16 682π	98	± 2
	± 2	5975.2	16 731σ			0	± 2
				6010.8[x]	16 632σ	99	$\pm 2'$
	0	6010.8[x]	16 632σ			0	± 2
				6023.3	16 598π	34	3
				6046.6	16 534σ	98	$\pm 2'$
$^1G_4$	± 1	10 191	9810π			0	± 2
				10 228[+]	9774σ	36	3
				10 297	9709π	101	$\pm 2'$
	± 2	10 228[+]	9774σ			0	± 2
				10 330°	9678σ	96	$\pm 2'$
	± 2	10 233	9769σ			0	± 2
				10 330°	9678σ	91	$\pm 2'$
	0	10 266	9738σ			0	± 2
				10 303	9703π	35	3
				10 371	9640σ	98	$\pm 2'$
$^3F_2$	± 1	14 735	6785π			0	± 2
				14 804	6753σ	32	3
				14 941	6691π	94	$\pm 2'$
	0	14 741	6782σ			0	± 2
				14 811	6750π	32	3
				14 947	6688σ	94	$\pm 2'$
	± 2	14 761	6773σ			0	± 2
				14 968	6679σ	94	$\pm 2'$
				15 053	6641π	132	± 1
$^3F_3$	± 1	15 751	6347π			0	± 2
				15 838	6312σ	35	3
				16 000•	6248π	99	$\pm 2'$
				16 080	6217σ	130	± 1
	± 2	15 875	6297σ			0	± 2
				16 134	6197σ	100	$\pm 2'$
				16 231	6160π	137	± 1
	0	15 923	6279σ			0	± 2
				16 000•	6248π	31	3
				16 188	6176σ	103	± 2
	3		(6296)[°]	16 216	6165σ		± 1
	3		(6292)[+]	16 232	6161σ		± 1
				16 266	6146π		

[a] [x] + [°] • Unresolvable accidental superpositions of pairs of lines.
[°] [+] Energies of the two $\mu=3$ upper levels if $\mu=\pm 1$ ground state level is correct.

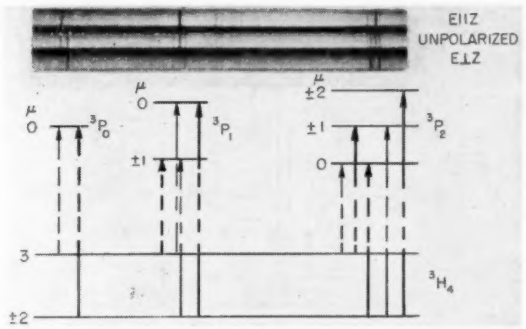

FIG. 2. Transitions from ground states to $^3P_{0,1,2}$ triplet of $PrCl_3$ in $LaCl_3$. Spectra of single crystal at 77°K; light transmitted perpendicular to unique, Z, axis of crystal.

The π polarized base lines, resulting from the upper levels with $\mu=\pm 1$, were both followed by some extremely weak σ polarized lines at an energy difference of 131 cm^{-1}. If these lines also arise from an electronic ground level it must be characterized either ± 1 or 3. Since no such line is seen associated with the $^3P_0$ state, this additional ground level is most probably ± 1. Identical spacing is encountered again in the strong transitions to the triplet F states. Here also the assignment ± 1 to the ground level of 131 cm^{-1} is consistent with the observations. The lines are so weak, however, that they may be only the result of vibrational coupling. Vibrationally coupled lines are nearly always in evidence to the blue of the base lines. They appear particularly strongly to the right of the $^3P_1$ group in Fig. 2. Hellwege and Hellwege[10] have made an analysis of these vibrationally coupled lines in the spectrum of praseodymium-zinc and magnesium nitrates.

THE $^1D_2$ STATE

At liquid helium temperature, one observes three lines at approximately 6000 A, one with π and two with σ polarization. At liquid nitrogen temperature, oppositely polarized lines appear 33 cm^{-1} to the red of the π polarized and one of the σ polarized lines, and all three of the original lines are repeated with their original polarization 97 wave numbers to the red. The transitions were weaker than those to the triplet P states, and no lines 131 cm^{-1} to the red were observed. This arrangement of lines is identical with that observed in the transitions to the $^3P_2$ state, and indicates the presence of three upper levels characterized by 0, ± 1, and ± 2. A state with a J of two would split into exactly such levels. However, a state with J equal to three would differ from this only in possessing two additional levels both characterized by a μ of 3. The selection rules do not allow a transition from any of the $+2$, 3, or $+2'$ ground levels to an upper level of 3. Therefore, within the limits of the measurements made on these particular crystals, upper states with J equal to two or three would produce identical line patterns. The state at 6000 A could only have a J of two because, being isolated, it cannot be part of a triplet and all of the singlet terms

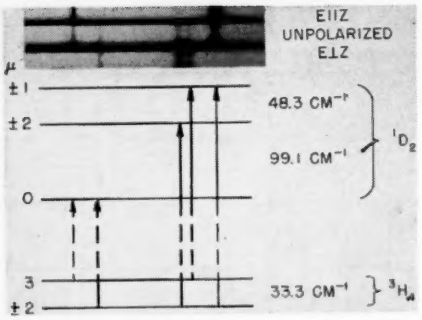

FIG. 3. Transitions from ground states to $^1D_2$ group of $PrCl_3$ in $LaCl_3$. Spectra of single crystal at 77°K; light transmitted perpendicular to unique, Z, axis of crystal.

available have even J values. The state must, therefore, be $^1D_2$. This is in agreement with the designation proposed by Hellwege and Hellwege. Figure 3 shows the strong lines of this group photographed at liquid nitrogen temperature.

THE $^1G_4$ STATE

The lines at approximately 10 000 A are extremely weak and diffuse. At liquid helium temperature, however, one can definitely resolve four lines, one with π and three with σ polarization. A densitometer tracing of these lines, photographed at 4°K, is shown in Fig. 4. The polarization was not complete in the spectrogram reproduced, so that the σ lines show up weakly in the π spectrum and vice versa. This spectrogram was selected purposely, however, because the resolution of the two middle lines shows up more clearly when they appear as weak residual lines. This distribution of base lines is consistent with an upper state of J equal to four, which would split into six levels with the following crystal quantum numbers, one of 0, one of ±1, two of ±2, and two of 3. The lines observed coincide with transitions to the first four of these upper levels, those to the last two being prohibited. At higher temperatures the broadening of the lines and the coincidence that some upper state spacing agree very closely to the spacings in the ground state, results in the unresolvable superposition of some of the lines. Everything observed at liquid nitrogen temperature, however, is also consistent with the assignment of a J value of four to this state. The state is, therefore, identifiable as $^1G_4$. A check of this transition, the analysis of which was not as secure as for the others because of the weak and diffuse nature of its lines, was available in the additional observation of the spectrum of anhydrous praseodymium fluoride. The results of this observation[14] confirm the $^1G_4$ term designation.

THE TRIPLET F STATES

All of the calculations place the triplet F states in the range of 6000 to 7000 cm^{-1}. We were able to examine two states of the triplet through groups of lines at 14 750 and 15 850 A. The third group lay beyond the infrared limit of the spectrograph. The lines were intense and sharp as were the transitions from the triplet H ground state to the triplet P states. They are shown in Fig. 5. At liquid helium temperatures both groups of lines consisted of three lines of which two were σ polarized and one π. This is the familiar number and distribution of lines that characterized the transitions to the $^3P_2$ and $^1D_2$ states. Thus, if the transitions are of an electric dipole nature, one must assign to them a J either of two or three.

As explained previously, mechanical difficulties prevented the direct observation, at these wavelengths, of the axial spectrum of the crystal. However, from the knowledge of the characters of the ground levels, now well established, it is easy to pick out which of the two polarized components of the transverse spectrum must coincide with the axial spectrum. In electric dipole transitions the selection rules are $\Delta\mu=\pm2 \bmod(6)$ for $x+iy$ polarized transitions and $\Delta\mu=3$ for z polarized transitions. In the magnetic dipole case the rules are $\Delta\mu=\pm1 \bmod(6)$ for $x+iy$ and $\Delta\mu=0 \bmod(6)$ for z. From these rules Table II has been derived which shows the number of lines of each polarization allowed for a transition from the lowest ground level, characterized by $\mu=+2$, to upper states of various J's. The point to be made from the table is that in either the electric or magnetic dipole case the number of $x+iy$ polarized transitions always equals or exceeds the number of z polarized transitions. The $x+iy$ polarized transitions in either electric or magnetic dipole radiation are the ones that will appear in the axial spectrum. Therefore, since in both groups, at helium temperatures, the σ polarized transverse spectrum component contains twice as many lines as the π polarized component, it must be the one that will coincide with the axial spectrum. As was argued previously, when the σ component of the transverse spectrum coincides with the

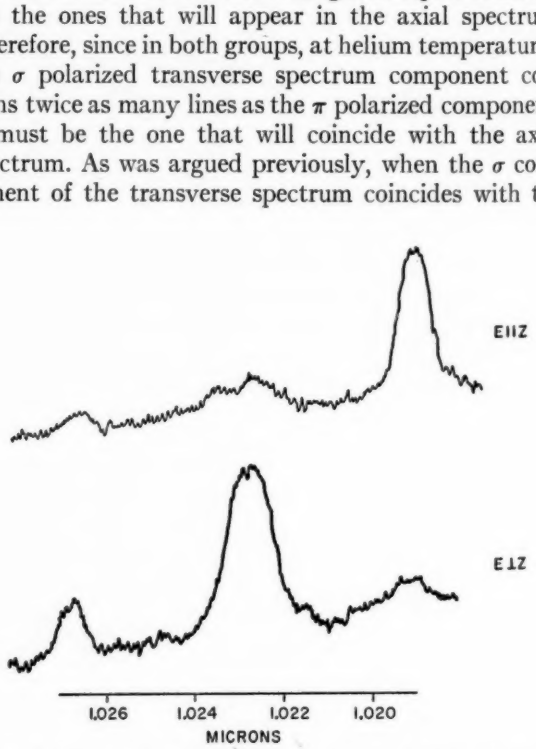

FIG. 4. Transitions from lowest lying ground level to $^1G_4$ state of $PrCl_3$ in $LaCl_3$. Spectra of single crystal at 4°K; light transmitted perpendicular to unique, Z, axis of crystal.

axial spectrum, the character of the radiation must be electric dipole. Thus both sets of transitions must be electric dipole radiation. In fact, it is only within the electric dipole transitions that one would expect exactly three transitions from the lowest ground state to an upper state. Similar arguments could be based upon the transitions from the next higher ground level with μ of three; the sets of lines would not make sense as magnetic dipole transitions.

One would have expected the higher energy group of lines about 14 750 A to have been transitions to the $^3F_4$ state. However, the number of lines observed, two σ and one π at helium temperatures, are too few to indicate a J of four. The lines are consistent only with a J of two or three. This suggests that perhaps the F triplet is inverted, with its highest energy state corresponding to a J of two. At liquid nitrogen temperatures the group about 14 750 A showed no lines not accountable for on the basis of an upper state with a J of two, even if the possible ground level characterized by ± 1 at 131 cm^{-1} is included. The spectra are shown in Fig. 5, and the interrelation of the lines is given in Table I. The spectrum of anhydrous praseodymium fluoride[14] also suggests a J of two for this state. Therefore, one is forced to accept the unexpected conclusion that the F triplet is reversed in energy with respect to the P and H triplets, its highest energy term being $^3F_2$.

Whether the F triplet is normal or inverted its middle term at approximately 15 850 A would be $^3F_3$, and the number and polarization of lines observed in this region are consistent with this designation. The lines are shown in Fig. 5 and tabulated in Table I. All lines consistent with upper levels of 0, ± 1, and ± 2 are present. In addition there are two extra σ lines, which are temperature dependent and lie well to the red and which could be the transitions from the possible ± 1 ground state at 131 cm^{-1} to the two upper ± 3 states. No transitions

TABLE II. Number and polarization of lines from the ground level, ± 2 character, to upper states of various J's for electric dipole and for magnetic dipole radiation.

J (upper state)	Electric dipole radiation		Magnetic dipole radiation	
	z	$x+iy$	z	$x+iy$
0	0	1	0	0
1	1	1	0	1
2	1	2	1	1
3	1	2	1	3
4	1	3	2	3

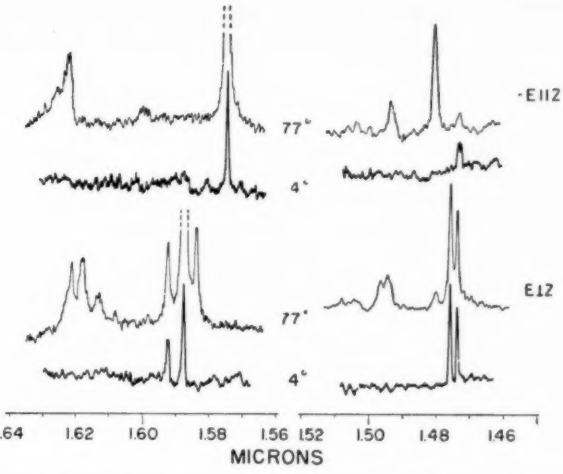

FIG. 5. Transitions from ground states to two ^3F states of $PrCl_3$ in $LaCl_3$. Polarized spectra of single crystal at 77° and 4°K; light transmitted perpendicular to unique, Z, axis.

are permitted between the other populated ground sublevels and these two additional upper levels so that this is the only direct evidence of their existence. If all assumptions concerning these lines are correct the energies of these two ± 3 upper levels would be 6296 and 6292 cm^{-1}. However, we also see an additional very weak π polarized line at 16 266 A for which we have no explanation, so we are not sure how heavily to weight these very weak lines which lie far to the red of the base lines. Even if these possible transitions to the ± 3 levels of the upper state are ignored, there seems adequate evidence to assign a $^3F_3$ term designation to the lines at 15 850 A.

Of the thirteen states predicted by Russell-Saunders coupling of the two $4f$ electrons in the praseodymium ion, energy levels have been substantiated for at least some of the states of all of the three triplets and also for $^1D_2$ and $^1G_4$. This leaves undetected only the $^1S_0$ and $^1I_6$ levels. One expects the $^1S_0$ to have very high energy, presumably lying below the 2200 A range of our spectrograph. The $^1I_6$ state might well lie beyond our infrared limit, 1.8 microns. In the light of the weakness and diffuseness of the transitions to the $^1G_4$ state it is possible that transitions to these missing states could have passed unseen.

ACKNOWLEDGMENTS

We are grateful to Professor F. H. Spedding for providing us with specially pure rare earth oxides.

Absorption Spectrum and Quantum States of the Praseodymium Ion. II. Anhydrous Praseodymium Fluoride in Films*

EDWARD V. SAYRE AND SIMON FREED
Department of Chemistry, Brookhaven National Laboratory, Upton, Long Island, New York
(Received February 7, 1955)

The absorption spectra of anhydrous praseodymium fluoride were examined to confirm term designations derived from the spectra of anhydrous praseodymium chloride. In the fluoride, praseodymium ion is at the center of a micro-field of C_{2v} symmetry and in the chloride it is in a field of C_{3h} symmetry. There was complete consistency in the interpretations of the spectra of the two compounds.

A new phenomenon appeared in the spectrum of the fluoride, however. The selection rules prohibiting some of the possible transitions of an ion in a field of C_{2v} symmetry valid at the temperature of liquid nitrogen were lifted at the temperature of liquid helium, where in fact all possible transitions occurred. There is evidence against any gross crystallographic transformation.

It is surmised that the positions of energy minimum for the ions lie slightly off the symmetric positions possibly due to higher order interactions such as occurs in the case of barium titanate.

A STUDY of the absorption spectrum of anhydrous praseodymium fluoride was undertaken to confirm some of the quantum state assignments of the praseodymium ion that had been indicated by the spectrum of single crystals of praseodymium chloride.[1] The crystal structure of praseodymium fluoride is known, making possible a quantitive interpretation of its spectrum. In addition to furnishing this confirmation, however, the spectrum exhibited an interesting and unexpected property. In cooling the fluoride from the temperature of liquid nitrogen to that of liquid helium some lines increased in intensity many fold. The lines exhibiting this effect were all extremely weak at liquid nitrogen temperatures, so that the change had the appearance of forbidden transitions becoming allowed at the much lower temperature. An example of this effect is shown in Fig. 1 in the transitions to the $^1D_2$ upper state at approximately 6000 A. A densitometer tracing of these lines reveals that the strong line to the blue develops a recognizable shoulder on its high energy side at helium temperature, so that the group is composed of five lines at liquid helium temperature but of only three strong lines at liquid nitrogen temperature. The appearance and disappearance of the extra lines was reversible with temperature. After carefully warming the fluoride from helium temperature to nitrogen temperature the same spectrum was observed as after cooling to nitrogen temperature from room temperature. The lines all remained invariant in wavelength; there was no evidence of any gross structural changes.

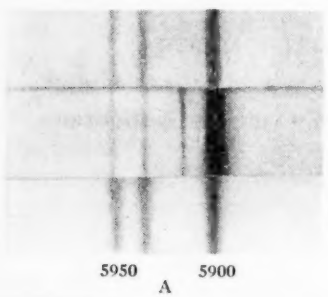

FIG. 1. Transitions to $^1D_2$ state in praseodymium fluoride: A, after cooling to 77°K; B, at 4°K, C, after warming from 4°K to 77°K.

PREPARATION OF FILMS

It was difficult to prepare praseodymium fluoride free of oxyfluoride, as evidenced by the failure of the preparations to melt fully even at temperatures one hundred or more degrees in excess of the melting point, 1370°C. The following procedure proved successful. Anhydrous praseodymium chloride was prepared by the method described in the preceding paper.[1] The chloride was dissolved in excess molten ammonium fluoride, which had been fumed for some period to free it of water. The residual ammonium fluoride was removed by distillation in a vacuum. The praseodymium fluoride was then suspended in a small platinum crucible within a vertical quartz tube which in turn was surrounded by the coil of an induction heater. The fluoride was distilled in a high vacuum from the crucible onto the cool walls of the quartz tube. An x-ray diffraction pattern taken of the distilled fluoride showed no lines not reported for the anticipated LaF_3-type structure.

OBSERVATION OF THE SPECTRUM

The spectrum was taken over the range of 2200 A to 18 000 A on a one meter Baird grating spectrograph described in the preceding paper.[1] Since the fluoride films were inert to hydrolysis by atmospheric moisture, they were immersed directly in liquid nitrogen or helium while the spectra were being taken.

The spectra at liquid nitrogen temperature were characterized by few strong absorption lines and by greater splitting between lines, indicating stronger crystalline fields than for praseodymium chloride. The appearance of only a few strong absorption lines within each group was in part the result of the greater separation of levels within the ground state. As shown in Table I, the separation of the lowest ground level and

* Research carried out under the auspices of the U. S. Atomic Energy Commission.

[1] Sayre, Sancier, and Freed, J. Chem. Phys. **23**, 2060 (1955), preceding paper.

the one closest to it is 66 cm^{-1}, while the next split level lies at 87.5 cm^{-1}. These separations are sufficiently great so that only the lowest ground level is appreciably populated at the temperature of liquid nitrogen; the transitions from the next lowest levels are correspondingly very weak. Transitions from these upper ground levels were investigated only to the degree of determining the energies of the levels.

The point symmetry of the metal ion site in LaF_3-crystal structure is C_{2V}.[2] This low symmetry would result in the complete splitting of the quantum states of the ion into their full $2J+1$ substates.

TRANSITIONS TO THE $^3P_{0,1,2}$ STATES

At approximately 77°K, the temperature of liquid nitrogen, one observes from the lowest ground level only a very weak transition to the $^3P_0$ level, three strong transitions to the $^3P_1$ level, and three strong transitions to the $^3P_2$ level. The three upper levels in a field of C_{2V} symmetry would split into one, three, and five levels, respectively, characterized group theoretically by A_1; A_2, B_1, and B_2; $2A_1$, A_2, B_1, and B_2. Assignment of A_2 character to the ground state would be in full accordance with the appearance of these numbers of lines since transitions are forbidden between levels characterized by A_2 and A_1 but allowed between A_2 and A_2, B_1, and B_2.

In liquid helium, at approximately 4°K, the weak basic transition from the lowest ground level to the $^3P_0$ state increases greatly in intensity, the three strong transitions to $^3P_1$ remain unchanged and in the transitions to the $^3P_2$ state two lines, weak at 77°K, now have become prominent, making five transitions in all. Thus at this very low temperature one observes transitions to all of the $2J+1$ levels of the upper states. It is as if the lowering of the temperature removes the prohibitions imposed by the selection rules. The frequencies of these transitions from the lowest ground level to all of the upper levels are given in Table II.

In the transitions to the $^3P_0$ state an exception occurs to the rule that all transitions except from the lowest ground level are weak at 77°K. The transition 66 cm^{-1} to the red of that from the lowest ground level is strong, and, although it is diminished greatly upon cooling to 4°K, it still remains visible. We do not know why this transition is so strong, although we suspect that, because the only transition from the true ground level to the upper $^3P_0$ level is forbidden, some of the energy that would go into it is conserved by entering into the transition from the first excited level.

TABLE I. The first two energy intervals within the ground state of praseodymium ion in the fluoride.

Lines eliminated upon cooling λ(A)	Lines eliminated upon cooling ν(cm^{-1})	Lines retained upon cooling λ(A)	Lines retained upon cooling ν(cm^{-1})	Δν(cm^{-1})
4444.6	22 493.1	4431.4	22 560.1	67.0
4793.3	20 856.8	4778.1	20 923.1	66.3
10 043	9954	9976.5	10 021	67
10 138.5	9861	10 072	9926	65
10 360	9650	10 289	9716	66
14 978	6675	14 826	6743	68
15 257	6553	15 111	6616	63
15 285	6540	15 138	6604	64
15 518	6443	15 359	6509	66
				Av. 65.8
4664.4	21 432.1	4645.2	21 521.6	89.5
5957.8	16 780.2	5926.7	16 868.2	88.0
9561	10 456	9483	10 542	86
15 567	6422	15 359	6509	87
15 680	6376	15 468	6463	87
				Av. 87.5

TABLE II. Transitions arising from the lowest ground level in praseodymium fluoride.

Term of upper state	A (in air)	cm^{-1} (in vacuum)
$^3P_2$	4371.1[a]	22 871.3
	4396.7[a]	22 738.1
	4404.7	22 696.8
	4417.8	22 629.6
	4431.4	22 560.1
$^3P_1$	4636.6	21 561.5
	4645.2	21 521.6
	4658.5	21 460.1
$^3P_0$	4778.1[a]	20 923.1
$^1D_2$	5910[ab]	16 916
	5915.8	16 899.3
	5926.7[a]	16 868.2
	5939.7	16 831.3
	5949.6	16 803.3
$^1G_4$	9483	10 542
	9808.5	10 193
	9924	10 074
	9976.5	10 021
	10 072	9926
	10 114	9884
	10 181	9819
	10 250	9753
	10 289	9716
$^3F_2$	14 826[a]	6743
	15 111[a]	6616
	15 138	6604
	15 359	6509
	15 468	6463

[a] Lines noticeably stronger at 4°K than at 77°K.
[b] Not fully resolved from the line at 5915.8.

TRANSITIONS TO THE $^1D_2$ STATE

The transitions at 6000 A to the $^1D_2$ upper state have already been shown in Fig. 1 and discussed to some extent. They are characterized by three strong transitions at 77°K and five at 4°K. One of the latter transitions is not fully resolved but appears as a well-defined shoulder on one of the temperature independent lines. This pattern of lines, the same as that of the

[2] I. Oftedal, Z. physik. Chem. **6**, 272 (1929); **13**, 190 (1931). Oftedal reported the structure only slightly distorted from a more symmetric one in which the rare earth ion would be at a site of D_{3h} point symmetry. K. Schlyter, Arkiv Kemi **5**, 73 (1953), has claimed the more symmetric structure is the correct one. If the symmetry of charge about the praseodymium ion were D_{3h}, however, we should observe smaller numbers of lines throughout our spectrum than we do. The number of lines we see at liquid nitrogen temperature confirms the original C_{2v} designation of Oftedal, for the crystal at that temperature.

transitions to the $^3P_2$ state, can be considered characteristic of an upper state of $J=2$.

TRANSITIONS TO THE $^1G_4$ STATE

The lines at 10 000 A were both relatively diffuse and weak as they had been in anhydrous praseodymium chloride. At 4°K, however, one could clearly count nine lines, confirming the J value of 4 required for the $^1G_4$ term assignment. None of these residual lines changed greatly in intensity with increasing temperature. The reason for this may be related to the general weakness of all of the lines of this group. None of the lines have much greater intensity than one we have called forbidden in other groups. It may be that these transitions are already so forbidden that the additional prohibitions arising from C_{2V} symmetry no longer greatly diminish line intensities.

TRANSITIONS TO THE $^3F_2$ STATE

The F triplet had shifted sufficiently to the red in praseodymium fluoride, that with our spectrograph it was possible to observe transitions only to its state of highest energy. These transitions were characterized by three strong lines at 77°K and five lines in all at 4°K, the same pattern observed in transitions to the $^1D_2$ and $^3P_2$ states. This observation, then, confirms that the highest energy state of the F triplet is $^3F_2$ and that the multiplet is inverted. There is then consistency throughout in the interpretations of the spectra of praseodymium chloride and praseodymium fluoride. In addition there is agreement with the term designations of Hellwege and Hellwege[3] for those groups in the visible, $^3P_{0,1,2}$ and $^1D_2$.

Transitions are forbidden in C_{2V} symmetry only because of the presence of vertical planes of reflection. A possible explanation as to why lines so forbidden might appear at very low temperatures is that positions of true minimum energy for the lattice ions might lie slightly off the planes of symmetry. At high temperature one would observe only the time average positions of the ions, which would possess more nearly full C_{2V} symmetry. At sufficiently low temperatures, however, the ions freeze into these slightly less symmetric positions. This would result in the lifting of the selection rules observed. If this explanation is correct, one might expect the salt to possess ferroelectric properties at low temperatures as exhibited by barium titanate.[4]

ACKNOWLEDGMENTS

The authors are grateful to Dr. Norman Elliott for his aid in the taking of x-ray diffraction pictures.

[3] A. M. Hellwege and K. H. Hellwege, Z. Physik **130**, 549 (1951); **133**, 174 (1952); **135**, 92 (1953).
[4] J. C. Slater, Phys. Rev. **78**, 748 (1950).

THE JOURNAL OF CHEMICAL PHYSICS VOLUME 23, NUMBER 11 NOVEMBER, 1955

Hybrid π Orbitals and Partial Double Bond Character in Covalent Complexes

GIOVANNI GIACOMETTI*,†
Gates and Crellin Laboratories of Chemistry, California Institute of Technology, Pasadena, California
(Received February 3, 1955)

Angular parts of p- and d-orbitals are hybridized to form a set of tetrahedrally oriented π orbitals. These orbitals are suitable for explaining partial double bond character in compounds such as nickel tetracarbonyl. It is shown that up to three of these orbitals may exist, each possessing the required properties of orthogonality and linear independence. The maximum partial double bond character allowed is, in this way, 75%. The strength of these orbitals, according to a modified Pauling's criterion, is discussed. Also the cases of trigonal bipyramidal and octahedral symmetry are discussed. An attempt is made to interprete semiquantitatively bond lengths in Cr, Fe, and Ni carbonyls.

THERE exists much experimental evidence of partial double bond character in coordination complexes of various symmetries, the central atom belonging to the upper periods of the table.

Many authors have discussed this fact on the basis of π-bond formation involving d orbitals.[1] However, in the case of tetrahedral structures, the problem of describing the double bonds by appropriate spd hybrids having the correct directional properties has not, so far, been solved.

We might take as an example, in order to illustrate the problem, the case of nickel carbonyl. The evidence for double bond between Ni and C comes from the observed distance of 1.82 ± 0.03 A,[2] which is 0.18 A smaller than the sum of the covalent bond radii. Brock-

* Smith-Mundt Fellow 1953–1954.
† Present address: Institute of Physical Chemistry, University of Padua, Padua, Italy.
[1] (a) L. Pauling, *The Nature of the Chemical Bond* (Cornell University Press, Ithaca, New York, 1939), Chap. VII. (b) Craig, Maccoll, Niholm, Orgel, and Sutton, J. Chem. Soc. 332 (1954). (c) H. H. Jaffè, J. Phys. Chem. **58**, 185 (1954).
[2] (a) L. O. Brockway and P. C. Cross, J. Chem. Phys. **3**, 828 (1935). (b) Ledell, Post, and Fankuchen, Acta Cryst. **5**, 795 (1952).

way and Cross suggested resonance between structures I and II,

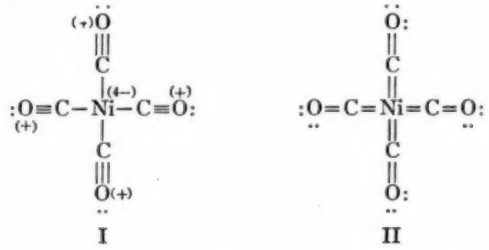

I

II

stating that ". . . structure I probably predominates in the resonance . . ." and ". . . its directional properties determine those of the normal state of the molecule . . .", but ". . . in fact, the observed tetrahedral structure cannot be used as a criterion for the proposed resonance." Furthermore, a description of this kind is not satisfactory because it is quite unlikely that structure I predominates, due to the large formal charge on the Ni atom, which is certainly not compensated by the partial ionic character of the bonds. The question is thus: is it possible to construct four equivalent double bonds from d^4sp^3 hybridization, with the correct properties for the tetrahedral symmetry and explain in this way the more reasonable structure II, or, at least, some intermediate structure with less amount of double bond character? The purpose of the present investigation was to give an answer to this question.

A completely similar problem arises in the case of the oxygen acids. π bonding in these compounds has been discussed by Pauling,[3] who gives semiempirical equations for calculating the bond distances and the amount of double bond character. Wolfsberg and Helmholz[4] treated the cases of CrO_4^{--}, MnO_4^-, ClO_4^-, computing molecular orbital combinations of symmetry T_d and solving the secular equations by use of semiempirical parameters for the integrals. Their result with respect to the π bonding is characterized by the existence of one set of strongly bonding orbitals (symmetry E) capable of holding four electrons and one other set, of only slightly bonding orbitals (symmetry T_2), holding six electrons. There are in this way two strong and three weak π bonds. It is to be remarked however, that the stability of the E-orbitals is much greater than is ordinarily attributed to π electrons in a double bond in the valence bond treatment. The authors emphasize the importance of double bonding in these structures, but they complain that ". . . the term double bond loses much of its meaning since the structure can only with difficulty be considered as resulting from the resonance of localized double bonds."

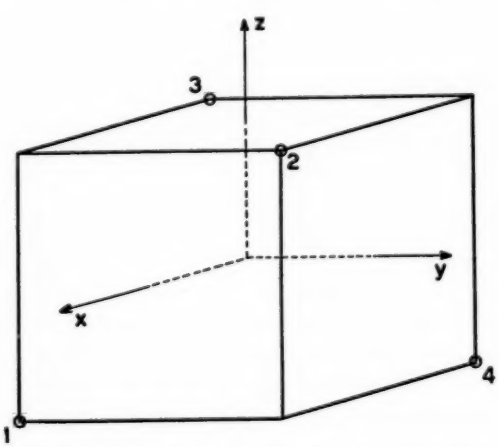

FIG. 1. Tetrahedron of reference inscribed in an oriented cube.

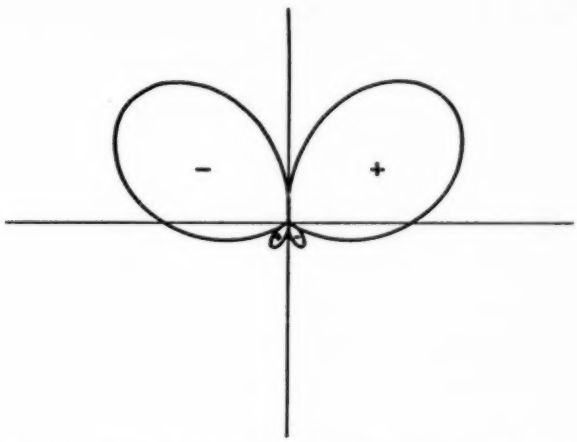

FIG. 2. General shape of orbitals of the type $(1-a^2)^{\frac{1}{2}}p+ad$. In the case of tetrahedral symmetry the plane of antisymmetry should contain one direction of the tetrahedron.

TETRAHEDRAL π ORBITALS

On a purely group-theoretical basis, Kimball[5] gives a method for determining all the allowed combinations of simple atomic orbitals which result in hybrids with the given symmetry character, including possibilities for π hybrids. According to the reduction table for the group T_d we can form σ hybrids from s, p, and d orbitals; the only allowed d's being d_{xz}, d_{xy}, and d_{yz}.‡ Furthermore, there is the possibility of a set of five π bonds, which can be made from any combination of p- and d orbitals.

We shall refer to a tetrahedron inscribed in a cube with the coordinate axes and the corners labeled as indicated in Fig. 1.

We shall also assume that π orbitals of the type that we are looking for must have the general shape shown in Fig. 2. In this figure the antisymmetry plane will contain, for example, the direction $(1\bar{1}\bar{1})$ of the cube (corner 1 of the tetrahedron). An orbital of this kind,

[3] L. Pauling, J. Phys. Chem. **56**, 361 (1952).
[4] Wolfsberg and Helmholz, J. Chem. Phys. **20**, 837 (1952).
[5] G. Kimball, J. Chem. Phys. **8**, 188 (1939).

‡ The notation here adopted for the d orbitals is

$$d_{xz}=(15)^{\frac{1}{2}}\sin\theta\cos\theta\cos\varphi$$
$$d_{yz}=(15)^{\frac{1}{2}}\sin\theta\cos\theta\sin\varphi$$
$$d_{xy}=[(15)^{\frac{1}{2}}/2]\sin^2\theta\sin 2\varphi$$
$$d_{z^2}=(\sqrt{5}/2)(3\cos^2\theta-1)$$
$$d_{x^2-y^2}=[(15)^{\frac{1}{2}}/2]\sin^2\theta\cos 2\varphi.$$

TABLE I. Transformation properties of p and d orbitals under the operations of group T_d.[a]

E	C_3	C_2	σ_d	S_4
p_x	$-p_z$	p_x	p_x	$-p_z$
p_y	$-p_x$	$-p_y$	p_z	p_z
p_z	p_y	$-p_z$	p_y	$-p_y$
d_{yz}	$-d_{xy}$	d_{yz}	d_{yz}	$-d_{yz}$
d_{xz}	$-d_{yz}$	$-d_{xz}$	d_{xy}	d_{xy}
d_{xy}	d_{yz}	$-d_{xy}$	d_{xz}	$-d_{xz}$
$d_{x^2-y^2}$	A[b]	$d_{x^2-y^2}$	$-A$	$-A$
d_{z^2}	A'[b]	d_{z^2}	A'	A'

[a] Only one example for each class is given. The notations for the classes are those of Eyring, Walter, and Kimball, *Quantum Chemistry* (John Wiley and Sons, Inc., New York).
[b] $A=(\sqrt{3}/2)d_{z^2}-(1/2)d_{x^2-y^2}$; $A'=(-1/2)d_{z^2}-(\sqrt{3}/2)d_{x^2-y^2}$.

pointing towards another direction in space (namely the negative z-direction), is obviously

$$\pi_{\bar{z}}=(1-a^2)^{\frac{1}{2}}p_x-ad_{xz}.$$

By rotating this function through an angle of 45° around the z-axis we obtain the new orbital

$$\pi_{\bar{z}}'=(1/\sqrt{2})[(1-a^2)^{\frac{1}{2}}(p_x+p_y)-a(d_{xz}+d_{yz})].$$

Now, the function which arises from rotating $\pi_{\bar{z}}'$ around the axis $x=y$ through an angle of 54°44′ will be our tetrahedral π orbital, if it can be expressed in terms of the orbital functions p and d. The transformation matrix for such a rotation is the similarity transformation $T^{-1}RT$, where

$$T\equiv\begin{vmatrix} 0 & -\sqrt{2}/2 & \sqrt{2}/2 \\ 0 & \sqrt{2}/2 & \sqrt{2}/2 \\ -1 & 0 & 0 \end{vmatrix}$$

is a transformstion of coordinates which brings z to coincide with the axis $x=y$, and

$$R\equiv\begin{vmatrix} 1/\sqrt{3} & \sqrt{2}/\sqrt{3} & 0 \\ -\sqrt{2}/\sqrt{3} & 1/\sqrt{3} & 0 \\ 0 & 0 & 1 \end{vmatrix}$$

is a rotation through 54°44′ around the new z-axis. Under the transformation $T^{-1}RT$ the function:

$$p_x+p_y\equiv\sqrt{3}(x+y)$$

TABLE II. Tetrahedral π functions.[a]

Function	p_x	p_z	p_y	d_{xz}	d_{yz}	d_{xy}	$d_{x^2-y^2}$	d_{z^2}	Corner[b]
1	0	a	a	$-b/\sqrt{3}$	$-b/\sqrt{3}$	0	$-2b/\sqrt{3}$	0	1
2	$-a$	$-a$	0	0	$b/\sqrt{3}$	$b/\sqrt{3}$	$2b/\sqrt{3}$	$-b$	1
3	a	0	$-a$	$b/\sqrt{3}$	0	$-b/\sqrt{3}$	$2b/\sqrt{3}$	b	1
4	0	a	$-a$	$b/\sqrt{3}$	$-b/\sqrt{3}$	0	$-2b/\sqrt{3}$	0	2
5	a	$-a$	0	0	$b/\sqrt{3}$	$-b/\sqrt{3}$	$2b/\sqrt{3}$	$-b$	2
6	$-a$	0	a	$-b/\sqrt{3}$	0	$b/\sqrt{3}$	$2b/\sqrt{3}$	b	2
7	0	$-a$	a	$-b/\sqrt{3}$	$b/\sqrt{3}$	0	$-2b/\sqrt{3}$	0	3
8	a	a	0	0	$-b/\sqrt{3}$	$-b/\sqrt{3}$	$2b/\sqrt{3}$	$-b$	3
9	$-a$	0	a	$b/\sqrt{3}$	0	$b/\sqrt{3}$	$2b/\sqrt{3}$	b	3
10	0	$-a$	$-a$	$b/\sqrt{3}$	$b/\sqrt{3}$	0	$-2b/\sqrt{3}$	0	4
11	$-a$	a	0	0	$-b/\sqrt{3}$	$b/\sqrt{3}$	$2b/\sqrt{3}$	$-b$	4
12	a	0	a	$-b/\sqrt{3}$	0	$-b/\sqrt{3}$	$2b/\sqrt{3}$	b	4

[a] Each coefficient has to be multiplied by $1/[2(a^2+b^2)]^{\frac{1}{2}}$.
[b] The functions pointing toward the same corner are rotated through an angle of 60°, each with respect to the others.

goes into itself and

$$d_{yz}+d_{xz}\equiv(15)^{\frac{1}{2}}(yz+xz)$$

goes into

$$(15/3)^{\frac{1}{2}}(x^2-y^2+xz+yz)$$

which corresponds to

$$(2/\sqrt{3})d_{x^2-y^2}+(1/\sqrt{3})d_{xz}+(1/\sqrt{3})d_{yz}$$

since

$$d_{x^2-y^2}\equiv[(15)^{\frac{1}{2}}/2](x^2-y^2).$$

The orbital $\pi_{\bar{z}}'$ becomes

$$\tau_1=(1/\sqrt{2})[(1-a^2)^{\frac{1}{2}}(p_x+p_y)-(a/\sqrt{3})(d_{yz}+d_{xz}+2d_{x^2-y^2})]$$

which is an orbital capable of forming a π bond with an atom situated on the corner 1 of the tetrahedron.

In order to obtain all the possible functions of this kind we have to perform on τ_1 all the operations of the symmetry group T_d.

The transformation properties of p and d orbitals under such operations are shown in Table I. In Table II

TABLE III. Orthogonal couples of tetrahedral π functions.

Corners	Functions I set	II set	III set	IV set
1–2	1–6	2–6	3–4	3–5
1–3	2–9	3–8	1–8	2–7
1–4	3–10	1–11	2–10	1–12
2–3	5–7	4–9	6–7	4–8
2–4	4–11	5–10	5–12	6–11
3–4	8–12	7–12	9–11	9–10

the twelve functions arising from τ_1 are listed, together with the corners to which they point. By inspecting the table it becomes obvious that these functions are linearly independent only when taken in groups of three.

The next step is to determine the parameter a in such a way that each function is orthogonal to the maximum number of others. We see from the table that the function 1 could be orthogonal only to 6, 8, 9, 10, 11, and 12. The condition for being orthogonal to 6, 8, 11, 12 is unique and it is different from the ones for 9 and 10. We therefore choose $a=\sqrt{3}/2$, which makes the couples 1–6, 1–8, 1–11, 1–12 orthogonal; so we can now write down all the couples which are made orthogonal by this condition. These are listed in Table III, together with the corners to which they refer. There are eight groups of three functions each which are mutually orthogonal; furthermore, the functions in each group are linearly independent and correspond to three different corners. Table IV shows the two equivalent sets of four triads of functions.

ORTHOGONALITY TO THE σ ORBITALS

So far we have not considered the orthogonality with the σ orbitals. The most general set of tetrahedral

σ functions is

$$\sigma_{111}=(1/2)s+[(1/4-b^2)^{\frac{1}{2}}(p_x+p_y+p_z)+b(d_{yz}+d_{xz}+d_{xy})]$$

$$\sigma_{1\bar{1}\bar{1}}=(1/2)s+[(1/4-b^2)^{\frac{1}{2}}(p_x-p_y-p_z)+b(d_{yz}-d_{xz}-d_{xy})]$$

$$\sigma_{\bar{1}1\bar{1}}=(1/2)s+[(1/4-b^2)^{\frac{1}{2}}(-p_x+p_y-p_z)+b(-d_{yz}+d_{xz}-d_{xy})]$$

$$\sigma_{\bar{1}\bar{1}1}=(1/2)s+[(1/4-b^2)^{\frac{1}{2}}(-p_x-p_y+p_z)+b(-d_{yz}-d_{xz}+d_{xy})].$$

$$0\leq b\leq 1/2.$$

The value b which gives the maximum strength, according to Pauling's criterion,[6] is $b=\sqrt{5}/4\sqrt{2}$, the value of the maximum of the functions being 2.95.

Each one of the functions of Table II is already orthogonal to two of the σ's by symmetry; in order to make them orthogonal also to the two others one has to take $b=1/\sqrt{8}$.

This value of b does not change the strength of the σ orbitals very much, the maximum in the bond direction being now 2.93.

TABLE IV. Triads of mutually orthogonal π functions.

Corners	Functions I set	Functions II set
1, 2, 3	2, 6, 7	3, 4, 8
1, 2, 4	3, 5, 10	1, 6, 11
1, 3, 4	1, 8, 12	2, 9, 10
2, 3, 4	4, 9, 11	5, 7, 12

STRENGTH OF THE π ORBITALS

We shall assume as a criterion for the strength of the π orbitals the value of the maximum of the projection of the angular part of the function along the bond direction; this is in conformity with the adopted criterion for the σ orbitals. A somewhat similar criterion has been used by Kilpatrick and Spitzer[7] in discussing bent bonds in some cyclic hydrocarbons.

Without loss of generality, we can investigate the behavior of this maximum as it varies with a, by looking at the simpler function

$$\pi_z=(1-a^2)^{\frac{1}{2}}p_x+ad_{xz}$$

which points toward the positive z-direction. The maximum cross section for the angular part of π_z is at $\varphi=0$,

$$(1-a^2)^{\frac{1}{2}}\sqrt{3}\sin\theta+a(15)^{\frac{1}{2}}\sin\theta\cos\theta.$$

The projection along the z-axis is

$$\rho=(1-a^2)^{\frac{1}{2}}\sqrt{3}\sin\theta\cos\theta+a(15)^{\frac{1}{2}}\sin\theta\cos^2\theta.$$

By taking $\partial\rho/\partial\theta=0$ and putting $\cos\theta=k$, $(0\leq k\leq 1)$ we find

$$3\sqrt{5}ak^3+2(1-a^2)^{\frac{1}{2}}k^2-2\sqrt{5}ak-(1-a^2)^{\frac{1}{2}}=0.$$

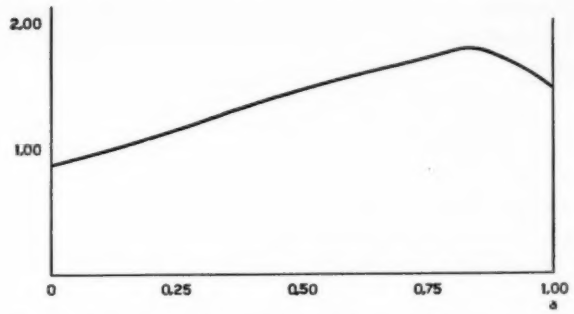

FIG. 3. Behavior with a of the maximum projection over the direction of the bond (which is indicated by ρ in the text), for orbitals of the general shape of Fig. 2.

The solution of this cubic in k for various values of a, introduced in the expression for ρ, gives us the desired behavior. This is illustrated in Fig. 3. The value of ρ for $a=\sqrt{3}/2$ is 1.77. The value of a which gives the maximum value for ρ is obtained by solving the system

$$\partial\rho/\partial\theta=0;\quad \partial\rho/\partial a=0.$$

It is found to be $a=0.845$, with $\rho=1.80$. It is important to note that these values are very close to the ones needed for orthogonality.

ORBITALS FOR THE LONE PAIRS

After the mutually orthogonal σ and π sets of orbitals have been established, we are left with a total of two orbitals to be made up by 2/8 of each one of the p- and d functions.

It is possible to hybridize these functions in order to obtain two mutually orthogonal orbitals each of which is orthogonal to the previous sets and suitable for filling with eventual lone pairs of electrons. These orbitals are

$$\lambda_1=(1/4)[(p_x-d_{yz})+(p_y-d_{xz})-2(p_z-d_{xy})+2d_{x^2-y^2}],$$

$$\lambda_2=(1/4)[\sqrt{3}(p_x-d_{yz})-\sqrt{3}(p_y-d_{xz})+2d_{z^2}],$$

or any two orthogonal linear combinations of them, such as the equivalent ones,

$$(1/\sqrt{2})(\lambda_1+\lambda_2)\quad\text{and}\quad(1/\sqrt{2})(\lambda_1-\lambda_2).$$

These orbitals are very probably not suitable for bonding, though their directional properties have not been determined.

CASE OF TRIGONAL BIPYRAMIDAL SYMMETRY

Precisely the same problem that has been treated for the tetrahedral case, applicable to nickel carbonyl, arises in the discussion of the molecule $Fe(CO)_5$. The geometrical configuration is here a trigonal bipyramid, symmetry group D_{3h}; the shortening of the bond distance with respect to the sum of the covalent bond radii is 0.16 ± 0.03 A.[8]

[6] L. Pauling, J. Am. Chem. Soc. **53**, 1367 (1931).
[7] Kilpatrick and Spitzer, J. Chem. Phys. **14**, 463 (1946).
[8] Ewens and Lister, Trans. Faraday Soc. **35**, 681 (1939).

TABLE V. Trigonal bipyramidal σ functions.[a]

Function	p_z	p_y	p_x	d_{xy}	$d_{x^2-y^2}$	d_{z^2}	s	
1	$(\sqrt{2}/\sqrt{3})b$	0	0	0	$\sqrt{2}(1-b^2)^{\frac{1}{2}}/\sqrt{3}$	$-a/\sqrt{3}$	$(1-a^2)^{\frac{1}{2}}/\sqrt{3}$	Eq.
2	$(-1/\sqrt{6})b$	$(1/\sqrt{2})b$	0	$-(1-b^2)^{\frac{1}{2}}/\sqrt{2}$	$-(1-b^2)^{\frac{1}{2}}/\sqrt{6}$	$-a/\sqrt{3}$	$(1-a^2)^{\frac{1}{2}}/\sqrt{3}$	Eq.
3	$(-1/\sqrt{6})b$	$-(1/\sqrt{2})b$	0	$(1-b^2)^{\frac{1}{2}}/\sqrt{2}$	$-(1-b^2)^{\frac{1}{2}}/\sqrt{6}$	$-a/\sqrt{3}$	$(1-a^2)^{\frac{1}{2}}/\sqrt{3}$	Eq.
4	0	0	$1/\sqrt{2}$	0	0	$(1-a^2)^{\frac{1}{2}}/\sqrt{2}$	$a/\sqrt{2}$	Axial
5	0	0	$-1/\sqrt{2}$	0	0	$(1-a^2)^{\frac{1}{2}}/\sqrt{2}$	$a/\sqrt{2}$	Axial

[a] The axis of the bipyramid is the z-axis, the function 1 points toward the x axis.

According to the reduction table for the group D_{3h},[5] we can form σ bonds from spd orbitals, the allowed d's being d_{z^2}, $d_{x^2-y^2}$, d_{xy}; it has to be noted that the p_z orbital must be used entirely in order to form the complete set of σ orbitals. For the π orbitals we can use only p_x, p_y, and any d's but d_{z^2}. The set of five σ orbitals has been actually written down by Duffey,[9] and is shown in Table V. In general the three equatorial orbitals are not equivalent to the two axial ones. However, if we take the values of a and b which make the function $3S_1+2S_2$ a maximum§ (S_1 and S_2 being the maxima of the equatorial and axial functions, respectively), we find $a=0.565$, $b=0.784$, and correspondingly $S_1=2.931$, $S_2=2.929$, so that the σ orbitals are almost equivalent, according to Pauling's criterion.

We shall again make the assumption, already made in the tetrahedral case, that a good π function must have general shape $(1-a^2)^{\frac{1}{2}}p+ad$. Owing to the fact that the orbital p_z has to be completely used in the σ orbitals formation, we conclude that it is impossible to have functions of this general shape outside of the plane xy. We have also in this case two classes of orbitals. The two orbitals d_{xz} and d_{yz} may form bonds with the axial atoms, but also (taking obvious linear combinations) with the equatorial ones. On the plane xy we have the orbital pointing toward the x direction (containing, for example, one of the equatorial atoms):

$$\pi_1=(1-c^2)^{\frac{1}{2}}p_y+cd_{xy}.$$

By applying to this function all the operations of group D_{3h} (see Table VI) we obtain the two other functions

TABLE VI. Transformation properties of p and d orbitals under the operations of group D_{3h}.[a]

E	σ_h	C_3[b]	S_3[b]	C_2	σ_v
p_x	p_x	$A(p_x,p_y)$	$A(p_x,p_y)$	p_x	p_x
p_y	p_y	$A'(p_x,p_y)$	$A'(p_x,p_y)$	$-p_y$	$-p_y$
d_{yz}	$-d_{yz}$	$A'(d_{xz},d_{yz})$	$-A'(d_{xz},d_{yz})$	d_{yz}	$-d_{yz}$
d_{xz}	$-d_{xz}$	$A(d_{xz},d_{yz})$	$-A(d_{xz},d_{yz})$	$-d_{xz}$	d_{xz}
d_{xy}	d_{xy}	$A(d_{xy},d_{x^2-y^2})$	$A(d_{xy},d_{x^2-y^2})$	$-d_{xy}$	$-d_{xy}$
$d_{x^2-y^2}$	$d_{x^2-y^2}$	$A'(d_{xy},d_{x^2-y^2})$	$A'(d_{xy},d_{x^2-y^2})$	$d_{x^2-y^2}$	$d_{x^2-y^2}$

[a] Only one example for each class is given. Notation as in Table I.
[b] $A(\zeta,\eta)=-\frac{1}{2}\zeta+(3/2)^{\frac{1}{2}}\eta$; $A'(\zeta,\eta)=-(3/2)^{\frac{1}{2}}\zeta-\frac{1}{2}\eta$.

[9] Duffey, J. Chem. Phys. **17**, 196 (1949).
§ Note that Duffey maximizes the function $3S_1^2+2S_2^2$. There is no obvious reason for taking the square because the orbitals matched in the bonds are in general different.

$$\pi_2=(1/2)[(1-c^2)^{\frac{1}{2}}(-\sqrt{3}p_x-p_y)+c(-d_{xy}+\sqrt{3}d_{x^2-y^2})],$$
$$\pi_3=(1/2)[(1-c^2)^{\frac{1}{2}}(\sqrt{3}p_x-p_y)+c(-d_{xy}-\sqrt{3}d_{x^2-y^2})].$$

These three functions are linearly independent only when taken by two's. However there is no way of making them orthogonal for any value of c. We conclude that there can be only one good π bond orbital lying in the equatorial plane, resonating among the three positions. The orbital for the lone pair of electrons will be, for each position,

$$\lambda_1=(1-c^2)^{\frac{1}{2}}p_x-cd_{x^2-y^2},$$
$$\lambda_2=(1/2)[(1-c^2)^{\frac{1}{2}}(-p_x+\sqrt{3}p_y)-c(-\sqrt{3}d_{xy}-d_{x^2-y^2})],$$
$$\lambda_3=(1/2)[(1-c^2)^{\frac{1}{2}}(-p_x-\sqrt{3}p_y)-c(\sqrt{3}d_{xy}-d_{x^2-y^2})],$$

orthogonal to the σ's and to the corresponding π. These orbitals are obviously not bonding; the shape of λ_1 being the one of Fig. 4.

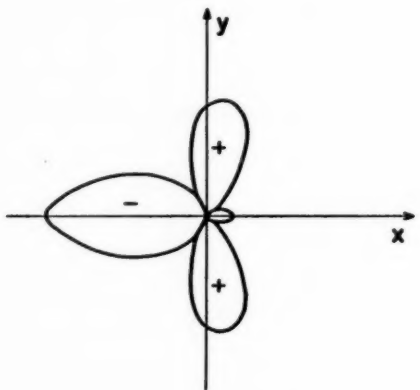

FIG. 4. Shape of the lone pair orbital λ_1 in the case of trigonal bipyramidal symmetry. This orbital is obviously not bonding since one of the atoms in the xy-plane has been supposed to be situated on the positive x-direction.

In order for the π functions to be orthogonal to all the σ's we must take $c=b=0.784$. The strength of the equatorial π orbital is in this way 1.70 (Fig. 3); the other two, being pure d's, have strength 1.50. One would thus expect a small difference in the corresponding bond lengths.

CASE OF OCTAHEDRAL SYMMETRY

Only a few words are needed in order to include the octahedral case which is applicable to the other car-

bonyls of the type $M(CO)_6$ (M=Cr,Mo,W). Here, in fact, only the orbitals d_{xy}, d_{xz}, d_{yz} are left for π bond formation. These orbitals are obviously suitable for forming bonds to atoms at the corners of the octahedron, the three bonds resonating among the six positions [see reference 1(c)].

DISCUSSION

For the results of our investigation we are now in a position to interpret the electronic structure of the three carbonyls by considering resonance structures of the type

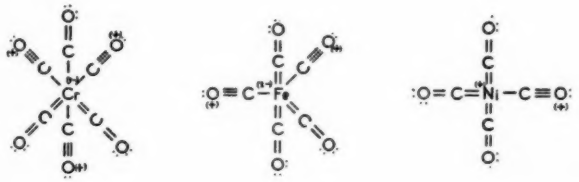

We can assume, in fact, that the d orbitals necessary for the double bonds will be used as much as possible, being of the same order of stability as $4s$ and $3p$. On the contrary, in the case of the oxygen acids of the elements of the second row the π bond formation will not be complete, since the d orbitals are in general less stable than s and p. Pauling[3] has calculated the amount of π bond formation in these cases, on the basis of charge neutralization considerations, and we have only to recall that this amount is never more than 75%, which is the maximum allowed for tetrahedral symmetry, according to our preceding arguments.

The proposed electronic structures for the carbonyls seem to give a good description of the molecules for two reasons.

(I). They reduce the formal negative charges on the metal atoms. These charges (3, 2, 1, going from the chromium to the nickel compound) are even more reduced by the effect of the electronegativity difference between the central atom and the carbon atom; this difference increases in the order Cr, Fe, Ni. By taking Haissinsky's values for the electronegativities of the metals[10] and assuming equal amounts of ionic character for the σ and π bonds,[11] we obtain the following values for the charges on the metals: 1.2 for Cr, 0.6 for Fe, no charge for Ni.

(II). They give a good qualitative account for the bond shortening, which increases in the order Cr, Fe, Ni, in agreement with increasing bond number.

[10] Haissinsky, J. chim. phys. 298 (1949).
[11] L. Pauling, *The Nature of the Chemical Bond* (Cornell University Press, Ithaca, New York, 1939), pp. 74–75.

TABLE VII. Bond number for coordination compounds of different symmetries containing penultimate d orbitals in the central atom.

Symm.	Strength σ	Strength π	Rel. strength σ	Rel. strength π	n	n corr.
Tetr.	2.930	1.77	1.00	1.00	1.75	1.75
Bipyr.	2.930[a]	1.57[a]	1.00	0.847	1.60	1.53
Oct.	2.923	1.50	0.998	0.847	1.50	1.42

[a] Average of the equatorial and axial strengths.

We have tried to provide a quantitative explanation on the basis of the equation

$$\Delta R=-\frac{0.63n_\pi+0.195n_\pi^2}{1+2n_\pi+(1/4)n_\pi^2}$$

used by Pauling for the oxygen acids.[3] This equation takes into account the fact that double bonds can resonate between the two perpendicular planes. In our case we have to take into account also the fact that the strength of the orbitals is different for the different compounds. In order to do this we shall use the bond number multiplied by the average strength of the orbitals involved, assuming the strength of the tetrahedral σ and π orbitals as unity. The bond numbers corrected in this way are given in Table VII.

By using these values of n_π in Pauling's equation we obtain the following figures for the shortenings:

Compound	ΔR calc	ΔR obs
$Cr(CO)_6$	0.16 A	0.10±0.04 A
$Fe(CO)_5$	0.18 A	0.16±0.03 A
$Ni(CO)_4$	0.22 A	0.18±0.03 A

The observed ΔR are based on the following values for the single bond radii of the metals: Fe, 1.18 A; Cr, 1.25 A; Ni, 1.23 A. Better quantitative agreement cannot be expected because of the uncertainty in these values and in the values to be assumed for the pure double and triple bond shortenings involved in Pauling's equation. He assumes 0.21 and 0.34 A, respectively; complete agreement could be obtained in the present case by taking the somewhat shorter values 0.17 and 0.28 A.

ACKNOWLEDGMENTS

The author is very thankful to Professor Linus Pauling for having suggested the problem and for his helpful advice and encouragement. Thanks are due also to Dr. J. D. Dunitz and Dr. L. Orgel for many illuminating discussions. Grants from the Institute of International Education and from the Fulbright program are gratefully acknowledged.

Molecular Theory of Light Scattering

MARSHALL FIXMAN*
Department of Chemistry, Yale University, New Haven, Connecticut
(Received January 20, 1955)

The Einstein-Smoluchowski phenomenological theory of light scattering is shown to agree with the molecular theory of light scattering for a one component system of isotropic scattering molecules.

INTRODUCTION

FOR more than twenty-five years the phenomenological theory of light scattering determined by Smoluchowski[1] and Einstein[2] has been subject to serious criticism.[3–6] These criticisms have entered into a current controversy over the absolute turbidities of pure liquids.[7] Such tribidities are widely used for the calibration of light scattering apparatus. Qualitatively, the objection to the phenomenological theory is this: Light scattering arises from density fluctuations in a region of linear dimensions small compared to the wavelength of the incident light; but in the Lorentz expression for the "local field" acting on a molecule (local field is $(n^2+2)\mathbf{E}/3$, where n is the index of refraction and $\mathbf{E}$ is the macroscopic electric field), the factor $(n^2+2)/3$ arises from the polarization of the fluid outside the region in question, and therefore does not fluctuate. This argument leads to the conclusion that the observed value of $\partial n^2/\partial v$ (where v is the fluid density) must be divided by $(n^2+2)/3$ to get the proper value of the density derivative of the dielectric constant, which enters into Einstein's formula for the turbidity. (The argument in the works[3–5] previously mentioned is usually more refined.)

Molecular theories of light scattering have been given by Zimm,[8] who consciously passed over the problem of the local field, and by Yvon,[9] who laid a magnificent foundation to which we shall constantly refer; but Yvon restored to drastic approximations near the end of his calculation, and so arrived at what we regard as an erroneous correction of Einstein's turbidity formula. Our molecular theory results in the generalized Einstein formula, which takes into account the possibility of fluctuations in the off-diagonal terms of the dielectric constant tensor.

We suppose that a large region of space is filled with optically isotropic molecules upon which acts a primary electric vector $\mathbf{E}_0$. We wish to compute the intensity of light scattered from a macroscopic volume V to a point within the fluid but far removed from V. We assume the presence of appropriate shielding so that the observer receives primary scattered light only from V, and further we neglect fluctuations in density or dielectric constant (which give rise to secondary scattering) in the fluid lying outside of V.

At each point in the fluid the electric and magnetic vectors $\mathbf{E}$ and $\mathbf{H}$, respectively, satisfy the microscopic Maxwell equations,[10] which are equivalent to the ordinary Maxwell equations in vacuum in the presence of a distribution of charge ρ given by $\rho=-\nabla\cdot\mathbf{P}$, $\mathbf{P}$ being the polarization vector, or dipole moment unit volume.[11] In mks units these equations are

$$\nabla\times\mathbf{E}+\mu_0\frac{\partial\mathbf{H}}{\partial t}=0, \tag{1}$$

$$\nabla\times\mathbf{H}-\epsilon_0\frac{\partial\mathbf{E}}{\partial t}=\frac{\partial\mathbf{P}}{\partial t}, \tag{2}$$

$$\nabla\cdot\mathbf{H}=0, \tag{3}$$

and

$$\nabla\cdot\mathbf{E}=-\frac{1}{\epsilon_0}\nabla\cdot\mathbf{P}. \tag{4}$$

In these equations, μ_0 and ϵ_0 are the magnetic and electric inductive capacities, respectively, of empty space. The time factor of the vectors in Eqs. (1)–(4) is assumed to be $\exp(-ik_0ct)$, where $c[=1/(\epsilon_0\mu_0)^{\frac{1}{2}}]$ is the velocity of light in vacuum; $k_0=2\pi/\lambda_0$, where λ_0 is the wavelength (in vacuum) of $\mathbf{E}_0$. After the standard substitutions Eqs. (1) and (2) lead to

$$\nabla^2\mathbf{E}+k_0^2\nabla\nabla\cdot\mathbf{E}=-k_0^2\mathbf{P}/\epsilon_0. \tag{5}$$

Since fluctuations are to be neglected outside V, the macroscopic equation, $\mathbf{P}=(\epsilon-\epsilon_0)\mathbf{E}$, holds outside V. We therefore perform a simple transformation of Eq. (5) so that $\mathbf{P}-(\epsilon-\epsilon_0)\mathbf{E}$ appears as a source function.

Let

$$k^2=n^2k_0^2$$

$$\epsilon=n^2\epsilon_0.$$

* F. B. Jewett Fellow, Yale University, 1953–1954.
[1] M. Smoluchowski, Ann. Physik **25**, 205 (1908).
[2] A. Einstein, Ann. Physik **33**, 1275 (1910).
[3] K. Ramanathan, Indian J. Phys. **1**, 413 (1927).
[4] Y. Rocard, Ann. phys. **10**, 158 (1928).
[5] J. Cabannes, *La Diffusion Moleculaire de la Lumière* (Presses Universitaires de France, Paris, 1929).
[6] H. A. Stuart and H. G. Trieschmann, *Hand-und-Jahrbuch der Chemischen Physik* (Akademische Verlagsgesellschaft, Leipzig, 1936), Vol. 8, Part 2.
[7] A. Rousset and R. Lochet, J. Polymer Sci. **10**, 319 (1953).
[8] B. H. Zimm, J. Chem. Phys. **13**, 141 (1945).
[9] J. Yvon, *Actualites Scientifiques et Industrielles* (Hermann Cie, Paris, 1937), Nos. 542, 543.
[10] P. Mazur and B. R. A. Nijboer, Physica **19**, 971 (1953) (with references).
[11] J. A. Stratton, *Electromagnetic Theory* (McGraw-Hill Book Company, Inc., New York, 1941), pp. 424–436.

[As before, n is the (average) index of refraction of the fluid.] The addition of $k_0^2(\epsilon-\epsilon_0)\mathbf{E}/\epsilon_0$ to both sides of Eq. (5) yields

$$\nabla^2\mathbf{E}+k^2\mathbf{E}-\nabla\nabla\cdot\mathbf{E}=-k_0^2[\mathbf{P}-(\epsilon-\epsilon_0)\mathbf{E}]/\epsilon_0.$$

Now express $\mathbf{E}$ in terms of the Hertz vector potential $\mathbf{\Pi}$,

$$\mathbf{E}=\nabla\nabla\cdot\mathbf{\Pi}+k^2\mathbf{\Pi}, \tag{6}$$

and

$$\nabla^2\mathbf{\Pi}+k^2\mathbf{\Pi}=-[\mathbf{P}-(\epsilon-\epsilon_0)\mathbf{E}]/\epsilon. \tag{7}$$

The r.h.s. of Eq. (7) is now a source function confined to V by virtue of our condition that fluctuations of dielectric constant outside V are to be ignored. The well-known solution for the scattered wave is[11]

$$\mathbf{\Pi}(\mathbf{D})=(4\pi\epsilon)^{-1}\int_V\frac{[\mathbf{P}-(\epsilon-\epsilon_0)\mathbf{E}]}{|\mathbf{R}-\mathbf{D}|}\times\exp(ik|\mathbf{R}-\mathbf{D}|)d\mathbf{R}. \tag{8}$$

We may subtract from Eq. (8) its average, and put $\boldsymbol{\pi}=\mathbf{\Pi}-\langle\mathbf{\Pi}\rangle_{Av}$, $\mathbf{e}=\mathbf{E}-\langle\mathbf{E}\rangle_{Av}$, $\mathbf{p}=\mathbf{P}-\langle\mathbf{P}\rangle_{Av}$. Suppose that the origin of a coordinate system is fixed in V, and that $\mathbf{D}$ is very large and has a direction specified by the unit vector $\mathbf{s}$. Then

$$\boldsymbol{\pi}=(4\pi\epsilon D)^{-1}e^{ikD}\int_V[\mathbf{p}-(\epsilon-\epsilon_0)\mathbf{e}]\times\exp(-ik\mathbf{s}\cdot\mathbf{R})d\mathbf{R}. \tag{9}$$

The scattered light is measured after it passed through an analyzer which has a direction specified by the unit vector $\mathbf{u}(\mathbf{u}\cdot\mathbf{s}=0)$. From Eqs. (6) and (9),

$$\mathbf{u}\cdot\mathbf{e}=k_0^2(4\pi\epsilon_0 D)^{-1}e^{ikD}\int_V\mathbf{u}\cdot[\mathbf{p}-(\epsilon-\epsilon_0)\mathbf{e}]\times\exp(-ik\mathbf{s}\cdot\mathbf{R})d\mathbf{R}. \tag{10}$$

The intensity of light scattered to $\mathbf{D}$ is proportional to $(\mathbf{u}\cdot\mathbf{e})(\mathbf{u}\cdot\mathbf{e}^*)$, where "*" indicates the complex conjugate.

We now turn to the detailed molecular evaluation of $[\mathbf{p}-(\epsilon-\epsilon_0)\mathbf{e}]$.

MOLECULAR THEORY

The oscillating dipole moment $\mathfrak{p}_j$, of molecule j centered at $\mathbf{R}_j$, produces a field $\mathbf{T}_{ij}\cdot\mathfrak{p}_j$ at $\mathbf{R}_i$, where $\mathbf{T}_{ij}$ is a dyadic operator given by

$$\mathbf{T}_{ij}=\mathbf{T}_{ji}=\frac{1}{4\pi\epsilon_0}(\nabla_i\nabla_i+k_0^2\mathbf{I})\frac{e^{ik_0R_{ij}}}{R_{ij}}, \tag{11}$$

$$R_{ij}=|\mathbf{R}_j-\mathbf{R}_i|.$$

The idemfactor or identity operator is "$\mathbf{I}$." Denote the polarizability of a molecule by α and use a primed sum to indicate a sum over $j\neq i$. We have for $\mathfrak{p}_i$,

$$\mathfrak{p}_i=\alpha(\mathbf{E}_{0i}+\sum{}'\,\mathbf{T}_{ij}\cdot\mathfrak{p}_j). \tag{12}$$

By the method of successive approximations to $\mathfrak{p}_i$, of which the first is $\alpha\mathbf{E}_{0i}$,[9,12] we get from Eq. (12):

$$\mathfrak{p}_i=\alpha\mathbf{E}_{0i}+\alpha^2\sum{}'\,\mathbf{T}_{ij}\cdot\mathbf{E}_{0j}+\alpha^3\sum{}'\sum{}'\,\mathbf{T}_{ij}\cdot\mathbf{T}_{jk}\cdot\mathbf{E}_{0k}+\cdots. \tag{13}$$

We now introduce three-dimensional Dirac δ functions with the object of expressing Eq. (13) in integral form. The density in molecules/unit volume at $\mathbf{R}_1$ is, in a particular configuration of molecular centers $\mathbf{R}_i$,[13] $\sum\delta(\mathbf{R}_1-\mathbf{R}_i)$. The instantaneous pair distribution function is $\sum\sum_{i\neq j}\delta(\mathbf{R}_1-\mathbf{R}_i)\delta(\mathbf{R}_2-\mathbf{R}_j)$, and so on. A δ function may be represented, for example, by

$$\delta(\mathbf{R}_1-\mathbf{R}_i)=\frac{1}{(2\pi)^3}\int_{-L}^{+L}\int\int e^{i\mathbf{K}\cdot(\mathbf{R}_1-\mathbf{R}_i)}dK_X dK_Y dK_Z,$$

where L is very large and in the ultimate averaging process is to approach infinity. The distribution of polarizability of molecule i is $\alpha\delta(\mathbf{R}_1-\mathbf{R}_i)$ and is spherically symmetrical around $\mathbf{R}_i$ and sharply peaked (but mathematically continuous) at $\mathbf{R}_i$.

Let

$$v_1=\langle\sum\delta(R_1-R_i)\rangle_{Av};\quad\delta_1=\sum\delta(\mathbf{R}_1-\mathbf{R}_i)-v_1$$

$$v_{12}=\langle\sum_{i\neq j}\sum\delta(\mathbf{R}_1-\mathbf{R}_i)\delta(\mathbf{R}_2-\mathbf{R}_j)\rangle_{Av};$$

$$\delta_{12}=\sum_{i\neq j}\sum\delta(\mathbf{R}_1-\mathbf{R}_i)\delta(\mathbf{R}_2-\mathbf{R}_j)-v_{12} \tag{14}$$

$$v_{123}=\langle\sum_{\substack{i\neq j,\ j\neq k\\ k\neq i}}\sum\sum\delta(\mathbf{R}_1-\mathbf{R}_i)\delta(\mathbf{R}_2-\mathbf{R}_j)\delta(\mathbf{R}_3-\mathbf{R}_k)\rangle_{Av};$$

$$\delta_{123}=\sum_{\substack{i\neq j,\ k\neq j\\ k\neq i}}\sum\sum\delta(\mathbf{R}_1-\mathbf{R}_i)\delta(\mathbf{R}_2-\mathbf{R}_j)\times\delta(\mathbf{R}_3-\mathbf{R}_k)-v_{123},\quad\text{etc.}$$

The averages are to be taken over the canonical ensemble appropriate to the temperature, volume, and number of particles in V. We may now obtain the polarization at $\mathbf{R}_1$ by multiplying Eq. (13) by $\delta(\mathbf{R}_1-\mathbf{R}_i)$ and summing over i.

$$\mathbf{p}_1=\alpha\delta_1\mathbf{E}_{01}+\alpha^2\int\delta_{13}\mathbf{T}_{13}\cdot\mathbf{E}_{03}d\mathbf{R}_3+\alpha^3\int\delta_{13}\mathbf{T}_{13}\cdot\mathbf{T}_{31}\cdot\mathbf{E}_{01}d\mathbf{R}_3+\alpha^3\int\delta_{135}\mathbf{T}_{13}\cdot\mathbf{T}_{35}\cdot\mathbf{E}_{05}d\mathbf{R}_3d\mathbf{R}_5+\cdots, \tag{15}$$

[12] J. G. Kirkwood, J. Chem. Phys. 4, 592 (1936).

[13] J. G. Kirkwood and F. P. Buff, J. Chem. Phys. 19, 744 (1951).

and $\langle \mathbf{P}_1 \rangle_{Av}$ is given by

$$\langle \mathbf{P}_1 \rangle = \alpha v_1 \mathbf{E}_{01} + \alpha^2 \int v_{13} \mathbf{T}_{13} \cdot \mathbf{E}_{03} d\mathbf{R}_3 + \cdots . \quad (16)$$

The average electric field vector, $\langle \mathbf{E}_1 \rangle$, is given by

$$\langle \mathbf{E}_1 \rangle = \mathbf{E}_{01} + \int \mathbf{T}_{13} \cdot \langle \mathbf{P}_3 \rangle d\mathbf{R}_3, \quad (17)$$

and

$$\mathbf{e}_1 = \int \mathbf{T}_{13} \cdot \mathbf{p}_3 d\mathbf{R}_3. \quad (18)$$

As an illustration of principles, and also because we need the result, we will review Yvon's calculation of the index of refraction. Equation (16) is inverted to obtain $\mathbf{E}_{01}$ in terms of $\langle \mathbf{P} \rangle$. The first of the successive approximations to $\mathbf{E}_{01}$ is $\langle \mathbf{P}_1 \rangle / \alpha v_1$. The result is

$$\begin{aligned} \alpha v_1 \mathbf{E}_{01} = \langle \mathbf{P}_1 \rangle &- \alpha \int v_3^{-1} v_{13} \mathbf{T}_{13} \cdot \langle \mathbf{P}_3 \rangle d\mathbf{R}_3 \\ &- a^2 \int v_1^{-1} v_{13} \mathbf{T}_{13} \cdot \mathbf{T}_{31} \cdot \langle \mathbf{P}_1 \rangle d\mathbf{R}_3 \\ &- \alpha^2 \int (v_5^{-1} \nu_{135} - v_3^{-1} v_5^{-1} v_{13} v_{35}) \\ &\times \mathbf{T}_{13} \cdot \mathbf{T}_{35} \cdot \langle \mathbf{P}_5 \rangle d\mathbf{R}_3 d\mathbf{R}_5 - \cdots . \end{aligned} \quad (19)$$

Substitution of this expression for $\mathbf{E}_0$ into Eq. (17) yields

$$\begin{aligned} \langle \mathbf{E}_1 \rangle = \frac{1}{\alpha v_1} \Big\{ \mathbf{I} &- \alpha \int (v_3^{-1} v_{13} - v_1) \mathbf{T}_{13} e^{i\mathbf{k} \cdot \mathbf{R}_{13}} d\mathbf{R}_3 \\ &- \alpha^2 \int v_1^{-1} v_{13} \mathbf{T}_{13} \cdot \mathbf{T}_{31} d\mathbf{R}_3 \\ &- \alpha^2 \int (v_5^{-1} v_{135} - v_3^{-1} v_5^{-1} v_{13} v_{35}) \\ &\times \mathbf{T}_{13} \cdot \mathbf{T}_{35} e^{i\mathbf{k} \cdot \mathbf{R}_{15}} d\mathbf{R}_3 d\mathbf{R}_5 + \cdots \Big\} \cdot \langle \mathbf{P}_1 \rangle . \end{aligned} \quad (20)$$

The dependence on position of $\langle \mathbf{P}_1 \rangle$ has been assumed to be $\exp(i\mathbf{k} \cdot \mathbf{R}_1)$. The first integral on the r.h.s. of Eq. (20) is readily evaluated. The integrand rapidly converges to zero (away from the critical point) as R_{13} increases, since v_{13} then approaches $v_1 v_3$ (to within terms whose order of magnitude is the reciprocal of the number of molecules in the system). The factor $\exp(i\mathbf{k} \cdot \mathbf{R}_{13})$ may be set equal to unity, and only the dominant term of $\mathbf{T}_{13}$ (at small R_{13}) which is $(4\pi\epsilon_0)^{-1} \nabla\nabla R_{13}^{-1}$ need be retained. Now

$$\nabla\nabla R_{13}^{-1} = R_{13}^{-3} (3\mathbf{u}_{13}\mathbf{u}_{13} - \mathbf{I}); \quad \mathbf{u}_{13} = \mathbf{R}_{13}/R_{13},$$

and a superficial integration over angles would lead to a value of zero for the integral. However, as the integral stands a separate integration over angles is not permissible. The quantity $(v_3^{-1} v_{13} - v_1)$ approaches $(-v_1)$ as $R_{13} \to 0$ (because repulsive forces make $v_{13} \to 0$), and so an integration over relative distances leads to infinity. The difficulty is easily circumvented in the standard way. The integration is first performed over an infinitesimal sphere surrounding $\mathbf{R}_1$;

$$\begin{aligned} &\int (v_3^{-1} v_{13} - v_1) \nabla\nabla R_{13}^{-1} d\mathbf{R}_3 \\ &= -v_1 \int_{s_1} \nabla\nabla R_{13}^{-1} d\mathbf{R}_3 + \int_{V_0 - s_1} (v_3^{-1} v_{13} - v_1) \\ &\qquad \times R_{13}^{-3} (3\mathbf{u}_{13}\mathbf{u}_{13} - \mathbf{I}) d\mathbf{R}_3 \quad (21) \\ &= \frac{4\pi}{3} v_1 \mathbf{I}. \end{aligned}$$

The second integral on the r.h.s. of Eq. (21), where V_0 is that part of the fluid illuminated by $\mathbf{E}_0 (V_0 > V)$, leads properly to zero, since the integration over relative distances is finite after the exclusion of s_1. The first volume integral may be converted to a surface integral with the application of Green's theorem, and so to the result. We may remark that the operational definition of $\mathbf{E}$ as the force acting on a unit charge led Kelvin to his cavity definition of $\mathbf{E}$. Although we have postponed the introduction of a cavity until its convenience became obvious, we could have introduced a cavity at the very beginning (as did Yvon in his refractive index and dielectric constant theories). Instead of Eqs. (17) and (18) we would have the equivalent equations

$$\langle \mathbf{E}_1 \rangle = \mathbf{E}_{01} + \int_{V_0 - s_1} \mathbf{T}_{13} \cdot \langle \mathbf{P}_3 \rangle d\mathbf{R}_3 - \frac{4\pi}{3} \langle \mathbf{P}_1 \rangle,$$

and

$$\mathbf{e}_1 = \int_{V_0 - s_1} \mathbf{T}_{13} \cdot \mathbf{p}_3 d\mathbf{R}_3 - \frac{4\pi}{3} \mathbf{p}_1.$$

Finally, we note that the more complicated integrands converge rapidly to zero, and the integrations result in multiples of the idemfactor.[14,15] There is then a scalar dielectric constant, independent of position and wavelength at optical frequencies (no absorption, naturally), and given by Yvon's expression,

$$\begin{aligned} (\epsilon - \epsilon_0)^{-1} &= \frac{\langle \mathbf{E}_1 \rangle}{\langle \mathbf{P}_1 \rangle} \\ &= \frac{1}{\alpha v_1} \Big\{ 1 - \frac{\alpha v_1}{3\epsilon_0} - \alpha^2 \int v_1^{-1} v_{13} \mathbf{T}_{13} \cdot \mathbf{T}_{31} d\mathbf{R}_3 \\ &\quad - \alpha^2 \int (v_5^{-1} v_{135} - v_3^{-1} v_5^{-1} v_{13} v_{35}) \\ &\qquad \times \mathbf{T}_{13} \cdot \mathbf{T}_{35} d\mathbf{R}_3 d\mathbf{R}_5 - \cdots \Big\}. \end{aligned} \quad (22)$$

[14] W. F. Brown, J. Chem. Phys. **18**, 1193 (1950).
[15] H. S. Green, *The Molecular Theory of Fluids* (Interscience Publishers Inc., New York, 1952), p. 207.

Before going on to the light scattering theory we wish to remark that there has been no step in this, Yvon's derivation, which would be invalid if the averages had been performed with the restriction that v be a slowly varying function of position. In particular, that part of the r.h.s. of Eq. (22) (the first and second term) which yields the Lorentz expression for the dielectric constant, involves only the density at $\mathbf{R}_1$, and not the density outside some large sphere surrounding $\mathbf{R}_1$. So it is indeed proper to speak of a "local" dielectric constant.

We now return to Eqs. (15) and (18) to obtain the source function $\mathbf{p}_1-(\epsilon-\epsilon_0)\mathbf{e}_1$. The bulky equations of the next few steps will be only briefly indicated. First, in Eq. (15), substitute for the primary wave $\mathbf{E}_0$ its expansion, in terms of the mean polarization vector, given by Eq. (19). Then Eq. (15) becomes

$$\mathbf{p}_1=\frac{\delta_1}{v}\langle\mathbf{P}_1\rangle-\cdots. \tag{23}$$

Next substitute Eq. (23) for $\mathbf{p}$ into Eq. (18) for $\mathbf{e}$. Then Eq. (18) becomes

$$\mathbf{e}_1=\frac{1}{v}\int\delta_3\mathbf{T}_{13}\cdot\langle\mathbf{P}_3\rangle d\mathbf{R}_3-\cdots. \tag{24}$$

Then we combine $\mathbf{e}_1$ and $\mathbf{p}_1$ to get $\mathbf{p}_1(\epsilon-\epsilon_0)\mathbf{e}_1$, which we need to compute the light scattering from Eq. (10). In order to avoid an inversion of the power series for $(\epsilon-\epsilon_0)^{-1}$, Eq. (20) or Eq. (22), the quantity $\mathbf{p}_1-(\epsilon-\epsilon_0)\mathbf{e}_1$ is factored into $(\epsilon-\epsilon_0)[\mathbf{p}_1(\epsilon-\epsilon_0)^{-1}-\mathbf{e}_1]$, and the multiplication by $(\epsilon-\epsilon_0)^{-1}$ is carried out using its series representation. In the resulting series for $\mathbf{p}_1(\epsilon-\epsilon_0)^{-1}-\mathbf{e}_1$, an integral,

$$\int\left(\frac{\delta_{13}}{v}-\frac{v_{13}}{v^2}\delta_1-\delta_3\right)\mathbf{T}_{13}e^{i\mathbf{k}\cdot\mathbf{R}_{13}}d\mathbf{R}_3,$$

which plays the role of a fluctuation in the value of

$$\int(v_3^{-1}v_{13}-v_1)\mathbf{T}_{13}e^{i\mathbf{k}\cdot\mathbf{R}_{13}}d\mathbf{R}_3,$$

is split into two parts as in the refractive index theory, an integration over an infinitesimal sphere surrounding $\mathbf{R}_1$, and the remainder:

$$\begin{aligned}&-\int_{s_1}\delta_3\mathbf{T}_{13}e^{i\mathbf{k}\cdot\mathbf{R}_{13}}d\mathbf{R}_3\\&+\int_{V_0-s_1}\left(\frac{\delta_{13}}{v}-\frac{v_{13}}{v^2}\delta_1-\delta_3\right)\mathbf{T}_{13}e^{i\mathbf{k}\cdot\mathbf{R}_{13}}d\mathbf{R}_3\\&=\frac{\delta_1}{3\epsilon_0}\mathbf{I}+\int_{V_0-s_1}\left(\frac{\delta_{13}}{v}-\frac{v_{13}}{v^2}\delta_1-\delta_2\right)\mathbf{T}_{13}e^{i\mathbf{k}\cdot\mathbf{R}_{13}}d\mathbf{R}_3.\end{aligned} \tag{25}$$

We then obtain

$$\begin{aligned}&\mathbf{p}_1-(\epsilon-\epsilon_0)\mathbf{e}_1\\&=\left\{\left[1+\frac{(\epsilon-\epsilon_0)}{3\epsilon_0}\right]\frac{\delta_1}{v}\mathbf{I}+\frac{(\epsilon-\epsilon_0)}{v}\right.\\&\times\left[\int_{V_0-s_1}\left(\frac{\delta_{13}}{v}-\frac{v_{13}}{v^2}\delta_1-\delta_3\right)\mathbf{T}_{13}e^{i\mathbf{k}\cdot\mathbf{R}_{13}}d\mathbf{R}_3\right.\\&+\alpha\int\left(\frac{\delta_{13}}{v}-\frac{v_{13}}{v^2}\delta_1\right)\mathbf{T}_{13}\cdot\mathbf{T}_{31}d\mathbf{R}_3\\&+\alpha\int\left(\frac{\delta_{135}}{v}-\frac{v_{135}}{v^2}\delta_1+\frac{2v_{13}v_{35}}{v^3}\delta_1\right.\\&\left.\left.-\frac{2v_{35}}{v^2}\delta_{13}+\frac{v_{35}}{v}\delta_3-\frac{v_{13}}{v}\delta_1+\delta_{13}-\delta_{35}\right)\right.\\&\left.\left.\times\mathbf{T}_{13}\cdot\mathbf{T}_{35}e^{i\mathbf{k}\cdot\mathbf{R}_{15}}d\mathbf{R}_3d\mathbf{R}_5+0(\alpha^2)+\cdots\right]\right\}\cdot\langle\mathbf{P}_1\rangle.\end{aligned} \tag{26}$$

The mean polarization $\langle\mathbf{P}_1\rangle$ may be replaced by $(\epsilon-\epsilon_0)\mathbf{E}_A\exp i\mathbf{k}\cdot\mathbf{R}_1$, where $\mathbf{E}_A$ is the *amplitude* of the mean, macroscopic electric vector in V. Equation (26) is completely accurate to the order of α which we have retained in the coefficient of $(\epsilon-\epsilon_0)/v$. Further, products of fluctuations have never entered, and therefore it has not been necessary to neglect them (as they are neglected at this stage in the phenomenological theory). We are now ready to compute the scattering. We need, by virtue of Eq. (10),

$$\begin{aligned}&\int_V\int_V\Big\langle\mathbf{u}\cdot[\mathbf{p}_1-(\epsilon-\epsilon_0)\mathbf{e}_1]\mathbf{u}\cdot[\mathbf{p}_2^*-(\epsilon-\epsilon_0)\mathbf{e}_2^*]\\&\times\exp[-i\mathbf{k}\mathbf{s}\cdot(\mathbf{R}_1-\mathbf{R}_2)]\Big\rangle_{\text{Av}}d\mathbf{R}_1d\mathbf{R}_2.\end{aligned} \tag{27}$$

In computing the averages we have the aid of Yvon's generalization[9] of the Ornstein-Zernike integral. In the equations that immediately follow, k' is Boltzmann's constant and $\beta=(\partial v/\partial P)_T$, where P is the pressure and T the temperature:

$$\begin{aligned}\int_V\langle\delta_1\delta_2\rangle_{\text{Av}}d\mathbf{R}_2&=v+\int_V(v_{12}-v^2)d\mathbf{R}_2\\&=k'Tv\beta\frac{\partial v}{\partial v}=k'Tv\beta,\end{aligned} \tag{28}$$

$$\begin{aligned}\int_V\langle\delta_{13}\delta_2\rangle_{\text{Av}}d\mathbf{R}_2&=2v_{13}+\int_V(v_{132}-v_{13}v)d\mathbf{R}_2\\&=k'Tv\beta\left(\frac{\partial v_{13}}{\partial v}\right)_T,\end{aligned} \tag{29}$$

and

$$\int_V \langle \delta_{135}\delta_2\rangle_{Av} d\mathbf{R}_2 = 3v_{135} + \int_V (v_{1352} - v_{135}v) d\mathbf{R}_2 = k'T v\beta \left(\frac{\partial v_{135}}{\partial v}\right)_T. \quad (30)$$

We now substitute $\mathbf{p}_1(\epsilon-\epsilon_0)\mathbf{e}_1$ as given by Eq. (26) into Eq. (27) and compute, term by term, the required averages. Let $(\mathbf{u}\cdot\mathbf{E}_0/E_0)=(\mathbf{u}\cdot\mathbf{E}_A/E_A)=\cos\gamma$. We need first

$$(\epsilon-\epsilon_0)^2 E_A^2 \cos^2\gamma \left(1+\frac{\epsilon-\epsilon_0}{3\epsilon_0}\right)^2 v^{-2} \int_V\int_V \langle \delta_1\delta_2\rangle_{Av} \times \exp[i(\mathbf{R}_1-\mathbf{R}_2)\cdot(\mathbf{k}-k\mathbf{s})] d\mathbf{R}_1 d\mathbf{R}_2. \quad (31)$$

Now

$$\langle \delta_1\delta_2\rangle = v\delta(\mathbf{R}_1-\mathbf{R}_2) + (v_{12}-v^2),$$

and so, because v_{12} reaches its asymptotic value of v^2 [always neglecting terms of $0(1/N)$], when R_{12} is as large as 20 or 30 A, expression (31) is very closely equal to, by virtue of Eq. (28),

$$(\epsilon-\epsilon_0)^2 E_A^2 \cos^2\gamma \left(1+\frac{\epsilon-\epsilon_0}{3\epsilon_0}\right)^2 \frac{k'T\beta V}{v}. \quad (32)$$

Next we need [with the appropriate constants such as $(\epsilon-\epsilon_0)$ in front]

$$\int_V\int_V\int_{\substack{V_0-s_1\\(\mathbf{R}_3)}} \langle [v^{-1}\delta_{13} - v^{-2}v_{13}\delta_1 - \delta_3]\delta_2\rangle \times \exp[i\mathbf{R}_{21}\cdot(\mathbf{k}-k\mathbf{s})]\mathbf{u}\cdot\mathbf{T}_{13}\cdot\mathbf{E}_A e^{i\mathbf{k}\cdot\mathbf{R}_{13}} d\mathbf{R}_3 d\mathbf{R}_2 d\mathbf{R}_1. \quad (33)$$

This expression is considerably more complicated than Eq. (31), and, although it could be handled in a straightforward way it is simpler to adopt a somewhat inverted procedure (which will also apply to succeeding averages). We set the exponents in Eq. (33) equal to zero, and compute the indicated average using Eqs. (28) and (29); in the course of the averaging we integrate over $\mathbf{R}_2$. We find in the resulting integral over $\mathbf{R}_1$ and $\mathbf{R}_3$ that the integrand differs appreciably from zero only when $R_{13}\ll\lambda$. Now if $R_{13}\ll\lambda$ the integral over $\mathbf{R}_2$ in Eq. (29) differs appreciably from zero only for $R_{12}\ll\lambda$. Since the exponents in Eq. (33) are effectively zero when $R_{13}\ll\lambda$ and $R_{12}\ll\lambda$, our neglect of them was justified. We apply this procedure to Eq. (33) and get

$$\int_V\int_{V_0-s_1}\int_V \langle [v^{-1}\delta_{13} - v^{-2}v_{13}\delta_1 - \delta_3]\delta_2\rangle_{Av} \times \mathbf{u}\cdot\mathbf{T}_{13}\cdot\mathbf{E}_A d\mathbf{R}_2 d\mathbf{R}_3 d\mathbf{R}_1$$
$$= k'T v\beta \int_V\int_{V_0-s_1} \left(v^{-1}\frac{\partial v_{13}}{\partial v} - v^{-2}v_{13} - 1\right) \times \mathbf{u}\cdot\mathbf{T}_{13}\cdot\mathbf{E}_A d\mathbf{R}_3 d\mathbf{R}_1$$
$$= k'T v\beta \frac{\partial}{\partial v}\int_V\int_{V_0-s_1} (v^{-1}v_{13} - v)\mathbf{u}\cdot\mathbf{T}_{13}\cdot\mathbf{E}_A d\mathbf{R}_3 d\mathbf{R}_1. \quad (34)$$

The integral (over $\mathbf{R}_3$) is the same as that which was set equal to zero in the refractive index theory and may be set equal to zero here for the same reasons.

Next is (we are to put $\mathbf{u}\cdot$ in front and $\cdot\mathbf{E}_A$ in back of the integral):

$$\int\int\int \langle [v^{-1}\delta_{13} - v^{-2}v_{13}\delta_1]\delta_2\rangle_{Av} \mathbf{T}_{13}\cdot\mathbf{T}_{31} d\mathbf{R}_1 d\mathbf{R}_2 d\mathbf{R}_3 = k'T v\beta \frac{\partial}{\partial v}\int\left[\int v^{-1}v_{13}\mathbf{T}_{13}\cdot\mathbf{T}_{31} d\mathbf{R}_3\right] d\mathbf{R}_1. \quad (35)$$

We again recognize an integral occurring in the refractive index theory, and the integrand rapidly converges to zero (Yvon gives a detailed discussion of the convergence in his refractive index theory.[16])

The final term which δ_2 multiplies gives rise to

$$\int\int\int\int \langle [v^{-1}\delta_{135} - v^{-2}v_{135}\delta_1 + \cdots - \delta_{35}]\delta_2\rangle \times \mathbf{T}_{13}\cdot\mathbf{T}_{35} d\mathbf{R}_1 d\mathbf{R}_3 d\mathbf{R}_5 d\mathbf{R}_2$$
$$= k'T v\beta \int\int\int \left[\frac{\partial}{\partial v}(v^{-1}v_{135}) - 2v^{-1}v_{35}\frac{\partial}{\partial v}(v^{-1}v_{13}) - v\frac{\partial}{\partial v}(v^{-1}v_{35}) + v\frac{\partial}{\partial v}(v^{-1}v_{13})\right] \mathbf{T}_{13}\cdot\mathbf{T}_{35} d\mathbf{R}_1 d\mathbf{R}_2 d\mathbf{R}_5.$$

Since $\mathbf{R}_{13}$ and $\mathbf{R}_{35}$ are dummy variables of integration, the contribution to the integral from $\partial(v^{-1}v_{35})/\partial v$ cancels that from $\partial(v^{-1}v_{13})/\partial v$; for the same reason we may replace $2v^{-1}v_{35}\partial(v^{-1}v_{13})/\partial v$, inside the integral signs, by $[v^{-1}v_{35}\partial(v^{-1}v_{13})/\partial v]+[v^{-1}v_{13}\partial(v^{-1}v_{35})/\partial v]$. We then have

$$k'T v\beta \frac{\partial}{\partial v}\int\int\int (v^{-1}v_{135} - v^{-2}v_{13}v_{35}) \times \mathbf{T}_{13}\cdot\mathbf{T}_{35} d\mathbf{R}_1 d\mathbf{R}_3 d\mathbf{R}_5, \quad (36)$$

which is a rapidly converging integral present in the refractive index theory.

We have next to take

$$\int_{V_0-s_2} (\delta_{24}v^{-1} - v^{-2}v_{24}\delta_2 - \delta_4)\mathbf{u}\cdot\mathbf{T}_{24}^*\cdot\mathbf{E}_A e^{-i\mathbf{k}\cdot\mathbf{R}_{24}} d\mathbf{R}_4 \quad (37)$$

and multiply it by, first, δ_1 and average. This leads to an integral like expression (34), that is, to zero. Then we are to multiply Eq. (37) by

$$\int_{V_0-s_1} (\delta_{13}v^{-1} - v^{-2}v_{13}\delta_1 - \delta_3)\mathbf{u}\cdot\mathbf{T}_{13}\cdot\mathbf{E}_A e^{i\mathbf{k}\cdot\mathbf{R}_{13}} d\mathbf{R}_3 \quad (38)$$

and average, and finally, by the coefficient of α in Eq. (26) and average. Both of the latter averages result in completely intractable combinations of distribution

[16] See reference 10, p. 76.

functions. However, as Yvon noted, we can keep the relative (or internal) coordinates of $(\mathbf{R}_2,\mathbf{R}_4,\mathbf{R}_1,\mathbf{R}_3)$ and $(\mathbf{R}_2,\mathbf{R}_4,\ \mathbf{R}_1,\ \mathbf{R}_3,\ \mathbf{R}_5)$ constant in the required integrals and average over all orientations of the respective configurations relative to an external coordinate system. Because of the small spheres excluded from the region of integration in Eqs. (37) and (38), we can be sure, at least, that the integrations over internal coordinates lead to finite results. We have to average over orientations relative to an external coordinate system the following quantities:

$$\mathbf{u}\cdot(3\mathbf{u}_{24}\mathbf{u}_{24}-\mathbf{I})\cdot\mathbf{E}_A\mathbf{u}\cdot(3\mathbf{u}_{13}\mathbf{u}_{13}-\mathbf{I})\cdot\mathbf{E}_A \tag{39}$$

and

$$\mathbf{u}\cdot(3\mathbf{u}_{24}\mathbf{u}_{24}-\mathbf{I})\cdot\mathbf{E}_A\mathbf{u}\cdot(3\mathbf{u}_{13}\mathbf{u}_{13}-\mathbf{I})(3\mathbf{u}_{35}\mathbf{u}_{35}-\mathbf{I})\cdot\mathbf{E}_A. \tag{40}$$

Here $\mathbf{u}_{24}$ is a unit vector pointing from $\mathbf{R}_2$ to $\mathbf{R}_4$, etc. The result of the averaging of both Eqs. (39) and (40) is a numerical multiple of $E_A^2(\cos^2\gamma+3)$.

The last required averages are

$$\int\int\int\int\langle[v^{-1}\delta_{246}-v^{-2}v_{246}\delta_2+\cdots-\delta_{46}]\delta_1\rangle \times\mathbf{T}_{24}\cdot\mathbf{T}_{46}d\mathbf{R}_2d\mathbf{R}_4d\mathbf{R}_6d\mathbf{R}_1 \tag{41}$$

and

$$\int\int\int\langle[v^{-1}\delta_{24}-v^{-2}v_{24}\delta_2]\delta_1\rangle\mathbf{T}_{24}\cdot\mathbf{T}_{42}d\mathbf{R}_2d\mathbf{R}_4d\mathbf{R}_1; \tag{42}$$

these expressions lead to exactly the same result as Eqs. (35) and (36). We may now add the averages computed in Eqs. (31) to (42):

$$|\mathbf{u}\cdot\mathbf{e}(D)|^2=\frac{k_0^4E_A^2k'T\beta vV\cos^2\gamma}{(4\pi\epsilon_0D)^2}\left\{\frac{(\epsilon-\epsilon_0)^2(\epsilon+2\epsilon_0)^2}{(3\epsilon_0v)^2}\right.$$
$$+\frac{2(\epsilon-\epsilon_0)^3(\epsilon+2\epsilon_0)}{3v^2\epsilon_0}\frac{\partial}{\partial v}\left[\int v^{-1}v_{13}\mathbf{T}_{13}\cdot\mathbf{T}_{31}d\mathbf{R}_3\right.$$
$$+\int\int(v^{-1}v_{135}-v^{-2}v_{13}v_{35})$$
$$\left.\left.\times\mathbf{T}_{13}\cdot\mathbf{T}_{35}d\mathbf{R}_3d\mathbf{R}_5\right]\right\}$$
$$+\frac{E_A^2V}{D^2}(\cos^2\gamma+3)F. \tag{43}$$

In F have been included those complicated integrals mentioned in Eqs. (37) to (40) as well as factors such as k_0^4, $(4\pi\epsilon_0)^{-2}$, etc. We are soon going to express F in terms of a familiar quantity, the depolarization. We recognize in curly brackets an expression for $(\partial\epsilon/\partial v)^2$ which may be obtained from Eq. (22) [valid, of course, only as far as we have carried the series in Eq. (22), which is as far as the first correction to the Lorentz-Lorenz formula]. The ratio of the intensity of scattered light at D to the intensity of light transmitted through V is $(i/i_0)=|\mathbf{u}\cdot\mathbf{e}|^2/E_A^2$, and Rayleigh's ratio $R=iD^2/i_0V$; we get (after replacing ϵ by ϵ_0n^2),

$$R=\frac{k_0^4k'T\beta v\cos^2\gamma}{(4\pi)^2}\left(\frac{\partial n^2}{\partial v}\right)^2+(\cos^2\gamma+3)F. \tag{44}$$

Let us now choose a y-axis in the direction of propagation of $\langle\mathbf{E}\rangle$, a z-axis parallel to plane of polarization of $\langle\mathbf{E}\rangle$, and an x-axis so as to form a right-handed coordinate system. We measure R far out on the x-axis, first with $\gamma=0$ (vertical $\mathbf{u}$), and call this R_0; next we measure R with $\gamma=\pi/2$ (horizontal $\mathbf{u}$), and call this $R_{\pi/2}$. Then the depolarization Δ_V (for vertically polarized incident light), is defined as $\Delta_V=R_{\pi/2}/R_0$.

$$\Delta_V=3F\left[(4\pi)^{-2}k_0^4k'T\beta v\left(\frac{\partial n^2}{\partial v}\right)^2+4F\right]^{-1}$$

and,

$$F=\frac{\Delta_V}{3-4\Delta_V}\left[(4\pi)^{-2}k_0^4k'T\beta v\left(\frac{\partial n^2}{\partial v}\right)^2\right].$$

Substitution of this value of F into Eq. (44) gives

$$R=\frac{k_0^4k'T\beta v[(1-\Delta_V)\cos^2\gamma+\Delta_V]}{(4\pi)^2(1-4\Delta_V/3)}\left(\frac{\partial n^2}{\partial v}\right)^2. \tag{45}$$

We may note that the correction factor takes what may be the more familiar form of the "Cabannes factor," $(6+6\Delta)/(6-7\Delta)$ for $\gamma=0$, if unpolarized incident light is used for the measurement of Δ. As an empirical fact, small, optically isotropic molecules almost always lead to a zero or near-zero value of Δ_V, and R will take the exact form given by Einstein:

$$R=(4\pi)^{-2}k_0^4k'T\beta v\cos^2\gamma(\partial n^2/\partial v)^2.$$

ACKNOWLEDGMENTS

The author is indebted to Professor J. G. Kirkwood and Professor R. F. Zwanzig for discussion and criticism of this work.

THE JOURNAL OF CHEMICAL PHYSICS VOLUME 23, NUMBER 11 NOVEMBER, 1955

Localizability of Electrons in Atoms and Molecules—Application to the Study of the Notion of Shell and of the Nature of Chemical Bonds

RAYMOND DAUDEL, HÉLÈNE BRION, AND SIMONE ODIOT
Centre de Chimie Theorique de France, 155 rue de Sèvres, Paris 15e, France
(Received January 24, 1955)

The importance of the correlations existing between the positions of electrons in atoms and molecules has recently been stressed. A new method for the study of these correlations is presented here. It consists in the decomposition of the space of an electronic system into small parts where there is a very large probability of finding one and only one electron of a given spin. This method allows the association of spherical rings to the shells of atoms and the association of space to the atomic core and to the bonds of molecules.

THE NOTION OF LOGE[1]

THE difficulties that arise when one seeks to define theoretically the idea of shell in an atom or that of bond in a molecule are connected essentially to the fact that electrons are simultaneously both mobile and indiscernible. As a result, on the average, any of them play exactly the same role as any other in the atom or molecule. Molecular architecture, as well as the structure of atoms, rests essentially on the correlation between the positions of electrons. This correlation contributes considerably to the establishment of the properties and the localizability of electrons as we propose now to indicate.

Let us consider a system of electrons (those of an atom, molecule, etc. . . .) in a stationary state and carve out in the space of the ensemble a certain volume V. Let us study the probability P to find in this volume one electron and one only of given spin. If V is very small this probability is very small, because V is generally empty. If V is very large, P again will be very small, because V now will contain generally more than one electron of the same spin. Thus intuitively it seems reasonable that only certain volumes V will correspond to a maximum value for P. It is assumed that the system is in such a state that the projection of the total spin is well defined. Let p be the number of electrons of spin $+1/2(h/2\pi)$ for example.

All space is cut up into p connex volumes (V_i) that do not overlap, and in each one of them the probability P_i to find one and only one electron of spin $+1/2(h/2\pi)$ is evaluated. We say that the space is divided into loges of order 1 and of character $+1/2(h/2\pi)$ with respect to the system. The same definition applies obviously to spin $-1/2(h/2\pi)$.

The quantity $\Omega=\sum_i P_i$ has an upper limit: the value p.

Let us suppose that $\eta=(p-\Omega)/p$; η is a positive quantity which we shall call *the lack of localization* of the decomposition of the space. We shall say that one decomposition is better than another as η is the smaller.

The ensemble of the possible decompositions of space thus defined for a system in a given state is very large. Practically we will content ourselves very often with considering the subensembles in imposing on the system of decomposition supplementary conditions that imply, for example, the symmetry properties of the system.

It thus will be often possible to find the best decompositions[2] of one such subensemble, that is to say that (or those) which corresponds to a minimum value of η when it exists.

Let $\psi(x_1,\omega_1,x_2,\omega_2\cdots x_j,\omega_j\cdots x_n,\omega_n)$ be the wave function describing the state of the system considered where x_j is the ensemble of the space coordinates associated with the jth electron. The probability P_i to find one and only one electron of spin $+1/2(h/2\pi)$ in the loge V_i is given by

$$P_i=C_p{}^n p\int_{V_i} d\tau_1\int_{\text{space}-V_i} d\tau_2\cdots d\tau_p \times\int_{\text{space}} d\tau_{p+1}\cdots d\tau_n\int_{+\frac{1}{2}(h/2\pi)} d\omega_1\cdots d\omega_p \times\int_{-\frac{1}{2}(h/2\pi)} d\omega_{p+1}\cdots d\omega_n|\psi|^2$$

APPLICATION TO ATOMS

A. First Excited State of Helium

Let us consider the first excited triplet state of helium in the case where the projection of total spin is $h/2\pi$. A decomposition of space in loges of order 1 and character $+1/2(h/2\pi)$ can be obtained in decomposing the space into two connex volumes. The symmetry of the problem suggests here to divide space either with a plane passing through the nucleus of the atom or by a sphere with the center at the nucleus which defines the loge V_1 which is inside the sphere, and the loge V_2 on the outside of the same sphere.

It is necessary to find (1) what the radius of the sphere giving the best corresponding loges is; (2) how the decomposition by the plane compares to the best spherical decomposition.

In a loge V_i the probability P_i to find one electron

[1] E. A. Hylleraas, Z. Physik **54**, 347 (1929).

[2] For details on this question see: Daudel, Odiot, and Brion, J. chim. phys. **51**, 74 (1954); Brion, Daudel, and Odiot, *ibid.* **51**, 358 (1954); Odiot and Daudel, *ibid.* **51**, 361 (1954).

and one only is given by the equation

$$P_i=2\int_{V_i} d\tau_1 \int_{\text{space}-V_i} d\tau_2|\psi|^2.$$

The first triplet state of helium will be represented by the function proposed by Hylleraas,[1,3]

$$\psi(r_1,r_2)=s\exp(-Z's)shct,$$

where r_1 and r_2 are the radii associated with the two electrons and where

$$s=\frac{r_1+r_2}{a_0},\quad t=\frac{r_1-r_2}{a_0}$$

$$c=0.825,\quad Z'=1.374,\quad a_0=0.53\text{ A}.$$

Readily there is found for the decomposition by a plane:

$$P_1=P_2=0.5$$

thus

$$\eta=(2-1)/2=0.5.$$

The probability of finding one and only one electron on one side of a plane is thus 0.5 which corresponds to a rather strong deviation from localization.

We can envisage then the case of spherical decomposition. Let R be the radius of the sphere. It can be readily shown that the quantity η is a simple function of R and the value of R which minimizes η is the best decomposition of space into spherical loges with the center at the nucleus. The curve of Fig. 1 represents the variation of $P=P_1=P_2$ with R.

It is seen that the maximum has a value of 0.93 for $R=1.7\ a_0$. It is at this place that η is a minimum and is

$$\eta=(2-2P)/2=0.07.$$

In the case of the first excited state of helium the sphere of radius $R=1.7\ a_0$ corresponds then to the best decomposition into spherical loges and the probability of finding one and only one electron in this sphere reaches 93%.

The probability of finding one and only one electron on the outside of this sphere is, equally, 93%.

The best spherical decomposition is better than the decomposition by a plane.

We are thus quite naturally led to think that the sphere of radius 1.7 a_0 can be associated with the K shell of helium in this state and the rest of space then being associated with the L shell. We thus give again to the idea of shell a certain precise geometric signification which was lost with the abandonment of atomic models based on the idea of orbits. Note that the geometric idea of shell envisaged here can be made starting from any type of wave function including the exact function, while the habitual energetic idea can only be realized starting from a very particular type of approximate wave function.

These results naturally follow from the form of the wave function used. As one of the referees has pointed out, it is very probable that if a better function than the Hylleraas function had been used, these precise results would not have been found. In particular, if a wave function specifically including r_{12} had been used it seems likely a 50% probability would not result from the decomposition by a plane. As is well known, the integration of such type of functions presents very great difficulties and this is particularly marked when, as here, the integration must be carried out over only a portion of space. We did not carry out this integration. However it does seem reasonable that the improved wave function would not materially alter the picture which we have found.

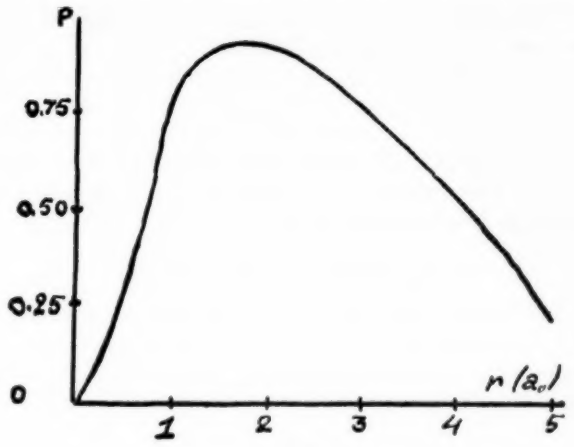

FIG. 1.

Furthermore, certain energetic properties can be obtained from the idea of loges. The average energy $\bar{E}_V$ of an electron in a loge V can in effect be defined:

$$\bar{E}_V=\frac{\int_{j\epsilon V}\psi^* H_j\psi d\tau}{\int_{j\epsilon V}\psi^*\psi d\tau}$$

where H_j is the part of the Hamiltonian that refers to the jth electron, where the symbol $j\epsilon V$ states that the point associated with the jth electron remains always on the inside of volume V. (This formula is only valuable because of the antisymmetric character of the function ψ.)

The following table compares the values obtained in the cases we have studied of the energies $\bar{E}$ with energy given by SCF[4] atomic orbitals and the energy of ionization I of the state of helium considered:

	E_k (SCF)	$\bar{E}_k$	I_k (exp)
$k=K$	−3.469	−3.565	−3.352
$k=L$	−0.30	−0.43	−0.35

B. Study of Another Excited State of Helium

As a check we have studied another state of helium corresponding to a projection of spin $h/2\pi$ and represented by the atomic antisymmetric term $(2s)\ (2p_z)$.

[3] R. Daudel, Compt. rend. 237, 601 (1953).

[4] Wilson and Lindsay, Phys. Rev. 47, 681 (1935).

This state corresponds to the classical idea of two electrons which belong to the same shell.

If the best spherical decomposition is compared to the decomposition formed by a plane perpendicular to the z axis it can be shown that the latter is the better. It presents a lack of localization of 0.22 while the best spherical decomposition obtained for $R=3.2\ a_0$ possesses a lack of localization of 0.48.

C. Application to Other Atoms[3]

The results previously obtained are susceptible to being generalized. It can be shown that in following this idea one is led to associate different shells of an atom with spherical rings with the center at the nucleus. Most of these rings can be decomposed into several loges where there is found to be a large probability of finding one and only one electron of given spin. The knowledge of the values of these probabilities P_i gives an idea of the localizability of electrons in these atoms.

If V is the volume of a loge and $\bar{F}$ the average electric potential of an electron in the loge, the following relation is obtained[5] $V\bar{F}^{\frac{1}{2}}=$constant, no matter what the shell of the atom considered.

Coulson[6] has shown that an analogous relation can be obtained theoretically from Thomas-Fermi statistics between the volume occupied by unity charge in the electronic ensemble of an atom and the average electrical potential in this volume. This fact shows that the properties resulting from the integration of a volume as large as a loge act in an analogous fashion in Thomas-Fermi statistics and in wave mechanics.

APPLICATION TO MOLECULES

A. The Lithium Molecule

In a good decomposition of a molecule into loges some of the loges which are representative of atoms before bonding will be found again in the molecule (with only small modifications). They can be called the loges of the core while the others make up the loges of the bond.

We shall discuss the case of the lithium molecule from this point of view. We shall in succession study the loges of the free atom lithium and of the molecule. For the ground state of the atom, we use a wave function having the form of a Slater determinant with the following monoelectronic functions[7]:

$$1s=(c^3/\pi)^{\frac{1}{2}}e^{-cr},\quad 2s=N(r-\alpha)e^{-dr}$$

with $c=2.694$, $d=0.767$, and $\alpha=0.867$.

We assume that the atom has two electrons of spin $+1/2(h/2\pi)$ and one of $-1/2(h/2\pi)$; the problem of decomposition into loges only concerns the first two.

In following the method already outlined it is easily found that the best spherical decomposition is made of a sphere with its center at the nucleus and with a radius $R=1.44\ a_0$; the probability of finding one and only one electron of spin $+1/2(h/2\pi)$ in this sphere is 0.97 which corresponds to a lack of localization of only 3%.

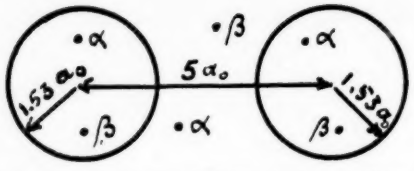

FIG. 2. $\cdot\alpha$ denotes an electron of spin $+\frac{1}{2}(h/2\pi)$. $\cdot\beta$ denotes an electron of spin $-\frac{1}{2}(h/2\pi)$.

For the molecule we shall use the function used by Coulson and Duncanson[7] which, among other qualities, is particularly interesting as it has a form comparable to that of the wave function for the atom.

In this molecule there are three electrons of each spin. Thus three loges can be envisaged. Let us imagine the decomposition into loges formed by two spheres with their centers respectively on each nucleus and a radius equal to R. The value of R corresponding to the best decomposition of this subensemble can be calculated and it is found that $R=1.53\ a_0$.

The two loges surrounding the nuclei of the molecule Li_2 are very similar to the loge K of the free atom. They can be considered as playing the role of loges of the core, the rest of the space of the molecule making up a loge of the bond.

The probability to find one and only one electron of given spin in one of the loges of the core thus defined is 0.98, that of finding one and only one electron of given spin in the loge of the bond is 0.95. The decomposition thus obtained is very good, the lack of localization being 3%.

One can say that for the majority of the time the electrons of the lithium molecule can be considered as occupying the positions corresponding to Fig. 2: one electron of each spin in each loge of the core; one electron of each spin in the loge of the bond.

It seems to us that this representation derived from wave mechanics is the closest approach to the representation of Lewis, the most in accord with the ideas of chemists.

B. Application to Other Problems of Molecular Structure

The same method has been utilized[8] to discuss the problem of the distinction between π and σ bond.

It can be shown that in the case of ethylene the decomposition of the double bond into two loges by the plane of the nuclei is better than the best decomposition obtained by an ellipsoid with the foci centered on the carbon nuclei.

This result is in satisfactory agreement with the conclusions of Altmann, Coulson, and March.[9] In effect it does not seem necessary to try to decompose the

[5] S. Odiot and R. Daudel, Compt. rend. **238**, 1384 (1954).
[6] C. A. Coulson, Compt. rend. **239**, 868 (1954).
[7] Coulson and Duncanson, Proc. Roy. Soc. (London) **A62**, 37 (1944) and **A181**, 378 (1943).
[8] Brion, Daudel, and Odiot, J. chim. phys. **51**, 553 (1954).
[9] Coulson, Altmann and March, Proc. Natl. Acad. Sci. U. S. **38**, 372 (1952).

space of a double bond into a σ region and a π region. It is not less true that it is quite justified to speak of σ orbitals and π orbitals at the same time on the basis of symmetry and the energetic point of view.

It seems intuitively reasonable that when equivalent orbitals exist they are localized in the different loges of a good decomposition[10]; therefore they are particularly suitable for writing the wave function with a view to the discussion of the geometric problems, although symmetry orbitals remain more adaptable to the discussion of energy problems.

The notion of loge may be used to establish a new general formalism for the description of bonds. This will be discussed elsewhere.

Thanks are due to Dr. Carl Moser for the translation from the French.

[10] See for example J. E. Lennard Jones, J. Chem. Phys. **20**, 1024 (1952).

THE JOURNAL OF CHEMICAL PHYSICS VOLUME 23, NUMBER 11 NOVEMBER, 1955

On the Fermi Resonance and Isotope Effect in the Infrared Spectrum of Carbon Tetrachloride

P. TUOMIKOSKI
Institute of Physics, University of Helsinki, Helsinki, Finland
(Received February 23, 1955)

The influence of intermolecular (solvent) interactions on the Fermi resonance in a number of CCl_4 infrared absorptions has been examined: it is discussed together with the incidence of isotopic frequencies.

THE Fermi resonance[1] of vibrational energy levels of polyatomic molecules is very sensitive to the difference between the corresponding unperturbed levels, as can be shown by the first-order perturbation theory. Thus it is to be expected that the amount of the resonance will depend upon the state of the substance, because it is known that the intermolecular forces influence the various vibrational modes to significantly different extents. On the other hand a comparison of the molecular spectra obtained from the same substance in different states should be useful when one has to settle if a resonance occurs or not.

A study of this kind is perhaps most easily performed for carbon tetrachloride. The Raman spectrum of liquid carbon tetrachloride shows a doublet 762, 791 cm^{-1} which Placzek[2] interpreted as resulting from the Fermi resonance. An interpretation of these frequencies as fundamentals would require a molecular structure differing from a regular tetrahedron,[3] which model gives indeed a very accurate agreement between the computed and observed electronic diffraction curves, obtained from gaseous carbon tetrachloride.[4]

The infrared spectra presented here were recorded with a Perkin-Elmer Model 12C single beam instrument provided with NaCl-optics. The double band referred to has been studied in the vapor in a 10-cm gas cell and in dilute solutions in a 0.1-mm liquid cell. To obtain a suitable low concentration the vapor was introduced into the cell in a stream of dry nitrogen. The first overtone region of the double band was investigated in liquid carbon tetrachloride using the same 0.1-mm cell while the vapor was studied in a 1-meter gas cell.

Appreciably differing spectra have been obtained in different states (Fig. 1) and some of them show interesting fine structures. Of the solution bands all except those obtained from hexane solution obey very accurately the forms predicted theoretically by Horiuti.[5] Although the low frequency component at about 765 cm^{-1} is flatter (because of the isotope effect) than the high frequency component at about 790 cm^{-1}, the areas under the bands seem to be nearly equal. The region between the peaks is partly filled with a third band of lower intensity in accord with the theory, although the middle band does not appear as a separate peak in the actual spectra. According to the figures in Horiuti's work, the separation of the side bands of the 1550 cm^{-1} band should be close to $(5/2)(791-762)=72$ cm^{-1}, whereas the measured value is $1587-1518=69$ cm^{-1}.

The hexane solution forms an intermediate between the gaseous state and the other liquid states studied. This is in accordance with some earlier observations on OH-stretching and NH-bending vibrations[6] when hexane or heptane have been used as solvents.

The vapor spectrum shows that carbon tetrachloride molecules are almost free from Fermi resonance when intermolecular actions are weak. The fine structure of the low-frequency "doublet" component is readily explained as caused by isotopes of chloride (Fig. 2).

[1] E. Fermi, Z. Physik **71**, 250 (1931).
[2] G. Placzek, *Handbuch der Radiologie VI*$_2$ (Leipzig, 1934), p. 205.
[3] Cl. Schaefer, Z. Physik **60**, 586 (1930); A. Langseth, *ibid.* **72**, 350 (1931).
[4] J. Karle and J. L. Karle, J. Chem. Phys. **17**, 1052 (1949).
[5] J. Horiuti, Z. Physik **84**, 380 (1933).
[6] P. Tuomikoski, Suomen Kemistilehti **B23**, 44 (1950); Tuomikoski, Pulkkinen, Hirsjärvi, and Toivonen, *ibid.* **B23**, 53 (1950); P. Tuomikoski, J. phys. radium **15**, 318 (1954).

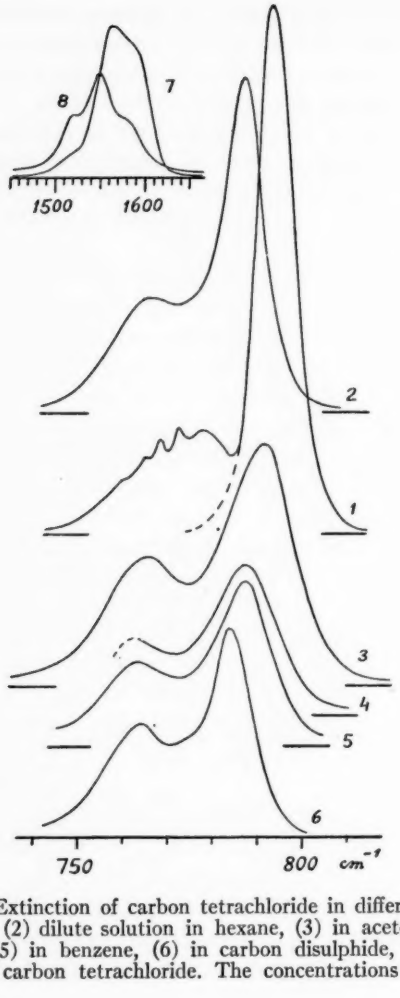

FIG. 1. Extinction of carbon tetrachloride in different states: (1) vapor, (2) dilute solution in hexane, (3) in acetone, (4) in pyridine, (5) in benzene, (6) in carbon disulphide, (7) vapor, (8) liquid carbon tetrachloride. The concentrations are undetermined.

The theoretical intensity lines of Fig. 2 are based on calculations of Wu and Sutherland[7] using the Urey and Bradley (1) potential function. The notations of these authors are used in Fig. 2, i.e., one dot indicates that the molecule has one Cl_{37}-atom and three Cl_{35}-atoms and so on. The abundances of the five isotopic molecules are 32.3, 42.2, 20.7, 4.5 and 0.37%. Thus the abundances of the molecules vibrating with the frequencies ν_{4ab}', ν_{4c}', ν_{4a}'', $\nu_{4b}''\cdots$ are successively practically 28.1, 14.1, 6.9, 6.9$\cdots$% owing to the small frequency differences. The position of the $\nu_1'''+\nu_{4ab}'''$ was estimated from Wu and Sutherland's results. The low spectral resolution does not permit a decision between the various potential functions discussed by these authors except that the Rosenthal and Voge model (2) is ruled out, the same conclusion as that to which the authors were led because of the sharpness of the ν_3 band.

The spreading of the band on the low-frequency side is very like that found by Langseth[3] and Menzies[8] in the case of the ν_1 Raman band, and maybe it is the result of various difference bands. The 779 cm^{-1} band can be explained as a $\nu_1+\nu_3-\nu_1$ difference band whose Boltzmann factor is 1:9.3, to be compared with the proportion of the observed areas of this and the ν_3 band which is 1 to 10.

It is futile to try to explain the structure of the first overtone gas band on account of the absence of any fine structure. The dissimilarity with the liquid band is even more marked here than in the case of the main bands.

Using the 1-meter gas cell, the following summation bands which, as far as the author is aware, have not been reported before, have been measured: 978, 1011, 1070, 1114, 1220, and 1250 cm^{-1}. (Schaefer and Kern[9] reported only the gas frequencies 768 and 797 cm^{-1}.) As these three pairs of frequency arise from the 775 cm^{-1} doublet in summation with the fundamentals ν_2, ν_4, and ν_1, respectively, these pairs could show similar resonance features to the 775 cm^{-1} doublet. In fact, in the gas the 1011 and 1250 cm^{-1} bands are considerably increased in intensity relatively to the lower frequency companions, whereas in the liquid carbon tetrachloride spectrum the intensities of the components are of the same magnitude.

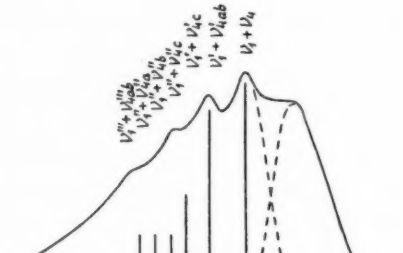

FIG. 2. The fine structure of the 750–785 cm^{-1} band of gaseous carbon tetrachloride explained as caused by difference bands and isotopic molecules. The relative theoretical intensities of the isotopic bands are assumed to be proportional to the abundance of the corresponding isotopic species and equally distributed in the vibrational modes of a particular species. The theoretical frequencies are based on Wu and Sutherland's[7] calculations and on the potential function proposed by Urey and Bradley.[7]

The author wishes to thank Professor Mansel Davies (University College of Wales, Aberystwyth, Wales) for kindly correcting the English manuscript.

Note added in proof.—The assumption of difference bands was rendered unlikely by a closer examination, as the bands remained practically unchanged in the temperature interval 20–100°C. In addition a ν_1 vapor frequency 1250−779=471 cm^{-1} exceeds significantly the earlier in the Raman effect measured ν_1 vapor frequencies. See a further discussion published in Suomen Kemistilehti **B28**, 152 (1955).

[7] C. K. Wu and B. B. M. Sutherland, J. Chem. Phys. **6**, 114 (1938); H. C. Urey and C. A. Bradley, Phys. Rev. **38**, 1969 (1931); H. H. Voge and J. E. Rosenthal, J. Chem. Phys. **4**, 137 (1936).

[8] A. C. Menzies, Proc. Roy. Soc. (London) **A172**, 89 (1939).

[9] Cl. Schaefer and R. Kern, Z. Physik **78**, 609 (1932).

On the Origin of the Electronically Excited C_2^* Radical in Hydrocarbon Flames

R. E. FERGUSON
National Bureau of Standards, Washington, D. C.
(Received February 18, 1955)

An isotopic tracer experiment, using carbon 13, has been performed to determine whether the excited C_2 radical in acetylene flames comes directly from the carbon pair of the acetylene burned. In the flame studied, the greater part of the C_2^* which radiates does not come from this source, but is produced in some series of reactions in which the $-C\equiv C-$ bond is broken prior to the appearance of C_2^*. It is shown further that most of the C_2^* cannot arise from the random breakup of polymers or incipient carbon particles formed by direct polymerization of acetylene. The results appear to favor the choice of a reaction between single-carbon fragments as the predominant source of C_2^*.

THE reaction steps leading to the production of the excited dicarbon radical, C_2^*, the emitter of the Swan bands in hydrocarbon flames, are not known. An experiment designed to throw some light on these steps is reported here. Although the results do not point to the detailed processes which occur, they set definite requirements which proposed mechanisms must satisfy, and in this way they provide means for evaluating some of the mechanisms currently considered.

The main object of this investigation was to find whether the excited C_2 radical in acetylene flames comes from the original carbon pair of the acetylene. The method used involves the measurement of relative intensities of C_2 emission due to $C^{12}C^{12}$, $C^{12}C^{13}$, and $C^{13}C^{13}$ in premixed flames with air of acetylene containing C^{13} distributed in various ways among the fuel molecules. This method provides a clear test, for if C_2^* comes directly from an acetylene molecule, the C^{13} will be distributed among the isotopic C_2 radicals in the same way as it is in the acetylene burned.

The bearing of the results obtained upon other possible mechanisms will be discussed in some detail because of the importance of probable connections, suggested mainly by Gaydon and Wolfhard,[1,2] between the presence of C_2^* and the excess excitation of other species in hydrocarbon flames.

EXPERIMENTAL

Samples of acetylene $-C^{13}$ were prepared from enriched $BaCO_3$ by the carbide method,[3] and were purified by three vacuum distillations at dry ice temperature into a trap at liquid nitrogen temperature. Table I shows the composition of the mixtures burned. Mixture 1 is acetylene$-C^{13}$ containing 22 atom percent C^{13} distributed randomly[4] among the acetylene molecules. It was prepared from $BaCO_3$ containing 22 atom percent C^{13}. Mixture 2 has about the same C^{13} concentration, but the relative concentrations of the isotopic acetylenes are different. This mixture was prepared by diluting a sample of acetylene$-C^{13}$ containing 66.6% C^{13} distributed randomly with twice the volume of ordinary acetylene$-C^{12}$. This gives a mixture of isotopic acetylenes much different from an equilibrium or random mixture; that is, it contains an excess of $HC^{12}C^{12}H$ and $HC^{13}C^{13}H$. Mixture 3 is another nonequilibrium mixture of lower C^{13} content prepared by diluting a sample of mixture 2 with acetylene$-C^{12}$.

The compositions of mixture 1 and 2 were obtained by mass spectrometric analysis both by low voltage measurements (only the molecule ions present) and by the usual 70 v method, and that of mixture 3 was calculated on the basis of the analysis of mixture 2 and the amount of acetylene$-C^{12}$ used for dilution. The analyses were in good agreement with the calculated concentrations of the different species and showed a maximum of 1% impurity, most of which was ethylene. The isotopic ethylene concentrations were

TABLE I.

A. Composition of acetylene mixtures burned, mole percent.

Component	Mixture 1	Mixture 2	Mixture 3
$HC^{12}C^{12}H$	61.1	68.9	83.5
$HC^{12}C^{13}H$	33.8	16.4	9.2
$HC^{13}C^{13}H$	5.1	14.7	7.3

B. Relative intensities of the 1, 0 band heads of C^2 in the flame.

Emitter	Mixture 1	Mixture 2	Mixture 3
$C^{12}C^{12}$	63.1±0.2[a]	61.7±0.2	77.7±0.5
$C^{12}C^{13}$	32.6±0.2	32.3±0.4	20.1±0.4
$C^{13}C^{13}$	4.3±0.2	6.0±0.2	2.1±0.1

[a] Average of three independent measurements, with standard deviation of the mean computed from $[\Sigma_i^3(x_i-\bar{x})^2/6]^{\frac{1}{2}}$.

or in C_2, and is given approximately in this case by

$$[HC^{12}C^{12}H]=[C^{12}]^2$$
$$[HC^{12}C^{13}H]=2[C^{12}][C^{13}]$$
$$[HC^{13}C^{13}H]=[C^{13}]^2,$$

where the brackets denote atom or mole fractions, and

$$[C^{12}]+[C^{13}]=1.$$

[1] A. G. Gaydon and H. G. Wolfhard, Proc. Roy. Soc. (London) A201, 570 (1950).
[2] A. G. Gaydon and H. G. Wolfhard, Proc. Roy. Soc. (London) A213, 366 (1952).
[3] M. Calvin *et al.*, *Isotopic Carbon* (John Wiley and Sons, Inc., New York, 1949), p. 205.
[4] 'Random distribution' is used here to mean the equilibrium distribution of carbon isotopes among the carbon pairs in acetylene

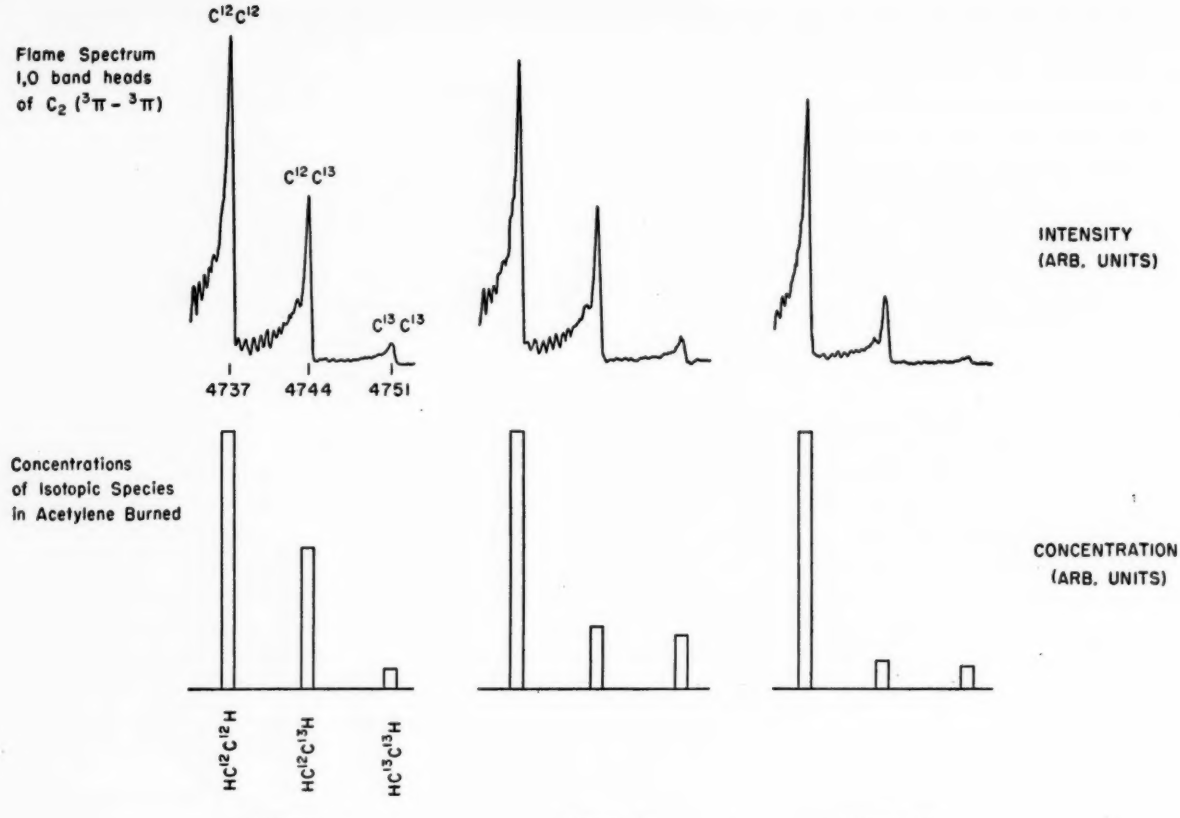

FIG. 1. Comparison of the carbon isotope distribution in C_2* in the flame with that in the acetylene burned.

added to those of the corresponding acetylenes to give the figures in Table I.

The mixtures were burned with air in a near stoichiometric flame on a small welding torch; the samples were delivered from a rubber gas expansion bag surrounded by nitrogen at 5 psig from a pressure-regulated tank. The same mixture ratio and total flow rate were used for all observations. The band heads of the 1, 0 transition of the C_2 Swan system ($^3\Pi_g - {}^3\Pi_u$) in the region 4735 to 4755 A were scanned (inner cone) using a grating monochromator with photoelectric detection, direct intensity recording and linear response.[5] The $C^{12}C^{12}$, $C^{12}C^{13}$, and $C^{13}C^{13}$ heads are separated by about 7 A in this band and overlapping of rotational lines is not serious for the C^{13} concentrations used.

Relative intensities were measured from the chart recordings; zero values for the separate band heads were taken as the lowest descent of the recording pen on the longer wavelength side of the band head. The numbers listed in the data tables are relative intensities calculated from the measured values by requiring the sum of the three band head intensities to be 100 units. An advantage of this presentation is that the numbers may be considered as apparent relative mole fractions of the isotopic C_2* radicals in the flame. The numbers given are averages for three separate scans of the region including one in a reverse direction; the reproducibility of the relative intensity measurements is indicated by the standard deviation of the mean in each case.

RESULTS

Figure 1 shows a typical spectral recording for each mixture listed in Table I. Below each recording is a bar graph representing the composition of the mixture burned.

Mixture 1 is the equilibrium sample. It was burned as a control sample in order to reveal possible complications in the method due to isotope effects. The isotope distribution in this sample is random. Further shuffling about of the carbon atoms will produce no change in the distribution except insofar as the difference in mass of the carbon isotopes affects the shuffling process. The results for this mixture, then, provide data for an estimate of the magnitude and direction of the over-all isotope effect in the reaction sequence $C_2H_2 \cdots \rightarrow (C_2$ radiation). The over-all effect will include: (1) isotope effects on chemical reaction rates, (2) the effect of differences in nuclear mass upon the relative populations of isotopic C_2 radicals in the upper state of the transition observed, (3) the isotope effect upon the transition

[5] W. Fastie, J. Opt. Soc. Am. 42, 641 (1952).

probability, (4) effects upon the measured band head intensities due to differences in rotational structure of the isotopic bands.

A comparison of the isotopic acetylene composition with the corresponding C_2 relative band head intensities for mixture 1 is given in the second column of Table I. The data show that the over-all isotope effect results in an apparent decrease in the relative abundance of C^{13} in the sample when measured by the C_2 band head intensities. Mass spectrometric analysis shows a C^{13} abundance of 22.0 atom percent, whereas the intensity measurements give 20.6 atom percent. However, the apparent distribution of the isotopes in C_2^* is still an equilibrium distribution, within the experimental error of the measurements, for a C^{13} content of 20.6 atom percent. One can conclude that the over-all isotope effect is in the expected direction (the lighter isotope is favored slightly), that there are no anomalies, and that the isotope effects in themselves do not alter the random nature of the isotope distribution in the carbon pairs. Therefore, anticipating the results with the nonequilibrium mixtures, a major change in this distribution as the result of the reactions $C_2H_2\cdots\longrightarrow C_2^*$ can be safely ascribed to a shuffling of the carbon atoms.

If one wishes to do so, it is easy to obtain empirical correction factors which bring the relative intensities into line with the corresponding isotopic acetylene concentrations in mixture 1, and to apply them to the results obtained with the nonequilibrium mixtures. However, the meaning of such corrections is certainly not clear and, when applied, they do not affect the conclusions to be drawn from the data. For these reasons, only the observed relative intensities are given here, and the discussion will neglect for the most part the rather small (in relation to the present problem) isotope effect suggested by the control experiment.

The spectra obtained with the flames of mixtures 2 and 3 can now be discussed. Their significance is most easily seen by reference to Fig. 1. It is at once apparent from the figure that a randomization process occurs in the flame. The carbon pairs of the C_2^* are not the same as those in the acetylene burned, showing that little of the C_2^* comes directly from the molecules of the fuel.

The extent of randomization of the isotope distribution is shown in the last two columns of Table II, where the measured band head intensities are compared with those calculated assuming a breaking of all the carbon-carbon bonds of the original fuel and a random recombination of single-carbon fragments (mechanism unspecified) to form C_2^*. The results for mixture 2 (22.9 atom percent C^{13}) are presented because for this case the $C^{13}C^{13}$ band head intensity can be measured most accurately. Three other nonequilibrium mixtures of 12, 6.3, and 3.6 atom percent C^{13} content gave comparable results in respect to the degree of randomization observed.

The measured relative intensities differ somewhat from those expected for the completely random case;

TABLE II. Comparison of observed isotopic C_2 relative intensities with those predicted for various mechanisms of C_2^* formation. Mixture 2. Sum of band head intensities = 100 units.

Emitter	From acetylene	From polymer	Random recombination	Observed
$C^{12}C^{12}$	68.9	64.2	59.4	61.7±0.2[a]
$C^{12}C^{13}$	16.4	25.9	35.3	32.3±0.4
$C^{13}C^{13}$	14.7	10.0	5.2	6.0±0.2

[a] Average of three independent measurements, with standard deviation of the mean computed from $[\Sigma_1^3(x_i-\bar{x})^2/6]^{\frac{1}{2}}$.

this deviation appears to be real and is difficult to explain in terms of isotope effects. However, it is clear that at some stage prior to the appearance of C_2^* most of the original carbon-carbon bonds must be broken; that is, under the conditions of these experiments most of the bonds in C_2^* are new bonds formed in the reaction zone.

It should be emphasized that the following discussion strictly applies only to $C_2(^3\Pi_g)$, since the measurements described were made using the 1, 0 band of the Swan system ($^3\Pi_g - {}^3\Pi_u$). The arguments do not necessarily apply to C_2 in the ground state or in other excited states. However, since at present there is no reason to suspect that other emission band systems might show a different isotope distribution in C_2, the symbol C_2^* is used here in place of the more strictly correct $C_2(^3\Pi_g)$.

DISCUSSION

The most obvious conclusion that can be drawn from the data is that reactions such as

$$HC\equiv C^- + H = C_2 + H_2,^6$$

in which the carbon-carbon bond in acetylene survives, must be rejected as the main source of C_2^* regardless of how the subsequent excitation of C_2 occurs. On the other hand a reaction involving single-carbon fragments such as

$$2CH = C_2 + H_2$$

would be consistent with the experimental results (neglecting for the time being the apparent slight deviation from the random case in the intensity distribution mentioned above). In fact any reaction producing C_2^* in which at least one free single-carbon fragment is incorporated into the C_2 radical will result in a complete reshuffling of the isotopes to give equilibrium relative concentrations of the isotopic C_2^* radicals and approximate agreement with experiment. Before discussing this and the apparent residue of old bonds in the C_2^*, another mechanism will be considered.

Gaydon and Wolfhard have suggested, on the basis of a variety of evidence,[1,2] that C_2^* results from the exothermic breakup of unsaturated polymers formed from the fuel in the reaction zone. This idea has been supported and developed by Thomas[7] who has discussed

[6] Herman, Hornbeck, and Laidler, Science **112**, 497 (1950).
[7] N. Thomas, J. Chem. Phys. **20**, 899 (1952).

the mechanism of decomposition of large unsaturated polymer chains. It is of interest now to find what relative concentrations of excited $C^{12}C^{12}$, $C^{12}C^{13}$, and $C^{13}C^{13}$ would be expected from such a process, starting with a nonequilibrium mixture of isotopic acetylenes such as mixture 2.

It will be assumed that the hypothetical polymer is formed from the fuel; i.e., that it is made up of the carbon pairs of the acetylene joined at random to make an infinite chain. Such a chain will consist of the original bonds (or pairs) and new bonds (or pairs). The set of old pairs is labeled in the sense that it displays a unique distribution of the carbon isotopes which differs from an equilibrium distribution. The set of new pairs is not so distinguished; it is made up of pairs $-C^{12}-C^{12}-$, $-C^{12}-C^{13}-$, and $-C^{13}-C^{13}-$ in relative concentrations corresponding to statistical equilibrium, the pairs having been formed by random joining of old pairs.[8]

If the chain polymer breaks up randomly to give C_2^* as one of the fragments, the process is equivalent to selecting, at random, a pair from the chain. Since for a large polymer the number of old pairs and new pairs is practically the same, the selection of an old or a new pair will be equally likely, and the isotopes will be only half shuffled in the aggregate of pairs selected. That is, the relative frequency of occurrence, P_i, of a pair of kind i in the randomly selected set will be given by $P_i=\frac{1}{2}[P_i(\text{old})+P_i(\text{new})]$. The relative isotopic C_2^* concentrations calculated on this basis are shown in Table II. Comparison with the experimental results shows that this mechanism cannot be the predominant one.[9]

The calculations were made for an infinite polymer, and do not hold for short chains. However, it is easy to see that as the chain length decreases the predicted intensity distribution shifts in a direction away from the experimentally determined distribution. In any chain formed from acetylene, the number of new bonds is one less than the number of old bonds. As the chain length decreases the ratio of new pairs to old decreases until for a chain length of two, only the original acetylene pair remains. Therefore short chains would favor the selection of old pairs in any scheme involving random breakup into pairs; i.e., the shuffling of isotopes would be less efficient for this case.

The calculations also neglect possible isotope effects in the hypothetical polymerization-decomposition reactions. This does not alter the conclusions drawn because the results with mixture 1 appear to rule out an over-all isotope effect of the magnitude and direction required to make the polymer hypothesis consistent with experiment.

In order to retain the polymerization-decomposition scheme of C_2^* formation as the predominant mechanism in flames, rather detailed assumptions about the process would have to be made. Two examples can be given to illustrate this. First, the polymer might not contain the original carbon pairs of the acetylene. According to the experimental results, most of the $-C\equiv C-$ bonds are broken at some stage before C_2^* appears, and although it seems unlikely, this might occur prior to polymer formation. Second, the breakup of the polymer might not be random. The results could be explained by a decomposition in which the new bonds were favored for survival. This could occur if the first step were the removal of an end carbon atom with subsequent release of the next pair as C_2^*. Or, the polymer in question could be considered as a collision complex made up of two two-carbon species each derived from acetylene, from which the newly formed bond survives as C_2^*. While both of these processes would give a random distribution of the carbon isotopes in C_2, such schemes are not comfortable subjects for speculation at present since there is no independent experimental evidence for either one.

It remains to discuss the apparent deviation from randomness of the isotope distribution in C_2^*, as shown in the last two columns of Table II. If the relative band head intensities correspond accurately to the concentrations of the isotopic C_2^* radicals in the flame, then the data indicate that a small fraction of the bonds in C_2^* are old bonds. This could be explained by the assumption of two separate reactions forming C_2^*: one which results in a complete shuffling of the isotopes and another in which the carbon-carbon bonds of the acetylene survive, the former reaction being the predominant source of C_2^* in a near stoichiometric acetylene-air flame.

In summary, the data show that the greater part of the C_2^* which radiates in the flames studied results

[8] This can be easily checked by a detailed probability calculation:

Let $C^{12}=A$ and $C^{13}=B$, denote the mole fractions (or relative frequencies) of AA, BB, and AB in the acetylene by p_1, p_2, and p_3, and assume that the original pairs are joined together at random. If all the ways a given new pair can result from combinations of old pairs are listed and the probabilities of these combinations summed, the relative frequency of occurrence, P, of new pairs is obtained:

$$P(AA)=\left(p_1+\frac{p_3}{2}\right)^2$$

$$P(BB)=\left(p_2+\frac{p_3}{2}\right)^2$$

$$P(AB)=2\left(p_1+\frac{p_3}{2}\right)\left(p_2+\frac{p_3}{2}\right);$$

but $p_1+(p_3/2)=[A]$ and $p_2+(p_3/2)=[B]$, where the brackets denote concentration in (atom percent)/100, and so

$$P(AA)=[A]^2$$
$$P(BB)=[B]^2$$
$$P(AB)=2[A][B].$$

Or, the isotope distribution in the set of new pairs is independent of that in the original pairs and is given by the statistical equilibrium distribution based on the atomic isotopic abundance in the acetylene.

[9] These arguments apply also to the hypothetical case of evaporation of C_2 from incipient carbon particles of graphitic structure made up of the carbon pairs of the acetylene *if* the possibility of pairing of carbon atoms from adjacent plane layers is excluded.

from a process in which the carbon-carbon bonds of the acetylene are broken prior to the appearance of C_2^*. The apparent residue of old bonds may mean that there is another reaction forming C_2^*, perhaps by some exothermic polymerization-decomposition process. If there really are in this sense two C_2^* populations in an acetylene flame, it will be of considerable interest to study their relative contribution to the total C_2 radiation as a function of pressure or acetylene/oxygen ratio in order to determine whether conditions expected to favor fuel polymerization also favor the survival of old bonds.

In respect to the predominant mechanism in these flames, the results show that it cannot be (1) one in which C_2^* comes directly from the acetylene molecule, nor (2) one in which it arises from the random breakup by pairs of a polymer containing the original carbon bonds of the fuel. The simplest choice of mechanism consistent with the data available is the recombination of single-carbon radicals.

ACKNOWLEDGMENTS

The writer expresses his thanks to Dr. H. P. Broida for helpful discussions and for making the recordings of spectra, to the Mass Spectrometry Section of the National Bureau of Standards for the isotopic acetylene analyses, and to the Statistical Engineering Laboratory, National Bureau of Standards, for advice on the probability calculation.

THE JOURNAL OF CHEMICAL PHYSICS VOLUME 23, NUMBER 11 NOVEMBER, 1955

On the Semiempirical Treatment of the Pi Electrons of Some Halogen Substituted Benzene*†

R. H. KNIPE‡
Department of Physics, Duke University, Durham, North Carolina
(Received February 14, 1955)

The pi moments of some halogen-substituted benzenes have been estimated from measured moments and compared to the predictions of a semiempirical molecular orbital theory of the pi electrons. Using parameters suggested by a perturbation treatment of these molecules, the results of two previous semiempirical molecular orbital treatments considering different molecular properties are compared with each other and with the estimated pi moments. The agreement is in general found to be good.

INTRODUCTION

THE pi electrons of some halogen-substituted benzenes have been treated in the semiempirical LCAO–MO approximation by several authors. In particular Robertson and Matsen[1] have evaluated parameters based on the location of the spectrum and its intensity. Wheland[2] has obtained parameters for chlorobenzene based on the directing properties of the chlorine atom. It is of interest to consider this method with respect to the dipole moments of some halogen substituted benzenes. Before beginning the treatment of these molecules, it was found desirable to obtain some results from an approach to the general perturbation problem.

SOME REMARKS ON PERTURBATION THEORY

We approach the general perturbation problem after the manner of Löwdin.[3] Assuming a set of linearly independent functions ϕ_i, we expand the wave function in the form

$$\psi=\sum_i \phi_i c_i. \tag{1}$$

Depending on whether the set of functions is complete or not, we may proceed from the variational form of the wave equation or from the variational principle to obtain

$$\sum_j (h_{ij}-\bar{H}\delta_{ij})c_j=0. \tag{2}$$

Here, $\bar{H}=\int\psi^*H\psi d\tau$, $h_{ij}=\int\phi_i^*H\phi_j d\tau$, where H is the Hamiltonian, and $\delta_{ij}=\int\phi_i^*\phi_j d\tau$ need not necessarily be the Kronecker symbol.

Let $u(E)_{ij}=h_{ij}-E\delta_{ij}$ and

$$(u)_{\alpha\beta^n}=\sum_{\lambda_1}\sum_{\lambda_2}^{\lambda_1}\cdots\sum_{\lambda_n}^{\lambda_{n-1}}\frac{u_{\alpha\lambda_1}u_{\lambda_1\lambda_2}u_{\lambda_2\lambda_3}\cdots u_{\lambda_n\beta}}{u_{\lambda_1\lambda_1}u_{\lambda_2\lambda_2}\cdots u_{\lambda_n\lambda_n}}, \tag{3}$$

where $\sum_{\lambda_j}^{\lambda_i}$ indicates the sum over λ_j, with $\lambda_j\neq\lambda_i$. Con-

---

* This work was supported in part by the Office of Naval Research under contract N6ori-107, T. O. I., with Duke University and in part by the E. I. du Pont de Nemours and Company under a predoctoral fellowship.

† Based on a thesis submitted in partial fulfillment of the requirement for the degree of Doctor of Philosophy in the Graduate School of Arts and Sciences of Duke University in 1954.

‡ Present address: Research Department, U. S. Naval Ordnance Test Station, Inyokern, China Lake, California.

[1] W. W. Robertson and F. A. Matsen, J. Am. Chem. Soc. **72**, 5252 (1950).

[2] G. W. Wheland, J. Am. Chem. Soc. **64**, 900 (1942).

[3] P.-O. Löwdin, J. Chem. Phys. **19**, 1396 (1951).

sider the set of functions ϕ_i to be chosen such that, for any value of E in the neighborhood of an eigenvalue of interest, the set may be divided into a finite set, denoted by the subscripts $(\alpha,\beta,\gamma,\cdots)$, and the remainder of the set, denoted by subscripts $(\kappa,\lambda,\mu,\cdots)$, where, for $n>N$ and for all α and β, $|(u)_{\alpha\beta}{}^n|/|(u)_{\alpha\beta}{}^{n-1}|<1$. If the set of functions ϕ_i be infinite, we assume the sum (3) to exist. Choosing $E=\bar{H}$ in the u_{ij}, (2) may be written for arbitrary α,

$$\sum_\beta u_{\alpha\beta}c_\beta=-\sum_\lambda u_{\alpha\lambda}c_\lambda, \tag{4}$$

and for arbitrary λ,

$$u_{\lambda\lambda}c_\lambda=-\sum_\beta u_{\lambda\beta}c_\beta-\sum_k{}^\lambda u_{\lambda k}c_k. \tag{5}$$

By virtue of the choice of the sets of functions, we may apply the expansion procedure used by Löwdin[3] to obtain by iterative substitution of (5) into (4)

$$\sum_\beta U_{\alpha\beta}c_\beta=0. \tag{6}$$

In the foregoing expression, $U_{\alpha\beta}=u_{\alpha\beta}-(u)_{\alpha\beta}{}^1+(u)_{\alpha\beta}{}^2-(u)_{\alpha\beta}{}^3+\cdots$. A similar expression is obtained from iterative substitution of (5) into itself. This expression, as can be readily shown, may be written

$$c_\lambda=\sum_\beta\frac{\partial U_{\beta\beta}}{\partial u_{\beta\lambda}}c_\beta. \tag{7}$$

The substitution of this result into (1) yields

$$\psi=\sum_\beta\psi_\beta c_\beta, \tag{1a}$$

where $\psi_\beta=\sum_i(\partial U_{\beta\beta}/\partial u_{\beta i})\phi_i$. Since $(\partial U_{\beta\beta}/\partial u_{\beta\alpha})=0$ for $\alpha\neq\beta$, the linear independence of the ϕ_i implies that the ψ_β are linearly independent.

Considering an arbitrary operator G, let $g_{ij}=\int\phi_i{}^*G\phi_j d\tau$, $G_{\alpha\beta}=\int\psi_\alpha{}^*G\psi_\beta d\tau$, and

$$\begin{aligned}(g)_{\alpha\beta}{}^n=\sum_{\lambda_1}\sum_{\lambda_2}^{\lambda_1}\cdots\sum_{\lambda_n}^{\lambda_{n-1}}&\frac{g_{\alpha\lambda_1}u_{\lambda_1\lambda_2}u_{\lambda_2\lambda_3}\cdots u_{\lambda_n\beta}}{u_{\lambda_1\lambda_1}u_{\lambda_2\lambda_2}\cdots u_{\lambda_n\lambda_n}}\\
&-\frac{u_{\alpha\lambda_1}g_{\lambda_1\lambda_1}u_{\lambda_1\lambda_2}u_{\lambda_2\lambda_3}\cdots u_{\lambda_n\beta}}{u_{\lambda_1\lambda_1}u_{\lambda_1\lambda_1}u_{\lambda_2\lambda_2}u_{\lambda_3\lambda_3}\cdots u_{\lambda_n\lambda_n}}\\
&+\frac{u_{\alpha\lambda_1}g_{\lambda_1\lambda_2}u_{\lambda_2\lambda_3}\cdots u_{\lambda_n\beta}}{u_{\lambda_1\lambda_1}u_{\lambda_2\lambda_2}\cdots u_{\lambda_n\lambda_n}}\\
&-\frac{u_{\alpha\lambda_1}u_{\lambda_1\lambda_2}g_{\lambda_2\lambda_2}u_{\lambda_2\lambda_3}\cdots u_{\lambda_n\beta}}{u_{\lambda_1\lambda_1}u_{\lambda_2\lambda_2}u_{\lambda_2\lambda_2}u_{\lambda_3\lambda_3}\cdots u_{\lambda_n\lambda_n}}+\cdots\\
&+\frac{u_{\alpha\lambda_1}u_{\lambda_1\lambda_2}\cdots u_{\lambda_{n-1}\lambda_n}g_{\lambda_n\beta}}{u_{\lambda_1\lambda_1}u_{\lambda_2\lambda_2}\cdots u_{\lambda_n\lambda_n}}.\end{aligned} \tag{8}$$

$$G_{\alpha\beta}=g_{\alpha\beta}-(g)_{\alpha\beta}{}^1+(g)_{\alpha\beta}{}^2-(g)_{\alpha\beta}{}^3+\cdots. \tag{9}$$

If the g_{ij} in (8) are replaced by the corresponding u_{ij}, this expression becomes identical with (3). Therefore, denoting the identity operator by Δ and assuming that the series $H_{\alpha\beta}$ and $\Delta_{\alpha\beta}$ converge in the same sense as the series $U_{\alpha\beta}$, we find $U_{\alpha\beta}=H_{\alpha\beta}-\bar{H}\Delta_{\alpha\beta}$. The substitution of this result into (6) yields

$$\sum_\beta(H_{\alpha\beta}-\bar{H}\Delta_{\alpha\beta})c_\beta=0. \tag{2a}$$

Thus, beginning with a set of linearly independent functions ϕ_i which may or may not be complete, by assuming a convergence property, we have arrived at a smaller number of linearly independent functions ψ_β which are equivalent to the original set for the representation of any particular eigenfunction of the system in question. This new set is considerably less general than the original set in that the functions are dependent on the eigenvalue. In a completely analytical approach to the perturbation problem, the new set is of little interest, since the necessary matrix elements would be obtained from the evaluation of expressions of the form of (9). In a semiempirical theory, however, these functions offer a conceptual advantage.

For example in benzene, Hückel[4] suggests that the pi electron orbitals may be represented as linear combinations of the carbon p_z functions. Subsequent studies using atomic orbitals have suggested that the atomic functions may better be replaced by distorted orbitals.[5] Thus, we might let the ϕ_β be the six degenerate p_z functions and the ϕ_λ be other functions in which the distortion may be expanded. The ψ_β are then the distorted orbitals which will in general be dependent on the particular molecular orbital in which they appear. If the $u_{\lambda\lambda}$ are sufficiently large compared to the energy differences between the different low lying molecular orbitals, these distorted orbitals would be approximately correct for all orbitals contributing to the ground state pi configuration and perhaps for some of the excited configurations as well. From this point of view it should not be surprising that discrepancies exist between molecular parameters determined semiempirically and by actual calculation using Slater p_z functions. In the case of substitution, the change of the Hamiltonian would result in changes in the h_{ij} as well as in the one-electron energies. These changes would correspond to changes in the distorted atomic orbitals. It is expected, however, that these changes would be most pronounced at the point of substitution. It is with this point of view that we shall proceed to discuss the halogen-substituted benzenes in the simplest one-electron molecular orbital approximation.

In an effort to minimize the appearance of the overlap in the semiempirical results, it is desirable to obtain some further general results from the perturbation theory. The series representation of the matrix elements (9) suggests an iterative process for the determination of the eigenvalue similar to the one used by Born, Heisenberg, and Jordan.[6] In what follows, we shall assume that the eigenvalue is known.

---

[4] E. Hückel, Z. Physik **70**, 204 (1931).

[5] See, for example, N. Rosen, Phys. Rev. **38**, 2099 (1931), and E. F. Gurnee and J. L. Magee, J. Chem. Phys. **18**, 142 (1950).

[6] Born, Heisenberg, and Jordan, Z. Physik **35**, 557 (1925).

Equations (6) are a system of linear homogeneous equations whose solutions, in the case where the eigenvalue is not degenerate, may be written

$$c_\beta = \rho_\alpha \bar{U}_{\alpha\beta}. \tag{10}$$

In (10), $\bar{U}_{\alpha\beta}$ is the cofactor of $U_{\alpha\beta}$ in $\det(U_{\alpha\beta})$ where α is chosen such that $\bar{U}_{\alpha\beta}$ is not zero. In the case of degeneracy, there are several possibilities. The matrix $U_{\alpha\beta}$ may be replaced by a sub-matrix of the same rank. In this case, a linearly independent set of degenerate wave functions may be constructed from a number of such sub-matrices. In the event that the series (9) and the eigenvalue are continuous functions of some element h_{ij} or δ_{ij} which will remove the degeneracy, this element may be varied to remove the degeneracy, and the result may be followed by continuity to the value of interest. The most satisfactory procedure appears to be to consider the equations in the form (2a). The eigenvalue in this equation, $\bar{H}$, is a continuous function of the $H_{\alpha\beta}$ and $\Delta_{\alpha\beta}$, as are the c_β. Varying an $H_{\alpha\beta}$ or $\Delta_{\alpha\beta}$ will remove the degeneracy to allow the c_β to be obtained by the use of (10) and a subsequent limit process. We proceed under the assumption that any degeneracy has been removed by this method.

It can be shown from the proportionality of similar cofactors of a singular determinant that the wave function determined by (10) is independent of the choice of α, except as it depends on the choice of the normalization factor ρ_α. To normalize this wave function, let $1=\sum_{\beta\gamma} c_\beta^* c_\gamma \Delta_{\beta\gamma}$ which becomes $1=|\rho_\alpha|^2 \bar{U}_{\alpha\alpha} \sum_{\beta\gamma} \bar{U}_{\beta\gamma}\Delta_{\beta\gamma}$. The linear independence of the ψ_β implies that the sum in this last expression is not zero; therefore,

$$|\rho_\alpha|^2 = (\bar{U}_{\alpha\alpha} \textstyle\sum_{\beta\gamma} \bar{U}_{\beta\gamma}\Delta_{\beta\gamma})^{-1}. \tag{11}$$

We now compute the mean value of an arbitrary operator G in the state described by this wave function; $\bar{G}=\sum_{\beta\gamma} c_\beta^* c_\gamma G_{\beta\gamma}$. Upon substitution from (10) and (11) and some rearrangement, we obtain

$$\bar{G} = (\textstyle\sum_{\beta\gamma} \bar{U}_{\beta\gamma} G_{\beta\gamma}) / (\sum_{\beta\gamma} \bar{U}_{\beta\gamma}\Delta_{\beta\gamma}). \tag{12}$$

$\sum_\beta \bar{U}_{\beta\gamma} G_{\beta\gamma}$ is a determinant of the same order as $\det.(U_{\alpha\beta})$ in which the $U_{\beta\gamma}$ in the γth column are replaced by the corresponding $G_{\beta\gamma}$. The numerator and denominator of (12) are sums of these determinants where γ is allowed to take on all values up to N, where N is the order of $\det.(U_{\alpha\beta})$. It is convenient to abbreviate these sums by $[G]$, so that (12) becomes

$$\bar{G} = [G]/[\Delta]. \tag{12a}$$

This is the form for which we shall find later use; however, we wish to point out another form which is of some interest.

If one multiplies (12a) by $[\Delta]$ and transposes, this equation becomes $[G-\bar{G}\Delta]=0$. As a particular case where G is replaced by H, this becomes $[H-\bar{H}\Delta] = N \det.(U_{\alpha\beta})=0$ which is essentially the secular equation for the system (2a). This similarity between the mean value of the arbitrary operator G in a particular energy eigenstate and the eigenvalue becomes even more pronounced when one considers that for the specific value of $\bar{G}$ satisfying (12a), the two polynomials in $\bar{H}$, $[G-\bar{G}\Delta]=0$ and $\det.(U_{\alpha\beta})=0$, have a common root. The mathematical expression of this fact is that the resultant of the two polynomials vanishes. The resultant of these polynomials is a polynomial of degree N in $\bar{G}$ where the coefficients do not involve the $\bar{H}$ explicitly. In fact, in the particular case of a finite number of functions ϕ_i, if the set $(\alpha,\beta,\gamma,\cdots)$ is chosen to include all of the set, the coefficients of the resultant with respect to the operator G are independent of the eigenvalue. Thus, in this particular case it is possible to compute the set of mean values, which are not necessarily eigenvalues, directly without first computing the set of energy eigenvalues.

Before going on to the particular problem of interest, we wish to point out that the derivations in this discussion are generally valid for any functions ϕ_i which yield to the necessary convergence properties upon which the derivations are based.

THE GENERAL SUBSTITUTION CASE

The dipole moment operator is a separable operator which does not mix the sigma and pi electrons of a plane molecule. Where the wave function may be written as the product of a sigma function and a pi function, the dipole moment is the vector sum of the dipole moments of the sigma function and the pi function. Where the pi function may be written as a single configuration of orthogonal one-electron functions, the pi moment is the vector sum of the moments of the one-electron functions. Thus we see that for a plane molecule, the dipole moment is particularly well adapted for discussion in terms of the Hückel approximation. We now proceed to discuss some halogen-substituted benzenes in this approximation formulating the problem semiempirically along the lines of Wheland and Pauling.[7]

Each halogen is considered to contribute two pi electrons and one semiempirical atomic pi orbital, and each carbon to contribute one pi electron and one pi orbital. We denote the halogen orbitals by the subscript x and the carbon orbitals by k. $k+1$ and $k-1$ denote the carbons adjacent to carbon k, and x_k and k_x denote that halogen x is bonded to carbon k and vice versa. We specify those important interaction integrals, which we do not neglect, as follows:

$\Delta_{ii}=|\lambda_i|^2$, where the λ_i are multipliers of the normalized ψ_i appropriate to the carbons in benzene and to the halogens, which leave the normalization of these orbitals in the substituted benzenes to be specified at our convenience;

$H_{kk}=\alpha_k|\lambda_k|^2$, where α_k is the Coulomb integral of the

[7] G. W. Wheland and L. Pauling, J. Am. Chem. Soc. **57**, 2086 (1935).

normalized function in the field of the nuclei and the average field of the other electrons;

$H_{kk\pm1}=\gamma\lambda_k^*\lambda_{k\pm1}$, where γ is the value appropriate for normalized functions in benzene;

$\Delta_{kk\pm1}=s\lambda_k^*\lambda_{k\pm1}$, where s is the value appropriate for normalized functions in benzene;

$H_{xx}=\alpha_x|\lambda_x|^2$; $H_{kx_k}=\gamma_k\lambda_k^*\lambda_{x_k}$; and $\Delta_{kx_k}=s_k\lambda_k^*\lambda_{x_k}$, where it is assumed on the basis of the similarity of the atomic orbitals involved that $\gamma_k s=\gamma s_k$. All other integrals of these types are assumed negligible. With respect to the similar integrals with the dipole moment operator, we use the hypothesis of Svartholm[8]—that is, $\mathfrak{y}_{ij}=\frac{1}{2}e(\mathbf{r}_i+\mathbf{r}_j)\Delta_{ij}$. Here, $\mathfrak{y}_{ij}=\int\psi_i^*\mathfrak{y}_0\psi_j d\tau$, e is the magnitude of the charge on the electron, and $\mathbf{r}_i$ is the vector from the origin to the nucleus designated by the subscript i. For the purpose of calculation, we take the origin to be the center of the ring.

To minimize the appearance of the overlap s in the equations (2a), we introduce the following transformation:

$\delta_i=(\alpha_i-\alpha)/(\gamma-\alpha_i s)$, which is a measure of the electronegativity of the atom i as compared to the carbon atoms in benzene;

$\lambda_i=(1+\delta_i s)^{\frac{1}{2}}$, which in the cases we consider is real;

$\rho_k=\gamma_k\lambda_k\lambda_{x_k}/\gamma$, which is a measure of the effectiveness of the exchange between the substituent orbital and the carbon orbital at the point of substitution as compared to the overlap between adjacent carbon orbitals; and $\bar{H}=(\alpha+\gamma y)/(1+sy)$.

These quantities with the exception of λ_i are similar to, though not precisely the same as, the analogous quantities used by Wheland.[2] Wheland's arguments as to the order of magnitude of the quantities carries over to these definitions essentially intact—that is, if α is taken to be the value of the α_k appropriate for normalized functions in benzene, the greater electronegativity of the halogen compared to the carbon implies that δ_x is positive. The effect of the halogen on the carbon at the substitution point in attracting sigma electrons to form the sigma bond should increase the apparent electronegativity of the carbon as seen by the pi electrons. This effect, however, should not make the carbon appear as electronegative as the halogen. Therefore, δ_k is positive but less than δ_x. The halogen-carbon distance is somewhat greater than the nearest neighbor carbon-carbon distance; therefore, the ratio γ_k/γ should be less than unity. Since the δ_i are positive, the λ_i are somewhat greater than one. Their effect on the ρ_k would be to keep its value near to one.

If the substitutions are made into (2a) in terms of these last defined parameters, these equations upon division by $(\gamma-\alpha s)$ become

$$\lambda_k\lambda_{k+1}c_{k+1}+(\delta_k-y)c_k+\lambda_k\lambda_{k-1}c_{k-1}+\rho_k c_{x_k}=0 \quad (13a)$$

and

$$\rho_{k_x}c_{k_x}+(\delta_x-y)c_x=0. \quad (13b)$$

These equations are recognizable as those which would be obtained for a fictitious molecule where $s=0$ and where the $H_{kk\pm1}$ are slightly altered from what they were in the unsubstituted benzene. It is assumed that the halogen lies along the extension of the line connecting the carbon at the point of substitution with the center of the ring, this molecule without overlap has the same dipole moment as the actual molecule we wish to treat in this simple molecular orbital approximation. This may be evidenced as follows:

The one-electron wave functions for the two molecules differ only in their normalization constants. If Δ_0 is the matrix of the Δ_{ij}, the corresponding matrix for the fictitious molecule is the identity I. If H is the Hamiltonian matrix for the fictitious molecule, $\Delta_0=I+sH$. Thus, averages with respect to the wave functions of the two molecules differ by the factor $1+sy$. Let averages with respect to a particular one-electron state of the actual molecule be indicated by brackets and with respect to the corresponding state of the fictitious molecule by angular brackets. If $\mathfrak{y}_0$ is the matrix of the components of $\mathfrak{y}_{ij}$ in the plane of the ring, $\mathfrak{y}$, the corresponding matrix for the fictitious molecule is obtained from $\mathfrak{y}_0$ by setting s equal to zero. With these definitions, it can be shown that $\{\mathfrak{y}_0\}=\mathfrak{y}+s.\langle\mathbf{J}\rangle/(1+sy)$ where the matrix $\mathbf{J}$ is $-y\mathfrak{y}+(\mathfrak{y}_0-\mathfrak{y})/s$. $\langle\mathbf{J}\rangle$ may be computed by (12a). The result is that $\langle\mathbf{J}\rangle=0$ for any y which is an eigenvalue of H. Therefore, $\{\mathfrak{y}_0\}=\bar{\mathfrak{y}}$. From the symmetry of the molecule, there is no dipole moment perpendicular to the ring. All of our subsequent calculations are with respect to the fictitious molecule.

To discuss the general substitution case as a perturbed benzene, we apply the transformation, which was used by Hückel[4] in obtaining the one-electron pi orbitals in benzene, to the atomic functions referred to the carbon atoms leaving the halogen atomic functions unchanged. Taking these transformed functions as ϕ's, an approximate dipole moment may be computed using the expansions (9). These calculations are simplified if, instead of computing the dipole moments of the occupied levels, one computes the moments of the unoccupied levels. If the nuclear charge is taken into account, it can be readily shown, from the invariance of the trace of a matrix under a unitary transformation, that the dipole moment of the ground state of the molecule is the negative of twice the sum of the moments of the unoccupied levels. Since the number of unoccupied levels is independent of the substitution case, these are the levels most readily treated for the general case. These levels correspond to those in benzene for which y is -2 and -1 (doubly degenerate in this approximation). Since the δ_x are greater than zero, these levels are less affected by the substitution than are the occupied levels which correspond to positive values of y.

To obtain an approximate dipole moment by em-

[8] N. Svartholm, Arkiv Kemi, Mineral. Geol. **A15**, N:O 13 (1941–42).

ploying the expansions (9) on the unoccupied levels, the following approximations were made: (1) where y appears in the u_{ij}, the benzene eigenvalues were used, (2) all terms involving products of the δ_k and ρ_k^2 were neglected. The result is that the moment is the vector sum of bond moments in the directions of the halogen carbon bonds. These bond moments are given by

$$\mu=\frac{ea\delta_k}{3}-\frac{ea\rho_k^2}{3}\left[\frac{2}{\delta_x+2}-\frac{1}{\delta_x+1}\right]$$
$$-\frac{e(a+b)\rho_k^2}{3}\left[\frac{1}{(\delta_x+2)^2}+\frac{2}{(\delta_x+1)^2}\right]. \quad (14)$$

In (14), a is the distance from the center of the ring to a carbon atom, b is the distance from the halogen atom to the carbon at the substitution point, and δ_x, δ_k, and ρ_k are the electronegativity and exchange parameters associated with this point. The sign is positive when the moment is directed toward the substituent, and negative when directed toward the center of the ring. The first term $ea\delta_k/3$ is recognizable as that obtained by Löwdin[9] for substitution which does not increase the number of pi electrons. It should be noted that in this approximation μ is independent of the overlap except as it appears in the definitions of the semiempirical parameters.

THE MONO- AND CERTAIN DI-SUBSTITUTED CASES

Our knowledge of the structure of the halogen-substituted benzenes is based on the work of Bastiansen and Hassel,[10] who investigated the structures of certain chlorine- and bromine-substituted benzenes in the vapor state by electron diffraction. They find the mono-substituted compounds and, where both substituents are the same, the di-substituted compounds, with the exception of *ortho*-substitution, to be planar. In the case of *ortho*-substitution, the two halogens are rotated 18° perpendicular to the ring such that they occupy equivalent positions on opposite sides of the ring. This rotation in the *ortho*-case tends to break down the distinction between sigma and pi electrons. The effects of this breakdown may not readily be included in a semiempirical theory of the type we are employing here; however, it is of interest to include the *ortho*-case in our considerations under the assumption that the angle of rotation is small enough to allow the effects due to this breakdown to be neglected. Since the halogens are on opposite sides of the ring, symmetry allows no permanent dipole moment perpendicular to the plane of the ring. Thus, our replacement of the molecule with overlap by an equivalent molecule without overlap carries over to the *ortho*-case when b in (14) is replaced by its projection on the plane of the ring.

To compare the observed moments with those predicted by (14), we estimate the sigma moments and subtract them from the observed moments to obtain estimated pi moments. The sigma moment is estimated under the assumption that it is the vector sum of the bond moments derived from aliphatic compounds. With this assumption and our result (14), the total moment should be representable as the vector sum of bond moments. Without prior knowledge of the C—H bond moment, all that can be determined from the measured moments is the difference between the halogen-carbon (C—X) moment and the C—H moment. It is these moments which are tabulated in Table I. The advantage of using the differences of the bond moments is that it tends to correct for changes in the individual bond moments due to changes in the carbon hybridization in going from the aliphatic to the aromatic compounds. Two estimates of the sigma moment are given. That which is conventionally used is the moment of the methylhalide (MeX). The other moment given is that of the tertiary butylhalide (tBX). The pi moment is estimated as the difference between the aliphatic moment and the aromatic moment under the assumption that in the aliphatic compounds the halogen is negative with respect to the carbon and that the pi moment is small. The sign convention is then that of (14).

The measured values of the moments of the substituted benzenes tend to vary within 0.02 Debye from observer to observer. Thus we expect the differences of the moments for the various substitution cases to have errors of this order of magnitude. In the estimates of the pi moments (φX-MeX and φX-tBX), we use only vapor data, since the differences in the moments obtained in vapor and solution are the order of magnitude of the quantity we wish to estimate. The differences of the *ortho*- and mono-moments and of the *meta*- and mono-moments in the case of chlorine substitution are,

TABLE I. A summary of dipole moment data for certain halogen-substituted benzenes.[a]

X	Cl_{vap}	F	Cl	Br	I
φX	1.72	1.45 $(1.57)_{vap}$	1.56	1.52 $(1.71)_{vap}$	1.34
o-φX_2	1.45	1.37	1.31	1.23	0.98
m-φX_2	1.67		1.48	1.46	1.27
MeX[b]		1.79	1.87	1.80	1.65
tBX[c]		2.05	2.15	2.21	2.13
φX-MeX	−0.15	$(-0.22)_{vap}$		$(-0.09)_{vap}$	
φX-tBX	−0.43	$(-0.52)_{vap}$		$(-0.05)_{vap}$	
ortho-mono	−0.27	−0.08	−0.25	−0.29	−0.36
meta-mono	−0.05		−0.08	−0.06	−0.07
ortho-mono +MeX(1 −cos18°)	−0.18	0.01	−0.16	−0.20	−0.28
ortho-mono +tBX(1 −cos18°)	−0.17	0.02	−0.15	−0.18	−0.26
[d]		1.34	1.69	1.88	2.00

[a] The tabulated values are bond moments in Debye units computed from recent determinations in the vapor (subscript vap) and in benzene solution quoted by G. L. Wesson, *Tables of Electric Dipole Moments*, The Technology Press, Cambridge, (1948) except as otherwise noted.

[b] Quoted by Gordy, Smith and Trambarulo, *Microwave Spectroscopy* (John Wiley and Sons, Inc., New York, 1953), pp. 361–362.

[c] Quoted by P. Kisliuk and C. H. Townes, *Molecular Microwave Spectra Tables* (NBS Circular 581, 1952) with the exception of tBF which was determined by Andersen, Andersen, Bak, Bastiansen, Risberg, and Smedvik, J. Chem. Phys. **21**, 373 (1953).

[d] C—X bond distances in angstrom units quoted by P. E. Allen and L. E. Sutton, Acta Cryst. **3**, 46 (1950). In the case of *o*-Cl, the projection of this distance inferred from Bastiansen and Hassel[10] is 1.63 A.

[9] P.-O. Löwdin, J. Chem. Phys. **19**, 1323 (1951).

[10] O. Bastiansen and O. Hassel, Acta chem. scand. **1**, 489 (1947).

to within the stated accuracy, independent of whether we use the moments measured in benzene solution or in the vapor. Assuming this to be true for the other halogens as well, we obtain estimates of these differences in the other cases. To estimate the contributions of the pi electrons to the *ortho*-mono differences in the case of the 18° angle, the contribution of the sigma moment must be added. This correction is approximately accomplished by adding the sigma moment multiplied by the factor $(1-\cos 18°)$. In applying the correction in this fashion, we neglect the fact that the C—H moment is not also bent out of the plane. Taking Pauling's estimate of the C—H moment of about 0.4 Debye,[11] we make an error of about 0.02 Debye which is of little consequence in this discussion. We see from Table I that the correction for the effect of the sigma moment is, to within the stated accuracy, independent of which aliphatic moment we use. From our present point of view, we consider the difference *meta*-mono as an estimate of the difference in the contributions of the pi electrons to the *meta*- and mono-moments.

On the basis of (14), we should expect the difference *meta*-mono to be zero, and the corrected difference *ortho*-mono to be different from zero and positive, since the value of b in the *ortho*-case is less than in the mono-case. We observe that the difference *meta*-mono is small, but its value may be significant. The only case for which the *ortho*-mono difference is positive is the fluorine substitution, and in this case it is so small as to be insignificant. Thus, it is only in the fluorine case, where we lack complete data even unto the molecular structure, that we might hope to explain the observed moments on the basis of the theory as developed thus far. Therefore, we investigate some of the effects which have been neglected as possible explanations of the discrepancies between what we have estimated from the measured moments and what we have predicted.

To check the validity of the expansion (14), the eigenvalue was computed from the secular equation corresponding to Eqs. (13) for a number of values of the parameters. This eigenvalue was then used to compute the moments and their partial derivatives with respect to the parameters using the bond distances for chlorine substitution and the empirical value of the overlap, $s=0.25$. Some of the moments and their differences are given in Table II. These numerical calculations also give us an opportunity to investigate the consequences of having large pi moments, a situation for which the expansion (14) does not hold. Our numerical calculations show that, in the case of the large moments, which would be predicted by reversing the directions of the total moments, one-half to one-quarter of an electron charge must migrate from the halogen into the ring per substituent. Such a migration should evidence itself in profound changes in the spectra and in the ionization potentials, but such changes have not been observed. A further difficulty with moments of this magnitude is the large *meta*-mono difference predicted but not observed. For small moments of the order of our estimates of Table I, the *ortho*-mono difference is positive rather than negative as observed. *Meta*-mono differences, the order of those observed, can be obtained by a careful balance of the effects of δ_k and ρ_k^2 in a reasonably large region about $\delta_x=2$. It is evident from Table II that (14) becomes valid to the accuracy of our estimated moments for δ_x somewhat larger than two.

TABLE II. Pi-bond moments and differences as functions of δ_x, δ_k, and ρ_k^2 using the chlorine bond distances.

ρ_k^2	δ_x	δ_k	μ_{mono}	*ortho*-mono	*meta*-mono	Eq. (14)
1	0	0	−6.36	−0.17	0.74	−11.12
½	0	0	−4.04	−0.15		
1	½	0	−4.20	0.06		−5.48
1	1	0	−2.95	0.09	0.15	−3.39
1	1	1	−0.97	0.42		
½	1	0	−1.59	0.07		
1	2	0	−1.60	0.24	−0.06	−1.78
1	4	0	−0.83	0.02	0.01	−0.83
1	8	0	−0.37	0.01	0.00	−0.37
ρ_k^2	∞	1		0.22	−0.04	
0	δ_x	1		0.22	−0.04	
0	δ_x	0	0	0	0	0

[11] L. Pauling, *The Nature of the Chemical Bond* (Cornell University Press, Ithaca, New York, 1940).

As seen from Table I, the estimated *ortho*-mono differences increase in the sequence F, Cl, Br, I. In other words, the discrepancy between what is observed and what is predicted increases as the principal quantum number of the atomic valence p-function increases. Since for fluorine-substitution, where the quantum number is that of the p-functions of carbon, the theoretical prediction is consistent with what is observed, one might consider that the discrepancy be connected with the breakdown of the two assumptions $\gamma_k s=\gamma s_k$ and $\mathfrak{y}_{ij}=1/2e(\mathbf{r}_i+\mathbf{r}_j)\Delta_{ij}$ for the carbon-halogen interaction integrals. These assumptions were based on the similarity of the semiempirical halogen and carbon orbitals. If the supposition were correct, however, *meta*-mono differences of the same order as the *ortho*-mono differences would be expected with a similar trend. Also, to remove these assumptions would overburden the semiempirical theory with parameters. Therefore, we examined some alternative explanations for these differences which are more in line with the ideas of a semiempirical theory.

As stated previously, in the *ortho*-case the C—X bonds are rotated 18° out of the plane of the ring such that the halogen atoms occupy equivalent positions on opposite sides of the ring. If it is assumed that the halogen pi orbital is perpendicular to the bond rather than to the plane of the ring, ρ_k could be estimated, in the further assumption that it is pure p, to be about 5% less than the ρ_k for the mono-case. If now the halogen orbital were rotated from the perpendicular to the bond, or if the carbon orbital were rotated into the C—X bond slightly, the decrease in ρ_k could be changed into

an increase (the amount being dependent on the difference in the sigma overlap and the pi overlap) and could explain the observed *ortho*-mono differences. This situation is complicated by the fact that these interactions may result in rotations of the sigma orbitals as well as the pi orbitals. What effect this might have on the sigma and pi moments we cannot estimate with the approximate theory developed here.

In our discussion of the parameters of importance, the δ_k were introduced in part to allow for changes in the Coulomb integral effected by the average field of the other electrons. It is of interest to consider the influence of the sigma electrons on this quantity. Since substitution at one point will affect the neighboring points to some extent, we investigate how this would appear in the bond moment formula (14) in the mono-substituted case. Let all but one ρ_k be equal to zero, and put the value of δ_k equal to δ_1, δ_o, δ_m, and δ_p corresponding to the position of substitution, the *ortho*-, the *meta*-, and the *para*-position. Adding the moments given by (14) for this set of parameters is equivalent to putting δ_k in (14) equal to $\delta_1+\delta_0-\delta_m-\delta_p$ and treating only the position of substitution. From the point of view of our present semiempirical approach, there would be no apparent change in the latter case. Thus we see the possibility of the inclusion of changes in the electronegativities of the carbon atoms upon substitution in the bond moment formula (14) through changes in δ_k dependent on the substitution cases.

In the mono-substituted case, the greater electronegativity of the halogen causes the halogen to remove sigma charge from the carbon at the point of substitution, thus increasing the apparent electronegativity of this carbon relative to its neighbor carbon atoms. This carbon will then attract sigma charge from its two neighbors to increase their apparent electronegativities, and so on. The carbon at the substitution point will not attract as much charge from its neighbors as did the halogen from it, and the neighbors will attact less than the substituted carbon, etc.; thus $\delta_1>\delta_o>\delta_m>\delta_p$.

Let us now consider this inductive effect in the *ortho*-case. Sigma charge has been removed from the adjacent carbons which are substitution points by the action of the substituted halogens. With respect to each other their apparent electronegativities are the same; hence, they can only attract sigma charge from their unsubstituted neighbors. Thus, in a first approximation, the net result in the bond moment formula (14) would be to decrease δ_k in the *ortho*-case by an amount δ_o from what it was in the mono-case. The results summarized in Table II indicate that there is some nonadditivity which is neglected in the approximate expression for the bond moments (14). For pi moments of the order of those we estimate from Table I, the *ortho*-mono nonadditivity is in the direction opposite to that which is observed. The *ortho*-mono difference due to the decrease in δ_k in the *ortho*-case is, however, in the observed direction and amounts to $-ea\delta_o/3$ or about $-2.2\delta_o$ in the approximation of (14). To estimate the order of magnitude of the δ_o necessary to account for the observed differences, we assume that all of the nonadditivity is due to the change in δ_k. Equating the corrected *ortho*-mono differences from Table I to $-2.2\ \delta_o$, we obtain the following estimates of δ_0: for F, Cl, Br, and I, the values are 0.00, 0.08, 0.09, and 0.12, in that order. That these values are in the reverse order from that of the electronegativities suggests that not all of the observed *ortho*-mono difference may be explained on the basis of the inductive effect alone.

Similar effects would contribute to the *meta*-mono differences of the moments. In the *meta*-case, there would be a competition between the two substituted carbons for the charge from the atom adjacent to both. In addition, the δ_m of one substituent would be suppressed when it refers to the same position as the δ_1 of the other substituent. The result would be to decrease the δ_k for this case by δ_m plus the difference between $2\delta_o$ and the apparent electronegativity of the carbon adjacent to both substituted carbons. The effect on the calculated difference in the pi moments would be to make it more negative than otherwise.

These changes in the sigma charge distribution will affect the sigma moment. The attraction of sigma charge by the carbon at the substitution point, and by the subsequent carbons, will tend to increase the sigma moment over that which would result if there were no carbons adjacent to the substitution point. The observed increase in the moments in the sequence methyl-, ethyl-, isopropyl-, tertiary butyl-halide may be interpreted as due to this effect. Examination of the amount of increase along the series shows that the effect tends to saturate. For this reason, we have included in Table I the tertiary butyl moment as a good estimate of the sigma moment in the substituted benzenes including the effect of induction. We point out, however, that there is an alternative explanation of this increase of the moment in this sequence.[12] As for variations of the sigma moments with type of substitution in the substituted benzenes, we mention that in the *ortho*-case the carbon-carbon bond which is most affected is perpendicular to the direction of the moment; hence a symmetric alteration of the charge in this bond such as we have described does not contribute to the total moment. In the *meta*-case, there would be a slight effect on the sigma electron distribution in the direction opposite to that of the very small effect which we have discussed with respect to the pi electrons.

SUMMARY AND CONCLUSION

In developing the approximate theory we have explicitly neglected those interactions between the sigma and pi electrons which might vary with the substitution

[12] Y. K. Syrkin and M. E. Dyatkina, *The Structure of Molecules and the Chemical Bond* (translation and revision by M. A. Partridge and D. O. Jordan) (Interscience Publishers Inc., New York, 1950), p. 216.

TABLE III. The value of the parameters for the mono-substituted benzenes.

Source	Robertson and Matsen[a]			Wheland[b]	
X	F	Cl	Br	Cl[d]	Cl[e]
ρ_k	1	1	1	0.85	1.18
δ_x	5	2.5	2.4	1.6	2.7
$\delta_{k(\text{mono})}$	1.1	0.8	0.6		0.72
δ_1				0.55	0.64
δ_o				0.075	0.076
$\tilde{\mu}_{\text{mono}}$[e]	1.9	0.4	−0.2		−0.17
					[−0.20 from (14)]
ortho-mono					−0.16
meta-mono					−0.00

[a] See reference 1.
[b] See reference 2.
[c] Except as noted above the moments are computed from (14).
[d] The parameters in this column are those analogous to ours as given by Wheland.
[e] The parameters in this column are adjusted to our definitions. The relations between Wheland's parameters (denoted by the subscript w) and ours are $\delta=\delta_w/(1-\delta_w s)$ and $\rho^2=\rho_w^2(1+\delta_x s)(1+\delta_1 s)$. The moments in this column are based on the numerical solution of Eq. (13)s.

case. Those interactions which were the same for all substitution cases were approximately incorporated in the theory as changes in the carbon Coulomb integrals as reflected in the electronegativity parameter δ_k. We found that the *meta*-mono moment differences predicted by the semiempirical theory are in good agreement with the estimated differences (based on measured total moments) for a range of values of the parameters in the neighborhood of $\delta_x=2$. It appeared, however, that the *ortho*-mono differences are not explained in a wholely satisfactory manner by the semiempirical theory of the pi electrons alone. Two possible sources were discussed for the breakdown of the simple theory in this case. One of these, the inductive effect, may be incorporated in a molecular orbital theory of the pi electrons alone by changing the apparent electronegatives of the carbon atoms with the substitution case. The other, a geometrical effect, deals with the breakdown of the distinction between pi electrons and sigma electrons in the *ortho*-substituted case. This effect cannot be incorporated into a theory of the pi electrons alone.

As mentioned in the Introduction, the semiempirical molecular orbital method has been used by other authors to describe properties other than the dipole moment of the mono-halogen-substituted benzenes. It is of interest to examine their results in terms of the dipole moments of these compounds. The values of their parameters and the moments computed therefrom are given in Table III.

Robertson and Matsen[1] treated the spectral shifts of the near ultraviolet absorption spectra of the mentioned compounds relative to benzene and the corresponding f-numbers. In these calculations they neglected the effect of overlap; therefore, we interpret their parameters as ours for the fictitious molecule without overlap. Wheland[2] treated the directing properties of chlorobenzene including the effects of overlap; therefore, we must adjust his parameters to our definitions using the empirical value of the overlap ($s=0.25$). It is of interest to note the close agreement between the parameters obtained from essentially different physical properties when our definitions are used. This suggests that the parameters as defined here lead to a favorable comparison between results obtained with and without the inclusion of overlap. The agreement between Wheland's δ_o and that which we estimated from the consideration of the effect of induction on the *ortho*-mono nonadditivity suggests, at least in the case of chlorine-substitution, that this effect is the principal cause of the observed nonadditivity.

Since we found (14) to give a satisfactory value of the mono-moment for parameters the order of magnitude of those given in Table III, the mono-moments have been computed from (14) using these parameters. The comparison between the results thus computed for chlorine-substitution from the parameters of Robertson and Matsen, and of Wheland, emphasizes the fact that a change of a few tenths in any one of the parameters results in a considerable change in the calculated moment.

The moment obtained for fluorobenzene based on the parameters of Robertson and Matsen is inconsistent with the measured moments given in Table I. The difference between the estimated moment and the computed moment indicates that large changes are necessary in the parameters if the semiempirical theory is to account for the measured moment. The results for chlorine and bromine suggest, on the other hand, that the estimated moments could be obtained with only small changes in the values of the parameters. We also recall that it was in the region about $\delta_x=2$ that we were able to fit the observed *meta*-mono differences. Therefore, we consider the pi moments calculated for these latter cases to be in good agreement with the estimates of Table I using either of the two estimates of the sigma moment.

The general agreement in the case of chlorobenzene between the semiempirical calculations for a number of physical properties suggests that in many respects the semiempirical molecular orbital method gives an adequate representation of the behavior of the pi electrons in the halogen-substituted benzenes. It must be remembered, however, that this agreement may be fortuitous.

ACKNOWLEDGMENTS

The author wishes to express his appreciation to Professor H. Sponer, who directed this research, and to Dr. P.-O. Löwdin for their valuable suggestions and continued interest in this work.

THE JOURNAL OF CHEMICAL PHYSICS VOLUME 23, NUMBER 11 NOVEMBER, 1955

Spectrum of Carbon Monoxide-Oxygen Explosion. I. The Visible Spectrum

R. H. KNIPE AND ALVIN S. GORDON
Chemistry Division, U. S. Naval Ordnance Test Station, China Lake, California
(Received February 14, 1955)

The effect of composition on the spectrum of the explosion of pure, dry CO and oxygen has been studied. In addition to the expected continuum with a superposed banded emission, a banded absorption has been observed. The absorber is probably the $a(^3\Pi_r)$ state of CO. The possibility that this excited state of CO is important in the production of the continuum is discussed.

INTRODUCTION

THE CO flame spectrum was first studied by Weston.[1] Extensive measurements and an analysis of the discrete emission spectrum, which is superposed on a continuum, were made by Gaydon[2] in the region 6250–3250 A. The hypothesis of Gaydon and earlier investigators[2] that the discrete emission is due to electronically excited CO_2 has recently been given further support by Walsh.[3] The source of the continuum is not so well understood. Previously suggestions have been made that it is due to direct association of CO and an oxygen atom[4] or of two oxygen atoms.[5] In this present work, the flame spectrum is studied as it appears in the explosion of pure, dry CO and oxygen for several different compositions of the gas.

MATERIALS

Carbon Monoxide

The CO was prepared by phosphoric acid dehydration of formic acid. After removal of acidic impurities and desiccation at about −160°C, the CO was liquified by liquid nitrogen. The first portion of the effluent gas was discarded to eliminate a slight trace of H_2. Part of the remaining liquid CO was then distilled directly to storage.

Oxygen

Tank oxygen was liquified. About one third of the liquid was boiled away to eliminate most of the nitrogen impurity. Part of the remaining liquid was distilled directly to storage, the low temperatures insuring efficient desiccation.

EXPERIMENTAL

The explosion was photographed by a ray control Raman spectrograph having an f/3.5 Schmidt-type camera. The dispersive elements are three extra dense flint 60° prisms. The spectrum was recorded on film strips (~4 in.×$\frac{3}{8}$ in.) of Ansco Triple-S-Pan developed in D-19. The dispersion was determined from a study of the mercury and argon spectra in the region of interest. Strong lines of these spectra were superposed on half of the exposed portion of the film to orient the exposures with respect to wavelength.

Flames of pure, dry CO-O_2 cannot be stabilized by the usual burner techniques. The spectrum was studied by admitting the premixed gases into a spherical quartz vessel 8 cm in diameter, set into a furnace at about 700°C. The compositions used were approximately $\frac{1}{4}$, 1, 2, and 4 CO to 1 O_2; the same final pressure was obtained for all compositions, except in the instance where the effect of final pressure was studied. From 20 to 60 explosions were used per exposure. A 50μ slit was used for the stoichiometric and the fuel rich mixtures; however, a 100μ slit was necessary for the lean mixtures in order to obtain an interpretable record without a prohibitive number of explosions per exposure. The useful region of the spectrum thus obtained was from about 5600 to 4300 A.

Because of the weakness of the discrete spectrum as compared to the underlying continuum, the most satisfactory method for studying the exposures has been by microphotometry. The central section of representative traces obtained using a Jarrell-Ash automatic recording microphotometer are shown in Fig. 1.[6] From observation of the mercury and argon lines it has been found that the scanning speed of the microphotometer was constant to about 0.4%. For scanning these exposures, the slit found most desirable was equivalent to a slit 2 mm×30μ at the plane of the emulsion. The scanning speed used was 2.5 mm/min. Various sections of film were scanned to observe the effects of photographic "noise." The traces through the section with the superposed atomic spectra together with the dispersion data obtained from these spectra alone furnished a wavelength calibration. The Na "D" lines, present in the explosion spectrum, as well as the pronounced features of the banded spectrum, allowed for orientation of the traces taken through those sections of the film which did not have the calibration lines.

RESULTS

A visual examination of the film strips suggests that the discrete spectrum superposed on the continuum

[1] F. R. Weston, Proc. Roy. Soc. (London) **A109**, 523 (1925).
[2] A. G. Gaydon, Proc. Roy. Soc. (London) **A176**, 505 (1940).
[3] A. D. Walsh, J. Chem. Soc. 2266 (1953).
[4] A. G. Gaydon, Proc. Roy. Soc. (London) **A183**, 111 (1944).
[5] G. A. Hornbeck, *Third Symposium on Combustion and Flame and Explosion Phenomena* (Williams and Wilkins, Baltimore, 1949), p. 501.

[6] We are indebted to Professor H. Sponer for the use of the Jarrell-Ash automatic recording microphotometer in her laboratory at Duke University.

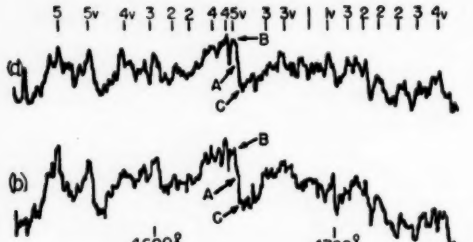

FIG. 1. Portion of the spectrum of the CO-O_2 explosion. (a) 1 CO to 4 O_2 showing the positions of the maxima of the flame bands as measured by Gaydon[2] with the intensities indicated for identification. (b) 2 CO to 1 O_2 (stoichiometric) with wavelength markers. (c) 4 CO to 1 O_2 showing the position of the heads of the triplet system of CO as measured by Herman and Herman.[8]

consists of several absorption bands in addition to the expected emission bands. A comparison of the spectra for different compositions indicates several distinct regions of absorption: ~20 500, ~21 500, ~21 800, and ~22 400K. Of these the band at about 21 500K, which is degraded to the red, presents the most promising head for measurement (*C* of Fig. 1). This head was measured on a number of tracings. Based on the reproducibility of the measurements of the known atomic lines used for comparison, its position was determined to be 4647 A with an error of at most 2 A. From the data quoted by Pearse and Gaydon,[7] CO is the only one of all known possible reaction species which has an observed band at this wavelength. The direction of degradation of the band strengthens this identification. The particular band in question belongs to the "triplet system" which has been observed in emission and is attributed to the transition from the $d(^3\Pi_i)$ to the lowest triplet $a(^3\Pi_r)$ of CO. The wavelength quoted is 4646.7 A.

In Fig. 1, the positions of the heads of the "triplet system" in CO measured by Herman and Herman[8] are indicated below the tracings. Asundi[9] showed that the v' values used by Herman and Herman should be increased by at least two, and suggested that an even further increase might be necessary. The assignments, as corrected by Asundi, are indicated for identification. Morse curves have been constructed using the molecular constants quoted by Herzberg.[10] These curves are in qualitative agreement with the relative intensities of the bands with the same v' as evidenced by the low temperature print given by Herman and Herman. The Morse curves predict qualitatively that the stronger bands in absorption should be in the neighborhood of the following:

Transitions	Sequence
7–0	$v'' = 0$
4–1 and 10–1	$v'' = 1$
1–2 and 13–2	$v'' = 2$
1–3 and 14–3	$v'' = 3$
0–4 and 18–4	$v'' = 4$
0–5 and 20–5	$v'' = 5$

Since the 0–0 appears from these curves to be Franck-Condon forbidden it is quite probable that the v' values of the observed bands should be increased further. Taking this uncertainty and the high temperature (~3000°K) into account, the relative intensities of the observed absorption bands are not unreasonable.

The positions of the maxima of the bands of the CO_2 emission, as well as their relative intensities as measured by Gaydon,[2] are indicated above the tracings exhibited in Fig. 1. It is evident that neither set of measurements alone gives a satisfactory description of this spectrum. Viewing the spectrum as a competition between an emission and an absorption spectrum is more satisfactory.

Approximate relative intensity in the continuum was obtained by a comparison of these tracings with tracings of photographs of the emission of a tungsten filament using the same optical system. The results,

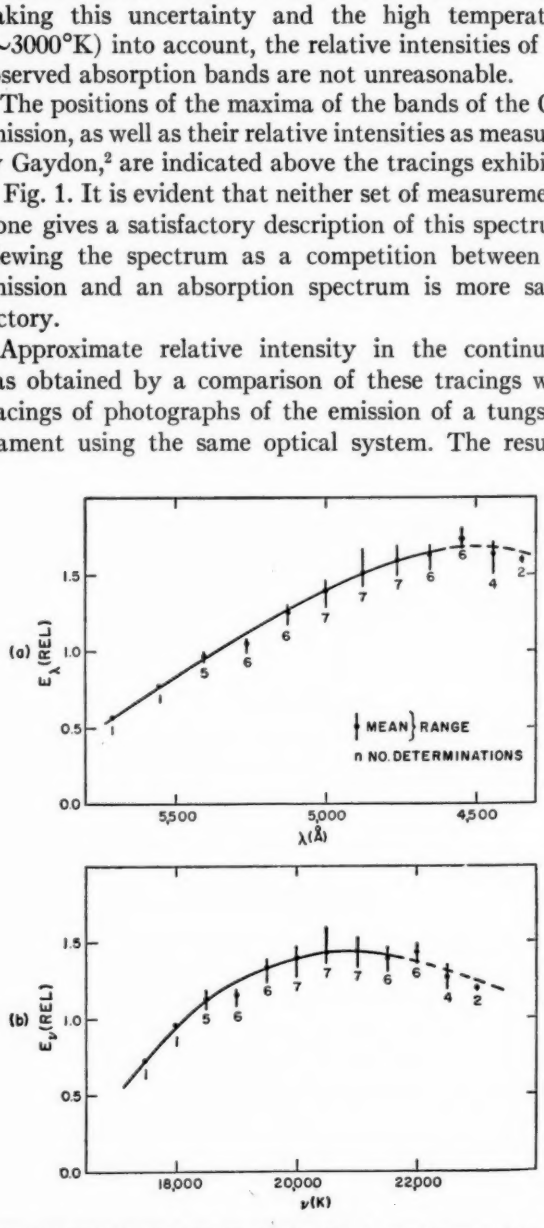

FIG. 2. Spectral distribution of the CO-O_2 continuum (a) per unit wavelength interval; (b) per unit energy interval.

[7] W. B. Pearse and A. G. Gaydon, *The Identification of Molecular Spectra* (Chapman and Hall, Ltd., London, England, 1950), second edition.

[8] R. Herman and M. L. Herman, J. phys. radium **9**, 160 (1948).

[9] R. K. Asundi, Proc. Indian Acad. Sci. **12A**, 491 (1940).

[10] G. Herzberg, *Spectra of Diatomic Molecules* (D. Van Nostrand Company, New York, 1950), second edition, p. 520.

assuming reciprocity, correcting for the dispersion of the spectrograph and the emissivity of tungsten, and neglecting the uncertainty inherent in the fact that the tungsten and explosion pictures were developed separately on individual film strips, are summarized in Figs. 2 and 3.

Figure 2 gives the relative intensity of the median of the discrete structure superposed on the continuum. Since the structure consists of emission and absorption of comparable intensity, this procedure represents our best estimate of the intensity of the continuum. As such, it is in agreement with other qualitative estimates of this intensity.[2] The relative intensity distributions of the continuum, as determined from the different exposures for various compositions, were fitted to an average curve which is presented in Fig. 2. The data are consistent to within 3%. There is no indication of consistent long-range deviations from the average curve as a function of composition. We conclude, therefore, that the relative intensity in the continuum is affected only slightly by composition.

The coefficients used in the foregoing fit, when corrected for the slit width and number of explosions used for the exposures, are estimates of the relative energy in the continuum as a function of composition. Again, assuming that composition does not affect the distribution of the continuum, a measurement of the intensity of the continuum at any point should give a second estimate of the relative energy as a function of composition. In a spectrum with both discrete emission and absorption superposed on a continuum as presented here, the determination of the intensity of the continuum at any point is rather uncertain. Figure 4 shows a situation which in appearance corresponds to the points A, B, and C in the vicinity of 21 500K (Fig. 1). For this case, the emission and absorption are separated so that the apparent absorption and emission heads (C and B) correspond to the real absorption and emission heads (C′ and B′), and there is a null point (A). If the absorption and emission were to overlap,

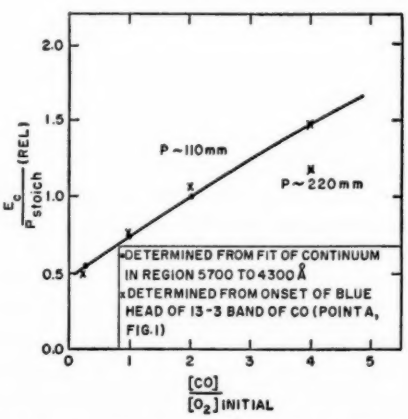

FIG. 3. Relative energy in the continuum divided by the partial pressure of the initial stoichiometric mixture *vs* the initial CO/O_2 ratio.

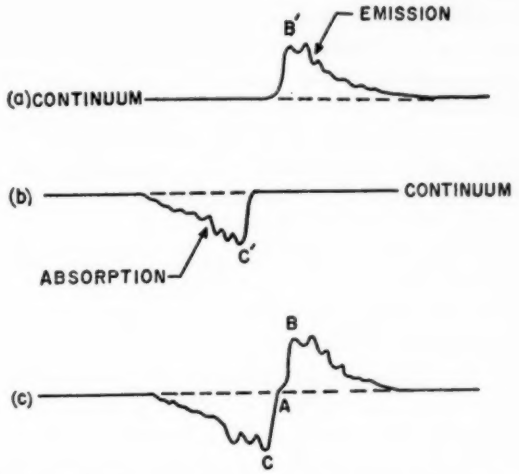

FIG. 4. Superposition of emission and absorption so as to give points A, B, and C of Fig. 1. (a) Emission alone. (b) Absorption alone. (b) Superposition.

the apparent absorption and emission heads would appear to be interchanged with a more complicated situation corresponding to point A. When one considers that the relative degradation of the emission and absorption bands may be reversed in some cases from that of Fig. 4, the complicated structure observed in Fig. 1, as well as some of the peculiar band shapes, is not unreasonable. The use of the point A in Fig. 1 as an estimate of the energy in the continuum leads to good agreement with that obtained from the previously described fitting procedure (Fig. 3). The curve (Fig. 3) is in qualitative agreement with the similar curve given by Kondratjewa and Kondratjew[11] although the results are not quantitatively comparable because of the differences in the experimental techniques.

It is evident from Fig. 1 that there is considerably more absorption in the rich mixture than in the stoichiometric mixture. In the case of the lean mixture, the position of point A would indicate that there is still considerable absorption. This may be due, in part, to the fact that a wider slit was used for this exposure than in any other exposures shown. Since the emission of the continuum and the distribution of absorbers may well have different dependences on time and location in the vessel, the interpretation of the observed absorption in terms of the number of absorbers could lead to erroneous results.

It is desirable, however, to consider the number of absorbers to some extent in order to discuss the possibility of the excited CO being thermal. The comparison which proceeds most readily involves a change of the quantity of exploded gas without changing the composition. For this case, little change in temperature is expected, and the number of absorbers should then be approximately proportional to the quantity of exploded gas. For a steady state situation, denoting the exposures

[11] H. Kondratjewa and V. Kondratjew, Acta Physicochim. U.R.S.S. **6**, 625 (1937).

with and without absorption by E_a and E_c and distinguishing between the results for two amounts of gas by using primes in one case, $\ln(E_a/E_c)=(n/n')\ln(E_a'/E_c')$ where n/n' is the ratio of the amounts of gas. A similar result follows if it is assumed that the distributions of radiators and absorbers are similar functions of time and position in the vessel for the two amounts of gas.

Data for this comparison were obtained for the mixture 4 CO:1 O_2 by doubling the amount of gas present. The ratio of the $\ln(E_a/E_c)$ as determined from the band head C of Fig. 1 was 0.4 rather than 2 as would be predicted by the foregoing consideration. We feel that this disagreement is striking enough to indicate that the absorber is not thermally excited. For chemical excitation, it would be expected that collisional quenching would increase with pressure to give the result which we observed.

A comparison of the trace for the stoichiometric mixture with Gaydon's published spectrogram[2] suggests that the absorption bands which we observed were also present in his work. As has been pointed out above, this added complexity could lead to some uncertainty as to the origin of the structure at any particular wavelength. This may, in turn, contribute to the lack of sharpness in the peaks in the distribution of the band differences as determined by Gaydon.

In Fig. 2, except for the point at 19 000 K and the region from 21 500 K toward higher energy, the points lie along a very smooth curve. The point at 19 000 K probably reflects the "green dip" in the film characteristic which has not been fully corrected. The structure on the high-energy side of 21 500 cannot be attributed to the calibration. It is to be noted in Fig. 1 that the appearance of this region is dramatically affected by composition. This suggests a competition between strong bands in both emission and absorption. In particular, the two bands 5 v and 5, which lie between heads of the 8–0 and 10–1 absorption bands, in addition to the high value of the continuum point in this region, suggest that the emission here may be an intense broad band from which the absorption is subtracted. The many overlapping absorption bands on the high-energy side of this emission would indicate that the continuum in this region should be somewhat more intense than indicated in Fig. 2.

It is difficult to obtain much information about the intensity of the banded emission with our crude calibration technique. However, the approximate measurements which we can make indicate that the discrete emission amounts to less than 10% of the total light in the region of our data.

DISCUSSION

It is observed that hydrogen contamination has a marked effect on the mechanism of the explosion. However, a comparison of the present spectra with the published spectrogram and measurements of Gaydon,[2] where hydrogen contamination is evidenced by the OH bands, shows no evidence of any marked structural changes due to our use of the pure gases. Further, the higher initial temperature of the explosive mixture does not affect the sharpness of the bands to any marked extent. The microphotometer traces show somewhat more of the structural detail than is evidenced by Gaydon's published spectrogram. The most pronounced spectroscopic effect which we observe is due to changing the CO/O_2 ratio. The evidence presented here indicates that this change in spectral character is due to absorption by excited CO.

In considering the presence of excited CO in the combustion, the mechanisms for its production and quenching are of interest. As to production, the reaction

$$CO_2{}^*+CO(^1\Sigma^+)\rightarrow CO_2(^1\Sigma_g{}^+)+CO(^3\Pi_r) \qquad (1)$$

is attractive as a bimolecular process. Excited CO could also be produced by the termolecular reaction

$$2CO(^1\Sigma^+)+O(^3P)\rightarrow CO_2(^1\Sigma_g{}^+)+CO(^3\Pi_r) \qquad (2)$$

which would be endothermic by about 13 kcal. The bimolecular collision of the excited CO with O and O_2 would tend to be deactivating; whereas the collision with normal CO would have a very small probability of deactivation because of the required multiplicity change.

The excited CO could react with O_2 in the following type of reaction:

$$CO(^3\Pi_r)+O_2(^3\Sigma_g{}^-)\rightarrow CO_3{}^*, \qquad (3)$$

followed by

$$CO_3{}^*\rightarrow[CO_2(^1\Sigma_g{}^+)+O(^3P)]$$

or (4)

$$[CO(^1\Sigma^+)+O_2(^3\Sigma_g{}^-)].$$

In (3) the two triplet reactant molecules should be very reactive. Further, a CO_3 molecule should have numerous opportunities for resonance stabilization. For example, in a roughly square spacial configuration $\begin{matrix}C & O\\ O & O\end{matrix}$, there would be the possibility of resonance between the two structures $\begin{matrix}C\text{–}O\\ O\text{–}O\end{matrix}$ and $\begin{matrix}C & O\\ | & |\\ O & O\end{matrix}$. Since there is no evidence for for a CO_3 molecule corresponding to the electronic configurations $CO_2(^1\Sigma_g{}^+)+O(^3P)$ and $CO(^1\Sigma^+)+O_2(^3\Sigma_g{}^-)$, the chemical combination of the two triplet molecules would be expected to dissociate radiatively to produce one of these lower configurations. These are the lowest configurations of the system CO_2 and O, and CO and O_2, and they are found to correlate. Energy considerations favor dissociation to the CO_2+O side, while, if the resonance mentioned in the foregoing is important for stabilization, dissociation to the $CO+O_2$ side would be favored. In either event a dissociative continuum would result. The energies available are about 147 and 139 kcal, respectively. Since the continuum has been ob-

served out to the order of 3000 A, it is expected that the reaction giving rise to the continuum must have at least the order of 100 kcal available. The length of the continuum (9000 to 3000 A)[12] suggests that, if the continuum is to be produced by dissociation, the upper state should have a moderate amount of binding energy. Thus, a dissociation continuum requires that the overall reaction have an energy significantly in excess of 100 kcal. The reactions (3) and (4) seem to be tailor-made to these requirements.

The need for third body stabilization in reaction (3) may be avoided by the crossing of potential energy surfaces which is thought to be particularly important for reactions involving electronically excited molecules.[13] The quantity of radiation per molecule of CO_2 formed appears to maximize at $\sim$40 mm[14] so that a termolecular reaction would not be expected to play an important role in the light formation. Thus if the reactions (3) and (4) are responsible for the major portion of the radiation (3) is expected to be bimolecular. The quenching processes for the CO_3* would be bimolecular, whereas its dissociation to form the continuum is unimolecular. However, the depth of well necessary to produce a continuum of the observed length should stabilize the molecule relative to quenching collision.

Since it appears that most of the light output is in the continuum, and that the order of 1 quantum is emitted per 100 CO_2 molecules formed,[15] it seems unlikely that the association processes mentioned in the Introduction, which proceed with a very low probability, could be responsible for the continuum. One would expect rather a dissociative process involving species produced during the reaction in moderate quantity. Quenching processes are rapid compared to an absorption process, so that the $CO(^3\Pi_r)$ must be present in relatively high concentration during the burning of CO.

Production of the continuum according to reactions (3) and (4) is consistent with the fact that it is not observed in the atomic flame, whereas the flame bands are,[16] since at low pressures reaction (3) is not competitive with the unimolecule production of the banded spectrum from CO_2*. For the association reactions to be responsible for the continuum, Broida and Gaydon[16] point out that an association reaction would have to have a high activation energy. This high activation energy would be a further deterrent at any temperature for these already improbable processes. In this connection, the continuum as well as the banded emission appears to be present in Gaydon's photographs of the pre-ignition glow.[17] Since the temperature at which the glow occurs is much lower than the temperature of the flame of the explosion, it does not appear that the activation energy for the production of the species responsible for the continuum is appreciably greater than that for the species responsible for the banded structure.

Figure 3 gives further evidence to support our contention that the continuum producing reaction is not any of the previously suggested association reactions. Both of these reactions depend on the production of O from O_2 in the reaction. It would be expected, therefore, that the curve would have a negative slope instead of the strong positive slope observed. The observed slope indicates that the continuum is produced by a reaction involving chemical preparation through CO or reaction with CO following a chemical preparatory process. It should be noted that the slight curvature observed in Fig. 3 is probably significant, since, for large values of the CO/O_2 ratio, the curve must approach a horizontal asymptote. Our assumption that excited CO is involved in the production of the continuum is consistent with the observation that the radiation is not thermal,[18] since we observe that the excited CO also is not thermal.

[12] M. W. Feast, Proc. Phys. Soc. (London) **A63**, 772 (1950).
[13] See, for example, K. E. Shuler, J. Chem. Phys. **21**, 624 (1953).
[14] E. Kondratjewa and V. Kondratjew, Acta Physicochim. U.R.S.S. **4**, 547 (1936).
[15] E. Kondratjewa and V. Kondratjew, Acta Physicochim. U.R.S.S. **6**, 748 (1937).
[16] H. P. Broida and A. G. Gaydon, Trans. Faraday Soc. **49**, 1190 (1953).
[17] A. G. Gaydon, Proc. Roy. Soc. (London) **A182**, 199 (1943–44).

Determination of the Velocity of Sound in Hydrazine-Water Mixtures by Means of the Debye-Sears Ultrasonic Light Diffraction Phenomenon

GEORGE G. KRETSCHMAR
Michelson Laboratory, U. S. Naval Ordnance Test Station, Inyokern China Lake, California
(Received February 7, 1955)

The velocity of sound has been determined at 4 megacycles for a large number of different concentrations of hydrazine in water from 8 to 99 weight percent of hydrazine. The velocities were determined from the diffraction of a monochromatic light beam which was projected through a glass-sided cell containing the liquid in which standing waves were set up by an oscillating quartz crystal. The light source was a sodium arc and the frequency of the ultrasonic wave train was determined with a precision frequency meter. The diffraction angles were measured on a Gaertner spectrometer, reading to one second of arc. The data can be represented by the equation

$$V = 1497.40 + 745.460H + 382.353H^2 - 556.3361H^3,$$

where V is the velocity of sound in the hydrazine-water mixture at 25°C and H is the fractional weight of hydrazine.

INTRODUCTION

THE velocity of sound has recently been determined for hydrazine-water mixtures throughout the range of concentrations from zero to 100 weight percent of hydrazine.[1] This work was done by making use of the ultrasonic interferometer which has been described in a previous publication.[2] One purpose of the experiments was to see if the velocity of sound data contained any discontinuities such as appear in the eutectic points of the freezing-point curve.[3] However, the data obtained by the sonic interferometer method were not sufficiently precise to determine with certainty if there were any variation from a smooth curve.

In order to increase the precision and obtain more accurate data on the velocity of sound and the compressibility of hydrazine and hydrazine-water mixtures, new sound velocity data were taken by making use of the Debye-Sears method of ultrasonic diffraction of a monochromatic light beam.[4] This method, making use of a known wavelength of light, and precise angular measurements, is inherently more sensitive and approaches optical measurements in precision. The method is essentially like the diffraction of light by a ruled grating in which the standing wave pattern of the ultrasonic waves through the liquid acts as the grating.[5] The ultrasonic waves are set up in the liquid by means of an oscillating quartz crystal which operates near its resonant frequency.

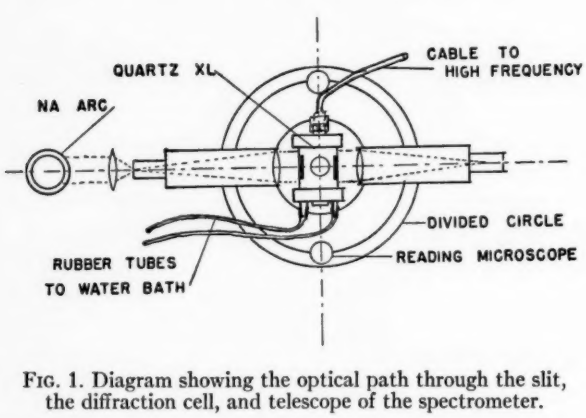

FIG. 1. Diagram showing the optical path through the slit, the diffraction cell, and telescope of the spectrometer.

DESCRIPTION OF THE APPARATUS

Figure 1 is a diagrammatic sketch of the diffraction cell mounted on the table of a spectrometer. The light from a sodium laboratory arc is received on a condensing lens which concentrates it on the slit of the spectrometer. Adjustments are made so that light going through the cell is essentially a parallel beam. The slit image is focused on the vertical cross hair in the telescope. When high frequency is applied to the crystal, and the oscillator tuned to produce a standing wave pattern, sharp diffraction lines are observed on both sides of the central slit image. The angular displacements can be accurately measured on the divided circular scale of the spectrometer, which is a precision Gaertner instrument provided with reading microscopes so that readings can be estimated to one second of arc.

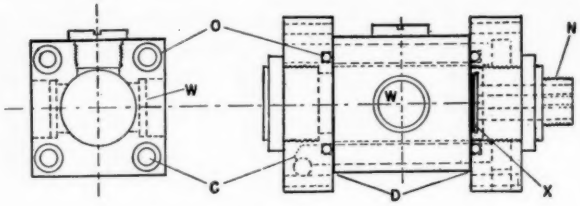

FIG. 2. Details of the diffraction cell.

Details of the diffraction cell are given in Fig. 2. It is cut out of a solid block of aluminum through which a

[1] George G. Kretschmar, J. Chem. Phys. **22**, 753 (1954).
[2] George G. Kretschmar, J. Am. Rocket Soc. **23**, 82 (1953).
[3] Paul H. Mohr and L. F. Andrieth, J. Phys. Colloid Chem. **53**, 901 (1949).
[4] P. Debye and F. W. Sears, Proc. Natl. Acad. Sci. U. S. **18**, 409–414 (1932).
[5] L. Bergmann, *Ultrasonics and their Scientific and Technical Applications*, English edition, translated by H. S. Hatfield (John Wiley and Sons, Inc., New York, 1938), p. 63.

round hole one inch in diameter is drilled. The four quarter-inch holes, *C*, through the four corners, are used as ducts for the water which is circulated to maintain a constant temperature of 25°C. Connections between the ducts are drilled into the endplates. The ends of the cell are sealed with thin aluminum diaphragms, *D*, which are held firmly in position by clamping between the endplates and the body of the cell. Tight contact seals, *O*, are made by the pressure of O-rings. The cell is equipped with two windows, *W*, placed transverse to the direction of the sound wave train. These windows, of selected plate glass, allow the light beam to be projected across the sound waves in the liquid. Pressing against one of the diaphragms is the crystal, *X* which is held in place by a brass crystal holder which makes contact with the central conductor of a coaxial cable from the driving amplifier through a modified Amphenol connector *N*.

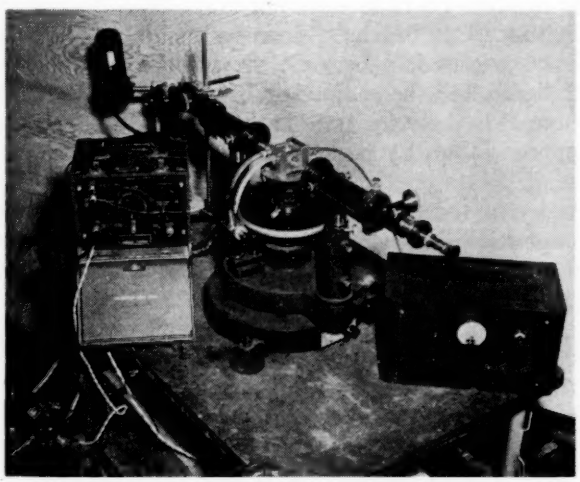

FIG. 3. The assembled apparatus.

Figure 3 shows the assembled equipment in which the diffraction cell is mounted upon the table of the spectrometer. The crystal is driven by a General Radio Type 700A beat frequency oscillator and a small amplifier which is similar to that described in recent work[6] on the compressibilities of solutions. The frequency was monitored by a Signal Corps type BC 221 A.H. frequency meter. The temperature was maintained constant to about one part in two thousand by pumping water through the cooling ducts of the cell from a water bath of about 80 liters capacity in which the temperature was regulated to 25°±0.01°C by means of an electronic regulating circuit.[7]

THEORY

Figure 4 is the diffraction pattern produced by the diffraction of the light beam passing through pure water and two different concentrations of hydrazine. It will be noted that there is a progressive decrease in the spacing of the lines, which is apparently due to the increasing wavelength of the sound wave train as the concentration of the hydrazine is increased. This is exactly analogous to the optical case where the different orders of diffraction are spaced more closely for the more coarsely ruled gratings.

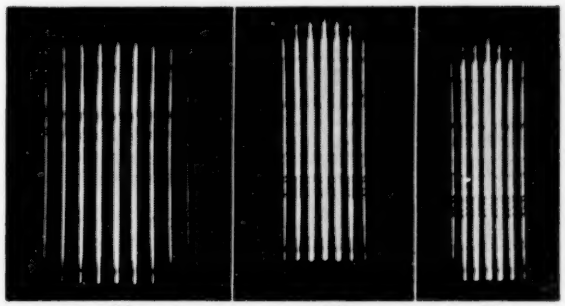

FIG. 4. The diffraction pattern. (1) the cell containing water, (2) the cell containing 46% hydrazine, (3) the cell containing 96% hydrazine.

In the original work of Lucas and Biquard[8] it was observed that the wavelength of the ultra sound and the wavelength of the transmitted light beam are related to the angle of diffraction exactly as in the case of optical diffraction with a ruled grating, according to the well-known relation

$$\frac{n\lambda}{d}=\sin\theta,$$

where λ = wavelength of the light, d = wavelength of the sound, n = the order of the diffraction image, and θ = the angle of the diffraction.

It will be observed from Fig. 4 that a number of equally spaced orders of diffraction are produced. The actual number of orders produced appears to depend on (1) the sharpness of tuning, (2) the liquid composition, that is, the number of orders is reduced as the concentration of hydrazine is increased, and (3) the state of the liquid, that is, with high concentrations of hydrazine, the number of orders decreases with time because of some effect of the ultrasonic oscillations on the hydrazine. For pure water the number of orders made visible with a narrow slit and the spectrometer adjusted for parallel light was a maximum of 20 on each side of the central image. This was accomplished by a small amount of tuning of the oscillator near the resonance fundamental of the crystal at approximately 4000 kc. For hydrazine mixtures of the higher concentrations the number of orders is less than half as many as for water, and this is reduced to as few as three to five after a few minutes of operation. The appearance of a few small bubbles after the reduction in number of orders leads one to the conclusion that a slight amount

[6] Frank T. Guker and Robert M. Hoag, J. Acoust. Soc. Am. **25**, 470 (1953).
[7] I. Sucher and H. S. Anker, Rev. Sci. Instr. **20**, 321 (1949).
[8] R. Lucas and P. Biquard, Compt. rend. **194**, 2132 (1932).

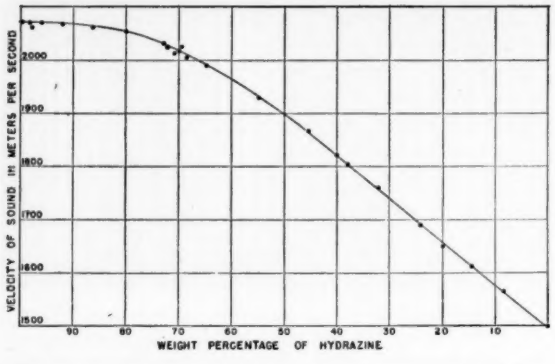

FIG. 5. The velocity of sound in hydrazine-water mixtures plotted against the concentration of hydrazine.

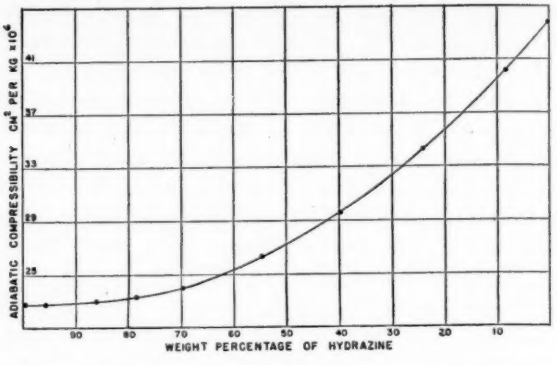

FIG. 6. The adiabatic compressibility of hydrazine-water mixtures plotted against the concentration of hydrazine.

of cavitation or dissociation has reduced the efficiency of the diffraction effect.

RESULTS

As a check on the accuracy of the method a large number of readings were taken on distilled water. The average velocity of sound computed from a group of ten readings on water was 1498.1 meters per second, with the maximum deviation from the mean of 3.68 meters per second. A second group of three gave an average of 1498.12, with maximum deviation of 1.58. A third group of three was 1498.00, with maximum deviation of 1.37. The average of these three groups of readings, taken on different days, is 1498.07 meters per second. Comparison with Table II of reference 5 shows a very satisfactory agreement with other published values.

A series of 23 readings was taken with various concentrations of hydrazine in water from 8 to 99 weight percent of hydrazine. The concentration at each point was determined by a separate chemical analysis making use of the direct iodate method.[9] Velocity-of-sound computations were made by multiplying the frequency as read on the frequency meter by the wavelength of the sound in the liquid as determined from the wavelength of the light (5893 angstroms) and the measured angle of the diffraction image. Each point is an average of four to six values obtained from independent measurements of the diffraction angle. These points are plotted in Fig. 5, and it will be observed that the data give a smooth curve which is linear up to 50% hydrazine and then curves rather abruptly at about 70% hydrazine, and is nearly horizontal for concentrations above 90% hydrazine.

An equation which fits the data closely is

$$V=1497.40+745.460H+382.353H^2-556.3361H^3,$$

where V is the velocity of sound in meters per second at 25°C and H is the fractional weight of hydrazine in the hydrazine-water mixture. The value 2074 meters per second for pure hydrazine is probably within less than five meters of the true value for this constant.

From the velocity-of-sound data one may compute the adiabatic compressibilities of the hydrazine-water mixtures. This has been done by making use of the known relationship between the velocity of sound in the liquid and the compressibility, which is $V^2=1/\rho\beta$, where V is the velocity, ρ is the density, and β is the compressibility. By taking velocities for a chosen number of points on the graph of Fig. 5, and using the density of the mixture at these points, the adiabatic compressibilities were computed. The densities were taken as the weighted average of the density of hydrazine and the density of water at 25°C at the point in question. The density of hydrazine[10] was taken as 1.004 at 25°C and that for water as 0.99707. The weighted mean density of the two components will give the density of the mixture to a reasonable approximation. Since both components are close to unity, the effect on the computed compressibilities will be small. The computed compressibility values have been plotted in Fig. 6.

The data plotted on the graph of Fig. 5 shows no evidence of variations from a smooth curve throughout the continuous dilution range of the hydrazine-water mixtures. Special attention was given to the upper eutectic point of 69 weight percentage of hydrazine, but the variations here are not more than would be accounted for by the experimental distribution of the data.

The velocity of sound in hydrazine is the highest of any liquid for which data are found in the literature. It is believed that the two end points of the curve of Fig. 5 give values for the velocity of sound in hydrazine, and in water at 25°C, which are within 0.1% of the true values for these constants.

The author wishes to express his appreciation to Martha J. Kenyon of the Computing Branch for the least squares fitting of the data to the equation given above. Dr. Howard W. Kruse of the Chemistry Division furnished the hydrazine used in the experiments.

[9] L. F. Andrieth and Betty Ackerson Ogg, *The Chemistry of Hydrazine* (John Wiley and Sons, Inc., New York, 1951), p. 157.

[10] George G. Kretschmar, Jet Propulsion 24, 175 (1954.)

Infrared Spectra and Structure of the Crystalline Sodium Acetate Complexes of U(VI), Np(VI), Pu(VI), and Am(VI). A Comparison of Metal-Oxygen Bond Distance and Bond Force Constant in this Series*

LLEWELLYN H. JONES
Los Alamos Scientific Laboratory, University of California, Los Alamos, New Mexico
(Received February 9, 1955)

Infrared spectra of solid $NaXO_2(Ac)_3$, with X=U, Np, Pu, and Am, have been observed. From the symmetric and asymmetric stretching frequencies of the O−X−O groups, approximate X−O force constants have been calculated and were found to decrease in the order $k_{U-O}>k_{Np-O}>k_{Pu-O}>k_{Am-O}$, the respective values being about 0.705, 0.698, 0.675, and 0.612 megadyne/cm. From the cell constants for $NaXO_2(Ac)_3$ it is apparent that the X−O bond distance decreases in the same order—$R_{U-O}>R_{Np-O}>R_{Pu-O}>R_{Am-O}$. Thus, a decrease in bond distance appears to be accompanied by a decrease in force constant, probably because the bond, though shortened by contraction of the electron shells of the metal, is weakened by interaction with the extra valence shell electrons.

IN a study of the infrared spectra of aqueous uranyl and transuranyl (V) and (VI) ions, Jones and Penneman[1] concluded that the X−O force constant decreased in the series $NpO_2^{++}>UO_2^{++}>PuO_2^{++}>AmO_2^{++}$. However, Zachariasen[2] found for $NaXO_2(Ac)_3$ crystals that the cell constant decreases in the order X=U, Np, Pu, suggesting a regular decrease in X−O distance from O−U−O to O−Np−O to O−Pu−O. In this laboratory[3] more precise values of these cell constants and the cell constant of $NaAmO_2(Ac)_3$ have been determined. They are listed in Table I.

This apparent regular decrease in X−O distance seemed to be anomalous in view of the fact that the infrared data pointed to a decrease in force constant while, assuming U, Np, Pu, and Am are similar type atoms, one would expect an increase in force constant as the bond distance is decreased. Since a comparison of the force constants of the XO_2^{++} ions in aqueous solution with their bond distances in solid $NaXO_2(Ac)_3$ is somewhat dubious, we observed the infrared spectra of the solid compounds, $NaXO_2(Ac)_3$, with X=U, Np, Pu, and Am. Also it seemed possible that the decrease in cell constant could arise from differences within the acetate group, which should show up as differences in the infrared spectra of the acetate vibrations.

EXPERIMENTAL

Sodium uranyl (and transuranyl) acetate was prepared by adding a large excess of saturated aqueous sodium acetate to a 2 formal solution of uranyl nitrate. The precipitate which formed was washed with sodium acetate several times and finally with 50% acetic acid to remove the sodium acetate. Though these compounds are relatively insoluble in saturated sodium acetate, they are appreciably soluble in 50% acetic acid and quite soluble in water.

Two types of samples were prepared for infrared spectral observations. In the first the washed slurry was spread out on a silver chloride plate and allowed to dry. For the second method, the dried powder was ground intimately with finely divided potassium chloride or bromide, and the mixture was then pressed into plates.

The spectra were observed with a Perkin-Elmer Model 12-C spectrometer converted to double-pass operation.

RESULTS

Part of the spectrum of $NaUO_2(Ac)_3$ is shown in Fig. 1. The spectra of $NaNpO_2(Ac)_3$, $NaPuO_2(Ac)_3$, and $NaAmO_2(Ac)_3$ are not shown, as they are almost identical with that of $NaUO_2(Ac)_3$ except for shifts in the O−X−O frequencies.

The vibrational frequency assignments resulting from these observations are listed in Table II, along with those of sodium acetate[4] for comparison.

The frequencies given in Table II show that the forces within the carboxyl groups of the acetates are considerably altered in going from sodium acetate to $NaXO_2(Ac)_3$. However, they also show that among the four $NaXO_2(Ac)_3$ complexes there is little difference

TABLE I. Cell constants for cubic $NaXO_2(Ac)_3$ at 25°C.[a]

X	a_0
U	10.6935±0.0002 A
Np	10.679 ±0.001
Pu	10.670 ±0.001
Am	10.653 ±0.002

[a] The temperature is fairly critical as Ellinger[3] determined that $NaUO_2(Ac)_3$ has a temperature coefficient of linear expansion of 52×10^{-6} per degree centigrade in the range 17–26°C.

* This work was sponsored by the U. S. Atomic Energy Commission.

[1] L. H. Jones and R. A. Penneman, J. Chem. Phys. **21**, 542 (1953).

[2] W. H. Zachariasen, Phys. Rev. **73**, 1104 (1948); A. F. Wells, *Structural Inorganic Chemistry* (Oxford University Press, London, 1950), second edition, p. 661.

[3] F. H. Ellinger, Los Alamos Scientific Laboratory (unpublished work).

[4] L. H. Jones and E. H. McLaren, J. Chem. Phys. **22**, 1796 (1954).

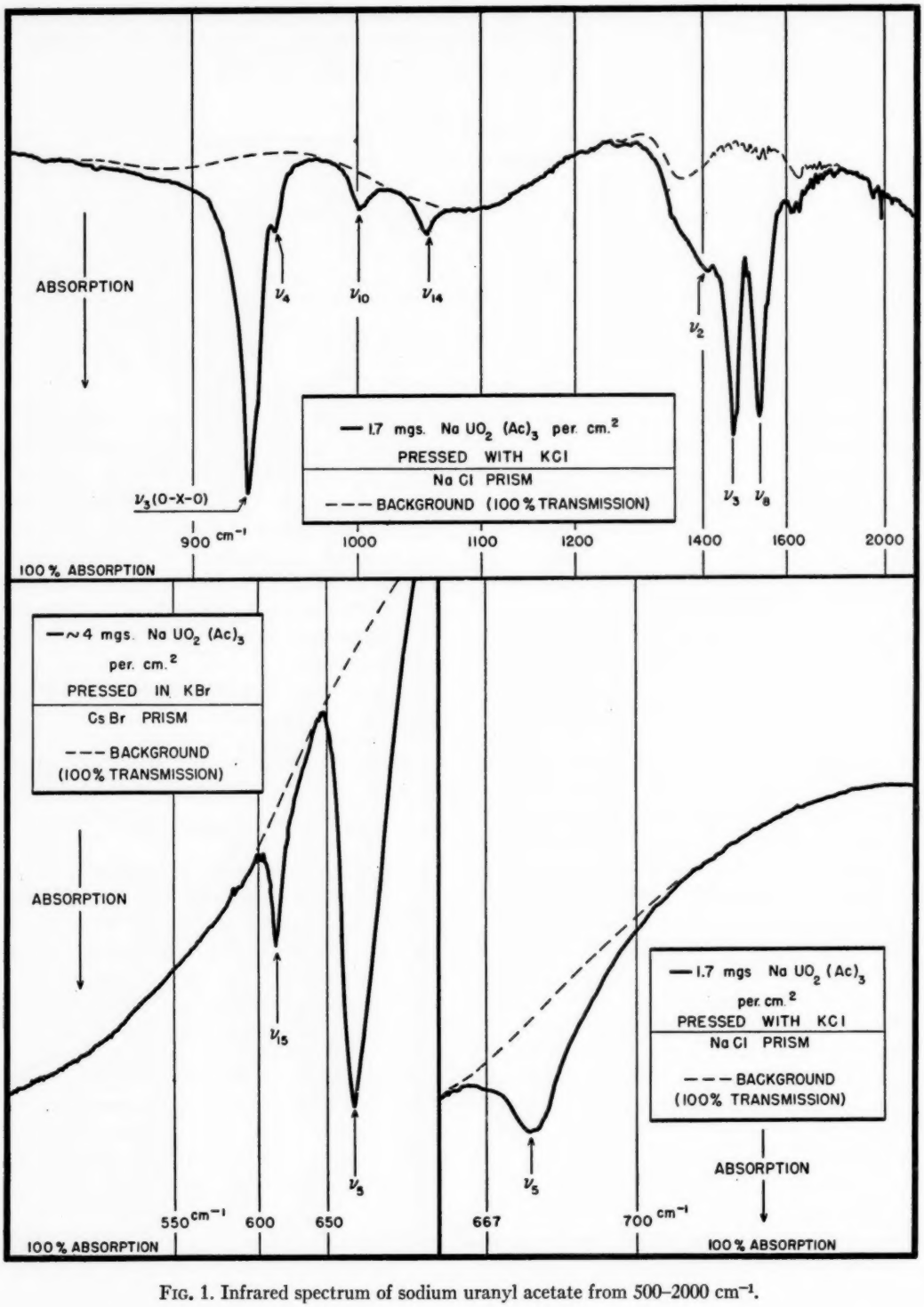

FIG. 1. Infrared spectrum of sodium uranyl acetate from 500–2000 cm^{-1}.

in the observed acetate frequencies. Thus the bonds within the acetate groups are not appreciably different in strength in the series X=U−Np−Pu−Am. Also we can say that there is no great difference in the force of binding of the acetate groups to the central atom (X), as this would be reflected as a change in the acetate frequencies. Therefore, the only explanation for the decrease in cell constant shown in Table I is that the X−O distance decreases in a fairly regular fashion over the series X=U, Np, Pu, Am.

The symmetric O−X−O stretching frequencies, ν_1, listed in Table II are somewhat uncertain as they are very weak. However, the combination frequencies $\nu_1+\nu_3$ observed for the U, Np, and Pu compounds serve

to confirm the assignments of ν_1. There can be no doubt that the assignments of the strongly infrared-active vibrations, ν_3, are correct.

Force constants were calculated for the X−O bonds, treating the linear O−X−O groups independently, using the valence force potential function,

$$2V=k_{X-O}[\Delta R_1^2+\Delta R_2^2]+k_{12}(\Delta R_1)(\Delta R_2)+k_\alpha(\Delta\alpha)^2. \quad (1)$$

The last term, of course, becomes zero for the two stretching vibrations. Using the frequencies ν_1(O−X−O) and ν_3(O−X−O) of Table II, the calculated force constants are as listed in Table III.

Thus, the X−O force constant appears to decrease in the order U>Np>Pu>Am, even though the X−O distance becomes smaller in the same order. Treating U, Np, Pu, and Am as similar type atoms, Badger's rule, relating force constant and bond distance, predicts

TABLE II. Vibrational frequencies of sodium acetate and the sodium acetate complexes of U(VI), Np(VI), Pu(VI), and Am(VI).

	Type of vibration	$NaAc^a$ cm^{-1}	$NaUO_2(Ac)_3$ cm^{-1}	$NaNpO_2(Ac)_3$ cm^{-1}	$NaPuO_2(Ac)_3$ cm^{-1}	$NaAmO_2(Ac)_3$ cm^{-1}
ν_1	C−H stretching	2933	2933	2935	2927	···
ν_2	CH_3 deformation	1425	1413	1410	1415	···
ν_3	C−O stretching	1408	1472	1472	1470	1467
ν_4	C−C stretching	924	948	948	948	948
ν_5	CO_2 deformation	645	678	677	677	675
ν_6	torsion about C−C bond	···	···	···	···	···
ν_7	C−H stretching	2999	2978	2980	2980	···
ν_8	C−O stretching	1578	1537	1536	1540	1541
ν_9	CH_2 deformation	1440	(1450?)	···	···	···
ν_{10}	CH_3 rocking	1012	1004	1004	1004	
ν_{11}	CO_2 rocking	465	···	···	···	···
ν_{12}	C−H stretching	2999	2978	2980	2980	···
ν_{13}	CH_3 deformation	1488	(1480?)	···	···	···
ν_{14}	CH_3 rocking	1045	1055	1054	1054	1052
ν_{15}	CO_2 rocking	615	612	610	609	···
ν_1	(O−X−O)	···	856[b]	844[b]	818[b]	749[b]
ν_3	(O−X−O)	···	931	934	930	914
$\nu_1+\nu_3$	(XO_2 group)	···	1781[b]	1770[b]	1739[b]	···

[a] The acetate frequency assignments are those of Jones and McLaren.[4]
[b] These absorption bands were observed only on very thick samples and are not shown in Fig. I.

that the X−O distance increases regularly in the series U−Np−Pu−Am, in direct contradiction with the x-ray diffraction results. Apparently Badger's rule is good for estimating approximate bond distances, but not good for determining small differences in bond distances where the bonded pair is not the same.

The explanation is probably that the bond distance becomes smaller because of increased nuclear charge and the resulting contraction of the electron shells, but the bond also becomes weaker because of interaction with the extra valence shell electrons.

Clark and Webb[5] have shown that the expression

$$k_e R_e^6 n = k_{qr}, \quad (2)$$

[5] C. H. D. Clark and K. R. Webb, Trans. Faraday Soc. **37**, 293 (1941).

TABLE III. Force constants for X−O bonds in $NaXO_2(Ac)_3$.

X	k_{X-O}	k_{12}
U	0.715×10^6 dynes/cm	-0.030×10^6 dynes/cm
Np	0.698	−0.054
Pu	0.675	−0.089
Am	0.612	−0.166

fits diatomic molecules quite well. k_e=force constant, R_e=equilibrium bond distance, n=number of electrons in the valence shell (10 for CO), and k_{qr}=a constant for a given type of bond. The (n) in this formula represents interaction of the electrons in the valence shell with the bond. An expression of this type would explain the behavior of the complexes, $NaXO_2(Ac)_3$. That is, (n) includes the extra electrons (presumably $5f$) in the valence shell and thus increases in the order $n_U<n_{Np}<n_{Pu}<n_{Am}$. Therefore, k_{X-O} and R_{X-O} can both decrease with k_{qr} remaining constant.

From the infrared studies of aqueous uranyl and transuranyl ions, Jones and Penneman[1] concluded that the X−O force constants decreased in the order $k_{Np-O}>k_{U-O}>k_{Pu-O}>k_{Am-O}$. These force constants were very approximate, as only the asymmetric stretching frequency was used in their calculation, so the interaction terms had to be neglected. In this work on the solid sodium acetate complexes, the symmetric stretching frequencies were also observed and, thus, one interaction constant was included in the potential function (see Eq. 1). This valence bond interaction appears to increase considerably in going from U−Np−Pu−Am (see k_{12} in Table III). When the results of Jones and Penneman[1] are corrected with these interaction constants, in aqueous perchloric acid solution of XO_2^{++} [as in solid $NaXO_2(Ac)_3$] the force constants decrease in the order $k_{U-O}>k_{Np-O}>k_{Pu-O}>k_{Am-O}$. Because the force constants change in a similar manner in the series (both in aqueous solution and in the solid state), it appears that the bond distances decrease in the same order as the force constants ($R_{U-O}>R_{Np-O}>R_{Pu-O}>R_{Am-O}$) as long as the series of ions are in similar surroundings (whether in solution or the solid state).

ACKNOWLEDGMENTS

The author is indebted to Dr. F. H. Ellinger of this laboratory for determination of the cell constants of the complexes $NaXO_2(Ac)_3$ and the temperature coefficient of linear expansion for $NaUO_2(Ac)_3$. He also wishes to thank Mr. Dale Armstrong of this laboratory for preparation of the figure. The purified plutonium was furnished by Mr. Joseph Leary of this laboratory.

Activation Cross Sections of Y^{90} and Pr^{142}†

R. R. SMITH AND S. D. REEDER
Atomic Energy Division, Phillips Petroleum Company, Idaho Falls, Idaho

(Received January 25, 1955)

The irradiation of Y^{89} and Pr^{141} under a sufficiently high thermal neutron flux produces small amounts of Y^{91} and Pr^{143} by secondary neutron capture. A measurement of the second-order activities, although completely unobservable at the end of the irradiation, may be made after the shorter lived first-order activities have disappeared. From relative measurements of the first- and second-order activities induced in Y^{89} and Pr^{141} values for the activation cross sections of Y^{90} and Pr^{142} have been established. For Pr^{142} a value of $\sigma_{act} = 18 \pm 3$ barns was found; for Y^{90} a value of 6.5 barns was established as an effective upper limit.

INTRODUCTION

THE theory and the difficulties associated with second-order neutron cross-section measurements have been treated in detail by Katcoff and by Yaffe *et al.*[2] In brief the method outlined and used by these investigators is based on the quantitative radiometric determination of the $A+2$, $Z+1$ activity formed as the result of second-order neutron capture in a known amount of material irradiated under a calibrated neutron flux. A factor of prime importance in measurements of this nature is the neutron flux since the production rate of second-order species is proportional to its square. In spite of the limited neutron fluxes available to earlier investigators several cross-section measurements based on the successive capture principle have been reported.[2–5] With the higher neutron fluxes currently available the relative production of second-order species is increased to the extent that in many instances second-order activities may be observed directly. Outstanding examples of the latter are given by Au and Ta where the $A+1$ cross sections are unusually large.[6,7] Under more usual circumstances where the $A+1$ cross sections are not large (i.e., 5 to 50 barns), a direct observation of the $A+2$ activity may still be possible if the neutron flux is sufficiently high and if the first-order activity decays with the shorter half-life.

The measurements reported here are those of the activation cross sections of Y^{90} and Pr^{142}, both of which result from a single neutron capture in the naturally occurring monoisotopes, Y^{89} and Pr^{141}. In each case the first-order species decay with the shorter half-lives and measurements of the second-order activities may be made after the first-order activities have disappeared. An additional feature making these isotopes adaptable for investigation in this manner is the relative simplicity of the decay schemes for the various nuclear species involved. In each case the first- and second-order species are pure or almost completely pure beta emitters and complications from gamma emission do not arise.

EXPERIMENTAL

Ten microgram portions of spectrographically pure Y_2O_3 and Pr_6O_{11}[8] sealed in separate quartz ampules were subjected to a total nvt of 3.2×10^{20} neutrons/cm^2 in a high flux facility of the Materials Testing Reactor. Following the irradiation the samples were dissolved in concentrated nitric acid, converted to the chlorides by treatment with hydrochloric acid, and were eluted from a Dowex-50 ($12X$) resin column with $0.24M$ citric acid maintained at 87°C with a boiling trichloroethylene refluxing system. Individual drops were collected on platinum plates at the rate of one drop per two minutes and were flamed free of citric acid to produce essentially weightless samples for counting. The plates containing the drops from the centers of the elution peaks were counted with an end-window, flow-type, proportional counter over a period of three months under geometry conditions ranging from five percent at the start of the counting to thirty percent after the bulk of the $A+1$ activity had disappeared. By using drops from the centers of the elution peaks, activities producible by (n,p) reactions and by (n,γ) reactions (on impurities) were effectively eliminated.

The resulting decay curves for yttrium and praseodymium are given in Figs. 1 and 2. Coincidence loss corrections amounting to 0.4% per 10^5 c/min have been applied to the data shown. Corrections for beta absorption in the rubber hydrochloride window (0.5 mg/cm^2) and in the air path separating the sample and the window have been estimated from aluminum absorption curve measurements and have been applied directly to the activity ratios. Back scattering corrections have not been applied since the back scattering from platinum has been shown to be approximately constant over the range of beta energies involved in the measure-

† Work carried out at the Materials Testing Reactor, Idaho Falls, Idaho, under contract with the U. S. Atomic Energy Commission.

[1] S. Katcoff, Paper No. 220, *Radiochemical Studies: The Fission Products* (McGraw-Hill Book Company, Inc., New York, 1951), p. 1391, National Nuclear Energy Series, Plutonium Project Record, Vol. 9, Div. IV.

[2] Yaffe, Sargent, Kirsch, Standil, and Grunlund, Phys. Rev. **76**, 617 (1949).

[3] N. Sugarman and A. Turkevich, reference 1, Paper No. 221.

[4] S. Katcoff, reference 1, Papers 222, 223, and 224.

[5] S. Katcoff, Phys. Rev. **87**, 886 (1952).

[6] R. D. Hill and J. W. Michelich, Phys. Rev. **79**, 275 (1950).

[7] DuMond, Hoyt, Marmier, and Murray, Phys. Rev. **92**, 202 (1953).

[8] Samples purchased from Jarrell-Ash Company, Newtonville, Massachusetts.

ments.[9] From Figs. 1 and 2 it may be seen that the gross decay curves are resolvable into pure components corresponding to the $A+1$ and $A+2$ activities. Extrapolation of the separated components back to zero time results in activity ratios (after correcting for absorption effects) of 1.94×10^4 and 6.14×10^3 for yttrium and praseodymium, respectively.

RESULTS

Regarding flux destruction of all nuclear species as negligible the ratio of the $A+1$ and $A+2$ activities after an irradiation of time t may be shown to be

$$R_0=\frac{A_1}{A_2}=\frac{\lambda_1(\lambda_1-\lambda_2)(1-e^{-\lambda_1 t})}{(nv)_{th}\sigma_1[\lambda_1(1-e^{-\lambda_2 t})-\lambda_2(1-e^{-\lambda_1 t})]}, \quad (1)$$

where $(nv)_{th}$ is the thermal neutron flux, i.e., the number of thermal neutrons/cm²sec, and the subscripts 0, 1, and 2 refer to the original monoisotope and the first- and second-order species, respectively. The effect of a routine reactor shutdown on the final $A+2$ activity was considered by subdividing the irradiation into the following segments: $t_1=9.83\times10^5$ seconds, the irradiation period prior to shutdown; $t_2=2.41\times10^5$ seconds, the shutdown period; and $t_3=1.45\times10^6$ seconds, the irradiation period following the shutdown. The total $A+2$ activity was regarded as arising from three independent sources: that generated during t_1 and remaining at the end of t_3, that generated during t_3 from the $A+1$ isotope remaining at the end of t_2, and that generated from the original monoisotope during t_3. The effect of the shutdown on the $A+1/A+2$ activity ratio given in Eq. (1) is easily considered by a simple but lengthy modification of the denominator. Corrections for the effect of the reactor shutdown on the final $A+1$ activities were unnecessary since in each case the saturation activities were closely approached.

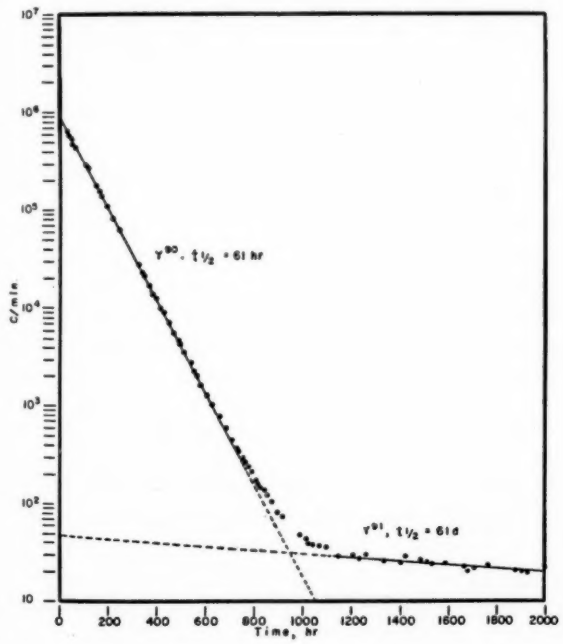

FIG. 1. Gross decay curve for pile-irradiated yttrium, corrected for background effects and showing the separated $A+1$ and $A+2$ activities.

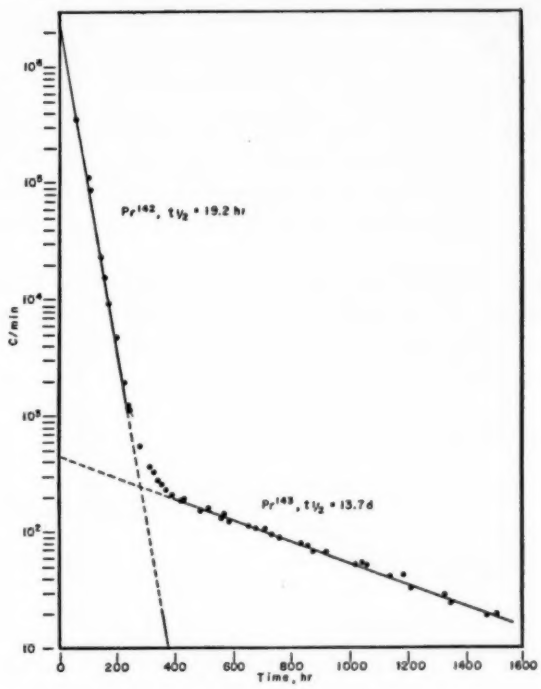

FIG. 2. Gross decay curve for pile-irradiated praseodymium, corrected for background effects and showing the separated $A+1$ and $A+2$ activities.

The thermal neutron flux was measured as 1.29×10^{14} neutrons/cm²sec with a cobalt wire monitor placed in the rabbit assembly with the samples. The specific activity of the monitor was determined with a high pressure ionization chamber calibrated against a National Bureau of Standards sample of Co^{60}. Conversion of the cobalt specific activity to thermal neutron flux involved the use of the following constants: $\sigma_{th}(Co)=34.0$ barns, and $T_{\frac{1}{2}}(Co^{60})=5.30$ years. Corrections for self-protection and for resonance neutron activation of cobalt have been applied to the thermal flux value given above.

The half-life of Y^{90} was taken to be 61 hours[10] although a recent value reported by Chetham-Strode and Kinderman[11] suggests that some uncertainty may be associated with the earlier value. The values used for the half-lives of Y^{91}, Pr^{142}, and Pr^{143} were 61 days,[12] 19.2 hours,[10] and 13.7 days,[13] respectively.

[9] B. P. Burtt, Nucleonics **5**, No. 2, 28 (1949).

[10] W. Bothe, Z. Naturforsch, **1**, 179 (1946).

[11] A. Chetham-Strode, Jr., and E. M. Kinderman, Phys. Rev. **93**, 1029 (1954).

[12] L. M. Langer and H. C. Price, Jr., Phys. Rev. **76**, 641 (1949).

[13] Feldman, Lidofsky, Macklin, and Wu, Phys. Rev. **76**, 1888 (1949).

Substitution of the experimental value of 6.14×10^3 found for the $A+1/A+2$ activity ratio of praseodymium into Eq. (1) (after a correction for the effects of reactor shutdown) results in a value of 18 ± 3 barns for the activation cross section of Pr^{142}. The precision limits take into consideration uncertainties inherent in the values used for decay constants, neutron flux, and the graphical determination of the $A+1/A+2$ activity ratio.

The situation for yttrium is complicated by the existence of two isomeric states of the $A+2$ nucleus. There is nothing in the experimental data that will permit a direct evaluation of the cross section for the formation of either state. However, by assuming a negligible cross section for the formation of one state an upper limit may be assigned to the cross section for the formation of the other isomer. Treating the data in this manner an upper limit of 6.5 barns was determined for the formation of each isomer of Y^{91}.

Appreciation is expressed to Mr. N. P. Alley and to Mr. R. H. Lewis for their assistance in these measurements.

THE JOURNAL OF CHEMICAL PHYSICS VOLUME 23, NUMBER 11 NOVEMBER, 1955

Gas Adsorption on Heterogeneous Surfaces

LOREN G. HEPLER
Cobb Chemical Laboratory, University of Virginia, Charlottesville, Virginia
(Received January 26, 1955)

The mathematical treatment of the adsorption of gas on nonuniform surfaces has been investigated with respect to the proper limits for the integration of the isotherm equation. The physical significance of these limits is discussed. Equations that relate the distribution of energy sites over the surface and the heat of adsorption are derived.

We begin by considering the treatment of noncooperative adsorption of gas on a heterogeneous surface after the manner of Halsey and Taylor.[1] For sites of a particular value of the heat of adsorption, ϵ, the coverage is given by the Langmuir equation. The total coverage is given by (1) where N_ϵ is a function which represents the distribution of adsorption energies for the surface sites.

$$\theta=\int\frac{N_\epsilon d\epsilon}{1+(a/p)e^{-\epsilon/kT}}. \tag{1}$$

We are especially concerned with the case where $N_\epsilon=c\exp(-\epsilon/\epsilon_m)$. The problem of deciding upon the best limits for the integration of the isotherm equation in this case is not an obviously simple one. Halsey and Taylor[1] and Halsey[2] have integrated from $-\infty$ to $+\infty$, for which limits the integration is not difficult. The use of this lower limit has been criticized by Hill[3] and others on the basis that this interval of integration improperly includes a range of repulsive energy sites.

The uncertainty about the proper lower limit for the integration can be resolved by determining whether the integral from $-\infty$ to 0 contributes appreciably to the total integral from $-\infty$ to $+\infty$. Neither the integral from $-\infty$ to 0 nor from 0 to $+\infty$ can be obtained in closed form.

Because we are interested in determining whether the integral from $-\infty$ to 0 is small in comparison to the integral from $-\infty$ to $+\infty$, the following procedure is adopted. It is seen that

$$c\int_{-\infty}^{0}\frac{e^{-\epsilon/\epsilon_m}d\epsilon}{1+(a/p)e^{-\epsilon/kT}}<c\int_{-\infty}^{0}\frac{e^{-\epsilon/\epsilon_m}d\epsilon}{(a/p)e^{-\epsilon/kT}}, \tag{2}$$

and that the right-hand expression in (2) can be integrated to give $-(cpkt\epsilon_m/a)/(kT-\epsilon_m)$. This last expression will be regarded as a correction to be applied to the integral of (1) from $-\infty$ to $+\infty$.

Equation (1) is integrated from $-\infty$ to $+\infty$ to obtain an uncorrected expression for the adsorption isotherm.[2] The correction term (it is seen from (2) that the term we have used is larger than the true correction term) is applied to the expression so obtained to give the corrected isotherm Eq. (3)

$$\theta=c\epsilon_m(p/a)^{RT/\epsilon_m}+(cpRT\epsilon_m/a)(RT-\epsilon_m). \tag{3}$$

The isotherms of Frankenburg[4] for hydrogen on tungsten have been used to evaluate c, a, and ϵ_m. The correction term in every case is less than 6% of the total and for all except the high pressure end of the high temperature isotherms is less than 1% of the total. The data of Homfray (taken from Brunauer[5]) for carbon monoxide on charcoal have been used in a

[1] G. Halsey and H. S. Taylor, J. Chem. Phys. **15**, 624 (1947).
[2] G. D. Halsey, *Advances in Catalysis* (Academic Press, Inc., New York, 1952), Vol. IV.
[3] T. L. Hill, J. Chem. Phys. **17**, 762 (1949).
[4] W. G. Frankenburg, J. Am. Chem. Soc. **66**, 1827 (1944).
[5] S. Brunauer, *The Adsorption of Gases and Vapors* (Princeton University Press, Princeton, New Jersey, 1945).

similar fashion to evaluate the correction term, which in this case is always less than 1% of the total.

The form of the correction term should be considered qualitatively in relation to the physical assumption involved in employing $-\infty$ as the lower limit of integration. The essential feature of any argument used to justify the use of this lower limit must be that it is permissible, if mathematically desirable, to integrate over a group of unattractive sites because these sites contribute almost nothing to the total amount of gas adsorbed. The fact that the integral from $-\infty$ to 0 turns out to be very small bears out the validity of this argument. We also see that the magnitude of the correction term increases with increasing pressure as should be expected.

The author is grateful to the referee who has pointed out that Danon and Zamith[6] have also recently investigated this problem. They actually carried out the integration of (1) from 0 to $+\infty$ for p/a and kT/ϵ_m less than unity. The resulting series expression was shown to reduce to the Freundlich isotherm expression of Halsey and Taylor for small values of the pressure.

It is apparent from (1) that there must be a complex relationship between the distribution function and the heat of adsorption. The usual practice has been to consider only the relation between the isotherm and the heat of adsorption. This has been done by solving the isotherm equation for p, differentiating with respect to T, and then using the Clausius-Clapeyron equation for the computation of the isosteric heat of adsorption. Even though this procedure is a valid one, it is nevertheless desirable to derive the direct relationship between the distribution function and the heat of adsorption.

The Clausius-Clapeyron equation for the calculation of the isosteric heat of adsorption is written

$$q_{st}=(RT^2/p)(\partial p/\partial T)_\theta. \tag{4}$$

The total differential of θ (a function of p and T) is

$$d\theta=(\partial\theta/\partial T)_p dT+(\partial\theta/\partial p)_T dp, \tag{5}$$

and at constant θ we obtain $(\partial p/\partial T)_\theta$ as desired.

$$(\partial p/\partial T)_\theta=-(\partial\theta/\partial T)_p/(\partial\theta/\partial p)_T. \tag{6}$$

We find $(\partial\theta/\partial T)_p$ and $(\partial\theta/\partial p)_T$ by performing the indicated differentiations on the expression for θ (1). In order to do this simply, N_ϵ and a are considered to be independent of pressure and temperature. The expressions so obtained are combined with (4) and (6) to give the relationship between q_{st} and N_ϵ (7).

$$q_{st}=\int\frac{\epsilon e^{-\epsilon/kT}N_\epsilon d\epsilon}{[1+(a/p)e^{-\epsilon/kT}]^2}\Big/\int\frac{e^{-\epsilon/kT}N_\epsilon d\epsilon}{[1+(a/p)e^{-\epsilon/kT}]^2}. \tag{7}$$

In order to obtain an expression for the isosteric heat of adsorption as a function of the pressure and temperature it is necessary to integrate (7). The required integrations with finite limits are easily carried out for the case where N_ϵ is a constant. The resulting complicated expression for q_{st} has one advantage over the almost equally complicated equations of Halsey and Taylor.[1] Because of the complexity of the isotherm equation, they found it expedient to make limiting high and low pressure approximations for use with the Clausius-Clapeyron equation. The one equation that is derived in the fashion outlined above has the advantage of being valid, for this particular case, for both high and low pressures as well as intermediate pressures.

It is seen from (1) that the total or integral heat of adsorption can be expressed as in (8). It is also possible to derive an equation

$$Q=\int\frac{\epsilon N_\epsilon d\epsilon}{1+(a/p)e^{-\epsilon/kT}}, \tag{8}$$

relating the differential isothermal heat of adsorption, q_T, and the distribution function. We express the physical meaning of a differential isothermal heat of adsorption with the aid of (1) and (8) and write the following expression for q_T:

$$q_T=(\partial Q/\partial p)_T dp/(\partial\theta/\partial p)_T dp. \tag{9}$$

We have already found $(\partial\theta/\partial p)_T$ and can obtain $(\partial Q/\partial p)_T$ by differentiating (8) with respect to p. This procedure yields an expression for q_T that is identical to the expression derived for q_{st} (7). Hence we write that $q_T=q_{st}$. This is as it should be.

In view of recent papers by Kington and Aston[7] and Hill[8] and others in which the differences between various kinds of differential heats of adsorption are discussed, an explanation about the stated equality of q_{st} and q_T is in order. The apparent disagreement with the conclusions of other authors is due to the fact that our q_T represents a different differential isothermal heat of adsorption than does Hill's q_{th}. Hill has considered the thermodynamics of a complete process taking place in a certain type of isothermal adsorption calorimeter. This process includes a compression of the gas in the calorimeter as well as the actual adsorption. It can be seen from Kington and Aston's Eqs. (1) and (26) that the differential isothermal *calorimetric* heat of adsorption and the isosteric heat of adsorption differ by only the heat of this compression process. Hence we see that the statement that $q_{st}=q_T$ (remembering that q_T does not include any heat of compression) is not in disagreement with the results of Kington and Aston and Hill.

ACKNOWLEDGMENTS

The author is grateful to Dr. Botts of this University and to Dr. Hugus of the University of Minnesota for their helpful discussions.

[6] J. Danon and A. Zamith, J. chim. phys. **51**, 260 (1954).

[7] G. L. Kington and J. G. Aston, J. Am. Chem. Soc. **73**, 1929 (1951).

[8] T. L. Hill, J. Chem. Phys. **17**, 520 (1949).

Resolution of $\nu_{11}(E)$ of Allene at 28μ

K. NARAHARI RAO* AND E. D. PALIK†
Department of Physics, The Ohio State University, Columbus, Ohio
(Received February 25, 1955)

The perpendicular band of allene at 28μ(ν_{11}) has been resolved for the first time. The average separation between successive Q branches, which represents essentially $2[A_v'(1-\zeta_v)-B_v']_{v=11}$ is found to be 1.2±0.2 cm^{-1}.

SPECTROSCOPISTS have for some time evinced considerable interest in the study of the rotation-vibration bands of allene (C_3H_4). Allene belongs to the point group V_d. A molecule of this symmetry type has four type E fundamental vibrations, recognized by the perpendicular bands. Three of these doubly degenerate vibrations have been well resolved by Miller and Thompson[1] with a grating spectrometer, and later reinvestigated by Lord and Venkateswarlu[2] in their survey of the entire infrared spectrum of allene between 2 and 35μ with a prism spectrometer. The low-frequency band at 28μ has, however, not been resolved until now. A knowledge of the separations of Q branches in this perpendicular band is necessary for the evaluation of the ζ factors of allene. Lord and Venkateswarlu had to base their conclusions only upon an estimated value for spacings between these Q branches. Using the far infrared spectrograph in this laboratory described by Oetjen *et al.*[3], it has been possible to resolve this low-frequency rotation-vibration band of allene. An echelette grating with 553 lines/inch ruled at the University of Michigan and a Golay detector equipped with a diamond window‡ have been used in this study.

Figure 1 is a reproduction of the band. The expected alternation of intensity in the Q branches is clearly seen. The statistical weights and relative intensities of lines have been considered by de Heer[4] who showed that lines with even K values[5] should be the stronger components. The band center is located at 351.3 cm^{-1}. This choice is made in order to maintain a symmetric distribution of lines on either side of the center. The assignments to the Q branches are given only near the center of the band, as the structure, especially on the low-frequency end of the band, seems to be complicated by factors not readily understood at the present time. Also, by making a record in a region of the spectrum free from allene bands it was noticed that a few of the strong pure rotation water lines appear weakly due to insufficient drying of the allene with P_2O_5. A separate background run was made in the region of the allene band, after introducing into the absorption cell enough water vapor to give rise to the water lines of the same intensity as those observed in the allene sample but in a region where allene did not absorb. It was noticed in the background run that three weak water lines occur at 349.8, 352.0, and 354.4 cm^{-1}. Measurements of the areas under these water lines indicate that, compared to the allene lines, the impurity lines are much weaker and do not affect the general conclusions reached in this note. The records have been obtained using slits having effective spectral widths of about 0.45 cm^{-1}. The positions of the lines are average values of the measurements taken on five traces of the band

TABLE I. Wave numbers of lines in ν_{11} (E) of allene at 28μ.

Serial number as in Fig. 1	ν_{vac} in cm^{-1}	Assignment	$\Delta\nu$
1	358.5		
2	357.3		
3	356.5	RQ_4	
			1.2
4	355.3	RQ_3	
			1.0
5	354.3	RQ_2	
			1.2
6	353.1	RQ_1	
			1.1
7	352.0	RQ_0	
			1.2
8	350.8	PQ_1	
			1.0
9	349.8	PQ_2	
			1.4
10	348.4	PQ_3	
			1.1
11	347.3	PQ_4	
			1.2
12	346.1	PQ_5	
13	345.2		
14	344.7		
15	344.0		
16	343.5		
17	342.3		

* Support received from Office of Ordnance Research through a contract with The Ohio State University Research Foundation.
† DuPont Fellow.
[1] C. H. Miller and H. W. Thompson, Proc. Roy. Soc. (London) **A200**, 1 (1949).
[2] R. C. Lord and Putcha Venkateswarlu, J. Chem. Phys. **20**, 1237 (1952).
[3] Oetjen, Haynie, Ward, Hansler, Schauwecker, and Bell, J. Opt. Soc. Am. **42**, 559 (1952).
‡ We wish to express our thanks to Elias Burstein of the Naval Research Laboratory, Washington, D. C., for making the detector available to us.
[4] J. de Heer, J. Chem. Phys. **20**, 637 (1952).
[5] For the notation used here, see, for example, G. Herzberg, *Infrared and Raman Spectra of Polyatomic Molecules* (D. Van Nostrand Company, Inc., New York, 1945).

obtained at different pressures ranging from 20 to 70 mm of Hg.

Table I summarizes the results. As can be seen, the average separations of the successive Q branches which represents essentially $2[A_v'(1-\zeta_v)-B']_{v=11}$, is 1.2 ± 0.2 cm^{-1}, compared to the estimate of 3.0 ± 0.6 cm^{-1} of Lord and Venkateswarlu. In view of this result, a re-evaluation of all the ζ factors of allene seems desirable.

A reinvestigation of the entire infrared spectrum of allene has been undertaken by one of us (KNR) at the University of Tennessee, Knoxville, Tennessee, under the partial sponsorship of the Office of Ordnance Research. The sample of allene used in the present work has come from that source. Our thanks are due to Professor Alvin H. Nielsen and Professor W. M. Fletcher in this connection. A discussion of the results obtained at the University of Tennessee and the work continued at this institution will be incorporated in a separate publication. The spectrograph was available for the present investigation through the courtesy of the Wright Air Development Center, who through a contract with the Ohio State University Research Foundation provide partial support for its construction and maintenance. Our thanks are also due to Professors Harald H. Nielsen and Alvin H. Nielsen for their interest in this problem and valuable discussions.

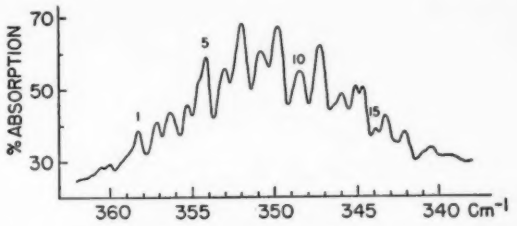

FIG. 1. ν_{11} of allene. Absorption path 20 cm. Pressure 25 mm Hg.

Note added in proof.—By cooling the absorbing gas to about $-80°C$ no change was noticed in the relative intensities of the Q branches, and so it is considered that any "hot" bands of allene occurring in the same spectral region as ν_{11} do not influence the main results of the above paper.

THE JOURNAL OF CHEMICAL PHYSICS VOLUME 23, NUMBER 11 NOVEMBER, 1955

Configuration of Polymer Molecules with Excluded Volume*

W. R. KRIGBAUM
Department of Chemistry, Duke University, Durham, North Carolina

(Received February 1, 1955)

The displacement distribution for a polymer molecule with excluded volume is derived by rejecting the unacceptable configurations available to random-flight chains. The fraction of those configurations corresponding to a displacement length L which are acceptable is calculated through use of a model which considers the chain to be composed of a sequence of identical subchains. Interactions between the elements of a given subchain, and between these and elements of the various possible clusters of adjacent subchains, are summed to obtain the total interference for all elements of the chain. The average interference encountered by the elements of one subchain is calculated therefrom. The resulting displacement distribution is considerably sharper than the corresponding Gaussian distribution for positive values of the excluded volume, but somewhat more extended than the corresponding Gaussian for negative excluded volumes. When the present treatment is compared with that of Flory, the former predicts smaller values for the mean-square displacement length, $\langle L^2\rangle$, at both the low and the high ends of the molecular weight scale, and a more marked dependence of $\langle L^2\rangle$ upon the thermodynamic interactions as embodied in the factor $(\frac{1}{2}-\chi_{12})$. Comparison with experiment confirms these predictions, and indicates the present treatment to be a significant improvement over that proposed earlier by Flory.

I. INTRODUCTION

THE theoretical description of any property of dilute polymer solutions ultimately requires a knowledge of the average configuration of the polymer molecules. The average configuration is characterized by a value for the mean-square distance $\langle L^2\rangle$ between the ends of the chain, or of the mean-square radius R^2, given for a chain of N elements by:

$$R^2=(1/N)\sum_{i=1}^{N}\langle r_i^2\rangle$$

where $\langle r_i^2\rangle$ is the mean-square distance from element i to the center of gravity of the molecule. However, the more complete information embodied in the respective distribution functions $W(L)$ or $W(R)$ is of interest in many applications.

At first sight, the configurational problem posed by a chain of N flexibly linked elements of length a would appear to be analogous to that of characterizing the three-dimensional path of a diffusing particle which makes N random jumps of length a. The theory of random flights yields a solution to this problem in the form of the radial distribution function for the displace-

* Presented at the 127th National Meeting of the American Chemical Society, Cincinnati, Ohio, April 4, 1955.

ment length L:

$$W_0(u)du=(4/\pi^{\frac{1}{2}})e^{-u^2}u^2du, \quad (1)$$

where

$$u^2=3L^2/(2Na^2). \quad (2)$$

From this distribution function one finds $\langle L_0^2\rangle=Na^2$.

Although the radial displacement distribution for a random flight chain can be expressed in closed form, this is not true for the distribution of elements about the center of gravity. Isihara[1] and Debye and Bueche[2] have obtained the probability $P_0(r_i)$ that element i will be found at a vector distance r_i from the center of gravity:

$$P_0(r_i)=\{(2/9)\pi Na^2[y^3+(1-y)^3]\}^{-\frac{3}{2}} \times\exp\{-9r_i^2/2Na^2[y^3+(1-y)^3]\},$$

where $y=i/N$. The expression for the radial distribution function for all elements therefore becomes:

$$W_0(v)dv=(4/\pi^{\frac{1}{2}})\left\{\int_{y=0}^{1}\exp[-(\rho v)^2](\rho v)^2\rho dy\right\}dv, \quad (3)$$

where $v=(2R^2/9Na^2)$ and $\rho=[y^3+(1-y)^3]^{-1}$. The integral appearing in square brackets in Eq. (3) could not be evaulated in closed form; however, Debye and Bueche[2] give the first terms in the power series expansions valid for v large or small.

Closer examination of the polymer configuration problem has revealed[3] that whereas a diffusing particle is permitted to cross its path numerous times, a configuration of the polymer molecule which involves one or more crossovers is forbidden because each element of the chain excludes a volume to all other elements. The problem posed by this excluded volume or long-range interference effect is one which has recently received considerable attention. Current treatments lead to two divergent conclusions, namely: (1) The result is the same as that introduced by "short-range" interactions, such as restricted rotation about the chain bonds and the requirement of fixed valence angles, so that $\langle L^2\rangle=ANa^2$. (2) When long-range interference is taken into account, $\langle L^2\rangle$ increases more rapidly than N, hence the ratio $\langle L^2\rangle/N$ increases with increasing N. For details of these treatments the reader is referred to several papers[4–6] in which excellent reviews are presented. The earlier statistical treatments leading to the third possible conclusion—that the long-range interference effects can be ignored so that $\langle L^2\rangle=Na^2$—have been adequately criticized elsewhere.[5]

[1] A. Isihara, J. Phys. Soc. Japan **5**, 201 (1950).
[2] P. Debye and F. Bueche, J. Chem. Phys. **20**, 1337 (1952).
[3] P. J. Flory, J. Chem. Phys. **17**, 303 (1949).
[4] Hermans, Klamkin, and Ullman, J. Chem. Phys. **20**, 1360 (1952).
[5] Zimm, Stockmayer, and Fixman, J. Chem. Phys. **21**, 1716 (1953).
[6] F. T. Wall, "Properties of Macromolecules in Solution," a chapter in *Annual Review of Physical Chemistry*, **5**, 267 (1954), published by Annual Reviews, Inc., Stanford, California.

The theoretical treatments have sometimes been classified on the basis of the predicted behavior of the ratio $\langle L^2\rangle/N$ in the limit as $N\to\infty$. It appears to the writer that this choice is unfortunate, since it does not permit the verification of either of the alternatives by direct experimental test. Once the behavior of $\langle L^2\rangle/N$ has been established for the range of N values amenable to experiment, some inferences may then be forthcoming concerning the more academic problem of the asymptotic behavior of this function.

Since excluded volume depends upon the thermodynamic interactions, the predicted dependence of $\langle L^2\rangle$ upon the thermodynamic variables offers a second test of theory. Zimm, Stockmayer, and Fixman[5] have clearly shown the intimate connection between the magnitude of $\langle L^2\rangle$, the excluded volume, and the thermodynamic parameters. They expose the artificiality of attempts to compare predicted values for $\langle L^2\rangle$ with "observed" values arbitrarily corrected to a constant value of the second virial coefficient. Thus, a satisfactory treatment should give an adequate account of the observed dependence of $\langle L^2\rangle/N$ upon the variables N, temperature, and the interaction parameters.

II. THEORETICAL

Equation (1) representing the displacement distribution for the unperturbed random flight chain will serve as a point of departure for the present treatment. If we consider a chain of N elements, then only a fraction $f_N(L)$ of the random flight configurations which correspond to a displacement length L will be allowed when the excluded volume is other than zero. Thus, the displacement distribution $W(L)$ for a chain with excluded volume can be constructed by rejecting the unacceptable configurations in $W_0(L)$; i.e.,

$$W(L)=\frac{f_N(L)W_0(L)}{\int_{L=0}^{\infty}f_N(L)W_0(L)dL}. \quad (4)$$

The success of such an approach depends entirely upon obtaining the correct form for $f_N(L)$. The calculation of $f_N(L)$ to be presented below follows that of Flory[3] in defining the radial distribution of elements or its equivalent at the outset; however, it differs from Flory's treatment in several important respects: (a) the simple Gaussian radial element distribution used by Flory will be replaced by a more realistic model, (b) $f_N(L)$ will not be replaced by an average value, and (c) it will not be assumed at the outset that $W(L)$ is related to $W_0(L)$ by a scale factor.

A. Calculation of $f_N(L)$

We wish to calculate the probability $f_N(L)$ that N elements will encounter no interference when placed in contiguous positions to form a random flight chain

having ends separated by a distance L. Flory[3] noted that his calculation of f evidently did not take all interferences into account, since it indicated $f_{2N}>f_N^2$, i.e., fewer interferences for a single chain of $2N$ elements than for two separate chains of N elements. He suggested that this was due to his neglect of "short-range" interactions, a point which we shall return to later. One can give a simple proof that on the basis of total interference $f_{2N}<f_N^2$; furthermore, this demonstration will suggest a model to be used for counting interferences.

If one imagines the chain of $2N$ elements to be subdivided into two subchains of N elements, then the total interference for the chain will be given by the sum of the interferences encountered by elements of the two separated subchains *plus* the additional interferences arising when these two subchains are joined and overlap. Hence $f_{2N}<f_N^2$. The foregoing suggests that for the purpose of counting interferences one may consider a chain of N elements to be composed of ω subchains, each consisting of ν elements, with the obvious restriction that ν be large enough so that statistical considerations apply within a subchain. Let us examine the interactions which arise during the formation of subchain i. We designate by f_1 the factor arising from interferences between the elements of any given subchain. There will be a certain density of segments belonging to subchain $(i-1)$ within the region to be occupied by subchain i. This adjacent subchain density is assumed to be independent of the length of the remaining chain, and gives rise to a factor f_2. Likewise, each more remote subchain contributes a characteristic density within the region to be occupied by subchain i, the contribution from subchain 1 at the other end of the chain giving rise to a factor f_i. The total contribution to the partition function for the molecule arising from the addition of subchain i is therefore $\prod_{\kappa=1}^{i} f_\kappa$, hence:

$$f_N=\prod_{i=1}^{\omega}\prod_{\kappa=1}^{i} f_\kappa=f_1^{\omega}f_2^{\omega-1}\cdots f_\omega. \tag{5}$$

Before proceeding with the calculation of the factors f, we recognize that if a lattice model is to be used in this calculation a relationship must be established between the respective sizes of the solvent molecule, the configurational element, and the lattice site.[7] The simplest model allows one solvent molecule to occupy a site; hence, each configurational element will in general be composed of p segments, each of which occupies a single site. A chain of N elements will thus consist of $x=pN$ segments, and its molecular volume will be pNV_1, where V_1 is the molecular volume of the solvent molecule. We next note that for any arbitrary distribution of x segments within a region of s sites, an *effective* density may be defined such that a uniform distribution of segments having this density would give rise to the same number of interferences as would be encountered for the actual distribution. The effective segment density may be calculated as follows:

$$\varphi=\frac{\int (dx/ds)dx}{\int dx}, \tag{6}$$

where dx segments reside within the region of ds sites.

Let each subchain be characterized by a displacement length l, so that $L^2=\omega l^2$. We assume that the radial distribution function for the $i\nu$ elements which form a chain composed of i subchains can be represented by:

$$W(r_i)dr_i=(4/\pi^{\frac{1}{2}})\sum_{\kappa=1}^{i}\beta_\kappa^3\exp(-\beta_\kappa^2 r_\kappa^2)r_\kappa^2 dr_\kappa. \tag{7}$$

On setting

$$\int_{r_\kappa=0}^{\infty} W(r_\kappa)r_\kappa^2 dr_\kappa=\langle r_\kappa^2\rangle,$$

there is obtained:

$$\beta_\kappa^2=3/2\langle r_\kappa^2\rangle. \tag{8}$$

For a system of chains, each composed of N elements of length a, characterized by displacement length L, Hermans and Overbeek[8] obtained:

$$R_L^2=(Na^2+L^2)/12. \tag{9}$$

If $L^2=\langle L_0^2\rangle=Na^2$, corresponding to the most probable displacement distribution, Eq. (9) reverts to $R_0^2=Na^2/6$ previously obtained by Debye.[9]

Comparison of Eqs. (8) and (9) suggests:

$$\beta_\kappa^2=18/\kappa\nu a^2(1+\xi^2), \tag{10}$$

where $\xi^2=l^2/\nu a^2$. To calculate the contribution φ_κ to the effective segment density within the domain of subchain i due to the $p\nu$ segments of subchain $(i-\kappa+1)$, we set

$$dx_\kappa=p\nu W(r_\kappa)dr_\kappa$$
$$ds_\kappa=4\pi r_\kappa^2 dr_\kappa/V_1,$$

where V_1 is the molecular volume of solvent. From Eq. (6) there is obtained:

$$\varphi_\kappa=\varphi/\kappa^{\frac{3}{2}} \tag{11}$$

where

$$\varphi=2C_M M_\nu^{\frac{1}{2}}(1/p\nu)[2/(1+\xi^2)]^{\frac{3}{2}}.$$

Here M_ν is the molecular weight of a ν element subchain and C_M is the same parameter which appears in the treatment of Flory,[10] i.e.,

$$C_M=(27/2^{5/2}\pi^{3/2})(\bar{v}^2/\mathbf{N}V_1)(M_\nu/\nu l^2)^{3/2},$$

[7] F. Bueche and W. R. Krigbaum, J. Chem. Phys. **23**, 1863 (1955).

[8] J. J. Hermans and J. Th. G. Overbeek, Rec. trav. chim. **67**, 761 (1948).

[9] P. Debye, J. Chem. Phys. **14**, 636 (1946).

[10] See P. J. Flory and W. R. Krigbaum, J. Chem. Phys. **18**, 1086 (1950).

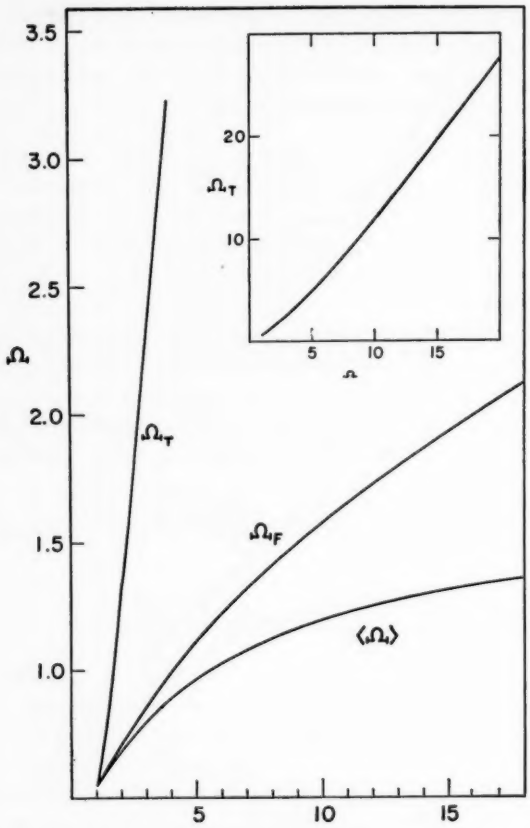

FIG. 1. Ω_T, Ω_F, and $\langle\Omega\rangle$ plotted against ω (see text).

where $\mathbf{N}$ is the Avogadro number, $\bar{v}$ the partial specific volume of polymer and $\mathbf{V}_1$ the *molar* volume of solvent. The effective segment density within the region to be occupied by subchain i is therefore:

$$\sum_{\kappa=1}^{i}\varphi_\kappa=\varphi\sum_{\kappa=1}^{i}(1/\kappa^{\frac{1}{2}}). \tag{12}$$

To proceed with the calculation of f_N, we note that the factor $\prod_{\kappa=1}^{i} f_\kappa$ appearing in Eq. (5) represents the contribution to the partition function for the molecule due to the addition of subchain i. Hence, we write:

$$\prod_{\kappa=1}^{i} f_\kappa=\exp(-\Delta F_i/kT),$$

where ΔF_i represents the free energy change on adding $p\nu$ segments to a chain composed of $(i-1)$ subchains to form a chain of i subchains. The entropy contribution to ΔF_i due to the interactions with segments of subchain $(i-\kappa+1)$ can be calculated from the probability P_κ that the $p\nu$ segments encounter no interference on entering the domain of s sites containing an effective segment density φ_κ:

$$P_1=\prod_{k=1}^{p\nu}[1-(k-1)/s_1]\cong\exp(-p\nu\varphi/2), \quad (\kappa=1) \tag{13}$$

$$P_\kappa=(1-\varphi_\kappa)^{p\nu}\cong\exp(-p\nu\varphi/\kappa^{\frac{1}{2}}), \quad (\kappa>1). \tag{14}$$

Representing the pair interaction free energy change due to interactions arising from the addition of subchain i by

$$-2kT\chi_{12}p\nu\varphi\left[\tfrac{1}{2}+\sum_{\kappa=2}^{i}(1/\kappa^{\frac{1}{2}})\right],$$

there is obtained for

$$\Delta F_i/kT=-\sum_{\kappa=1}^{i}\ln f_\kappa:$$

$$\Delta F_i/kT=2C_M M_\nu^{\frac{1}{2}}(1-2\chi_{12})\left[\tfrac{1}{2}+\sum_{\kappa=2}^{i}(1/\kappa)^{\frac{1}{2}}\right][2/(1+\xi^2)]^{\frac{1}{2}}. \tag{15}$$

According to Eq. (5),

$$\ln f_N=\sum_{i=1}^{\omega}(\omega-i+1)\ln f_i;$$

hence,

$$\ln f_N=-J\Omega_T M_\nu^{\frac{1}{2}}[2/(1+\xi^2)]^{\frac{1}{2}}, \tag{16}$$

where

$$J=2C_M(1-2\chi_{12}) \tag{17}$$

$$\Omega_T=\left[\frac{\omega}{2}+\sum_{i=2}^{\omega}\frac{\omega-(i-1)}{i^{\frac{1}{2}}}\right]. \tag{18}$$

Equation (16) should represent the total interference within a random-flight chain consisting of ω subchains, each having ν elements. Comparison with the expression derived by Flory[3] for the case of a random-flight chain, $\ln f_N=-JM^{\frac{1}{2}}/2$, where M is the molecular weight, reveals that the latter is equivalent to Eq. (16) when $\omega=1$ and $\xi=1$ (most probable distribution). However, for purposes of comparison we express Flory's result in the form:

$$\ln f_N=-J\Omega_F M_\nu^{\frac{1}{2}} \tag{19}$$

where $\Omega_F=(\omega^{\frac{1}{2}}/2)$. In Fig. 1 the molecular weight dependence of $\ln f_N$, represented by the factor Ω_T in Eq. (16), is compared with the corresponding factor Ω_F deduced for a random-flight chain by Flory. Evidently Ω_T as given by Eq. (18) does reflect the total interference, since it increases more rapidly then ω (as it must if $f_{2N}<f_N^2$).

We will now show that what is required for the calculation of the expansion due to interferences is the *average* interference encountered by elements of a subchain, rather than the total interference encountered by all elements of the chain. One might attempt to generate possible configurations for a real chain of N elements by placing each element in sequence on a lattice according to some random process, but taking interference into account at each step. Such a process

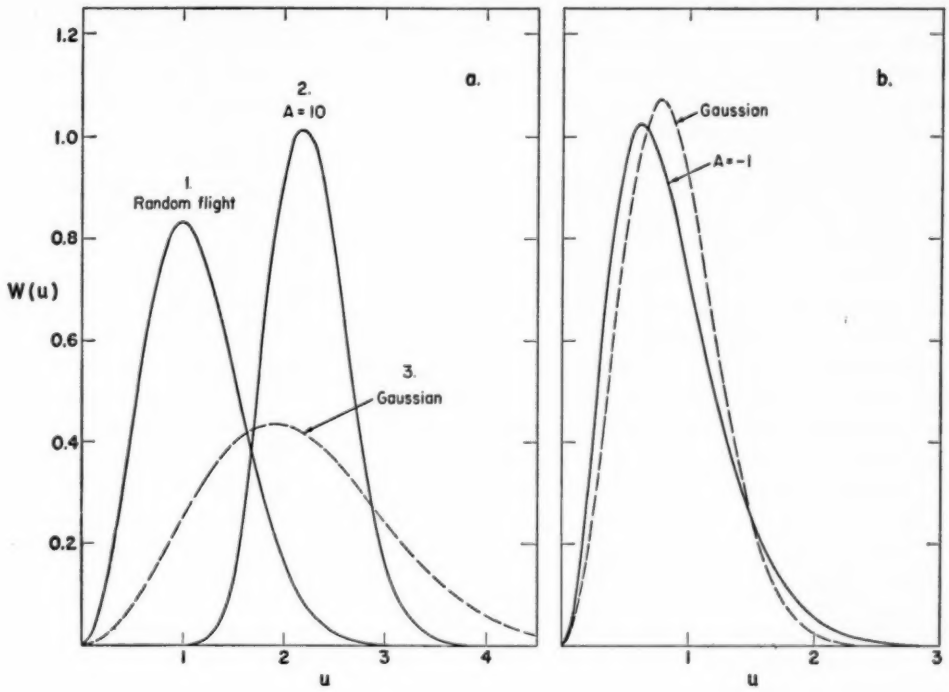

FIG. 2. (a) $W_0(u)$ for the random-flight chain (curve 1) compared with $W(u)$ for $\mathbf{A}=10$ (curve 2) and the corresponding Gaussian distribution (dashed curve 3). In (b) the full curve represents $W(u)$ for $\mathbf{A}=-1$ and the dashed curve the Gaussion distribution having the same value for $\langle L^2\rangle$.

would result in a rather improbable set of configurations, since each succeeding subchain would encounter more interference than the last, and thus the expansion factor for a subchain would increase from beginning to end of the chain. This, of course, is due to the fact that the configuration assumed by the elements of a given subchain, once having been assigned, does not reflect the effect of interferences arising from encounters with segments of the subchains subsequently added. The expansion factor characterizing the entire chain would be obtained from the appropriate sum of the expansion factors for the separate subchains. Evidently a more realistic set of configurations would result if each subchain were allowed to assume a new configuration reflecting the *average* interference encountered by the elements of that subchain. As a consequence of these remarks, we replace Eqs. (16) and (18) by

$$\ln\langle f_N\rangle=-J\langle\Omega\rangle M_\nu^{\frac{1}{2}}[2/(1+\xi^2)]^{\frac{3}{2}}, \tag{20}$$

$$\langle\Omega\rangle=\left[\frac{1}{2}+\frac{1}{\omega}\sum_{i=2}^{\omega}\frac{\omega-(i-1)}{i^{\frac{3}{2}}}\right]. \tag{21}$$

As shown in Fig. 1, the molecular weight dependence of the average f per subchain, represented by $\langle\Omega\rangle$, varies still more slowly with ω than does Ω_F.

Before leaving this section, we may anticipate that if ν is large there may exist a range of low molecular weights corresponding to less than one subchain (i.e., chains having $N<\nu$) for which the above treatment does not apply. We shall assume that Flory's calculation will serve as a sufficiently good approximation to $\langle\Omega\rangle$ within this range:

$$\langle\Omega\rangle=(\tfrac{1}{2})(N/\nu)^{\frac{1}{2}}, \quad (N<\nu). \tag{22}$$

B. The Displacement Distribution $W(L)$

Substituting $\langle f_N\rangle$ as given by Eq. (20) into Eq. (4), we make use of Eqs. (1) and (2) and note that

$$\xi^2=l^2/\nu a^2=L^2/Na^2=2u^2/3,$$

to obtain the following expressions for the displacement distribution $W(u)$, the mean-square displacement $\langle L^2\rangle$, and the square of the expansion factor, $\alpha^2=\langle L^2\rangle/Na^2$, for a chain with excluded volume:

$$W(u)=(4/\pi^{\frac{1}{2}})(1/I_1)\exp\{-u^2-\mathbf{A}[2/(1+2u^2/3)]^{\frac{1}{2}}\}u^2du, \tag{23}$$

$$\langle L^2\rangle=(I_2/I_1)Na^2, \tag{24}$$

$$\alpha^2=(I_2/I_1), \tag{25}$$

where $\mathbf{A}=J\langle\Omega\rangle M_\nu^{\frac{1}{2}}$ and

$$I_1=(4/\pi^{\frac{1}{2}})\int_{u=0}^{\infty}\exp\{-u^2-\mathbf{A}[2/(1+2u^2/3)]^{\frac{1}{2}}\}u^2du, \tag{26}$$

$$I_2=(8/3\pi^{\frac{1}{2}})\int_{u=0}^{\infty}\exp\{-u^2-\mathbf{A}[2/(1+2u^2/3)]^{\frac{1}{2}}\}u^4du. \tag{27}$$

We note that when $J=0$, corresponding to zero excluded volume, $\mathbf{A}=0$ and both I_1 and I_2 take the value unity, so that $W(u)=W_0(u)$ and $\langle L^2\rangle=Na^2$. In order to display the effect of nonzero excluded volume upon the displacement distribution, the integrals I_1 and I_2 were evaluated graphically for values of $\mathbf{A}=J\langle\Omega\rangle M_\nu^{\frac{1}{2}}$ ranging from -1 to $+10$. Figure 2(a)

shows $W_0(u)$ for the unperturbed random-flight chain (curve 1), $W(u)$ as calculated according to Eq. (23) for $\mathbf{A}=10$ (curve 2), and the expanded Gaussian displacement distribution having the same value for $\langle L^2\rangle$ (dashed curve 3). As predicted by James,[11] the displacement distribution is no longer Gaussian for $J>0$. The peak is shifted to larger values of u but the distribution is sharper than curve 1 instead of broader, as would be supposed from the expanded Gaussian distribution represented by curve 3. The physical explanation for this sharpening lies in the fact that there are few configurations corresponding to large L, and too many interferences in those configurations having small displacements. Thus, the majority of the acceptable configurations lie within a relatively narrow band of displacements between these two extremes. In Fig. 2(b) are compared $W(u)$ calculated according to Eq. (23) for $\mathbf{A}=-1$ and the corresponding Gaussian distribution. For this case, corresponding to a negative excluded volume, the Gaussian distribution is seen to be a better approximation, although it overestimates somewhat the sharpness of the displacement distribution. We further note that the relationship $\langle L^2\rangle/R^2=6$ derived by Debye makes use of the assumption that the mean-square displacement between any two elements i and j of the chain be given by $\langle l_{ij}^2\rangle=(j-i)a^2$. Since this is precisely true only for $J=0$, we may anticipate that the ratio $\langle L^2\rangle/R^2$ will be dependent to some extent upon both J and N.

III. COMPARISON WITH EXPERIMENT

Although all dilute solution properties depend upon the average configuration of the polymer molecules in the solution, it is nevertheless true that none of the methods currently employed to obtain a measure of $\langle L^2\rangle$ or R^2 is completely satisfactory. Some of the objections to these experimental procedures have been pointed out by Hermans, Klamkin, and Ullman.[12] Light scattering would appear to afford the most direct measurement of R; however, the precision of these results is not all that might be desired. Furthermore, Benoit[13] has recently pointed out that treatment of light scattering data may yield different averages for R^2. Unfortunately, there appears to be a range of molecular sizes for which the results correspond to no well-defined average.

The hydrodynamic properties offer a second possible experimental approach. The principle doubts concerning such an assignment of $\langle L^2\rangle$ or R^2 lie in uncertainties in the theoretical treatments rather than in the precision of the experimental measurements. The two hydrodynamic treatments[14,15] based on a random-flight model do not appear [16] to represent both sedimentation and viscosity data as well as the modification proposed by Flory.[17] Flory suggested the following alterations of the foregoing treatments: (a) that the hydrodynamic factors $xF(x)$ in the KR treatment and $\varphi(\sigma)$ and $\chi(\sigma)$ in the DB treatment are at their asymptotic limit for flexible-chain polymers over the molecular weight range of interest, (b) that the effective hydrodynamic radius is proportional to some number-average linear dimension of the coil, such as $\langle L^2\rangle^{\frac{1}{2}}$ or R, and (c) that R or $\langle L^2\rangle^{\frac{1}{2}}$ is expanded over the corresponding dimension for the unperturbed coil by a factor α which increases with N due to long range interferences.

Each of these proposed modifications has been subjected to experimental test. Intrinsic viscosity measurements[18] in "ideal" solvents at the Flory Θ temperature testify to the correctness of Flory's proposal (a), since $[\eta]_\Theta/M^{\frac{1}{2}}$ remains constant down to molecular weights of a few thousand. For intrinsic viscosity, assumption (b) may be stated in the form[19]:

$$\Phi=[\eta]\bar{M}_n/\langle L_n^2\rangle^{\frac{3}{2}}=6^{\frac{3}{2}}[\eta]\bar{M}_n/R_n^3. \qquad (28)$$

The majority of the experimental data [16,20–23] indicates that Φ is approximately a constant of magnitude 2.5×10^{21} for flexible-chain polymers, although Thurmond and Zimm[24] have suggested that Φ may increase as the solvent becomes poorer. Turning to assumption (c), though there is no doubt that flexible polymer molecules are more expanded in thermodynamically good solvents, the question of the precise dependence of the expansion factor α and N remains to be examined. The relationship proposed by Flory[3] indicates that α should increase monotonically with N. The observed[25] dependence of $[\eta]$ in "nonideal" solvents is in qualitative agreement with Flory's prediction, although the sensitive test furnished by a plot of the function $(\alpha^5-\alpha^3)/M^{\frac{1}{2}}$ reveals a considerable discrepancy for both the low and high molecular weights. In summary, Flory's proposed modification (a) appears to be well established, whereas there remains some doubt concerning (b). The relationship between α and N deduced by Flory represents an approximation which is only qualitatively correct; however, correctness of this relation is not a necessary condition for the deduction of R^2 or $\langle L^2\rangle$ from intrinsic viscosity data.

[11] H. M. James, J. Chem. Phys. **21**, 1628 (1953).
[12] Hermans, Klamkin, and Ullman, J. Chem. Phys. **20**, 1360 (1952).
[13] H. Benoit, J. Polymer Sci. **9**, 507 (1953); Benoit, Holtzer, and Doty, J. Phys. Chem. **58**, 635 (1954).
[14] J. G. Kirkwood and J. Riseman, J. Chem. Phys. **16**, 565 (1948).
[15] P. Debye and A. M. Bueche, J. Chem. Phys. **16**, 573 (1948).
[16] Mandelkern, Krigbaum, Scheraga, and Flory, J. Chem. Phys. **20**, 1392 (1952).
[17] P. J. Flory and T. G. Fox, J. Am. Chem. Soc. **73**, 1904 (1951). See also reference 3.
[18] Krigbaum, Mandelkern, and Flory, J. Polymer Sci. **9**, 381 (1952).
[19] P. J. Flory and T. G. Fox, J. Polymer Sci. **5**, 745 (1950).
[20] T. G. Fox and L. Mandelkern, J. Chem. Phys. **21**, 187 (1953).
[21] J. Bischoff and V. Desreux, J. Polymer Sci. **10**, 437 (1953).
[22] A. R. Shultz, J. Am. Chem. Soc. **76**, 3422 (1954).
[23] Newman, Krigbaum, Laugier, and Flory, J. Polymer Sci. **14**, 451 (1954).
[24] C. D. Thurmond and B. H. Zimm, J. Polymer Sci. **8**, 477 (1954).
[25] W. R. Krigbaum and P. J. Flory, J. Polymer Sci. **11**, 37 (1953).

A third, though less direct, test of the correctness of an assumed form for $W(R)$ is offered by studies of the second virial coefficient. Flory[26,27] has presented a theoretical treatment of the second virial coefficient analagous to that for imperfect gases. It is assumed that $W(R)$ for a real chain may be represented by a single Gaussian function expanded by a scale factor α. This theory yields an expression for the second virial coefficient of the form:

$$A_2=(\bar{v}^2/v_1)\psi_{12}(1-\Theta/T)F(X). \qquad (29)$$

This differs from the relationship obtained according to the original Flory-Huggins treatment through the additional factor $F(X)$. This factor introduces a dependence of A_2 upon molecular weight, molecular weight heterogeneity, and upon the thermodynamic parameters. Since the form of the $F(X)$ function depends upon the radial distribution function, the correctness of the assumed distribution may be judged by a comparison of the experimental and predicted dependences of A_2 upon molecular weight and the thermodynamic parameters. Osmotic pressure measurements[28] reveal that the form of the theoretical $F(X)$ function is qualitatively correct, although it does not allow an exact fit to be obtained for either the molecular weight or the thermodynamic dependence of A_2.

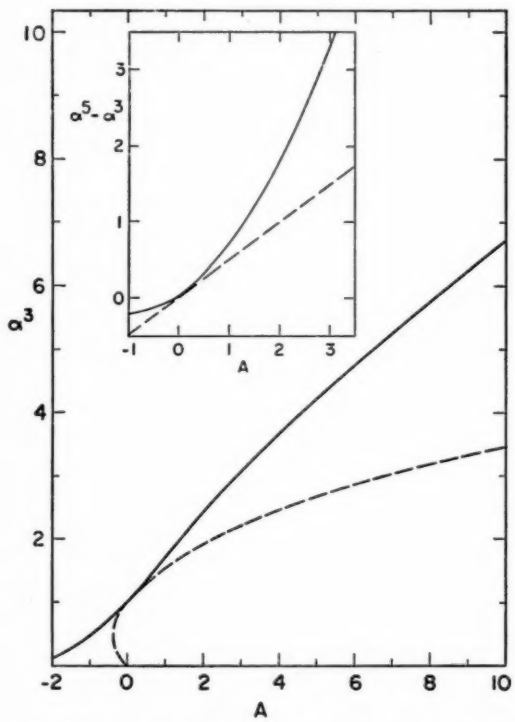

FIG. 3. $\alpha^3=[\langle L^2\rangle/N\alpha^2]^{\frac{3}{2}}$ shown as a function of **A**. The insert shows $\alpha^5-\alpha^3$ plotted against **A**. In each case the full curve is given by the present treatment and the dashed curve by that of Flory.

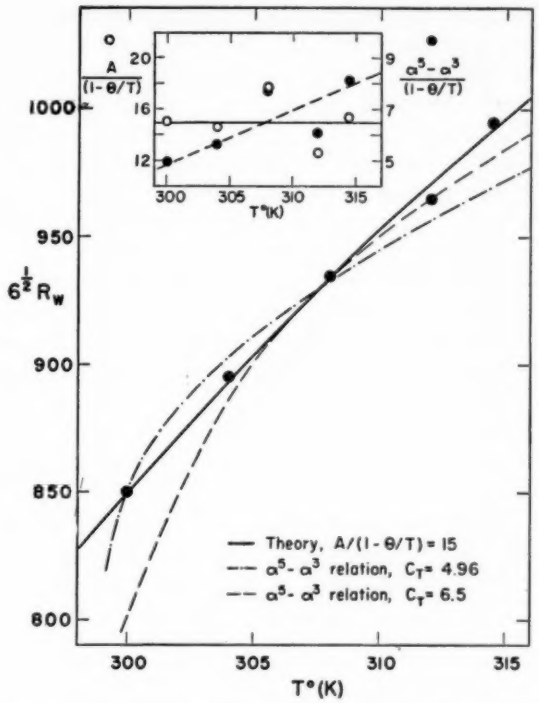

FIG. 4. The points represent $\langle L_w\rangle^{\frac{1}{2}}$ values for polystyrene-cyclohexane[31] plotted against T. The full curve is given by the present theory; the dashed curves are calculated according to Flory. Filled circles in the insert represent $(\alpha^5-\alpha^3)/(1-\Theta/T)$, a constant according to Flory, while the open circles represent $\mathbf{A}/(1-\Theta/T)$.

To summarize the above remarks, the writer feels that the results of light scattering and viscosity measurements are about equally reliable at the present time. Since there is considerable activity in the dilute solution field, we may anticipate that some of the questionable points mentioned above may be resolved in the near future. Although it is now known[1,2] that $W_0(R)$ for random-flight chains is not a simple Gaussian function, the form of $W(R)$ for chains with excluded volume has still to be determined.

With the foregoing comments in mind, we turn to a comparison of theory and experiment. Theoretical values for $\alpha^3=(I_2/I_1)^{\frac{3}{2}}$ obtained by graphical integration of the two integrals appearing in Eqs. (26) and (27) are plotted against $\mathbf{A}=J\langle\Omega\rangle M^{\frac{1}{2}}$ in Fig. 3. These are compared with the α^3 values (dashed curve) calculated according to Flory's relationship,[3] which when transformed into the present notation becomes:

$$\alpha^5-\alpha^3=J\Omega_F M^{\frac{1}{2}}, \qquad (30)$$

where J is given by Eq. (17) and $\Omega_F=(\omega^{\frac{1}{2}}/2)$. As shown in Fig. 3, the present treatment predicts a more rapid increase in α for increasing positive values of **A**, but a less drastic variation over the range of negative **A** values. Since **A** varies linearly with the factor J expressing the thermodynamic interactions, the curves

[26] P. J. Flory, J. Chem. Phys. **17**, 1347 (1949).
[27] P. J. Flory and W. R. Krigbaum, J. Chem. Phys. **18**, 1086 (1950).
[28] (a) W. R. Krigbaum and P. J. Flory, J. Am. Chem. Soc. **75**, 1775 (1953); (b) **75**, 5254 (1953); (c) W. R. Krigbaum, J. Am. Chem. Soc. **76**, 3758 (1954).

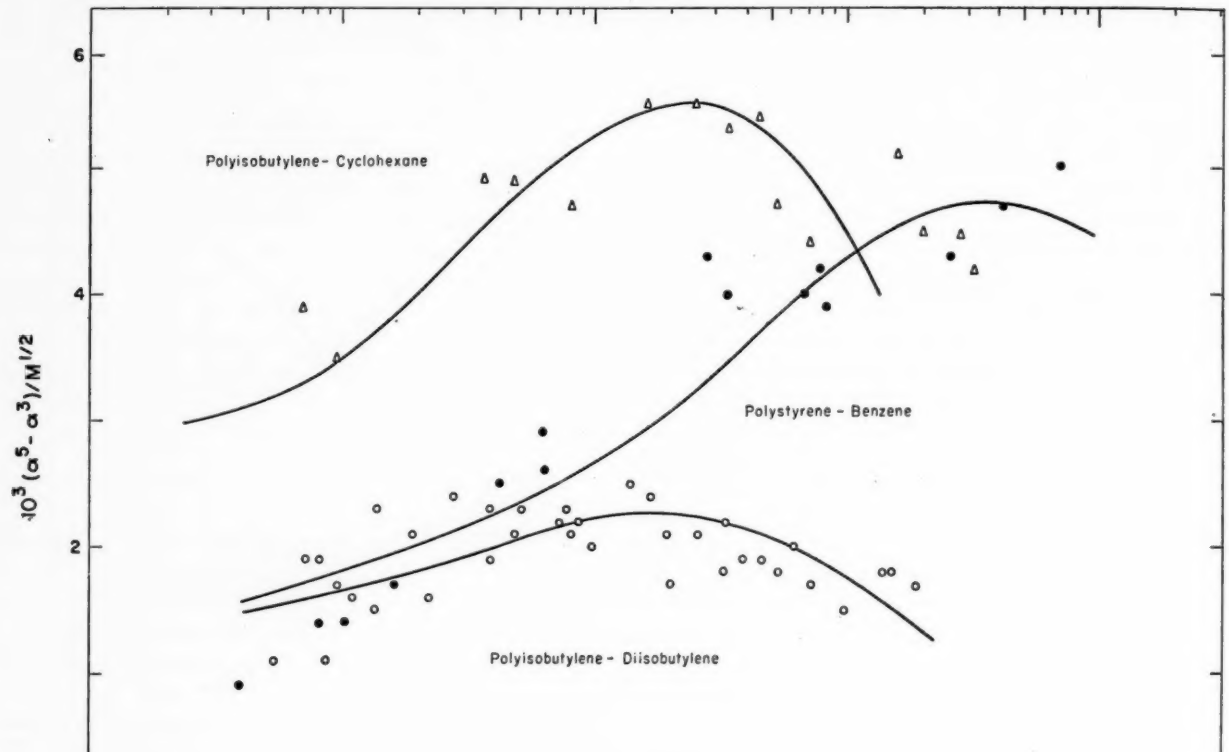

FIG. 5. Values[27] of $10^3(\alpha^5-\alpha^3)/M^{\frac{1}{2}}$ for polyisobutylene in diisobutylene at 20° (open circles), in cyclohexane at 30° (triangles) and for polystyrene in benzene at 25° (filled circles). Curves represent calculated values. Horizontal lines are predicted according to Flory.

in Fig. 3 represent the dependence of α^3 upon J as well. It should be noted that the thermodynamic factor J and the molecular weight dependent factor $\langle\Omega\rangle$ are separable, thus an error in the latter will not influence the form of the α^3 *vs* J curve. Values for the function $(\alpha^5-\alpha^3)$ as calculated according to these two treatments are shown plotted against $\mathbf{A}$ in the insert to Fig. 3.

A test of the predicted dependence of α^3 upon the thermodynamic factor J is possible only if both R^2 and the thermodynamic parameters are known for the same system. The light scattering data of Outer, Carr, and Zimm[29] for the system polystyrene-cyclohexane in the vicinity of the Flory Θ temperature fulfill these requirements. The Θ temperature has been evaluated for this system by Shultz and Flory[30] by means of precipitation temperature measurements, and by the writer[28] by osmotic pressure measurements. The two values may be represented by $\Theta=307.4\pm0.2$°K. If one writes for the interaction parameter $\chi_{12}=1/2-\psi_{12}\times(1-\Theta/T)$, where $1/2-\psi_{12}$ represents the entropy component and $\psi_{12}\Theta/T$ the enthalpy component of the pair interaction free energy, then Flory's treatment predicts that for a given molecular weight $(\alpha^5-\alpha^3)/(1-\Theta/T)$ should be a constant equal to $C_T=4C_M\Omega_F\times M_w^{\frac{1}{2}}\psi_{12}$ for all temperatures. The filled circles shown in the insert to Fig. 4 indicate that for these data this quantity actually increases substantially with increasing temperature. For a test of the present treatment, one may assign a value for $\mathbf{A}$ corresponding to each experimental α through use of the plot of α^3 *vs* $\mathbf{A}$ shown in Fig. 3. Recalling that $\mathbf{A}=J\langle\Omega\rangle M_w^{\frac{1}{2}}$, then according to Eq. (17) $\mathbf{A}/(1-\Theta/T)$ should be a constant equal to $4C_M\langle\Omega\rangle M_w^{\frac{1}{2}}\psi_{12}$. The open circles appearing in the insert to Fig. 4 represent a test of this prediction, and demonstrate that $\mathbf{A}/(1-\Theta/T)$ is indeed constant within experimental error for this particular system. The experimental values obtained for $\langle L_w^2\rangle^{\frac{1}{2}}=6^{\frac{1}{2}}R_w$ by Outer, Carr, and Zimm appear as filled circles in Fig. 4. The full curve represents the fit obtained by the present theory taking $\mathbf{A}/(1-\Theta/T)=15$, while the broken curves represent attempts to fit the data according to Flory's equation (30), using two different values for C_T. It appears from Fig. 4 that the temperature dependence of $\langle L_w\rangle^{\frac{1}{2}}$ exhibited by these data is better represented by the present treatment than by that of Flory, although a final decision must await a more extensive test. It should be pointed out that $(\alpha^5-\alpha^3)/(1-\Theta/T)$ could be maintained constant, as required by Flory's theory, by selecting a lower value for Θ. However, the Θ value for this system is well known, and the value $\Theta=306$°K

[29] Outer, Carr, and Zimm, J. Chem. Phys. **18**, 830 (1950).
[30] A. R. Shultz and P. J. Flory, J. Am. Chem. Soc. **74**, 4760 (1952).

required to render $(\alpha^5-\alpha^3)/(1-\Theta/T)$ a constant for these data appears to lie outside the experimental error. Furthermore, the A_2 values given for this system by Outer, Carr, and Zimm place Θ in the range 307.5 −308°K.

Finally, we turn to a test of the predicted dependence of $\langle L^2\rangle$ upon N. It is evident from Fig. 1, that $\langle\Omega\rangle$ is not a linear function of ω, and that the present treatment predicts a more gradual increase in α in the region of large N values than does that of Flory. The dependence of α upon N as predicted according to Flory's theory has previously[25] been subjected to an extensive test using intrinsic viscosity data for three polymer-solvent systems covering a wide range of molecular weights. According to Flory's treatment[17] of intrinsic viscosity, the expansion factor $\alpha=[\langle L^2\rangle/\langle L_0^2\rangle]^{\frac{1}{2}}$ should be determinable from intrinsic viscosity through use of the relation $\alpha^3=[\eta]/[\eta]_\Theta$, where $[\eta]_\Theta$ is the value which would be observed in a Θ solvent at the same temperature. The predicted molecular weight dependence of α or $[\eta]$ was found to be qualitatively correct, although as mentioned above the very sensitive test afforded by a plot of $(\alpha^5-\alpha^3)/M^{\frac{1}{2}}$ revealed that the observed α values fell below those predicted for both high and low molecular weights.

These same data are represented by the points shown in Fig. 5. According to Flory's treatment the points should fall on horizontal lines, whereas the molecular weight dependence predicted with the use of Eqs. (21) and (22) is represented by the curves shown in Fig. 5. The present theory has one adjustable parameter not available to Flory—the number ν of elements in a subchain. A value of ν has been assigned for each polymer so that the predicted maximum in the $(\alpha^5-\alpha^3)/M^{\frac{1}{2}}$ curve coincides approximately with that observed. The M_ν values required were 4×10^4 for polyisobutylene and 1×10^6 for polystyrene, corresponding to 700 and 10^4 repeating units per subchain, respectively. Polyisobutylene has been shown[31] by light scattering to have a more flexible chain than polystyrene, so the order of the ν values observed above is reasonable, although the significance of the magnitudes of these values is not immediately evident. Nevertheless, the agreement between theory and experiment shown in Fig. 5 is very gratifying. In view of the fact that this represents an exceedingly sensitive test, it is evident that the molecular weight dependence of $[\eta]$ or $\langle L^2\rangle$ for flexible chain polymers can be represented with considerable accuracy by the present treatment.

It should be noted that the present treatment predicts smaller α values for the range of small N values than does that of Flory, which allows $[\eta]$ to vary as M to a power no greater than 0.8. Thus, the viscosity behavior exhibited by the cellulosics, for which $[\eta]\approx M^{1.0}$, lies beyond the bounds of the present treatment as well as that of Flory. One infers from this hydrodynamic behavior that low molecular weight cellulose chains do not conform to the flexible chain model. One might suspect that for sufficiently high molecular weights a sufficient number of units would be present to ensure chain flexibility. Münster[32] has reported viscosity measurements for cellulose nitrate in acetone which indicate that the exponent a in the relation $[\eta]=KM^a$ does decrease from unity for sufficiently high molecular weights, suggesting that the transition to a flexible chain does occur.

In summary, comparison with experiment reveals that the molecular weight dependence of $[\eta]$, and by implication that of $\langle L^2\rangle$ and R^2, is accurately represented by the treatment presented here. The observed dependence of R^2 upon the thermodynamic variables also appears to be better represented by the present treatment. Application of this theory to intrinsic viscosity data will of course lead to a new set of interaction parameters from that source; however, consideration of this point will be deferred until a later time. It is hoped that the dilute solution treatment[26,27] can be re-examined, using the model proposed here for counting interferences, to obtain improved agreement with the observed values for the second virial coefficient.

ACKNOWLEDGMENT

The author wishes to express his gratitude to the E. I. du Pont de Nemours Company for a Grant-in-Aid during the summer months of 1954, at which time the majority of the work appearing in this paper was completed.

[31] E. D. Kunst, Rec. trav. chim. **69**, 125 (1950).

[32] A. Münster, J. Polymer Sci. **8**, 633 (1952).

THE JOURNAL OF CHEMICAL PHYSICS VOLUME 23, NUMBER 11 NOVEMBER, 1955

Vibrational Spectrum of 1-Fluoro-1-Chloroethylene*

D. E. MANN, N. ACQUISTA, AND EARLE K. PLYLER
National Bureau of Standards, Washington 25, D. C.

(Received February 16, 1955)

The infrared spectrum of gaseous $FClC:CH_2$ has been investigated in the range 1.6–52μ. A satisfactory vibrational assignment has been achieved. The planar fundamentals occur at 3069, 3016, 1656, 1383, 1186, 947, 699, 432, and 371 cm^{-1}; the out-of-plane fundamentals are at 836, 607, and 515 cm^{-1}. A table of the thermodynamic functions for the ideal gas is given from 200 to 1500°K.

INTRODUCTION

RELATIVELY complete spectral data and vibrational assignments have recently become available for several fluorinated ethylenes. The fluorochloro series of compounds is represented by $F_2C:CF_2$,[1,2] $F_2C:CFCl$,[3] $F_2C:CCl_2$,[4,5] $FClC:CCl_2$,[5] and $Cl_2C:CCl_2$.[2] Other simple fluoroethylenes for which fairly complete interpretations have recently appeared are $F_2C:CFH$,[6] $F_2C:CH_2$,[7] and $FHC:CH_2$.[8,9] Only a few ethylenes containing H, F, and Cl appear to have been studied. Nielsen, Liang, and Smith have published spectral data and an assignment for $F_2C:CClH$.[10] A partial survey of the infrared spectrum of $FClC:CH_2$ has been reported by Torkington and Thompson.[8] They examined its spectrum from 3 to 20 μ and suggested an assignment for 8 of the 12 fundamentals. In the present work its infrared spectrum has been investigated more extensively and the complete vibrational assignment given.

EXPERIMENTAL

The sample of $FClC:CH_2$ was made available to us by the M. W. Kellogg Company and was used without further purification. The infrared absorption spectrum of its vapor at various pressures was studied over the range 1.6–52 μ with equipment and methods previously described.[3] Prisms of LiF, CaF_2, CsBr, and CsI were used with a Perkin-Elmer 12C spectrometer, NaCl with a Perkin-Elmer 21 spectrophotometer, and KBr with a Baird Associates instrument. The infrared spectrum, replotted on a scale linear in wave number, is presented in Fig. 1. The absence of any significant absorption in the region 30−52 μ is indicated by the termination of the trace just below the band at 371 cm^{-1}. The wave number measurements of all the observed bands are given in Table I together with their assignments. The Raman spectrum was not obtained.

RESULTS

Where the two are comparable, the infrared spectrum reported here agrees well with that given by Torkington and Thompson.[8] The discrepancies in the wave number measurements of some of the bands are not regarded as serious, and probably result chiefly from differences in the resolution achieved. Many more absorption maxima and shoulders are listed in Table I than were recorded by Torkington and Thompson. It is quite likely that the few very faint bands for which satisfactory interpretations are not given are caused by traces of unidentified impurities.

Three perpendicular or type C bands are clearly evident at 836, 607, and 515 cm^{-1} in Fig. 1. Each is characterized by a prominent central branch flanked by much less pronounced P and R wings. The unusual appearance of the 836 cm^{-1} band recalls that of the corresponding type C band at 803 cm^{-1} in the infrared spectrum of vinylidene fluoride.[7] The 803 cm^{-1} band seems to have 4 secondary zero branches symmetrically disposed about the central Q branch. In the present case, the peak at 824 cm^{-1} on the P wing of the 836 cm^{-1} band appears to be a secondary zero branch. By analogy with the 803 cm^{-1} band of $F_2C:CH_2$ another submaximum might be expected at about 848 cm^{-1} in the R wing of the 836 cm^{-1} band, but it does not seem to be present. The appearance of this suggests considerable overlapping.

INTERPRETATION

Preliminary Discussion

The structure of $FClC:CH_2$ has not yet been determined although a microwave investigation[11] of the pure rotation spectra of its Cl^{35} and Cl^{37} isotopic species has yielded, among other things, the values for $(A+C)/2$, and the asymmetry parameter $\kappa=2(B-(A+C)/2)/(A-C)$, where A, B, and C are the rotational constants inversely proportional to the least, intermediate, and largest effective moments of inertia, I_A, I_B, and I_C, respectively. That the effective aplanarity of the molecule may, for our purposes, be neglected is clear

* This work has been supported in part by the Office of Naval Research.

[1] Nielsen, Claassen, and Smith, J. Chem. Phys. **18**, 812 (1950).
[2] Mann, Acquista, and Plyler, J. Research Natl. Bur. Standards **52**, 67 (1954).
[3] Mann, Acquista, and Plyler, J. Chem. Phys. **21**, 1949 (1953).
[4] Nielsen, Claassen, and Smith, J. Chem. Phys. **18**, 485 (1950).
[5] D. E. Mann and E. K. Plyler, J. Chem. Phys. **23**, 1989 (1955).
[6] Mann, Acquista, and Plyler, J. Chem. Phys. **22**, 1586 (1954).
[7] Smith, Nielsen, and Claassen, J. Chem. Phys. **18**, 326 (1950).
[8] P. Torkington and H. W. Thompson, Trans. Faraday Soc. **41**, 236 (1945).
[9] A. R. H. Cole and H. W. Thompson, Proc. Roy. Soc. (London) **A200**, 10 (1949).
[10] Nielsen, Liang, and Smith, J. Chem. Phys. **20**, 1090 (1952).
[11] Bragg, Madison, and Sharbaugh, Phys. Rev. **77**, 148 (1950).

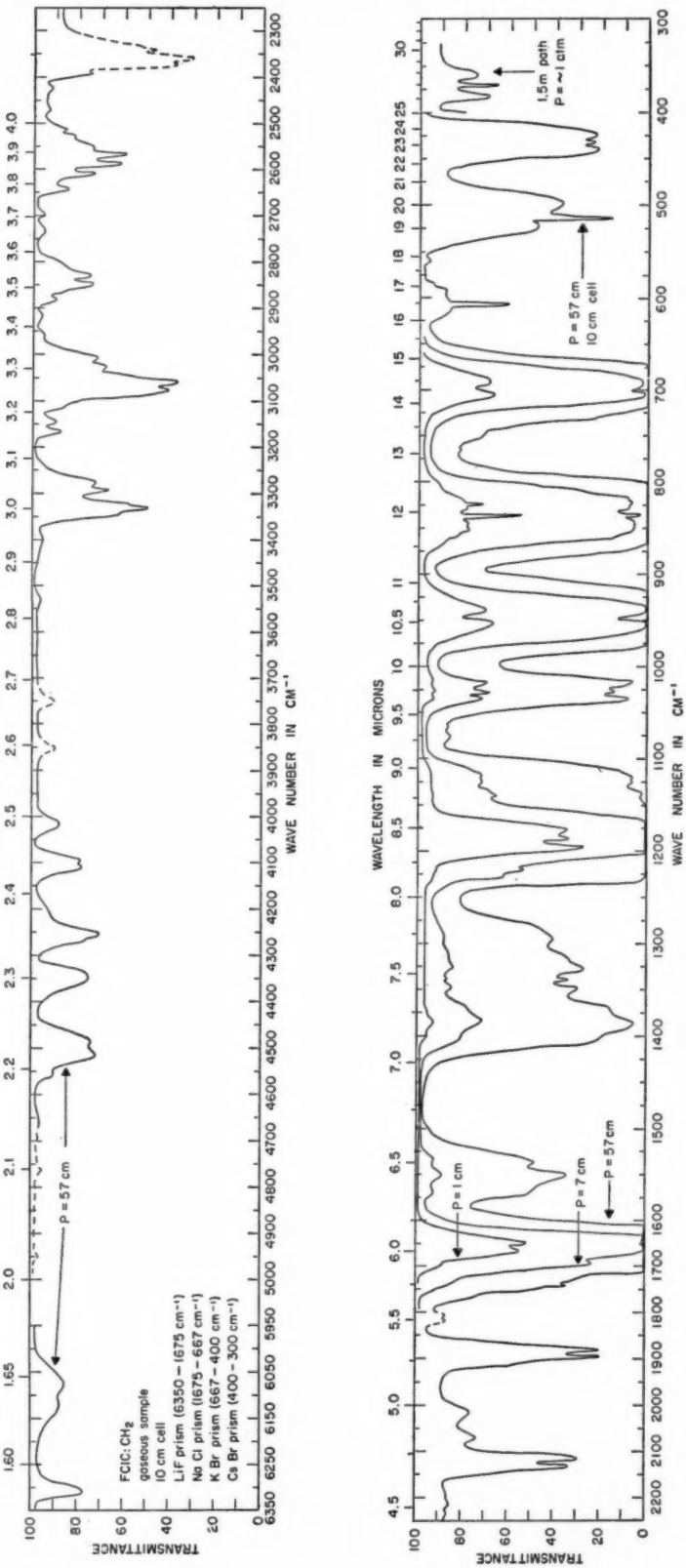

FIG. 1. Infrared spectrum of $FClC{:}CH_2$ (gas) from 1.6 to 30 microns.

TABLE I. Infrared spectrum of $FClC:CH_2$ (gas).

Wave number (cm^{-1})	Intensity		Interpretation
360	vvw	P	
371	vvw	Q	$\nu_9(a')$[a]
380	vvw	R	
424	m	P	
432	m	Q	$\nu_8(a')$
440	m	R	
500	w	P	
515	m	Q	$\nu_{12}(a'')$
521	w	R	
560	vvw		?[b]
~ 586 sh[c]	vvw		?
593	vvw		$\nu_{11}+\nu_i-\nu_i$
~		P	
607	vw	Q	$\nu_{11}(a'')$
~		R	
691	s	P	
$(699)_c$[d]			$\nu_7(a')$
705	s	R	
~ 727 sh	vvw		?
~ 750	vvw		$2\times371=742$[e]
~ 761	vvw		?
~ 765	vvw		?
802	vvw		$371+432=803$
820	s		
824	s	Q	$\nu_{10}+\nu_j-\nu_j$
828	s		
836	s	Q	$\nu_{10}(a'')$
853	s		
860 sh	vvw		$2\times432=864$
938	s	P	
$(947)_c$			$\nu_6(a')$
954	s	R	
1017	m	P	
1028	m	Q	$2\times515=1030$
1035	m	R	
1076	vvw		$371+699=1070$
~1120	vw		$515+607=1122$
1140	vw		?
1176	s	P	
1186	s	Q	$\nu_5(a')$
1195	s	R	
1221	vw	Q	$515+699=1214(A'')$; $2\times607=1214$
1227	vw	R	
1295	w		? $607+699=1306(A'')$
1319 sh	w		? $371+947=1318$
1326	w		?
1337	w		? $515+824=1339$
1346	w		? $515+836=1351$
1375 sh	m	P	
1383	m	Q	$\nu_4(a')$
1395	m	R	
1538	w		$699+836=1535(A'')$
1550	w		$371+1186=1557$; $607+947=1554(A'')$
1567	w		?
1650	s	P	
$(1656)_c$			$\nu_3(a')$
1667	s	R	
1695	m		$2\times836=1672$[f]; $515+1186=1701(A'')$
~1725 sh	vw		? $2\times515+699=1729$
1742	vw		?
~1750 sh	vw		? $371+1383=1754$
1805	vvw	P	
$(1812)_c$			$432+1383=1815$
1818	vvw	R	
1882	w	P	
$(1890)_c$			$2\times947=1894$
1895	w	R	
1910 sh	vvw		$371+699+836=1906(A'')$; $515+2\times699=1913(A'')$
2012	vw		$836+1186=2022(A'')$
2068	vw		$371+1695=2066$
2116	w	P	
$(2124)_c$			$947+1186=2133$
2132	w	R	
2217	vvw		$836+1383=2219(A'')$
2232	vvw		$2\times699+836=2234(A'')$
2333 sh	vvw		
2340	vw		$947+1383=2330$
2357	w		$699+1656=2355$
2372	w		$2\times1186=2372$
2391	vvw		$371+836+1186=2393(A'')$
2424	vvw		$432+607+1383=2422(A'')$
2469	vvw		
2513	vvw	P	
$(2520)_c$			$432+699+1383=2514$
2527	vvw	R	
2552	vvw		$515+853+1186=2554$
2567	vw		$1186+1383=2569$
2587	vw		$699+2\times947=2583$; $2\times699+1186=2584$
2608	vw		$947+1656=2603$
2642	vvw		$947+1695=2642$; $515+947+1186=2648(A'')$
2698	vvw		$371+947+1383=2701$
2734	vvw		$836+2\times947=2730(A'')$; $607+947+1186=2740(A'')$; $371+2\times1186=2743$
2827	vw	P	
$(2837)_c$			$1186+1656=2842$
2846	vw	R	
2880	vvw		$1186+1695=2881$
2924	vvw		$699+836+1383=2918(A'')$
2959	vvw		$607+699+1656=2962(A'')$; $836+947+1186=2969(A'')$
3006	vw	P	
$(3016)_c$			$\nu_2(a')$
3025	vw	R	
3059	w	P	
$(3069)_c$			$\nu_1(a')$
3075	w	R	
3112 sh	vvw		$515+947+1656=3118(A'')$
3145	vvw		$371+2\times1383=3137$
3166	vvw		$836+947+1383=3166(A'')$
3275	vw		$2\times947+1383=3277$; $432+1186+1656=3274$
3291	vw		$947+699+1656=3302$
3320 sh	vvw	P	
3330	vw		$2\times1656=3312$
3342 sh	vw	R	
3397	vvw		$371+3016=3397$
3529	vvw		$515+3016=3531(A'')$
3750	vvw		$2\times1186+1383=3755$; $699+3069=3768$
3852	vvw		$836+3016=3852(A'')$
4016	vvw		$947+3069=4016$
4093	vw	P	
$(4101)_c$			$2\times515+3069=4099$
4108	vw	R	
~4200 sh	vvw		$1186+3016=4202$
4255	vw	Q	$1186+3069=4255$
4266 sh	vw	R	
4348	vw		$2\times515+2\times1656=4342$
4484	vw	P	
$(4498)_c$			$1186+2\times1656=4498$
4513	vw	R	
4554 sh	vvw		$699+836+3016=4551(A'')$
~4762	vvw		$1695+3069=4764$
~4950	vvw		$699+1186+3069=4954$
~5181	vvw		$515+1656+3016=5187(A'')$; $947+1186+3069=5202$
6075	vvw		$3016+3069=6085$
6120	vvw		$2\times3069=6138$
6309	vw		$2\times1656+3016=6328$

[a] The planar fundamentals are numbered, in order of decreasing magnitude, from 1 to 9. The a'' fundamentals are similarly numbered from 10 to 12.
[b] The question mark indicates the absence of a plausible interpretation. A good many of these questioned bands are attributable to impurities. For example, the absorption at 1750, 1742, 1346, 1337, 750, 586 cm^{-1} could result from the presence of $F_2C:CClH$; that at 1742, 1725, 1319, 1295 cm^{-1} from $F_2C:CH_2$, that at 1750, 1326, 1140, and 560 from $F_2C:CCl_2$; or perhaps some closely related substance is responsible.
[c] The designation "sh" means shoulder. The tilde (~) is used to indicate that the measured quantity may be more than normally uncertain, and usually applies to weak shoulders or broad bands.
[d] A wave number given in the form $(\cdots)_c$ is the measured value of the minimum between two related branches.
[e] The species of the combination or overtone is understood to be A' unless A'' is given explicity.
[f] Fermi resonance. See text.

TABLE II. Vibrational assignments for gaseous $F_2C{:}CH_2$, $FClC{:}CH_2$, $Cl_2C{:}CH_2$, and $Br_2C{:}CH_2$.[a]

$F_2C{:}CH_2$		$FClC{:}CH_2$[b]		$Cl_2C{:}CH_2$		$Br_2C{:}CH_2$	
cm^{-1}	Species and mode character[c]	cm^{-1}	Species and mode character[c]	cm^{-1}	Species and mode character[c]	cm^{-1}	Species and mode character[c]
3100[d]	$b_1(\nu\ CH)$	3069	$a'(\nu\ CH)$	3130[f]	$b_1(\nu\ CH)$	3108[f]	$b_1(\nu\ CH)$
3058[d]	$a_1(\nu\ CH)$	3016	$a'(\nu\ CH)$	3035[f]	$a_1(\nu\ CH)$	3023[f]	$a_1(\nu\ CH)$
1728[d]	$a_1(\nu\ CC)$	1656	$a'(\nu\ CC)$	1620[e]	$a_1(\nu\ CC)$	1593[f]	$a_1(\nu\ CC)$
1414[e]	$a_1(\delta\ CH_2)$	1383	$a'(\delta\ CH_2)$	1391[e]	$a_1(\delta\ CH_2)$	1379[f]	$a_1(\delta\ CH_2)$
1302[e]	$b_1(\nu\ CF)$	1186	$a'(\nu\ CF)$	1094[e]	$b_1(\rho\ CH_2)$	1065[f,g]	$b_1(\rho\ CH_2)$
955[e]	$b_1(\rho\ CH_2)$	947	$a'(\rho\ CH_2)$	794[e]	$b_1(\nu\ CCl)$	696[f]	$b_1(\nu\ CBr)$
926[e]	$a_1(\nu\ CF)$	699	$a'(\nu\ CCl)$	605[e]	$a_1(\nu\ CCl)$	467[f]	$a_1(\nu\ CBr)$
550[e]	$a_1(\delta\ CF_2)$	432	$a'(\delta-\rho\ CFCl)$	375[f]	$b_1(\rho\ CCl_2)$	322[f]	$b_1(\rho\ CBr_2)$
438[e]	$b_1(\rho\ CF_2)$	371	$a'(\rho-\delta\ CFCl)$	299[f]	$a_1(\delta\ CCl_2)$	184[f]	$a_1(\delta\ CBr_2)$
803[e]	$b_2(\beta\ CH_2)$	836	$a''(\beta\ CH_2)$	872[e]	$b_2(\beta\ CH_2)$	886[f]	$b_2(\beta\ CH_2)$
714[f]	$a_2(\tau)$	607	$a''(\tau)$	686[f]	$a_2(\tau)$	668[f]	$a_2(\tau)$
611[e]	$b_2(\beta\ CF_2)$	515	$a''(\beta\ CFCl)$	458[f]	$b_2(\beta\ CCl_2)$	405[f]	$b_2(\beta\ CBr_2)$

[a] For $F_2C{:}CH_2$ see reference 7, for $Cl_2C{:}CH_2$ see reference 14, and for $Br_2C{:}CH_2$ see reference 15.
[b] Present results from infrared spectrum of vapor.
[c] The symbols used to refer to stretchings, planar deformations or scissors motions, planar rockings, nonplanar bendings or waggings, and the torsion or twisting are, respectively: ν CC, CX, CY (X or Y=H, F, Cl, Br), δ CXY, ρ CXY, β CXY, and τ. It need hardly be emphasized again that these convenient, conventional characterizations of the various modes are usually only approximate and should not be taken too literally.
[d] From Raman spectrum of vapor.
[e] From infrared spectrum of vapor.
[f] From Raman spectrum of liquid.
[g] Corrected for Fermi resonance shift.

from the small value of the defect $\Delta=I_C-(I_A+I_B)=0.317\times10^{-40}$ g cm^2. Without additional data or assumptions the details of the configuration and dimensions cannot be fixed. However, if the structural details found by Karle and Karle for $F_2C{:}CF_2$,[12] $F_2C{:}CH_2$,[12] and $Cl_2C{:}CCl_2$[13] are considered, it is possible to estimate a set of distances and angles which are quite plausible for $FClC{:}CH_2$ and which satisfy very well the conditions imposed by the microwave results. We have assumed strict planarity, and that the CC, CF, CCl, CH distances and the CCF, CCCl, CCH angles are 1.31 A, 1.32 A, 1.734 A, 1.07 A, and 124.4°, 123°, 121°, respectively. This set of assumptions leads to the following rotational constants, A, B, and C in Mc/sec): 10 680.89, 5092.86, 3448.53 for the Cl^{35} species, and 10 680.87, 4945.40, 3380.28 for the heavier isotope. The corresponding results obtained from the microwave data with the assumption of planarity are 10 681.62, 5092.36, 3448.38, and 10 681.33, 4945.75, 3380.49, respectively. The principal axis of the least moment of inertia lies very nearly along the CCl bond, and passes through the Cl atom, for either isotopic species.

Since $FClC{:}CH_2$ has no symmetry elements other than its molecular plane it belongs to the point group C_s, and its 12 fundamental vibrations include 9 planar a' and 3 nonplanar a'' modes. All 12 fundamentals are permitted to appear in both infrared and Raman spectra, the a' ones giving hybrid infrared bands with compound type A to type B envelopes, and polarized Raman lines. The 3 a'' modes give type C bands and depolarized Raman lines.

The location of each of the fundamentals is predictable from a careful examination and correlation of the spectra and assignments for $F_2C{:}CH_2$,[7] $Cl_2C{:}CH_2$,[14] and $Br_2C{:}CH_2$.[15] The results for $FClC{:}CH_2$ as well as the earlier data for the other vinylidene compounds are discussed in the next section and summarized in Table II.

ASSIGNMENT OF FUNDAMENTALS

The strong band whose center occurs near 1656 cm^{-1} is certainly to be associated with the CC stretching motion. Torkington and Thompson[8] observed that the CC stretching frequency of a fluorinated ethylene may be characterized by its dependence on the number of F atoms attached to the C atoms, and that it is relatively independent of the nature of the other substituents. Thus the CC stretching mode occurs at about 1650 cm^{-1} for $FHC{:}CH_2$, 1645 cm^{-1} for $FClC{:}CCl_2$, and 1656 cm^{-1} for the present compound.

It is well known that the CH_2 planar deformation or scissors mode occurs characteristically in a variety of ethylenic molecules near 1400 cm^{-1}. In $F_2C{:}CH_2$, $Cl_2C{:}CH_2$, and $Br_2C{:}CH_2$ this fundamental is located at 1414, 1391, and 1379 cm^{-1}. The corresponding a' band of $FClC{:}CH_2$ is found at 1383 cm^{-1}. The expected strong infrared band in the vicinity of 1200 cm^{-1} and which presumably arises largely from CF stretching motion is actually found at 1186 cm^{-1}. The next lower a' fundamental may be directly assigned to the doublet band at 947 cm^{-1}. The weaker but clearly resolved band at 1028 cm^{-1} is explained as 2×515.

The highest out-of-plane wagging mode is certainly to be associated with the strong type C band at 836 cm^{-1}. Attention has already been drawn to the prominent so-called secondary Q branch at 824 cm^{-1} on its

[12] I. L. Karle and J. Karle, J. Chem. Phys. **18**, 963 (1950).
[13] I. L. Karle and J. Karle, J. Chem. Phys. **20**, 63 (1952).
[14] P. Joyner and G. Glockler, J. Chem. Phys. **20**, 302 (1952).
[15] de Hemptinne, Velghe, and van Riet, Bull. Class. Sci. Acad. Roy. Belg. **30**, 40 (1944).

TABLE III. Thermodynamic functions in dimensionless units for $FClC:CH_2$ in the ideal gas state.

$T°K$	$C_p°/R$	$(H°-E_0°)/RT$	$-(F°-E_0°)/RT$	$S°/R$
200	5.975	4.552	26.79	31.34
273.16	7.310	5.115	28.29	33.41
298.16	7.724	5.317	28.75	34.07
300	7.754	5.332	28.78	34.11
400	9.170	6.122	30.43	36.55
500	10.26	6.845	31.87	38.72
600	11.10	7.486	33.18	40.66
700	11.77	8.052	34.38	42.43
800	12.31	8.551	35.48	44.03
900	12.77	8.995	36.52	45.51
1000	13.15	9.392	37.49	46.88
1100	13.48	9.749	38.40	48.15
1200	13.76	10.07	39.26	49.33
1300	14.00	10.36	40.08	50.44
1400	14.20	10.63	40.86	51.49
1500	14.38	10.87	41.60	52.47

P wing. The remaining 2 nonplanar modes may be assigned without difficulty to the clearly defined perpendicular bands at 607 and 515 cm^{-1}. In common with several other fluorinated ethylenes the 1st overtones of the wagging fundamentals are fairly prominent in the infrared spectrum. Indeed, in certain instances the upper level exceeds its parent in intensity, as is the case for the lower wagging mode of $F_2C:CH_2$. The explanation of the well-resolved band at 1030 cm^{-1} in Fig. 1 as 2×515 has already been given. The overtone of 836 cm^{-1}, which would be expected near 1872 cm^{-1}, is probably largely obscured and somewhat shifted by the very strong CC stretching fundamental at 1656 cm^{-1}. The side band at 1695 cm^{-1} could well be 2×836, shifted by Fermi resonance with the adjacent fundamental.

Inspection of Table II indicates the plausibility of assigning the band at 699 cm^{-1} to the CCl stretching fundamental. Equally good correlations exist which suggest the assignment of the a' bands at 432 and 371 cm^{-1} to the remaining 2 planar angular modes. Although the lower of these bands seems especially weak there is no doubt of its reality and little question about its assignment.

Almost all of the bands in the region below the CH stretchings that remain unassigned can be accounted for in terms of the 8 planar and 3 nonplanar fundamentals already given. In a number of cases ternary combinations are invoked but it is to be noted that most of them have at least one binary component of appreciable infrared intensity. The few very faint bands for which no reasonable explanation is apparent probably result from impurities.

The symmetric and antisymmetric CH stretchings of $F_2C:CH_2$ are known to occur as infrared bands of medium intensity at 3060 and 3103 cm^{-1}, respectively. Likewise, those of $Cl_2C:CH_2$ fall at 3035 and 3130 cm^{-1}, and those of $Br_2C:CH_2$ at 3023 and 3108 cm^{-1}, respectively. From Fig. 1 it is clear that only the band system in the neighborhood of 3050 cm^{-1} can be ascribed to the CH stretching fundamentals. The band at 2837 is certainly too low, while that at 3291 is obviously too high. Moreover, the absorption near 3155 may be discounted as being due to a fundamental on the basis of its low intensity. The prominent doublet at 3069 may be taken as one of the CH fundamental bands, while the weaker branches near 3016 cm^{-1} are ascribed to the other CH mode. The present spectra do not permit the more precise location of these fundamentals, and it may be expected that the Raman spectrum would be more helpful in this respect. Nevertheless, it seems reasonably certain that the location of the 2 CH stretching fundamentals cannot be in error by more than 10 or 15 cm^{-1}.

The final assignment for $H_2C:CFCl$ is compared in Table II, with the results for $H_2C:CF_2$, $H_2C:CCl_2$, and $H_2C:CBr_2$.†

THERMODYNAMIC FUNCTIONS

The bond distances, interbond angles, and point-group symmetry of $FClC:CH_2$ have been discussed in a previous section. The principal moments of inertia for the Cl^{35} and Cl^{37} isotopic species are, in units of 10^{-40} g cm^2 and with the assumption of strict planarity, 78.564, 164.768, 243.332, and 78.565, 169.681, 248.245, respectively. For the actual calculations, however, the translational and rotational contributions to the entropy and free energy functions were obtained from averaged values based on the natural abundance ratio for Cl^{35} to Cl^{37}. The final expression used for $[S°/R]_{T,R}$ is $9.4342+9.2103\log T$. The wave numbers used are given in Table II. The thermodynamic functions, to the usual rigid rotator, harmonic oscillator approximation, were computed for the ideal gaseous state with the National Bureau of Standards' electronic digital computer, the SEAC. An abridged version of the results is presented in Table III.

ACKNOWLEDGMENTS

The authors are grateful to the M. W. Kellogg Company for providing the sample of $FClC:CH_2$.

† Correlation similar to those used in the present work in connection with $FClC:CH_2$ may be used to predict with some assurance the fundamentals of $ClBrC:CH_2$. We place the planar modes near 3120, 3030, 1610, 1390, 1085, 750, 550, 350, and 250 cm^{-1}, and the nonplanar modes near 880, 680, and 440 cm^{-1}.

Infrared and Raman Spectra of Dicyanoacetylene. II

FOIL A. MILLER, ROY B. HANNAN, JR.,* AND LAUREN R. COUSINS
Department of Research in Chemical Physics, Mellon Institute, Pittsburgh 13, Pennsylvania

(Received Februrary 17, 1955)

The infrared spectrum of dicyanoacetylene has been extended downward to 320 K, and one more combination tone located. Fifteen Raman frequencies have now been observed in place of the four reported earlier, allowing the vibrational assignments to be revised and extended. All but one of the fundamentals have now been observed directly, and that one (107 K) is well established from combination tones. The totally symmetric fundamentals have been reassigned to 2290, 2119, and 692 K.

AN earlier paper on this subject by two of the authors[1] (hereafter referred to as I) describes the spectra and gives an assignment of the frequencies of dicyanoacetylene, $N\equiv C-C\equiv C-C\equiv N$. This paper presents some new data, and confirms or alters several of the earlier assignments. The present assignments are summarized in Table I. The notation is the same as in I, except that the symbol K (for kayser) is used everywhere in place of cm^{-1}.[2]

INFRARED SPECTRUM

Portions of the infrared spectrum of the vapor have been reexamined with a Perkin-Elmer Model 112 double-pass spectrometer. A small sample of dicyanoacetylene was prepared especially for this purpose. It was not purified because of its small volume, but fortunately the few impurity bands could be readily identified by comparison with the earlier work.

A CsBr prism was used to extend the spectrum from 420 to 320K. There are two infrared-active binary combination tones which are calculated to come in this range. Both involve the 107K fundamental (ν_9): $\nu_7+\nu_9=370$ and $\nu_6-\nu_9=397$K. There was no indication of a band near 370K, but a band of medium intensity was found at 398K (see Fig. 1). The parallel structure was resolved, the P to R spacing being 8.3K. Because it is a difference tone, it provides further confirmation for the value of 107K for ν_9.

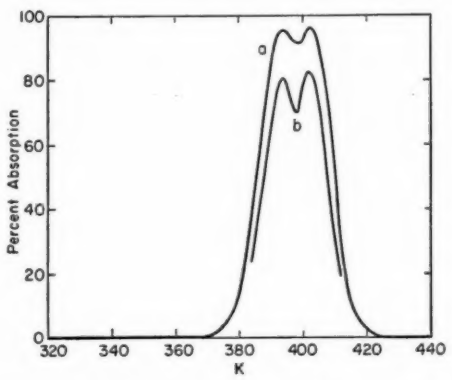

FIG. 1. Portion of the infrared spectrum of dicyanoacetylene. Cell length = 100 cm, a = 90 mm, b = 45 mm pressure.

A portion of the spectrum was also re-examined with the CaF_2 prism, and slightly different frequencies were obtained for some of the bands. All the new infrared observations are given in Table II. The new frequencies are more accurate because of the greater dispersion available. In several cases they improve the agreement with the calculated assignments. The bands reported in I at 3007 and 2978K were not found, and apparently were due to impurities in I. On the other hand, the band at 2850K is decidedly more intense in this sample than in I, and is therefore at least partly the result of an impurity. The weak fundamental at 2241K was overlaid by another impurity band so that it was difficult to measure accurately.

RAMAN SPECTRUM

The Raman spectrum in I was incomplete. The small volume of sample then available (2 ml) produced a weak spectrum, and the use of an inferior grating gave rise to a very bothersome background consisting of a multitude of fine lines. Both of these objections have been overcome. One of the new Bausch and Lomb transfer gratings is now employed, having a ruled area 5 in. high by 6 in. wide, 600 lines/mm, and blazed for 4700 A in the first order. Its performance is excellent. There is complete freedom from the fine-line ghosts mentioned previously, and with a clean sample Raman shifts as low as 100K can be observed. We have remeasured the spectrum of a 7-ml sample of dicyanoacetylene, and have found 15 Raman frequencies in place of the four reported earlier. These are tabulated,

TABLE I. Summary of the fundamental frequencies for dicyanoacetylene.

Species	Activity	Notation	Frequency, K	Description
Σ_g^+	R, p	ν_1	[~2290][a]	C≡N stretch
		ν_2	2119	C≡C stretch
		ν_3	692	C−C stretch
Σ_u^+	i.r.(∥)	ν_4	2241	C≡N stretch
		ν_5	1154	C−C stretch
Π_g	R, dp	ν_6	504	Bending
		ν_7	263	Bending
Π_u	i.r.(⊥)	ν_8	472	Bending
		ν_9	[107][b]	Bending

[a] Estimated from the 2267–2333 resonance pair (see text).
[b] Calculated from combination tones (see I).

* Present address: Research Laboratories, Standard Oil Company of Indiana, Whiting, Indiana.

[1] F. A. Miller and R. B. Hannan, Jr., J. Chem. Phys. **21**, 110 (1953).

[2] Recommendation of the Joint Commission for Spectroscopy, J. Opt. Soc. Am. **43**, 410 (1953).

TABLE II. Frequencies of some of the infrared bands of dicyanoacetylene vapor (in K).

From I	This work	I	Assignment[a]
3276	3278	w	2119+1154=3273
3007	...	vw	Impurity
2978	...	vw	Impurity
2858	2850	vw	Impurity, or 2119+730=2849
2808	2803	w	2333+472=2805
2735	2738	w	2267+472=2739 2119+612=2731
2591	2590	w	2119+472=2591
2505	2500	w	2241+263=2504
2442	2435	w	2333+[107]=2440
2375	2369	w	2267+[107]=2374
2241	~2238	w	ν_4
2226	2226	w	2333−[107]=2226 2119+[107]=2226
2162	2157	w	2267−[107]=2160
	402.1 (max) 398.2 (min) 393.8 (max)	m	504−[107]=397

[a] See Table I for the fundamentals. They are not the same as in I.

together with our assignments, in Table III. Exposure times up to one hour were used. The sample became distinctly yellow in three hours, even though it was distilled and sealed in the Raman tube under vacuum. Polarization measurements were not made because of this complication.

ASSIGNMENT OF THE RAMAN FREQUENCIES

ν_7, ν_9, and ν_3

In the earlier work there were three frequencies which were not observed directly. ν_7, a Raman-active bending frequency, was estimated from combination tones to be at 260K. It has now been observed at 263K. ν_9, an infrared-active bending vibration estimated quite certainly to be at 107K, is still unobserved. However it is used once more to explain a Raman-active combination tone (2137K), and 263K is used twice, so their assignments are even more firmly established.

The third frequency, ν_3, belongs to the Raman-active C−C stretching mode. No value whatever could be deduced for this from the earlier data. We feel now that it is responsible for the medium intensity line at 692K. There are, in fact, only three possibilities for ν_3 among the observed Raman lines: 1018, 759, and 692K. 692 is the most intense of these. It has a very weak counterpart in the infrared spectrum of the liquid at 693 which is missing in the vapor. It cannot be explained as a combination tone, whereas 759 can be attributed to 504+263=767. Also a normal coordinate calculation demands a low frequency. 1018 is completely unacceptable on this basis, but 692 appears reasonable. Although 692 seems surprisingly low for a C−C stretching frequency, the antisymmetric C−C stretching at 1154 seems correspondingly high. Their average is 928, which is a reasonable value for this bond. Presumably this is an example of resonance occurring between the two single-bond vibrations because of the mechanical coupling provided by the connecting triple bond. As a result the energy levels "repel" one another, resulting in one being abnormally high and the other abnormally low.[3] A similar case of two C−C single bonds being coupled by a triple bond occurs in dimethylacetylene, and the corresponding frequencies for it are astonishingly close to those for dicyanoacetylene:

Dicyanoacetylene 692, 1154K
Dimethylacetylene[4] 693, 1152K.

This provides additional support for the choice of 692 as ν_3.

Triple-Bond Stretching Frequencies

It appears now that the assignment of the high Raman frequencies in I needs modification. The line at 2119K, which was originally reported as very weak, is now judged to be of medium intensity. We attribute it to ν_2 rather than to a ternary combination as before. Dr. S. R. Polo[5] has very kindly pointed out that combinations of 2119K with the strong infrared bands agree with other observed infrared bands. The three

Raman		i.r.		i.r.(calc)	i.r.(obs)
2119	+	[107]	=	2226	2226
2119	+	472	=	2591	2590
2119	+	612	=	2731	2738
2119	+	730	=	2849	2850
2119	+	1154	=	3273	3278

cases that are underlined are distinct improvements over the explanations in I. The very intense Raman pair at 2267 and 2333K would then be interpreted as due to Fermi resonance between $2\nu_5$ and ν_1. Their average is 2300, whereas $2\nu_5$ is 2308. The unperturbed ν_1 would therefore have been about 2290K. This is supported by the observation that 2267K is somewhat more intense than 2333K. It is quite reasonable to find strong interaction between ν_1 and $2\nu_5$. The symmetry and frequency requirements are fulfilled, of course. Also, because ν_5 is a stretching mode of the two C−C single bonds and ν_1 is the stretching mode of the triple bond that links them, it is not surprising that the mechanical coupling between ν_1 and $2\nu_5$ is relatively strong.

There are several additional advantages to this interpretation. In the first place, 2267 and 2333K seem too close together to be fundamentals of the same species, especially since both would be due to stretching modes which would be expected to interact strongly. Secondly, this assignment agrees more nearly with what one would expect from characteristic frequencies.

[3] G. Herzberg, *Infrared and Raman Spectra of Polyatomic Molecules* (D. Van Nostrand Company, Inc., New York, 1945), p. 196.

[4] I. M. Mills and H. W. Thompson, Proc. Roy. Soc. (London) **A226**, 306 (1954).

[5] Private communication from Dr. Santiago R. Polo, Harvard University.

The unconjugated C≡C stretch usually occurs at 2260–2200K and the unconjugated C≡N stretch near 2250K.[6,7] When three such groups are conjugated in a molecule their stretching motions will interact in a manner that will be difficult to predict if the force constants are not known. However it would be surprising if both ν_1 and ν_2 were higher than these characteristic values. The choice of [2290] and 2119K (where one is higher and one lower than the frequencies of the isolated groups) is more reasonable. Thirdly, if the wave functions for the levels 2267 and 2333K have been mixed by Fermi interaction, both frequencies would be expected to give rise to analogous combination tones. This is found to be the case. Both appear as (and only as) $\nu+\nu_9$, $\nu-\nu_9$, and $\nu+\nu_8$ in the infrared (see Table II). Conversely, this is slight evidence that the wave functions have been mixed—that there has been Fermi interaction. Finally somewhat more reasonable values of the stretching-force constants are obtained if the newer assignment is used.

There is a serious obstacle to this explanation of 2267–2333K as a resonance pair, however, and that is the presence of a very weak line between them at 2309K. The only explanation for this that has been found is $2\nu_5=2308$. It is indeed difficult to explain how $2\nu_5$ can be observed at its calculated position and still be participating in the resonance.† This is an objection which we have not been able to overcome without postulating that 2309K is the result of an impurity. In spite of it, the weight of evidence seems to be in favor of the proposed new assignments, and they are adopted.

TABLE III. Raman spectrum of dicyanoacetylene.

K	Intensity	Excitation[a]	Assignment
2886	vw	e	?
2333	vs	e	ν_1[b]
2309	vw	e	2×1154=2308?
2267	vs	e,f,g	ν_1[b]
2137	w	e	2241−[107]=2134
2119	m	e	ν_2
2070	vw	e	2333−263=2070
2023	vvw Real?	e	?
1018	vw	e	263+759=1022
759	w	e	263+504=767
692	m	e	ν_3
618	vw, diffuse	e	?
570	w	e	472+[107]=579. k−2337=570(?)
504	vs	e,f	ν_6
263	w	e	ν_7

[a] e=Hg 4358 A, f=4347 A, g=4339 A, k=4047 A.
[b] 2333 and 2267 are a resonance pair.

Assignment of the Remaining Raman Lines

All but four of the remaining frequencies can be reasonably accounted for, as shown in Table III. The exceptions are 618, 1018, 2023, and 2886K, for which no satisfactory explanation has been found. All of them are very weak and could be due to an impurity. Frequency 618 may be a counterpart of the strong infrared band at 624K in the liquid (612 in the vapor) appearing in violation of selection rules. This would be the only case of such violation in this Raman spectrum. 1018K can be explained as a ternary combination as shown, but ternary combinations are unlikely in the Raman effect.

This concludes the assignments. They are all quite certain, except for the three in the totally symmetric species. Polarization measurements on the Raman lines might be of help in assigning 692K, but probably will not aid with 2119, 2267, or 2333K, since these latter three are totally symmetric in the assignments of either this paper or of I.

[6] W. Otting, *Der Raman Effekt* (Springer-Verlag, Berlin, Germany, 1952), pp. 45–46.
[7] L. J. Bellamy, *Infrared Spectra of Complex Molecules* (John Wiley and Sons, Inc., New York, 1954), pp. 50, 223.

† The authors do not know of any reason why a portion of the intensity would remain at 2308K if resonance actually does occur. If $2\nu_5$ had several sublevels, one of which had a symmetry other than Σ_g^+, that one level would not interact (see reference 3, p. 217). This is not the case, however, since ν_5 is not degenerate. Neither does it help to attribute 2308 to ν_1 of an isotopic molecule having one or more C^{13} or N^{15} atoms. (Approximately 5% of the molecules have one heavier isotopic atom.) Ordinarily the lines due to these isotopic molecules are not seen because they are close to the lines of the light molecule and are much weaker. In this special case the line of the light molecule is presumed to have been moved aside by the resonance. In order to explain why the line of the isotopic molecule is not similarly shifted, it is necessary to assume that the resonance is much less effective in the isotopic molecule (of symmetry $C_{\infty v}$). This requires in effect that ν_5 and/or ν_1 must be considerably different in the two molecules, which seems unlikely. Another difficulty with this is that 2308 is appreciably higher than the estimated position of unperturbed ν_1(~2290), whereas for a heavier isotopic molecule it should be lower.

THE JOURNAL OF CHEMICAL PHYSICS VOLUME 23, NUMBER 11 NOVEMBER, 1955

Nature of the Hydrogen Bond. II. The Effect of Hydrogen Bonding and Other Solute-Solvent Interactions upon the Shape and Intensity of the Infrared OH Band of Phenol

HIROSHI TSUBOMURA
Tokyo Institute of Technology, Oh-okayama, Meguroku, Tokyo, Japan
(Received February 8, 1955)

The hydrogen-bonded OH bands of phenol are studied in ternary systems, each of which is composed of phenol, a proton acceptor, and a solvent. The acceptors used are ethyl ether, ethyl acetate, acetonitrile, and hexamethylene tetramine. It is confirmed that the frequency, shape, and molecular extinction coefficient of the band are not changed by the concentration of the acceptor, as far as the latter is smaller than *ca* 2 mole/liter. The spectra are slightly modified by further increase of the concentration of the acceptor. These modifications are in all cases far smaller than the modification due to the hydrogen bonding, and the peak intensities remain nearly constant. The equilibrium constants for the formation of the hydrogen bond are determined for all acceptors and the heat of formation is determined for the case of hexamethylene tetramine. It is found that the decrease of frequencies of the hydrogen-bonded OH bands is not strictly parallel to the increase of equilibrium constants.

EXTENSIVE studies have been made on the change of the infrared OH and NH bands due to the hydrogen bonding. Until now, however, only few quantitative measurements of the change of integrated intensities have been made. S. A. Francis[1] reports that the integrated intensity of the bonded OH band of *n*-propyl alcohol is about ten times larger than that of the free one. Coggeshall[2] calculated the ratio of the squares of the matrix elements of dipole moment for the hydrogen-bonded and free OH bands of alcohols by the use of the point-charge model. The calculated value of 1.16 contradicts seriously the observed one, indicating that the marked increase of intensity cannot be explained by such a simple model.

In the first paper of this series,[3] the author has calculated the contribution of the charge-transfer energy (the delocalization energy, in other words) to the hydrogen bonding between water molecules and proposed an idea that, for the energy of the hydrogen bond, this charge-transfer energy is of nearly the same importance as the electrostatic one. Here the charge transfer means the partial electron transfer from the lone-pair orbital of the proton-acceptor to the OH orbital of the proton-donor, or, in other words, the contribution of the dative-bond resonance structure such as $(X-O^{-}H-Y^{+})$ to the ground state of the two hydrogen-bonded molecules $(X-O-H\cdots Y)$. Now, it may be supposed that this charge transfer plays an important role in increasing the intensity, since it can produce an oscillating electric dipole of the same frequency as that of the vibration of the proton. At the present stage, however, more experimental knowledge is necessary to make further analyses of this problem.

The intensity of the bonded OH band can be measured with the ternary system composed of a proton-donor, a proton-acceptor, and a solvent. In this system, the concentration of the proton-donor must be so small that the association of donors are negligible. In a dilute solution, one can expect that Beer's law for the bonded OH band holds. But even if the concentration of the donor is very small, it is somewhat ambiguous whether or not Beer's law holds for a wide range of the concentration of the acceptor, say 0.01 to 5 mole/liter. For it seems probable that, in solutions containing large amount of the acceptor, the electrostatic force exerted by the acceptors which surround the donor-acceptor complex modifies the OH band. Therefore, it was thought necessary to ascertain these points before proceeding to our original aim. For this end, and also for the purpose of obtaining some thermochemical data concerning the hydrogen bonds in solutions, the intensities of the OH bands of the ternary systems composed of phenol and some proton-acceptors in a variety of the concentrations have been measured.

EXPERIMENTAL

Throughout this work, measurements were made by the Perkin Elmer Model 112 infrared spectrophotometer equipped with a lithium fluoride prism. The slit width used ranged from 0.07 to 0.1 mm, and were kept constant for each sequence of dilution. A 0.5-mm fixed cell with potassium bromide windows and a 10-mm quartz cell were used. The thickness of the former was measured by the interference method.[4] For each measurement of the ternary system, a background trace of the corresponding blank solution (the solution that contained the same concentration of the acceptor) was run so that it was superimposed. The point by point measurement of the absorbance a, that is, $\log_{10} I_0/I$, was made from the chart. The curve of a *versus* wave numbers was plotted and the half-width of the band was measured from it.

The compounds used as proton-acceptors were ethyl ether, ethyl acetate, acetonitrile, and hexamethylene tetramine. Carbon tetrachloride and *n*-heptane were

[1] S. A. Francis, J. Chem. Phys. **19**, 505 (1951).
[2] N. D. Coggeshall, J. Chem. Phys. **18**, 978 (1950).
[3] H. Tsubomura, Bull. Chem. Soc. Japan **27**, 445 (1954).
[4] G. B. B. M. Sutherland and H. A. Willis, Trans. Faraday Soc. **41**, 181 (1945).

used as solvents. All materials used in this work were purified by either fractional distillation or recrystallization, and carefully dried.

The determination of the molecular extinction coefficients* of the bonded OH bands can be made by the use of ternary solutions which contain relatively large amount of the acceptor. In a ternary system, the following equilibrium formula may be applied:

$$K=\frac{C_x}{(C_p^0-C_x)\cdot(C_a^0-C_x)}, \quad (1)$$

where C_p^0, C_a^0, and C_x are the concentrations of total proton-donor, total proton-acceptor, and hydrogen-bond complex, respectively. Usually, the equilibrium constants range from 10 to 20 (mole/liter)$^{-1}$. Hence, when C_a^0 is, for example, about 2 mole/liter and K is 10, it can be hoped from Eq. (1) that *ca* 95% of the donor are hydrogen bonded.† This is confirmed qualitatively by the extreme weakness of the free OH band in such solutions. Therefore, if one assumes $C_x=C_p^0$ in such solutions, the error is the order of 5%. And, of course, more accurate results may be obtained if one

TABLE I. Results for the OH band of the phenol-ethyl ether system. C_p^0: 0.0324 mole/l. Cell: 0.503 mm. Solvent: *n*-heptane. 30°C.

No. of solution	C_a^0 (mole/l)	ν_{max} (cm^{-1})	Half-width (cm^{-1})	a_{max}	ϵ_{max}	K
1	4.840	3354	134	0.312	194	···
2	2.420	3359	116	0.304	191	···
3	1.210	3360	115	0.299	191	···
4	0.0980	3364	114	0.139	···	9.4
5	0.0490	3361	···	0.088	···	9.8

corrects the C_x's by use of Eq. (1) and appropriately assumed K values.

After the peak molecular extinction coefficients ϵ_{max} were calculated in this way, the concentrations of the bonded phenol in solutions in which the acceptor was very dilute were calculated by the formula $C_x=a_{max}^0/\epsilon_{max}$, where a_{max}^0 is the absorbance at the peak per unit thickness of the solution, and from the values thus obtained the equilibrium constants were calculated.

In the case of using hexamethylene tetramine as an acceptor, the above described method cannot be applied because of the very little solubility of this compound in nonpolar solvents. In this case, therefore, the molecular extinction coefficient and the equilibrium constant were calculated directly from the measurement of the isothermal dilution change: When there are two solutions which contain the same concentration of phenol (C_p^0) and different concentrations of acceptor (C_a^0 and $C_a^{0\prime}$, respectively), then from Eq. (1) we can derive the following equation:

$$(x-x^2)C_x^2-x(C_a^0-C_a^{0\prime})C_x+C_p^0(x\cdot C_a^0-C_a^{0\prime})=0. \quad (2)$$

Here, C_x is the concentration of the bonded phenol in the solution in which the concentration of the acceptor is C_a^0, and x is a value defined by the formula, $x=C_x'/C_x$, where C_x' is the concentration of the bonded phenol in another solution. For dilute solutions, this ratio may be regarded to be equal to the ratio of the absorbances at a certain wave number for the two solutions. Solving (2), we can obtain C_x and from it the K and ϵ can be calculated.

When *n*-heptane is used as a solvent, the CH absorption makes it difficult to use thick cells. For this reason, about 0.03 mole/liter was chosen for the most convenient concentration of phenol, though it was desirable to use more dilute solutions in order to avoid the phenol-phenol association completely. For the present measurements, however, the error that arises from the association is of the same order of magnitude of the error due to the instrument.

TABLE II. Results for the OH band of the phenol-ethyl acetate system. Cell: 0.503 mm. Solvent: *n*-heptane. 30°C.

No. of solution	C_p^0 (mole/l)	C_a^0 (mole/l)	ν_{max} (cm^{-1})	Half-width (cm^{-1})	a_{max}	K
1	0.03290	1.024	3468	171	0.217	(ϵ_{max}=145)
2	0.03283	0.1698	3462	158	0.163	17.2
3	0.03283	0.0849	3460	162	0.123	17.4
4	0.03283	0.0424	3460	···	0.081	18.0

EXPERIMENTAL RESULTS

The numerical results are tabulated in Tables I–VI. In these tables a_{max} and ν_{max} are the absorbance and wave number at the band maximum. The ϵ_{max}'s given in Tables I, II, and III are the values calculated from the results of measurements for the solutions containing large amount of acceptor and from the concentrations of the bonded phenol corrected by use of Eq. (1), and K is the value calculated by these ϵ_{max}'s.

As for the case of hexamethylene tetramine, the measurements of the absorbances were made at three different temperatures in order to obtain the heat of formation. In Table IV, the results of the measurement are tabulated. Using Eq. (2), K and ϵ were calculated

TABLE III. Results for the OH band of the phenol-acetonitrile system. Cell: 0.503 mm. Solvent: *n*-heptane. 30°C.

No. of solution	C_p^0 (mole/l)	C_a^0 (mole/l)	ν_{max} (cm^{-1})	Half-width (cm^{-1})	a_{max}	K
1[a]	0.0316	···	3410	160	0.286	(ϵ_{max}=180)
2	0.0324	0.1865	3478	76	0.180	9.4
3	0.0324	0.1243	3478	80	0.149	9.5
4	0.0324	0.0932	3478	74	0.123	9.1

[a] The solution 1 is the acetonitrile solution of phenol.

* A molecular extinction coefficient, ϵ, is defined by the following formula: $\epsilon=a/$(cell thickness in cm)·(concentration in mole/liter).

† Of course, in order that Eq. (1) strictly holds, one must use activities rather than concentrations. In dilute solutions, however, the former may be considered to be equal to the latter. Even for solutions in which the concentration of the solute is of the order of 2 mole/liter, this assumption will not give serious errors.

TABLE IV. Results for the intensity of the OH band of the phenol-hexamethylene tetramine system. C_p^0: 0.00523 mole/l. Cell: 10.00 mm. Solvent: Carbon tetrachloride.

No. of solution	C_a^0 (mole/l)	a (at 3093 cm^{-1}) 27°C	40°C	50°C
1	0.0335	0.494	0.421	0.383
2	0.0251	0.452	0.369	0.313
3	0.01675	0.382	0.303	0.240
4	0.00838	0.262	0.203	0.175

from the experimental data of some pairs of solutions. The results for 27°C are shown in Table V. The ϵ's and K's are in good agreement. However, we could not obtain constant ϵ's and K's for higher temperatures. Hence, assuming that ϵ is unchanged with temperature, the C_x's for all solutions and temperatures were calculated again by the use of the averaged value of ϵ at 27°C. The K values calculated from these C_x's are shown in Table VI. It is a matter of course that constant K's are obtained for 27°C. But the K values for higher temperatures are also in endurably good agreement.

Using the averaged values of K's thus obtained, $R\ln K$ is plotted against the inverse of the absolute temperature. The points lie on a straight line and, as is usually done, from its tangent and its intersection with the ordinate axis, the heat of formation, ΔH, and the change of entropy, ΔS, for the hydrogen bond are obtained as follows: $\Delta H = -6.9$ kcal/mole, $\Delta S = -13.6$ cal/deg mole. As is expected, the absolute value of ΔH obtained is considerably greater than those for the hydrogen-bond of phenol with ethers or esters. But the entropy change is nearly the same in all cases (*ca* − 13 cal/deg mole).[5]

From the results of Table V and the complete absorption curve of the bonded OH band of this system, following results are obtained: $\nu_{max} = 3070$ cm^{-1}, $\epsilon_{max} = 140$, and the half-width = 310 cm^{-1}.

DISCUSSIONS

The results tabulated in Table I indicate that the frequency and the half-width of the bonded OH band for the phenol-ether system are practically unaltered by the concentration of the acceptor as far as it is less than *ca* 2 mole/liter. For the solution in which C_a^0 is 4.8 mole/liter, the band shifts towards longer wavelength and increases in half-width. Such changes are, however, considerably smaller than the change caused by the hydrogen bonding. It is considered that the electrostatic field of the acceptor molecules which surround the donor-acceptor complex is the main cause, although other solvent-solute interactions (van der Waals force, for instance,) are superimposed on it.

TABLE V. Calculated K and ϵ for the phenol-hexamethylene tetramine system at 27°C.

	K	ϵ (at 3093 cm^{-1})
From solutions 2 and 4	112	126
1 and 4	113	123
3 and 4	119	118
	Average: 122	

[5] S. Nagakura, J. Chem. Soc. Japan **74**, 153 (1953).

For the phenol-acetonitrile system, we notice that the frequency and the half-width for the first solution in Table III are considerably different from those of the other solutions. This solution is an acetonitrile solution of phenol,‡ and the cause of the modification of the spectrum will be the same as that described in the case of the phenol-ethyl ether system. The large difference between the first solution and others may be due in part to the fact that the first solution does not contain any quantity of the nonpolar solvent. But, even if this is taken into account, the difference is so large that it can be concluded that the effect of the acetonitrile molecules which are outside the hydrogen-bond complex upon the OH vibration is greater than that of ethyl ether molecules. This conclusion seems to be consistent with the fact that the former is much more polar and smaller in size than the latter.

As is indicated in Table II, the frequency and the half-width for the OH bands of the phenol-ethyl acetate system are also unchanged as far as C_a^0 is less than 1 mole/liter. Owing to the absorption of ethyl acetate, it is difficult to examine the OH band for solutions in which C_a^0 is larger than this value.

TABLE VI. Calculated K values for the phenol-hexamethylene tetramine system for various temperatures and concentrations.

No. of solution	27°C	40°C	50°C
1	116	69	55
2	114	65	47
3	110	71	44
4	112	73	58
Average	113	69	51

From these tables we can also see that the K values obtained are practically constant for all cases, showing that the ϵ_{max} remains constant for all concentrations of the acceptor. The agreement of the ϵ_{max}'s of solution 1 and 2 for phenol-ethyl ether system provides another evidence for this conclusion. This constancy of the ϵ_{max} will perhaps be due to the accidental cancellation of the effect of the increase of the transition probability by that of the band-broadening.

The large absolute value of ΔH obtained for hexamethylene tetramine is in agreement with the series of the strengths of acceptors determined by Tsuboi,[6] in which the tertiary amine is regarded as the strongest. This result is very likely to support the idea that the charge transfer makes certain contribution to the hydrogen bonding, since strong bases tend to stabilize the dative bond such as (H—Y$^+$), which was previously described in this paper, and consequently increase the charge transfer energy.

It is widely recognized that the shift of the OH fre-

‡ Acetonitrile is not largely miscible with *n*-heptane.

[6] M. Tsuboi, Kagaku-no-Ryôiki **7**, 611 (1953).

quency due to the hydrogen bond is a measure of its strength. The equilibrium constant is also closely related to the energy of the hydrogen bond. However, it is worthwhile to note that the shift and the equilibrium constant are not strictly parallel to each other for some of the systems studied in the present work.

In later communications, the integrated intensities of the various hydrogen-bonded OH bands will be discussed in detail.

The author would like to acknowledge sincerely the valuable advices given by Professor K. Kozima in the course of this work.

THE JOURNAL OF CHEMICAL PHYSICS VOLUME 23, NUMBER 11 NOVEMBER, 1955

Absolute Thermal Decomposition Rates of Solids. Part II. The Vacuum Sublimation Rate of Molecular Crystals*

ROBERT D. SCHULTZ AND ALBERT O. DEKKER
Aerojet-General Corporation, Azusa, California

(Received February 8, 1955)

The linear rates of sublimation of rhombic benzene and rhombic sulfur have been calculated by use of absolute reaction rate theory in reasonable agreement with rates derived from published experimental data. Required mean torsional oscillation and translational oscillation frequencies for the molecules in the crystal lattice were obtained by an analysis of the available heat capacity and Raman spectral data. A detailed comparison of this treatment with Penner's treatment of the sublimation process is included.

INTRODUCTION

THE thermal decomposition and gasification of a solid involves at least four steps which may in certain cases occur simultaneously. The processes are:

A. Formation of an intermediate complex which is physically adsorbed on the decomposition surface

B. Decomposition of the intermediate complex into products also physically adsorbed on the decomposition surface

C. Desorption or evaporation of one or more of these physically adsorbed products

D. Diffusion of the product through the ambient gas.

Theoretically, it is possible for any one of the above steps to be a rate-controlling process. As part of a systematic study of the mechanism of solid decomposition, this paper is concerned with the rate and mechanism of a reaction in which there is no doubt that the desorption step (C) is rate-controlling, namely, the sublimation of a molecular crystal in a vacuum.

LINEAR RATES OF SUBLIMATION OBTAINED BY EXPERIMENT OR INDIRECTLY BY MEASUREMENT OF THE EVAPORATION COEFFICIENT

The rate of sublimation of rhombic sulfur in a vacuum has been measured by R. S. Bradley.[1] The temperature dependence of the linear rate of regression of the interface was found to correspond to the Arrhenius type of equation

$$B_{\substack{\text{rhombic sulfur}\\ \text{sublimation}}} = 1.1\times10^{10}\exp\left(\frac{-23\,890}{RT}\right) \text{ cm sec}^{-1}, \quad (1)$$

where $288°\text{K} < T < 306°\text{K}$ and $R = 1.99$ cal g-mole^{-1} °K^{-1}. Within experimental accuracy, the activation energy is the same as the enthalpy of sublimation. With the assumption that the same situation holds true for solid benzene, the Arrhenius type of equation for the linear rate of regression of the surface of the rhombic benzene crystal during sublimation is

$$B_{\substack{\text{rhombic benzene}\\ \text{sublimation}}} = 3.9\times10^{8}\exp\left(\frac{-11\,200}{RT}\right) \text{ cm sec}^{-1}, \quad (2)$$

where $T_{\text{average}} = 217°\text{K}$. The following procedure was used to obtain Eq. (2) from available experimental data. The heat of sublimation of solid benzene was calculated as 11.2 kcal g-mole^{-1} from vapor pressure data compiled by Stull.[2] The linear rate of sublimation of benzene in a vacuum was calculated to be 2.41×10^{-3} cm sec^{-1} at 217°K by means of the Knudsen equation, which equates the number of molecules subliming from unit area of the crystal surface per unit time to αn_g, where n_g is the number of gaseous molecules which strike a unit area of the surface per unit time at the equilibrium vapor pressure p_s and where α, the accommodation coefficient, is the fraction of these molecules which undergo condensation. The specific form of the Knudsen equation em-

* This work was supported under Contract AF18(600)1026 by the United States Air Force, through the Office of Scientific Research of the Air Research and Development Command, OSR-TN-54-367.

[1] R. S. Bradley, Proc. Roy. Soc. (London) **A205**, 553–563 (1951).

[2] D. R. Stull, Ind. Eng. Chem. **39**, 517–550 (1947).

TABLE I.

Investigators	Method or theory	Calculated rate equation
Bradley[a]	Experiment	$B_{\text{rhombic sulfur}} = 1.1\times10^{10}\exp\left(-\frac{23\,890}{RT}\right)$ cm sec^{-1}
Frenkel[b]	Simple lattice vibration model	$B = 6\times10^{4}\exp(-E/RT)$ cm sec^{-1}
Herzfeld[c]	Helmholtz free energy of an assembly of three-dimensional oscillators	$B = 1\times10^{7}\exp(-E/RT)$ cm sec^{-1}
Polanyi and Wigner[d] Pelzer[e]	Improvement of Herzfeld treatment	$B = 4.8\times10^{6}\exp(-E/RT)$ cm sec^{-1}

[a] See reference 1.
[b] J. Frenkel, *Kinetic Theory of Liquids* (Clarendon Press, Oxford, 1946), p. 5.
[c] K. F. Herzfeld, *Kinetische Theorie der Wärme* (Vieweg, 1946), p. 233.
[d] M. Polanyi and F. Wigner, Z. physik. Chem. **A139**, 439 (1928).
[e] H. Pelzer, see Volmer, *Kinetik der Phasenbildung* (Steinkopff, Leipzig, 1939), p. 37.

ployed was

$$B=\frac{\alpha}{\rho}\left(\frac{M}{2\pi RT}\right)^{\frac{1}{2}}p_s \text{ cm sec}^{-1}, \qquad (3)$$

where $\alpha=0.622$, the accommodation coefficient measured by Baranaev[3]
$\rho=1.015$ g cm^{-3} = the density of solid benzene
$p_s=1.50\times10^{2}$ dynes cm^{-2}, the equilibrium vapor pressure at 217°K
$M=78.11$ g mole^{-1}, the molecular weight of benzene
$R=8.314\times10^{7}$ erg °K^{-1} mole^{-1}, the gas constant per mole
$T=217$°K.

The pre-exponential factor of Eq. (2) was calculated from the sublimation rate at 217°K using an 11.2 kcal g-mole^{-1} activation energy assumed equal to the heat of sublimation.

PREVIOUS THEORIES OF THE SUBLIMATION MECHANISM: A COMPARISON

Results of sublimation rate calculations for rhombic sulfur based on various published theories have been reported by R. S. Bradley.[1] These results are briefly summarized and compared with the experimental rate in Table I.

It is evident that sublimation rates calculated for a molecular crystal such as rhombic sulfur by the theories listed above are in extremely poor agreement with the experimentally determined rates.

[3] M. K. Baranaev, Chem. Abstracts **40**, 6911 (1946).

ABSOLUTE RATE THEORY FOR THE SUBLIMATION PROCESS

In Part I of this series,[4] the following absolute rate expression was derived for the linear rate of regression of the surface of a solid undergoing thermal decomposition:

$$B=L\frac{kT_s}{h}\frac{F^*}{F}\exp(-E_s/RT_s) \text{ cm sec}^{-1}, \qquad (4)$$

where L is the average thickness of the monomolecular surface layer
k is the Boltzmann constant
T_s is the absolute temperature of the surface
h is Planck's constant
F^* is the partition function for the activated complex in the monomolecular surface layer over all degrees of freedom except the one corresponding to motion along the reaction coordinate
F is the corresponding partition function for the normal state over all degrees of freedom
E_s is activation energy for the surface reaction, cal mole^{-1}
R is the gas constant = 1.99, cal °K^{-1} mole^{-1}.

Equation (4) is an extension and generalization of the hypothesis advanced by Wilfong, Penner, and Daniels[5] for the purpose of explaining the burning rate of double-base propellants, and is based on the Eyring formulation of the transition-state rate theory.[6]

Equation (4) may be applied to the calculation of the absolute sublimation rate of molecular crystals by setting E_s equal to $(\Delta H_{c0}-RT)$, where ΔH_{c0} is the enthalpy of sublimation, so that

$$B_{\text{sublimation}}=eL\frac{kT_s}{h}\frac{F^*}{F}\exp(-\Delta H_{c0}/RT_s) \text{ cm sec}^{-1}. \qquad (5)$$

Penner has derived an equation similar to (5) for calculating the absolute rates of evaporation of liquid compounds.[7] A basic postulate of Penner's treatment for liquids is that the activated complex consists of gas-like molecules which can move freely in a plane of area $v^{*\frac{2}{3}}$, where $v^*=v$ is the volume per molecule in the condensed state. In the present treatment for the solid state, however, the activated complex is regarded as an

[4] R. D. Schultz and A. O. Dekker, "The absolute thermal decomposition rates of solids," Part I: "The hot-plate pyrolysis of ammonium chloride and the hot-wire pyrolysis of polymethyl methacrylate (Plexiglas IA)," to be published in the Fifth International Symposium on Combustion, University of Pittsburgh, Pennsylvania (1954) (Reinhold Publishing Corporation, New York, 1955).
[5] Wilfong, Penner, and Daniels, J. Phys. & Colloid Chem. **54**, 863–872 (1950).
[6] Glasstone, Laidler, and Eyring, *The Theory of Rate Processes* (McGraw-Hill Book Company, Inc., New York, 1941).
[7] S. S. Penner, J. Phys. Chem. **52**, 950 (1948); **52**, 1262 (1948); **56**, 475 (1952).

S_8 or C_6H_6 molecule which is precisely in the act of leaving the surface. It is recognized that the direction of the escape velocity vector may differ from molecule to molecule. For any given molecule, however, the escape velocity vector may be resolved into three mutually perpendicular components, two of which are parallel to the plane of the crystal surface and one of which is perpendicular to this surface. The latter component will be considered to correspond to motion along the reaction coordinate. The components parallel to the crystal surface will be considered as originating from the normal-state lattice vibrations of the center of gravity of the molecule in the plane of the crystal surface. On this assumption, the energies and partition functions of the two components of the escape velocity parallel to the crystal surface will be equated respectively to the energies and partition functions of two vibrational modes of the center of gravity of the molecule in the normal crystal. Moreover, the intramolecular vibrations of the molecule will be virtually unaffected by the transition from the condensed to the vapor state.[8] Thus, Eq. (5) may be simplified by cancellation of equivalent terms in the numerator and denominator to

$$B_{\text{sublimation}}=eL\frac{kT_s}{h}\frac{F_r^*}{f(\nu_\phi)f(\nu_\beta)f(\nu_\gamma)f(\nu_L)}\times\exp(-\Delta H_{c_0}/RT_s)\ \text{cm sec}^{-1}, \quad (6)$$

where

$$F_r^*=\frac{\pi^{\frac{1}{2}}}{\sigma}\frac{(8\pi^2 I_\phi kT)^{\frac{1}{2}}}{h}\frac{8\pi^2 I_{\beta\gamma}kT}{h^2}\Bigg\}\text{rotational partition function for activated state,}$$

σ = symmetry number of gaseous molecule

$f(\nu)$ = a partition function for one vibrational mode. $f(\nu)$ has the conventional form $[1-\exp(-h\nu/kT)]^{-1}$

I_ϕ = moment of inertia of the molecule about the principal axis perpendicular to the plane of the molecule

I_β, I_γ = moments of inertia about a principal axis in the plane of the molecule (for C_6H_6 and S_8, $I_\beta=I_\gamma=I_{\beta\gamma}$)

ν_ϕ = torsional oscillation frequency for normal state about the principal axis perpendicular to the plane of the molecule

ν_β, ν_γ = torsional oscillation frequencies for normal state about the two principal axes in the plane of the molecule (note that for rhombic benzene and rhombic sulfur ν_β does not equal ν_γ because of anisotropy of crystal)

ν_L = lattice vibration frequency for translation oscillation of the center of gravity of the molecule.

[8] Lord, Ahlberg, and Andrews, J. Chem. Phys. **5**, 649–654 (1937).

The following section will be devoted to the evaluation of the frequencies ν_ϕ, ν_β, ν_γ, and ν_L for rhombic benzene and rhombic sulfur on the basis of an analysis of published heat-capacity data and comparison with Raman and far-infrared spectral data.

ESTIMATION OF TRANSLATIONAL AND TORSIONAL OSCILLATION LATTICE FREQUENCIES FROM LOW-TEMPERATURE HEAT-CAPACITY DATA: COMPARISON WITH RAMAN AND FAR-INFRARED SPECTRAL DATA

Since intra-molecular frequencies are comparatively high, the contribution of the corresponding Einstein vibrational terms to the heat of a molecular crystal is usually negligible below about 50°K. The heat capacity below this temperature should depend, therefore, only on the set of $3N$ low-frequency torsional modes of vibration and the set of $3N$ translational modes of vibration. On this assumption, Lord, Ahlberg, and Andrews[8] found that the molar heat capacity of solid benzene in this temperature region could be fitted closely by the single Debye term

$$C_v(C_6H_6)=6Rf_d\frac{\theta_D}{T}, \quad (7)$$

where f_d is the Debye function and $\theta_D=h\nu_m/k=150$°K. The corresponding Debye frequency, $\nu_m(C_6H_6)$, is 104 $\text{cm}^{-1}=3.12\times10^{12}$ sec^{-1}. Equation (7) is based on the assumption that the average torsional oscillation frequency is about equal to the average translational oscillation frequency. This assumption is consistent with the data of Ichishima and Mizushima[9] for four principal low-frequency Raman lines of the benzene crystal. The mean frequencies of these lines and their temperature dependence are

$$\begin{aligned}\nu_1&=69-0.100T,\\ \nu_2&=89-0.083T,\\ \nu_3&=112-0.127T,\\ \nu_4&=141-0.128T.\end{aligned} \quad (8)$$

If the assignment of these lines to torsional oscillation frequencies as proposed by Fruhling[10] is accepted tentatively, the average torsional oscillation frequency ν_γ at absolute zero is approximately

$$\nu_\gamma(C_6H_6)=\frac{69+89+112+141}{4}=103\ \text{cm}^{-1} \quad (9)$$

in excellent but somewhat fortuitous agreement with the Debye frequency proposed by Lord, Ahlberg, and Andrews[8] to explain the low-temperature heat capacity of crystalline benzene. Unfortunately, the precise assignment of these Raman lines is still controversial.[9,10]

[9] I. Ichishima and S. Mizushima, J. Chem. Phys. **18**, 1686–1687 (1950).

[10] A. Fruhling, Ann. phys. **6**, 401–480 (1951).

For this reason, the mean Debye frequency ν_m from Eq. (7) will be used to approximate ν_ϕ, ν_β, ν_γ, and ν_L. It is noted that the frequency ν_m pertains to an ideal solid whose interatomic distance is kept constant as the temperature changes. In the actual crystal at constant pressure, however, the expansion of the lattice with increasing temperature will result in a decrease in the mean lattice frequency. It seems logical to assume that this temperature dependence is about equal to the average temperature dependence of the Raman lines for benzene discussed above. Moreover, above about $1.4\,\theta_D$ the Debye frequency is approximately equal to the corresponding Einstein frequency. Accordingly, in this approximation

$$\nu_L(C_6H_6)\approx\nu_\phi\approx\nu_\beta\approx\nu_\gamma\approx\nu_m-0.11T \text{ cm}^{-1}. \quad (10)$$

At 217°K, therefore,

$$\nu_L(C_6H_6)\approx\nu_\phi\approx\nu_\beta\approx\nu_\gamma\approx\nu_m\approx 79 \text{ cm}^{-1} \approx 2.37\times10^{12} \text{ sec}^{-1}. \quad (11)$$

Similarly, for rhombic sulfur, the heat capacity of the crystal at low temperatures is approximated as

$$C_v(S_8)=6Rf_D\left(\frac{\theta_D}{T}\right). \quad (12)$$

Equation (12) is considered valid for rhombic sulfur only below about 20°K (rather than below 50°K for benzene) because the S_8 molecule has some intramolecular frequencies around 100 cm^{-1} whose Einstein terms contribute to the heat capacity in the range 20–50°K. From the heat-capacity data of Eastman and McGavock,[11] $\theta_D(S_8)$ is estimated to be about 108°K. The corresponding Debye frequency $\nu_m(S_8)$ is 75 cm^{-1} = 2.26×10^{12} sec^{-1}. Unfortunately there are no Raman spectral data available for the low-frequency torsional oscillation modes of the S_8 molecule as a whole with respect to the crystal lattice. For this reason, a comparison of $\nu_m(S_8)$ with the Raman frequencies and an approximation of the temperature dependence of the lattice frequencies is not possible at the present time. Tentatively, then, the mean lattice frequencies for rhombic sulfur at 298°K are estimated as

$$\nu_L(S_8)\approx\nu_\phi\approx\nu_\beta\approx\nu_\gamma\approx\nu_m\approx 75 \text{ cm}^{-1} \approx 2.25\times10^{12} \text{ sec}^{-1}. \quad (12)$$

It is interesting to note that Barnes[12] has observed an absorption band in the far-infrared for rhombic sulfur at room temperature, which starts at about 81 cm^{-1} and extends through the limit of the observations at 75 cm^{-1}. However, it is not possible as yet to make a definite assignment for the vibrational modes responsible for this band.

[11] E. D. Eastman and W. C. McGavock, J. Am. Chem. Soc. **59**, 145–151 (1937).

[12] R. B. Barnes, Phys. Rev. **39**, 562–575 (1932).

EVALUATION OF ABSOLUTE SUBLIMATION RATE EQUATION FOR RHOMBIC BENZENE AND RHOMBIC SULFUR

The experimental and estimated constants necessary to evaluate the absolute sublimation rate Eq. (6) may now be summarized in Table II.

The comparison between the linear sublimation rate for benzene calculated by the absolute rate Eq. (6) and that calculated from vapor pressure data by the Knudsen Eq. (3) using an experimental evaporation coefficient ($a=0.622$) determined by Baranaev[3] is

$$B_{\substack{\text{rhombic}\\\text{benzene}}}=0.8\times10^8\exp(-\Delta H_{cg}/RT) \text{ cm sec}^{-1} \text{ (abs. rate theory)}; \quad (13)$$

$$B_{\substack{\text{rhombic}\\\text{benzene}}}=3.9\times10^8\exp(-11\,200/RT) \text{ cm sec}^{-1} \text{ (Knudsen equation)}. \quad (14)$$

The comparison between the linear sublimation rate for rhombic sulfur calculated by the absolute rate Eq. (6) and that measured by Bradley[1] is

$$B_{\substack{\text{rhombic}\\\text{sulfur}}}=0.3\times10^{10}\exp(-\Delta H_{cg}/RT) \text{ cm sec}^{-1} \text{ (abs. rate theory)}; \quad (15)$$

$$B_{\substack{\text{rhombic}\\\text{sulfur}}}=1.1\times10^{10}\exp(-23\,890/RT) \text{ cm sec}^{-1} \text{ (experiment)}. \quad (16)$$

COMPARISON OF PRESENT THEORY WITH PENNER'S TREATMENT OF THE SUBLIMATION PROCESS

Penner[7] has presented an interesting picture of the sublimation process for monatomic solids based on the Einstein approximation for oscillators in the normal state and the Lennard-Jones equation[13] relating the vibration frequency of these oscillators to the free volume of the solid. A modification of this picture (along the lines suggested by Penner for evaporation of associated liquids with hindered rotation) yields an absolute rate equation for the sublimation of molecular crystals similar in form to the Knudsen equation (3). This extension of Penner's treatment is given below and the differences in the concepts from those of the authors are discussed in detail. The authors are indebted to Pro-

TABLE II.

	Rhombic benzene	Rhombic sulfur
L	5.05×10^{-8}	5.9×10^{-8} cm
T_S (average)	217	298°K
I_ϕ	2.95×10^{-38}	24.4×10^{-38} g cm^2
$I_\beta=I_\gamma=I_{\beta\gamma}$	1.47×10^{-38}	13.0×10^{-38} g cm^2
$\nu_L\approx\nu_\phi\approx\nu_\beta\approx\nu_\gamma$	2.37×10^{12}	2.25×10^{12} sec^{-1}
σ (symmetry number)	12	8
ΔH_{cg}	11 200	23 890 cal g mole^{-1}

[13] J. E. Lennard-Jones, Proc. Phys. Soc. (London) **52**, 729 (1940).

fessor Penner for a valuable discussion which provided a basis for the following presentation.

Again one starts with the sublimation equation

$$B=eL\frac{kT}{h}\frac{F^*}{F}\exp(-\Delta H_{c_0}/RT)\text{ cm sec}^{-1}. \quad (5)$$

If the activated surface complex and the original surface state consist of Einstein oscillators, then

$$\frac{F^*}{F}=\frac{[1-\exp(-h\nu_L^*/kT)]^{-2}f(\nu_\phi^*)f(\nu_\beta^*)f(\nu_\gamma^*)}{[1-\exp(-h\nu_L/kT)]^{-3}f(\nu_\phi)f(\nu_\beta)f(\nu_\gamma)}. \quad (17)$$

The frequencies ν_L^*, ν_ϕ^*, ν_β^*, and ν_γ^* are those of the activated state and correspond to the frequencies ν_L, ν_ϕ, ν_β, and ν_γ defined previously. As an approximation (valid if $kT\gg h\nu_L^*$ and $kT\gg h\nu_L$)

$$\frac{F^*}{F}\approx\frac{(kT/h\nu_L^*)^2f(\nu_\phi^*)f(\nu_\beta^*)f(\nu_\gamma^*)}{(kT/h\nu_L)^3f(\nu_\phi)f(\nu_\beta)f(\nu_\gamma)}. \quad (18)$$

Let

$$ZF_r^*=f(\nu_\phi^*)f(\nu_\beta^*)f(\nu_\gamma^*), \quad (19)$$

$$\theta F_r^*=f(\nu_\phi)f(\nu_\beta)f(\nu_\gamma), \quad (20)$$

where F_r^*, the rotational partition function for the gaseous molecule, has been defined in an earlier discussion. If it were assumed that $Z=1$ and $\nu_L^*=\nu_L$, an equation essentially the same as (6) above would be obtained. (It is noted that Penner[7] has made the assumption $\nu_L^*\approx\nu_L$ in his treatment of the kinetics of fusion of monatomic solids but not in his treatment of the sublimation process.) However, instead of assuming that $Z=1$ and $\nu_L^*=\nu_L$, Eq. (5) is now written as

$$B=eL\frac{\nu_L^3}{\nu_L^{*2}}\frac{Z}{\theta}\exp(-\Delta H_{c_0}/RT)\text{ cm sec}^{-1}. \quad (21)$$

Following Penner, it is now postulated arbitrarily that the center of gravity of the activated complex, although confined to the crystal surface, can move freely as a gas-like molecule throughout a two-dimensional enclosure of area $v^{*\frac{2}{3}}$ where $v^*=v$ is the volume per molecule in the condensed state. The frequency ν_L^* is now approximated as the mean collision frequency

$$\nu_L^*=(dx/dt)_{Av}/v^{\frac{1}{3}}=(kT/2\pi m)^{\frac{1}{2}}/v^{\frac{1}{3}}, \quad (22)$$

where $(dx/dt)_{Av}$ is the mean translation velocity in a given direction of a molecule of mass m at temperature T. Similarly, the center of gravity of the molecule in the initial surface state is considered to move freely throughout a two-dimensional enclosure of area $v_f^{\frac{2}{3}}$, where v_f is the Lennard-Jones[13] free volume of the solid, so that

$$\nu_L\approx\frac{(dx/dt)_{Av}}{v_f^{\frac{1}{3}}}=(kT/2\pi m)^{\frac{1}{2}}/v_f^{\frac{1}{3}}. \quad (23)$$

Insertion of Eqs. (22) and (23) into Eq. (21) gives

$$B=eL\left(\frac{kT}{2\pi m}\right)^{\frac{1}{2}}\frac{v^{\frac{1}{3}}}{v_f}\frac{Z}{\theta}\exp(-\Delta H_{c_0}/RT)\text{ cm sec}^{-1}. \quad (24)$$

It is now postulated that the Kincaid and Eyring[14] treatment of restricted rotation of molecules in the liquid phase is also valid for the solid phase so that

$$v_f\theta=\frac{kT}{p_s}\exp(-\Delta H_{c_0}/RT), \quad (25)$$

where θ is now identified with the Kincaid-Eyring free angle ratio. The average thickness of the monomolecular surface layer L is

$$L=v^{\frac{1}{3}}=\left(\frac{m}{\rho}\right)^{\frac{1}{3}}. \quad (26)$$

Insertion of Eqs. (25) and (26) into (24) yields

$$B=\frac{eZ}{\rho}\left(\frac{m}{2\pi kT}\right)^{\frac{1}{2}}p_s\text{ cm sec}^{-1}, \quad (27)$$

which is identical in form to the Knudsen equation (3). If it is assumed that Hirschfelder's[15] nonequilibrium theory of reaction rates applies to sublimation, then Eq. (27) gives rates which are too large by a factor of 1/0.387. Application of this correction factor to Eq. (27) gives

$$B\approx\frac{\kappa Z}{\rho}\left(\frac{m}{2\pi kT}\right)^{\frac{1}{2}}p_s\text{ cm sec}^{-1}. \quad (28)$$

Equation (28) now includes κ (heretofore assumed to be unity) where κ is the transmission coefficient for sublimation. If the assumptions thus far are valid, the accommodation coefficient α of the Knudsen equation may now be identified with κZ, where Z is the ratio of the partition function for torsional oscillation in the activated state to the partition function for rotation in the gas phase. It is emphasized that although Eq. (21) may be reduced to the form of the Knudsen equation in the manner described, this fact in itself does not constitute proof of the correctness of the free volume concept as applied to sublimation. The authors will now demonstrate that the alternative assumptions that $Z=1$

[14] J. F. Kincaid and H. Eyring, J. Chem. Phys. **6**, 620–629 (1938).

[15] J. O. Hirschfelder, J. Chem. Phys. **16**, 22–25 (1948).

and $\nu_L^*=\nu_L$ (where ν_L is a normal lattice frequency), which lead to Eq. (6), are also consistent with the Knudsen equation. Moreover, it will be demonstrated that any other reasonable choice of the frequencies ν_L^* and ν_L is also consistent with the Knudsen equation.

Let Eqs. (22) and (23) be replaced by

$$\nu_L^*=C_1(kT/2\pi m)^{\frac{1}{2}}/v^{\frac{1}{3}} \tag{29}$$

and

$$\nu_L=C_2(kT/2\pi m)^{\frac{1}{2}}/v_f^{\frac{1}{3}}, \tag{30}$$

where ν_L^* and ν_L are now the correct frequencies involved in the sublimation process, and C_1 and C_2 are constants of equality. Similarly, replace Eq. (25) by

$$v_f\theta=C_3\frac{kT}{p_s}\exp(-\Delta H_{c0}/RT), \tag{31}$$

where C_3 is also a constant of equality. Insertion of Eqs. (29), (30), and (31) into (21) gives

$$B=\left(\frac{C_2^3\kappa Z}{C_1^2C_3}\right)\frac{1}{\rho}\left(\frac{m}{2\pi kT}\right)^{\frac{1}{2}}p_s \text{ cm sec}^{-1}, \tag{32}$$

which also has the same form as the Knudsen equation except that α, the accommodation coefficient, must now be identified with the quantity $(C_2^3\kappa Z/C_1^2C_3)$ containing the correction constants C_1, C_2, and C_3. Since these constants are unknown, any reasonable choice of the frequencies ν^* and ν is consistent with the Knudsen equation.

Thus, Penner's treatment and that of the authors have both been reduced to the form of the Knudsen equation [see Eqs. (28) and (32)]. However, each equation contains numerical factors which could be identified with the accommodation coefficient. Sufficient data on accommodation coefficients and transmission coefficients are not available for making a comparison of the merits of the two treatments.

SUMMARY

The advantage of the foregoing absolute rate treatments over the older sublimation rate theories previously discussed is evident. The absolute rate treatment as embodied in Eq. (6) gives sublimation rates which agree within a factor of five with rates derived for benzene from vapor pressure data or obtained directly for sulfur by a vacuum sublimation technique. This factor of five is within the generally recognized uncertainty inherent in the Eyring transition state theory. The model of the activated state used in both cases is a gas molecule possessing three rotational degrees of freedom and moving away from a horizontal surface with an escape velocity whose vertical component can be treated statistically by inclusion in the kT/h factor, and whose horizontal components are considered to arise solely from the normal state vibrations with respect to adjacent molecules. The partition functions for the horizontal components of the escape velocity in the activated state are, therefore, treated statistically as two normal-state translational lattice vibrations. The mean translational and torsional oscillation lattice frequencies for the normal state were derived from low-temperature heat-capacity data and compared with the available Raman and far-infrared spectral data. The authors' treatment of the sublimation process has been compared with Penner's treatment (as modified to apply to molecular crystals) and the differences have been discussed in detail.

The authors wish to express their appreciation to Dr. S. Burket of Aerojet-General Corporation for stimulating discussions during the course of this work and for reviewing the final manuscript, and again to Professor S. S. Penner of the California Institute of Technology for the discussion which provided the basis for a comparison with his theory of the sublimation process.

Note added in proof.—The reader's attention is called to a paper by R. S. Bradley, Trans. Faraday Soc. **50**, 1182–87 (1954), which contains an improved statistical treatment of the specific heat of rhombic sulfur in terms of two Debye frequencies ν_m of 1.41×10^{12} and 3.16×10^{12} sec^{-1}. These values neatly bracket the value of $\nu_m=2.25\times10^{12}$ sec^{-1} used in the above calculations.

Infrared Spectrum and Molecular Constants of CD_4†

HOYT M. KAYLOR* AND ALVIN H. NIELSEN
Department of Physics, The University of Tennessee, Knoxville, Tennessee

(Received February 7, 1955)

The infrared spectrum of CD_4 has been examined from 900 cm^{-1} to 8500 cm^{-1}. A total of twenty-eight bands were observed, including four originally measured by Nielsen and Nielsen under somewhat lower resolving power. Twenty-three bands were attributed to CD_4, two to CD_3H, two to CH_4, and one was unassigned. With the aid of the band centers of the corresponding fundamentals in CH_4, the following vibrational constants of CD_4 were obtained: the normal frequencies $\tilde{\omega}_1=2143.2$, $\tilde{\omega}_2=1109.4$, $\tilde{\omega}_3=2336.8$, $\tilde{\omega}_4$ 1026.8 cm^{-1}; the harmonic potential energy constants $k_1=2.093\times10^5$, $k_2=2.841\times10^5$, $k_3=8.463\times10^5$, $k_4=2.790\times10^5$, $k_5=1.329\times10^5$ dynes/cm. From the rotational analysis of nine bands, the B values of the upper states for these modes of vibration were found as well as the following rotational constants: the vibration-rotation interaction constants $\alpha_1=-0.017$, $\alpha_2=-0.015$, $\alpha_3=0.014$, $\alpha_4=0.017$ cm^{-1}; $B_0=2.591$ cm^{-1}; $B_e=2.614$ cm^{-1}; $I_e=10.70\times10^{-40}$ g-cm^2; $r_{C-D}=1.095\times10^{-8}$ cm; $r_{D-D}=1.788\times10^{-8}$ cm; and the moduli of the internal angular momentum $\zeta_3=0.14_5$, $\zeta_4=0.35_5$.

I. INTRODUCTION

THE original infrared measurements on the deuterated form of methane, CD_4, were made by Nielsen and Nielsen[1] who observed three regions of absorption; at 10μ, 4.4μ, and 3μ. They resolved four bands, two being identified as the fundamentals $\tilde{\nu}_3$ and $\tilde{\nu}_4$ at 2260 cm^{-1} and 996 cm^{-1}, respectively, with the remaining two bands in the 3μ region being assigned as combination bands. There was some question regarding the assignment of the combination bands, as the authors stated in their paper. The fine structure in one of these bands had abnormally large spacing, much larger than would be expected from the fine structure of the observed fundamentals, and it was suggested that this band might be caused by an impurity of CD_3H in the gas sample.

Investigations of other molecules with the same type symmetry as CD_4; silane,[2] germane,[3] and ordinary methane[4,5]; revealed the presence in the infrared of the normally infrared inactive fundamental, $\tilde{\nu}_2$. The only data for $\tilde{\nu}_2$ of CD_4 were those from the Raman spectrum of the first overtone of this fundamental.[6] The combined data on CD_4 were not sufficient to yield accurate information concerning the molecular constants of the molecule. In an attempt to remove any discrepancy in the assignments of previously observed bands, and to observe as many new bands as possible, new measurements on CD_4 were undertaken. It was thought that this new information on CD_4 in conjunction with already known data on the isotopic form, CH_4, would permit calculation of both the vibrational and rotational constants of the molecule.

II. EXPERIMENTAL DETAILS

The instrument used in these measurements was The University of Tennessee prism-grating spectrograph.[7] Three replica gratings were used. One, ruled with 3600 lines-per-inch was used to cover the region from 11μ to 5.5μ. From 5.5μ to 2.7μ, a 7200 lines-per-inch grating was employed, and a 15 000 lines-per-inch grating was used for all wavelengths less than 2.7μ. A lead sulfide photoconductive cell with a Wilson type amplifier[8] constituted the detector system for use with the 15 000 lines-per-inch grating, whereas a Golay detector[9] was used for the rest of the spectral region observed. All records were made with a Leeds and Northrup Type-G Speedomax recorder.

Glass cells varying in length from 10 cm to 40 cm and fitted with polished rocksalt windows were used with the Golay detector. In the lead sulfide region, a multiple reflection cell 50 cm in length of the type discussed by White[10] was used, with the number of traversals varying from 8 to 40.

In regions where atmospheric bands of H_2O and CO_2 normally obscured observations, the instrument was dried with P_2O_5 and Ascarite in conjunction with dry nitrogen gas. It was not possible to eliminate these bands completely, but their levels of absorption were reduced to a sufficient degree that absorption due to CD_4 was distinguishable from the background. Slit widths of less than 0.5 cm^{-1} were used for most of the observations, the exceptions occurring with the multiple reflection cell. Because of the loss of energy with a large number of traversals, the use of slit widths of 0.6 to 0.8 cm^{-1} was required for sufficient energy at the detector. In Table I, which gives the wave numbers and the assignments of the observed bands, is also given the slit widths and the path lengths used in their observation.

The sample of CD_4 gas used was prepared by allowing

† This paper is a condensation of a Ph.D. thesis submitted to the Physics Department, The University of Tennessee.

* Present address: Department of Physics, Birmingham-Southern College, Birmingham, Alabama.

[1] A. H. Nielsen and H. H. Nielsen, Phys. Rev. **54**, 118 (1938).
[2] Tindal, Straley, and Nielsen, Phys. Rev. **62**, 151 (1942).
[3] Straley, Tindal, and Nielsen, Phys. Rev. **62**, 161 (1942).
[4] J. S. Burgess, Phys. Rev. **76**, 302 (1949).
[5] Burgess, Bell, and Nielsen, J. Opt. Soc. Am. **43**, 1058 (1953).
[6] G. E. MacWood and H. C. Urey, J. Chem. Phys. **4**, 402 (1936).
[7] A. H. Nielsen, J. Tenn. Acad. Sci. **22**, 241 (1947).
[8] Kuiper, Wilson, and Cashman, Astrophys. J. **106**, 243 (1947).
[9] M. J. E. Golay, J. Opt. Soc. Am. **39**, 437 (1949).
[10] J. U. White, J. Opt. Soc. Am. **32**, 285 (1942).

TABLE I. Assignment of bands.

Band	Band center	Meter atmospheres	Slit widths	$(B'-\zeta_4 B')$	$(B''-\zeta_4 B')$	B'	ζ_4
$\tilde{\nu}_4$	996.0 cm^{-1}	0.01	0.3 cm^{-1}	1.684 cm^{-1}	1.701 cm^{-1}	2.574 cm^{-1}	0.355
$\tilde{\nu}_2+$	1092	0.12	0.3	2.605	2.592	2.605	
$\tilde{\nu}_2-$				2.608	2.592	2.608	
$2\tilde{\nu}_4$	1986.8	0.7	0.4	3.529	3.576	2.544	−0.387
$\tilde{\nu}_1$	2084.7 (R)[a]						
$\tilde{\nu}_2+\tilde{\nu}_4$	2097*	0.3	0.4				
$\tilde{\nu}_3$	2259.3	0.01	0.4	2.180	2.194	2.577	0.145
$3\tilde{\nu}_4$?	2940*	0.3	0.5				
$\tilde{\nu}_3\|$ of CD_3H	2992*	0.3	0.5				
$\tilde{\nu}_3$ of CH_4	3020*	0.3	0.5				
$\tilde{\nu}_1+\tilde{\nu}_4$	3105.2	0.3	0.5	1.659	1.656	2.594	0.360
$\tilde{\nu}_3+\tilde{\nu}_4$	3255*	0.3	0.5				
$\tilde{\nu}_2+\tilde{\nu}_3$	3338*	0.3	0.5				
$\tilde{\nu}_1+2\tilde{\nu}_4$	3986*	1.2	0.4				
$\tilde{\nu}_1+\tilde{\nu}_2+\tilde{\nu}_4$?	4162*	1.2	0.3				
$\tilde{\nu}_3+2\tilde{\nu}_4$	4212*	1.2	0.3				
$\tilde{\nu}_1+\tilde{\nu}_3$	4331*	1.2	0.3				
$\tilde{\nu}_2+\tilde{\nu}_3+\tilde{\nu}_4$		1.2	0.3				
$2\tilde{\nu}_2+\tilde{\nu}_3$	4389*	1.2	0.3				
$2\tilde{\nu}_3$	4496.4	0.1	0.35	2.979	3.013	2.557	−0.165
$\tilde{\nu}_1+3\tilde{\nu}_4$	5045*	6.4	0.7				
$\tilde{\nu}_2+2\tilde{\nu}_3$	5566.7	6.4	0.6	2.982	3.030	2.541	−0.174
$2\tilde{\nu}_3\|$ of CD_3H	5865*	8.0	0.8				
$2\tilde{\nu}_3$ of CH_4	6006*	8.0	0.8				
$2\tilde{\nu}_1+\tilde{\nu}_3$	6283*	6.4	0.6				
$2\tilde{\nu}_3+2\tilde{\nu}_4$	6380*	6.4	0.6				
$\tilde{\nu}_1+2\tilde{\nu}_2+\tilde{\nu}_3$	6430*	6.4	0.6				
$\tilde{\nu}_1+2\tilde{\nu}_3$	6536.8	6.4	0.6	2.738	2.862	2.467	−0.100
$3\tilde{\nu}_3$	6661.8	6.4	0.6	2.758	2.760	2.589	−0.065
?	6767*	6.4	0.6				

* The band centers of the bands marked with an asterisk were determined from Q branch positions.
[a] See reference 6.

heavy water of 99.5% purity to react with aluminum carbide. To obtain as pure gas as possible, the aluminum carbide was maintained at a temperature of 450°–500°C under vacuum for several days to drive off any volatile impurities, and the glass generating system was torched at regular intervals to remove any ordinary water from the system. Even with the precautions taken, there were impurities in the sample. In the main, these were CHD_3 and CH_4; the other isotopic forms CH_2D_2 and CH_3D, were not detected.

A minimum of three records was made for the determination of the wave numbers of the spectral lines. The spectral curves shown herein are tracings of representative original records. Because of the large number of observed bands, and in the interest of conservation of space, the tables of wave numbers of the rotation-vibration lines are not included. They may be found in the Ph.D. thesis entitled "The Infrared Spectrum and Rotational Analysis of CD_4" by Hoyt M. Kaylor, in the Library of The University of Tennessee. The lines shown in the figures herein are numbered to agree with the wave numbers listed in these tables.

III. DISCUSSION OF OBSERVED BANDS

The infrared region was scanned from 900 cm^{-1} to 8500 cm^{-1} with absorption being observed over the range 900 cm^{-1} to 6900 cm^{-1} under a variety of conditions of resolving power and path length of gas. A total of twenty-eight bands was observed, twenty-three of which were attributed to CD_4, two to CD_3H, two to CH_4, and one was unassigned.

$\tilde{\nu}_4$

The infrared active fundamental $\tilde{\nu}_4$, the details of which are shown in Fig. 1, was observed with considerably better resolving power than that obtained by Nielsen and Nielsen.[1] All three branches of the band show rather complex structure. In the R branch especially, it can be noted how the lines split into components as the value of J increases. The first four lines in this branch (lines 81, 80, 79, 75) appear as individual lines; $R(4)$ shows indications of splitting, and all lines of higher J in this branch are separated into at least two resolved components. Normally, one would expect a spacing of $2B(1-\zeta_4)$, where B is the rotational constant and ζ_4 is the modulus of internal angular momentum, with each of these single lines being highly degenerate. The fundamental $\tilde{\nu}_2$, however, causes a perturbation which removes the degeneracy in each of the rotational levels of the state $\tilde{\nu}_4$, and the close proximity of $\tilde{\nu}_2$ to $\tilde{\nu}_4$ makes this perturbation of sufficient magnitude that the fine structure of the individual lines is resolved to some extent. In actuality, each of these "individual" components is composed of several lines falling so close to one another that complete resolution is highly improbable with present facilities available for infrared spectroscopy.

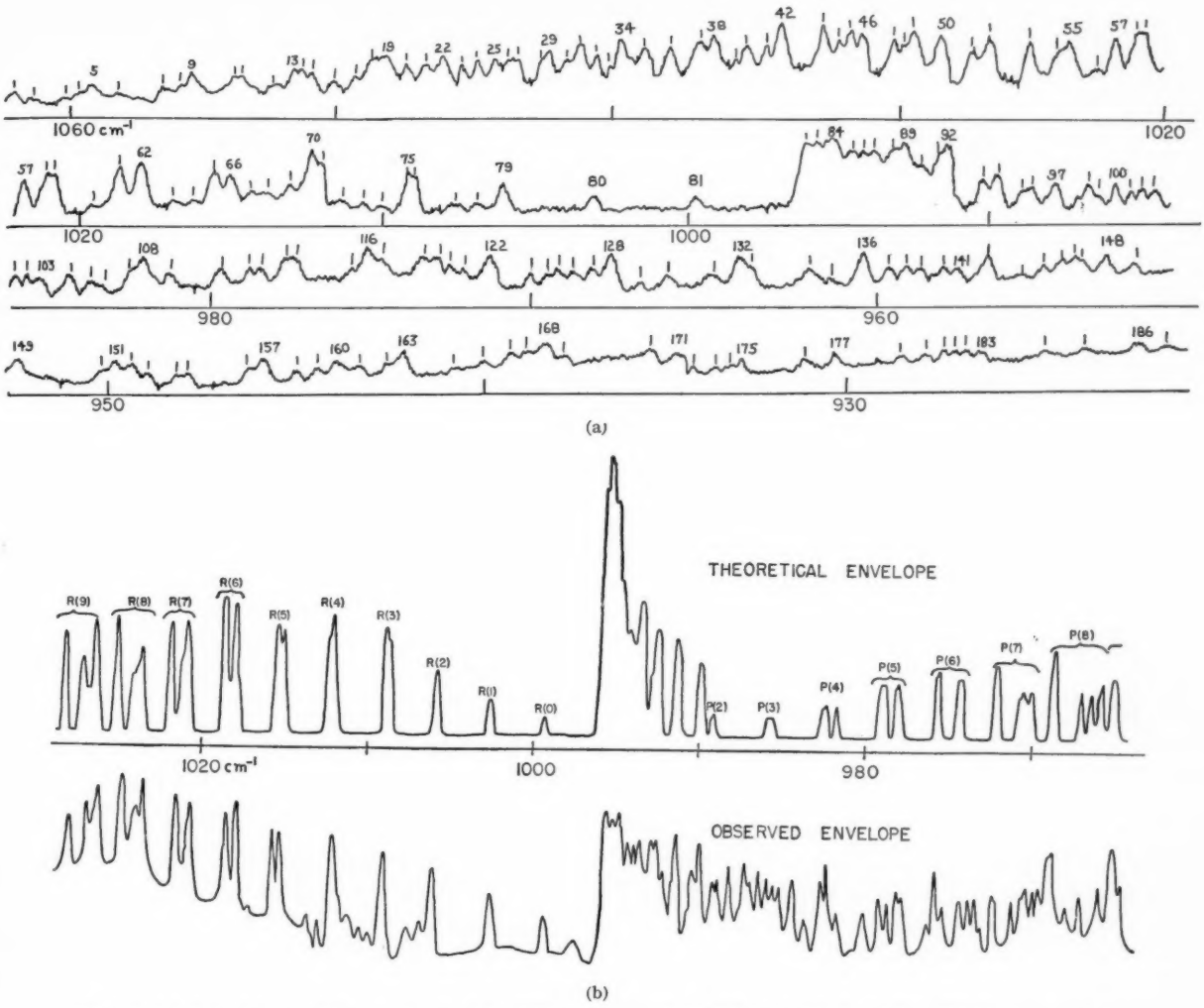

FIG. 1. (a) Actual trace of the spectrum of $\tilde{\nu}_4$ of CD_4 taken with 3600 lines-per-inch grating. (b) Comparison of actual trace of $\tilde{\nu}_4$ with a theoretically computed envelope.

The Q branch has a sharp leading edge at approximately 996 cm^{-1} and then degrades toward lower wave numbers, overlapping far into the P branch of the band. This spreading of the Q branch further increases the complexity of the structure in the P branch. The interaction between $\tilde{\nu}_2$ and $\tilde{\nu}_4$ apparently causes a repulsion between the two bands and accounts for the fact that the Q branch has such a wide spread. Because of this repulsion between the two bands, it is thought that the highest wave number component of a particular transition best represents the wave number of a rotation line in the P and R branches of $\tilde{\nu}_4$ for purposes of rotational analysis.

In Fig. 1(b) is shown a theoretical spectrum of $\tilde{\nu}_4$ which was computed and drawn by adapting the calculations of Childs and Jahn[11] for the energy changes in the rotational levels of $\tilde{\nu}_4$ of CH_4 caused by the Coriolis interaction between $\tilde{\nu}_2$ and $\tilde{\nu}_4$. The figure also shows the observed spectrum drawn to the same scale. The agreement between the two representations is, on the whole, excellent, verifying that the resonance interaction of these two close fundamental bands is the primary cause of the rotational level splitting.

$\tilde{\nu}_2$

The presence in the infrared of the band corresponding to the excitation of the vibration $\tilde{\nu}_2$ is an example of the occurrence of a forbidden vibrational transition. This breakdown of the vibrational selection rules takes place because of the strong interaction between the levels $\tilde{\nu}_2$ and $\tilde{\nu}_4$. It was first pointed out by Childs and Jahn[11] that a Coriolis interaction term in the Hamiltonian linked $\tilde{\nu}_2$ and $\tilde{\nu}_4$. Thus, the wave functions describing a state are linear combinations of the unperturbed wave functions of $\tilde{\nu}_2$ and $\tilde{\nu}_4$ which enables $\tilde{\nu}_2$ to combine with the ground state to an extent dependent upon the wave number interval between the vibrations $\tilde{\nu}_2$ and $\tilde{\nu}_4$.

[11] W. H. T. Childs and H. A. Jahn, Proc. Roy. Soc. (London) A169, 451 (1939).

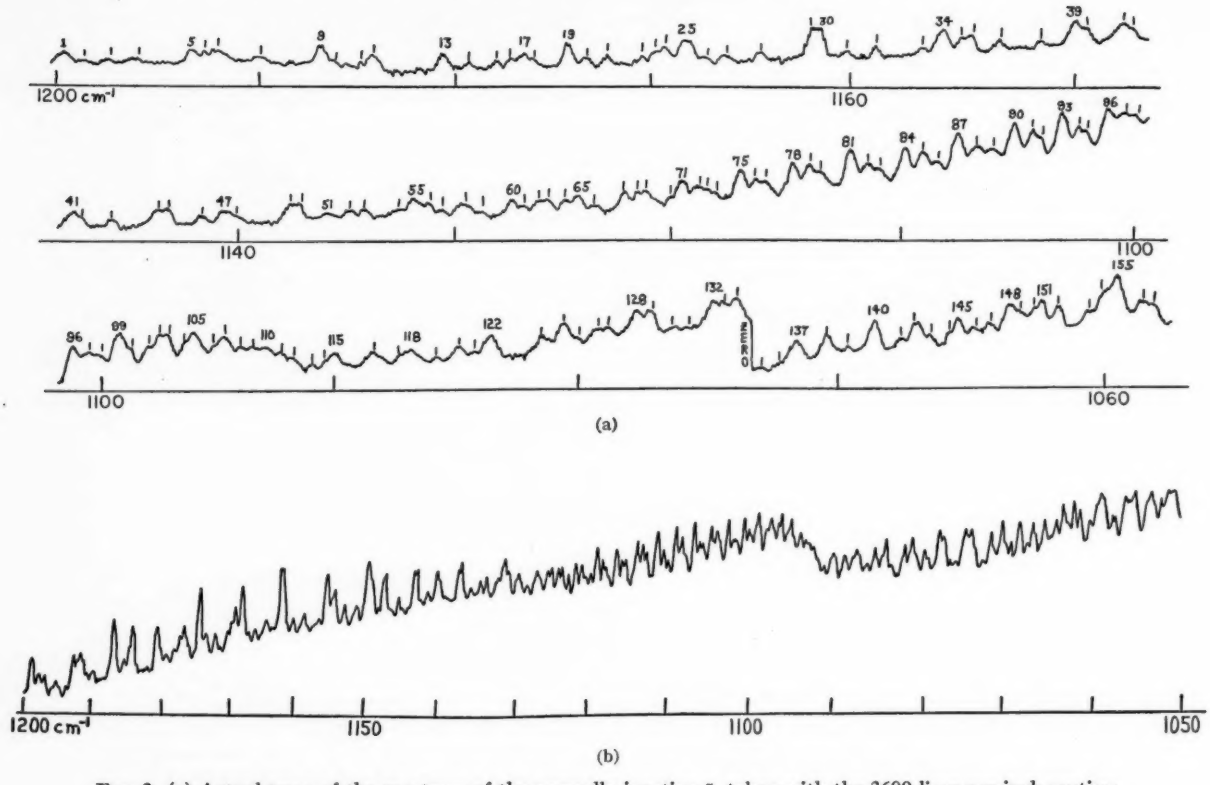

FIG. 2. (a) Actual trace of the spectrum of the normally inactive $\tilde{\nu}_2$ taken with the 3600 lines-per-inch grating. (b) Same as 2*a* (fast scan).

In Fig. 2 is shown the absorption band which is assigned as $\tilde{\nu}_2$. Because of the large dispersion, two different representations, (a) and (b), of the band are given so that the over-all structure as well as the detailed structure may be seen. In the lower representation (b), it may be seen that the Q branch of this band is quite different from that of the band $\tilde{\nu}_4$. It is not nearly so sharp and also shades toward the high wave number end of the spectrum. This shading in the opposite direction is to be expected on the assumption of a perturbation or repulsion which increases with J.

The separation between the rotational lines in the $\tilde{\nu}_2$ band should be $2B$ because there is no internal angular momentum associated with this mode of vibration. There appear to be two sets of lines, which are apparently independent of one another, which have this spacing. A rotational analysis of each set gives the same value for B'', the rotational constant for the ground

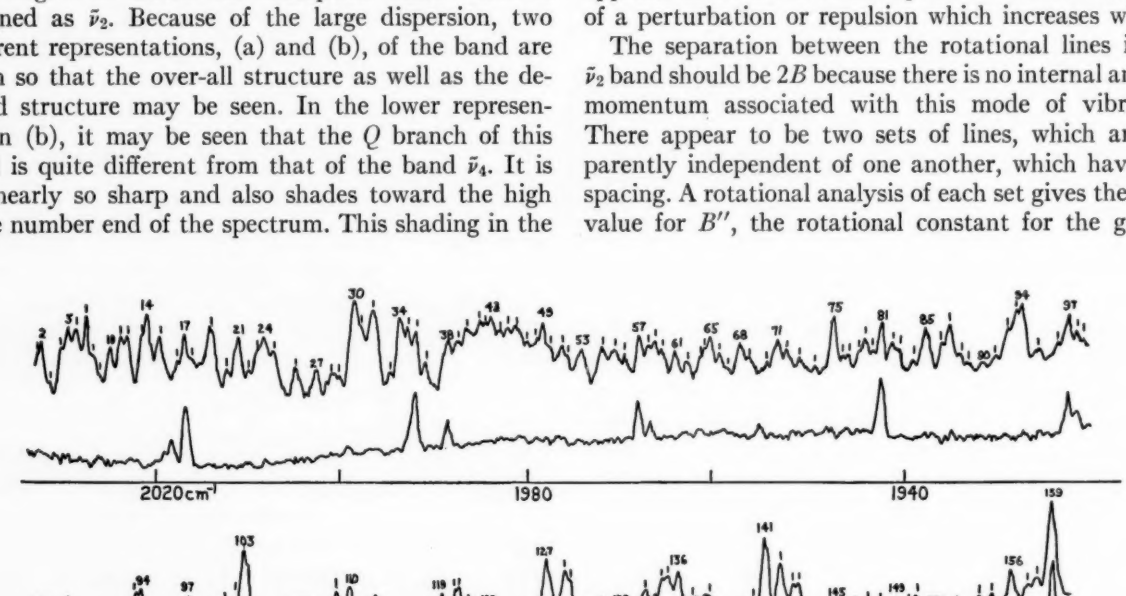

FIG. 3. Trace of the spectrum of the overtone band $2\tilde{\nu}_4$ (3600 lines/inch grating). The lower curve in the figure is the background absorption by water vapor.

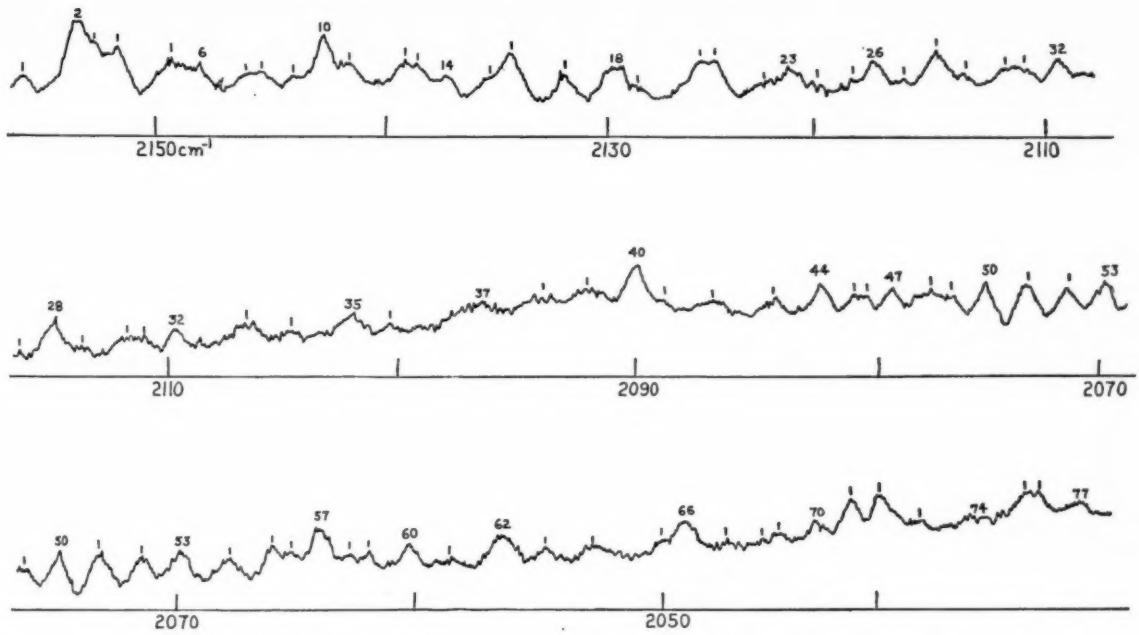

FIG. 4. Trace of the spectrum of the combination band $\tilde{\nu}_2+\tilde{\nu}_4$ (7200 lines/inch grating).

state, but the values of B' are slightly different in the two component upper levels. The phenomenon of the doubling of the lines is almost certainly related to the phenomenon of l-type doubling in axially symmetric molecules. The theory of this effect is incomplete and a detailed interpretation cannot be given at this time. The forbidden transition has been observed also in silane,[2] germane,[3] and methane,[5] with component bands being observed in silane and methane, but not in germane.

$2\tilde{\nu}_4$

The band $2\tilde{\nu}_4$ is shown in Fig. 3. This band lies on the high wave number end of the 6.3μ water vapor band and the background due to water vapor is shown underneath the envelope. The structure of this band is quite complex, but some semblance of order can be seen upon close examination. On looking at the low wave number side, or P branch, it is seen that there are clusters or groups of lines with intervals between them that are relatively free of absorption. If one considers each group as arising from transitions to sublevels belonging to the same J values in the excited state, then a value of J may be assigned to the group. This seems a reasonable assumption when it is remembered that second-order effects can produce just such a splitting. The spacing between the centers of these groups appears to be of the order of 7 cm^{-1}, which is in agreement with the predictions of Johnston and Dennison[12] for the active overtones of XY_4 molecules with spherical symmetry. It also agrees with the spacing of one of the subbands which would occur according to the treatment of Shaffer, Nielsen, and Thomas[13] for the XY_4 molecule. However, the intensities do not agree with those predicted by Shaffer, Nielsen, and Thomas.

The Q branch of this band has its head at about 1988 cm^{-1}. Just as in the band $\tilde{\nu}_4$, the Q branch extends well into the P branch and prevents the identification of the first two lines of the P branch. The high wave number end of the band is overlapped by the band $\tilde{\nu}_2+\tilde{\nu}_4$. A curious structural feature is noted at wave numbers just higher than that of the band center. There are two very intense absorption regions, the first being that containing the lines 30, 31, 32, and the other containing lines 34, 35, 36, 37. No satisfactory explanation can be given for this seemingly abnormal absorption at this time. This strong absorption hides any lines which could be assigned as $R(0)$, but at higher wave numbers reasonable assignments of lines in the R branch may be made even though there is an overlap of bands occurring. Other members of the R branch of this band are found in Fig. 4.

$\tilde{\nu}_2+\tilde{\nu}_4$

The band $\tilde{\nu}_2+\tilde{\nu}_4$ should occur in the vicinity of 2086 cm^{-1}, this number being the sum of the band centers of the two fundamentals, $\tilde{\nu}_2$ and $\tilde{\nu}_4$. In Fig. 4 is shown the band which is ascribed to this combination band. One would expect the spacing in this band to be the same as that in the fundamental $\tilde{\nu}_4$, for the mode $\tilde{\nu}_2$, has no internal angular momentum connected with it. A set of lines corresponding to this spacing (3.4 cm^{-1})

[12] M. Johnston and D. M. Dennison, Phys. Rev. **48**, 864 (1935).

[13] Shaffer, Nielsen, and Thomas, Phys. Rev. **56**, 895, 1051 (1939).

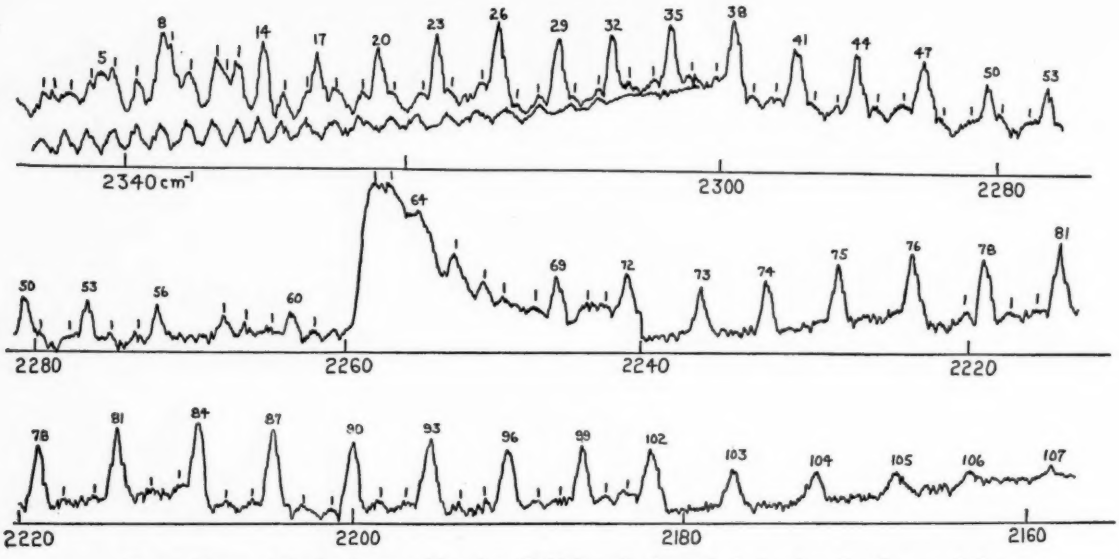

FIG. 5. Trace of the fundamental band $\tilde{\nu}_3$ (7200 lines/inch grating) showing also the remainder of the atmospheric band $\tilde{\nu}_3$ of CO_2 not removed by Ascarite.

cannot be found in the band. A possible explanation for this is also found in the work of Shaffer, Nielsen, and Thomas.[13] Only to the first order of approximation, i.e., taking into consideration only the Coriolis interaction between degenerate modes of vibration of the same band, would the spacing in a combination band involving one of the infrared active fundamentals and an inactive fundamental be expected to be that of the active fundamental involved. In case of a combination band involving $\tilde{\nu}_2$, because of second-order interaction, it is possible that there are two sets of independent lines just as was the case in the fundamental $\tilde{\nu}_2$. If the band is approached from this viewpoint, in the P branch, there are a number of regularly spaced lines extending from line 41 to line 55 which have an average spacing of 1.8 cm^{-1}, a value which is in fair agreement with the spacing expected from $\tilde{\nu}_4$. It is not possible to extend this spacing into the band center, and further extension toward lower wave numbers is obscured because of the overlap of this combination band with the overtone $2\tilde{\nu}_4$.

The Q branch of this band is not as sharp as those of most bands of CD_4. The gentle rise in absorption starting between lines 36 and 37 and extending toward lower frequency is due to the Q branch. This position is chosen as the band center and has a value of 2097 cm^{-1}.

In the R branch, there occurs an overlap of bands also. Here the offending band is the fundamental $\tilde{\nu}_3$. The very strong line numbered 2, for example, is $P(23)$ of $\tilde{\nu}_3$. No rotational analysis has been attempted for this band.

$\tilde{\nu}_3$

The beautiful band shown in Fig. 5 is that of the infrared active fundamental $\tilde{\nu}_3$. It has a Q branch with a sharp leading edge shading toward lower wave numbers, which is characteristic of molecules for which the B value of the upper state is smaller than that of the ground state. If $(B'-B'')$ is negative, then each successive line making up the Q branch falls at a lower wave number than the one just preceding it.

In the R branch of the band there is underlying absorption due to the very intense CO_2 band at 4.25μ. The optical path was dried with Ascarite during the recording of the spectrum, and the intensities of the CO_2 lines were reduced to a sufficient extent to make positive identification of at least seventeen lines in this branch. A background run shows the CO_2 lines quite plainly and was of aid in the identification. The Q branch obscures the first line in the P branch, but all others can be readily identified. The very weak lines which extend just above the noise level cannot be accounted for positively. They may possibly arise from some second-order effect.

3.0–3.4μ Region

The region of the spectrum of CD_4 shown in Fig. 6 is a portion of the spectrum which was examined originally by Nielsen and Nielsen.[1] A number of overlapping bands due to CD_4 occur in this region as well as a strong band due to the impurity of CD_3H. The fundamentals, $\tilde{\nu}_2$ and $\tilde{\nu}_4$, are of nearly the same frequency, and $\tilde{\nu}_1$ and $\tilde{\nu}_3$ are also quite close to one another at a wave number approximately double that of $\tilde{\nu}_2$ and $\tilde{\nu}_4$, hence the overlap of the combination bands. Identifiable in this region are the bands $\tilde{\nu}_2+\tilde{\nu}_3$, $\tilde{\nu}_3+\tilde{\nu}_4$, $\tilde{\nu}_1+\tilde{\nu}_4$, and the impurity band due to CD_3H at 2992 cm^{-1}.

Considering the impurity band first, the spacing of the lines in the R branch of this band, where the Q branch is line 131, is of the order of 5.5 cm^{-1}, which is

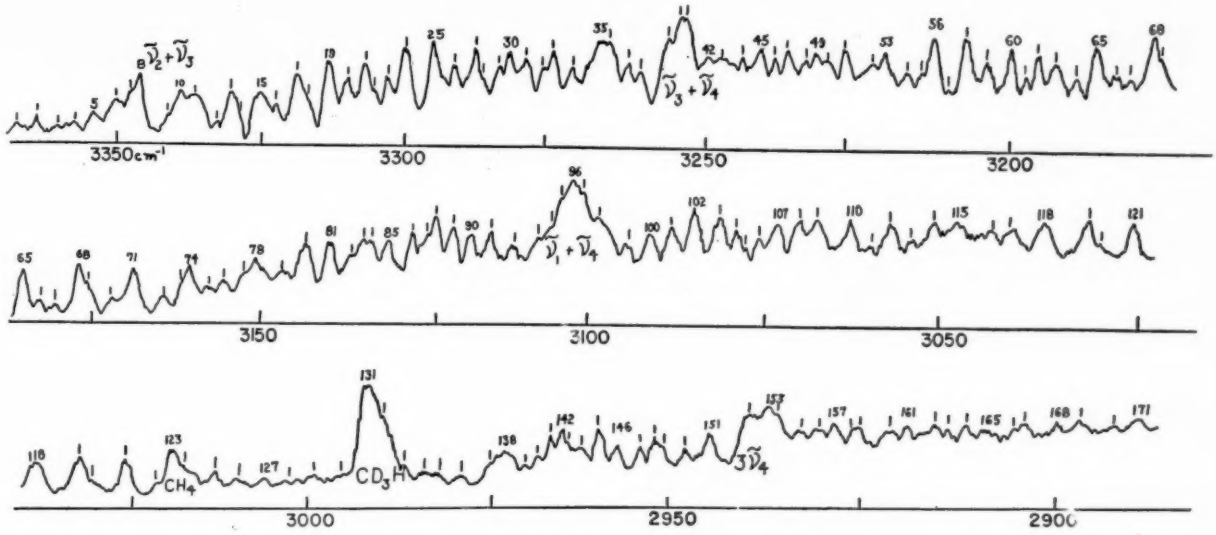

FIG. 6. Trace of the 3.0−3.4μ region (7200 lines/inch grating).

too large for any CD_4 combination bands which can arise in this region, for the spacing would have to be that of $\tilde{\nu}_3$ or $\tilde{\nu}_4$. The position of the band center is in agreement with an observed fundamental of CD_3H.[14]

The line numbered 123 of the CD_3H band is not as symmetrically shaped as the lines in the R branch, and this may be caused by just a trace of CH_4 in the gas sample. The line is located at a wave number of 3020 which is precisely the frequency of the Q branch of $\tilde{\nu}_3$ of CH_4. At 2940 cm^{-1} there also appears to be an indication of a Q branch. None of the possible isotopic forms of CH_4 has fundamentals occurring at this wave number, and the only combination of the fundamentals of CD_4 which could produce a band at this place is the second overtone, $3\tilde{\nu}_4$, and that is the tentative assignment made.

The impurity band of CD_3H and the band which has the Q branch in the neighborhood of 3100 cm^{-1} were the two bands in this region which were assigned by Nielsen and Nielsen.[1] Their assignments for these two bands were $\tilde{\nu}_1+\tilde{\nu}_4$ for the band with its center at 2992 cm^{-1}, and $\tilde{\nu}_3+\tilde{\nu}_4$ for the band centering at 3100 cm^{-1} as these are the strongest combination bands of CD_4 which should occur in this wave number region. As an alternative, they suggested that the assignments could be an impurity band of CD_3H for the lower frequency member, and $\tilde{\nu}_1+\tilde{\nu}_4$ of CD_4 for the band of higher frequency. Their alternative assignments turn out to be the correct ones. The 3100 cm^{-1} band has clean P and R lines near the band center, making it possible to perform a rotational analysis. The spacing of the lines is almost the same as the spacing found in the fundamental $\tilde{\nu}_4$, and the assignment of $\tilde{\nu}_1+\tilde{\nu}_4$ is here given.

Another prominent Q branch is present at a wave number of 3255. The vibration giving rise to this band is assigned as $\tilde{\nu}_3+\tilde{\nu}_4$. According to the theory of Shaffer, Nielsen, and Thomas,[13] this band is ninefold degenerate, with all the degeneracy removed by the first-order Coriolis interaction, as ζ_3 and ζ_4 are both quite different from zero. Were either ζ_3 or ζ_4 zero or nearly so, the rotational levels would coincide in groups of three, so that instead of nine subbands, only three would be present. A rotational analysis of this band in SiH_4 has been made on the basis of only three subbands being present.[2] In CD_4, both ζ_3 and ζ_4 are appreciably different from zero, but the resolving power is not sufficiently high to indicate clearly all of the component lines, if the removal of the degeneracy follows the theory of Shaffer, Nielsen, and Thomas.[13] Johnston and Dennison,[12] who considered only one of the subbands which has been given by Shaffer, Nielsen, and Thomas,[13] calculated the proper value of $\zeta(\tilde{\nu}_3+\tilde{\nu}_4)$ to be $-\frac{1}{2}(\zeta_3+\zeta_4)$ or $-\frac{1}{4}$. According to their treatment, the spacing between the lines should be $2.5B$. In the P branch there appears to be a set of lines of some prominence which will fit this spacing. Listing them, they are the lines marked 44, 47, 50, 53, 56, 59, 62, 65, 68, 71, 74, and 77. It is not possible to pick out a similar set of lines in the R branch because of the overlap of this branch with $\tilde{\nu}_2+\tilde{\nu}_3$. The value of $-\frac{1}{4}$ for the modulus of internal angular momentum of the vibration-rotation band was found to fit prominent lines in the spectrum of the corresponding band in CH_4.[15] There, as in CD_4, this value for the modulus left many lines with no identification. The leading edge of the Q branch has been taken as the band center, the above noted value of 3255 cm^{-1}.

The other band due to CD_4 which should appear in this region is the combination band $\tilde{\nu}_2+\tilde{\nu}_3$. Such a band appears to be present with the Q branch located at 3338 cm^{-1}. The P branch is badly intermingled with the R branch of the $\tilde{\nu}_3+\tilde{\nu}_4$ band. The R branch should be

[14] N. Ginsberg and E. F. Barker, J. Chem. Phys. **3**, 668 (1935).

[15] A. H. Nielsen and H. H. Nielsen, Phys. Rev. **48**, 864 (1935).

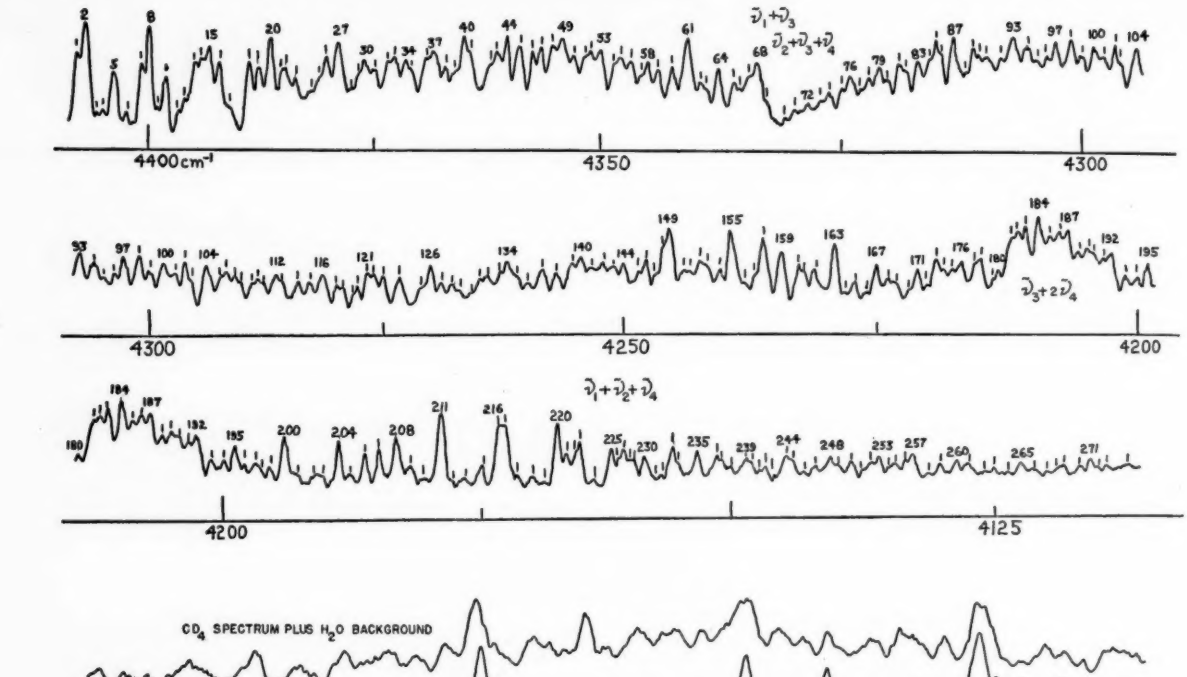

FIG. 7. Trace of the 2.27−2.53μ region (15 000 lines/inch grating).

clear, but for some undetermined reason, the band cuts off quite sharply if the above assignment is the correct one. The record shown in Fig. 6 was made with a sample of gas at 0.3 meter atmospheres. In an attempt to find more lines in the R branch, this portion of the spectrum was mapped with 0.6 meter atmospheres, but no additional lines appeared. The only effect was to raise the general absorption level.

2.27−2.53μ Region

In the 2.27−2.53μ region of the spectrum of CD_4, there is a possibility of a number of combination bands. Figure 7 shows the observed spectral envelope, and the structure there exhibited amply illustrates the complexity which arises in the spectrum of CD_4 because of overlapping bands.

No satisfactory rotational analysis has been made of the bands falling in this region, but some salient features may be pointed out. At the high wave number end, around 4400 cm^{-1}, the very strong lines, 2, 8, 15, 20, 27, and some of the lines of intermediate strength in between, are $P(13)$, $P(14)$, $P(15)$, $P(16)$, $P(17)$, respectively, of $2\tilde{\nu}_3$. Undoubtedly, the P branch of $2\tilde{\nu}_3$ extends considerably further into this region, since these identifiable lines are so strong. Also around 4400 cm^{-1} should occur the band center of $2\tilde{\nu}_2+\tilde{\nu}_3$. This band is a tertiary combination band and should be rather weak, with only the Q branch having any particular prominence. At 4389 cm^{-1}, there occurs too much absorption to be attributed to the lines of $2\tilde{\nu}_3$ alone, and this can be reasonably associated with the Q branch of the tertiary band.

An obvious band center is present at 4331 cm^{-1}. No pronounced Q branch is in evidence and this is ascribed to the fact that two bands, $\tilde{\nu}_1+\tilde{\nu}_3$ and $\tilde{\nu}_2+\tilde{\nu}_3+\tilde{\nu}_4$, have almost the same wave number. The band $\tilde{\nu}_1+\tilde{\nu}_3$ should be comparatively strong since it is a binary combination band, but the slightly displaced superposition of the two bands would destroy the sharp leading edge of either Q branch. This band center is assigned to both $\tilde{\nu}_1+\tilde{\nu}_3$ and $\tilde{\nu}_2+\tilde{\nu}_3+\tilde{\nu}_4$.

The Q branch occurring at 4212 cm^{-1} is assigned to $\tilde{\nu}_3+2\tilde{\nu}_4$. In the P branch some regularity of structure can be found. The prominent lines, 187, 192, 200, 204, 208, have an average interval of 4.7 cm^{-1}. From the spacing in one branch alone, it is not possible to draw

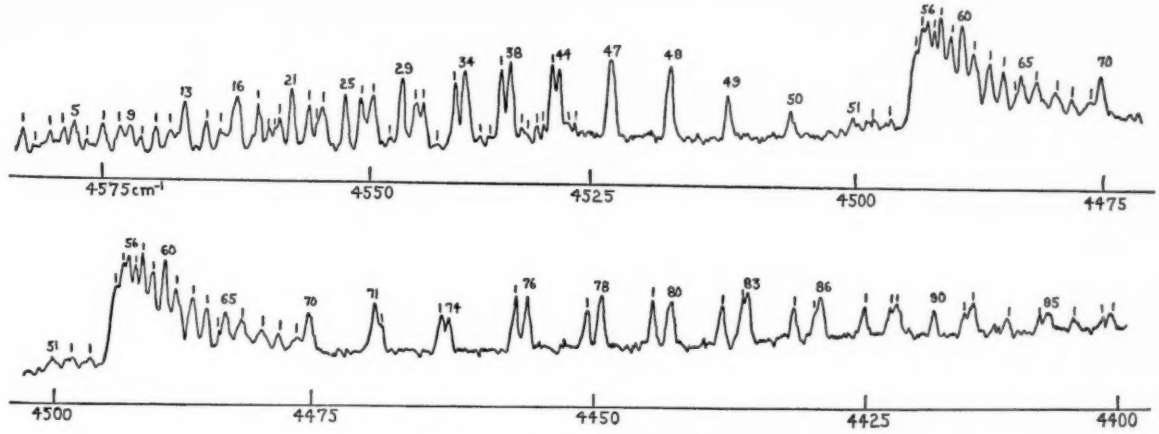

FIG. 8. Trace of the overtone band $2\tilde{\nu}_3$ (15 000 lines/inch grating).

any conclusion concerning the B value for a mode of excitation, since the internal angular momentum modulus cannot be determined. It is interesting to note, however, that this spacing is close to that which occurs in the fundamental band, $\tilde{\nu}_3$, where the average spacing is 4.4 cm^{-1}. No theory has been developed for such a combination band, which could exhibit an eighteen-fold degeneracy, so it is not known if one would expect the spacing of this band to follow the spacing of $\tilde{\nu}_3$.

Three other bands are possible in the mapped region shown in Fig. 7, $\tilde{\nu}_1+\tilde{\nu}_2+\tilde{\nu}_4$, $2\tilde{\nu}_2+2\tilde{\nu}_4$, and $\tilde{\nu}_1+2\tilde{\nu}_4$. The intensity of $2\tilde{\nu}_2+2\tilde{\nu}_4$ should be so weak that it would not cause any noticeable absorption. The other bands, however, could well give rise to Q branches with the conditions under which the region was recorded (1.2 meter atmospheres). One possible Q branch which falls in the proper wave number range is the absorption at 4162 cm^{-1}. This absorption serves to break up the regularity in the lines of $\tilde{\nu}_3+2\tilde{\nu}_4$, and a tentative assignment of $\tilde{\nu}_1+\tilde{\nu}_2+\tilde{\nu}_4$ is given to this absorption. A portion of this region is covered by the 2.7μ H_2O band, as indicated in the lower portion of Fig. 7, and interspersed among the strong water vapor lines is a Q branch at 3986 cm^{-1} which is believed to be the remaining band that was thought to be present in this general region, $\tilde{\nu}_1+2\tilde{\nu}_4$.

$2\tilde{\nu}_3$

The band $2\tilde{\nu}_3$ is the only overtone or combination band which is entirely free of both atmospheric absorption bands and overlap with some other band or bands of CD_4. In Fig. 8 is shown the reproduction of the observed band with the lines identified in terms of the rotational number J. Again, one notes the Q branch which has a sharp leading edge on the high wave number side and then shades off well into the P branch. It is noted also that with increasing J, the individual lines of the P and R branches split into components in a manner to suggest doubling. A rotational analysis has been made of this band assuming that each of the groups of lines represents a value of J.

Because this band is free of other CD_4 bands and of atmospheric absorption bands, it was thought that it would serve excellently for comparison of a theoretical spectrum with that which was observed experimentally. In plotting the theoretical band envelope the relations of Shaffer, Nielsen, and Thomas[13] for the positions of the individual lines relative to the band center and for the line intensities were used. The theoretical envelope computed in this manner had a fairly complicated pattern whereas the observed band exhibits fairly simple structure in the P and R branches as shown in Fig. 8. The basic spacing of the lines in the P and R branches is quite accurately given by $2(1+\zeta_3)B$ which is the value given by Johnston and Dennison[13] and is also the spacing of one of the subbands which occurs in the theoretical band envelope. However, the intensities of the other subbands which are likewise present in the theoretical spectrum are comparable to the one which follows the observed spacing, and their presence appears to obscure any regularity.

$\tilde{\nu}_1+3\tilde{\nu}_4$

A small region of very weak absorption was observed on the low wave number end of the 1.8μ water vapor band, and its envelope is shown in Fig. 9. A Q branch

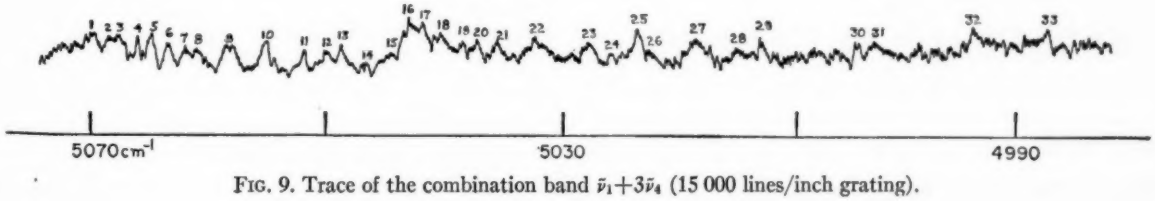

FIG. 9. Trace of the combination band $\tilde{\nu}_1+3\tilde{\nu}_4$ (15 000 lines/inch grating).

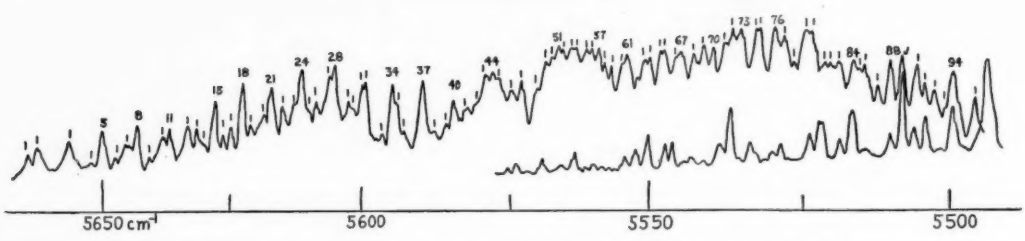

FIG. 10. Trace of the combination band $\tilde{\nu}_2+2\tilde{\nu}_3$ (15 000 lines/inch grating) showing the atmospheric water vapor background.

is located at 5045 cm^{-1} and the position of its leading edge is taken as the band center. The general absorption in the neighborhood of 5070 cm^{-1} is due to water vapor.

The weakness of the absorption suggests that this band must be a higher order combination band. From the addition of the fundamental frequencies the only band of CD_4 found which could occur in this region was $\tilde{\nu}_1+3\tilde{\nu}_4$. This addition leads to a value of 5071 cm^{-1} which is in reasonable agreement with the observed band center of 5045 cm^{-1}. This assignment is, therefore, given to this band.

$\tilde{\nu}_2+2\tilde{\nu}_3$

On the high wave number end of the 1.8μ water vapor band, there is a region of relatively strong absorption. Although the optical path was dried with P_2O_5, it was not possible to remove the water vapor in the spectrograph to an extent that it would not interfere with observations. The background due to the water vapor and the absorption with the cell in the optical path are both shown in Fig. 10. (It can be seen that the Q branch and portions of the P branch exhibit too much absorption for the best observation of rotational structure. However, because of the loss of gas which occurred each time that the number of traversals in the multiple reflection cell was changed, an attempt to observe this band at lower pressure or shorter path length was not made.) The assignment made for this band is $\tilde{\nu}_2+2\tilde{\nu}_3$, and this assignment is borne out by the rotational analysis. In the clear R branch, the lines show the same sort of splitting with increasing J that was noted in the band $2\tilde{\nu}_3$.

The same curious phenomenon is noted in this band that was found in the band $2\tilde{\nu}_4$. At frequencies just higher than that at which the Q branch is considered to terminate, there is a group of strong absorption lines (43, 44, 45, 46, 47) for which no explanation can be given at the present time.

1.63−1.73μ Region

The observed bands in this region are two impurity bands, and their envelopes are shown in Fig. 11. The band with the strong Q branch at 5865 cm^{-1} is assigned as the first overtone of the fundamental of CD_3H which occurs at 2992 cm^{-1}. The average spacing of the lines in the P and R branches of this band is the same as that in the band at 2992 cm^{-1}. The very sharpness of the Q branch, the regular structure in both the P and R branches, and the spacing of the rotational lines in both the P and R branches, all lead to the conclusion that this band could not be a member of the CD_4 family.

The other band at 6006 cm^{-1} is due to $2\tilde{\nu}_3$ of CH_4. The apparent intensity alternation between the two Q branches comes about because every other line of the R branch of CD_3H band and the lines of the P branch of the CH_4 band coincide. A comparison of this band with the corresponding band $2\tilde{\nu}_3$ of CD_4 illustrates very strikingly the effect of internal angular momentum. In CH_4, ζ_3 is only 0.05 as compared with a value of 0.14_5 in CD_4. The removal of the degeneracy by the Coriolis interaction between vibration and rotation is practically negligible, and if subbands are present, their lines coincide with one another to the degree of resolution here employed. The only noticeable effect with the wide spectral slit widths used in mapping this region is a slight broadening of the spectral lines. In CD_4, however, the lines of this corresponding band split into components at rather low values of J. The band $2\tilde{\nu}_3$ of CH_4 has been observed with very high resolving power by Nelson, Plyler, and Benedict.[16]

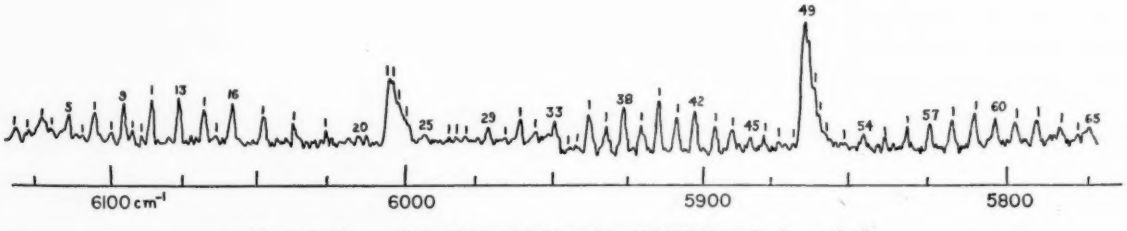

FIG. 11. Trace of the 1.63−1.73μ region (15 000 lines/inch grating).

[16] Nelson, Plyler, and Benedict, J. Research Natl. Bur. Standards **41**, 615 (1948).

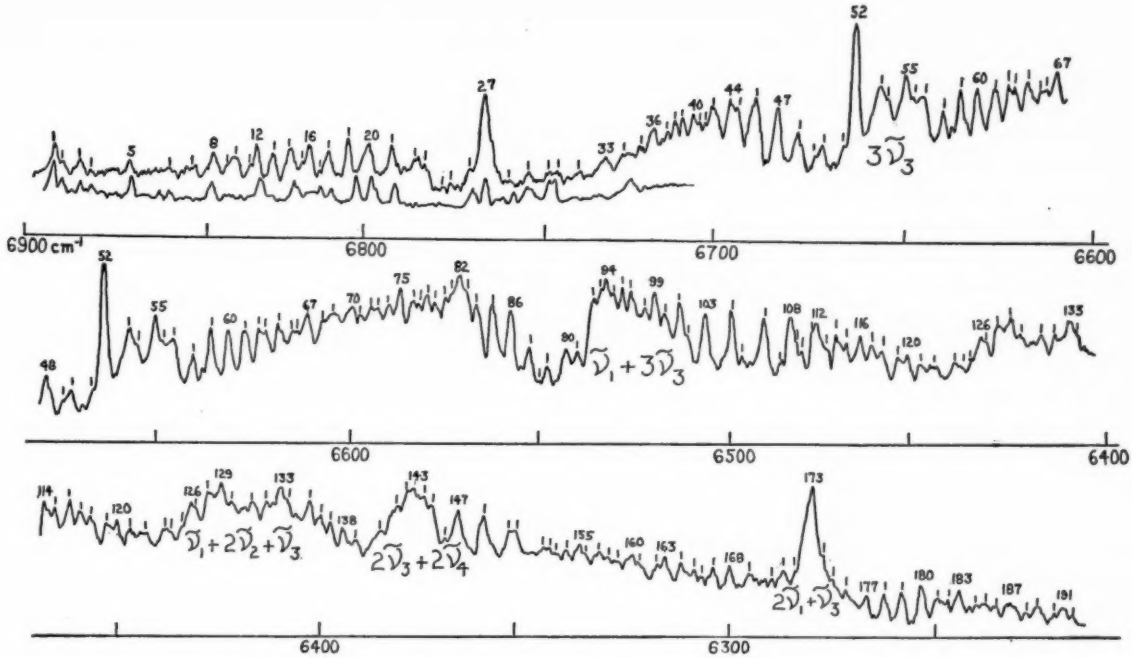

FIG. 12. Trace of the 1.45−1.61μ region (15 000 lines/inch grating) showing some atmospheric water vapor background.

Although these impurity bands appear quite strong in Fig. 11, it must be remembered that they were recorded at 8.0 meter atmospheres, corresponding to 40 traversals in the multiple cell, and with slit widths of 0.8 cm^{-1} in order to show the fine structure above the background.

1.45−1.61μ Region

The region shown in Fig. 12 lies at wave numbers just below the 1.4μ water vapor band. The slight absorption due to water vapor is shown as a separate trace beneath the envelope obtained with the CD_4 sample. This is another region in which many bands occur because the potential function of CD_4 is such that $\tilde{\nu}_1$ and $\tilde{\nu}_3$ have frequencies which are very nearly twice those of $\tilde{\nu}_2$ and $\tilde{\nu}_4$. In attempting assignments in this region, combinations of the fundamentals were made so as to include all the possible active bands not exceeding quaternary combinations, which would have wave numbers in the range which this region covers. Of these, three are tertiary bands, $2\tilde{\nu}_1+\tilde{\nu}_3$, $\tilde{\nu}_1+2\tilde{\nu}_3$, and $3\tilde{\nu}_3$, and one would expect that these three would exhibit the strongest absorption.

The Q branch at 6770 cm^{-1} lies at a wave number which is very nearly that obtained by multiplying the fundamental frequency of $\tilde{\nu}_3$ by three. However, it is difficult to accept this band as being $3\tilde{\nu}_3$ for two reasons. First, the shape of the Q branch itself is quite symmetrical whereas the typical Q branch of CD_4 is like the one occurring at 6537 cm^{-1}. In the second place, it is hard to conceive of a potential function which would cause the first overtone to be separated from the fundamental by a frequency interval which is less than that of the fundamental itself, and then cause the second overtone to be separated from the first overtone by an interval which is greater than that of the fundamental. For these reasons this band is not assigned as $3\tilde{\nu}_3$, but that assignment is given to the strong band at 6667 cm^{-1}. The average spacing of the lines in the R branch of the band with the Q branch at 6770 cm^{-1} is 6.3 cm^{-1}.

A rotational analysis has been made of the band assigned as $3\tilde{\nu}_3$. No specific theory has been developed for second overtones of active fundamentals of XY_4 molecules nor does the rotational analysis of $3\tilde{\nu}_3$ of CH_4, the only other XY_4 molecule in which the second overtone of $\tilde{\nu}_3$ has been observed, furnish any enlightment of what the B value of $3\tilde{\nu}_3$ of CD_4 should be. The second overtone of $\tilde{\nu}_3$ of CH_4 was observed by Childs[17] in the photographic infrared and analyzed. However, since ζ_3 is so near zero in CH_4, all of the overtones of this fundamental have the same spacing as the fundamental itself.

A very interesting feature is present near the Q branch of $3\tilde{\nu}_3$ in the strong line, 52. In other bands of the spectrum of CD_4, there has been unusual absorption on the high-frequency side of the Q branch, but none of these lines were as sharp or as intense as line 52. In fact, it very much looks like a Q branch which for the present remains unidentified.

The next strong band is the one which has the leading edge of its Q branch at 6537 cm^{-1}. This band has been assigned as $\tilde{\nu}_1+2\tilde{\nu}_3$, and a rotational analysis has been made for it. The R branch of this band is confused

[17] W. H. J. Childs, Proc. Roy. Soc. (London) **153**, 555 (1936).

because this branch overlaps with the P branch of $3\tilde{\nu}_3$, and there is also the possibility of the Q branch of $2\tilde{\nu}_2+2\tilde{\nu}_3$ in this region between the two band centers. The P branch is, however, relatively clean.

Between 6450 cm^{-1} and 6400 cm^{-1} is an interval where strong absorption takes place; too much, it is believed, to be accounted for altogether by the overlap of P and R branches. What appears to be a crude Q branch formed by lines 126, 127, 128, 129, is tentatively assigned as the Q branch of the band, $\tilde{\nu}_1+2\tilde{\nu}_2+\tilde{\nu}_3$. The band which contributes the Q branch at 6380 cm^{-1} is assigned as $2\tilde{\nu}_3+2\tilde{\nu}_4$. The average spacing of the regular lines, 145, 147, 148, 149–150, in the P branch is 7.5 cm^{-1} which is of the order of the separation of the lines in the overtone $2\tilde{\nu}_4$. Whether this has any significance is not known, for no theoretical treatment has been made for this quaternary combination band.

The band at 6283 cm^{-1} is assigned as $2\tilde{\nu}_1+\tilde{\nu}_3$. The spacings of the regular lines in the P branch and the intervals between two clean lines in the R branch support this assignment, for they agree within 0.2 cm^{-1} with the spacing of the fundamental $\tilde{\nu}_3$.

The assignment of all the observed bands, their band centers, and the data for the bands for which a rotational analysis has been made, are collected in Table I. Those bands in which the assignment is questionable are followed by a question mark. An asterisk is used to mark those frequencies which were estimated from the position of Q branches. The wave number of $\tilde{\nu}_1$ is from the Raman spectrum of CD_4.[6]

IV. VIBRATIONAL CONSTANTS

The determination of the normal frequencies and the harmonic potential energy constants is the extent to which the vibrational problem of CD_4 can be solved at the present time. The normal frequencies are required in order to calculate the potential constants in the general form of the potential[13]

$$2V_0=k_1\sum_{i=1}^{3}\xi_i^2+2k_2\sum_{i=1}^{3}\eta_i\xi_i+k_3\sum_{i=1}^{3}\eta_i^2 +k_4\sum_{i=1}^{3}\zeta_i^2+k_5\sum_{i=1}^{3}{}'\zeta_i\zeta_j, \quad (1)$$

where the k_i are linear combinations of the nine spring constants $K_1\cdots K_9$.

The usual method of determining the potential constants is to determine the anharmonic constants directly from the observed data. Once the anharmonic constants are known, the normal frequencies may be calculated from the observed fundamental band centers, and these normal frequencies are then used to establish the constants of the harmonic portion of the potential function. This method cannot be used with CD_4 because sufficient bands have not been observed to obtain the anharmonic constants, and no theoretical expressions are available which relate such constants to the observed bands. Dennison,[18] however, has devised a method for approximating the normal frequencies from the observed fundamental frequencies when observed frequencies are known for two isotopic forms of the molecule. He proposed the relation between the normal harmonic frequency $\tilde{\omega}_k$ and the observed frequency $\tilde{\nu}_k$ of a fundamental band to be $\tilde{\omega}_k=\tilde{\nu}_k(1+\beta_k)$, where the term $\tilde{\nu}_k\beta_k$ is a correction for the anharmonicity and β_k is the anharmonic constant (denoted as α_k by Dennison).

Accurate wave numbers of the fundamental vibrations of both CH_4 and CD_4 are now known, and the complete relations given by Dennison lead to the following β_k values for CD_4: $\beta_1=0.0281$, $\beta_2=0.0159$, $\beta_3=0.0343$, and $\beta_4=0.0300$. These values in turn give for the normal frequencies: $\tilde{\omega}_1=2143.2$ cm^{-1}, $\tilde{\omega}_2=1109.4$ cm^{-1}, $\tilde{\omega}_3=2336.8$ cm^{-1}, $\tilde{\omega}_4=1026.8$ cm^{-1}. The relations between the harmonic potential energy constants, the normal frequencies, and the moduli of internal angular momentum have been given by Shaffer, Nielsen, and Thomas.[13] Application of these relations to CD_4 leads to the following values of the constants $k_1\cdots k_5$: $k_1=2.093\times10^5$, $k_2=2.841\times10^5$, $k_3=8.463\times10^5$, $k_4=2.790\times10^5$, $k_5=1.329\times10^5$ dynes/cm.

For completeness, the normal frequencies and the potential constants of CH_4 have likewise been included. These constants are gathered together in Table II. The constants k_4 and k_5 are determined directly from the normal frequencies $\tilde{\omega}_1$ and $\tilde{\omega}_2$ and, using Dennison's method, their values should be exactly the same for the two isotopes. The constants k_1, k_2, k_3 require knowledge not only of the normal frequencies $\tilde{\omega}_3$ and and $\tilde{\omega}_4$, but also of the moduli of internal angular momentum, ζ_3 and ζ_4. The values used for CH_4 were those determined by Childs[17] from the average spacing of the lines in the fundamental, $\tilde{\nu}_3$ and $\tilde{\nu}_4$, and the observed convergence of these bands: $\zeta_3=0.05$, $\zeta_4=0.45$. The disagreement between the force constants for the two isotopic forms would indicate that there may be a small discrepancy in the ζ values of the two molecules.

TABLE II. Vibrational constants of CD_4 and CH_4.

Constant	CD_4	CH_4
$\tilde{\omega}_1$	2143.2 cm^{-1}[a]	3029.8 cm^{-1}[a]
$\tilde{\omega}_2$	1109.4 cm^{-1}	1566.2 cm^{-1}[b]
$\tilde{\omega}_3$	2336.8 cm^{-1}	3156.9 cm^{-1}[a]
$\tilde{\omega}_4$	1026.8 cm^{-1}	1357.6 cm^{-1}[a]
k_1	2.093×10^5 dynes/cm	2.116×10^5 dynes/cm
k_2	2.841×10^5 dynes/cm	2.740×10^5 dynes/cm
k_3	8.463×10^5 dynes/cm	8.132×10^5 dynes/cm
k_4	2.790×10^5 dynes/cm	2.790×10^5 dynes/cm
k_5	1.329×10^5 dynes/cm	1.329×10^5 dynes/cm
ζ_3	0.14[5]	0.05[c]
ζ_4	0.35[5]	0.45[c]
r_{X-Y}	1.095×10^{-8} cm	1.0929×10^{-8} cm[d]

[a] See reference 18.
[b] See reference 5.
[c] See reference 17.
[d] See reference 19.

[18] D. M. Dennison, Revs. Modern Phys. **12**, 175 (1940).

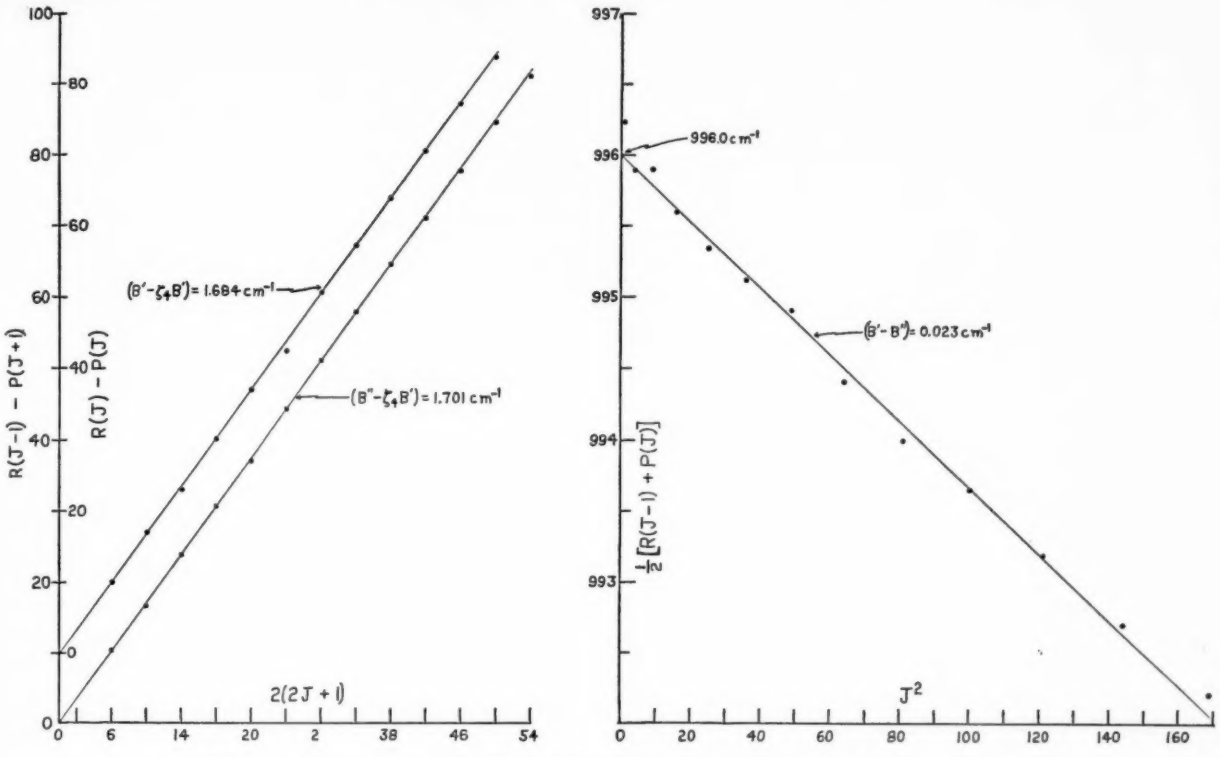

FIG. 13. Typical graphs of combination relations from which molecular constants were obtained.

V. ROTATIONAL CONSTANTS

The assignments given to the normal modes of vibration of a tetrahedrally symmetric XY_4 molecule are well established. There are four normal modes, one nondegenerate $\tilde{\omega}_1$, one doubly degenerate $\tilde{\omega}_2$, and two triply degenerate, $\tilde{\omega}_3$ and $\tilde{\omega}_4$, with only these triply degenerate modes being infrared active to a first order of approximation. The zero-order energy of the vibrating-rotating molecule is the sum of the vibrational energy and the rotational energy considering the molecule as a rigid rotator:

$$T=G(V_1,V_2,\cdots)+F(J)$$
$$=\sum_i \omega_i(V_i+d_i/2)+B_eJ(J+1), \quad (2)$$

where d_i is the order of degeneracy, V_i is the vibrational quantum number of the vibration $\tilde{\omega}_i$, J is the rotational quantum number and the rotational constant B_e is $h/8\pi^2cI_e$, I_e being the equilibrium value of the moment of inertia of the rotator.

During vibration the average positions of the nuclei composing the molecule do not coincide with their equilibrium positions. The effect is to change the moment of inertia by a small amount and, hence, to change the rotational constant, B, so that it has a slightly different value for different vibrational levels. This variation in B is a linear function of the vibrational quantum numbers to a first order of approximation

$$B_v=B_e-\sum_i \alpha_i(V_i+d_i/2), \quad (3)$$

where α_i is the vibration-rotation interaction constant associated with the normal harmonic frequency $\tilde{\omega}_i$ of degeneracy d_i. Again, the sum is over-all vibrations with the degenerate ones being counted only once.

Another effect which plays an important role in the vibration-rotation spectrum is the Coriolis interaction between total angular momentum and the internal angular momentum associated with degenerate modes of vibration. This Coriolis interaction removes the degeneracy in the rotational levels of the infrared active fundamentals, and in the combination bands $V_1\tilde{\nu}_1+V_2\tilde{\nu}_2+\tilde{\nu}_3$, $V_1\tilde{\nu}_1+V_2\tilde{\nu}_2+\tilde{\nu}_4$, causing each level to split into three sublevels.[13,18] The rotational energy values of these sublevels are

$$F_+(J)=B_vJ(J+1)+2\zeta_iB_v(J+1)$$
$$F_0(J)=B_vJ(J+1)-2\zeta_iB_v \quad (4)$$
$$F_-(J)=B_vJ(J+1)-2\zeta_iB_vJ.$$

The selection rule for the rotational quantum number J is $\Delta J=0,\pm1$ and the permitted transitions are such that for $\Delta J=+1$ only the $F_-(J)$ sublevels combine with the ground state; for $\Delta J=0$, on the $F_0(J)$ sublevels, and for $\Delta J=-1$ only the $F_+(J)$ sublevels. Bearing in mind the above selection rules for the $F_+(J)$, $F_0(J)$, and $F_-(J)$ sublevels, the equations for the frequencies of the absorption lines may be found by subtraction of the ground state energies from those of the upper state. From these transitions, certain combination relations are derivable which are useful in the

TABLE III. Rotational constants of CD_4.

$\alpha_1 = -0.017$ cm^{-1}	$I_e = 10.70 \times 10^{-40}$ g-cm^2
$\alpha_2 = -0.015$ cm^{-1}	$r_{C-D} = 1.095 \times 10^{-8}$ cm
$\alpha_3 = 0.014$ cm^{-1}	$r_{D-D} = 1.788 \times 10^{-8}$ cm
$\alpha_4 = 0.017$ cm^{-1}	$\zeta_3 = 0.14_5$
$B_0 = 2.591$ cm^{-1}	$\zeta_4 = 0.35_5$
$B_e = 2.614$ cm^{-1}	

determination of the rotational constants of the molecule. These relations are

$$\begin{aligned} R(J)-P(J) &= 2(2J+1)(B'-\zeta_i B') \\ R(J-1)-P(J+1) &= 2(2J+1)(B''-\zeta_i B') \\ \tfrac{1}{2}[R(J-1)+P(J)] &= \tilde{\nu}_0+(B'-B'')J^2. \end{aligned} \tag{5}$$

The left-hand side of the first two of these combination relations when plotted *versus* $2(2J+1)$ yield straight lines whose slopes give numerical values for $(B'-\zeta_i B')$ and $(B''-\zeta_i B')$ where B' is the rotational constant of the excited state and B'' is the rotational constant for the ground state. The third relation when the left-hand side is plotted against J^2, likewise yields a straight line having as its intercept the band center and as its slope the difference in the B values of the excited state and the ground state, $(B'-B'')$. This latter slope is the convergence factor of the rotational lines in a particular band, and its negative is the vibration-rotation interaction constant (the α_i of (3)). Equations (5) have been plotted for a number of bands and the results of these plots are given in Table I. Typical plots for $\tilde{\nu}_4$ are shown in Fig. 13.

The rotational constants of the CD_4 molecule which can be obtained from the data of this article are the values of the moduli of the internal angular momentum, ζ_3 and ζ_4, the rotational constant of the ground state, B'' or B_0, the vibration-rotation interaction constants α_i, the equilibrium rotational constant B_e, and the B values of certain of the excited states. From B_e in turn, the moment of inertia of the molecule, I_e, and the internuclear distances are readily available.

The ground-state B value should be given directly by the combination differences when they are applied to the band $\tilde{\nu}_2$, since this band has no internal angular momentum. The value of B'' can be obtained also from the fundamentals $\tilde{\nu}_3$ and $\tilde{\nu}_4$, so there is a check available on its value. Considering this latter source, the slopes of the lines from the combination differences contain B', B'', and the magnitude of the internal angular momentum of the excited state. For these infrared active fundamentals the four equations are $B'_{\tilde{\nu}_3}-\zeta_3 B'_{\tilde{\nu}_3} = 2.180$ cm^{-1}, $B'_{\tilde{\nu}_4}-\zeta_4 B'_{\tilde{\nu}_4} = 1.684$ cm^{-1}, $B''-\zeta_3 B'_{\tilde{\nu}_3} = 2.194$ cm^{-1}, $B''-\zeta_4 B'_{\tilde{\nu}_4} = 1.701$ cm^{-1}. These four equations involve five unknowns, but a further relation exists between ζ_3 and ζ_4, $\zeta_3+\zeta_4=\frac{1}{2}$. The simultaneous solution of these five equations gives the following values: $B''=2.591$ cm^{-1}, $B'_{\tilde{\nu}_3}=2.577$ cm^{-1}, $B'_{\tilde{\nu}_4}=2.574$ cm^{-1}, and $\zeta_3=0.14_5$, $\zeta_4=0.35_5$. The value of B'' obtained by this method agrees well with the value of 2.592 cm^{-1} from $\tilde{\nu}_2$. The value of 2.591 cm^{-1} is taken as the better value.

The combination relations yield α_2, α_3, and α_4 but the value of α_1 cannot be obtained directly, because the vibration $\tilde{\nu}_1$ is inactive in the infrared. It is calculated from the combination band $\tilde{\nu}_1+\tilde{\nu}_4$ by the subtraction of α_4 from $(\alpha_1+\alpha_4)$. The values of the α_i are: $\alpha_1 = -0.017$, $\alpha_2 = -0.015$, $\alpha_3 = 0.014$, $\alpha_4 = 0.017$ cm^{-1}. Using these values in (3), the value of B_e is 2.614 cm^{-1}. There is some doubt as to the correctness of α_1 for it can be obtained only from combination bands which occur in regions of the spectrum where considerable overlapping of bands takes place. It is believed that the value from the combination band $\tilde{\nu}_1+\tilde{\nu}_4$ is a better value than that which would be obtained from the only other combination containing $\tilde{\nu}_1$ which was analyzed, the band $\tilde{\nu}_1+2\tilde{\nu}_3$.

The rotational constant B_e is related to the moment of inertia by $B_e = h/8\pi^2 c I_e$. The resulting calculation yields a value for I_e of 10.70×10^{-40} g-cm^2. The moment of inertia is a function of the internuclear distances in the following manner: $I_e = (8/3) m_D (r_{C-D})^2 = m_D (r_{D-D})^2$. These expressions lead to the values of the internuclear distances of $r_{C-D} = 1.095 \times 10^{-8}$, $r_{D-D} = 1.788 \times 10^{-8}$ cm. All of these constants are listed in Table III. It is of interest to compare these values with those of other isotopic forms. For methane, the r_{C-H} distance is 1.0929×10^{-8} cm[19] and in the isotopic molecule CH_3D, r_{C-H} has a value of $1.0935_6 \times 10^{-8}$ cm.[20]

VI. ACKNOWLEDGMENTS

The authors express their appreciation to Dr. W. H. Fletcher of the Department of Chemistry for his continued interest and helpful discussions throughout the course of this investigation.

[19] G. Herzberg, *Infrared and Raman Spectra of Polyatomic Molecules* (D. Van Nostrand Company, Inc., New York, 1945), p. 455.

[20] D. R. Boyd and H. W. Thompson, Trans. Faraday Soc. 49, 1281 (1953).

Iron-Catalyzed Reaction between Nitrosyl Disulfonate and Hydroxylamine Monosulfonate Ions*

WILLIAM J. RAMSEY† AND DON M. YOST
Gates and Crellin Laboratories of Chemistry, California Institute of Technology, Pasadena, California
(Received February 25, 1955)

An investigation of the kinetics of the iron-catalyzed reaction between the purple-colored, paramagnetic nitrosyl disulfonate ($ON(SO_3)_2^=$) ions and hydroxylamine monosulfonate ($HONHSO_3^-$) ions has been made. [W. J. Ramsey and D. M. Yost, J. Chem. Phys. **21**, 957 (1953)]. At a temperature of 20°C, an ionic strength of 0.026, and total added iron concentrations less than 3.5×10^{-7} *VF*, the initial rate of disappearance of $ON(SO_3)_2^=$ is well represented by the equation:

$$-\frac{d(ON(SO_3)_2^=)}{dt}=2\left\{\frac{k_2h_1(H^+)+k_3h_1h_2}{(H^+)^2+h_1(H^+)+h_1h_2}\right\}(\Sigma Fe^{+3})(HONHSO_3^-),$$

where h_1 and h_2 are the first and second hydrolysis constants for ferric iron and where k_2 and k_3 are the specific second-order rate constants for the reactions of $HONHSO_3^-$ with $Fe(OH)^{++}$ and $Fe(OH)_2^+$, respectively. Under the above conditions, and if a value of 3×10^{-3} is assumed for h_1; h_2, k_2, and k_3 have the values, 7×10^{-4} l·mole^{-1}, $13.7\pm1.0\times10^4$ l·mole^{-1}·min^{-1}, and $1.5\pm0.5\times10^4$ l·mole^{-1}·min^{-1}, respectively.

INTRODUCTION

THE iron catalyzed reaction between the purple-colored, paramagnetic nitrosyl disulfonate ions and hydroxylamine monosulfonate ions, $ON(SO_3)_2^=$ and $HONHSO_3^-$, respectively, is interesting for two reasons. First, the concentration of iron necessary to cause the reaction to proceed at an easily measurable rate is on the order of 10^{-7} mole per liter. Second, the ability of iron to catalyze the reaction is dependent upon hydrogen-ion concentration in a way that indicates that predominantly one of the hydrolyzed species of iron (III), $Fe(OH)^{++}$, is responsible for the catalysis. The stoichiometry of the reaction is,

$$4ON(SO_3)_2^=+2HONHSO_3^-+H_2O=N_2O+4HON(SO_3)_2^=+2HSO_4^-. \quad (1)$$

This iron-catalyzed reaction was investigated as part of a study of the autocatalytic decomposition of nitrosyl disulfonate ion. However, the iron-catalyzed reaction is of interest by itself, and further, is of little or no significance in the autocatalytic decomposition. A kinetic investigation of the autocatalytic decomposition of nitrosyl disulfonate ion has been reported in some detail by Murib and Ritter[1]; our own independent, unpublished study is in substantial agreement with the results of Murib and Ritter.

For the above reasons, the details of our investigation of the iron-catalyzed reaction between nitrosyl disulfonate and hydroxylamine monosulfonate ions are described below.

EXPERIMENTAL

Reagents

Potassium nitrosyl disulfonate was prepared by the method of Raschig,[2] and the preparation was further purified by recrystallizing it from 0.1-*VF* (formula weights per liter of solution) potassium hydroxide between 40° and 0°C. The resulting orange-colored crystalline product was washed three times with absolute alcohol and three times with absolute ether, and was then stored in a vacuum desiccator. In this way, a salt of purity greater than 99% is obtained.[3]

Anhydrous sodium hydroxylamine monosulfonate was prepared by the method of Raschig.[4] Salt samples thus prepared were found by iodometric titration to be about 75% pure, the principal impurity being sodium sulfate. Further purification was obtained by equilibrating the impure material with a 50–50 weight percent solution of methanol and water. Excess solid material was filtered off, and the relatively pure (93–97%) product was precipitated by adding excess absolute methanol. Again the main impurity was sodium sulfate as indicated by testing with barium chloride solution.

Iron-free potassium perchlorate, used to adjust the ionic strength, was prepared by adding a ten percent excess of concentrated perchloric acid to a saturated solution of potassium chloride. The precipitate was filtered, and washed several times with ice water and then recrystallized from water.

Standard 0.0167-*VF* lanthanum perchlorate solution was prepared by weighing out just 5.43 gm of lanthanum sesquioxide, just dissolving and neutralizing this solid with standard 0.100-*VF* perchloric acid, and diluting

* Taken in part from a thesis by William J. Ramsey submitted in partial fulfillment of the requirements for the Ph.D. degree at the California Institute of Technology in 1952.

† Present address: University of California Radiation Laboratory, Livermore, California.

[1] J. H. Murib and D. M. Ritter, J. Am. Chem. Soc. **74**, 3394 (1952).

[2] F. Raschig, *Schwefel- und Stickstoffstudien* (Verlag Chemie, G. m. b. H., Leipzig-Berlin, 1924), pp. 148–9.

[3] H. J. Tauber and G. Jellinek, Naturwiss. **38**, 259 (1951).

[4] Raschig, see reference 2, pp. 154–5.

the resulting solution to 1.00 liter. The lanthanum sesquioxide was labeled 99.9% pure and was obtained from Research Chemicals, Incorporated, Burbank, California.

Tap-distilled water was redistilled from alkaline permanganate in an all-pyrex still. Water thus purified had a specific conductance of about 5×10^{-5} mho, and a *p*H value of about 6.5. This water was stored in a bottle fitted with a soda-lime tube.

A solution of ferric perchlorate was prepared in the following way. Reagent-grade ferric chloride was twice resublimed. To the resulting solid was added a 20% excess of concentrated perchloric acid, and the mixture was fumed almost to dryness. More concentrated perchloric acid was added, and the mixture again fumed almost to dryness. Excess perchloric acid was then filtered off, and the precipitate was weighed and dissolved in enough 0.1-*VF* perchloric acid to make the solution obtained 0.1 *VF* in ferric perchlorate. This solution gave a negative test for chloride with silver nitrate.

A dilute solution of ferric perchlorate was prepared by adding one milliliter of the 0.1-*VF* solution to a liter of 1.0×10^{-3} *VF* perchloric acid. The authors are indebted to Mr. J. K. Rowley, who standardized the dilute stock solution by a coulometric method. This dilute stock solution underwent no significant change with time, as was indicated by the constancy of rate measurements made at the beginning and end of the period of its use.

A standard 0.0100-*VF* perchloric acid solution was prepared by diluting concentrated, vacuum-distilled perchloric acid, and was standardized against recrystallized borax, using a Beckman Model H *p*H meter to determine the end point.

Iron in the various reagents was tested for by the method of Appleman.[5] This test is sensitive to about one part per million of iron and, therefore, was useful only when relatively large amounts of iron were present.

Apparatus

All rate runs were carried out in a Beckman Model DU spectrophotometer, in ten-centimeter optical cells. A solution to be used in any rate run was first thermostated in a water bath. The cell compartment of the spectrophotometer was carefully thermostated. Temperature variations were within 0.05°C, provided that the temperature of the room was not more than a few degrees from the thermostating temperature.

Glassware was carefully cleaned in the following way. First the object was rinsed with chromic-acid cleaning solution, then with tap-distilled water, then with concentrated hydrochloric acid, then with acidified Versene Fe-3 Specific, then with more distilled water, and finally with several portions of redistilled water. When working with very small concentrations of iron, it was found desirable to rinse the reaction vessels in advance with a solution of the same concentration of iron (III) as that to be used in a rate run. This procedure largely eliminated any effects which may have been due to surface-adsorbed iron.

[5] See reference 8 in paper by Ramsey, Colichman, and Pack, J. Am. Chem. Soc. **68**, 1695 (1946).

OPTICAL PROPERTIES OF POTASSIUM NITROSYL DISULFONATE SOLUTIONS

Extinction coefficients of the purple solutions of potassium nitrosyl disulfonate were measured over a range of wavelengths and of concentrations. Values obtained for the coefficients are shown graphically in Fig. 1 and are in substantial agreement with those found in the visible region by Murib and Ritter.[3] There is a shoulder on the curve of coefficient *vs* wavelength at 2450 A, at which point it has the value 1690 ± 15 $l\cdot mole^{-1}\cdot cm^{-1}$. At 2450 A, the value of the extinction coefficient is independent of the concentration of potassium nitrosyl disulfonate in the range of concentrations between 2 and 6×10^{-5} *VF*.

Procedure for Rate Runs

In running any particular rate, all of the solutions to be used in establishing the conditions of the run, exclusive of that containing potassium nitrosyl disulfonate, were mixed in a reaction vessel, and the vessel was placed in the thermostat. A blank solution was prepared which was identical to the reaction mixture except that the volume of potassium nitrosyl disulfonate solution to be used was replaced by the same volume of water. Blank solutions were always placed in the same optical cell. The cell which was to contain the reaction mixture was first allowed to stand in the thermostated cell compartment for several minutes. An appropriate quantity of potassium nitrosyl disulfonate solution was then added to the reaction mixture, and the clock was started. Reaction mixtures were rapidly stirred, and portions were then placed in the reaction cell. First measurements of optical density

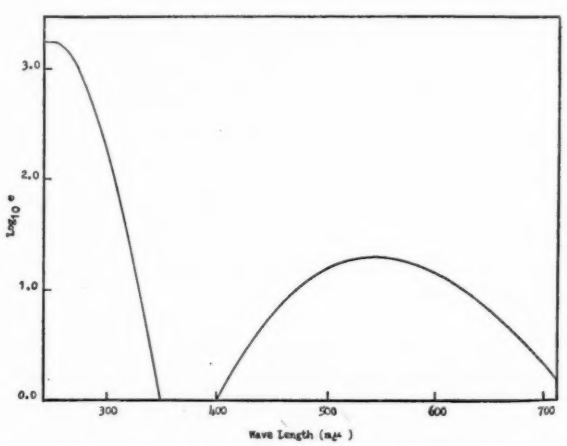

FIG. 1. Logarithm of extinction coefficient ($l\cdot mole^{-1}\cdot cm^{-1}$) of nitrosyl disulfonate ion *vs* wavelength ($m\mu$).

were usually obtained one and one-half minutes after the addition of the potassium nitrosyl disulfonate solution. Readings of optical density were made periodically, and the dark current and "zeroing" of the spectrophotometer were checked at appropriate intervals.

During the period of preparing for a rate run, and during the run itself, room temperature was kept within 2°C of the temperature at which the run was to be carried out.

Nitrosyl disulfonate ion undergoes slow, autocatalytic decomposition in dilute aqueous solution, and therefore solutions of this ion are used within one hour after their preparation.

Rates of disappearance of nitrosyl disulfonate were measured under the following initial conditions: Perchloric acid concentration, between 2.5×10^{-4} and 2.5×10^{-3} *VF*; ferric perchlorate, as high as 1.46×10^{-6} *VF*; sodium hydroxylamine monosulfonate, between 1.03 and 4.59×10^{-5} *VF*; potassium nitrosyl disulfonate, between 1.1 and 4.7×10^{-5} *VF* (determined spectrophotometrically); various concentrations of potassium perchlorate and lanthanum perchlorate to adjust the ionic strength; and the thermostating temperature, 20.00±0.03 or 30.00±0.03°C. In Table I are presented the time and concentration data for two typical experiments.

DISCUSSION

A reaction takes place between iron (III) and hydroxylamine monosulfonate which is entirely analogous to the reaction between iron (III) and hydroxylamine.[6] This reaction is,

$$4Fe(OH)^{++}+2HONHSO_3^- = N_2O+4Fe^{++}+2HSO_4^-+3H_2O. \quad (2)$$

TABLE I. Representative time-concentration data for rate measurements at 20°C.

Experiment No. 56 initial conditions		Experiment No. 88 initial conditions	
$(H^+)=5.0\times10^{-4}$ *VF*		$(H^+)=5.0\times10^{-4}$ *VF*	
$(HONHSO_3^-)=4.60\times10^{-5}$ *VF*		$(HONHSO_3^-)=4.58\times10^{-5}$ *VF*	
$(\Sigma Fe^{+3})_a=1.46\times10^{-7}$ *VF*		$(\Sigma Fe^{+3})_a=3.65\times10^{-7}$ *VF*	
$(KClO_4)=2.50\times10^{-2}$ *VF*		$(KClO_4)=2.50\times10^{-2}$ *VF*	
$(ON(SO_3)_2^=)=1.83\times10^{-5}$ *VF*		$(ON(SO_3)_2^=)=2.21\times10^{-5}$ *VF*	
Time (min)	$(ON(SO_3)_2^=)$ $\times10^5$ *VF*	Time (min)	$(ON(SO_3)_2^=)$ $\times10^5$ *VF*
1.50	1.71	1.50	1.85
2.00	1.65	2.00	1.72
2.50	1.60	2.50	1.60
3.00	1.54	3.00	1.49
3.50	1.49	3.50	1.37
4.00	1.43	4.00	1.26
4.50	1.37	4.50	1.14
5.00	1.32	5.00	1.05
5.50	1.26	5.50	0.93
6.00	1.20	6.00	0.82

[6] Bray, Simpson, and MacKenzie, J. Am. Chem. Soc. 41, 1363 (1919).

TABLE II. Values of R' at various concentrations of reactants (temperature 20°C; solutions 0.025 *VF* in $KClO_4$) initial concentrations (*VF*).

Experiment number[a]	$(H^+)\times10^3$	$(\Sigma Fe^{+3})_a$ $\times10^6$	$(HONHSO_3^-)$ $\times10^5$	$(ON(SO_3)_2^=)$ $\times10^5$	$R'\times10^2$ (min^{-1})
1	2.45	1.46	1.08	2.68	14.2
2	2.45	1.46	1.08	3.41	14.5
3	2.45	1.46	1.08	3.04	14.2
4	2.45	1.46	2.21	2.55	14.0
5	2.45	1.46	2.21	3.10	14.2
40–43	2.45	0.73	1.15	3.42	9.5
9–12	2.45	0.73	2.27	1.88	9.2_4
13–16	2.45	0.36_5	2.28	2.96	5.12
36–39	2.45	0.36_5	4.58	3.78	5.04
17–19	2.45	0.14_6	2.30	1.93	2.32
28–31	2.45	0.14_6	4.60	2.88	2.26
20–23	2.45	0.00	2.31	1.42	0.24
194–195	1.94	1.46	2.21	3.94	15.0
192–193	1.94	0.73	2.27	4.14	9.7
184–187	1.94	0.36_5	4.58	3.32	5.44
180–183	1.94	0.14_6	4.60	2.07	2.30
188–191	1.94	0.00	4.61	3.43	0.24
162–163	1.55	1.46	2.21	3.31	15.6
160–161	1.55	0.73	2.27	3.37	10.5
168–171	1.55	0.36_5	4.58	2.80	5.76
164–167	1.55	0.14_6	4.60	2.07	2.36
140–143	0.99	1.46	2.21	4.60	18.6
136–139	0.99	0.73	2.27	3.02	10.3
132–135	0.99	0.36_5	4.58	3.22	5.60
44–51	0.99	0.14_6	4.60	2.06	2.44
96–98	0.50	1.46	2.21	4.65	18.6
99	0.50	1.46	2.21	4.02	18.5
116–119	0.50	0.73	2.27	1.82	9.8
92–95	0.50	0.73	2.27	2.52	9.8
88–91	0.50	0.36_5	4.58	2.21	5.12
56–59	0.50	0.14_6	4.60	1.83	2.44
100–103	0.50	0.00	4.61	3.14	0.48
128–131	0.25	1.46	2.21	2.82	17.7
120–123	0.25	0.73	2.27	2.07	9.4
112–115	0.25	0.36_5	4.58	1.82	4.96
104–111	0.25	0.14_6	4.60	2.34	2.58

[a] Where a series of experiments is indicated, the initial conditions were the same for the series, and the value of R' is the average for the series.

A rapid reaction takes place between iron (II) and nitrosyl disulfonate ion in neutral or acid solutions:

$$Fe^{++}+ON(SO_3)_2^=+H_2O\rightarrow Fe(OH)^{++}+HON(SO_3)_2^=. \quad (3)$$

A quantitative determination of nitrosyl disulfonate ion could be based upon this reaction were it not for an indirect slow reaction between iron (III) and hydroxylamine disulfonate ion, $HON(SO_3)_2^=$.

Thus the stoichiometry of the iron-catalyzed reaction between nitrosyl disulfonate and hydroxylamine monosulfonate ions is obtained from Eqs. (2) and (3).

$$4ON(SO_3)_2^=+2HONHSO_3+H_2O = N_2O+4HON(SO_3)_2^=+2HSO_4^-. \quad (1)$$

In the majority of experiments the *initial* rate of disappearance of nitrosyl disulfonate ion was measured because of the complex reactions between the various products and the initial reactants. The value of the initial rate was determined by one of two methods. When the hydroxylamine monosulfonate ion concentration was greater than that of the nitrosyl disulfonate ion, the rate of disappearance of the latter was very

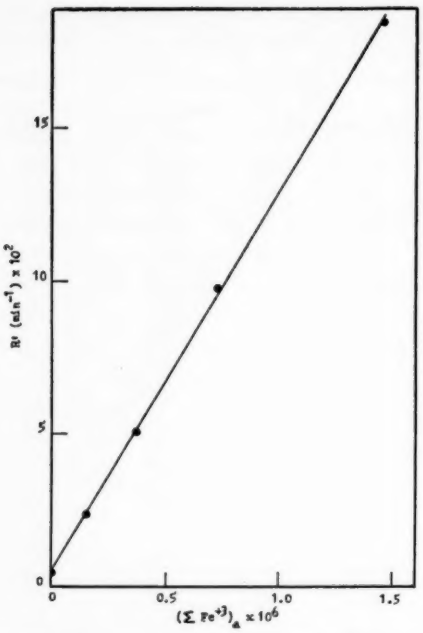

FIG. 2. R' *vs* $(\Sigma Fe^{+3})_a$, slope equals k_0. $((H^+)=0.50\times10^{-3}\ VF$; $(KClO_4)=0.0250\ VF$; $t=20°C.)$

nearly constant for the first three minutes of the reaction. Therefore, since spectrophotometric determinations of nitrosyl disulfonate ion concentration were made every half minute, the average amount disappearing in half a minute determined the rate. When the hydroxylamine monosulfonate ion concentration was not greater than the nitrosyl disulfonate ion concentration, a plot of the latter concentration *vs* time was constructed. This plot was extrapolated to zero time, and the slope at zero time was taken as the initial rate of the reaction.

When the initial concentration of nitrosyl disulfonate ion was of the same order of magnitude as that of the hydroxylamine monosulfonate ion, the initial rate of disappearance of the former ion was independent of its own concentration.

Initial rates were found to be proportional to initial concentrations of hydroxylamine monosulfonate ion. A quantity, R', is defined as the *initial* rate of disappearance of nitrosyl disulfonate ion divided by the initial concentration of hydroxylamine monosulfonate ion.

The quantity $(\Sigma Fe^{+3})_a$ is defined as the total concentration of added iron, i.e., it is the formula weights of ferric perchlorate added per liter of reaction mixture, while (ΣFe^{+3}) represents the total concentration of iron in the reaction mixture including the relatively small amounts in the other reagents.

In Table II are presented the values of R' obtained. The independence of R' upon the nitrosyl disulfonate ion concentration is shown by the first five and twenty-sixth through twenty-ninth entries in the table. The independence of R' upon hydroxylamine monosulfonate ion concentration is shown by the first eleven entries in the table.

At each of the lower hydrogen-ion concentrations, 2.5 and $5.0\times10^{-4}\ VF$, the values of R' are directly proportional to the total iron concentration, as shown for the latter case in Fig. 2. At higher hydrogen-ion concentrations, plots of R' *vs* $(\Sigma Fe^{+3})_a$ are not linear. At low total iron concentrations the plots are very nearly linear, but at higher total iron concentrations they deviate considerably from linearity. An example of this behavior is shown in Fig. 3. At these higher hydrogen ion concentrations, the slope of the curve of R' *vs* $(\Sigma Fe^{+3})_a$ was measured at $(\Sigma Fe^{+3})_a$ equal zero. This slope is defined as k_0. In the case of the linear plots of R' *vs* $(\Sigma Fe^{+3})_a$, obtained for the lower hydrogen-ion concentrations, the slope of the line is k_0.

There is at present no certain explanation of the curvature of the plots of R' *vs* $(\Sigma Fe^{+3})_a$. The curvature is not due to any slowness of the reaction between ferrous ion and nitrosyl disulfonate ion because the rate of disappearance of the latter is independent of its own concentration. Also, it is not due to complex formation between iron (III) species and hydroxylamine monosulfonate ion because the values of R' were independent of the concentration of the latter ion. It would seem to be due to the removal of Fe^{+++}, because the curvature increases with increasing hydrogen-ion concentration, and indeed, vanishes at low hydrogen-ion concentration.

The intercept of the extrapolated curve of R' *vs* $(\Sigma Fe^{+3})_a$ on the abscissa axis is numerically equal to the amount of iron due to the reagents. That amount was, on the average, $3\times10^{-8}\ VF$.

That the rate-determining step in this iron-catalyzed reaction is the reaction between iron (III) and hydroxylamine monosulfonate ion is proved by the following facts. The rate is independent of nitrosyl disulfonate ion

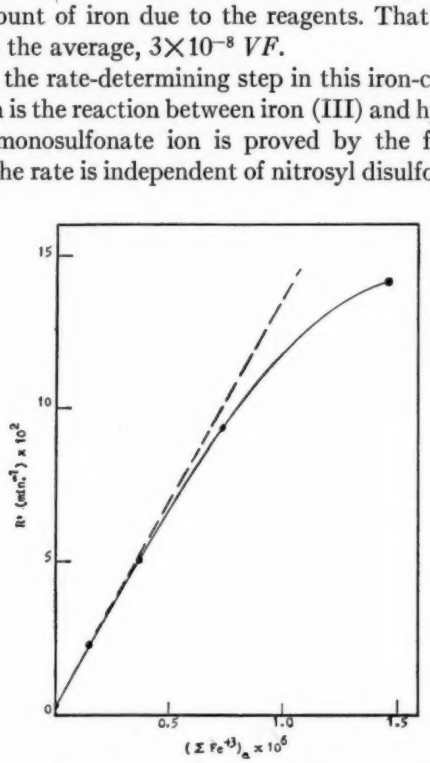

FIG. 3. $\hat{R}'$ *vs* $(\Sigma Fe^{+3})_a$, slope of dashed line equals k_0. $((H^+)=2.54\times10^{-3}\ VF$; $(KClO_4)=0.0250$; $t=20°C.)$

concentration; it is directly proportional to hydroxylamine monosulfonate ion concentration, and at low concentrations of added iron, the rate is directly proportional to these concentrations. Thus, at a given hydrogen-ion concentration, temperature, and ionic strength, and at total iron concentrations less than 3.5×10^{-7} VF, the rate of disappearance of nitrosyl disulfonate ion is well represented by the equation,

$$-\frac{d(ON(SO_3)_2^=)}{dt}=k_0(\Sigma Fe^{+3})(HONHSO_3^-). \quad (4)$$

Dependence of k_0 in Eq. (4) upon hydrogen-ion concentration, as shown graphically in Fig. 4, indicates that predominantly one of the hydrolyzed species of iron (III) is responsible for the catalysis. Since k_0 has a maximum value at a pH of about three, $Fe(OH)^{++}$ must be the principal catalytic species.

The problem of the dependence of k_0 upon hydrogen-ion concentration, may be treated mathematically in the following way. Let the three species, Fe^{+3}, $Fe(OH)^{++}$, and $Fe(OH)_2^+$, react with hydroxylamine monosulfonate ion with specific rate constants, k_1, k_2, and k_3, respectively. Futher, let h_1 and h_2 be the equilibrium constants, respectively, for the two reactions,

$$Fe^{+3}+H_2O=Fe(OH)^{++}+H^+ \quad (5)$$

and

$$Fe(OH)^{++}+H_2O=Fe(OH)_2^+ +H^+. \quad (6)$$

Under the conditions of these experiments, and assuming no $Fe(OH)_3$ to be present,

$$(\Sigma Fe^{+3})=(Fe^{+++})+(Fe(OH)^{++})+(Fe(OH)_2^+). \quad (7)$$

Making use of the equilibrium constants, and assuming that enough acid is present so that the hydrolysis of the iron does not change the hydrogen-ion concentration significantly, the following are obtained for the concentrations of the various iron (III) species:

$$(Fe^{+++})=\frac{(H^+)^2(\Sigma Fe^{+3})}{(H^+)^2+h_1(H^+)+h_1h_2}, \quad (8)$$

$$(Fe(OH)^{++})=\frac{h_1(H^+)(\Sigma Fe^{+3})}{(H^+)^2+h_1(H^+)+h_1h_2}, \quad (9)$$

$$(Fe(OH)_2^+)=\frac{h_1h_2(\Sigma Fe^{+3})}{(H^+)^2+h_1(H^+)+h_1h_2}. \quad (10)$$

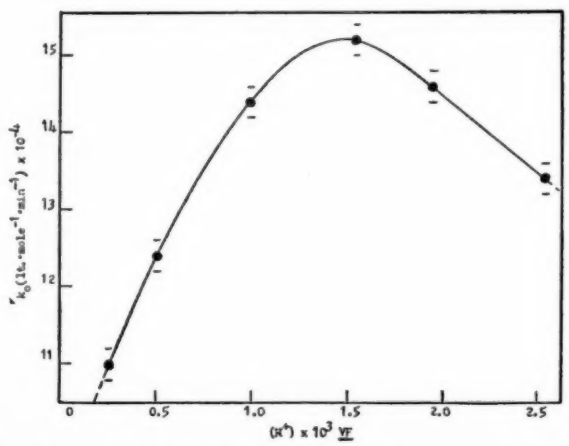

FIG. 4. k_0 *vs* (H^+), bars above and below point are equivalent to $\pm2\%$ error in k_0. $((KClO_4)=0.0250\ VF;\ t=20°C.)$

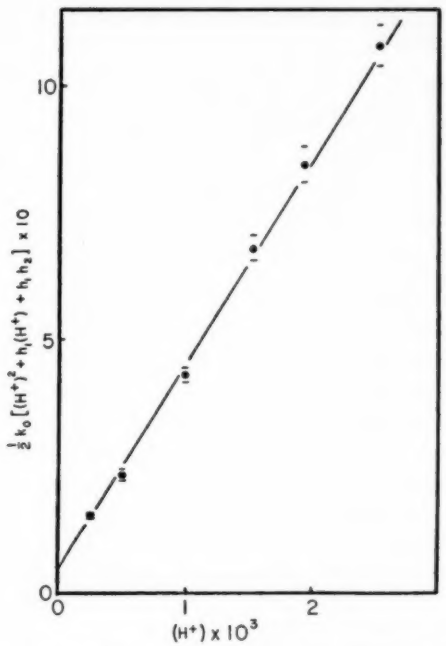

FIG. 5. A plot of the function $\frac{1}{2}k_0[(H^+)^2+h_1(H^+)+h_1h_2]$ *vs* (H^+). Bars above and below the points represent an error in k_0 of $\pm4\%$.

As shown above, the rate-determining step is the reaction between the various iron (III) species and hydroxylamine monosulfonate ion, also according to the stoichiometry of the over-all reaction (Eq. (1)), two moles of nitrosyl disulfonate ion are reduced per mole of the monosulfonate reacting with iron (III). Therefore, the rate of disappearance of nitrosyl disulfonate ion will be twice the rate of reaction between iron (III) and hydroxylamine monosulfonate ion, and

$$\frac{1}{2}k_0(\Sigma Fe^{+3})=k_1(Fe^{+++})+k_2(Fe(OH)^{++})+k_3(Fe(OH)_2^+). \quad (11)$$

By substituting Eqs. (8), (9), and (10) into Eq. (11), and simplifying, k_0 is related to the hydrogen-ion concentration by the expression,

$$\frac{1}{2}k_0=\frac{k_1(H^+)^2+k_2h_1(H^+)+k_3h_1h_2}{(H^+)^2+h_1(H^+)+h_1h_2}. \quad (12)$$

If it is assumed that both k_1 and k_3 are zero, k_0 will have a maximum value when (H^+) is equal to $\sqrt{h_1h_2}$.

TABLE III. Effect of ionic strength on k_0.

$(H^+)\times10^3$ VF	$\mu\times10^3$	$k_0\times10^{-4}$ $l\cdot mole^{-1}\cdot min^{-1}$
1.94	2.70 ($KClO_4$, 2.5×10^{-2} VF)	14.6
1.94	2.70 ($La(ClO_4)_3$, 4.17×10^{-3} VF	14.4
1.94	0.20	18.7
0.50	2.55 ($KClO_4$, 2.5×10^{-2} VF)	12.5
0.50	2.55 ($La(ClO_4)_3$, 4.17×10^{-3} VF)	12.5
0.50	0.06	19.8

The maximum value of k_0 occurs when (H^+) equals 1.5×10^{-3} VF. Although there is general disagreement about the value of h_1,[7] a value of about 3×10^{-3} is reasonable for a temperature of 20°C and an ionic strength of 0.025. Therefore, if k_1 and k_3 are zero, h_2 has the value, 7×10^{-4}. This value of h_2 might appear to be higher than expected, but recently, a value for the ratio of h_1 to h_2 of only 1.67 for somewhat different conditions has been reported.[8]

Using the values of h_1 and h_2 stated above, a plot of $\frac{1}{2}k_0[(H^+)^2+h_1(H^+)+h_1h_2]$ *vs* (H^+) was constructed, and is shown in Fig. 5. That the plot is very nearly linear indicates that Fe^{+++} is insignificant in the catalysis. The slope of the curve is equal to k_2h_1, and the intercept is equal to $k_3h_1h_2$. The least-squares method was used to fit the line. Calculated values of k_2 and k_3 are $13.7\pm1.0\times10^4$ $l\cdot mole^{-1}\cdot min^{-1}$ and $1.5\pm0.5\times10^4$ $l\cdot mole^{-1}\cdot min^{-1}$. The limits of error in the rate constants are estimated on basis of the accuracy of the least-squares calculation.

Values of k_2 and k_3 obtained by the above calculations depend critically upon the value chosen for h_1, and since there does exist disagreement about the value of h_1, the values of k_2 and k_3 must remain tentative.

A value other than zero for k_3 would be expected to change the value found for h_1h_2, and, therefore, change the evaluation of k_3. However, when k_3 is not zero the maximum value of k_0 occurs at,

$$(H^+)=\left[\frac{k_3^2h_2^2}{k_2^2}+\frac{h_1h_2}{k_2}(k_2-k_3)\right]^{\frac{1}{2}}-\frac{k_3h_2}{k_2}. \qquad (13)$$

Using the values determined above for k_2, k_3, h_1, and h_2, k_0 should have a maximum value when the hydrogen-ion concentration is 1.4×10^{-3} VF, which agrees with the experimental value within the limits of experimental error.

The following mechanism is in accord with the experimental data:

$$Fe(OH)^{++}+HONHSO_3^- \xrightarrow{k_2} \text{reactive products}+Fe^{++} \qquad (14)$$

$$Fe(OH)_2^{+}+HONHSO_3^- \xrightarrow{k_3} \text{reactive products}+Fe^{++} \qquad (15)$$

[7] T. H. Siddall, III, and W. C. Vosburgh, J. Am. Chem. Soc. **73**, 4270 (1951).
[8] B. O. A. Hedström, Arkiv Kemi **6**, 1 (1953).

$$\text{reactive products}+ON(SO_3)_2^= \rightarrow N_2O+HON(SO_3)_2^= \qquad (16)$$

$$\text{reactive products}+Fe(III) \rightarrow N_2O+Fe^{++} \qquad (17)$$

$$Fe^{++}+ON(SO_3)_2^=+H_2O \rightarrow Fe(OH)^{++}+HON(SO_3)_2^=. \qquad (3)$$

Equation (17) summarizes the reactions which may take place between various species of iron (III) and the reactive products of the initial oxidation of hydroxylamine monosulfonate ion. The reactions represented by Eqs. (3) and either (16), (17), or both must be fast compared to those represented by Eqs. (14) and (15).

Effects of ionic strength upon the rate of reaction would be expected to be complex, because of the nature of k_0. Further, there is disagreement about the quantitative effect of "inert" electrolytes upon the hydrolysis of ferric ion[9,10] and upon ionic reactions in general.[10] Therefore, the experimental results summarized in Table III are useful primarily in determining the magnitude of any errors resulting from small changes in ionic strength. From the values shown it is evident that a change in ionic strength of ten percent would cause a change of about one percent in the value of k_0. Also, there is no measurable difference between the effects of lanthanum perchlorate and potassium perchlorate at the same ionic strength.

Effects of temperature changes upon the rates of the reaction would be expected to be complex, again because of the nature of k_0. Effects of a ten degree change in temperature upon the values of k_0 obtained at hydrogen-ion concentrations of 1.94 and 0.50×10^{-3} VF are shown in Table IV. Also, an apparent activation energy, ΔE_a, has been calculated by use of the equation,

$$\Delta E_a=\frac{-R\Delta \ln k_0}{\Delta\frac{1}{T}}, \qquad (18)$$

TABLE IV. Effect of temperature on k_0 ($KClO_4=2.5\times10^{-2}$ VF).

$(H^+)\times10^3$ VF	t°C	$k_0\times10^{-4}$ $l\cdot mole^{-1}\cdot min^{-1}$	$\Delta E_a=\frac{R\Delta \ln k_0}{\Delta\frac{1}{T}}$
1.94	20.0	14.6	
1.94	30.0	48.6	21.4 kcal
0.50	20.0	12.5	
0.50	30.0	41.7	21.4

[9] A. R. Olson and T. R. Simonson, J. Chem. Phys. **17**, 1322 (1949).
[10] A. R. Olsen and T. R. Simonson, J. Chem. Phys. **17**, 1167 (1949).

where T is the absolute temperature, and R the gas constant. That ΔE_a has the same value for the two hydrogen-ion concentrations is quite probably fortuitous.

An estimate of the possible error due to incomplete temperature control shows that a 0.08°C error in temperature gives rise to an error of one percent in the value of k_0.

The authors wish to express their appreciation to the Research Corporation, the Shell Oil Company, and E. I. Du Pont de Nemours and Company for grants which supported this work.

THE JOURNAL OF CHEMICAL PHYSICS VOLUME 23, NUMBER 11 NOVEMBER, 1955

Mass Spectrometric Study of Barium Oxide Vapor*

MARK G. INGHRAM, WILLIAM A. CHUPKA, AND RICHARD F. PORTER
Department of Physics, University of Chicago, Chicago, Illinois and Argonne National Laboratory, Lemont, Illinois

(Received February 17, 1955)

Ions formed by electron bombardment of the vapor in thermodynamic equilibrium with BaO solid have been studied mass spectrometrically. The BaO solid was heated in a Knudsen cell and a sample of the effusing vapor entered the ion source of a mass spectrometer. At cell temperatures between 1500°K and 1800°K, ion currents of Ba^+, BaO^+, Ba_2O^+, $Ba_2O_2^+$, and $Ba_2O_3^+$ were observed. The variations of ion intensities with temperature were measured and appearance potential curves were obtained. Possible mechanisms of ion formation were considered, and evidence for the existence of gaseous molecular species of BaO, Ba_2O, Ba_2O_2, and Ba_2O_3 was obtained. The major molecular species, effusing from the Knudsen cell, was BaO. A thermodynamic treatment of ion currents yields the following heats of reaction

$$BaO(s)=BaO(g); \quad \Delta H_0^\circ=104\pm4 \text{ kcal/mole}$$
$$BaO(g)=Ba(g)+O(g); \quad \Delta H_0^\circ=130\pm5 \text{ kcal/mole}$$
$$Ba_2O_2(g)=2BaO(g); \quad \Delta H_{1700}^\circ=89\pm11 \text{ kcal}$$
$$Ba_2O(g)=Ba(g)+BaO(g); \quad \Delta H_{1700}^\circ=93\pm17 \text{ kcal.}$$

INTRODUCTION

THE species evaporating from heated metal surfaces coated with barium oxide have been studied by earlier workers employing mass spectrometric methods. These workers[1–4] found that BaO^+ was the predominant ion formed by electron bombardment of the vapor. This indicated that BaO gas is the principal vaporizing species. In addition to BaO^+, Aldrich[2] observed less intense currents of Ba_2O^+ and $Ba_2O_2^+$. Pelchowitch[3] measured the temperature dependence of $Ba_2O_2^+$ and obtained further evidence that the oxide vaporizes to a small degree as gaseous Ba_2O_2.

Our purpose has been to extend the work on barium oxide by studying the vapor in thermodynamic equilibrium with BaO solid inside a Knudsen cell. A sample of this vapor effusing from the Knudsen cell enters directly into an ion source of a mass spectrometer. With this experimental arrangement, observation of ions and measurements of ion currents offer both a means of identifying the molecular species in the vapor and of obtaining thermodynamic data for the gaseous equilibria inside the Knudsen cell. In this experiment the activities (or partial pressures) of the gaseous species involved in the equilibria are measured. Only one assumption regarding the activity of a component is made. It is assumed that the activity of the BaO solid phase is nearly unity. Since BaO solid is present in large quantity, this should be a good assumption. Experimental evidence in support of the assumption can be obtained by x-ray and chemical examination of material removed from the inside of the cell after completion of an experiment. It is further assumed that the gaseous species reach equilibrium with each other and with the BaO solid phase. The use of a Knudsen cell with a large ratio of internal BaO surface area to effusion-hole area justifies this assumption.

This method of approach differs from the filament-type experiment in that here one is dealing with equilibrium concentrations of gases while the filament work deals principally with rates of vaporization. Thus, while the Knudsen cell method generally yields the true ΔH of vaporization, the surface-evaporation method yields only the activation energy of vaporization which may be equal to or greater than the true ΔH of vaporization. For calculation of such quantities as dissociation energies, it is, of course, necessary to know the true ΔH of vaporization.

EXPERIMENTAL

The Knudsen cell assembly for the mass spectrometer has been described earlier by Chupka and Inghram[5]

* This work was supported in large part by a grant from the National Science Foundation.

[1] R. H. Plumlee and L. P. Smith, J. Appl. Phys. **21**, 811 (1950).
[2] L. T. Aldrich, J. Appl. Phys. **22**, 1168 (1951).
[3] I. Pelchowitch, Philips Research Repts. **9**, 42 (1954).
[4] P. W. Bickel and L. V. Holroyd, J. Chem. Phys. **22**, 1793 (1954).
[5] W. A. Chupka and M. G. Inghram, J. Phys. Chem. **59**, 100 (1955).

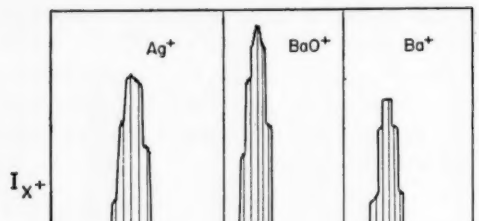

FIG. 1. Shutter "profiles" of Ag^+, Ba^+, and BaO^+. The Ba^+ and BaO^+ "profiles" are essentially the same as that of Ag^+, showing that Ba^+ and BaO^+ are formed by electron impact of gases coming from the orifice of the Knudsen cell. The position of maximum intensity of the Ba^+ and BaO^+ curves is slightly shifted from that of Ag^+. This shift is due to motion of the Knudsen cell, caused by thermal expansion due to heating. The small "shoulder" on the Ba^+ curve is due to Ba(g) re-evaporated from radiation shields.

and Porter, Schissel, and Inghram.[6] A significant feature of the apparatus is the shutter arrangement by means of which one may distinguish between ion currents formed from gases coming out of the Knudsen cell and ion currents formed from background gases.[5] In each run a weighed amount of silver was first vaporized from the crucible. Introduction of the silver serves as a method of obtaining a shutter "profile" and a sensitivity calibration of the mass spectrometer. The shutter consists of a movable plate with a 0.020 inch by 0.75 inch slit in the center. It is mounted between the Knudsen cell and the ion source. The shutter is operated manually. The shutter "profile" is the correlation between the intensity of the ion beam and the position of the shutter. The ion intensity is a maximum when the shutter slit is on a line between the effusion hole of the Knudsen cell and the entrance to the ionization chamber of the ion source. The intensity decreases rapidly as the slit is moved to either side of this position. Figure 1 shows examples of shutter "profiles" obtained in this work. Ions formed from gaseous species coming from the crucible region, but not from the effusion hole, will have a shutter "profile" different from that of the Ag^+ used for calibration purposes. Only intensity data for those ions having the same shutter "profile" as Ag^+ were treated. The sensitivity calibration was made in terms of the ion current of Ag^{107+} per atmosphere of silver vapor and was obtained by dividing the ion current of Ag^{107+} (averaged over the time required for all the silver to vaporize) by the pressure of Ag^{107} inside the Knudsen cell calculated from the effusion equation.

Knudsen cells constructed of alumina crucibles and covers were used in the majority of experiments. In one set of experiments, however, a Knudsen cell consisting of a thoria crucible and a tantalum cover was used. The quoted purity of the alumina was 99.5% Al_2O_3. The crucibles were 2.5 cm deep and had an internal diameter of 1 cm. The cover had a "knife edge" effusion hole with an area of 0.011 cm^2. The inner surface of the crucible was completely covered with a pressed layer of barium oxide powder about 1 mm thick. The ratio of the geometrical surface area of BaO to the area of the effusion hole, at the beginning of an experiment, was greater than 200 to 1. The effusion cells were placed in a tantalum oven which was heated by high-voltage electron bombardment.[5]

After completion of one of the longest high-temperature experiments, the crucible was disassembled and the contents were examined by x-ray, spectroscopic, and chemical methods. The x-ray analysis showed the presence of only barium hydroxide in samples taken from the bottom of the crucible. The hydroxide presumably resulted from hydration of BaO(s) when the samples were exposed to air. In addition, a poorly crystallized phase was present as a smooth layer adjacent to the alumina. This layer was fragile and was easily separated from the alumina surface. Chemical analysis showed it to be 72.1 mole percent BaO and 27.9 mole percent Al_2O_3. The presence of excess BaO(s) indicates that even after heating the crucible for a long period of time, a BaO(s) phase still existed on the inner surface of the Knudsen cell. These observations substantiate the assumption that in the early phase of the experiment when absolute pressures were measured, the activity of BaO(s) could be considered to be unity.

In addition to the runs with pure BaO(s), one run was made in which a piece of Ba metal was heated with BaO(s) in an alumina Knudsen cell.

Temperatures of the oven were read with an optical pyrometer, and emissivity and window corrections were added. The estimated uncertainty in quoted temperatures (including corrections and systematic errors) is $\pm 1\%$.

RESULTS FROM ALUMINA KNUDSEN CELLS

As in the filament experiments of earlier workers, ion currents of Ba^+, BaO^+, Ba_2O^+, and $Ba_2O_2^+$ were observed. In addition, an ion current of $Ba_2O_3^+$ was observed under certain conditions.

Ba^+ and BaO^+

Appearance potential curves for Ba^+ and BaO^+ are shown in Fig. 2. The intensity of the BaO^+ ion beam was found to be a function of temperature only. Since (as is shown later) the BaO^+ beam is a measure of BaO pressure in the cell, this observation shows that the activity of the BaO(s) did not change appreciably during an experiment. On the other hand, the Ba^+ was a function of both temperature and time. At the

[6] Porter, Schissel, and Inghram, J. Chem. Phys. 23, 339 (1955).

beginning of each run when the crucible was first brought to operating temperature, the Ba^+ was approximately an order of magnitude lower than BaO^+. After the crucible had been maintained for some time at a constant temperature, however, the Ba^+ increased relatively and eventually became as intense as the BaO^+. The Ba^+ (1) curve in Fig. 2 was obtained shortly after the crucible had been brought to the operating temperature and under these conditions a major fraction of Ba^+ is formed by dissociative ionization, presumably of BaO, as is indicated by the break in the appearance potential curve. The Ba^+ (2) curve was obtained after the crucible has been heated for some time, and under these conditions the Ba^+ formed by dissociative ionization is only about ten percent of the Ba^+ formed from Ba gas. The rise of Ba^+ intensity with time is probably due to the reduction of $BaO(s)$ by some impurity which slowly diffuses into the Knudsen cell, as is also indicated by a discoloration which appeared on the outer walls of the alumina cell and which progressively decreased toward the inner surfaces. The Ba^+ intensity eventually approached a constant value at a given temperature, indicating that the diffusion process finally approached a steady state. It is unnecessary to consider the details of the reaction producing the Ba gas, even though it is a nonequilibrium process, so long as the Ba gas reaches equilibrium with the other species inside the Knudsen cell.

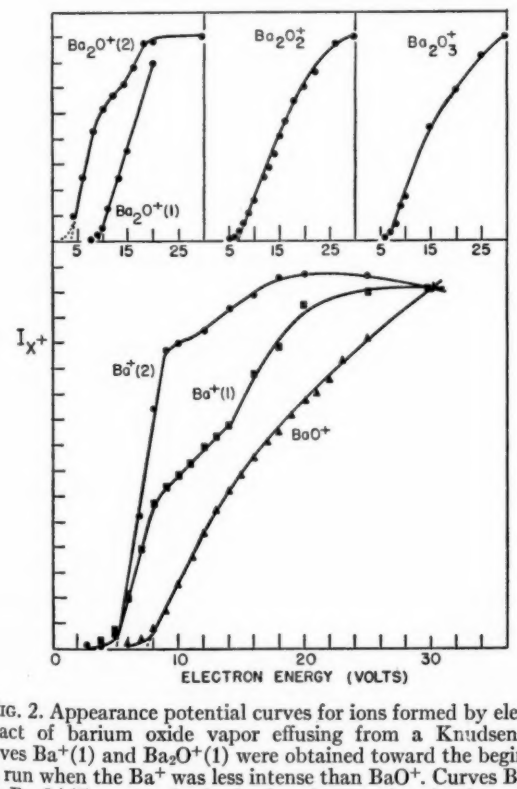

FIG. 2. Appearance potential curves for ions formed by electron impact of barium oxide vapor effusing from a Knudsen cell. Curves $Ba^+(1)$ and $Ba_2O^+(1)$ were obtained toward the beginning of a run when the Ba^+ was less intense than BaO^+. Curves $Ba^+(2)$ and $Ba_2O^+(2)$ were obtained after increased reduction of the BaO solid by impurities, when the Ba^+ and BaO^+ intensities were approximately equal.

The appearance potential of the BaO^+ is only about 2.5 volts higher than that of Ba^+. The relatively low value of this appearance potential is evidence that the BaO^+ is being formed by simple ionization of BaO gas rather than by dissociative ionization of other species. The fact that the BaO^+ ion intensity is more than two orders of magnitude greater than the intensities of Ba_2O^+, $Ba_2O_2^+$, and $Ba_2O_3^+$ further indicates that the amount of BaO^+ resulting from dissociative ionization of the heavier species must be small.

It is possible to calculate the partial pressure of the BaO gas inside the Knudsen cell from the sensitivity calibration with silver and an estimate of the relative ionization cross sections of Ag and BaO. The partial pressure of a gaseous species, x, is obtained from the ion current, $I_{x^{i+}}$, by the relationship:

$$P_x=\frac{1}{r_i k}\left(\frac{\sigma(\mathrm{Ag})}{\sigma(x)}\right)\left(\frac{T(x)}{T(\mathrm{Ag})}\right)\left(\frac{S(\mathrm{Ag}^+)}{S(x^+)}\right)I_{x^{i+}}.$$

The symbols in the equation are defined as follows:

P_x = the partial pressure of gaseous species, x.

x^{i+} = ion of isotopic species of molecule x having mass i.

r_i = the isotopic fraction of molecules having mass i.

$\sigma(\mathrm{Ag})/\sigma(x)$ = the ratio of ionization cross sections for Ag and x. Electron energies were selected from appearance potential curves for Ag^+ and x^+ and correspond to approximately maximum ionization cross sections. The maximum for Ag^+ occurs at about 80 volts.

$T(x)$ = temperature of the Knudsen cell during during observation of x^+.

$T(\mathrm{Ag})$ = temperature of the Knudsen cell during observation of Ag^+, approximately 1400°K.

$S(\mathrm{Ag}^+)/S(x^+)$ = a correction due to different electron multiplier efficiencies of Ag^+ and x^+ (estimated from reference 7).

k = the sensitivity in arbitrary units of Ag^{107+} ion intensity for 80-volt electrons per atmosphere of silver vapor.

$I_{x^{i+}}$ = observed ion intensity of x^{i+} in same units as used for Ag^+.

Results of the BaO pressure calculation are given in Table I. An estimated value of $\frac{1}{2}$ was taken for $\sigma(\mathrm{Ag})/\sigma(\mathrm{BaO})$, and $S(\mathrm{Ag}^+)/S(\mathrm{BaO}^+)$ was taken to be 1.2.

Free energy functions for BaO solid were calculated above 298°K from Lander's heat capacity equation as published by Drummond and Barrow.[8] This heat capacity equation was extrapolated above 1400°K.

[7] Inghram, Hayden, and Hess, Mass Spectroscopy in Physics Research, Natl. Bur. Standards Circular 522, p. 257 (1953).

[8] G. Drummond and R. F. Barrow, Trans. Faraday Soc. 47, 1275 (1951).

TABLE I. Calculation of BaO pressure and $\Delta H_0°$ of sublimation.

Run	Sensitivity, k, in units of Ag^{107+} ion intensity per atmos of Ag vapor	BaO^{154+} ion intensity	Temp. °K	BaO pressure (in atmos)	$\frac{-(\Delta Fr°-\Delta H_0°)_{BaO(s)}}{T}$ $=BaO(g\,^1\Sigma)$	$\Delta H_0°$ kcal/mole
1	3.9×10^{11}	6.5×10^{4}	1530	1.5×10^{-7}	36.44	103.5
1	3.9×10^{11}	4.9×10^{5}	1667	1.3×10^{-6}	36.11	105.0
2	5.4×10^{11}	5.2×10^{5}	1655	9.4×10^{-7}	36.13	105.5
3	1.3×10^{12}	9.8×10^{6}	1758	7.9×10^{-6}	35.89	104.0

The value of $H_{298}°-H_0°$ for BaO solid was obtained from the data of Anderson.[9] For the gas, the vibrational and rotational contributions to the free energy functions were calculated from spectroscopic constants[10] for the lowest $^1\Sigma$ state of BaO. No electronic contribution has been included for the gas. The total probable error in the calculated pressure of BaO, including the uncertainty in ionization cross section, is about a factor of three. Averaging results, we obtain for the reaction

$$BaO(s)=BaO(g,\,^1\Sigma),\quad \Delta H_0°=104\pm4\text{ kcal/mole}.$$

The heat of sublimation of BaO gas was also obtained from the conventional Clapeyron-Clausius plot. A plot of $\log I_{BaO^+}T$ *versus* $1/T$ is shown in Fig. 3. By the slope method we obtain for the reaction

$$BaO(s)=BaO(g),\quad \Delta H_{1700}°=102\pm8\text{ kcal/mole},$$

and correcting this value to 0°K,[11] $\Delta H_0°=109\pm9$ kcal/mole. The slope method serves as an independent check on the absolute-pressure method. In particular, the results of the slope method may be used as a crude check on the accuracy of the estimated relative ionization cross sections of Ag^+ and BaO^+, since the slope method requires no estimate of these quantities.

Ba_2O^+ and $Ba_2O_2^+$

The small intensities of Ba_2O^+ and $Ba_2O_2^+$ permitted only rough appearance potential measurements, as shown in Fig. 2. Only one higher mass peak, $Ba_2O_3^+$, was observed. The $Ba_2O_3^+$ peak had a different temperature dependence from either Ba_2O^+ or $Ba_2O_2^+$ (see Table II). For this reason, the amount of Ba_2O^+ or $Ba_2O_2^+$ formed by dissociative ionization of Ba_2O_3 must be small. The fact that $Ba_2O_3^+$ was about an order of magnitude less intense than either Ba_2O^+ or $Ba_2O_2^+$ is further evidence that the amount of Ba_2O^+ and $Ba_2O_2^+$ formed by dissociative ionization of Ba_2O_3 is small.

The possibility that $Ba_2O_2^+$ is formed by the reaction $BaO^+ + BaO(g)\rightarrow Ba_2O_2^+$ in the ionization chamber was considered. If most of the $Ba_2O_2^+$ were formed by this mechanism, the $Ba_2O_2^+$ peak should increase as the square of the BaO^+ peak, and the slope of the temperature-dependence curve for $Ba_2O_2^+$ should be twice that of the BaO^+ curve. From the curves in Fig. 2 it is observed that the $Ba_2O_2^+$ curve has nearly the same slope as the BaO^+ curve rather than twice the value, showing that $Ba_2O_2^+$ cannot be formed in appreciable amounts by a second-order mechanism involving BaO. The only reasonable mechanism by which $Ba_2O_2^+$ can be formed is by simple ionization of Ba_2O_2 gas. As in the case of BaO^+ the $Ba_2O_2^+$ was found to be a function of temperature only, indicating that the activity of $BaO(s)$ remained essentially constant during the course of an experiment.

The fact that within the experimental uncertainty BaO^+ and $Ba_2O_2^+$ increase at the same rate with increasing temperature does not contradict the previous argument that BaO^+ is not formed appreciably by dissociative ionization of Ba_2O_2. This simply indicates that $BaO(g)$ and $Ba_2O_2(g)$ have nearly equal heats of sublimation. From the temperature-dependence curve for $Ba_2O_2^+$ (as shown in Fig. 3) we obtain for the reaction,

$$2BaO(s)=Ba_2O_2(g),\quad \Delta H_{1700}°=105\pm10\text{ kcal}.$$

Using the graphically determined heat of sublimation of $Ba_2O_2(g)$ and the heat of sublimation of $BaO(g)$ from Table I,[11] we obtain for the reaction

$$Ba_2O_2(g)=2BaO(g),\quad \Delta H_{1700}°=89\pm11\text{ kcal}.$$

This value is considered to be more accurate than the value obtained by combining twice the graphical heat of sublimation of BaO(g) with the graphical heat of sublimation of $Ba_2O_2(g)$. Although there may be a partial cancellation of systematic errors by combining

TABLE II. Ion intensity data[a] for Ba_2O^+, $Ba_2O_2^+$, and $Ba_2O_3^+$.

Ion	Relative ion intensity	Temperature °K	$\frac{(I_{Ba_2O^+})(I_{Ba_2O_3^+})}{(I_{Ba_2O_2^+})^2}$
Ba_2O^+	31.0		
$Ba_2O_2^+$	13.0	1775	0.38
$Ba_2O_3^+$	02.1		
Ba_2O^+	13.5		
$Ba_2O_2^+$	06.0	1721	0.56
$Ba_2O_3^+$	01.5		
Ba_2O^+	6.5		
$Ba_2O_2^+$	3.1	1689	0.61
$Ba_2O_3^+$	0.9		
Ba_2O^+	22.5		
$Ba_2O_2^+$	13.0	1762	0.37
$Ba_2O_3^+$	02.8		

[a] All ion current produced with 30-volt electrons.

[9] C. T. Anderson, J. Am. Chem. Soc. **57**, 429 (1935).

[10] G. Herzberg, *Molecular Spectra and Molecular Structure, I. Spectra of Diatomic Molecules* (D. Van Nostrand Company, Inc., New York, 1950), p. 507.

[11] Heat-capacity data for BaO solid were taken from references 8 and 9, and a heat capacity of 9 cal/deg was used for BaO gas.

graphical values, the probable error in the heat of dimerization of $BaO(g)$ by this method is still larger than that obtained in the former manner.

At the beginning of a run, the Ba_2O^+ was less intense than $Ba_2O_2^+$. As the crucible was held at a constant temperature, the Ba_2O^+ intensity increased and eventually became greater than that of the $Ba_2O_2^+$. Appearance potential curves in Fig. 2 for Ba_2O^+ show that Ba_2O^+ is formed by two mechanisms. The $Ba_2O^+(1)$ curve was obtained at the beginning of the run when the Ba_2O^+ peak was an order of magnitude lower than the $Ba_2O_2^+$ peak. Under these conditions Ba_2O^+ appears at approximately 10 volts and is probably formed by dissociative ionization of Ba_2O_2. The $Ba_2O^+(2)$ curve was obtained after the crucible had been heated for some time and the Ba_2O^+ intensity had become comparable to the $Ba_2O_2^+$ intensity. Under these conditions Ba_2O^+ appears at approximately 4 volts and only a small fraction of the Ba_2O^+ intensity can be formed, even at higher voltages, by dissociative ionization. It is believed that the part of the $Ba_2O^+(2)$ appearance potential curve below ten volts in Fig. 2

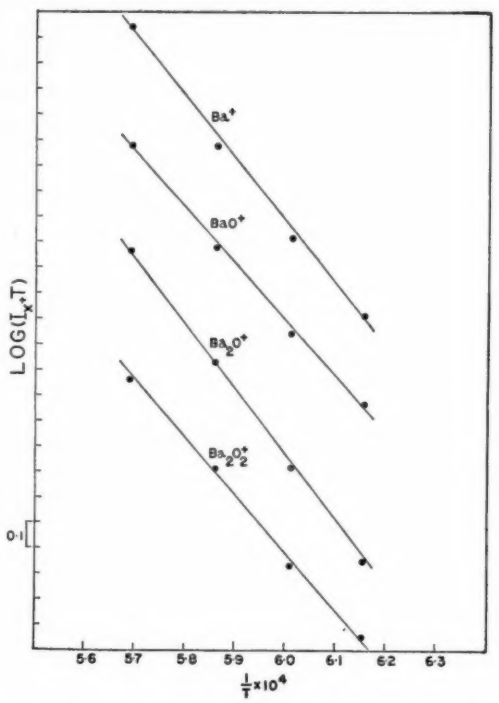

FIG. 3. Temperature-dependence curves for ions formed by electron impact on barium oxide vapor effusing from a Knudsen cell. Ions were formed by 30-volt electrons. The partial pressure of gaseous species, x, is related to the ion current, I_x^+, by the equation: $P_x = cI_x^+T$, where T is the temperature of the Knudsen cell and c is a proportionality constant. No direct thermodynamic significance, i.e., heats of vaporization, should be attached to the slopes of Ba^+ and Ba_2O^+ curves separately. However, the difference of these two slopes combined with the BaO slope (see Fig. 4), does have thermodynamic significance. The conditions prevailing in the Knudsen cell were those of curve (2) of Fig. 2. For convenience of plotting, intensities for each curve were multiplied by an arbitrary constant factor, and the position of one curve with respect to the others is not significant.

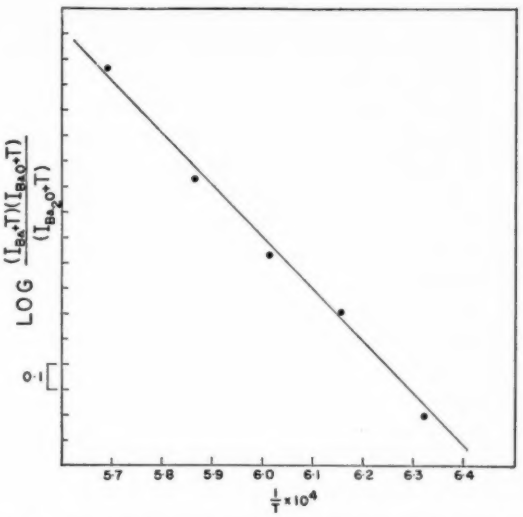

FIG. 4. Graphical determination of ΔH_{1700}^0 for the reaction $Ba_2O(g) = BaO(g) + Ba(g)$.

actually represents the process of simple ionization of Ba_2O gas and that the increase in Ba_2O^+ during the run is due to an increase in Ba_2O pressure inside the crucible.

If Ba_2O^+ were formed in a second-order mechanism involving Ba^+ and BaO, the slope of the temperature-dependence curve for Ba_2O^+ should equal the sum of the slopes of these curves for Ba^+ and BaO^+. From the curves in Fig. 3 it is obvious that this is not the case.

Further evidence for the existence of gaseous Ba_2O was obtained from the run in which Ba metal was added to the BaO. Because of the high volatility of Ba metal, it was necessary to use temperatures so low that BaO^+ was undetectable. Nevertheless, Ba_2O^+ was detected, and the ratio Ba^+/Ba_2O^+ was about 3×10^3 for ionizing electron energy of 20 volts and cell temperatures of 1250°K. This ratio was multiplied by the value of the vapor pressure of BaO calculated from our results at higher temperatures. The resulting equilibrium constant falls, within experimental error, on an extrapoation of the line of Fig. 4.

The equilibrium constant for the reaction, $Ba_2O(g) = BaO(g) + Ba(g)$, is proportional to $(I_{BaO^+}T)(I_{Ba^+}T)/(I_{Ba_2O^+}T)$. A plot of the logarithm of this quantity *versus* $1/T$ is shown in Fig. 4. From the slope of the curve we obtain for the reaction

$$Ba_2O(g) = BaO(g) + Ba(g) \quad \Delta H_{1700}^\circ = 93 \pm 17 \text{ kcal.}$$

It should be emphasized that although the Ba and the Ba_2O pressures were not constant in time, the equilibrium constant plotted in Fig. 4 remained constant and was reproducible under varying conditions.

$Ba_2O_3^+$

At higher temperatures an ion peak, not previously reported, was observed and identified as $Ba_2O_3^+$. At temperatures between 1690°K and 1780°K the three peaks, Ba_2O^+, $Ba_2O_2^+$, and $Ba_2O_3^+$, increased in

intensity as the temperature of the Knudsen cell was raised. Above 1780°K, however, the intensity of $Ba_2O_3^+$ began to decrease with increasing temperature while the Ba_2O^+ and $Ba_2O_2^+$ peaks continued to increase. A possible explanation of this effect is that conditions inside the crucible change suddenly above 1780°K and that the observed ion intensities no longer pertain to the equilibrium concentration of gaseous molecules. It is difficult to propose any mechanism by which $Ba_2O_3^+$ can be formed other than that of simple ionization of Ba_2O_3 gas. The data which have been obtained are good evidence for the existence of Ba_2O_3 gas, although we have not satisfactorily explained the anomalous temperature behavior.

Table II gives the intensity data for Ba_2O^+, $Ba_2O_2^+$, and $Ba_2O_3^+$ below 1780°K. The Knudsen cell was maintained at each temperature for several minutes while successive intensity measurements of each peak were made. The simplest method of treating the data is to consider the reaction,

$$2Ba_2O_2(g)=Ba_2O(g)+Ba_2O_3(g).$$

The quantity $(I_{Ba_2O^+})(I_{Ba_2O_3^+})/(I_{Ba_2O_2^+})^2$ will be nearly equal to the true equilibrium constant since the ionization cross sections for the three species would be expected to be nearly equal and will approximately cancel.

VAPOR PRESSURE CALCULATIONS

The partial pressures of gaseous species in equilibrium with BaO solid at different temperatures were calculated by use of the equation described earlier. Table III gives the result of the calculations from data obtained using alumina Knudsen cells. The following estimated relative ionization cross sections were used: $\sigma(Ag^+):\sigma(Ba^+):\sigma(BaO^+):\sigma(Ba_2O^+):\sigma(Ba_2O_2^+)=1:1:2:4:4$. The ions, Ba^+, Ba_2O^+, and $Ba_2O_2^+$, were formed with 30-volt ionizing electrons, and BaO^+ was formed with 60-volt electrons. At these voltages the ionization cross sections of each of these species are approximately at a maximum.

RESULTS FROM THORIA KNUDSEN CELLS

An additional experiment was made in which a Knudsen cell consisting of a thoria crucible and a tantalum cover was used. This cell provided, not only a different crucible material, but also stronger reducing conditions than an alumina cell. This was indicated by the fact that the Ba^+ was approximately ten times more intense than the BaO^+ in this case, while these ions were roughly equal in intensity when alumina crucibles were used. At the same temperature the partial pressures of BaO and Ba_2O_2 and the Ba^+/Ba_2O^+ ratios, obtained in the two sets of experiments, were reproducible and agreed to within 30%. This is well within the experimental error. However, the $Ba_2O_3^+$ peak behaved anomalously, as in the experiments with alumina cells. Although it did not decrease in intensity at higher temperatures, as in experiments with alumina cells, it was not reproducible and the equilibrium constant $(Ba_2O_3^+)(Ba_2O^+)/(Ba_2O_2)^2$ varied with time.

An x-ray analysis of solid removed from the inner surface of the thoria crucible after an experiment revealed only lines attributed to barium oxide (as the hydroxide).

In addition to the above mentioned species, a relatively intense beam of $BaTaO^+$ ions was observed. The ratio of BaO^+ to $BaTaO^+$ at 1780°K was about 2.3. The appearance potential of $BaTaO^+$ was below 6 ev. Traces of ions of higher molecular weight were observed but at 1780°K were present in intensities less than 1/50 that of $BaTaO^+$. Aldrich[2] observed species such as $BaTaO_2^+$ and higher species but did not report $BaTaO^+$. However, his experimental arrangement and conditions were considerably different from those of this work.

Table III. Partial pressures of gaseous species over BaO solid.[a]

Gaseous species (x)	x^{i+} peak observed	x^{i+} ion intensity[b]	Temperature °K	Pressure (in atmos)
Ba	Ba^{138+}	1.5×10^6	1664	2.2×10^{-6}
BaO	BaO^{154+}	1.8×10^6	1664	1.4×10^{-6}
Ba_2O	Ba_2O^{292+}	1.0×10^4	1664	7.3×10^{-9}
Ba_2O_2	$Ba_2O_2^{308+}$	1.3×10^4	1664	9.8×10^{-9}
Ba	Ba^{138+}	1.0×10^7	1758	1.5×10^{-5}
BaO	BaO^{154+}	9.8×10^6	1758	7.9×10^{-6}
Ba_2O	Ba_2O^{292+}	6.5×10^4	1758	5.0×10^{-8}
Ba_2O_2	$Ba_2O_2^{308+}$	6.5×10^4	1758	5.2×10^{-8}

[a] These intensities were measured under conditions indicated by curve (2) of Fig. 2.
[b] k, the sensitivity constant, is 1.3×10^{12} units of Ag^{107+} ion intensity for 80-volt electrons per atmosphere of silver vapor.

DISCUSSION AND CONCLUSIONS

The dissociation energy of BaO(g) was obtained by combining the following thermochemical data:

Heat of formation of BaO(s) (-133 ± 2 kcal/mole) selected by Brewer.[12]
$\Delta H_0°$ of sublimation of BaO(g) (104 ± 4 kcal/mole) obtained in this work.
$\Delta H_{298}°$ of sublimation of Ba(s) (42 kcal/mole) given by Brewer.[13]
Dissociation energy of O_2 (117.96 ± 0.04 kcal/mole) given by Brix and Herzberg.[14]
$H_{298}°-H_0°$ for O_2 and Ba(g) tabulated by Brewer.[13]
$H_{298}°-H_0°$ for BaO(s) from data of reference 9.

Thus, we obtain for the reaction

$$BaO(g, {}^1\Sigma)=Ba(g)+O(g),$$
$$\Delta H_0°=130.2\pm4.5 \text{ kcal/mole or } D_0°(BaO)=5.65\pm0.20 \text{ ev.}$$

In Table IV vapor-pressure data for BaO(g) and $D_0°(BaO)$ values obtained in this work are compared

[12] L. Brewer, Chem Revs. **52**, 13 (1953).
[13] L. Brewer, Paper 3, *National Nuclear Energy Series*, Vol. 19B, Edited by L. L. Quill (McGraw-Hill Book Company, Inc., New York, 1950).
[14] P. Brix and G. Herzberg, Can. J. Phys. **32**, 110 (1954).

with results obtained by other workers. The total spread in $D_0°$ values obtained by three independent methods is only 0.35 ev.

It should be re-emphasized that the mechanism by which BaO is being reduced need not be known. Gaseous species inside the Knudsen cell will reach equilibrium with the BaO solid if the accommodation coefficient of a gaseous species on BaO solid is greater than the ratio of effusion-hole area to total BaO surface area. Our ratio of effusion-hole area to BaO surface area at the beginning of a run was less than 5×10^{-3}. Ion intensities were measured before any appreciable amount of $BaO(s)$ had been removed from the inner surface of the Knudsen cell by reaction with Al_2O_3 or impurities. Thus, the partial pressures obtained refer to true equilibrium pressures for gaseous species, except those whose accommodation coefficients on $BaO(s)$ are less than 5×10^{-3}. It is considered rather improbable, however, that the gaseous species observed here, with the possible exception of Ba_2O_3, have accommodation coefficients less than 5×10^{-3}. In particular, the $BaO(g)$ species must have an accommodation coefficient near unity. This is shown by the fact that the vapor pressure of $BaO(g)$ obtained by Knudsen effusion and rate-of-vaporization methods agree closely (see Table IV).

It should also be re-emphasized that even though the Ba pressure was varied by orders of magnitude in different experiments and Knudsen cells of different material were used, the equilibrium constants measured in this work were constant and reproducible at a given temperature. The only exception to this statement is the equilibrium constant involving Ba_2O_3, which has an anomalous temperature dependence.

Because of the reduction of the BaO solid, the partial pressure of $Ba(g)$ inside the Knudsen cell was several orders of magnitude higher than the partial pressure of $O_2(g)$ and was nearly equal to the partial pressure of $BaO(g)$ in the alumina cell. Under conditions where the partial pressures of $Ba(g)$ and $O_2(g)$ are equal, $BaO(g)$ will be the predominant species in the vapor. Under highly oxidizing conditions where the partial pressure of $O_2(g)$ is several orders of magnitude higher than the partial pressure of $Ba(g)$, $Ba_2O_3(g)$ may be the most abundant species in the vapor. The formation of Ba_2O_3 gas under these conditions may account for the results of Thompson and Armstrong.[19] They measured the volatility of $BaO(s)$ in air and reported pressures two orders of magnitude higher than values obtained by others under vacuum conditions.

TABLE IV. Comparison of $BaO(g)$ vapor-pressure data and $D_0°(BaO)$ values.

Investigator	Method	$P_{BaO(g)}$ over $BaO(s)$ at T = 1530°K (in atmos)	$D_0°(BaO)$ ev
Claassen and Veenemanns[a]	Rate of vaporization from platinum surface	1.3×10^{-7} [e]	5.70±0.15[f]
Blewett, Liebhafsky, and Hennelly[b]	Platinum Knudsen cells	1.2×10^{-7} [e]	5.70±0.15[f]
This work	Mass spectrometric+ Knudsen effusion	1.5×10^{-7}	5.65±0.20
Huldt and Lagerqvist[c]	Flame	···	5.50
James[d]	Flame	···	5.85

[a] See reference 15.
[b] See reference 16.
[c] See reference 17.
[d] See reference 18.
[e] Obtained from investigators' vapor-pressure equation.
[f] Calculated using free energy functions.

No attempt has been made to explain the stability of Ba_2O, Ba_2O_2, and Ba_2O_3 in terms of chemical bonding. The relatively high concentration of Ba_2O in the vapor is rather surprising in light of bond energy calculations[20] which indicate instability for Ba_2O_3. In order to account for the stability of the Ba_2O species on the basis of bond energy calculations the structural model and approximations used previously need to be modified.

[15] A. Claassen and C. F. Veenemans, Z. Physik **80**, 342 (1933).
[16] Blewett, Liebhafsky, and Hennelly, J. Chem. Phys. **7**, 478 (1939).
[17] L. Huldt and A. Lagerqvist, Arkiv Fysik **2**, 333 (1950).
[18] G. James, Thesis, Cambridge, England (1954).
[19] M. de K. Thompson and W. G. Armstrong, Trans. Am. Electrochem. Soc. **54**, 85 (1928).
[20] L. Brewer and D. F. Mastick, J. Am. Chem. Soc. **73**, 2045 (1951).

Thermodynamic Properties of Krypton Adsorbed on Titanium Dioxide (Rutile)

E. L. Pace, Kent S. Dennis, and W. T. Berg
Morley Chemical Laboratory, Western Reserve University, Cleveland, Ohio

(Received August 16, 1955)

The zero point entropy of krypton adsorbed on titanium dioxide (rutile) has been determined at a coverage of 0.57 of the monolayer capacity from calorimetric measurements of the heat capacity, differential heat of adsorption, and from adsorption isotherms. The value is 0.4 cal deg^{-1}mole^{-1} with an experimental uncertainty of the order of $\pm$0.8 cal deg^{-1}mole^{-1}. Within this high uncertainty, the result is in essential agreement with the results of Morrison and co-workers for argon adsorbed on rutile and Aston and co-workers with neon adsorbed on rutile.

THE present study is one of a series of thermodynamic studies involving gases with approximately the same physical properties adsorbed on a finely divided solid surface. Low temperature calorimetric techniques are used to obtain the experimental data. Previous work[1,2] has involved methane adsorbed on titanium dioxide (rutile). The present work is concerned with krypton, a monatomic gas, adsorbed on titanium dioxide (rutile). It has been carried out in greater detail than any of the preceding work in that a zero point entropy has been evaluated from the experimental data.

Recent work directly comparable to that being presented is that of Aston *et al.* with the nitrogen-rutile[3] and neon-rutile[4] systems and that of Morrison and co-workers with argon, oxygen, and nitrogen adsorbed on rutile.[5–7]

Morrison and co-workers conclude that the value of zero point entropy of argon adsorbed on rutile for coverages less than a monolayer is zero within the experimental error. The results of Aston *et al.* with neon adsorbed on rutile are in essential agreement with this conclusion.

EXPERIMENTAL

The krypton was purchased from the Matheson Chemical Company, East Rutherford, New Jersey. The analysis supplied with the gas indicated a total impurity of 0.08 mole percent. No further analysis or purification was attempted.

The titanium dioxide used was a sample of rutile obtained from Dr. W. K. Nelson of the National Lead Company. It was 94.3% titanium dioxide, the remainder being adsorbed or coordinately bound water. The titanium dioxide was activated by evacuation to a sustained pressure of 10^{-5} mm at 190°C. The monolayer capacity determined by the BET method with krypton at 120°K was 0.0283 mole.

The calorimeter used was of the adiabatic type. The construction did not differ significantly from the calorimeter previously described.[1] The experimental technique and derivation of the thermodynamic quantities from the measurements have been adequately described elsewhere.[1,2,5,6]

RESULTS AND DISCUSSION

It was assumed in the succeeding treatment and discussion that the adsorbed gas was a one-component system. Thus, the thermodynamic properties of the solid were considered to be unaffected by the presence of the adsorbed phase; the surface area of the solid was assumed independent of temperature and pressure.

The experimentally observed heat capacity (c_{N_s}, cal deg^{-1}) for 0.0163 mole of krypton adsorbed on titanium dioxide (rutile) with a monolayer capacity of 0.0283 mole ($\theta=0.57$) is shown in Fig. 1. The average precision in the measurements of $\pm$0.005 calorie is roughly represented by the diameter of the circles in the graph. The molar heat capacity of the adsorbed krypton (C_{N_s}), as well as that for the bulk phases, is plotted against the temperature in Fig. 1.

The zero point entropy (S_0) of the adsorbed krypton was calculated from the expression

$$S_0=S_G(T,P_0)-\int_0^T C_{N_s}/T dT-Q_{N_s}(T)/T - R/N_s\int_0^{N_s}\ln P/P_0 dN_s' \quad (1)$$

in which $S_G(T,P_0)$ is the molar entropy of the gas phase at absolute temperature T and equilibrium pressure P_0; C_{N_s}, the molar heat capacity of the adsorbed gas at a constant number of moles adsorbed (N_s); $Q_{N_s}(T)$, the molar integral heat of adsorption at temperature T; and P, the equilibrium pressure of the system consisting of N_s' moles of gas adsorbed on the solid at temperature T.

The term $S_G(T,P_0)$ was computed for krypton from the Sackur-Tetrode equation at a temperature of 126°K and a reference pressure (P_0) of 21.45 mm corresponding

[1] Pace, Sasmor, and Heric, J. Am. Chem. Soc. **74**, 4413 (1952).
[2] Pace, Heric, and Dennis, J. Chem. Phys. **21**, 1225 (1953).
[3] Aston, Szasz, and Kington, J. Am. Chem. Soc. **73**, 1937 (1951).
[4] Tykodi, Aston, and Schreiner, J. Am. Chem. Soc. **77**, 2168 (1955).
[5] Morrison, Los, and Drain, Trans. Faraday Soc. **47**, 1023 (1951).
[6] L. E. Drain and J. A. Morrison, Trans. Faraday Soc. **48**, 316 (1952).
[7] L. E. Drain and J. A. Morrison, Trans. Faraday Soc. **49**, 654 (1953).

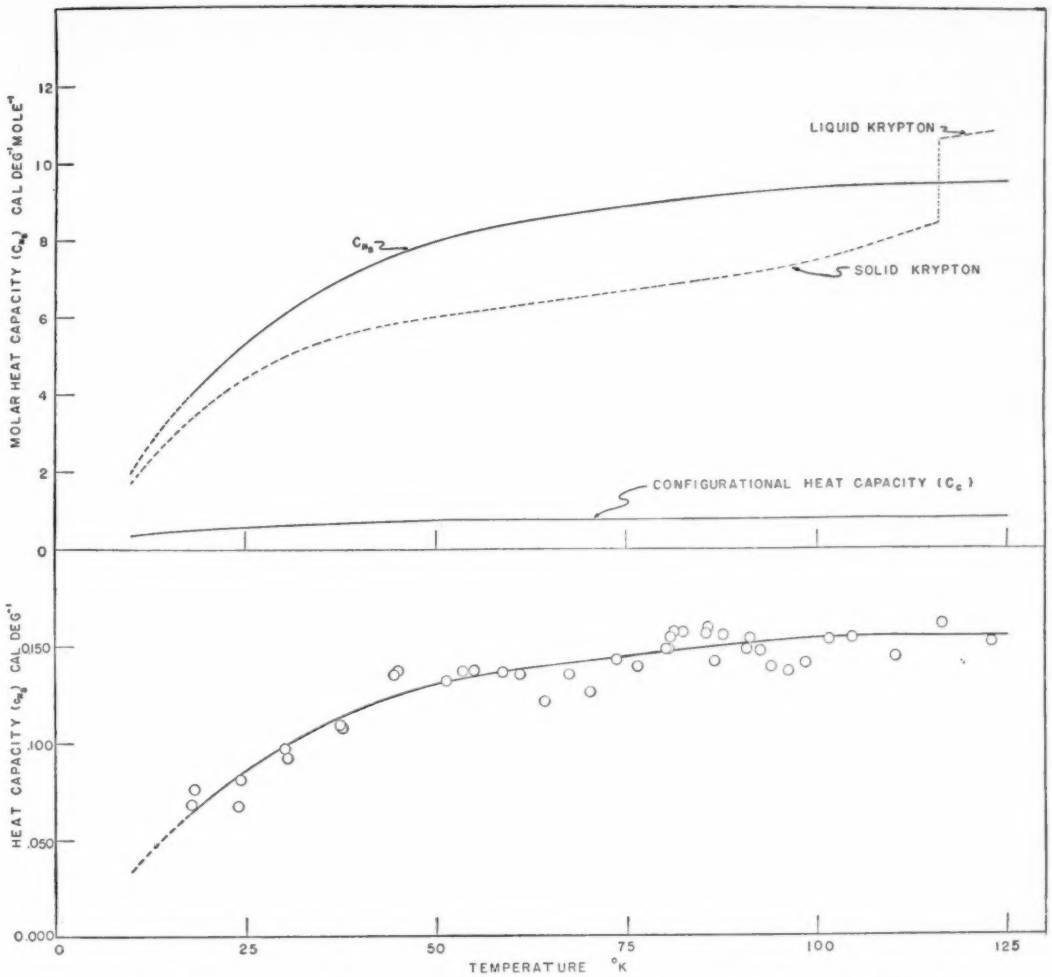

FIG. 1. Heat capacity of krypton adsorbed on titanium dioxide. 0.0163 mole of krypton; monolayer capacity, 0.0283 mole; $\theta=0.57$.

to the equilibrium pressure for the system with 0.0163 mole of adsorbed gas.

The entropy contribution from the heat capacity was evaluated in two parts. For the interval between 18 and 126°K, the integral was evaluated graphically by Simpson's rule from the experimental heat-capacity temperature data. For temperatures below 18°K, the entropy was assumed to be that of a three-dimensional isotropic oscillator with a frequency of 8.2×10^{11}sec^{-1} determined from the experimental heat capacity value at 18°K.

The molar integral heat (Q_{N_s}) at 126°K was determined from the experimental integral heat obtained in the usual manner by summing the thermal effects produced by successive adsorptions of small increments of krypton and dividing by the total moles adsorbed. The last term in (1) is a cumulative entropy term involved in bringing the sample of ideal adsorbed gas reversibly to the reference pressure (P_0). The values of the equilibrium pressures were taken from an adsorption isotherm determined at 126°K. The integration was performed in two parts. From $N_s'=0$ to $N_s'=0.0025$ mole, the adsorption isotherm was assumed linear and an analytical integration was carried out; the remainder of the term was evaluated graphically by use of the adsorption isotherm data.

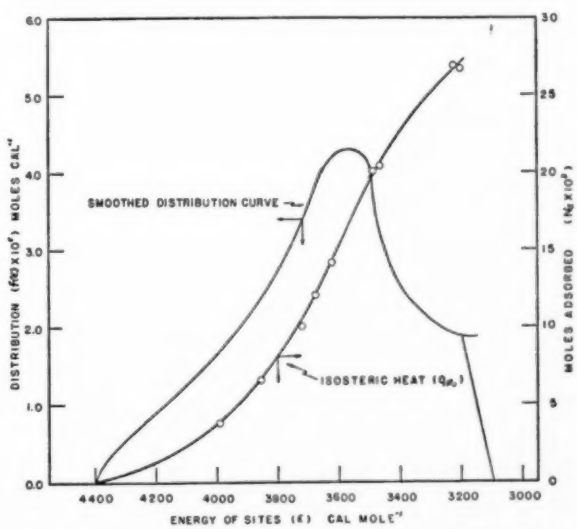

FIG. 2. Distribution of energy among adsorption sites for krypton adsorbed on titanium dioxide (rutile).

The zero point entropy (S_0) thus computed from the experimental data is 0.4 cal deg^{-1}mole^{-1}. The uncertainty in this value is of the order of ± 0.8 cal deg^{-1} mole^{-1}. Despite the smaller mobility of krypton as compared to neon and argon, the result is essentially the same as that for neon[4] and argon[5] adsorbed on rutile. A value of 2.4 cal deg^{-1}mole^{-1} can be calculated for the zero point entropy for a uniform surface with a coverage of 0.57 monolayer providing that molecular interaction is neglected. The smaller experimental value is not surprising when one considers the nature of the surface and the possibility of nearest neighbor interaction.

Differential heats of adsorption were measured experimentally at 126°K and reduced to 0°K by use of the experimental heat capacity data (assuming $(\partial C_{N_s}/\partial N_s)_T$ equal to zero). The differential heat curve at 0°K is shown in Fig. 2. The method of Morrison and co-workers[6] was used to obtain the energy distribution curve shown in Fig. 2 and the configurational heat capacity curve shown in Fig. 1.

ACKNOWLEDGMENTS

We are pleased to acknowledge the support of this work by the U. S. Atomic Energy Commission under Contract No. AT(30-1)-824. The hydrogen liquefier was loaned for the work by the Office of Naval Research (Contract No. 182(00)). We are indebted also to Dr. W. K. Nelson of the National Lead Company for the sample of rutile.

THE JOURNAL OF CHEMICAL PHYSICS VOLUME 23, NUMBER 11 NOVEMBER, 1955

Near Infrared Spectrum of Liquid Diborane*

HAROLD C. BEACHELL AND EUGENE J. LEVY
Department of Chemistry, University of Delaware, Newark, Delaware
(Received Februrary 7, 1955)

The infrared spectrum of liquid diborane has been obtained between 4500–10 500 cm^{-1}. A complete assignment for the observed overtone and combination bands is presented.

INTRODUCTION

THE structure of diborane and its vibrational spectrum have been under discussion for many years.[1–8] A recent electron diffraction study tends to support the D_{2h} or nonplanar bridge models,[9] as opposed to the earlier D_{3h} or ethane-like structure.[10] The selection rules for the symmetry-point group D_{2h} permit the even overtones of the diborane fundamentals to be active in the infrared but forbid the appearance of the odd overtones. In this investigation the near infrared spectrum of diborane liquid is obtained and a complete assignment of the observed bands to overtones and combinations is presented.

EXPERIMENTAL

The diborane was prepared by the method of Shapiro and Smith.[11] After purification by trap to trap distillation the vapor pressure of B_2H_6 at -111.8°C was 225 mm.

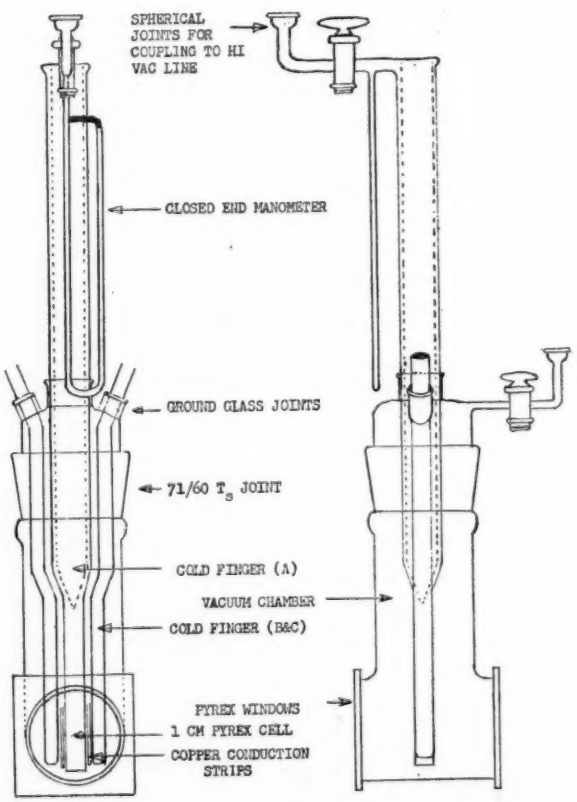

FIG. 1. Low temperature near infrared liquid cell.

* Based on a thesis submitted by Eugene J. Levy in partial fulfillment of the requirements for the degree of Doctor of Philosophy.

[1] T. F. Anderson and A. B. Burg, J. Chem. Phys. **6**, 586 (1938).
[2] F. Stitt, J. Chem. Phys. **9**, 780 (1941).
[3] R. P. Bell and H. C. Longuet-Higgins, Proc. Roy. Soc. (London) **A183**, 357 (1945).
[4] W. C. Price, J. Chem. Phys. **16**, 894 (1948).
[5] Webb, Neu, and Pitzer, J. Chem. Phys. **17**, 1007 (1949).
[6] W. E. Anderson and E. F. Barker, J. Chem. Phys. **18**, 698 (1950).
[7] R. C. Lord and E. Nielsen, J. Chem. Phys. **19**, 1 (1951).
[8] W. N. Lipscomb, J. Chem. Phys. **22**, 985 (1954).
[9] K. Hedberg and V. Schomaker, J. Am. Chem. Soc. **73**, 1482 (1951).
[10] S. H. Bauer, J. Am. Chem. Soc. **59**, 1896 (1937); Chem. Revs. **31**, 46 (1942).
[11] Shapiro, Weiss, Schmich, Skolnik, and Smith, J. Am. Chem. Soc. **74**, 901 (1952).

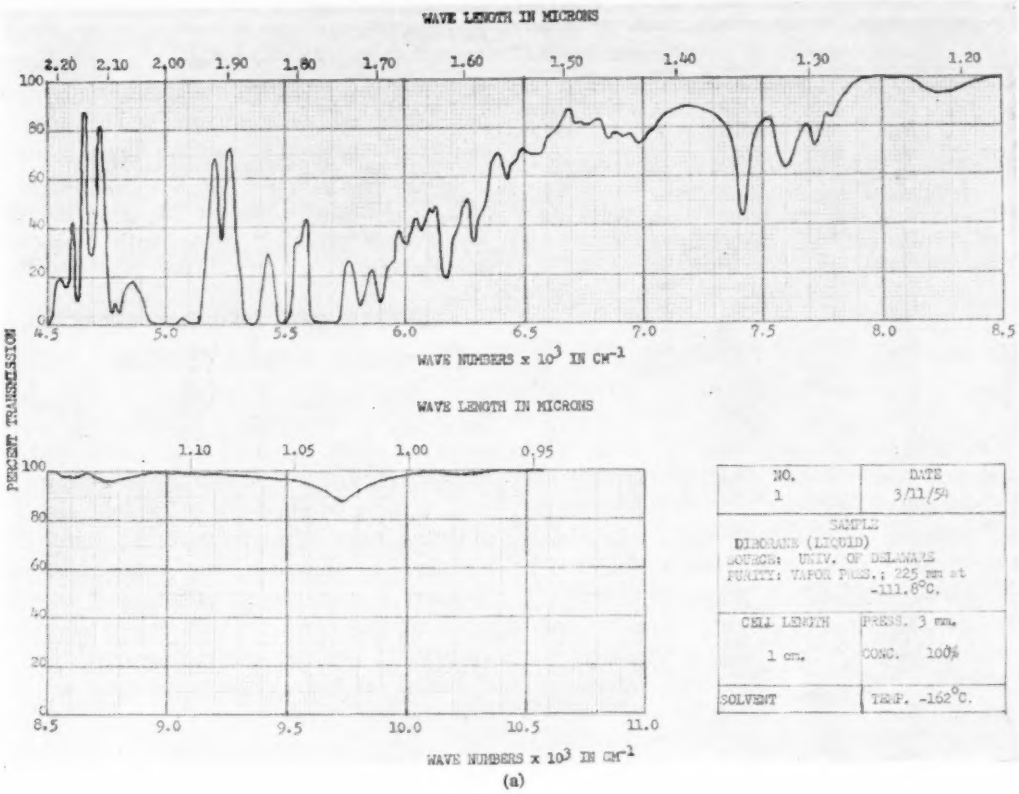
WAVE LENGTH IN MICRONS
2.20 2.10 2.00 1.90 1.80 1.70 1.60 1.50 1.40 1.30 1.20
100 80 60 40 20 0
4.5 5.0 5.5 6.0 6.5 7.0 7.5 8.0 8.5
WAVE NUMBERS x 10³ IN CM⁻¹
PERCENT TRANSMISSION
WAVE LENGTH IN MICRONS
1.10 1.05 1.00 0.95
100 80 60 40 20 0
8.5 9.0 9.5 10.0 10.5 11.0
WAVE NUMBERS x 10³ IN CM⁻¹
NO. 1
DATE 3/11/54
SAMPLE
DIBORANE (LIQUID)
SOURCE: UNIV. OF DELAWARE
PURITY: VAPOR PRES.; 225 mm at -111.8°C.
CELL LENGTH 1 cm.
PRESS. 3 mm.
CONC. 100%
SOLVENT
TEMP. -162°C.

(a)

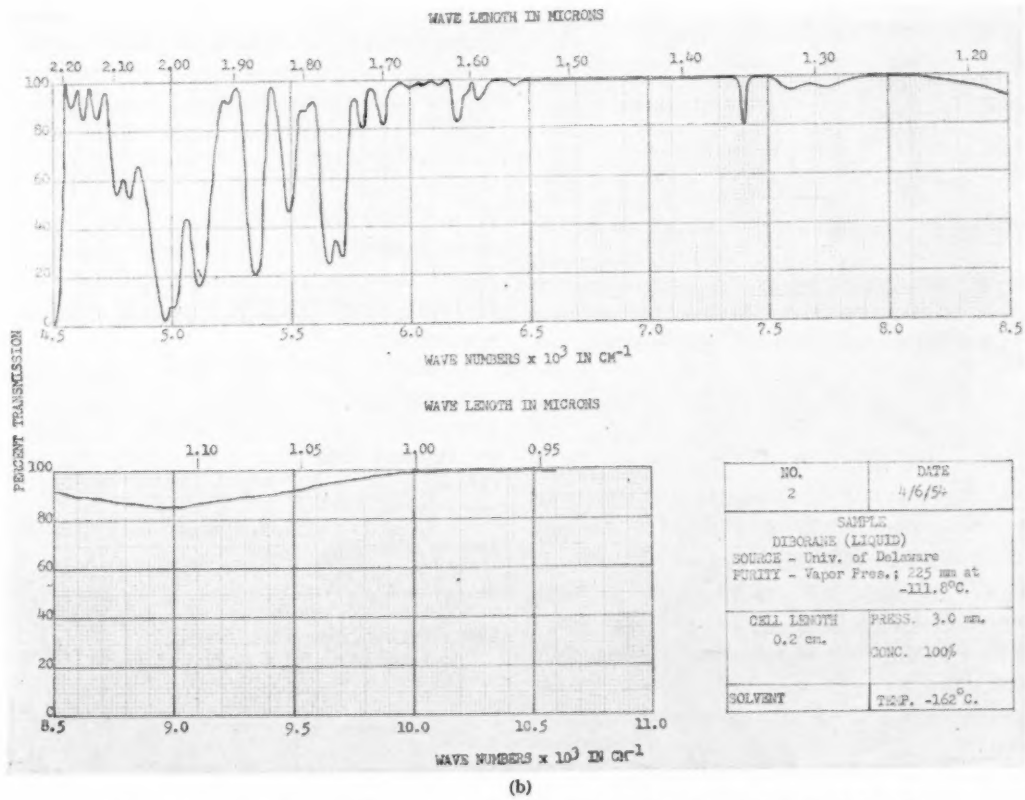
WAVE LENGTH IN MICRONS
2.20 2.10 2.00 1.90 1.80 1.70 1.60 1.50 1.40 1.30 1.20
100 80 60 40 20 0
4.5 5.0 5.5 6.0 6.5 7.0 7.5 8.0 8.5
WAVE NUMBERS x 10³ IN CM⁻¹
PERCENT TRANSMISSION
WAVE LENGTH IN MICRONS
1.10 1.05 1.00 0.95
100 80 60 40 20 0
8.5 9.0 9.5 10.0 10.5 11.0
WAVE NUMBERS x 10³ IN CM⁻¹
NO. 2
DATE 4/6/54
SAMPLE
DIBORANE (LIQUID)
SOURCE - Univ. of Delaware
PURITY - Vapor Pres.; 225 mm at -111.8°C.
CELL LENGTH 0.2 cm.
PRESS. 3.0 mm.
CONC. 100%
SOLVENT
TEMP. -162°C.

(b)

FIG. 2. Spectra of liquid diborane: (a) at 1-cm path length, (b) at 0.2-cm path length.

TABLE I. Assignments for diborane.

Number	Symmetry	ν_c(cm^{-1})	ν_{obs}(cm^{-1})	Relative intensity	$(\nu_c-\nu_{obs})$ $\Delta\nu$ cm^{-1}
1. $\nu_8+\nu_{10}$	B_{3u}	4566	4500	vs	66
2. $\nu_2+\nu_{16}$	B_{3u}	4629	4594	w	35
3. $\nu_{16}+\nu_{18}+\nu_{13}$	B_{2u}	4652	4637	w	25
4. $\nu_2+\nu_{12}$	B_{2u}	4716	4689	w	27
5. $(\nu_{17})^3$	B_{3u}	4806	4793	m	13
6. $\nu_{16}+(\nu_{18})^2$	B_{3u}	4879	4830	m	49
7. $\nu_1+\nu_{16}$	B_{3u}	5050	4987	vs	63
8. $\nu_{16}+\nu_{17}+\nu_{13}$	B_{2u}	5077	5036	sh	41
9. $\nu_1+\nu_{12}$	B_{2u}	5137	5122	s	15
10. $\nu_{16}+\nu_{17}+\nu_{18}$	B_{3u}	5304	5242	w	62
11. $\nu_{17}+\nu_{18}+\nu_{12}$	B_{2u}	5391	5360	s	31
12. $\nu_{12}+\nu_{14}+\nu_{16}$	B_{3u}	5505	5482	ms	23
13. $\nu_8+\nu_9+\nu_{12}$	B_{2u}	5560	5553	wsh	7
14. $\nu_{16}+\nu_{18}+\nu_8$	B_{1u}	5677	5656	s	21
15. $\nu_{16}+(\nu_{17})^2$	B_{2u}	5729	5706	s	23
16. $(\nu_{17})^2+\nu_{12}$	B_{2u}	5816	5805	m	11
17. ν_8^3	B_{1u}	5925	5900	m	25
18. $\nu_6+\nu_{12}+\nu_{16}$	B_{1u}	5966	5962	wsh	4
19. $(\nu_{16})^2+\nu_9$	B_{1u}	6023	6000	w	23
20. $\nu_{12}+\nu_{13}+\nu_{16}$	B_{3u}	6087	6054	w	33
21. $\nu_1+\nu_{12}+\nu_{15}$	B_{1u}	6148	6110	w	38
22. $\nu_{12}+\nu_{13}+\nu_9$	B_{1u}	6197	6180	m	17
23. $\nu_{16}+\nu_{18}+\nu_{12}$	B_{2u}	6314	6283	m	31
24. $(\nu_8)^2+\nu_{16}$	B_{3u}	6429	6429	w	46
25. $\nu_2+\nu_6+\nu_{12}$	B_{3u}	6484	6465	vwsh	19
26. $\nu_8^2+\nu_{12}$	B_{2u}	6562	6508	vw	54
27. $\nu_1+\nu_2+\nu_8$	B_{1u}	6603	6552	vw	51
28. $(\nu_{16})^2+\nu_{17}$	B_{3u}	6652	6621	vw	31
29. $\nu_{16}+\nu_{17}+\nu_{12}$	B_{2u}	6739	6700	w	39
30. $\nu_{16}^2+\nu_{17}$	B_{3u}	6784	6749	w	35
31. $\nu_1+\nu_6+\nu_{12}$	B_{3u}	6904	6843	w	61
32. $\nu_6+\nu_{10}+\nu_{12}$	B_{1u}	6971	6918	w	53
33. $\nu_1^2+\nu_8$	B_{1u}	7023	6955	w	68
34. $\nu_{10}^2+\nu_8$	B_{1u}	7025	7010	wsh	15
35. ν_{16}^3	B_{3u}	7575	7368	m	207
36. $\nu_{16}^2+\nu_{12}$	B_{2u}	7662	7531	w	131
37. $\nu_{12}^2+\nu_{16}$	B_{3u}	7749	7600	wsh	149
38. ν_{12}^3	B_{2u}	7836	7657	w	179
39. $\nu_{10}+\nu_{16}+\nu_{17}+\nu_{18}$	B_{1u}	7895	7733	vw	162
40. $\nu_4+(\nu_{16})^3$	B_{3u}	8369	8169	vw	200
41. $\nu_4+(\nu_{12})^3$	B_{2u}	8630	8498	vw	142
42. $\nu_{15}+(\nu_{12})^3$	B_{1u}	8848	8668	vw	180
43. $\nu_2+(\nu_{12})^3$	B_{2u}	9940	9644	w	296

The infrared measurements in the 1- to 2-micron region of liquid diborane were obtained by using a low-temperature liquid cell designed in this laboratory (see Fig. 1). An essential feature of this cell is the attached closed end manometer which measures the pressure of the vapor in equilibrium with the liquid at cell temperature. The insertion of this measured vapor pressure into known pressure-temperature equations gives a good indication of the temperature of the sample. The cooling is accomplished by using liquid nitrogen in the side cold fingers (B and C) and liquid nitrogen with a small amount of ethyl bromide in the inner cold finger A. The diborane was distilled directly into the cell after preparation and purification in a high-vacuum line.

The design of the infrared spectrophotometer employed in this investigation is essentially that described by Lauer and Rosenbaum.[12] The instrument was calibrated using the emission lines of mercury as a primary standard and the sharp bands of chloroform and 1,2,4-trichlorobenzene as secondary standards.[13] The actual resolving power of this instrument is 775 at 1.7μ.

RESULTS AND SPECTRAL INTERPRETATION

The spectra of liquid diborane at 0.2-cm and 1-cm path lengths are reproduced in Fig. 2. Using the fundamental assignments of Lord and Nielsen[7] and the selection rules for a molecule possessing D_{2h} symmetry,[14] the frequencies for the allowed harmonics and combination bands were calculated. In Table I the observed near infrared bands of liquid diborane are assigned to suitable overtones and combinations. Column I lists the overtones and combinations of fundamentals to which the observed bands are assigned. Column II lists the resultant symmetry of the modes. Columns III and IV are tabulations of the calculated and observed frequencies. Column V lists the relative intensities of the observed bands and column VI shows the frequency difference between the calculated and observed values.

The criteria used in assigning an observed band to a given summation or overtone frequency are selection rules and relative intensities.[15] The more intense bands are assigned to overtones and combinations of slightly higher frequencies. If a number of combination bands are possible that particular combination is chosen which has all or most of its fundamental modes active. In all cases binary combinations were selected before ternary, and ternary before quaternary combinations. Alternative assignments may be made for the weaker bands, however, the combinations selected seemed most appropriate.

It may be noted that all the observed bands have been assigned on the basis of a D_{2h} symmetry point group. This is therefore additional evidence tending to support the D_{2h} or ethylene-like structure for diborane.

[12] J. L. Lauer and E. J. Rosenbaum, Soc. Appl. Spectroscopy Bull. **6**, 27 (1952).
[13] E. K. Plyler and C. W. Peters, J. Research, Natl. Bur. Standards **45**, No. 6 (December, 1950), Research Paper 2159.
[14] G. Herzberg, *Infrared and Raman Spectra* (D. Van Nostrand Company, Inc., New York, 1949).
[15] G. Gauthier, J. phys. radium **14**, 19, 85 (1953).

Pyramidal $XY(CH_3)_2$ Molecular Model Classical Vibration Problem

HAROLD C. BEACHELL, BERNARD KATLAFSKY, AND JAMES L. LAUER
Chemistry Department, University of Delaware, Newark, Delaware

(Received February 7, 1955)

Symmetry coordinates are set up from the standpoint of group theory for describing the normal modes of vibration of a valence force pyramidal $XY(CH_3)_2$ molecular model in such a way that maximum factorization of the secular determinant is accomplished. The kinetic energy matrix is set up and an analytical expression is given for each matrix element in terms of the reciprocal bond distances, reciprocal masses of the atoms, and the bending and twisting angles. A valence force and a Urey-Bradley field potential is discussed.

I. INTRODUCTION

THE pyramidal $XY(CH_3)_2$ molecular model has the symmetry C_S and includes, as examples, dimethyl amine, dimethyl phosphine, and others. The complete normal vibrational pattern of this molecular model and the quantum-mechanical evaluation of its allowed rotation-vibration energies have not been treated in the literature. This paper is intended to form the classical part of the basis for the interpretation of both the gross vibrational and fine rotational structure of the Raman and infrared spectra of pyramidal $XY(CH_3)_2$ molecules. Furthermore, this paper deals with the purely vibrational aspects of the problem of a valence force model and includes discussions of the molecular symmetry, characteristic modes of vibration, valence type symmetry coordinates, and potential and kinetic energy functions.

II. GEOMETRY AND SYMMETRY

The equilibrium configuration assumed for the pyramidal $XY(CH_3)_2$ model is shown in Fig. 1 along with a right-handed cartesian coordinate system, xyz, whose origin coincides with the center of the apex atom. The respective atoms are indicated by the arbitrary index X for the apex atom, Y for the single base atom, C_1 and C_2 for the two methyl carbon atoms, and H_{ij} ($i=1, 2$ and $j=1, 2, 3$) for the six methyl hydrogen atoms. For convenience in assigning the twisting angles, it is assumed that atoms C_1, C_2, H_{13}, H_{23}, and X lie in the xz plane, while atom Y lies in the yz plane below the xz plane, and atoms H_{11} and H_{21} lie below and H_{12} and H_{22} lie above the xz plane.

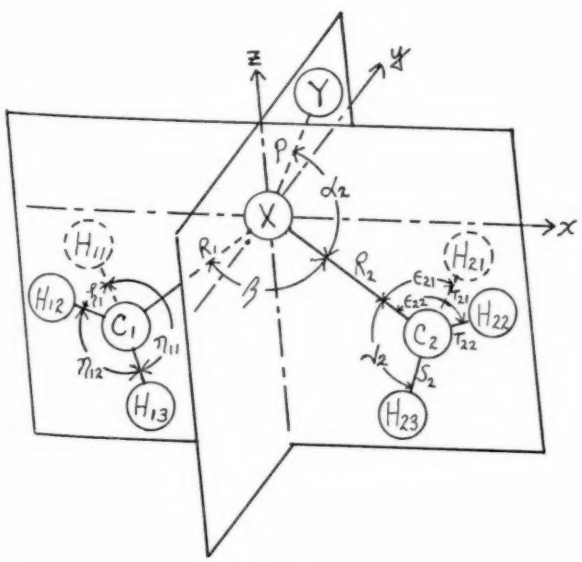

FIG. 1.

A plane of reflection is the only element of symmetry inherent to a pyramidal $XY(CH_3)_2$ molecular model. Therefore, this model can be classified under the C_S symmetry point group. The two covering operations of the C_S point group form two classes as follows: E, the identity operation; and σ, reflection in the yz plane, the plane containing the y-axis and atoms X and Y. Table I contains the characters of the various classes of covering operations performed on the two possible types (A' and A'') of physical quantities. The vibrational species types A' and A'' are both nondegenerate.

TABLE I. Characters of point group C_S.

	E	σ
A'	1	1
A''	1	−1

III. VALENCE SYMMETRY COORDINATES

The body-fixed cartesian coordinate system introduced in Sec. II for the description of the equilibrium configuration of the pyramidal $XY(CH_3)_2$ model is unsuitable for the analytical discussion of the modes of vibration of this molecule unless the detailed geometry of the model is known. The coordinates for the normal vibrations of this system can be expressed simply in terms of infinitesimal changes in the internal coordinates. The internal coordinates of the pyramidal $XY(CH_3)_2$ molecular model, changes in the equilibrium values of the 9 bond lengths, 15 bond angles, and 2 twisting angles during the period of vibration, are given in Table II.

The methods of group theory show that the twenty-four normal modes of vibration of the pyramidal $XY(CH_3)_2$ model of symmetry C_S have thirteen modes of species type A' and eleven modes of type A''. The

TABLE II. Internal coordinates of the pyramidal $XY(CH_3)_2$ model.

Type	Symbol	Number	Description
Stretching	P	1	X−Y
Stretching	R_i	2	X−C_i
Stretching	S_i	2	C_i−H_{i3}
Stretching	T_{ij}	4	C_i−H_{ij}
Bending	α_i	2	C_i−X−Y
Bending	β	1	C_i−X−C_j
Bending	γ_i	2	X−C_i−H_{i3}
Bending	ϵ_{ij}	4	X−C_i−H_{ij}
Bending	ζ_i	2	H_{i1}−C_i−H_{i2}
Bending	η_{ij}	4	H_{i3}−C_i−H_{ij}
Twisting	τ_i	1	H_{i3}−C_i−X−$C_j(\pm)$

complete secular determinant can accordingly be broken up at once, if one uses coordinates with proper symmetry properties, into one thirteen-fold step and one eleven-fold step. Applying the characters of the covering operations of the C_S symmetry point group to the symmetry transformations of the internal coordinates, twenty-six symmetry coordinates can be constructed from linear transformations of the internal coordinates. This indicates that one of the bending coordinates about each carbon atom is not independent of the other five bending coordinates. This condition can be rectified by setting up the following two conditions of restraint to satisfy the limit that the total angular change about each carbon atom is zero:

$$\sum\Delta(\gamma_1+\epsilon_{11}+\epsilon_{12}+\zeta_1+\eta_{11}+\eta_{12})=0, \quad (1)$$

$$\sum\Delta(\gamma_2+\epsilon_{21}+\epsilon_{22}+\zeta_2+\eta_{21}+\eta_{22})=0. \quad (2)$$

It follows that the sum and difference of (1) and (2) are also equal to zero. These two conditions can be used to represent two new bending coordinates:

$$S_i=\Delta(\gamma_1+\gamma_2+\epsilon_{11}+\epsilon_{12}+\epsilon_{21}+\epsilon_{22}+\zeta_1+\zeta_2+\eta_{11}+\eta_{12}+\eta_{21}+\eta_{22})\equiv 0 \text{ (redundant coordinate)}, \quad (3)$$

$$S_j=\Delta(\gamma_1-\gamma_2+\epsilon_{11}+\epsilon_{12}-\epsilon_{21}-\epsilon_{22}+\zeta_1-\zeta_2+\eta_{11}+\eta_{12}-\eta_{21}-\eta_{22})\equiv 0 \text{ (redundant coordinate)}. \quad (4)$$

Ten other bending coordinates can now be constructed which are orthogonal to (3) and (4). The redundant coordinates can now be disregarded without destroying

TABLE III. g^{-1} matrix for the pyramidal $XY(CH_3)_2$ molecular model.

	P	R_1	R_2	S_1	S_2	T_{11}	T_{12}	T_{21}	T_{22}	α_1	α_2	β
P	gP	gPR	gPR	0	0	0	0	0	0	$gP\alpha$	$gP\alpha$	$gP\beta$
R_1		g^1R	g^2R	gRS	0	gRT	gRT	0	0	$g^1R\alpha$	$g^2R\alpha$	$gR\beta$
R_2			g^1R	0	gRS	0	0	gRT	gRT	$g^2R\alpha$	$g^1R\alpha$	$gR\beta$
S_1				gS	0	gST	gST	0	0	$gS\alpha$	0	$gS\beta$
S_2					gS	0	0	gST	gST	0	$gS\alpha$	$gS\beta$
T_{11}						g^1T	g^2T	0	0	$g^1T\alpha$	0	$gT\beta$
T_{12}							g^1T	0	0	$g^2T\alpha$	0	$gT\beta$
T_{21}								g^1T	g^2T	0	$g^1T\alpha$	$gT\beta$
T_{22}									g^1T	0	$g^2T\alpha$	$gT\beta$
α_1										$g^1\alpha$	$g^2\alpha$	$g\alpha\beta$
α_2											$g^1\alpha$	$g\alpha\beta$
β												$g\beta$

TABLE III—*Continued.*

	γ_1	γ_2	ϵ_{11}	ϵ_{12}	ϵ_{21}	ϵ_{22}	ζ_1	ζ_2	η_{11}	η_{12}	η_{21}	η_{22}	τ_1	τ_2
P	$gP\gamma$	$gP\gamma$	$g^1P\epsilon$	$g^2P\epsilon$	$g^1P\epsilon$	$g^2P\epsilon$	0	0	0	0	0	0	$g^1P\tau$	$g^2P\tau$
R_1	$g^1R\gamma$	$g^2R\gamma$	$g^1R\epsilon$	$g^1R\epsilon$	$g^2R\epsilon$	$g^2R\epsilon$	$gR\zeta$	0	$gR\eta$	$gR\eta$	0	0	0	0
R_2	$g^2R\gamma$	$g^1R\gamma$	$g^2R\epsilon$	$g^2R\epsilon$	$g^1R\epsilon$	$g^1R\epsilon$	0	$gR\zeta$	0	0	$gR\eta$	$gR\eta$	0	0
S_1	$gS\gamma$	0	$gS\epsilon$	$gS\epsilon$	0	0	$gS\zeta$	0	$gS\eta$	$gS\eta$	0	0	0	0
S_2	0	$gS\gamma$	0	0	$gS\epsilon$	$gS\epsilon$	0	$gS\zeta$	0	0	$gS\eta$	$gS\eta$	0	0
T_{11}	$gT\gamma$	0	$g^1T\epsilon$	$g^2T\epsilon$	0	0	$gT\zeta$	0	$g^1T\eta$	$g^2T\eta$	0	0	$g^1T\tau$	$g^2T\tau$
T_{12}	$gT\gamma$	0	$g^2T\epsilon$	$g^1T\epsilon$	0	0	$gT\zeta$	0	$g^3T\eta$	$g^1T\eta$	0	0	$g^2T\tau$	$g^4T\tau$
T_{21}	0	$gT\gamma$	0	0	$g^1T\epsilon$	$g^2T\epsilon$	0	$gT\zeta$	0	0	$g^1T\eta$	$g^2T\eta$	$g^4T\tau$	$g^2T\tau$
T_{22}	0	$gT\gamma$	0	0	$g^2T\epsilon$	$g^1T\epsilon$	0	$gT\zeta$	0	0	$g^2T\eta$	$g^1T\eta$	$g^3T\tau$	$g_1T\tau$
α_1	$g^1\alpha\gamma$	$g^2\alpha\gamma$	$g^1\alpha\epsilon$	$g^2\alpha\epsilon$	$g^3\alpha\epsilon$	$g^4\alpha\epsilon$	$ga\zeta$	0	$g^1\alpha\eta$	$g^2\alpha\eta$	0	0	$g^1\alpha\tau$	$g^3\alpha\tau$
α_2	$g^2\alpha\gamma$	$g^1\alpha\gamma$	$g^3\alpha\epsilon$	$g^4\alpha\epsilon$	$g^1\alpha\epsilon$	$g^2\alpha\epsilon$	0	$ga\zeta$	0	0	$g^1\alpha\eta$	$g^2\alpha\eta$	$g^4\alpha\tau$	$g^2\alpha\tau$
β	$g\beta\gamma$	$g\beta\gamma$	$g\beta\epsilon$	$g\beta\epsilon$	$g\beta\epsilon$	$g\beta\epsilon$	$g\beta\zeta$	$g\beta\zeta$	$g\beta\eta$	$g\beta\eta$	$g\beta\eta$	$g\beta\eta$	0	0
γ_1	$g^1\gamma$	$g^2\gamma$	$g^1\gamma\epsilon$	$g^1\gamma\epsilon$	$g^2\gamma\epsilon$	$g^2\gamma\epsilon$	$g\gamma\zeta$	0	$g\gamma\eta$	$g\gamma\eta$	0	0	0	0
γ_2		$g^1\gamma$	$g^2\gamma\epsilon$	$g^2\gamma\epsilon$	$g^1\gamma\epsilon$	$g^1\gamma\epsilon$	0	$g\gamma\zeta$	0	0	$g\gamma\eta$	$g\gamma\eta$	0	0
ϵ_{11}			$g^1\epsilon$	$g^2\epsilon$	$g^3\epsilon$	$g^4\epsilon$	$g\epsilon\zeta$	0	$g^1\epsilon\eta$	$g^2\epsilon\eta$	0	0	$g^1\epsilon\tau$	$g^3\epsilon\tau$
ϵ_{12}				$g^1\epsilon$	$g^4\epsilon$	$g^3\epsilon$	$g\epsilon\zeta$	0	$g^2\epsilon\eta$	$g^1\epsilon\eta$	0	0	$g^2\epsilon\tau$	$g^4\epsilon\tau$
ϵ_{21}					$g^1\epsilon$	$g^2\epsilon$	0	$g\epsilon\zeta$	0	0	$g^1\epsilon\eta$	$g^3\epsilon\eta$	$g^4\epsilon\tau$	$g^2\epsilon\tau$
ϵ_{22}						$g^1\epsilon$	0	$g\epsilon\zeta$	0	0	$g^3\epsilon\eta$	$g^1\epsilon\eta$	$g^3\epsilon\tau$	$g^1\epsilon\tau$
ζ_1							$g\zeta$	0	$g\zeta\eta$	$g\zeta\eta$	0	0	0	0
ζ_2								$g\zeta$	0	0	$g\zeta\eta$	$g\zeta\eta$	0	0
η_{11}									$g^1\eta$	$g^2\eta$	0	0	$g^1\eta\tau$	$g^3\eta\tau$
η_{12}										$g^1\eta$	0	0	$g^2\eta\tau$	$g^4\eta\tau$
η_{21}											$g^1\eta$	$g^2\eta$	$g^4\eta\tau$	$g^2\eta\tau$
η_{22}												$g^1\eta$	$g^3\eta\tau$	$g^1\eta\tau$
τ_1													$g^1\tau$	$g^2\tau$
τ_2														$g_1\tau$

the symmetry of the remaining ten bending coordinates since they were chosen in such a way that they are identically zero and therefore make no contribution to the kinetic and potential energy of the system.[1] The following twenty-four linear combinations of internal coordinates form a set of orthogonal, normalized valence-type symmetry coordinates for setting up the normal vibration problem of a pyramidal $XY(CH_3)_2$ molecular model.

Type A':

$$
\begin{aligned}
S_1&=P\\
S_2&=1/(2)^{\frac{1}{2}}(R_1+R_2)\\
S_3&=1/(2)^{\frac{1}{2}}(S_1+S_2)\\
S_4&=1/(2)^{\frac{1}{2}}(T_{11}+T_{21})\\
S_5&=1/(2)^{\frac{1}{2}}(T_{12}+T_{22})\\
S_6&=1/(2)^{\frac{1}{2}}(\alpha_1+\alpha_2)\\
S_7&=\beta\\
S_8&=1/(12)^{\frac{1}{2}}(+\gamma_1+\gamma_2+\epsilon_{11}-\epsilon_{12}+\epsilon_{21}-\epsilon_{22}\\
&\qquad+\zeta_1+\zeta_2-\eta_{11}-\eta_{12}-\eta_{21}-\eta_{22})\\
S_9&=1/(12)^{\frac{1}{2}}(-\gamma_1-\gamma_2+\epsilon_{11}+\epsilon_{12}+\epsilon_{21}+\epsilon_{22}\\
&\qquad-\zeta_1+\zeta_2-\eta_{11}+\eta_{12}-\eta_{21}-\eta_{22})\\
S_{10}&=1/(12)^{\frac{1}{2}}(-\gamma_1-\gamma_2-\epsilon_{11}-\epsilon_{12}+\epsilon_{21}-\epsilon_{22}\\
&\qquad+\zeta_1+\zeta_2+\eta_{11}+\eta_{12}+\eta_{21}-\eta_{22})\\
S_{11}&=1/(12)^{\frac{1}{2}}(+\gamma_1-\gamma_2+\epsilon_{11}-\epsilon_{12}+\epsilon_{21}-\epsilon_{22}\\
&\qquad-\zeta_1-\zeta_2-\eta_{11}+\eta_{12}+\eta_{21}+\eta_{22})\\
S_{12}&=1/(12)^{\frac{1}{2}}(+\gamma_1+\gamma_2-\epsilon_{11}-\epsilon_{12}+\epsilon_{21}+\epsilon_{22}\\
&\qquad-\zeta_1-\zeta_2+\eta_{11}+\eta_{12}-\eta_{21}-\eta_{22})\\
S_{13}&=1/(2)^{\frac{1}{2}}(\tau_1+\tau_2)
\end{aligned}
\tag{5}
$$

Type A'':

$$
\begin{aligned}
S_{14}&=1/(2)^{\frac{1}{2}}(R_1-R_2)\\
S_{15}&=1/(2)^{\frac{1}{2}}(S_1-S_2)\\
S_{16}&=1/(2)^{\frac{1}{2}}(T_{11}-T_{21})\\
S_{17}&=1/(2)^{\frac{1}{2}}(T_{12}-T_{22})\\
S_{18}&=1/(2)^{\frac{1}{2}}(\alpha_1-\alpha_2)\\
S_{19}&=1/(12)^{\frac{1}{2}}(-\gamma_1+\gamma_2+\epsilon_{11}+\epsilon_{12}+\epsilon_{21}-\epsilon_{22}\\
&\qquad-\zeta_1-\zeta_2+\eta_{11}-\eta_{12}+\eta_{21}-\eta_{22})\\
S_{20}&=1/(12)^{\frac{1}{2}}(-\gamma_1+\gamma_2+\epsilon_{11}-\epsilon_{12}-\epsilon_{21}+\epsilon_{22}\\
&\qquad+\zeta_1-\zeta_2-\eta_{11}+\eta_{12}+\eta_{21}-\eta_{22})\\
S_{21}&=1/(12)^{\frac{1}{2}}(-\gamma_1+\gamma_2-\epsilon_{11}+\epsilon_{12}+\epsilon_{21}-\epsilon_{22}\\
&\qquad+\zeta_1-\zeta_2-\eta_{11}+\eta_{12}-\eta_{21}+\eta_{22})\\
S_{22}&=1/(12)^{\frac{1}{2}}(+\gamma_1-\gamma_2-\epsilon_{11}+\epsilon_{12}+\epsilon_{21}+\epsilon_{22}\\
&\qquad+\zeta_1-\zeta_2-\eta_{11}-\eta_{12}+\eta_{21}-\eta_{22})\\
S_{23}&=1/(12)^{\frac{1}{2}}(+\gamma_1+\gamma_2-\epsilon_{11}+\epsilon_{12}-\epsilon_{21}-\epsilon_{22}\\
&\qquad-\zeta_1+\zeta_2-\eta_{11}+\eta_{12}+\eta_{21}-\eta_{22})\\
S_{24}&=1/(2)^{\frac{1}{2}}(\tau_1-\tau_2).
\end{aligned}
\tag{6}
$$

[1] A. G. Meister and F. F. Cleveland, Am. J. Phys. **14**, 13 (1946).

IV. KINETIC ENERGY MATRIX

Wilson[2] has shown that the vibrational kinetic energy of a system can be expressed as a quadratic function of the masses of the atoms and unit vectors directed along the chemical bonds by:

$$2T=G=Ug^{-1}U', \tag{7}$$

where U is the matrix of the coefficients of the valence-type symmetry coordinates taken from (5) and (6); U' is the transpose of the U matrix (rows and columns interchanged); g^{-1} is the inverse kinetic energy matrix element defined by:

$$g_{qq'}{}^{-1}=\sum S_{qk}S_{q'k}\mu_k \tag{8}$$

where g^{-1} is the matrix element associated with coordinates q and q'; S_{qk} is a vector representing the contribution of the kth atom to coordinate q; and μ_k is the reciprocal mass of the kth atom.

The g^{-1} matrix for the pyramidal $XY(CH_3)_2$ molecule is given in Table III, only half the matrix being shown since it is symmetrical. The zeros in the matrix arise simply because the pairs of coordinates involved have no common atom. The matrix elements involving coordinate pairs $R_i\tau_i$, $S_i\tau_i$, $\beta_i\tau_i$, $\gamma_i\tau_i$, and $\zeta_i\tau_i$ also vanish since they represent interactions of either a stretching or bending coordinate with a twisting coordinate, and the configurations of the atoms defining them contain a plane of symmetry. The analytical expressions for these g^{-1} kinetic energy matrix elements, obtained by substituting the proper ϕ and τ values into the general Decius tables for acyclic structures,[3] are given in Table IV. In the evaluation of these expressions, it was assumed that all the C−H distances were equal; the reciprocal of such a distance being represented by S_0. The reciprocal of the X−Y distance is designated by P_0 and that of the C−X distance by R_0. Furthermore, the equilibrium C−X−Y and the C−X−C bond angles are designated by α and β, respectively; the angles $\gamma=\epsilon=\zeta=\eta=109°28'$; and the twisting angles are $0°$, $\pm120°$, $\pm\tau'$, and $[\pm\tau'\mp n(120°)$, where τ' can be

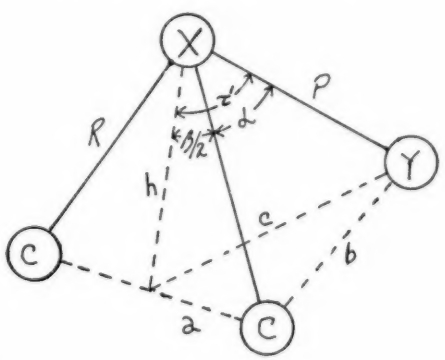

FIG. 2.

[2] E. B. Wilson Jr., J. Chem. Phys. **7**, 1047 (1939); **9**, 76 (1941).
[3] J. C. Decius, J. Chem. Phys. **16**, 1025 (1948).

TABLE IV. g^{-1} elements of the kinetic energy matrix.

Type	g^{-1} element	Formula
$g_{rr}{}^{2}$	gP	$\mu_X+\mu_Y$
	g^1R	$\mu_X+\mu_C$
	$gS=g^1T$	$\mu_H+\mu_C$
$g_{rr}{}^{1}$	gPR	$\cos\alpha\mu_X$
	g^2R	$\cos\beta\mu_X$
	$gRS=gRT=gST=g^2T=(-\mu_C/3)$	
$g_{r\phi}{}^{2}$	$gP\alpha$	$-R_0\sin\alpha\mu_X$
	$g^1R\alpha$	$-P_0\sin\alpha\mu_X$
	$gR\beta$	$-R_0\sin\beta\mu_X$
	$g^1R\gamma=g^1R\epsilon=gS\eta=gT\zeta=g^1T\eta$	$-(8)^{\frac{1}{2}}S_0\mu_C/3$
	$gS\gamma=g^1T\epsilon$	$-(8)^{\frac{1}{2}}R_0\mu_C/3$
$g_{r\phi}{}^{1}\binom{1}{2}$	$gP\gamma$	$R_0\sin\alpha\cos\tau^1\mu_X$
	$g^1P\epsilon$	$R_0\sin\alpha\cos(\tau^1-120°)\mu_X$
	$g^2P\epsilon$	$R_0\sin\alpha\cos(240°-\tau^1)\mu_X$
	$g^2R\epsilon$	$-R_0\sin\beta\mu_X/2$
	$g^2R\gamma$	$R_0\sin\beta\mu_X$
	$gS\alpha$	$(8)^{\frac{1}{2}}R_0\cos\tau^1\mu_C/3$
	$g^1T\alpha$	$(8)^{\frac{1}{2}}R_0\cos(\tau^1-120°)\mu_C/3$
	$g^2T\alpha$	$(8)^{\frac{1}{2}}R_0\cos(240°-\tau^1)\mu_C/3$
	$gT\beta$	$-(2)^{\frac{1}{2}}R_0\mu_C/3$
$g_{r\phi}{}^{1}\binom{1}{1}$	$gP\beta$	$-R_0\cos\alpha\mu_X/\sin\beta[1-\cos\beta]$
	$g^2R\alpha$	$-\mu_X/\sin\alpha[R_0\cos\alpha(1-\cos\beta)+P_0(\cos\beta-\cos^2\alpha)]$
	$gR\zeta=gR\eta=gS\zeta=g^2T\eta$	$(8)^{\frac{1}{2}}S_0\mu_C/3$
	$gS\epsilon=gT\zeta=g^2T\epsilon$	$(2)^{\frac{1}{2}}(S_0+R_0)\mu_C/3$
$g_{\phi\phi}{}^{3}$	$g^1\alpha$	$P_0{}^2\mu_Y+R_0{}^2\mu_C+(P_0{}^2+R_0{}^2-2P_0R_0\cos\alpha)\mu_X$
	$g\beta$	$2R_0{}^2[\mu_C+(1-\cos\beta)\mu_X]$
	$g^1\gamma=g^1\epsilon$	$S_0{}^2\mu_H+R_0{}^2\mu_X+(3S_0{}^2+3R_0{}^2+2S_0R_0)\mu_C/3$
	$g\zeta=g^1\eta$	$2S_0{}^2\mu_H+8S_0{}^2\mu_C/3$
$g_{\phi\phi}{}^{2}\binom{1}{1}$	$g^2\alpha$	$\frac{\cos\beta-\cos^2\alpha}{\sin^2\alpha}\left\{P_0{}^2\mu_Y+\left[P_0{}^2-2P_0R_0\cos\alpha+\frac{\cos^2\alpha(\cos\beta-1)+\sin^2\alpha}{\cos\beta-\cos^2\alpha}R_0{}^2\right]\mu_X\right\}$
	$g\alpha\beta$	$\frac{\cot\alpha(1-\cos\beta)}{\sin\beta}\left\{R_0{}^2\mu_C+\left[R_0{}^2(1-\cos\beta)-P_0R_0\cos\alpha+\frac{\cos^2\alpha(\cot\beta-1)+\sin^2\beta}{\cos\alpha(1-\cos\beta)}P_0R_0\right]\mu_X\right\}$
	$g^1\gamma\epsilon=g^2\epsilon$	$-1/6[3R_0{}^2\mu_X+(3R_0{}^2+2R_0S_0-5S_0{}^2)\mu_C]$
	$g\gamma\eta=g\epsilon\zeta=g\epsilon\eta$	$-1/6[3S_0{}^2\mu_H+4(S_0{}^2-R_0S_0)\mu_C]$
	$g\zeta\eta=g^2\eta$	$-S_0{}^2\mu_H/2$
$g_{\phi\phi}{}^{2}\binom{1}{0}$	$g^1\alpha\gamma$	$-R_0\cos\tau^1/3[(3R_0+S_0)\mu_C+3(R_0-P_0\cos\alpha)\mu_X]$
	$g^1\alpha\epsilon$	$-R_0\cos(\tau^1-120°)/3[(3R_0+S_0)\mu_C+3(R_0-P_0\cos\alpha)\mu_X]$
	$g^2\alpha\epsilon$	$-R_0\cos(240°-\tau^1)/3[(3R_0+S_0)\mu_C+3(R_0-P_0\cos\alpha)\mu_X]$
	$g\beta\gamma$	$-R_0/3[(3R_0+S_0)\mu_C+3R_0(1-\cos\beta)\mu_X]$
	$g\beta\epsilon$	$R_0/6[(3R_0+S_0)\mu_C+3R_0(1-\cos\beta)\mu_X]$
$g_{\phi\phi}{}^{1}\binom{2}{2}$	$g^2\gamma$	$-R_0{}^2\cos\beta\mu_X$
	$g^2\gamma\epsilon$	$R_0{}^2\cos\beta\mu_X/2$
	$g^3\epsilon$	$(3-\cos\beta)R_0{}^2\mu_C/4$
	$g^4\epsilon$	$-(3+\cos\beta)R_0{}^2\mu_C/4$
$g_{\phi\phi}{}^{1}\binom{2}{1}$	$g^2\alpha\gamma$	$R_0\mu_X/\sin\alpha[\sin\alpha\cos\tau^1(\cos\alpha P_0-R_0)+\sin\beta(R_0\cos\alpha-P_0)]$
	$g^3\alpha\epsilon$	$R_0\mu_X/\sin\alpha[\sin\alpha\cos(\tau^1-120°)(P_0\cos\alpha-R_0)-\frac{1}{2}\sin\beta(R_0\cos\alpha-P_0)]$
	$g^4\alpha\epsilon$	$R_0\mu_X/\sin\alpha[\sin\alpha\cos(240°-\tau^1)(P_0\cos\alpha-R_0)-\frac{1}{2}\sin\beta(R_0\cos\alpha-P_0)]$
	$g\alpha\zeta$	$-4R_0S_0\mu_C/3[\cos(\tau^1-120°)+\cos(240°-\tau^1)]$
	$g^1\alpha\eta$	$-4R_0S_0\mu_C/3[\cos\tau^1+\cos(\tau^1-120°)]$
	$g^2\alpha\eta$	$-4R_0S_0\mu_C/3[\cos\tau^1+\cos(240°-\tau^1)]$
	$g\beta\zeta$	$4R_0S_0\mu_C/3$
	$g\beta\eta$	$-2R_0S_0\mu_C/3$
$g_{\phi\phi}{}^{1}\binom{1}{1}$	$g\gamma\zeta=g^2\epsilon\eta$	$-4S_0(S_0+R_0)\mu_C/3$

TABLE IV—*Continued.*

Type	g^{-1} element	Formula
$g_{\tau\tau}{}^{1}\binom{1}{3}$	$g^{3}T_{\tau}=-g^{4}T_{\tau}$	$-(6)^{\frac{1}{2}}R_0\mu_C/3\sin\beta$
$g_{\tau\tau}{}^{1}\binom{1}{2}$	$g^{1}P_{\tau}=-g^{2}P_{\tau}$	$-[R_0\sin\alpha\sin\tau^{1}\mu_X/4\sin\beta][4(1-\cos\beta)+(2)^{\frac{1}{2}}\sin\beta]$
	$g^{1}T_{\tau}=-g^{2}T_{\tau}$	$(3)^{\frac{1}{2}}\mu_C/6\{3S_0+[1-(8)^{\frac{1}{2}}\cot\beta]R_0\}$
$g^{2}{}_{\phi\tau}\binom{1}{2}$	$g^{3}\alpha_{\tau}=-g^{4}\alpha_{\tau}$	$\sin\tau^{1}\{R_0/\sin\beta[(R_0-P_0\cos\alpha)\mu_X+R_0\mu_C]+R_0\mu_X/4[R_0-P_0\cos\alpha][(2)^{\frac{1}{2}}-4\cot\beta]\}$
	$g^{1}\eta_{\tau}=-g^{2}\eta_{\tau}$	$-(3)^{\frac{1}{2}}\mu_X/6[(2)^{\frac{1}{2}}S_0(3S_0-R_0)+4R_0S_0\cot\beta]-3(6)^{\frac{1}{2}}S_0{}^{2}\mu_H/8$
$g_{\phi\tau}{}^{2}\binom{1}{1}$	$g^{1}\alpha_{\tau}=-g^{2}\alpha_{\tau}$	$-\sin\tau^{1}\{\mu_C/4[4R_0{}^{2}\cot\beta-(2)^{\frac{1}{2}}R_0(R_0+3S_0)]+R_0\mu_X/4\sin\beta[R_0-P_0\cos\alpha]\times[4(\cos\beta-1)-(2)^{\frac{1}{2}}\sin\beta]\}$
	$g^{1}\epsilon_{\tau}=-g^{2}\epsilon_{\tau}$	$(3)^{\frac{1}{2}}R_0{}^{2}/8\sin\beta\{[\mu_C+\mu_X][4\cot\beta-(2)^{\frac{1}{2}}]-4\mu_X\}+(3)^{\frac{1}{2}}S_0\mu_C/24\{R_0[4\cot\beta-10(2)^{\frac{1}{2}}]-3(2)^{\frac{1}{2}}S_0\}$
$g_{\phi\tau}{}^{2}\binom{1}{0}$	$g^{3}\epsilon_{\tau}=-g^{4}\epsilon_{\tau}$	$(3)^{\frac{1}{2}}R_0/24\sin\beta\{4\mu_C(3R_0+S_0)+3R_0\mu_X[4(1-\cos\beta)+(2)^{\frac{1}{2}}\sin\beta]\}$
$g_{\phi\tau}{}^{1}\binom{1}{3}$	$g^{3}\eta_{\tau}=-g^{4}\eta_{\tau}$	$2(3)^{\frac{1}{2}}R_0S_0\mu_C/3\sin\beta$
$g_{\tau\tau}{}^{4}$	$g^{1}\tau$	$9(\mu_C+\mu_H)S_0{}^{2}/8+(\mu_C+\mu_X)R_0{}^{2}/8[9+16\cot^{2}\beta-4(2)^{\frac{1}{2}}\cot\beta]+R_0{}^{2}\mu_X/2\sin\beta[(2)^{\frac{1}{2}}-4\cot\beta]+3R_0S_0\mu_C/4[1-6(2)^{\frac{1}{2}}\cot\beta]$
$g_{\tau\tau}{}^{3}\binom{1}{0}$	$g^{2}\tau$	$(\mu_C-\mu_X)R_0{}^{2}/2\sin\beta[4\cot\beta-(2)^{\frac{1}{2}}]+R_0{}^{2}\mu_X/8[9+16\cot^{2}\beta-4(2)^{\frac{1}{2}}\cot\beta]-3(2)^{\frac{1}{2}}R_0S_0\mu_C/2\sin\beta$

found by:

$$\cos\tau'=\frac{h^2+P^2-c^2}{2hP} \tag{9}$$

where $h=R\cos(\beta/2)$; R and P are the equilibrium C−X and X−Y bond lengths; $c^2=(b^2-a^2)$; $a=R\sin(\beta/2)$; $b^2=P^2+R^2-2PR\cos\alpha$; and α and β are the equilibrium C−X−Y and C−X−C bond angles (see Fig. 2).

V. VALENCE POTENTIAL FUNCTION

The most general quadratic potential function satisfying the symmetry conditions is given in terms of the valence-type symmetry coordinates by:

$$\begin{aligned}2V=&k_P(P^2)+\sum_R\{k_R(R_i^2)+2\sum k_{RR}(R_iR_j)\}\\&+\sum_{S+T}\{k_S(S_i^2+T_{ij}^2)+2\sum k_{SS}[S_i(T_{ij}+T_{ik})+T_{ij}T_{ik}]\}\\&+\sum_{\alpha}\{PRk_{\alpha}(\alpha_i^2)+2\sum PRk_{\alpha\alpha}(\alpha_i\alpha_j)\}+R^2k_{\beta}(\beta^2)\\&+\sum_{\gamma+\epsilon}\{RSk_{\gamma}(\gamma_i^2+\epsilon_{ij}^2)+2\sum RSk_{\gamma\gamma}[\gamma_i(\epsilon_{ij}+\epsilon_{ik})+\epsilon_{ij}\epsilon_{ik}]\}\\&+\sum_{\zeta+\eta}\{S^2k_{\zeta}(\zeta_i^2+\eta_{ij}^2)+2\sum S^2k_{\zeta\zeta}[\zeta_i(\eta_{ij}+\eta_{ik})+\eta_{ij}\eta_{ik}]\}\\&+\sum_{\tau}\{RSk_{\tau}(\tau_i^2)+2\sum RSk_{\tau\tau}(\tau_i\tau_j)\}\end{aligned} \tag{10}$$

in which cross products occur only between symmetry coordinates of the same type. The complete valence-type potential function for the pyramidal $XY(CH_3)_2$ molecular model can be written as:

$$\begin{aligned}2V=&k_P(P^2)+\sum_R\{k_R(R_i^2)+2\sum k_{RR}(R_iR_j)\}\\&\sum_{S+T}\{k_S(S_i^2+T_{ij}^2)+2\sum k_{SS}[S_i(T_{ij}T_{ik})+T_{ij}T_{ik}]\}\\&+\sum_{\alpha}\{PRk_{\alpha}(\alpha_i^2)+2\sum PRk_{\alpha\alpha}(\alpha_i\alpha_j)\}+R^2k_{\beta}(\beta^2)\\&+\sum_{\gamma+\epsilon}\{RSk_{\gamma}(\gamma_i^2+\epsilon_{ij}^2)+2\sum RSk_{\gamma\gamma}[\gamma_i(\epsilon_{ij}+\epsilon_{ik})+\epsilon_{ij}\epsilon_{ik}]\}\\&+\sum_{\zeta+\eta}\{S^2k_{\zeta}(\zeta_i^2+\eta_{ij}^2)+2\sum S^2k_{\zeta\zeta}[\zeta_i(\eta_{ij}\eta_{ik})+\eta_{ij}\eta_{ik}]\}\\&+\sum_{\tau}\{RSk_{\tau}(\tau_i^2)+2\sum RSk_{\tau\tau}(\tau_i\tau_j)\}\\&+2\sum k_{PR}[P(R_i)]+2\sum k_{RS}[R_i(S_i+T_{ij})]\\&+2\sum PRk_{\alpha\beta}[\beta(\alpha_i)]+2\sum RSk_{\alpha\gamma}[\alpha_i(\gamma_i+\epsilon_{ij})]\end{aligned}$$

(*continued on next page*)

$$
\begin{aligned}
&+2\sum RSk_{\alpha\gamma}'[\alpha_j(\gamma_i+\epsilon_{ij})]+2\sum RSk_{\alpha\xi}[\alpha_i(\zeta_i+\eta_{ij})]\\
&+2\sum RSk_{\beta\gamma}[\beta(\gamma_i+\epsilon_{ij})]+2\sum RSk_{\beta\xi}[\beta(\zeta_i+\eta_{ij})]\\
&+2\sum RSk_{\gamma\gamma}'[(\gamma_i+\epsilon_{ij})(\gamma_j+\epsilon_{jk})]\\
&+2\sum RSk_{\gamma\xi}[(\gamma_i+\epsilon_{ij})(\zeta_i+\eta_{ij})]\\
&+2\sum Rk_{P\alpha}[P(\alpha_i)]+2Rf_{P\beta}[P(\beta)]\\
&+2\sum Pk_{R\alpha}[(R_i)(\alpha_i)]+2\sum Pk_{R\alpha}'[(R_i)(\alpha_j)]\\
&+2\sum Rk_{R\beta}[\beta(R_i)]+2\sum Rk_{P\gamma}[P(\gamma_i+\epsilon_{ij})]\\
&+2\sum Sk_{R\gamma}[R_i(\gamma_i+\epsilon_{ij})]+2\sum Sk_{R\gamma}'[R_j(\gamma_i+\epsilon_{ij})]\\
&+2\sum k_{R\xi}[R_i(\zeta_i+\eta_{ij})]+2\sum Rk_{S\gamma}[S_i\gamma_i+T_{ij}\epsilon_{ij}]\\
&+2\sum Rk_{S\gamma}'[S_i(\epsilon_{ij}+\epsilon_{ik})+T_{ij}(\gamma_i+\epsilon_{ik})]\\
&+2\sum Sk_{S\xi}[(S_i\eta_{ij})+(T_{ij}\zeta_i)]\\
&+2\sum Sk_{S\xi}'[(S_i\zeta_i)+T_{ij}(\eta_{ij}+\eta_{ik})].
\end{aligned}
\tag{11}
$$

VI. UREY-BRADLEY FIELD-TYPE POTENTIAL FUNCTION

Following the method of Simanouti,[4] the Urey-Bradley field-type potential energy function for the pyramidal $XY(CH_3)_2$ molecular model can be expressed as:

$$
\begin{aligned}
V=&\sum[K_1'P(\Delta P)+\tfrac{1}{2}K_1(\Delta P)^2]\\
&+\sum[K_2'R_i(\Delta R_i)+\tfrac{1}{2}K_2(\Delta R_i)^2]\\
&+\sum\{K_3'[S_i(\Delta S_i)+T_{ij}(\Delta T_{ij})]\\
&\qquad+\tfrac{1}{2}K_3[(\Delta S_i)^2+(\Delta T_{ij})^2]\\
&+\sum[H_1'PR(\Delta\alpha_i)+\tfrac{1}{2}H_1PR(\Delta\alpha_i)^2]\\
&+\sum[H_2'R^2(\Delta\beta)+\tfrac{1}{2}H_2R^2(\Delta\beta)^2]\\
&+\sum\{H_3'[RS(\Delta\gamma_i)+RT(\Delta\epsilon_{ij})]\\
&\qquad+\tfrac{1}{2}H_3[RS(\Delta\gamma_i)^2+RT(\Delta\epsilon_{ij})^2]\}\\
&+\sum\{H_4'[ST(\Delta\eta_{ij})+T^2(\Delta\zeta_i)]\\
&\qquad+\tfrac{1}{2}H_4[ST(\Delta\eta_{ij})^2+T^2(\Delta\zeta_i)^2]\}\\
&+\sum[H_\tau'RS(\Delta\tau_i)+\tfrac{1}{2}H_\tau(\Delta\tau_i)^2]\\
&+\sum[F_1'q_{PR}(\Delta q_{PR})+\tfrac{1}{2}F_1(\Delta q_{PR})^2]\\
&+\sum[F_2'q_{RR}(\Delta q_{RR})+\tfrac{1}{2}F_2(\Delta q_{RR})^2]\\
&+\sum\{F_3'[q_{RS}(\Delta q_{RS})+q_{RT}(\Delta q_{RT})\\
&\qquad+\tfrac{1}{2}F_3[(\Delta q_{RS})^2+(\Delta q_{RT})^2]\}\\
&+\sum\{F_4'[q_{ST}(\Delta q_{ST})+q_{TT}(\Delta q_{TT})]\\
&\qquad+\tfrac{1}{2}F_4[(\Delta q_{ST})^2+(\Delta q_{TT})^2]\}
\end{aligned}
\tag{12}
$$

where P and R are the equilibrium X−Y and C−X bond distances; S and T are the equilibrium C−H bond distances; α and β are the equilibrium C−X−Y and C−X−C bond angles; γ and ϵ are the equilibrium X−C−H bond angle; ζ and η are the equilibrium H−C−H bond angle; q_{ij} is the distance between atoms not directly bonded; and K_i', K_i, H_i', H_i, H_τ, F_i', and F_i are force constants, the last two being repulsion constants between nonbonded atoms.

Through the relationship:

$$q_{ij}^2=r_i^2+r_j^2-2r_ir_j\cos\phi_{ij} \tag{13}$$

we can represent Δq_{ij} by Δr_i, Δr_j, and $\Delta\phi_{ij}$:

$$
\begin{aligned}
\Delta q_{PR}=&x_{11}\Delta_P+x_{12}\Delta R_i+(y_{11}y_{12})^{\frac{1}{2}}(PR)^{\frac{1}{2}}\Delta\alpha_i+\{y_{11}^2(\Delta P)^2+y_{12}(\Delta R_i)^2-x_{11}x_{12}[PR(\Delta\alpha_i)^2]\\
&-2y_{11}y_{12}(\Delta P)(\Delta R_i)+2y_{11}x_{12}(\Delta P)(R\Delta\alpha_i]+2y_{12}x_{11}(\Delta R_i)(P\Delta\alpha_i)\}/2q_{PR}
\end{aligned}
\tag{14a}
$$

$$
\begin{aligned}
\Delta q_{RR}=&x_{21}(\Delta R_i+\Delta R_j)+y_{21}(R\Delta\beta)+\{y_{21}^2[(\Delta R_i)^2+(\Delta R_j)^2]-x_{21}^2(R\Delta\beta)^2\\
&-2y_{21}^2(\Delta R_i)(\Delta R_j)+2x_{21}y_{21}(\Delta R_i+\Delta R_j)(R\Delta\beta)\}/2q_{RR}
\end{aligned}
\tag{14b}
$$

$$
\begin{aligned}
\Delta q_{RS}=&x_{31}\Delta R_i+x_{32}\Delta S_i+(y_{31}y_{32})^{\frac{1}{2}}(RS)^{\frac{1}{2}}\Delta\gamma_i+\{y_{31}^2(\Delta R_i)^2+y_{32}^2(\Delta S_i^2)-x_{31}x_{32}[RS(\Delta\gamma_i)^2]\\
&-2y_{31}y_{32}(\Delta R_i)(\Delta S_i)+2y_{31}x_{32}(\Delta R_i)(S\Delta\gamma_i)+2y_{32}x_{31}(\Delta S_i)(R\Delta\gamma_i)\}/2q_{RS}
\end{aligned}
\tag{14c}
$$

$$
\begin{aligned}
\Delta q_{RT}=&x_{31}\Delta R_i+x_{32}\Delta T_{ij}+(y_{31}y_{32})^{\frac{1}{2}}(RT)^{\frac{1}{2}}\Delta\epsilon_{ij}+\{y_{31}^2(\Delta R_i)^2+y_{32}^2(\Delta T_{ij})^2-x_{31}x_{32}[RT(\Delta\epsilon_{ij})^2]\\
&-2y_{31}y_{32}(\Delta R_i)(\Delta T_{ij})+2y_{31}x_{32}(\Delta R_i)(T\Delta\epsilon_{ij})+y_{32}x_{31}(\Delta T_{ij})(R\Delta\epsilon_{ij})\}/2q_{RT}
\end{aligned}
\tag{14d}
$$

$$
\begin{aligned}
\Delta q_{ST}=&x_{41}(\Delta S_i+\Delta T_{ij})+y_{41}(ST)^{\frac{1}{2}}\Delta\eta_{ij}+\{y_{41}^2[(\Delta S_i)^2+(\Delta T_{ij})^2]-x_{41}^2[ST(\Delta\eta_{ij})^2]\\
&-2y_{41}^2(\Delta S_i)(\Delta T_{ij})+2x_{41}y_{41}(\Delta S_i)(T\Delta\eta_{ij})+2x_{41}y_{41}(\Delta T_{ij})(S\Delta\eta_{ij})\}/2q_{ST}
\end{aligned}
\tag{14e}
$$

$$
\begin{aligned}
\Delta q_{TT}=&x_{41}(\Delta T_{ij}+\Delta T_{ik})+y_{41}(T\Delta\zeta_i)+\{y_{41}^2[(\Delta T_{ij})^2+(\Delta T_{ik})^2]-x_{41}^2(T\Delta\zeta_i)^2\\
&-2y_{41}^2(\Delta T_{ij})(\Delta T_{ik})+2y_{41}x_{41}(\Delta T_{ij})(T\Delta\zeta_i)+2y_{41}x_{41}(\Delta T_{ik})(T\Delta\zeta_i)\}/2q_{TT}
\end{aligned}
\tag{14f}
$$

[4] T. Simanouti, J. Chem. Phys. **17**, 245 (1949).

where q_{PR} is the C_i-Y distance; q_{RR} is the C_i-C_j distance; $q_{RS}=q_{RT}=q_{HX}$, the $H_{ij}-Y$ distance; $q_{ST}=q_{TT}=q_{HH}$, the $H_{ij}-H_{ik}$ distance; γ, ϵ, ζ, and η are the tetrahedral carbon atoms; $S_i=T_{ij}$; and:

$$x_{11}=(P-R\cos\alpha)/q_{PR} \qquad y_{11}=R\sin\alpha/q_{PR}$$
$$x_{12}=(R-P\cos\alpha)/q_{PR} \qquad y_{12}=P\sin\alpha/q_{PR}$$
$$x_{21}=(1-\cos\beta)R/q_{RR} \qquad y_{21}=R\sin\beta/q_{RR} \tag{15}$$
$$x_{31}=(3R+S)/3q_{HX} \qquad y_{31}=(2)^{\frac{1}{2}}S/3q_{HX}$$
$$x_{32}=(3S+R)/3q_{HX} \qquad y_{32}=(2)^{\frac{1}{2}}R/3q_{HX}$$
$$x_{41}=4S/3q_{HH} \qquad y_{41}=(2)^{\frac{1}{2}}S/3q_{HH}.$$

From Eqs. (12) and (13) the potential energy is obtained as a function of valence-force coordinates:

$$\begin{aligned}
V=&\sum[K_1'P+F_1'x_{11}q_{PR}](\Delta P)\\
&+\sum[K_2'R_i+F_1'x_{12}q_{PR}+F_2'x_{21}q_{RR}+F_3'x_{31}q_{HX}](\Delta R_i)\\
&+\sum[K_3'S_i+F_3'x_{32}q_{HX}+F_4'x_{41}q_{HH}](\Delta S_i+\Delta T_{ij})\\
&+\sum[H_1'(PR)^{\frac{1}{2}}+F_1'(y_{11}y_{12})^{\frac{1}{2}}q_{PR}][(PR)^{\frac{1}{2}}\Delta\alpha_i]\\
&+\sum[H_2'R+F_2'y_{21}q_{RR}](R\Delta\beta)\\
&+\sum[H_3'(RS)^{\frac{1}{2}}+F_3'(y_{31}y_{32})^{\frac{1}{2}}q_{HX}][(RS)^{\frac{1}{2}}(\Delta\gamma_i+\Delta\epsilon_{ij})]\\
&+\sum[H_4'S+F_4'y_{41}q_{HH}][S(\Delta\zeta_i+\Delta\eta_{ij})]\\
&+\tfrac{1}{2}\sum[K_1+F_1'y_{11}^2+F_1x_{11}^2](\Delta P)^2\\
&+\tfrac{1}{2}\sum[K_2+F_1'y_{12}^2+F_1x_{12}^2+F_2'y_{21}^2+F_2x_{21}^2+F_3'y_{31}^2+F_3x_{31}^2](\Delta R_i)^2\\
&+\tfrac{1}{2}\sum[K_3+F_3'y_{32}^2+F_3x_{32}^2+F_4'y_{41}^2+F_4x_{41}^2][(\Delta S_i)^2+(\Delta T_{ij})^2]\\
&+\tfrac{1}{2}\sum[H_1-x_{11}x_{12}F_1'+y_{11}y_{12}F_1][PR(\Delta\alpha_i)^2]\\
&+\tfrac{1}{2}\sum[H_2-x_{21}^2F_2'+y_{21}^2F_2](R\Delta\beta)^2\\
&+\tfrac{1}{2}\sum[H_3-x_{31}x_{32}F_3'+y_{31}y_{32}F_3]\{RS[(\Delta\gamma_i)^2+(\Delta\epsilon_{ij})^2]\}\\
&+\tfrac{1}{2}\sum[H_4-x_{41}^2F_4'+y_{41}^2F_4]\{S^2[(\Delta\zeta_i)^2+(\Delta\eta_{ij})^2]\}\\
&+\sum[-y_{11}y_{12}F_1'+x_{11}x_{12}F_1](\Delta P)(\Delta R_i)\\
&+\sum[-y_{21}^2F_2'+x_{21}^2F_2](\Delta R_i)(\Delta R_{ij})\\
&+\sum[-y_{31}y_{32}F_3'+x_{31}x_{32}F_3][\Delta R_i(\Delta S_i+\Delta T_{ij})]\\
&+\sum[-y_{41}^2F_4'+y_{41}^2F_4][\Delta S_i(\Delta T_{ij}+\Delta T_{ik})+\Delta T_{ij}\Delta T_{ik}]\\
&+\sum[y_{11}x_{12}F_1'+y_{12}x_{11}F_1](\Delta P)(R\Delta\alpha_i)\\
&+\sum[y_{12}x_{11}F_1'+y_{11}x_{12}F_1](\Delta R_i)(P\Delta\alpha)\\
&+\sum[x_{21}y_{21}(F_2'+F_2')](\Delta R_i)(R\Delta\beta)\\
&+\sum[y_{31}x_{32}F_3'+y_{32}x_{31}F_3]\{(\Delta R_i)[S(\Delta\gamma_i+\Delta\epsilon_{ij})]\}\\
&+\sum[y_{32}x_{31}F_3'+y_{31}x_{32}F_3]\{(\Delta S_i)[R(\Delta\gamma_i+\Delta\epsilon_{ij})]\}\\
&+\sum[y_{41}x_{41}(F_4'+F_4)]\{[\Delta S_i+\Delta T_{ij}][S\Delta\eta_{ij}]\}\\
&+\sum[y_{41}x_{41}(F_4'F_4)][(\Delta T_{ij})(S\Delta\zeta_i)]\\
&+\tfrac{1}{2}\sum(H_\tau)[RS(\Delta\tau_i)^2]+\sum[(RS)^{\frac{1}{2}}H_\tau][(RS)^{\frac{1}{2}}\Delta\tau].
\end{aligned} \tag{16}$$

In this equation ΔP, ΔR, ΔS, ΔT, $\Delta\alpha$, and $\Delta\beta$ are independent variables, but $\Delta\gamma$, $\Delta\epsilon$, $\Delta\zeta$, and $\Delta\eta$ are not. Since it is assumed that the last four bond angles are tetrahedral in the equilibrium position, denoting these by θ, the following relationship among the six $\Delta\theta$'s about each carbon atom can be obtained, neglecting the higher terms of $\Delta\theta$

$$\sum_{i<j}(\Delta\theta_{ij})+(2)^{\frac{1}{2}}/8\{3\sum_{i<j}(\Delta\theta_{ij})^2+4\sum_{i\neq j\neq k}(\Delta\theta_{ij})(\Delta\theta_{ik})\}=0. \tag{17}$$

As the atoms are in the equilibrium position, from (16) and (17) are obtained:

$$r_iK_i'+\sum x_{ij}q_{ij}F_i'=0 \tag{18}$$

$$r_ir_jH_i'+(r_ir_j)^{\frac{1}{2}}q_{ij}(y_{ij}y_{ji})^{\frac{1}{2}}F_i'+\lambda=0 \tag{19}$$

where r_i is an equilibrium bond length; Eq. (19) applies only to those terms containing $\Delta\gamma$, $\Delta\epsilon$, $\Delta\zeta$, and $\Delta\eta$; and λ is the Lagrangian multiplier (called the "intermolecular tension" by Simanouti[4]). The potential energy can be expressed finally as:

$$
\begin{aligned}
V=&\tfrac{1}{2}\sum[K_1+y_{11}^2F_1'+x_{11}^2F_1](\Delta P)^2\\
&+\tfrac{1}{2}\sum[K_2+y_{12}^2F_1'+x_{12}^2F_1+y_{21}^2F_2'+x_{21}^2F_2+y_{31}^2F_3'+x_{31}^2F_3](\Delta R_i)^2\\
&+\tfrac{1}{2}\sum[K_3+y_{32}^2F_3'+x_{32}^2F_3+y_{41}^2F_4'+x_{41}^2F_4][(\Delta S_i)^2+(\Delta T_{ij})^2]\\
&+\tfrac{1}{2}\sum[H_1-x_{11}x_{12}F_1'+y_{11}y_{12}F_1][PR(\Delta\alpha_i)^2]\\
&+\tfrac{1}{2}\sum[H_2-x_{21}^2F_2'+y_{21}^2F_2](R\Delta\beta)^2\\
&+\tfrac{1}{2}\sum\{H_3-x_{31}x_{32}F_3'+y_{31}y_{32}F_3+[3\lambda/(8)^{\frac{1}{2}}RS]\}\{RS[(\Delta\gamma_i)^2+(\Delta\epsilon_{ij})^2]\}\\
&+\tfrac{1}{2}\sum\{H_4-x_{41}^2F_4'+y_{41}^2F_4+[3\lambda/(8)^{\frac{1}{2}}S^2]\}\{S^2[(\Delta\zeta_i)^2+(\Delta\eta_{ji})^2]\}\\
&+\sum[-y_{11}y_{12}F_1'+x_{11}x_{12}F_1](\Delta P)(\Delta R_i)\\
&+\sum[-y_{21}^2F_2'+x_{21}^2F_2](\Delta R_i)(\Delta R_j)\\
&+\sum[-y_{31}y_{32}F_3'+x_{31}x_{32}F_3][\Delta R_i(\Delta S_i+\Delta T_{ij})]\\
&+\sum[-y_{41}^2F_4'+x_{41}^2F_4][\Delta S_i(\Delta T_{ij}+\Delta T_{ik})+\Delta T_{ij}\Delta T_{ik}]\\
&+\sum[y_{11}x_{12}F_1'+y_{12}x_{11}F_1](\Delta P)(R\Delta\alpha_i)\\
&+\sum[y_{12}x_{11}F_1'+y_{11}x_{12}F_1](\Delta R_i)(P\Delta\alpha_i)\\
&+\sum[x_{21}y_{21}(F_2'+F_2)](\Delta R_i)(R\Delta\beta)\\
&+\sum[y_{31}x_{32}F_3'+y_{32}x_{31}F_3]\{(\Delta R_i)[S(\Delta\gamma_i+\Delta\epsilon_{ij})]\}\\
&+\sum[y_{32}x_{31}F_3'+y_{31}x_{32}F_3]\{(\Delta S_i)[R(\Delta\gamma_i+\Delta\epsilon_{ij})]\}\\
&+\sum[y_{41}x_{41}(F_4'+F_4)][(\Delta S_i+\Delta T_{ij})(S\Delta\eta_{ij})+\Delta T_{ij}(S\Delta\zeta_i)]\\
&+\sum[\lambda/(2)^{\frac{1}{2}}RS][RS(\Delta\gamma_i)(\Delta\epsilon_{ij})]\\
&+\sum[\lambda/(2)^{\frac{1}{2}}S^2][S^2(\Delta\zeta_i)(\Delta\eta_{ij})]\\
&+\sum[\lambda/(2)^{\frac{1}{2}}R^{\frac{1}{2}}S^{\frac{1}{2}}][R^{\frac{1}{2}}S^{\frac{1}{2}}(\Delta\gamma_i+\Delta\epsilon_{ij})(\Delta\zeta_i+\Delta\eta_{ij})]\\
&+\sum\{[H_1'(PR)^{\frac{1}{2}}+F_1'(y_{11}y_{12})^{\frac{1}{2}}q_{PR}][H_2'R+F_2'y_{21}q_{RR}]\}[P^{\frac{1}{2}}R^{\frac{1}{2}}(\Delta\alpha_i)(\Delta\beta)]\\
&+\tfrac{1}{2}\sum(H_\tau)[RS(\Delta\tau_i)^2]._{i}
\end{aligned}
$$

VII. THE NORMAL MODES OF VIBRATION

Following the Wilson method,[2] the potential energy is expressed in matrix form as:

$$2V=F=UfU' \qquad (21)$$

where U is the matrix of the coefficients of the valence-type symmetry coordinates obtained from Eqs. (5) and (6); U' is the transpose of this matrix; and f is the matrix of the potential force constants obtained from either the valence force potential function, Eq. (11), or from the Urey-Bradley field-type potential function, Eq. (20).

In the analysis of the experimental data it is necessary to assume that some of the force constants are negligible, or that several of them can be grouped together as a summation term into a new constant as a first approximation, since sufficient data are not available for the evaluation of all the constants.

The frequencies γ_i of the normal or characteristic modes of vibration are obtained from the solution of the Wilson determinantal equation[2] $|GF-\omega^2|=0$, $\omega_i^2-4\pi^2c^2\nu_i^2$, if c is the velocity of light in cm/sec and ν_i is the frequency in cm^{-1}.

Use of Interpolation Theory in the Analysis of Gas Adsorption Isotherms. II. Estimation of Certain Parameters

J. M. HONIG AND P. C. ROSENBLOOM
Department of Chemistry, Purdue University, Lafayette, Indiana, and Department of Mathematics and Mechanics, University of Minnesota, Minneapolis 14, Minnesota

(Received January 27, 1955)

In an extension of the interpolation theory described elsewhere, upper and lower bounds have been placed on a number of physical quantities of interest in adsorption theory.

INTRODUCTION

IN a recent publication[1] it was shown that the interpolation theory developed by Rosenbloom[2] can be usefully applied to the analysis of gas adsorption isotherms. In particular, it is possible to ascertain whether certain models describing the adsorption process can be used in the interpretation of adsorption data. The interpolation theory shows that if one wishes to analyze such data by use of the modified Langmuir model[3–10]

$$\frac{n}{n_m}=\theta(p,T)=\int_0^\infty \frac{dF(\epsilon)}{1+\dfrac{\beta(\epsilon,T)}{p}e^{-\epsilon/kT}}; \quad dF(\epsilon)=f(\epsilon)d\epsilon \tag{1}$$

one can construct two extremal isotherms θ_a and θ_b by choosing the corresponding distributions $F_a(\epsilon)$ and $F_b(\epsilon)$ of Eq. (1) to be step functions. Complete details for the construction of θ_a and θ_b are provided in reference 1. If the actual distribution of adsorption energies among surface sites differs from F_a or F_b, then the experimental isotherm must lie between the two bounding isotherms θ_a and θ_b on a θ *vs* p diagram. Failure of the data to lie within the limits dictated by the mathematical analysis indicates clearly the inapplicability of the model associated with the use of Eq. (1). The interpolation theory should thus aid in establishing the limits of usefulness of the modified Langmuir model.

In the present paper the interpolation theory is extended to obtain upper and/or lower bounds on a variety of quantities of interest in gas adsorption; a numerical analysis of data in terms of the theory will be presented in a companion paper.[11] Of necessity, the concepts and notations developed in reference 1 will be adopted here. By way of review, it suffices to note that the integral (1) can be converted to the simple form[10]

$$L(y,T)=\int_0^\infty \frac{dG(\lambda,T)}{\lambda+y}=\int_0^\infty \frac{g(\lambda,T)d\lambda}{\lambda+y} \tag{2}$$

by use of the substitutions[10]

$$\begin{aligned}\eta&=\epsilon-\epsilon_0,\\ \alpha(\eta,\epsilon_0,T)&=\beta(\epsilon_0+\eta,T)e^{-\epsilon_0/kT},\\ \alpha_0&=\alpha(0,\epsilon_0,T),\\ y&=\alpha_0/p+1,\\ \lambda&=(\alpha_0/\alpha)e^{\eta/kT}-1,\\ L(y,T)&=\theta(\alpha_0/(y-1),T).\end{aligned} \tag{3}$$

The quantity dG appearing in Eq. (2) defines a function

$$G=\int_0^\infty dG(\lambda,T)\equiv\int_0^\infty g(\lambda,T)d\lambda, \tag{4}$$

where

$$\begin{aligned}dG(\lambda,T)&=g(\lambda,T)d\lambda=(\alpha_0/\alpha)e^{\eta/kT}\cdot f(\eta+\epsilon_0)d\eta\\ &=(\lambda+1)\cdot dF(\epsilon).\end{aligned} \tag{5}$$

BOUNDS OBTAINED FROM THE DISTRIBUTION FUNCTIONS USED IN THE SECOND ORDER THEORY

In this section the theory of reference 1 will be utilized to place bounds on the following quantities: (a) $\alpha_0=\beta(\epsilon_0,T)\exp(-\epsilon_0/kT)$, where β is given by[8]

$$\beta(\epsilon,T)=(2\pi mkT/h^2)^{\frac{3}{2}}\cdot kT\cdot j_g(T)/j_s(\epsilon,T) \tag{6}$$

j_g and j_s being the internal partition functions of the gaseous and adsorbed species respectively; ϵ_0 is the minimum adsorption energy encountered on the surface. (b) λ_m, related by Eq. (3) to ϵ_m, the maximum value of the adsorption energy. (c) n_m, the number of adsorbate molecules required for monolayer coverage of the surface. The second order theory of reference 1 adjusts the limiting curves θ_a and θ_b to a set of experimental data by requiring the curves to cross at one experimental "reference point," (θ_1,p_1), selected at random from the adsorption data. The corresponding point on the L *vs* y diagram will be designated by (C_1,y_1), $C_1\equiv L(y_1,T)$. A second constraint arises from the requirement that

[1] J. M. Honig and P. C. Rosenbloom, Can. J. Chem. **33**, 193 (1955).
[2] P. C. Rosenbloom, Bull. Soc. Math. France (to be published).
[3] E. Cremer and S. Flügge, Z. physik. Chem. **B41**, 453 (1938).
[4] E. Cremer, J. chim. phys. **46**, 411 (1949).
[5] M. Temkin and V. Levich, Zhur. Fiz. Khim. **20**, 1441 (1946).
[6] G. D. Halsey and H. S. Taylor, J. Chem. Phys. **15**, 624 (1947).
[7] R. Sips, J. Chem. Phys. **16**, 490 (1948); **18**, 1024 (1950).
[8] T. L. Hill, J. Chem. Phys. **17**, 762 (1949).
[9] F. C. Tompkins, Trans. Faraday Soc. **46**, 569 (1950).
[10] J. M. Honig and E. L. Hill, J. Chem. Phys. **22**, 851 (1954).
[11] J. M. Honig, J. Chem. Phys. (to be published).

$F(\epsilon)$ be normalized, i.e.,

$$\int_0^\infty dF(\epsilon)=\int_0^\infty f(\epsilon)d\epsilon=1. \tag{7}$$

With these constraints it can be shown[1] that to obtain the limiting isotherm $L_b(y,T)$, one must require $G_b(\lambda,T)$ to be a function which is everywhere constant except at the extreme ends of the λ spectrum, $\lambda=\lambda_0=0$ and $\lambda=\lambda_m$, where the function G experiences discontinuities given respectively by (see Eq. (14) of reference 1)

$$\begin{aligned}\Delta G_0&=[1+\lambda_m-C_1(y_1+\lambda_m)]y_1/\lambda_m(y_1-1),\\ \Delta G_m&=(C_1y_1-1)(y_1+\lambda_m)(1+\lambda_m)/\lambda_m(y_1-1).\end{aligned} \tag{8}$$

Since G is of the form indicated above, it follows as one of the elementary deductions[12] in the theory of Stieltjes integrals that Eq. (4) degenerates into a summation of the type

$$G=\sum_{i=1}^{k}\Delta G_i(\lambda_i,T)=\sum_{i=1}^{k}(\lambda_i+1)\Delta F(\epsilon_i) \tag{9}$$

k being the number of discontinuities in the step function. In the present case, $G=\Delta G_0+\Delta G_m$. From combination of (9) and (8), the definition of y, and from the fact that $\lambda_0=0$ it follows that the first step in the sum satisfies

$$\Delta G_0=\frac{[1+\lambda_m-\theta_1(\alpha_0/p_1+1+\lambda_m)][\alpha_0/p_1+1]}{\lambda_m(\alpha_0/p_1)}=\Delta F(\epsilon_0)<1, \tag{10}$$

the inequality on the right resulting from the normalization condition (7). The above inequality can be rearranged to read $(\lambda_m+1+\alpha_0/p_1)[\theta_1(\alpha_0/p_1+1)-1]>0$, from which one finds

$$\theta_1(\alpha_0/p_1+1)-1>0 \quad \text{or} \quad \alpha_0>p_1(1-\theta_1)/\theta_1, \tag{11}$$

and

$$\lambda_m>-(\alpha_0/p_1+1). \tag{12}$$

The inequality for λ_m is of course trivial.

By considering the second step in the sum G, another set of inequalities may be obtained; thus,

$$\Delta G_m=\frac{[\theta_1(\alpha_0/p_1+1)-1][\alpha_0/p_1+1+\lambda_m][1+\lambda_m]}{\lambda_m(\alpha_0/p_1)}=(\lambda_m+1)\cdot\Delta F(\epsilon_m)<\lambda_m+1, \tag{13}$$

which can be rearranged into the equivalent forms;

$$\begin{aligned}&\theta_1(\alpha_0/p_1+1)-1<\lambda_m(1-\theta_1),\\ &\alpha_0/p_1<(1-\theta_1)(1+\lambda_m)/\theta_1,\end{aligned} \tag{14}$$

or

$$\lambda_m>[\theta_1(\alpha_0/p_1+1)-1]/(1-\theta_1).$$

[12] D. V. Widder, *The Laplace Transform* (Princeton University Press, Princeton, 1946).

BOUNDS OBTAINED BY USE OF LIMITING ISOTHERMS IN THE SECOND ORDER THEORY

An alternate procedure for specification of lower and/or upper bounds involves the use of the inequalities obtained from the limiting isotherms themselves. It was shown in reference 1 that the second order theory leads to the limiting relations;

$$\theta_a=p\theta_1/[p_1(1-\theta_1)+p\theta_1]=1/[1+p_1(1-\theta_1)/p\theta_1] \tag{15}$$

and

$$\theta_b=\frac{p_1/\alpha_0}{\lambda_m}\left\{\left(\frac{\alpha_0/p_1+1}{\alpha_0/p+1}\right)[(1+\lambda_m)(1-\theta_1)-\theta_1(\alpha_0/p_1)]+\left(\frac{\alpha_0/p_1+1+\lambda_m}{\alpha_0/p+1+\lambda_m}\right)\times(1+\lambda_m)[\theta_1(\alpha_0/p_1+1)-1]\right\}. \tag{16}$$

It was further shown[1] by a plausibility argument that θ_a and θ_b satisfied the relations;

$$\text{for}\quad \begin{aligned}&\theta_a<\theta<\theta_b, \quad 0<p<p_1,\\ &\theta_a>\theta>\theta_b, \quad p_1<p<\infty.\end{aligned} \tag{17}$$

The first task will thus be to establish Eq. (17) more rigorously. Since $\lambda_m>0$, the inequality (14) guarantees that $(1+\lambda_m)(1-\theta_1)-\theta_1(\alpha_0/p_1)$ remains positive. Hence, if $\alpha_0/p+1$ in (16) is replaced by $\alpha_0/p+1+\lambda_m$, the resulting expression is diminished with respect to (16). On introducing this replacement one finds

$$\theta_b>\left\{\frac{p_1/\alpha_0}{\alpha_0/p+1+\lambda_m}\right\}\{(1+\lambda_m)[\theta_1(\alpha_0/p_1+1)-1]+\theta_1(\alpha_0/p_1)(\alpha_0/p_1+1)\}. \tag{18}$$

The inequality (11) indicates that all terms in (18) are positive. Hence, one may replace λ_m in the numerator by its lower bound (14) without altering the direction of the inequality. This leads to

$$\theta_b>(\theta_1\alpha_0/p_1)[(\alpha_0/p+1+\lambda_m)(1-\theta_1)]^{-1}. \tag{19}$$

At very low pressure (19) becomes

$$\lim_{p\to\delta>0}\theta_b>\theta_1p/p_1(1-\theta_1). \tag{20}$$

On the other hand, (15) yields

$$\lim_{p\to\delta>0}\theta_a=\theta_1p/p_1(1-\theta_1) \tag{21}$$

On comparing (20) and (21) and recalling the interlacing properties of θ_a and θ_b discussed in reference 1, the relations (17) follow at once.

It is now possible to combine Eq. (15) and Eq. (17) into an inequality for n_m. Introduce the definition

$\theta=n/n_m$; then

$$\frac{n}{n_m}\lessgtr\frac{pn_1}{p_1(n_m-n_1)+pn_1} \quad \text{for } p\gtrless p_1. \tag{22}$$

This relation can be solved for

$$n_m>nn_1(p-p_1)/[pn_1-np_1], \tag{23}$$

the inequality sign being the same regardless of whether $p<p_1$ or $p>p_1$.

Bounds pertaining to α_0 can be found in principle by similar combination of (16) and (17). However, the relation for θ_b is too cumbersome for immediate use, and a simplification will have to be effected. Two methods of approach are presented as follows.

In the first method, the quantity $-\theta_1(\alpha_0/p_1)$ will be deleted from (16); let the resultant expression be denoted by θ_s, then $\theta_b<\theta_s$. Now choose p such that $p<p_1$. It follows from (17) that $\theta<\theta_b$ and hence, that $\theta<\theta_s$. Then replace p in θ_s by p_1; since all terms in θ_s are positive, as shown by (11) and by the relation $\theta_1<1$, the indicated replacement would maintain the direction of the inequalities. For present purposes it is important to apply this substitution only to the factor $Q(\lambda_m)=(\alpha_0/p_1+1+\lambda_m)/(\alpha_0/p+1+\lambda_m)$. One then obtains

$$\theta<[(p_1/\alpha_0)(1+\lambda_m)/\lambda_m][(\alpha_0/p_1+1)\times(\alpha_0/p+1)^{-1}(1-\theta_1)+\theta_1(\alpha_0/p_1+1)-1]. \tag{24}$$

It is desirable to eliminate from (24) the unknown λ_m so that the resulting expression will contain only the unknown α_0. Let γ be some number $\gamma>(1+\lambda_m)/\lambda_m$; under normal physical conditions one would expect $\lambda_m\gg1$, so that γ will be a number somewhat in excess of unity. In the large majority of cases encountered experimentally, $\lambda_m>1$, so that γ will not exceed the value 2. For most experimental work it therefore appears safe to set $\gamma=2$ without running the risk of violating the inequality (24). Replacing $(1+\lambda_m)/\lambda_m$ by γ and solving (24) for α_0, one then finds

$$\alpha_0>\{\gamma(p_1-p)-(\gamma p_1\theta_1-\theta p)\}/(\gamma\theta_1-\theta) \quad \text{with } \theta<\theta_1. \tag{25}$$

An alternative procedure consists in choosing $p>p_1$ so that $\theta>\theta_1$ and $\theta>\theta_b$, as indicated in (17). Now delete λ_m from the quantity $Q(\lambda_m)$ defined in conjunction with (24). Since by choice $p>p_1$, $Q(0)>Q(\lambda_m)$. It follows that θ_b is diminished by substitution of $Q(\lambda_m)$ for $Q(0)$ in (16). One finds $\theta>\theta_b>\theta_1\cdot Q(\lambda_m)$, which can be solved for α_0;

$$\alpha_0<\frac{(\theta-\theta_1)(1+\lambda_m)}{\theta_1/p_1-\theta/p} \quad (p>p_1). \tag{26}$$

Owing to the fact that the slope of the θ vs p plot diminishes monotonically with increasing p, the denominator in (26) will always remain positive.

It should be noted that in the limit of large α_0 and λ_m, $\theta_b=\theta_1$, independent of pressure. This shows very clearly the over-simplification associated with the use of the second-order theory, which utilizes information based on only one isotherm point. When unfavorable circumstances prevail, the mathematical analysis may yield only trivial information.

Equations (11), (14), (23), (25), and (26) thus represent a set of inequalities which can be utilized in numerical calculations. Further inequalities relating λ_m and α_0 are available by combining (17) with (16), or (18), or (9). Numerical calculations will yield a check on the determination of these quantities by other methods.

DEVIATION OF ENERGY DISTRIBUTIONS FROM THE LANGMUIR MODEL

If a set of experimental points lies very close to the second-order limiting isotherm θ_a, and if the postulates of the modified Langmuir model are applicable, then the actual energy distribution must be close to the Langmuir distribution, in which all adsorption energies have the value $\epsilon=\epsilon_1$. We wish to estimate the proportion of sites whose energies lie in an interval $I=(\epsilon_l,\epsilon_u)$ which does not include ϵ_1.

From (5) it follows that

$$F(I)=\int_{\epsilon_l}^{\epsilon_u}dF(\epsilon)=\int_{\lambda_l}^{\lambda_u}\frac{dG(\lambda,T)}{1+\lambda}=\int_I\frac{dG(\lambda,T)}{1+\lambda}. \tag{27}$$

In estimating $F(I)$ one notes that if all sites were associated with a value λ_1 not included in I, the above integral would be required to vanish identically. Further, the more sites are associated with λ's lying in I, the larger would $F(I)$, the distribution function over the interval, have to be. This suggests that the quantity $F(I)$ could be estimated by use of a positive function which vanishes at $\lambda=\lambda_1$ and which increases with the number of sites whose energies fall in the interval I. It will now be shown that such a function is given by the relation;

$$h(\lambda)\equiv N(\lambda)/D(\lambda)=z_0/(1+\lambda)+z_1/(y_1+\lambda)+z_2/(y+\lambda) \tag{28}$$

for $1<y<y_1$.

In (28) N and D satisfy the relations;

$$\begin{aligned}D(\lambda)&=(1+\lambda)(y_1+\lambda)(y+\lambda),\\ N(\lambda)&=A\lambda^2+B\lambda+C,\\ A&=z_0+z_1+z_2,\\ B&=z_0(y+y_1)+z_1(y+1)+z_2(y_1+1),\\ C&=z_0yy_1+z_1y+z_2y_1.\end{aligned} \tag{29}$$

In order that h have the desired properties, the parameters z_0, z_1, and z_2 must be determined such that $h(\lambda)\geqslant0$ and $h(\lambda_1)=0$, i.e., such that the positive function h has a minimum at $\lambda=\lambda_1$. Thus, one can determine

the z's by use of the equations;

$$\begin{aligned} h(\lambda_1)&=z_0/(1+\lambda_1)\\ &\quad+z_1/(y_1+\lambda_1)+z_2/(y+\lambda_1)=0,\\ -h'(\lambda_1)&=z_0/(1+\lambda_1)^2\\ &\quad+z_1/(y_1+\lambda_1)^2+z_2/(y+\lambda_1)^2=0, \end{aligned} \tag{30}$$

which lead to the set of relations,

$$\begin{aligned} Z&=\frac{z_0}{\begin{vmatrix}(y_1+\lambda_1)^{-1}(y+\lambda_1)^{-1}\\(y_1+\lambda_1)^{-2}(y+\lambda_1)^{-2}\end{vmatrix}}=\frac{z_1}{\begin{vmatrix}(y+\lambda_1)^{-1}(1+\lambda_1)^{-1}\\(y+\lambda_1)^{-2}(1+\lambda_1)^{-2}\end{vmatrix}}\\ &=\frac{z_2}{\begin{vmatrix}(1+\lambda_1)^{-1}(y_1+\lambda_1)^{-1}\\(1+\lambda_1)^{-2}(y_1+\lambda_1)^{-1}\end{vmatrix}} \end{aligned} \tag{31}$$

(Z an arbitrary constant) from which one obtains,

$$\frac{z_0}{(1+\lambda_1)^2(y_1-y)}=\frac{z_1}{(y_1+\lambda_1)^2(y-1)}=\frac{z_2}{(y+\lambda_1)^2(1-y_1)}=Z. \tag{32}$$

Equation (32) in turn can be solved for z_0, z_1, z_2 in terms of Z, λ_1, y, and y_1. These results can be substituted into the definitions for A, B, and C, and $h(\lambda)$ can then be found from (28). Using (32) in (29) one obtains;

$$A=Z(y_1-y)(1-y_1)(1-y),\quad B=-2\lambda_1 A,\quad C=\lambda_1^2 A. \tag{33}$$

It remains to be shown that the function (28), calculated from (29) via (33), does satisfy all the requirements imposed on it. Direct substitution of (32) into (28) shows that h and h' vanish identically at $\lambda=\lambda_1$ and only at that point. That h is non-negative can be shown readily: from (29) it follows that $D(\lambda)>0$. Hence, the sign of h will be determined by that of the parabolic function $N(\lambda)$. As was just demonstrated, h, and therefore N, is either a maximum or a minimum at $\lambda=\lambda_1$ where it has the value 0. Hence, the entire parabola N lies either above or below the axis $N=0$, depending on the sign of A. By (33) and the choice of $1<y<y_1$ (see (28)) it follows that A is positive and hence that $N(\lambda)\geqslant 0$.

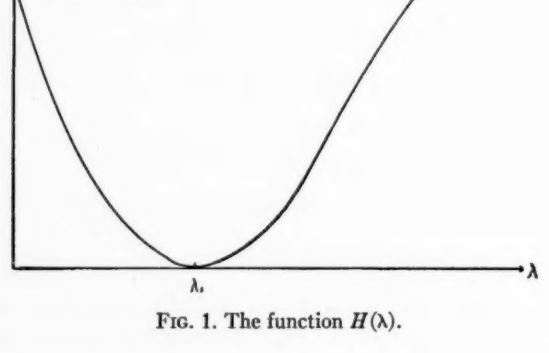

FIG. 1. The function $H(\lambda)$.

Having established that $h(\lambda)$ has the desired properties, we can return to the task of determining $F(I)$. For this purpose consider the following set of inequalities;

$$\begin{aligned} \int_0^\infty h(\lambda)dG(\lambda,T)&\geqslant\int_I h(\lambda)dG(\lambda,T)\\ &\equiv\int_I\frac{1+\lambda}{1+\lambda}h(\lambda)dG(\lambda,T)\geqslant\mu F(I), \end{aligned} \tag{34}$$

where

$$\mu=\min_{\lambda\epsilon I}(1+\lambda)h(\lambda). \tag{35}$$

Hence,

$$\begin{aligned} F(I)&\leqslant(1/\mu)\int_0^\infty h(\lambda)dG(\lambda,T)\\ &=(1/\mu)\int_0^\infty\left[\frac{z_0}{1+\lambda}+\frac{z_1}{y_1+\lambda}+\frac{z_2}{y+\lambda}\right]dG(\lambda,T)\\ &=(1/\mu)[z_0+z_1C_1+z_2L(y,T)], \end{aligned} \tag{36}$$

where $C_1=L(y_1,T)$.

To calculate an upper bound on $F(I)$ from (36) one thus proceeds as follows: A reference point $(\theta_1 p_1)$ is selected; C_1, y_1 are determined from Eq. (3); and λ_1 is calculated from the relation (see reference 1, Eq. (13))

$$\lambda_1=(C_1y_1-1)/(1-C_1). \tag{37}$$

Next, another experimental point L, y is chosen such that $y<y_1$; z_0, z_1, and z_2 can now be computed from (32). To evaluate μ in (35) one determines $h(\lambda)$ from (28), multiplies the result by $(1+\lambda)$ and takes the minimum of the function $H(\lambda)\equiv(1+\lambda)\cdot h(\lambda)=z_0+z_1(1+\lambda)/(y_1+\lambda)+z_2(1+\lambda)/(y+\lambda)$ in the interval I.

A rough sketch of $H(\lambda)$ is shown in Fig. 1. It is seen that if the interval $I=(\lambda_l,\lambda_u)$ is chosen from a range of $\lambda<\lambda_1$, $\mu=H(\lambda_u)$; while for an interval of λ values $\lambda>\lambda_1$, $\mu=H(\lambda_l)$.

In actual calculations the numerical values are specified only to within an arbitrary parameter Z. This means in effect that one can obtain only the relative fraction of all sites whose energies lie in the interval I. Such a specification is useful in comparing the results for different intervals.

Vibrational Intensities in Halogenated Methanes. I. Methylene Chloride

JOSEPH W. STRALEY
Department of Physics, The University of North Carolina, Chapel Hill, North Carolina
(Received February 25, 1955)

The absolute infrared absorption intensities of four fundamental bands in CH_2Cl_2 have been measured in the vapor state. The intensities that have been observed are

A_6 (CH stretching) $=48.0\times10^{10}$ cycles/sec at NTP
A_7 (CH rocking) $=13.0\times10^{10}$ cycles/sec at NTP
A_8 (CCl stretching) $=1420.0\times10^{10}$ cycles/sec at NTP
A_9 (CCl rocking) $=375.0\times10^{10}$ cycles/sec at NTP.

These data indicate that the bond moments and bond derivatives are

$\mu_{CH}=+0.45\times10^{-18}$ esu
$\mu_{CCl}=-0.95\times10^{-18}$ esu
$\partial\mu_{CH}/\partial r_{CH}=+0.3\times10^{-10}$ esu or -0.2×10^{-10} esu
$\partial\mu_{CCl}/\partial r_{CCl}=+3.7\times10^{-10}$ esu.

It was not possible to resolve the ambiguity in signs that lead to the alternate values of $\partial\mu_{CH}/\partial r_{CH}$.

INTRODUCTION

THE intensity of an absorption band in the infrared is determined by the change in dipole moment associated with the vibration of the molecule. This fact may be expressed quantitatively by

$$A_i=\frac{N\pi}{3c}\left(\frac{\partial\mu}{\partial Q_i}\right)^2, \qquad (1)$$

where A_i represents the intensity of fundamental associated with the normal mode Q_i, N is the number of molecules per cubic centimeter, and μ is the dipole moment of the molecule.

The absolute intensity of an infrared absorption band may be measured either in the vapor state[1] or in solution.[2] For some compounds one has no choice as to which of these techniques he will employ. Where choice exists there can be little doubt that the intensities measured in the vapor state are to be preferred over those measured in solution all other factors being equivalent.

Experience has justified in some cases the assumption that one may associate a "bond moment" with each valence bond in the molecule, and that the vector sum of all bond moments equals the total dipole moment of the molecule. While many doubts exist regarding the significance of these bond moments and the extent to which the assumptions that are made regarding their properties can be validated, there can be little doubt of the usefulness of this model in certain special cases.

Wherever this model is used it is accepted that

(a) the bond moment lies directly along the bond and continues to do so when the molecule is deformed by vibration, and

(b) the electric anharmonicity of the dipole moment is small, perhaps of the same order of magnitude as the anharmonicity of the force constants.

The near failure of the model for ethylene[3,4] may serve to indicate the need for modification of the model when applied to more complex molecules. Its success in HCN and DCN[5] and in C_2H_2 and C_2D_2[6] demonstrates that the model may be successfully employed at least in special cases.

EXPERIMENTAL PROCEDURE

The intensities of all bands reported in this paper were determined by the extrapolation method of Wilson and Wells.[1] A double-pass Perkin-Elmer Infrared Spectrometer was employed in securing all of the data. A high-pressure cell 5.122 centimeters long containing methylene chloride at a partial pressure of a few centimeters of mercury and containing nitrogen gas at a total pressure of 100 psi was placed in the path. The region in which the bands were located was scanned; the cell was evacuated and the region rescanned immediately. The instrument was in every case operated at minimum slit-maximum gain consistent with securing an intelligible record. The equivalent slit width employed in the various regions are indicated in Table I.

TABLE I.

Band	Location cm^{-1}-(microns)	Slit width (cm^{-1})	Intensity (cycles/sec at NTP)	$\frac{\partial\mu_T}{\partial Q_i}$
6	3048–(3.28)	2.4	48.0×10^{10}	±22.6
7	898–(11.14)	1.7	13.0×10^{10}	±11.7
8	742–(13.48)	2.4	1420.0×10^{10}	±123.0
9	1262–(7.92)	2.8	375.0×10^{10}	±63.1

[1] E. B. Wilson and A. J. Wells, J. Chem. Phys. **14**, 578 (1946).
[2] D. A. Ramsay, J. Am. Chem. Soc. **74**, 72 (1952).
[3] Thorndike, Wells, and Wilson, J. Chem. Phys. **15**, 157 (1947).
[4] D. F. Eggers, J. Chem. Phys. **23**, 221 (1955).
[5] G. E. Hyde and D. F. Hornig, J. Chem. Phys. **20**, 647 (1952).
[6] E. C. Wingfield and J. W. Straley, J. Chem. Phys. **23**, 731 (1955).

Each band was observed at least five times at a range of partial pressures chosen in such a way as to produce approximately 30% maximum absorption at one extreme and 90% maximum absorption at the other.

It was found that when sample gas was admitted to the previously evacuated cell a direct correlation could be established between the percent absorption at any given point in an absorption band and the pressure observed on the manometer. That gas was not being absorbed on the walls of the cell or absorbed in stopcock grease, etc., was apparent from the fact that when the cell was closed the percent absorption would remain constant over long periods of time.

When nitrogen gas was admitted to the cell an initial decrease in absorption was observed due to incomplete mixing. After thirty minutes the value of $\ln(I_0/I)$ was found to have attained an equilibrium value. Error from this source is included in judgment of the probable error in the measurements.

Values of the quantity $\ln(T_0/T)$ were determined at equal wave number intervals along the record.[7] The integral $\beta_i=\int \ln(T_0/T)d\nu$ was determined by numerical integration. Values of these integrated absorption areas were plotted against the equivalent paths L_e, defined as the path length which at NTP would contain the same number of molecules per unit cross section as the actual path. The intensity of the band is given by the slope of the curve thereby determined at $L_e=0$ in accordance with the equation

$$A_i=\lim_{L_e\to 0}\left(\frac{\beta_i}{L_e}\right). \tag{2}$$

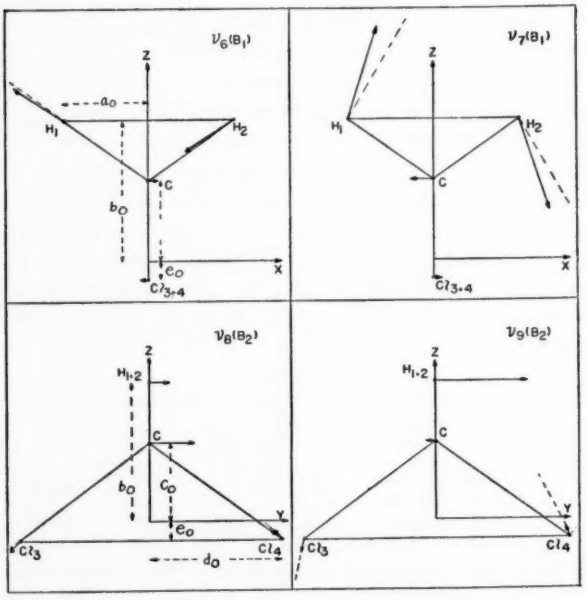

FIG. 1. Classical vibrational modes in CH_2Cl_2 of species B_1 and B_2. The scale chosen to represent amplitudes is 5× that used to represent interatomic distances.

[7] E. C. Wingfield, Rev. Sci. Instr. **25**, 1036 (1954).

The intensities of bands measured in this way are given in Table I.

The fundamental ν_6 is partially overlapped by ν_1 though the absorption maxima of each was clearly resolved. The bands were of approximately equal intensity. The value $A_6=48.0\times10^{10}$ cycles/sec at NTP was determined by measuring the entire contour of both bands and allotting half the observed intensity to ν_6. The probable error in this measurement was estimated at 20%.

NORMAL COORDINATES

The methylene chloride molecule belongs to the point group C_{2v}. The intrabond angles have been assumed to be tetrahedral. The bond lengths as indicated by electron diffraction data were taken to be $r_{oCCl}=1.75\times10^{-8}$ cm and $r_{oCH}=1.093\times10^{-8}$ cm. These quantities and the force constants used in this work were those quoted by Decius[8] with one correction supplied by Plyler and Benedict.[9]

The normal coordinates were determined in terms of a set of intermediate generalized coordinates by methods that have been described by Shaffer and Herman.[10] In this investigation it was necessary only to secure information regarding the vibrations of species B_1 and B_2; consequently, it was necessary only to determine normal coordinates that describe the B_1 and the B_2 vibrations. The intermediate coordinates that possess the proper symmetry are

$$\begin{aligned}\eta_6&=(x_1'+x_2')/2,\\ \eta_7&=(x_3'+x_4')/2,\\ \zeta_8&=(y_1'+y_2')/2,\\ \zeta_9&=(y_3'+y_4')/2,\end{aligned} \tag{3}$$

where x_i' represents the x-displacement of the ith particle from its equilibrium position, etc. These intermediate coordinates were found to be related to the normal coordinates as follows[11]:

$$\begin{aligned}\eta_6&=42.32\times10^{10}Q_6+17.94\times10^{10}Q_7,\\ \eta_7&=0.0233\times10^{10}Q_6+1.396\times10^{10}Q_7\end{aligned} \tag{4a}$$

for the B_1 vibrations, and

$$\begin{aligned}\zeta_8&=8.272\times10^{10}Q_8+52.68\times10^{10}Q_9,\\ \zeta_9&=3.524\times10^{10}Q_8-0.605\times10^{10}Q_9\end{aligned} \tag{4b}$$

for the B_2 vibrations.

[8] J. C. Decius, J. Chem. Phys. **16**, 214 (1948).

[9] E. K. Plyler and W. S. Benedict, J. Research Natl. Bur. Standards **47**, 202 (1951).

[10] W. H. Shaffer and R. C. Herman, J. Chem. Phys. **12**, 494 (1944).

[11] The expressions for the quantities N_k and N_l in reference 10 should be corrected as follows:

$N_k=[\mu_6(\lambda_k\mu_7-k_7)^2+\mu_7(\lambda_k\mu_{67}-k_{67})^2-2\mu_{67}(\lambda_k\mu_7-k_7)(\lambda_k\mu_{67}-k_{67})]^{\frac{1}{2}}$

$N_l=[\mu_8(\lambda_l\mu_9-k_9)^2+\mu_9(\lambda_l\mu_{89}-k_{89})^2-2\mu_{89}(\lambda_l\mu_9-k_9)(\lambda_l\mu_{89}-k_{89})]^{\frac{1}{2}}$.

The sign in the expression for n_{9l} should be changed to a minus sign.

When these normal coordinates are interpreted geometrically they yield the classical vibrations shown in Fig. 1.

BOND MOMENTS AND BOND DERIVATIVES

We associate bond moments μ_{CH} and μ_{CCl} with the interatomic bond CH and CCl and assume that these bond moments lie at all times directly along the bonds to which they relate. When the molecule vibrates it follows that the displacement of the bond generates a change in dipole moment perpendicular to the bond which is proportional to the magnitude of the bond moment and to the change in the angle which describes the orientation of the bond. Where the motion produces a change in length of the bond it is assumed that a component of dipole moment parallel to the bond is generated that is equal to the product of the change in length of the bond and the bond derivative, defined by $\partial\mu_{CH}/\partial r_{CH}$ or $\partial\mu_{CCl}/\partial r_{CCl}$.

It can be seen that for small oscillations the B_1 vibrations involve no change in the CCl bond length and that the B_2 vibrations involve no change in the CH bond length. Geometrical considerations make it possible to express the quantities that contribute to the change in total dipole moment as follows

$$\partial\mu_T/\partial Q_k = D_k\mu_{CCl} + E_k\mu_{CH} + F_k\partial\mu_{CH}/\partial r_{CH} \quad (k=6,7) \quad (5)$$

for the B_1 vibrations and

$$\partial\mu_T/\partial Q_l = D_l\mu_{CCl} + E_l\mu_{CH} + G_l\partial\mu_{CCl}/\partial r_{CCl} \quad (l=8,9) \quad (6)$$

for the B_2 vibrations. The constants in these expressions are given by

$$D_k = \frac{2}{r_{oCCl}}\left\{\frac{2m}{M}\frac{\partial\eta_6}{\partial Q_k} + \left(\frac{2n}{M}+1\right)\frac{\partial\eta_7}{\partial Q_k}\right\}, \quad (7a)$$

$$E_k = \frac{2\cos\frac{\beta}{2}}{r_{oCH}}\left\{\left[\left(\frac{2m}{M}+1\right)\cos\frac{\beta}{2} - \left(\frac{b_0-c_0}{a_0}\right)\sin\frac{\beta}{2}\right]\frac{\partial\eta_6}{\partial Q_k} + \left[\frac{2n}{M}\cos\frac{\beta}{2} + \frac{n}{m}\frac{(e_0+c_0)}{a_0}\sin\frac{\beta}{2}\right]\frac{\partial\eta_7}{\partial Q_k}\right\}, \quad (7b)$$

$$F_k = 2\sin\frac{\beta}{2}\left\{\left[\left(\frac{2m}{M}+1\right)\sin\frac{\beta}{2} + \left(\frac{b_0-c_0}{a_0}\right)\cos\frac{\beta}{2}\right]\frac{\partial\eta_6}{\partial Q_k} + \left[\frac{2n}{M}\sin\frac{\beta}{2} - \frac{n}{m}\left(\frac{e_0+c_0}{a_0}\right)\cos\frac{\beta}{2}\right]\frac{\partial\eta_7}{\partial Q_k}\right\}, \quad (7c)$$

and

$$D_l = \frac{2\cos\frac{\beta}{2}}{r_{oCCl}}\left\{\left[\frac{2m}{M}\cos\frac{\beta}{2} + \frac{m}{n}\frac{(b_0-c_0)}{d_0}\sin\frac{\beta}{2}\right]\frac{\partial\zeta_8}{\partial Q_l} + \left[\left(\frac{2n}{M}+1\right)\cos\frac{\beta}{2} - \left(\frac{e_0+c_0}{d_0}\right)\sin\frac{\beta}{2}\right]\frac{\partial\zeta_9}{\partial Q_l}\right\}, \quad (8a)$$

$$E_l = \frac{2}{r_{oCH}}\left\{\left(\frac{2m}{M}+1\right)\frac{\partial\zeta_8}{\partial Q_l} + \frac{2n}{M}\frac{\partial\zeta_9}{\partial Q_l}\right\}, \quad (8b)$$

$$G_l = 2\sin\frac{\beta}{2}\left\{\left[\frac{2m}{M}\sin\frac{\beta}{2} - \frac{m}{n}\left(\frac{b_0-c_0}{d_0}\right)\cos\frac{\beta}{2}\right]\frac{\partial\zeta_8}{\partial Q_l} + \left[\left(\frac{2n}{M}+1\right)\sin\frac{\beta}{2} + \left(\frac{e_0+c_0}{d_0}\right)\cos\frac{\beta}{2}\right]\frac{\partial\zeta_9}{\partial Q_l}\right\}, \quad (8c)$$

where m, n, and M represent the masses of the hydrogen, chlorine, and carbon atoms, respectively, β represents the tetrahedral angle and r_{oCH} and r_{oCCl} represent the equilibrium CH and CCl bond lengths.

In addition to these expressions, an additional equation relating bond moments to the known permanent dipole moment can be written as follows

$$2\cos\frac{\beta}{2}(\mu_{CH}-\mu_{CCl}) = \mu_T. \quad (9)$$

From the measured[12] value of $\mu_T = 1.62\pm0.02\times10^{-18}$ esu, this equation becomes

$$\mu_{CH}-\mu_{CCl} = 1.40\times10^{-18}. \quad (10)$$

The choice of a positive sign for μ_T is equivalent to assuming the chlorine atom to be more electronegative with respect to carbon than hydrogen.

Introducing known quantities into Eqs. (7) and substituting into Eqs. (5), we find,

$$8.30\times10^{18}\mu_{CCl} + 5.20\times10^{18}\mu_{CH} + 93.4\times10^{10}\frac{\partial\mu_{CH}}{\partial r_{CH}} = \pm22.6, \quad (11a)$$

$$14.5\times10^{18}\mu_{CCl} + 54.6\times10^{18}\mu_{CH} - 1.56\times10^{10}\frac{\partial\mu_{CH}}{\partial r_{CH}} = \pm11.7. \quad (11b)$$

In like manner Eqs. (6) become

$$7.34\times10^{18}\mu_{CCl} + 20.4\times10^{18}\mu_{CH} + 33.0\times10^{10}\frac{\partial\mu_{CCl}}{\partial r_{CCl}} = \pm123.0, \quad (12a)$$

$$2.36\times10^{18}\mu_{CCl} + 106\times10^{18}\mu_{CH} + 5.19\times10^{10}\frac{\partial\mu_{CCl}}{\partial r_{CCl}} = \pm63.1. \quad (12b)$$

TABLE II.

B_1		B_2	
Signs 11a and 11b	μ_{CH}	Signs 12a and 12b	μ_{CH}
+ +	$+0.470\times10^{-18}$	+ +	$+0.437\times10^{-18}$
+ −	+0.132	+ −	−0.776
− +	+0.459	− +	+0.809
− −	+0.121	− −	−0.405

[12] R. J. Myers and W. D. Gwinn, J. Chem. Phys. **20**, 1421 (1952).

TABLE III.

	Equations (11a) and (11b) (+ +)	Equations (11a) and (11b) (− +)	Equations (12a) and (12b) (+ +)
μ_{CH}	$+0.47(\pm0.02)\times10^{-18}$	$+0.46(\pm0.02)\times10^{-18}$	$+0.44(\pm0.04)\times10^{-18}$
μ_{CCl}	$-0.93(\pm0.03)\times10^{-18}$	$-0.94(\pm0.03)\times10^{-18}$	$-0.96(\pm0.04)\times10^{-18}$
$\partial\mu_{CH}/\partial r_{CH}$	$+0.30(\pm0.03)\times10^{-10}$	$-0.20(\pm0.03)\times10^{-10}$	...
$\partial\mu_{CCl}/\partial r_{CCl}$	...	...	$+3.7(\pm0.2)\times10^{-10}$

One may now solve for μ_{CH}. The ambiguity in sign is resolved by securing two sets of solutions, the first, using Eqs. (10), (11a), and (11b); the second using Eqs. (10), (12a), and (12b). The values secured for various combinations of signs appear in Table II. Inasmuch as we expect each species to manifest the same bond moment, we can eliminate all sign combinations except those associated with bond moments +0.437, +0.459, and $+0.470\times10^{-18}$.

One may now solve for the bond derivatives. Having narrowed the choice of signs in Eqs. (11a) and (11b) to + + and − + and having determined the signs in Eqs. (12a) and (12b) to be + + we may secure solutions for bond moments and bond derivatives as shown in Table III.

The judgment of probable error shown in the table is based on the assumption that the error in the weaker B_1 vibrations was approximately 20% and that in the B_2 vibrations was 12%. The assumed error in μ_T was as quoted by Myers and Gwinn and indicated in Eq. 9.

DISCUSSION OF RESULTS

As one may observe in Table III it was not possible to unambiguously make a choice between the combination of signs that leads to a positive CH bond derivative and that which leads to a negative CH bond derivative. Of the two, the positive sign would seem to be the more reasonable in the light of the positive CH bond moment.

However, the fact that one cannot in every case conclude that the bond moment must have the same sign as the bond derivative is revealed in the B_2 vibrations where the CCl bond is negative, and the bond derivative is positive. One is left to conclude that a classical picture of this particular CCl stretching vibration would show the postively charged core associated with the chlorine nucleus and its bound electrons vibrating within a relatively stationary negative charge cloud. This tendency toward incomplete "following" does not seem to occur in the bending vibrations. The author is not aware of a previous case in which the sign of a bond derivative was determined and found to exhibit this anomalous behavior.* In the case of C_2F_6, for example, Williams, Person, and Crawford[13] reported that the CF bond moment and the CF bond derivative have the same sign.

Work which may contribute to our picture of the makeup of the carbon-hydrogen and the carbon-halogen bond is in progress on other molecules of this type.

ACKNOWLEDGMENTS

The author expresses his appreciation to Professor Wave Shaffer, Professor Wayne Bowers, Dr. Nand Lal Singh, and Mr. Tom True for helpful suggestions and discussions. This work has been supported by a grant from the National Science Foundation.

[13] Williams, Person, and Crawford, J. Chem. Phys. **23**, 179 (1955).

* *Note added in proof.*—I. C. Hisatsune and D. F. Eggers, Jr., J. Chem. Phys. **23**, 492 (1955) have recently reported a similar anomaly in formaldehyde.

Letters to the Editor

THIS section will accept reports of new work, provided these are terse and contain few figures, and especially few half-tone cuts. The Editorial Board will not hold itself responsible for opinions expressed by the correspondents. Contributions to this section should not exceed 600 words in length and must reach the office of the Editor not later than the 15th of the second month preceding that of the issue in which the Letter is to appear. No proof will be sent to the authors. The publication charge for Letters is $25 per page, with a minimum of $25 per Letter. If honored, the Institution will be entitled to 100 reprints without covers.

Thermoluminescence Induced by Pressure and by Crystallization

EDWARD J. ZELLER, JOHN L. WRAY, AND FARRINGTON DANIELS
Department of Chemistry, University of Wisconsin, Madison, Wisconsin
(Received September 12, 1955)

IN trying to determine the age of coral limestones from the intensity of thermoluminescence and the alpha-ray activity it was found that the younger limestones gave abnormally bright thermoluminescence. This observation led to the unexpected discovery that calcium carbonate, freshly precipitated in the laboratory, is also thermoluminescent, even without exposure to radiation. A variety of related phenomena are under further investigation in this laboratory.

When calcium carbonate is precipitated from calcium nitrate by sodium carbonate and the washed and dried crystals exposed to gamma radiation, prominent peaks are found in the thermoluminescence glow curve which are associated with impurities, such as iron, manganese, strontium, barium, and magnesium. The middle fraction of the precipitated crystals contains the fewest impurities[1] and does not show radiation induced (gamma-ray) thermoluminescence. However, the precipitated $CaCO_3$ crystals, whether exposed to gamma radiation or not, exhibit some thermoluminescence around 250° shortly before blackbody radiation obscures further detection. A typical glow curve of this type is shown in Curve 1, Fig. 1.

When the crystals are subjected to high pressure (50 tons per square inch) the thermoluminescence observed on heating is much greater as shown in Curve 2, Fig. 1. This pressure-induced thermoluminescence, without previous exposure to radiation, occurs even with the highly purified calcium carbonate which shows no radiation-induced thermoluminescence.

In old limestones (older than 100 million years) the thermoluminescence induced by alpha particles from uranium is always *decreased* by application of high pressures. This pressure effect is useful because it distinguishes between the radiation-induced thermoluminescence on which the age determination is based and the complicating crystallization- or pressure-induced thermoluminescence. The radiation-induced thermoluminescence is decreased while the crystallization-(nonradiation) induced thermoluminescence is increased.[2] New possibilities are opened up for determining the age of minerals based on the several different types of thermoluminescence and the influence of pressure.

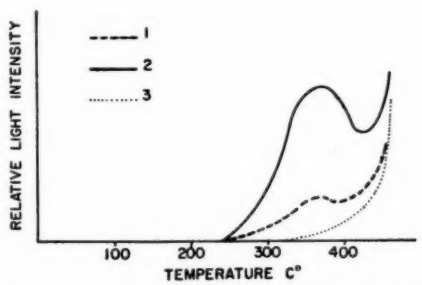

FIG. 1. Curve 1. The natural glow curve of a calcium carbonate precipitate before exposure to radiation or pressure. Curve 2. The glow curve of the same precipitate after pressure of 50 tons/sq in. but without exposure to radiation. Curve 3. Blackbody radiation curve.

More experimental facts are being accumulated on which to base a theory of pressure-induced and crystallization-induced thermoluminescence. It is suggested now that high pressures applied to a mass of crystals creates, by friction and point contact effects, high electrostatic voltages in local areas which are greater than the voltage necessary to release electrons in the crystal lattice. Triboluminescence is a well-known phenomenon in which light is emitted in the crushing of certain crystals such as cane sugar. The presence of pressure-induced thermoluminescence suggests that triboluminescence was produced initially, and that accumulated thermoluminescence is easier to detect than transient triboluminescence.

The crystallization-induced thermoluminescence merits further study. One theory suggests that strains of crystal growth may be set up which generate local electrostatic charges sufficient to release electrons; and according to another hypothesis a double layer involving ions attached to a growing crystal surface may, under certain conditions, generate a high enough charge to release electrons and give rise to subsequent thermoluminescence. Where crystallization-induced thermoluminescence exists, it is suggested that crystallization luminescence may be detected at the time of crystallization if the detection techniques with photomultiplier tubes are sufficiently improved. The pressure effects, in addition to releasing electrons in the crystal, may also create new holes or imperfections for the trapping of electrons, leading to new peaks in the thermoluminescence glow curves. Moreover, under certain conditions the application of pressure, causing plastic flow, may "heal" some of the imperfections already present and cause a decrease in some types of radioactivity-induced thermoluminescence.

The effects on thermoluminescence of pressure and crystallization described here are very small and could easily escape detection in earlier work with less sensitive equipment. By analogy with γ-induced thermoluminescence, it is estimated[3] that of the order of one electron may be released and trapped among 10^9 atoms.

[1] E. J. Zeller and J. L. Wray, Bull. Am. Assoc. Petroleum Geol. (to be published).
[2] E. J. Zeller, Symposium on Geochemistry, American Chemical Society, Minneapolis, Minnesota (September 12, 1955).
[3] Morehead and F. Daniels, J. Phys. Chem. **56**, 546 (1952).

Spectroscopic Studies of Some Aromatic Acids with a Heteroatom in the Side-Chain

A. I. KISS AND B. R. MUTH
Central Research Institute for Physics, Budapest, Hungary
(Received September 6, 1955)

THE purpose of our investigations has been to establish the part played by the elements of the main group in the column VI of the periodic system (O, S, Se) in the absorption of light by these compounds and to show how this appears in their ultraviolet absorption spectra. The compounds observed can be divided into two groups: (1) Compounds of the phenylglycolic acid type, (2) those of the salicylic acid type.

The spectrum of benzene, the basic compound has two bands in the ultraviolet and a third one in the Schuman violet region. The quantum-mechanical interpretation of the excitation processes corresponding to these bands was given recently by Craig.[1]

On substituting a carboxylic group in the benzene ring, its electron distribution changes on account of mesomeric and inductive effects.[2] In the benzoic acid (I) however, no new excitation

TABLE I.

		Maximum λmμ	Maximum loge	Maximum λmμ	Maximum loge	Maximum λmμ	Maximum loge
I	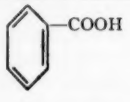	272	2936	227	4031		
II	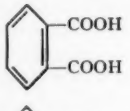	275	3047	229	3875	205	4318
III	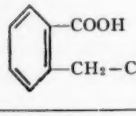	277	2999	229	3800	204	4227

		Minimum λmμ	Minimum loge	Minimum λmμ	Minimum loge
I	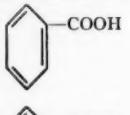	255	2758	209	3700
II	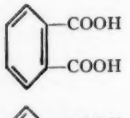	263	2926	221–26	3870
III	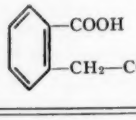	260	2812	222	3779

TABLE II.

		Maximum λmμ	Maximum loge	Maximum λmμ	Maximum loge	Maximum λmμ	Maximum loge
IV	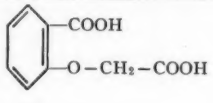	288	3304	230	3698	208	4132
V	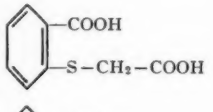	316	3414	258	3814	223	4201
VI	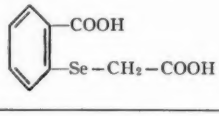	323	3548	264	3787	228	4214

		Minimum λmμ	Minimum loge	Minimum λmμ	Minimum loge
IV	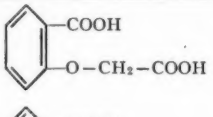	260	2751	220	3653
V	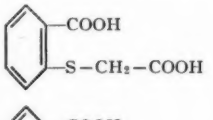	281	2892	241	3617
VI	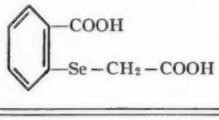	287	3005	247	3685

processes appear (see Table I). A π electron configuration is formed, which persists in the further derivates.

The substitution of the second carboxylic group in *ortho*-position has a bathochromic effect causing a shift of the band lying in the Schuman violet and consequently increases the number of bands in the ultraviolet region. The nearly identical extinction of the phthalic acid (II) with the benzoic acid is probably due to the interaction disturbing the simultaneous mesomerism of the two substituents.

If one of the carboxylic groups is separated by a methylenic group from the ring (homophthalic acid III), the latter reduces the mesomeric interaction compared with the phthalic acid, resulting in some decrease in the extinction too.

Introducing a heteroatom into the molecule, there will be no possibility for new excitation, but the relative height of the bands will be changed. The character of the spectrum of the *o*-carboxymethoxy benzoic acid (IV) (see Table II) is mainly determined—besides the two carboxylic groups—by the presence of the oxygen atom. Exchanging the oxygen atom in the ring with a sulfur or selen atom no change is to be observed in the structure of the curve of phenylthioglycolic (V) and phenylselenoglycolic *ortho*-carboxylic (VI) acids, respectively. The change takes place in the position of the curve. The curve is shifted towards the longer wavelengths with the decrease in the negative character of the heteroatom. It can be stated that the difference between the positions of the curves IV and V is considerably greater than that between V and VI; this being in complete accordance with the rule of the periodic system.

A new electronic system will be formed in the benzoic acid molecule in case of a substitution with a hydroxylic group in *ortho*-position. The spectrum of the salicylic acid (VII) (see Table III) shows three bands like that of the phthalic acid, their positions however being different owing to the mesomeric effect of the hydroxylic group. Substituting the hydroxylic group with mercapto group the structure of the spectrum will be greatly changed. The curve of the thiosalicylic acid (VIII) shows a shift towards the longer wavelength and the number of the bands increases with one. The appearing of the fourth band might be attributed to the excitation of the free electron pairs of the sulfur atom. We assume the low-intensity band near 275 mμ is to be assigned to this excitation process whereas the other three bands correspond to those of the salicylic acid with an approximately uniform shift. The selenosalicylic acid, being an unstable compound, can be produced only in its alkalic salt form[3] and so no comparison could be made.

TABLE III.

		Maximum λmμ	Maximum loge	Maximum λmμ	Maximum loge	Maximum λmμ	Maximum loge	Maximum λmμ	Maximum loge
VII	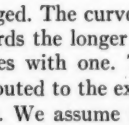	304	3574			236	3852	205	4498
VIII	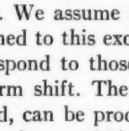	313	3153	275	3288	242	3653	220	4024

		Minimum λmμ	Minimum loge	Minimum λmμ	Minimum loge	Minimum λmμ	Minimum loge
VII	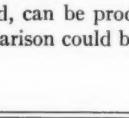	262	2469			220	3660
VIII	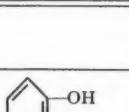	294	2990	268	3264	236	3634

Experimental.—Homophthalic acid.[4] Nearly colorless plates or prisms; m.p. 181–183°C. Carboxymethoxy benzoic acid.[5] Well-grown plates; m.p. 190–192°C. Phenylthioglycolic-*o*-carboxylic acid.[6] White needles; m.p. 217°C. Phenylselenoglycolic-*o*-carboxylic acid.[3] White crystalline powder; m.p. 233°C. Thiosalicylic acid.[7] Yellow thick needles or plates. Will be oxidized in air. M.p. 164–165°C.

A detailed paper on the foregoing subject will be published in *Acta Chimica Hungarica.*

[1] D. P. Craig, Discussions Faraday Soc. **9**, 5 (1950).
[2] A. Kiss and E. Csetneky, Acta Univ. Szeged **2**, 37 (1948).
[3] R. Lesser and R. Weiss, Ber. deut. chem. Ges. **45**, 1833 (1912).
[4] A. I. Vogel, *The Textbook of Practical Organic Chemistry* (1951), second edition, pp. 731–732.
[5] R. Meyer and C. Duczmel, Ber. deut. chem. Ges. **46**, 3366 (1913).
[6] H. E. Fierz-David and L. Blangey, *Farbenchemie* (Springer-Verlag, Vienna, 1952), eighth edition, p. 324.
[7] Org. Syntheses **2**, 580.

Spectroscopic Studies of Aromatic Sulfides and Selenides

A. I. Kiss and B. R. Muth
Central Research Institute for Physics, Budapest, Hungary
(Received September 6, 1955)

In this paper the effect on the ultraviolet absorption spectrum, resulting from one or two heteroatoms connecing two benzene rings, will be discussed.

Several opinions can be found in the literature concerning the interpretation of the spectrum of the basic compound diphenylsulfide.[1] We assume that the band at 276 mμ corresponds to the first band of benzene influenced by the electron pairs of the sulfur atom taking part in the mesomerism. The band at 250 mμ corresponds to the simultaneous excitation of the benzene-electrons and the free electrons of the sulfur atom. This assumption is supported by the high degree of resemblance of the curve to that of the thiophenol.

In the spectrum of the diphenylselenide the two bands appear fused, and a bathochromic effect takes place owing to the lower energy of excitation of the selen electrons.

The spectrum (Table I) of the diphenylsulfide-*o*, *o*'-dicarboxylic acid (I) shows an entirely different structure from the basic compound as the two carboxylic groups in *ortho*-position destroy the planar structure of the diphenylsulfide molecule. Thus the spectrum will be characteristic of the dicarboxylic acid structure.

The curve of the diphenylselenide-*o*, *o*'-dicarboxylic acid (II) shows a similar difference with respect to the basic compound. The exchange of the heteroatom in the molecule Se instead of S produces a shift towards the longer wavelength.

The interpretation of the spectrum of diphenyldisulfide has been given by Koch.[2] The steric effect is negligible between the diphenyl disulfide and its dicarboxylic derivate, because the basic compound already is not planar. The change in the structure of the spectrum of diphenyldisulfide-*o*, *o*'-carboxylic acid (III) is the result of the inductive and mesomeric effect of the carboxylic group. Here also the characteristics of dicarboxylic-type predominate in the spectrum.

The spectrum of the diphenyldiselenide-*o*, *o*'-dicarboxylic acid (IV) similarly to the foregoing, conforms to the rules prevailing in the spectra of the sulfuric and selenic compounds.

Comparing the spectra of the dicarboxylic acids containing one or two sulfur and selen atoms, respectively, it can be stated that changing the numbers of the heteroatoms results in the increase of extinction.

Experimental.—Diphenylsulfide-*o*, *o*'-dicarboxylic acid.[3] White crystals; m.p. 229–230°C. Diphenylselenide-*o*, *o*'-dicarboxylic acid.[4] Pale yellow microcrystals; m.p. 228–229°C. Diphenyldisulfide-*o*, *o*'-dicarboxylic acid.[5] Powder of microcrystals; m.p. 288–290°C.

Table I.

		Maximum λmμ	Maximum log ε	Maximum λmμ	Maximum log ε	Maximum λmμ	Maximum log ε
I	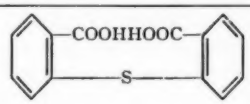	316	3.566	252	3.871	219	4.223
II	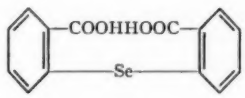	331	3.654	262	3.777	227	4.230
III	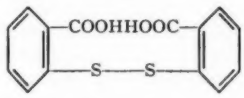	310	3.842	253	4.164	222	4.495
IV	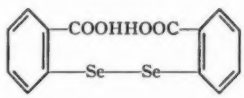	318	3.980	257	4.232	228	4.527

		Minimum λmμ	Minimum log ε	Minimum λmμ	Minimum log ε
I	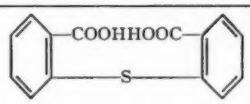	284	3.320	246	3.865
II	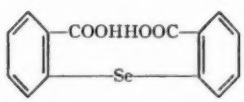	285	3.330	250	3.714
III	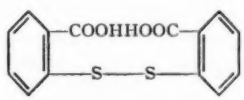	280	3.468	240	4.106
IV	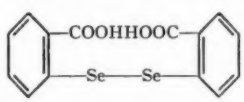	281	3.528	244	4.165

Diphenyldiselenide-*o*, *o*'-dicarboxylic acid.[4] Nearly colorless microcrystals; m.p. 296°C. A detailed paper on this subject will be published in *Acta Chimica Hungarica.*

[1] W. W. Robertson and F. A. Matsen, J. Am. Chem. Soc. **72**, 5250 (1950); H. P. Koch, J. Chem. Soc. 387 (1949); E. A. Fehnel and M. Carmack, J. Am. Chem. Soc. **71**, 84 (1949).
[2] H. P. Koch, J. Chem. Soc. 394 (1949).
[3] F. Mayer, Ber. deut. chem. Ges. **43**, 584 (1910).
[4] R. Lesser and R. Weiss, Ber. deut. chem. Ges. **45**, 1833 (1912).
[5] Org. Syntheses **2**, 580.

X-Ray Crystallographic Study of Phase Transformation of Borax during Thermal Treatments

D. R. Dasgupta and B. K. Banerjee
Indian Association for the Cultivation of Science Jadavpur, Calcutta 32, India
(Received August 24, 1955)

SYSTEMATIC studies of different types of sodium diborate have been made by many workers. It is well known that borax is decahydrate of sodium diborate having a monoclinic crystal structure with $a=11.82\pm0.04$ A, $b=10.61\pm0.03$ A, $c=12.30\pm0.04$ A, and $\beta=106°\,35'\pm0.4$. Besides decahydrate and anhydrous sodium diborate, different hydrates of borax, such as pentahydrate, tetrahydrate, dihydrate, and monohydrate are

known. In the earlier investigations, McIntosh and Mathews (1948),[1] Menzel and Schutze (1940),[2] Cole and Taylor (1935),[3] Minder (1935),[4] and a few others contributed valuable information concerning the method of formation and crystal structure of some types of sodium diborate, both hydrous and anhydrous. In the present investigation an attempt has been made to give information concerning the phase transformation of boraxdecahydrate after different thermal treatments and along with that the structural details of some sodium diborate determined by the x-ray method.

To start with, a preliminary differential thermal analysis of decahydrate of sodium diborate is made so as to find the temperature zone where structural change or any other change occurs. The differential thermal curve showed only one exothermic peak at 50°C and three endothermic peaks at 75°C, 162°C, and 202.5°C. In keeping with that information, borax powder was dehydrated at different temperatures up to 750°C for 12 to 16 hours in an electric oven until a constant weight was obtained. All these temperature heated products were then examined by the x-ray diffraction method. The decahydrate transformed into pentohydrate above 50°C, which could be identified easily from the x-ray picture. For the samples heated up to 150°C and 200°C, it was seen that, in the x-ray diffraction patterns for those two samples, the number of powder lines decreased and the evidence of an amorphous phase was indicated by the presence of diffuse bands by the sides of the strongest powder lines. It is interesting to note that if these samples were kept for some days, and then examined by the x-ray diffraction method, the diffuse bands in the diffraction pattern disappeared and the number of lines in the pattern increased. This pattern was similar to that of pentahydrate. Thus it is likely that the transformations which were indicated by the differential thermal analysis at 162 and 202.5°C are reversible transformations. After that, even up to 320°C, the pattern did not change. But when that specimen was heated further the x-ray picture revealed the presence only of bands. The most interesting thing that was noted in the present investigation was that there was an abrupt crystallization of the amorphous phase in the temperature zone of 675°C. The chemical composition of that specimen indicated it to be anhydrous $Na_2B_4O_7$. The Bragg angle, spacings, and intensity of the powder pattern of anhydrous borax are given in Table I.

The structural detail of the foregoing products were found out by the application of the method suggested by Lipson (1948).[5] This crystalline variety of anhydrous borax was found to have an orthorhombic symmetry with the axial parameters as $a=6.468$ A, $b=8.720$ A, and $c=11.54$ A. The density of the anhydrous borax, together with the above unit cell dimension allow only 4 molecules in the unit cell. There was no systematic absence of any kind of reflections in the x-ray pattern except for $l\neq 2n$, which showed the most suitable space-group for anhydrous borax to be $p/222_1$. It is to be noted here that the x-ray pictures were taken with the help of Cu radiation.

TABLE I. Bragg angle, spacings, and intensity of the powder pattern of anhydrous $Na_2B_4O_7$.

θ	d in A	v. Int
5°4′	8.730	vw
6°46′	6.533	s
7°40′	5.772	vw
8°26′	5.250	s
9°12′	4.816	vw
10°15′	4.328	s
11°25′	3.890	s
12°52′	3.457	m
13°37′	3.271	w
14°32′	3.068	w
15°3′	2.960	w
15°52′	2.816	m
16°51′	2.658	m
17°32′	2.557	w
18°38′	2.410	mw
21°4′	2.142	m
22°15′	2.036	m
23°34′	1.926	m
24°13′	1.877	w
25°18′	1.892	w
26°32′	1.724	vw

The authors wish to express their sincerest gratitude to Professor K. Banerjee and to Dr. A. Bose for their keen interests and suggestions during the progress of the work.

[1] A. O. McIntosh and F. W. Mathews, Am. Mineralogist **33**, 747 (1948).
[2] H. Menzel and H. Schu!ze, Z. anorg. u allgem. Chem. **245**, 157 (1940).
[3] S. S. Cole and N. W. Taylor, J. Am. Ceram. Soc. **18**, 79 (1935).
[4] W. Minder, Z. Krist. **92**, 30 (1935).
[5] H. Lipson, Acta Cryst. **2**, 43 (1949).

Study of Phase Transformation of Orthoboric Acid by X-Ray Diffraction Method

D. R. DASGUPTA AND B. K. BANERJEE
Indian Association for the Cultivation of Science
Jadavpur, Calcutta 32, India
(Received August 24, 1955)

SOME aspects of physico-chemical properties of oxyacids of boron have been studied by Kracek, Morey, and Merwin (1938),[1] McCulloch (1937),[2] and a few others. The crystal structure of orthoboric acid is triclinic (Zachariasen 1954[3]) with $a=7.04$ A, $b=7.04$ A, $c=6.56$ A, and $\alpha=92°\ 30'$, $\beta=101°\ 10'$, and $\gamma=120°$. The other important oxyacid of boron is metaboric acid which is formed by the thermal dehydration of orthoboric acid at 100°C–125°C. The thermal dehydration of orthoboric acid possibly takes place in the following way:

$$4H_3BO_3 \rightarrow 4H_2O+4HBO_2$$
$$4H_3BO_3 \rightarrow 5H_2O+H_2B_4O_7$$
$$4H_3BO_3 \rightarrow 6H_2O+2B_2O_3.$$

It is worthwhile to mention it here that the existence of $H_2B_4O_7$ is very doubtful. The condition of formation of metaboric acid and boric anhydride is determined by the temperature and the duration of heat treatment. Again unlike orthoboric acid, metaboric acid is said to exist in three monotropic forms to each other. But so far no detailed x-ray study of the dehydrated products of orthoboric acid has been carried out with the exception of that by McCulloch (1937), who gives only some planar spacings of metaboric acid. In the present investigation an attempt has been made to give further information on the structural details of the dehydrated products of orthoboric acid from x-ray study of those specimens. But prior to the x-ray study, a preliminary thermal and differential thermal analysis of orthoboric acid has been made so as to obtain valuable information over the temperature ranges where structural change may occur; when orthoboric acid was heated it was seen that up to a temperature of 100°C, the loss in weight was small. The differential thermal analysis curve of orthoboric acid also showed only one exothermic peak in this temperature region. From chemical analysis also it was seen that at this temperature, orthoboric acid was changed into metaboric acid. By the application of Hesse (1948)[4] and Stosick's (1949)[5] method to the x-ray diffraction data of metaboric acid, thus found, it was seen to have a tetragonal crystal symmetry with the axial parameters as $a=b=9.865$ A and $c=7.427$ A. The axial lengths and density of metaboric acid allow only 16 molecules in the unit cell. There were no systematic absence in any order of reflecting planes, suggesting the most suitable space-group for metaboric acid as D_{4h}^1 or $P4/mmm$. It is quite evident from the x-ray analysis that the crystallographic structure of each specimen depends on the thermal history. Metaboric acid obtained by the dehydration gives rise to an x-ray diffraction pattern which is distinct from that of the orthoboric acid. Again, the x-ray pattern of the dehydrated products obtained from 140°C upwards is quite different from that of metaboric acid. It is also observed that the specimens prepared at 145°C for 15 hours give only diffuse bands. But in the case of other specimens prepared at a still higher temperature, having the same period of heating, some lines also appear in the picture as

TABLE I.

θ	Int.	d in A
7°27′	s	5.933
8°4′	w	5.100
10°6′	mw	4.388
10°49′	w	4.103
12°46′	ms	3.485
14°17′	vs	3.119
15°32′	w	2.873
10°7′	m	2.476
19°21′	m	2.324
20°26′	m	2.206
21°57′	vw	2.060
23°0′	m	1.970
24°31′	mw	1.956
25°25′	vvw	1.793
27°5′	m	1.692
29°35′	w	1.560
35°5′	vvw	1.340
41°38′	mw	1.159

well as the other bands. The spacings of bands can be satisfactorily compared with those of pure B_2O_3 glass (4.1 A (s) and 2.1 A (w) bands) and again some lines which are present along with bands in some specimens have been compared with those of metaboric acid. In the x-ray analysis, only Cu targets were used in a Hadding tube, run at a voltage of 60 kv with a tube current of 15 ma. Table I gives the x-ray data of metaboric acid.

In conclusion, the authors express their thanks to Professor K. Banerjee and Dr. A. Bose for their keen interests during the progress of work.

[1] Kracek, Morey, and Merwin, Am. J. Sci. **35A**, 143 (1938).
[2] L. McCulloch, J. Am. Chem. Soc. **59**, 2650 (1937).
[3] W. H. Zachariasen, Acta Cryst. **7**, 305 (1954).
[4] R. Hesse, Acta Cryst. **1**, 200 (1948).
[5] A. J. Stosick, Acta Cryst. **2**, 271 (1949).

Internal Rotation in Methyl-Trifluoromethyl Acetylene

DAVID R. LIDE, JR., *National Bureau of Standards, Washington, D. C.*
AND
DANIEL KIVELSON, *Research Laboratory of Electronics and Department of Physics, Massachusetts Institute of Technology, Cambridge, Massachusetts**

(Received September 6, 1955)

THE microwave spectrum of $CH_3-C\equiv C-CF_3$ has been discussed in a recent communication by Bak, Hansen, and Rastrup-Andersen.[1] Microwave absorption was found at frequencies which corresponded to the $J=6\rightarrow7$, $7\rightarrow8$, and $8\rightarrow9$ transitions in a symmetric-rotor molecule, in agreement with the expected geometric configuration. For each $J\rightarrow J+1$ transition the observed spectrum was reported to consist of six "subgroups" of absorption lines, each subgroup containing a large number of overlapping lines which extended over a region of 15 to 20 mc. This complex pattern was interpreted by Bak, Hansen, and Rastrup-Andersen as indicating that the internal rotation of the CH_3 group with respect to the CF_3 group was hindered by a finite potential barrier.

Since the presence of an appreciable potential barrier in this molecule is in conflict with the evidence of a number of related molecules,[2] as well as with general notions of internal barriers, we have attempted to find an alternative explanation for the microwave spectrum. While the vibrational spectrum of $CH_3-C\equiv C-CF_3$ is apparently unknown, there are certain to be a number of low-lying skeletal vibrational levels which are well-populated even at dry-ice temperature. Thus the rotational spectrum of molecules in these excited vibrational states should appear with reasonable intensity. We therefore propose that each of the "subgroups" found by Bak, Hansen, and Rastrup-Andersen corresponds to a particular (nontorsional) vibrational state. If the molecule were a truly rigid symmetric rotor, a single absorption line would be observed for each $J\rightarrow J+1$ transition in a given vibrational state. In a rigid symmetric rotor, motion about the molecular figure axis cannot affect the perpendicular moment of inertia which alone determines the absorption frequencies; hence this observed line would actually be a superposition of lines from molecules in which the CH_3 and CF_3 groups are in different states of motion about the figure axis. When centrifugal distortion is considered, however, the component lines corresponding to the various states of motion about the figure axis occur at slightly different frequencies. Thus even if the CH_3 and CF_3 groups are able to rotate independently, a large number of closely-spaced absorption lines is to be expected for each vibrational state. The structure of the "subgroups" in the observed spectrum could in principle be explained by these centrifugal distortion effects, regardless of the magnitude of the internal potential barrier.

If the potential barrier is assumed to be zero, the contribution of centrifugal distortion to the frequency of the $J\rightarrow J+1$ transition may be written as[3]

$$2(J+1)\left[-D_{JK}(m_1+m_2)^2+G_V\left(\frac{I_1m_2-I_2m_1}{I_1+I_2}\right)^2\right].$$

Here I_1 and I_2 are the moments of inertia of the CH_3 and CF_3 groups about the figure axis, and m_1, m_2 are the corresponding angular momenta ($m_1+m_2=K$). D_{JK} is the usual symmetric-rotor distortion constant,[4] while G_V is the distortion constant arising from internal rotation.[3] From consideration of related molecules we have estimated $D_{JK}\simeq1$ kc and $G_V\simeq15$ kc. With these values we have calculated the frequencies and intensities for the $J=6\rightarrow7$ transition. The predicted spectrum consists of over one hundred lines of significant intensity extending over a range of about 15 mc. This is in reasonable agreement with the description of the observed spectrum.

We thus feel that it is possible to explain the microwave spectrum of $CH_3-C\equiv C-CF_3$ on the basis of a zero, or very low potential barrier. We hope to refine these calculations when more detailed experimental data are available.

We are grateful to Dr. Bak for several helpful communications.

* Present address: Department of Chemistry, University of California, Los Angeles, California.

[1] Bak, Hansen, and Rastrup-Andersen, J. Chem. Phys. **21**, 1612 (1953), and private communication.
[2] G. B. Kistiakowsky and W. W. Rice, J. Chem. Phys. **8**, 618 (1940); H. S. Gutowsky, J. Chem. Phys. **17**, 128 (1949).
[3] Daniel Kivelson, J. Chem. Phys. **22**, 1733 (1954).
[4] H. H. Nielsen, Revs. Modern Phys. **23**, 90 (1951).

Infrared Spectrum of Plutonium Hexafluoride

N. J. HAWKINS, H. C. MATTRAW, AND W. W. SABOL
Knolls Atomic Power Laboratory, Schenectady, New York*

(Received August 23, 1955)

PLUTONIUM hexafluoride was prepared at KAPL by the method of A. Florin.[1] It was handled in an all metal vacuum system.

Infrared spectra were obtained from 2 to 23 μ on a standard Baird spectrophotometer equipped with NaCl and KBr prisms. The cell design[2] and the technique of heating the gas in equilibrium with condensed phase[3] have been described in earlier reports. There was no optical effect on AgCl-windows to temperatures of 65°C; however, KRS-5 windows became opaque to infrared in about eight hours when exposed to PuF_6 at 100 mm.

The intensity and relative position of the bands in the spectrum of PuF_6 are very similar to all of the other heavy metal hexafluorides; namely, MoF_6,[4,5] WF_6,[4,5] UF_6,[3-5] ReF_6,[5] and IrF_6[2]; and the molecule can readily be assigned to O_h-symmetry. The one major difference between this spectrum and that of UF_6 is the relatively weak intensity of the $\nu_2+\nu_6$ combination band which is anomalously high in only the latter hexafluoride. The weak $\nu_1+\nu_4$ in all of the other hexafluorides is calculated to be blocked by the relatively stronger $\nu_3+\nu_5$. The observed frequencies are

TABLE I. Observed infrared bands of PuF_6.

Observed frequency	Assignment	Intensity[a]	Symmetry
1242 cm^{-1}	$\nu_1+\nu_3$	M	F_{1u}
1139	$\nu_2+\nu_3$	M	$F_{1u}+F_{2u}$
828	$\nu_3+\nu_5$	W	$A_{2u}+E_u+F_{1u}+F_{2u}$
727	$\nu_2+\nu_4$	W	$F_{1u}+F_{2u}$
698	$\nu_2+\nu_6$	W	$F_{1u}+F_{2u}$
617	ν_3	VS	F_{1u}

[a] Symbols: M = medium, W = weak, VS = very strong.

given in Table I. The fundamental frequencies, except for the directly observed ν_3, were calculated from appropriate combination bands and are listed and compared with UF_6 in Table II. The ν_3 had PQR structure at low pressure.

TABLE II. Fundamental vibration frequencies.

	Species	PuF_6[a]	UF_6[b]
1	A_{1g}	625 cm^{-1}	665 cm^{-1}
2	E_g	522	536
3	F_{1u}	617	623
4	F_{1u}	205	186
5	F_{2g}	211	202
6	F_{2u}	176	136

[a] This study.
[b] KAPL–1041.

It was noted that the stretching frequencies (ν_1, ν_2, ν_3) are higher in UF_6 while the bending frequencies are higher in PuF_6. This indicates that the repulsion between the nonbonded fluorine atoms in PuF_6 is higher than in UF_6 and hence a possibly shorter internuclear distance.

The vibrational contributions to the heat capacity, entropy, and free energy were calculated (Table III) from the fundamental vibration frequencies using the harmonic oscillator approximation. With the assumption that the Pu–F distance is 1.97 A; i.e., 0.03 A less[6] than Gaunt's[5] value for the U–F distance in UF_6 one would obtain (exclusive of magnetic terms) at 298°K for Cp^0, 30.901; S^0, 88.03; and $-(F^0-E_0^0)/T$, 67.24 all in cal/deg/mole.

A study of the OVFF force constants and the possibility of a difference in the nature of the orbital following between UF_6

TABLE III. Vibrational contributions to the thermodynamic properties of PuF_6.

T°K	Cp^0	S^0	$-(F-E_0^0)/T$
	all in cal/deg/mole at 1 atmos of perfect gas		
273	22.04	20.38	8.42
298	22.95	22.35	9.51
350	24.43	26.16	11.71
400	25.48	29.50	13.72
500	26.86	35.32	17.45

and PuF_6 will be the subject of a later communication. A high-resolution infrared study is now in progress.

The infrared spectrum of PuF_6 was also obtained by H. H. Claassen, J. G. Malm, and B. Weinstock at the Argonne National Laboratory a short time after our data was obtained. The spectral observations and values of the fundamental vibration frequencies agree rather well with our results.

* Operated by the General Electric Company for the U. S. Atomic Energy Commission.

[1] A. E. Florin and co-workers, J. Inorg. Nuclear Chem. (to be published).
[2] Mattraw, Hawkins, Carpenter, and Sabol, J. Chem. Phys. **23**, 985 (1955)
[3] Hawkins, Mattraw, and Carpenter, "Infrared spectrum of UF_6 at elevated temperatures," KAPL–1041, February 1, 1954.
[4] Burke, Smith, and Nielsen, J. Chem. Phys. **20**, 447 (1952).
[5] J. Gaunt, Trans. Faraday Soc. **49**, 1122 (1953); **50**, 209 (1954).
[6] W. H. Zachariasen, Phys. Rev. **73**, 1104 (1948).

Infrared Spectra of NpF_6 and PuF_6†

JOHN G. MALM, BERNARD WEINSTOCK, AND HOWARD H. CLAASSEN*
Argonne National Laboratory, Lemont, Illinois
(Received September 15, 1955)

THE infrared spectra of the transuranium hexafluorides, NpF_6 and PuF_6, have been studied with a Perkin-Elmer Model 21 spectrophotometer from 2 to 38 microns using CaF_2, NaCl, KBr, and CsBr optics. The hexafluorides were prepared by the reaction between the tetrafluorides and fluorine at elevated temperatures; the details of the preparations and purifications will be described elsewhere. A nickel absorption cell nine cm long was used, fitted alternately with AgCl and with KRS-5 windows. No indication of interfering chemical attack on the AgCl windows was observed for PuF_6 either at room temperature or at 70°C. With KRS-5, however, a reaction with PuF_6 occurred at room temperature which increased in rate at 70°C. This was evidenced by a serious decrease in optical transmission. For NpF_6 a similar reaction occurred with the KRS-5 but at a much slower rate.

An attempt was made to obtain the Raman spectrum of PuF_6, but this failed because of difficulties associated with the absorption in the visible region and because of rapid photochemical decomposition even in light of λ5461. Preliminary experiments indicate that these difficulties are less severe with NpF_6 and work is in progress on a multiple reflection cell suitable for obtaining the Raman spectrum.

Figures 1 and 2 are tracings of the infrared spectra except that the curves in the region from 275 to 450 cm^{-1} are calculated by comparison of the transmittances of the empty and filled cell. The observed infrared spectra are very similar to that obtained for UF_6[1–3] and on this basis both NpF_6 and PuF_6 are believed to have the symmetry of a regular octahedron (point group O_h). Although only one of the six fundamentals for each molecule is observed directly in the infrared, it is possible, as Gaunt[1] showed for UF_6, to evaluate all six fundamentals from active combination bands. Because of the similarity of the present spectra to that of UF_6, the combination bands can be assigned with confidence even without Raman data.

In Table I are listed the observed infrared frequencies, their assignment, and calculated values for both compounds. The fundamental frequencies are listed in Table II; they were chosen so as to minimize the sum of the squares of the deviations between calculated and observed values in Table I. The infrared spectra are satisfactorily interpreted except for one or two very weak bands. We have no very plausible interpretation for the NpF_6

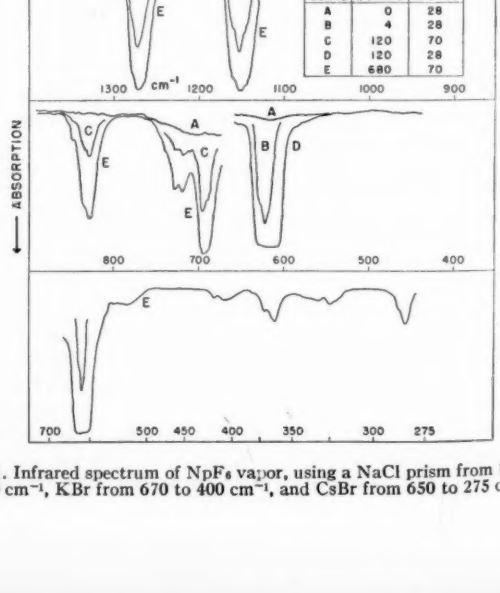

FIG. 1. Infrared spectrum of NpF_6 vapor, using a NaCl prism from 1300 to 670 cm^{-1}, KBr from 670 to 400 cm^{-1}, and CsBr from 650 to 275 cm^{-1}.

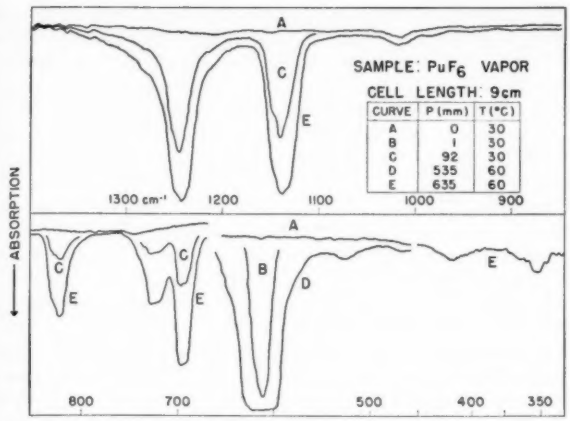

FIG. 2. Infrared spectrum of PuF_6 vapor, using a NaCl prism from 1400 to 670 cm^{-1}, KBr from 670 to 450 cm^{-1}, and CsBr from 450 to 325 cm^{-1}.

band at 284 cm^{-1}, but this band must be considered somewhat uncertain since it was observed near the transmission limit and since there was considerable absorption by the windows due to chemical attack. It may be significant that Burke, Smith, and Nielsen[2] observed a band for UF_6 at 279 cm^{-1} for which their interpretation is not plausible in the light of later work.

TABLE I. The infrared spectra.

Frequencies, cm^{-1} NpF_6 Observed	NpF_6 Calculated	PuF_6 Observed	PuF_6 Calculated	Assignment	Symmetry species
284 vw?					?
323 to 345 vvw	324	—	320	$\nu_2-\nu_6$	$F_{1u}+F_{2u}$
364 vw	364	353 w	352	$\nu_2-\nu_6$	$F_{1u}+F_{2u}$
371 vw	370	—	382	$\nu_5+\nu_6$	$A_{1u}+E_u+F_{1u}+F_{2u}$
407 vvw	406	418 vw	414	$\nu_4+\nu_5$	$A_{2u}+E_u+F_{1u}+F_{2u}$
418 vvw	418	—	404	$\nu_3-\nu_5$	$A_{2u}+E_u+F_{1u}+F_{2u}$
531 vvw	534	530 vw	531	$\nu_2+\nu_5-\nu_4$	$A_{1u}+A_{2u}+2E_u+2F_{1u}+2F_{2u}$
624 vs	—	615 vs	—	ν_3	F_{1u}
690 s 695	692	693 s 698	694	$\nu_2+\nu_6$	$F_{1u}+F_{2u}$
719 m 728	728	721 m 728	726	$\nu_2+\nu_4$	$F_{1u}+F_{2u}$
827 m	830	822 w	826	$\nu_3+\nu_5$	$A_{2u}+E_u+F_{1u}+F_{2u}$
849 vw	848	828 w	831	$\nu_1+\nu_4$	$A_{2u}+E_u+F_{1u}+F_{2u}$
1153 s	1152	1138 m	1138	$\nu_2+\nu_3$	$F_{1u}+F_{2u}$
1272 s	1272	1246 m	1243	$\nu_1+\nu_3$	F_{1u}
—	—	1279 vvw	—	?	
—	—	1346 vvw?	1349	$\nu_2+\nu_3+\nu_5$	$A_{1u}+A_{2u}+2E_u+2F_{1u}+2F_{2u}$
—	—	1656 vvw?	1661	$2\nu_2+\nu_3$	$2F_{1u}+F_{2u}$
2337 vvw?	2328	—	—	$2\nu_2+\nu_1+\nu_3$	$2F_{1u}+F_{2u}$

Nielsen's observed a band for UF_6 at 279 cm^{-1} for which their interpretation is not plausible in the light of later work.

The fundamental frequencies for PuF_6 derived by Hawkins, Mattraw, and Sabol[4] of Knolls Atomic Power Laboratory which are based on a less complete spectrum are in satisfactory agreement with the values given in Table II. Their results were made known to us while the present work was in progress.

Gas absorption spectra in the visible and near infrared at high resolution, and magnetic susceptibility measurements on the solid have also been obtained in this Laboratory for PuF_6, and are under way for NpF_6. The interpretation of these data is in progress and will permit an evaluation of the contributions of the degeneracy of the ground state and the electronic transitions to the thermodynamic functions. The values of the thermodynamic functions will therefore be included in a more complete publication, as well as a discussion of molecular potential functions.

TABLE II. Fundamental vibration frequencies.

Designation	Symmetry species	Spectral activity	Frequencies, cm^{-1} UF_6[a]	NpF_6	PuF_6
ν_1	a_{1g}	Raman, p	668	648	628
ν_2	e_g	Raman, dp	532	528	523
ν_3	f_{1u}	Infrared	626[b]	624[b]	615[b]
ν_4	f_{1u}	Infrared	189	200	203
ν_5	f_{2g}	Raman, dp	202	206	211
ν_6	f_{2u}	Inactive	144	164	171

[a] The frequencies for UF_6 are taken from reference 1.
[b] This is the only fundamental directly observed in the infrared.

† Work performed under the auspices of the U. S. Atomic Energy Commission.
* On leave from Wheaton College, Wheaton, Illinois.
[1] J. Gaunt, Trans. Faraday Soc. **49**, 1122 (1953).
[2] Burke, Smith, and Nielsen, J. Chem. Phys. **20**, 447 (1952).
[3] Bigeleisen, Mayer, Stevenson, and Turkevich, J. Chem. Phys. **16**, 442 (1948).
[4] Hawkins, Mattraw, and Sabol, J. Chem. Phys. **23**, 2191 (L) (1955).

Multiple Thio-Radicals in Sulfuric Acid Solution*

JOHN E. WERTZ AND JUANA L. VIVO†
School of Chemistry, University of Minnesota, Minneapolis, Minnesota
(Received September 13, 1955)

THE spin resonance absorption in a magnetic field due to unpaired electrons of free radicals is at present the most sensitive method of their detection. At high fields the resonance condition is given by the equation:

$$h\nu = g\mu_B H,$$

where h is Planck's constant, g is the spectroscopic splitting factor, μ_B is the Bohr magneton and ν and H are corresponding values of frequency and field for resonance. For free electrons, g has the value 2.0023, and for every organic free radical for which precise g-values have been reported, it has been within 3 parts per thousand of this value. One might therefore expect that with absorption lines commonly of the order of five gauss or more wide that one would not usually be able to resolve lines from different radicals in the same solution. To date no such multiple lines in the same solution have been reported.

The electron spin resonance absorption of radicals arising from thiophenol, diphenyldisulfide, and related compounds in sulfuric acid has been observed.[1] However, only one line was reported, though we have observed two when the samples are sealed out of contact with air. Figure 1 gives a trace of the derivative of the absorption lines for p-thiocresol, each having hyperfine structure. These hyperfine components are not as clearly shown in the absorption lines of Fig. 2. The line centers are separated by about 10 gauss. The g-values for the low- and high-field lines are respectively 2.0151 and 2.0081, based on a g-value of diphenylpicryl hydrazyl of 2.0036. For reference, we shall call these lines A and B respectively. The A line of thiophenol slowly disappears, while the B line has been observed after a month. Line B appears to be the

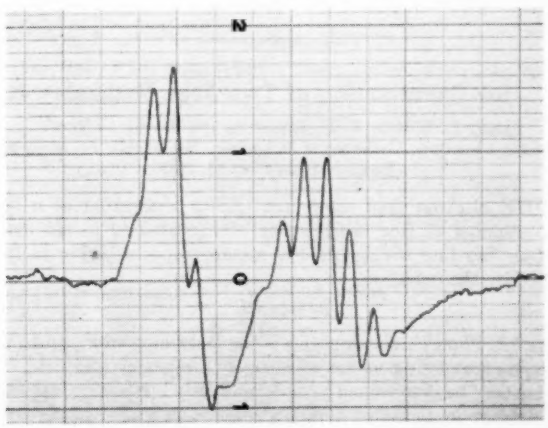

FIG. 1. Derivative curve of the electron spin resonance absorption of two free radicals formed from p-thiocresol in concentrated sulfuric acid.

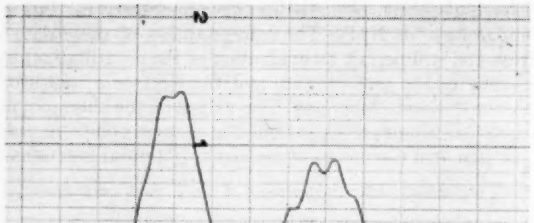

FIG. 2. The integrated absorption curve for the solution in Fig. 1.

same as one obtained from thianthrene and having a g-value of 2.0078. According to Fries and Volk,[2] thianthrene is the final oxidation product of thiophenol in H_2SO_4. Diphenyldisulfide gives two lines similar to those of thiophenol, and presumably the radicals which produce them involve at least the same oxidation state as a disulfide. Other substances giving two lines are α- and β-thionaphthol. Whereas the ratio of intensity of A and B lines early after preparation of the solutions is 0.14 for thiophenol, that of the two lines in p-thiocresol is nearly unity (0.97). The A lines in the thionaphthols are weak.

Line B for thiophenol, diphenyldisulfide, and thianthrene has five hyperfine components, suggesting that the unpaired electron is associated with a four-proton system, much as in the semiquinone radical of hydroquinone.[3] This would appear reasonable if the electron were confined to one of the thianthrene rings. The high g-value of line B would suggest less delocalization than in other organic radicals. If this is so, then the electron responsible for line A is still more localized.

Tentatively, it is suggested that the A line arises from a radical of the type $(C_6H_5S\cdot)H^+$, a proton complex of the type suggested by Mulliken,[4] but also a radical. Work is in progress to verify this assumption.

This research has been made possible by grants-in-aid from the Graduate School of the University. Thanks are due Theodore Hines for obtaining the traces of Figs. 1 and 2 and for maintaining electronic equipment.

* This research is supported in part by the United States Air Force under Contract AF18(600)–479, monitored by the Office of Scientific Research, Air Research and Development Command.

† Proctor and Gamble Fellow, 1955.

[1] Hirshon, White, and Fraenkel, J. Am. Chem. Soc. **75**, 4115 (1953).
[2] K. Fries and W. Volk, Chem. Ber. **42**, 1170 (1909).
[3] B. Venkataraman and G. K. Fraenkel, J. Chem. Phys. **23**, 588 (1955).
[4] R. S. Mulliken, J. Phys. Chem. **56**, 801 (1952).

Re-Examination of Two Free Radicals*

JOHN E. WERTZ, C. F. KOELSCH, AND JUANA L. VIVO†
School of Chemistry, University of Minnesota, Minneapolis 14, Minnesota
(Received September 13, 1955)

THE electron spin resonance (ESR) absorption of a large number of free radicals has been examined to the extent of observing line width and the spectroscopic splitting factor g defined by the equation,

$$h\nu = g\mu_B H,$$

where h is Planck's constant, μ_B is the Bohr magneton, and ν and H are corresponding values of resonant frequency and field. The g-value may be determined by independently measuring frequency and field or in terms of a radical of known g and possessing a narrow line. Diphenyl picryl hydrazyl (DPPH) is commonly used for this purpose, assuming $g=2.0036$. Of the g-values of organic free radicals which have been determined to four significant figures or more, none has been reported outside the range 2.0023 to 2.0151. The lower value corresponds to that of an entirely free electron, while the higher belongs to a thio-radical.[1] Therefore, we suspected two lower reported values, respectively 1.95 and 1.99 for the radicals pentaphenylcyclopentadienyl[2] $(C_6H_5)_5C_5$ and tri-t-butylphenoxyl[3] $(t\text{-}C_4H_9)_3C_6H_5\text{-}O\text{-}$. Their given line widths also appeared too broad.

Pentaphenyl cyclopentadienyl (PPCPD) was the first free radical in which ESR absorption was detected. It had been shown by magnetic susceptibility experiments to be completely dissociated in the solid state.[4] The published absorption line appears to have a half-width of over a hundred gauss. We have observed the line width at half-height ($\Delta H_{\frac{1}{2}}$) to be 0.96 gauss at 9000 Mc while the width between points of maximum slope ΔH_{ms} is 0.62 gauss. The saturated solution in benzene shows a ΔH_{ms} value of 2.3 gauss. For comparison, DPPH has $\Delta H_{\frac{1}{2}}=2.70$ gauss and $\Delta H_{ms}=1.99$ gauss. The ESR absorption of PPCPD was also observed at 30 Mc and 10.7 gauss. At this low field the ratio of $\Delta H_{\frac{1}{2}}$ of DPPH to PPCPD is 4.0. A similar reduction of width at low field relative to DPPH was noted for the radical BDPA.[1] Its g-factor was found to be 2.0025, identical with that of the radical α,γ-bis-diphenylene-β-phenylallyl (BDPA) recently examined by us. Surprisingly, the latter has the even narrower line width of 0.66 gauss for $\Delta H_{\frac{1}{2}}$. The g-value of PPCPD is satisfyingly close to the free-electron value, since for its molecular composition one could hardly write a structure which would allow for more delocalization of the unpaired electron.

The tri-t-butyl phenoxyl (TTBP) was reported[3] to be present as a monoradical to the extent of 85%, with no line-width data being given. With sufficient care taken in its preparation, we have found it to be wholly in the radical form. Its line width $\Delta H_{\frac{1}{2}}$ is 7.7 gauss, a not unreasonable value in view of the fact that one has only a single ring system to take part in electronic exchange which gives rise to narrowing in the solid state. We find its g-factor to be 2.0052, rather greater than the free-electron g. The related compound 2, 6 di-t-butyl-4-phenyl phenoxyl has $\Delta H_{\frac{1}{2}}=4.4$ gauss and $g=2.0043$. No previous data have been reported on this compound, or for other radicals of the $-\overset{|}{\underset{|}{C}}-O$-type. Thio-radicals usually have somewhat larger g-values.[1]

One may thus remark that no known organic free radical has a spectroscopic splitting factor differing from the free-electron value by as much as 1%.

This research was made possible by grants-in-aid from the Graduate School of the University. Thanks are due to Fred Welland who assisted with the preparation of the pentaphenylcyclopentadienyl, and to William Witsiepe for preparing the phenoxyls. Theodore Hines gave valuable electronic assistance and did the 30 Mc experiments.

* This research was supported in part by The United States Air Force under Contract Af18(600)–479, monitored by the Office of Scientific Research, Air Research and Development Command.

† Procter and Gamble Fellow, 1955.

[1] Wertz, Koelsch, and Vivo (to be published).
[2] B. M. Kozyrev and S. G. Salikhov, Doklady Akad. Nauk S. S. S. R. **58**, 1023 (1947).
[3] E. Müller, and K. Ley, Chem. Ber. **87**, 922 (1954).
[4] E. Müller and I. Müller-Rodloff, Chem. Ber. **69B**, 665 (1936).

Successive Excitation by Low-Energy Electrons: General Principle*

MILTON BURTON AND JOHN L. MAGEE
Department of Chemistry, University of Notre Dame, Notre Dame, Indiana
(Received September 8, 1955)

RECENT studies of the electric discharge reaction in methane[1] have necessitated consideration of the effects of low-energy electrons. As had been customary also in radiation chemistry

the latter had been assumed to be without significant effect. More recently, the importance of such electrons in radiation chemistry has been recognized; they have been named *sub-excitation* electrons[2] and the suggestion has been made[2-4] that they may have special effects on minor constituents with sufficiently low-lying electronic energy levels. The purpose of this communication is to indicate the low-energy electrons may generally be more important than has heretofore been presumed.

Let us consider a system in which there are free electrons of rather low average energy (e.g., 0.5–4 ev). The energy source for these electrons is external to the system and the rate of energy input is sufficiently small so that the system has a moderately low "temperature." The "temperature" is determined from the molecules, which we assume are in equilibrium in all degrees of freedom except electronic. The electrons have a higher "temperature."

We are interested in production of electronic excitation by impacts of these low-energy electrons. We assume that their energy distribution function is skewed as in glow discharges so that few electrons have energy above the most probable energy. It is then essentially impossible to excite a molecular electronic state by direct impact if its energy is appreciably above the average electron energy. Nevertheless it is possible to excite electronic states of considerably higher energy by moving a molecule up a succession of closer-spaced electronic energy steps. For such a process to be possible it is necessary for electron impacts to furnish the most rapid mechanism for change of state (i.e., radiative processes must be slower than impact excitation of the states which form the latter). We note that multiplicity selection rules of optical transitions do not apply to slow electron impacts. Radical intermediates, such as CH_2 found in methane decomposition, furnish examples of systems which have ladders of low-lying electronic states.

Consider a species A which has a ladder of electronic states A', A'', $A'''\cdots$ below a state $A^{(n)}$ which decomposes rapidly compared with all other processes in which it may be involved.

$$A^0 \rightarrow A' \rightarrow A'' \rightarrow A''' \rightarrow \cdots \rightarrow A^{(n)} \rightarrow \text{products.} \qquad (1)$$

Under constant bombardment the species A will certainly decompose, since there will always be a finite probability that the state $A^{(n)}$ will be reached in any finite time increment and then decomposition follows with certainty. An approximate treatment of the decomposition rate can be set up as a problem in random walk of the system between A^0 and $A^{(n)}$, with a reflecting barrier at A^0 and an absorbing barrier at $A^{(n)}$. It can be shown[5] that for n approximately 2–5, the number of inelastic collisions required for half-decomposition of A is likely to be ten or less.

It should be noted that the mechanism discussed here has a rate directly proportional to the electron concentration and not proportional to the square of electron concentration. It is, therefore, not to be confused with the process which has been called "cumulative ionization" in the glow-discharge literature.[6]

An important special case is energy transfer from the species $A^{(n)}$ rather than direct decomposition. By this means, a small component of a mixture can sensitize the decomposition of a species which has an excitation potential too high to be affected directly.

It is typical of the electronic levels of most species that the energy difference between levels decreases as the excitation increases. This decrease in spacing increases the ease of motion up an excitation ladder.

* Contribution from the Radiation Project of the University of Notre Dame, supported in part under U. S. Atomic Energy Commission contract AT-(11-1)-38 and Navy equipment loan contract Nonr-06900.

[1] H. Wiener and M. Burton, J. Am. Chem. Soc. **75**, 5815 (1953).
[2] R. L. Platzman, Radiation Research **2**, 1 (1955).
[3] J. Weiss, Nature **174**, 78 (1954).
[4] M. Burton, NRC, Nuclear Science Series. No. 305: "Physical and chemical aspects of basic mechanisms in radiobiology." Pp. 9–11 (1953).
[5] This calculation is discussed in detail in forthcoming publications from this laboratory.
[6] R. M. Howe, J. Appl. Phys. **24**, 881 (1953).

Successive Excitation by Low-Energy Electrons: Application to Electric Discharge in Methane*

MILTON BURTON AND JOHN L. MAGEE
Department of Chemistry, University of Notre Dame, Notre Dame, Indiana
(Received September 8, 1955)

IN explanation of high yields reported by Schoch[1] for electric-discharge-induced production of acetylene from methane and as a result of an experimental study of some of the details of the chemical mechanism, Wiener and Burton[2] suggested that energy was transferred into the methane from the electron stream via the intermediary of free methyl radicals. Detailed reconsideration now makes it apparent that the velocity of reaction on such a scheme would be far below the observed one.[3]

The purpose of the present communication is to present a purely *ad hoc* explanation of the $CH_4 \rightarrow C_2H_2$ process consistent with the Wiener-Burton results and based essentially on the use of successive excitations[4] of methylene, which it appears has a succession of low-lying electronic energy states starting below 2 ev energy. The explanation outlined here indicates the demands which must ultimately be made on any complete mechanism submitted in explanation of this typical discharge process.

Consider a model *steady-state* process in which a stream of methane passing through a dc discharge between two planar electrodes is decomposed exclusively to acetylene by the over-all process

$$CH_4 \sim\!\!\rightarrow \tfrac{1}{2}C_2H_2 + \tfrac{3}{2}H_2. \qquad (0)$$

Secondary decomposition to carbon is not considered, since it is known to be unimportant under conditions of interest.[1,2] Under such circumstances it has been found that the rate of acetylene formation follows the law[2]

$$r_7 = \kappa I^{\frac{1}{2}}(CH_4) \qquad 1$$

where I is the current and κ is a constant.

The ladder of successive excitation processes[4] is

$$CH_2^0 \sim\!\!\rightarrow CH_2^{\,i} \sim\!\!\rightarrow CH_2^{\,ii} \sim\!\!\rightarrow CH_2^{\,iii} \sim\!\!\rightarrow CH_2^{\,iv} \qquad (1)$$

with the subsequent chemical steps

$$CH_2^{\,i} + CH_3 \rightarrow C_2H_3 + H_2 \qquad (2)$$

$$C_2H_3 \rightarrow C_2H_2 + H \qquad (3)$$

$$CH_2^{\,ii} + CH_3 \rightarrow CH_2 + CH_3^* \qquad (4)$$

$$CH_3 \rightarrow CH_2 + H \qquad (5)$$

$$CH_2^{\,iii} \rightarrow CH + H \qquad (6)$$

$$CH + CH_2 \rightarrow C_2H_2 + H \qquad (7)$$

$$CH_2^{\,iv} + CH_4 \rightarrow CH_2 + CH_4^* \qquad (8)$$

$$CH_4^* \rightarrow CH_3 + H \qquad (9)$$

$$H + CH_4 \rightarrow CH_3 + H_2 \qquad (10)$$

$$R + R + M \rightarrow R_2 + M. \qquad (11)$$

Noting that in the steady state, chain initiation and termination proceed at equal rates,

$$r_8 = r_{11} = k_{11}(R)^2(M), \qquad 2$$

$$(R) = \left(\frac{r_8}{k_{11}}\right)^{\frac{1}{2}}\left(\frac{1}{(M)}\right)^{\frac{1}{2}}, \qquad 3$$

and the rate of acetylene formation is essentially equal to r_7

$$r_7 \approx \tfrac{1}{2}r_{10} = \tfrac{1}{2}k_{10}(H)(CH_4). \qquad 4$$

Taking (H) proportional to (R) and assuming

$$r_8 \propto I(CH_4) \qquad 5$$

it follows that

$$r_7 \propto I^{\frac{1}{2}}(CH_4) \qquad 6$$

if M is taken justifiably to be CH_4.

Lack of space prevents an adequate discussion of this mechanism here, but it can be shown that with this scheme the maximum

100-ev yield of CH_4 decomposed is ≈ 50; i.e., very near the thermochemical limit.[3] Assumption *5* asserts that there is a linear relationship between the number of highest excited CH_2 radicals and the current, and that the fraction of such radicals which decompose via (8) is proportional only to the methane concentration. The key to the mechanism clearly lies in this assumption. Whether it is attributable to a fundamental characteristic of the discharge or is the approximate result of compensating factors cannot be said at present.

* Contribution from the Radiation Project of the University of Notre Dame supported in part under U. S. Atomic Energy Commission contract AT(11-1)-38 and Navy equipment loan contract Nonr-06900.

[1] L. S. Daniells, Petroleum Refiner **29**, No. 9, 221 (1950); E. P. Schoch *et al.*, University of Texas Publication, No. 5011, "Acetylene from hydrocarbons" (June 1, 1950).
[2] H. Wiener and M. Burton, J. Am. Chem. Soc. **75**, 5815 (1953).
[3] H. L. Weisbecker and M. Burton, (to be published).
[4] M. Burton and J. L. Magee, J. Chem. Phys. **23**, 2192 (1955).

Examination of the Isotope Effect in the Condensation of *o*-Benzoylbenzoic Acid-Carboxyl-C^{14} to Anthraquinone-9-C^{14}

GUS A. ROPP
Chemistry Division, Oak Ridge National Laboratory, Oak Ridge, Tennessee
(Received August 15, 1955)

TWO previously reported[1] "reverse isotope effects" which we failed to verify in this laboratory[2] apparently resulted from assay errors in the original work.[1]

It seemed probable that the more recently reported[3] reverse effect in the condensation of *o*-benzoylbenzoic acid-carboxyl-C^{14} to anthraquinone-9-C^{14} might have resulted from an isotopic dilution *after* synthesis of the acid. The possible effects of such dilutions should be pointed out at once to users of isotopic tracers because errors might thereby be introduced into various types of tracer experiments.

In the reported study[3] *o*-benzylbenzoic acid-carboxyl-C^{14} (I) was oxidized to *o*-benzoylbenzoic acid-carboxyl-C^{14} (II) which was then diluted several-fold with unlabeled acid II and recrystallized from 15% ethanol. In spite of recrystallization, the diluted acid II might have retained some of the unoxidized, several-times-more radioactive acid I.

Cyclization of I,

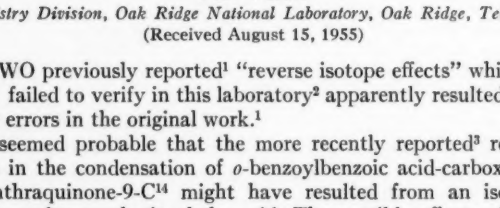

may well be more rapid[4] than cyclization of II.

TABLE I.

Compound	Representing	μc per mole[a] Run 1[b]	Run 2
Benzylbenzoic acid	Intermediate in synthesis	...	3.345±0.02
Benzoylbenzoic acid	Acid used in cyclization	6.95±0.01	3.36 ±0.01
Anthraquinone	Product from *ca* 100% reaction	6.89±0.01	3.345±0.02
Anthraquinone	Product from stated % reaction	6.76±0.01 (42%)	3.22 ±0.02 (16.5%)
Benzoylbenzoic acid	Recovered unreacted acid	7.11±0.03	3.39 ±0.01

[a] O. K. Neville, J. Am. Chem. Soc. **70**, 3501 (1948); V. F. Raaen and Gus A. Ropp, Anal. Chem. **25**, 174 (1953).
[b] Run 1 and Run 2 were entirely independent and used benzoylbenzoic acid samples prepared by separate syntheses and purified by different methods.

Hence, cyclization of II containing some several-times-more radioactive I might yield a crude product which at 12% reaction would contain more anthrone, and therefore more radioactivity per unit weight, than at 100% reaction. If recrystallization of the crude anthraquinone from alcohol failed to remove all the anthrone, then the higher percentage of anthrone remaining in the product of 12% reaction could account for the apparent "reverse isotope effect." Since the dilution ratio is not stated[3] it is not possible to estimate how much excess anthrone remaining in the 12% reaction product would correspond to the reported 7% "reverse isotope effect." A *normal* isotope effect ($k_{12}/k_{14}=1.03$ to 1.04) was indicated when we repeated the study using very pure acid II. Radiochemically pure acid I was synthesized and diluted *before* oxidation to acid II to avoid the possibility of an error resulting from isotope dilution as just described. Table I presents the experimentally measured isotope effect ratios. The observed fractionation factor may be the result of an isotope effect in the equilibrium[5] preceding the rate step:

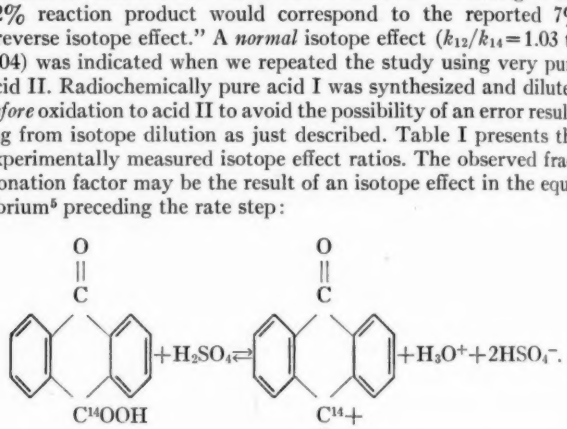

A crude calculation,[6] considering merely that there is one less carbon-14 to oxygen bond (assumed stretching frequency 850 cm^{-1}) in the charged organic structure, yields a value of K_{12}/K_{14} of about 1.035 at 80°C in reasonable agreement with our experimentally determined value. It is assumed that there is little or no isotope selectivity in the subsequent rate step which, so far as the labeled atom is concerned, involves pure bond formation. In accord with the mechanism[5] and the theory as discussed by Bigeleisen[7] and Bigeleisen and Mayer,[6] the net fractionation factor may be treated as the product of three factors arising from: (a) the isotope effect on the pre-rate equilibrium, (b) the temperature independent rate factor or "reduced mass factor," and (c) the temperature dependent rate factor of "zero point energy effect." All of these have been defined and discussed repeatedly in the literature, and it should suffice to say that for the present case of a rate process involving bond formation, factors (b) and (c) could very well have a product of about unity.

The absence of carbon isotope fractionation in other addition reactions[8] which have been reported by this laboratory may also be explainable on this basis and further studies of fractionation in addition reactions of labeled compounds are in progress.

A joint investigation with the original authors[3] is planned to study this reaction in greater detail.

[1] A. Roe and E. L. Albenesius, J. Am. Chem. Soc. **74**, 2402 (1952); Abstracts of Papers, 124th Meeting of the American Chemical Society, Chicago, Illinois, September 6–11, 1953, p. 65–0, 66–0, 67–0.
[2] Ropp, Bonner, Clark, and Raaen, J. Am. Chem. Soc. **76**, 1710 (1954).
[3] W. H. Stevens and D. A. Crowder, Can. J. Chem. **32**, 792 (1954).
[4] F. C. Whitmore, *Organic Chemistry* (D. Van Nostrand Company, Inc., New York, 1937), p. 868. The keto group should retard cyclization. In hydrogen fluoride as a condensing agent, I is cyclized but II fails to react.
[5] M. Newman, J. Am. Chem. Soc. **64**, 2324 (1942). The occurrence of the structure

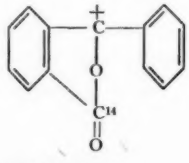

is not considered in the present argument.
[6] J. Bigeleisen and M. Mayer, J. Chem. Phys. **15**, 261 (1947).
[7] J. Bigeleisen, J. Chem. Phys. **17**, 675 (1949).
[8] Ropp, Raaen, and Weinberger, J. Am. Chem. Soc. **75**, 3694 (1953).

Quenching of Biacetyl Fluorescence in Solution

HANS L. J. BÄCKSTRÖM AND KJELL SANDROS
Laboratory of Physical Chemistry, Chalmers Institute of Technology, Gothenburg, Sweden
(Received September 9, 1955)

THE decay of biacetyl fluorescence in solution at 20°C has been studied using single flashes from a Philips stroboscope lamp as exciting light. Solutions were contained in an evacuated glass system and were carefully degassed at −78°C. Filters confined exciting light to the region 3800–5000 A. Fluorescent light was filtered to remove wavelengths below 5000 A before impinging on the photomultiplier tube. A Tektronix Type 514D oscilloscope was used to register the photomultiplier signal. Oscillograph traces were photographed and analyzed, registration beginning 50 μsec after flash initiation, when exciting intensity had dropped to <0.5% of its maximum value.

Decay curves were strictly exponential. Dilute solutions in highly purified benzene gave values of mean life (τ) varying between 1.03×10^{-3} and 0.98×10^{-3} sec. For biacetyl vapor at 25°C 1.80×10^{-3} sec has been reported[1] as against 2.25×10^{-3} sec for a rigid solution at 77°K.[2]

Self-quenching was slight and variable, indicating that it was caused by remaining traces of impurities in the biacetyl. In studying quenching by foreign substances the biacetyl concentration was kept so low that self-quenching was negligible.

Other weak quenchers studied as solvents gave for τ in μsec: Carbon tetrachloride 784, chlorobenzene 447, anisole 307, methyl benzoate 278, water 229. Stronger quenchers were studied in benzene solution. The relation between τ and quencher concentration (C) was given by the formula: $1/\tau=1/\tau_0+kC$. Table I gives observed values of k.

The long-lived fluorescence of biacetyl was ascribed by Lewis and Kasha[3] to a forbidden transition from a triplet of biradical state to the singlet ground state of the molecule. Earlier it had been pointed out by one of us[4] that a large number of photochemical reactions of carbonyl compounds can best be interpreted by assuming that the molecule on light absorption is transformed into a biradical: $R'R''C=O\rightarrow R'R''\dot{C}-\dot{O}$.[5] Due to the odd electron on oxygen this biradical will react with many substances by hydrogen abstraction, the radicals thus formed subsequently undergoing dimerization or disproportionation. Thus biacetyl reacts photochemically with ethanol[6] to give acetaldehyde and the compound

$$\begin{matrix}CH_3CH_2\\ CH_3CO.C.C.COCH_3.\\ OH\ \ OH\end{matrix}$$

The results of the quenching experiments indicate that for a large group of quenchers (alcohols, amines, phenols) the act of quenching consists in a chemical reaction between the biradical and the quencher involving abstraction of a hydrogen atom from the latter. This will account for the general parallelism between quenching power and inhibitory action in autoxidation reactions.

The remaining efficient quenchers are known to undergo additional reactions with free radicals.[7] We feel therefore that their quenching action must be connected with the biradical nature of the fluorescent state. Experiments are under way to establish whether stable compounds are formed in a photochemical reaction between biacetyl and quenchers of this type.

Values of k for the most efficient quenchers closely approach the value of 1.0×10^{10} l. mole^{-1} sec^{-1} estimated for a diffusion-controlled reaction in benzene at 20°C.[8] Values for weaker quenchers must be regarded as maximum values in cases where the presence of traces of chemically similar substances with strong quenching action may be suspected. This applies particularly to triphenylamine, naphthalene, and phenanthrene.

TABLE I. Quenching constants in l. mole^{-1} sec^{-1}.

Oxygen	4.8×10^9
Methanol	2.6×10^2
Isopropanol	2.7×10^3
Benzyl alcohol	6.9×10^3
Phenol	8.9×10^7
Resorcinol	3.5×10^8
Hydroquinone	5.3×10^9
Aniline	1.8×10^9
Diphenylamine	6.8×10^9
Triphenylamine	3.9×10^4
Perchloroethylene	3.5×10^4
Cyclohexene	$\sim1.0\times10^5$
Nitrobenzene	4.4×10^4
m-Dinitrobenzene	$\sim3.6\times10^5$
1,3,5-Trinitrobenzene	1.1×10^6
Stilbene	4.4×10^9
Naphthalene	3.8×10^8
Phenanthrene	2.3×10^8
Anthracene	8.1×10^9
Chrysene	2.4×10^8
Pyrene	7.5×10^9
Benzpyrene	8.2×10^9
1,2-Benzanthracene	3.8×10^9

[1] W. E. Kaskan and A. B. F. Duncan, J. Chem. Phys. **18**, 427 (1950).
[2] D. S. McClure, J. Chem. Phys. **17**, 905 (1949).
[3] G. N. Lewis and M. Kasha, J. Am. Chem. Soc. **67**, 994 (1945).
[4] H. L. J. Bäckström, Z. physik. Chem. **B25**, 99 (1934).
[5] This assumption will also explain the retarding effect of oxygen on the photochemical reaction of alcohols with oxygen, sensitized by benzophenone. H. L. J. Bäckström, *The Svedberg 1884–1944* (Almquist och Wiksells Boktryckeri, Uppsala, 1944), p. 45.
[6] W. D. Cohen, Chem. Weekblad **13**, 590 (1916).
[7] Key reference: M. Levy and M. Szwarc, J. Am. Chem. Soc. **77**, 1949 (1955).
[8] P. Debye, Trans. Electrochem. Soc. **82**, 265 (1942).

Note on the Absorption Spectra of the Methyl Radical

JIRO HIGUCHI
Laboratory of Physical Chemistry, Tokyo Institute of Technology, Ookayama, Meguro-ku, Tokyo, Japan
(Received September 12, 1955)

METHYL radical is one of the most elementary and important free radicals in chemistry. There have, however, been no spectroscopic data on it, and the structure is not yet determined. Recently, the electronic structures of CH[1] and NH, NH_2 and NH_3[2] were studied by the present author using the LCAO–SCF method[3] with reasonable results in spite of the approximation on the two-electron three-center integrals. The same method has been applied to lower electronic states of the methyl radical for the planar form, since the structure has generally been considered nearly planar.[4] The procedures used were similar to those for the CH radical.[1] The symmetry group of the radical was assumed as D_{3h}, and the internuclear distance between the carbon and hydrogen was taken as 1.124 A as in the CH radical.[1] The orthogonality relationship between the 1*s* orbitals of carbon and hydrogen was assumed. The one- and two-center integrals used were the same as in the case of the CH radical, but the one-electron three-center integrals were obtained from Hirschfelder-Weygandt's table[5] and by Oohata's method,[6] while the two-electron three-center integrals were approximately deduced from the above-mentioned integrals as in the case of NH_n.[2]

The LCAO–SCF calculation was carried out for the ground state $^2A_2''$ $(1a_1')^2(2a_1')^2(1e')^4(1a_2'')^1$ and the LCAO MOs and orbital energies obtained are shown in Table I. These MOs indi-

TABLE I. LCAO–SCF MOs and orbital energies.

LCAO–SCF MOs	Orbital energies (in a.u.)[c]
$(1a_1')=(a_1'c)$	...
$(2a_1')=0.63_4(a_1's)+0.34_8(a_1'h)$[a]	−0.959
$(3a_1')=1.54_7(a_1's)-1.33_8(a_1'h)$	0.252
$(1e')=0.64_8(e'p)+0.51_4(e'h)$[b]	−0.610
$(2e')=1.15_3(e'p)-1.41_7(e'h)$	0.309
$(1a_2'')=(a_2''p)$	−0.446

[a] $(a_1'h)=3^{-\frac{1}{2}}(h_1+h_2+h_3)$.
[b] $(e'h)=3^{-\frac{1}{2}}(h_1+h_2\varepsilon^{\pm 2\pi i/3}+h_3\varepsilon^{\pm 4\pi i/3})$.
[c] 1 atomic unit = 27.204 ev.

cate the large contribution from the sp^3 configuration of carbon atom, especially from the valence state $V_4(s\sigma\pi\pi')$, to the radical. The orbital energy of the $1a_2''$ MO is calculated as -12.13 ev, while the ionization potential observed is 10.1 ev,[7] and the discrepancy is mainly attributed to the difference between the calculated and the observed value for the ionization energies of the carbon atom.

Using the LCAO MOs given in Table I, the lower electronic states were calculated without *CI*. The dissociation energy of the ground state [relative to the energy of $C(^3P)+3H(^2S)$ without *CI*] was computed as 12.6 ev, which is very close to the observed value of 12.7 ev.[8] The first excited state $^2E'(1a_1')^2(2a_1')^2(1e')^3(1a_2'')^2$ was calculated to be 6.8 ev above the ground state but the $^2A_2''\rightarrow{}^2E'$ transition is forbidden. If the isoelectronic ion NH_3^+ is calculated without *CI* by using the NH_3 ground state MOs,[2] the energy of the ground state $^2A_1$ at $\angle HNH'=110°$ does not exceed that of the planar structure by more than 0.4 ev, and the energy of the first excited state ^2E at $\angle HNH'=110°$ is not lower than 0.3 ev as compared with that of the planar structure. Referring to this fact together with the results of the previous work,[4] it is evident that the methyl radical has an equilibrium bond angle of 110°∼120° and so the first absorption will be extremely weak and shorter than 2100 A. The second excited state $^2A_1'(1a_1')^2(2a_1')^2(1e')^4(3a_1')^1$ is calculated to be 10.5 ev above the ground state. The transition $^2A_2''\rightarrow{}^2A_1'$ is allowed but the energy is very high and is almost the same as the ionization energy of the radical. Consequently, the effect of the 3*s* orbital of carbon cannot be disregarded and the result is not conclusive.

In conclusion, the absorption spectra of the free methyl radical will be very difficult to be observed, because of the nearly forbidden transition to the first excited state and of the high location of the second excited state, although the concentration of the radical obtained is considerable.

The author wishes to thank Professor S. Shida for his continued interest in this work.

[1] J. Higuichi, J. Chem. Phys. **22**, 1339 (1954).
[2] J. Higuichi, J. Chem. Phys. (to be published).
[3] C. C. J. Roothaan, Revs. Modern Phys. **23**, 69 (1951).
[4] A. D. Walsh, J. Chem. Soc. 2296 (1953); Itoh, Ohno, and Kotani, J. Phys. Soc. Japan **8**, 41 (1953).
[5] J. O. Hirschfelder and C. N. Weygandt, J. Chem. Phys. **6**, 806 (1938).
[6] K. Oohata, Busseiron Kenkyu **50**, 38 (1952).
[7] J. D. Waldron, Trans. Faraday Soc. **50**, 97 (1954).
[8] K. J. Laidler and E. J. Cassey, J. Chem. Phys. **17**, 1087 (1949).

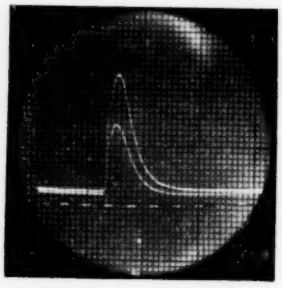

FIG. 1.

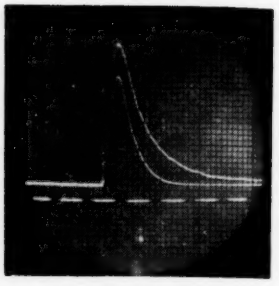

FIG. 2.

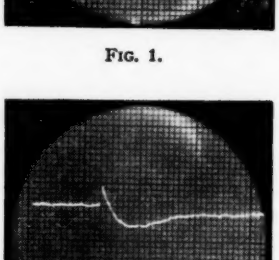

FIG. 3.

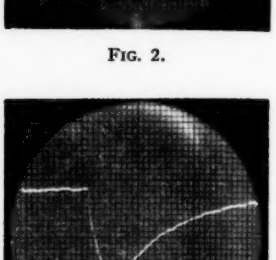

FIG. 4.

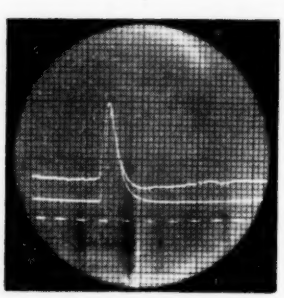

FIG. 5.

FIGS. 1–5. Changes in transmission through chlorophyll-B solutions at various wavelengths following flash illumination. Solvent: deoxygenated 95% methanol. Upper sweep: flash plus measuring light. Middle sweep: flash alone (base line, including scattered and any fluorescent light). Lower sweep: 10 000 cycle timing marker. Vertical distance between initial (flat) portions of upper and middle sweeps represents transmission of solutions before flash. Wavelengths and concentrations: (1) 655 mμ (red peak), 1.2×10^{-5} M; (2) 470 mμ (blue peak), 5.0×10^{-6} M; (3) 700 mμ, 1.2×10^{-5} M; (4) 525 mμ, 1.2×10^{-5} M; (5) 405 mμ, 7.9×10^{-6} M.

Reversible Flash Bleaching of Chlorophyll*

EDWIN W. ABRAHAMSON AND HENRY LINSCHITZ
Department of Chemistry, Syracuse University, Syracuse, New York
(Received September 12, 1955)

RECENT experiments on spectral changes of chlorophyll solutions either under steady-state illumination in rigid solvents[1] or following flash illumination,[2–4] have given direct evidence for a long-postulated metastable state.[5] In this note we wish to confirm and extend the flash illumination studies of Livingston *et al.*, and to demonstrate, by the flash technique, the existence in the metastable state of a far red absorption band previously observed in the steady-state bleaching studies.

The flash apparatus was as follows. A collimated beam of light was passed through a shutter, a 50-mm absorption cell containing the degassed, sealed-off chlorophyll solution, thence through a monochromator, and finally onto a photomultiplier tube connected to an oscilloscope. The absorption cell was mounted inside a helical xenon-filled flash tube operated at 200 joules. A suitable pulsing circuit first triggered the oscilloscope sweep and then fired the flash tube. Scattered and fluorescent light entering the monochromator were minimized by a system of baffles, and by placing the monochromator entrance slit some distance from the flash unit. In recording data, flashes and sweeps were taken with the shutter in the measuring beam first open and then closed. Any changes in the vertical distance between the two traces thus represent true changes in transmission. A third timing sweep was then added.

Typical results on chlorophyll-B in 95% methanol are shown in Figs. 1–5. Reversible bleaching of chlorophyll-B at the main absorption peaks (655 mμ and 470 mμ) is evident. By careful solvent purification irreversibility could be kept below 5%. New absorption bands appear in the far red (∼700 mμ), in the green (∼525 mμ), and in the violet (∼405 mμ). The precise location of these peaks is uncertain, particularly in the far red and violet where cell sensitivity and light are limiting. The strong transient absorption in the green and the order of magnitude of the lifetime check previous observations[2–4] but the 700 mμ band has hitherto been reported only in the low temperature steady-state cross-illumination studies.[1]

Similar experiments on chlorophyll-A show the same general features of the new absorption spectrum (far red and green bands). Measurements beyond the Soret peaks could not be taken on *A*, due to insufficient light.

These data, obtained with improved signal-to-noise ratio, are not in disagreement with the indications of Livingston and Ryan[2] that more than one transient product is formed following the flash, since lifetimes for decay and recovery measured at different wavelengths (525 and 470 mμ, for example) do not agree. However, considerably shorter duration flashes are necessary to obtain reliable kinetics. Such work is now in progress.

Flash bleaching of chlorophyll-B was also studied in wet and

dry hydrocarbon solvents (methylcyclohexane) and the preliminary results in the exhaustively dried solvent are noteworthy. Confirming earlier findings, the fluorescence of chlorophyll in dry hydrocarbon was very low[6] and the "dry" absorption spectrum showed a new band at 665 mμ.[7] After flashing, the rate of return of the "dry band" corresponded closely to the decay of the transient green band. It would appear that only one metastable intermediate is formed under these conditions.

Since extensive conversion under flash illumination occurs in both polar and nonpolar solvents,[3] one may conclude that at least one intermediate is formed by an intramolecular process, rather than by a reaction in which the solvent participates.[1,5] This transition may involve triplet-state formation, internal rearrangement, or both. In any event these studies obviate previous difficulties in understanding, on the basis of reasonable interpretations of the metastable state, the presumed disappearance of absorption in the red.

* This work is supported by a grant from the U. S. Atomic Energy Commission, Contract No. AT(30-1)-820.
[1] H. Linchitz and J. Rennert, Nature **169**, 193 (1952).
[2] R. Livingston and V. A. Ryan, J. Am. Chem. Soc. **75**, 2176 (1953).
[3] Livingston, Porter, and Windsor, Nature **173**, 485 (1954).
[4] R. Livingston, J. Am. Chem. Soc. **77**, 2179 (1955).
[5] E. Rabinowitch, *Photosynthesis* (Interscience Publishers, Inc., New York, 1945), Vol. I, Chap. 18.
[6] Livingston, Watson, and McArdle, J. Am. Chem. Soc. **71**, 1542 (1949).
[7] S. Freed and K. Sancier, J. Am. Chem. Soc. **76**, 198 (1954).

Homogeneity Condition in Thermodynamics

HENRY A. BENT*
Department of Chemistry, University of Connecticut, Storrs, Connecticut
(Received August 29, 1955)

A LARGE part of thermodynamics rests on the fact the energy of a stable system is a homogeneous function[1] of its entropy, volume, and mass numbers:

$$E(\lambda S,\lambda V,\lambda n_1,\cdots,\lambda n_c)=\lambda E(S,V,n_1,\cdots,n_c). \tag{1}$$

This relation follows directly from the additivity of E, S, V, and n_i, and the equilibrium condition $\delta E_{S,V,n_i}\geqq 0$.

Proof.—For simplicity, consider a one-component system. It is stable when E is small as S, V, and n allow. Change these, and presumably the minimum value of E will change; i.e., for stable states E is a function of S, V, and n: $E=E(S,V,n)$.

Now consider the system in two parts, a and b. Part a is stable when E^a is small as S^a, V^a, and n^a permit. The minimum value for E^a can be calculated from the formula $E^a=E(S^a,V^a,n^a)$; and likewise for part b: $E^b=E(S^b,V^b,n^b)$ when part b is stable. Observe, however, that E^{ab}, the total energy, cannot be calculated from the formula $E^{ab}=E(S^{ab},V^{ab},n^{ab})$ unless system is stable. But when

$$\begin{aligned} T^a\equiv\partial E^a/\partial S^a &= \quad T^b\equiv\partial E^b/\partial S^b,\\ -P^a\equiv\partial E^a/\partial V^a &= -P^b\equiv\partial E^b/\partial V^b, \end{aligned} \tag{2}$$

and

$$\mu^a\equiv\partial E^a/\partial n^a = \quad \mu^b\equiv\partial E^b/\partial n^b,$$

E^{ab} is small as S^{ab}, V^{ab}, and n^{ab} permit[2]; and hence ($X^{ab}=X^a+X^b$, $X=E$, S, V, or n)

$$E(S^a+S^b,\ V^a+V^b,\ n^a+n^b)=E(S^a,V^a,n^a)+E(S^b,V^b,n^b), \tag{3}$$

reminiscent of relation (1).[2]

We state these results as a theorem. Given that

$$f(X_1^a+X_1^b,\ X_2^a+X_2^b,\ X_3^a+X_3^b) = f(X_1^a,X_2^a,X_3^a)+f(X_1^b,X_2^b,X_3^b) \tag{3'}$$

whenever

$$f_i(X_1^a,X_2^a,X_3^a)=f_i(X_1^b,X_2^b,X_3^b),\quad i=1,2,3; \tag{2'}$$

then

$$f(\lambda X_1,\lambda X_2,\lambda X_3)=\lambda f(X_1,X_2,X_3), \tag{1'}$$

λ any positive rational number.

Proof.—Condition (2′) is satisfied by $X_i^a=X_i^b=X_i$.[3] Hence, (3′), $f(2X_i)=2f(X_i)$. Differentiating, $f_i(2X_i)=f_i(X_i)$; i.e., $X_i^a=2X_i^b=2X_i$ also satisfies condition (2′), giving in (3′) $f(3X_i)=f(2X_i)+f(X_i)=3f(X_i)$, etc. For fractional values, set $X_i^a=2X_i^b=X_i$, etc.

Alternatively, we could start with the fact the f_i are uniform at equilibrium ($f_i=$constant, N_i), regardless of how the subdivision is conceived. It follows from this that the derivatives are homogeneous to the zeroth degree; which implies, when $f(0)=0$, that $f(\lambda X_i)=\lambda f(X_i)$.

For suppose a and b are parts of a stable system. If $f_i(X_i^a)=N_i$, then also $f_i(X_i^b)=N_i$; moreover, $f_i(X_i^a+X_i^b)=N_i$ too. Putting $X_i^a=X_i^b$, etc., we find, very much as before, that $f_i(\lambda X_i)=f_i(X_i)$, so that $df(\lambda X_i)=\Sigma f_i(\lambda X_i)d(\lambda X_i)=\lambda\Sigma f_i(X_i)dX_i=\lambda df(X_i)$, giving on integration $f(\lambda X_i)=\lambda f(X_i)+C(\lambda)$. Setting $\lambda=0$, then differentiating with respect to λ and setting $X_i=0$, we find that $C(0)=f(0)$, and that $C'(\lambda)=-f(0)$; i.e., C is a constant, equal to zero, if $f(0)=0$; and hence $f(\lambda X_i)=\lambda f(X_i)$.

Proofs in the literature of this relation[4–6] assume properties of T, P, and u_i that seemingly can be derived only from the homogeneity condition itself, or its equivalent. The following argument is perhaps less circular.

Consider, as in the literature, a stable system, part by part. Then

$$\begin{aligned} f(X_i)&=\sum_j \Delta f^j && \text{(additivity of } f\text{)}\\ &=\sum_j\sum_i f_i^j(\Delta X_i^j)\cdot\Delta X_i^j && \text{(calculus applied to each little part, assuming } f(0)=0\text{)}\\ &=\sum_i\{f_i(X_i)\cdot\sum_j \Delta X_i^j\} && \text{(uniformity condition on } f_i\text{)}\\ &=\sum_i f_i(X_i)\cdot X_i && \text{(additivity of } X_i\text{)}, \end{aligned}$$

which implies that $f(\lambda X_i)=\lambda f(X_i)$.[1]

* Present address: Department of Chemistry, University of Minnesota, Minneapolis 14, Minnesota.
[1] D. V. Widder, *Advanced Calculus* (Prentice-Hall, Inc., New York, 1947), p. 15.
[2] J. Willard Gibbs, *Thermodynamics* (Yale University Press, New Haven, 1948), Vol. 1, p. 65.
[3] If X_i is allowed the value 0, then $f(0,0,0)$ must vanish (Eq. 3′), corresponding to $E=0$ when $S=V=n=0$.
[4] Gibbs, see reference 2, p. 77.
[5] G. N. Lewis and M. Randall, *Thermodynamics* (McGraw-Hill Book Company, Inc., New York, 1923), p. 42.
[6] E. A. Guggenheim, *Thermodynamics* (Interscience Publishers, Inc., New York, 1949), p. 23.

Entropy Requirements of the Hammett Relationship

JOHN E. LEFFLER
Department of Chemistry, Florida State University, Tallahassee, Florida
(Received September 1, 1955)

THE Hammett equation relating reaction rate constants to structural parameters is essentially a linear free energy relationship. It can be written in the form

$$\Delta\Delta F^{\ddagger}=\rho\Delta\Delta F_s, \tag{1}$$

in which $\Delta\Delta F^{\ddagger}$ is the effect of a certain substituent on the free energy of activation, $\Delta\Delta F_s$ is the effect of that same substituent in an arbitrarily chosen standard reaction, and ρ is a constant characteristic of the reaction being correlated.

The existence of a Hammett relationship for a reaction implies a constraint on the variation of the entropy of activation, but the entropy of activation need not, as has sometimes been assumed, be constant, but may be (a) constant or nearly constant, or (b) variable but linearly related to the activation enthalpy.[1] It is also possible for a reaction to give a Hammett relationship by coincidence, both the enthalpy and entropy being random variables. Such coincidences will be rare, especially when more than three structural variations are correlated. Furthermore, the coincidence

will then hold only at one temperature, giving place to a scatter diagram as the temperature is changed.

If the existence of a Hammett relationship at a given temperature is assumed, it is possible to derive the constraint on the entropy necessary to make the relationship hold at another temperature. In Eq. (1) $\Delta\Delta F_s$ is independent of temperature because the temperature of the standard reaction is specified. But ρ and $\Delta\Delta F^{\ddagger}$ are not always independent of the temperature.

$$\Delta\Delta F_1^{\ddagger}=\Delta\Delta H^{\ddagger}-T_1\Delta\Delta S^{\ddagger} \quad (2)$$

$$\Delta\Delta F_2^{\ddagger}=\Delta\Delta H^{\ddagger}-T_2\Delta\Delta S^{\ddagger} \quad (3)$$

$$\Delta\Delta F_1^{\ddagger}-\Delta\Delta F_2^{\ddagger}=(T_2-T_1)\Delta\Delta S^{\ddagger}. \quad (4)$$

From Eqs. (1) and (4),

$$\Delta\Delta S^{\ddagger}=\frac{\rho_1-\rho_2}{T_2-T_1}\Delta\Delta F_s\equiv\lambda\Delta\Delta F_s. \quad (5)$$

If $\lambda=0$, $\Delta S^{\ddagger}$ is constant and we have case (a). If λ is not zero, combination of Eqs. (1) and (5) gives

$$\Delta\Delta H^{\ddagger}=\left(\frac{\rho_1+\lambda T_1}{\lambda}\right)\Delta\Delta S^{\ddagger}. \quad (6)$$

Hence $\Delta H^{\ddagger}$ is a linear function of $\Delta S^{\ddagger}$ (case b).

When $\Delta S^{\ddagger}$ is constant, the Hammett relationship will not only hold at different temperatures but with the same value of ρ, as can be seen from Eq. (5).

[1] H. H. Jaffé, Chem. Revs. **53**, 191 (1953).

Metastable Ions in Mass Spectra

H. M. ROSENSTOCK, *Oak Ridge National Laboratory, Oak Ridge, Tennessee*
AND
A. L. WAHRHAFTIG AND H. EYRING, *Department of Chemistry, University of Utah, Salt Lake City, Utah*
(Received August 22, 1955)

THE term "metastable ions" in mass spectra denotes those ions which in the conventional Nier type mass spectrometer are detected as small diffuse peaks often occurring at nonintegral values of m/e. These peaks arise from ions which decompose spontaneously after electrostatic acceleration but before entering the magnetic field.[1-4] Hipple[2] and, more recently, Donnally and Carr[5] measured half-lives of such ions, both reporting values of about 2×10^{-6} sec. These authors pointed out that the measured lifetimes were determined essentially by the ion optics of the mass spectrometer.

The general theory of mass spectra previously presented[6] leads quite naturally to the concept of several classes of parent ions formed by electron impact: ions with excitation energy insufficient to decompose in appreciable number before collection, ions with enough energy to decompose essentially before leaving the ionization chamber and, lastly, ions which have a rather small intermediate range of energy such that they decompose primarily in transit. Those of this last group which decompose in the correct region appear as "metastable ions" and the remainder are either lost or contribute to the mass spectrometer background. One would predict, then, that with suitable ion optics metastable transitions could be detected, having a continuous range of half-lives from perhaps 10^{-12} sec to an upper limit determined only by instrumental problems. Further, any discussion in terms of isolated sets of electronic states is precluded by the high probability of radiationless transitions among the many closely spaced electronic states of a large molecule-ion.

As the intervals of time during which an ion is in the ionizing region or in the region giving rise to metastables are of the same order of magnitude, ion decomposition leading to daughter ions collected both as such and as metastable ions should be detected at the same electron voltage, *if one operates at constant mass spectrometer sensitivity*. However, since at high electron voltage the daughter peak is the larger by several orders of magnitude, the conventional manner of determining appearance potentials will result in a much lower sensitivity being used for the daughter ion.[7,8] We can estimate from reaction rates previously calculated[6,9] that this would result in an increase of several tenths of a volt in the observed appearance potential. These conclusions are consistent with the experimental observations of Fox and Langer.[7]

In terms of the theory presented, of the several possible reaction paths for an ion only the lowest energy path, and perhaps those paths with activation energy not over a few tenths of a volt higher than the lowest, will give observable metastable product ions. Ions with excitation energy necessary to yield metastable ions over higher energy paths will be removed by the lower energy competing processes. Since low activation energy also favors the formation of normal daughter ions, metastable ion transitions in general will correspond to reactions having high probability in the parent ion decomposition scheme. However, as any given reaction rate depends both upon an energy and a frequency term, it is possible with the distribution in parent ion excitation energies obtained at usual electron energies for a higher energy reaction to be favored by the frequency term and so predominate. Thus, no simple relation can be given between metastable ion peak intensity and the intensities of the corresponding initial and daughter ion peaks.

This work was supported in part by the U. S. Atomic Energy Commission.

[1] J. A. Hipple, J. Phys. & Colloid Chem. **52**, 456 (1948).
[2] J. A. Hipple, Phys. Rev. **71**, 594 (1947).
[3] J. A. Hipple and E. U. Condon, Phys. Rev. **68**, 54 (1945).
[4] Bloom, Mohler, Wise, and Wells, J. Research Natl. Bur. Standards **43**, 65 (1949).
[5] B. L. Donnally and H. E. Carr, Phys. Rev. **93**, 111 (1954).
[6] Rosenstock, Wallenstein, Wahrhaftig, and Eyring, Proc. Natl. Acad. Sci. **38**, 667 (1952).
[7] R. E. Fox and A. Langer, J. Chem. Phys. **18**, 460 (1950).
[8] D. P. Stevenson, Discussions Faraday Soc. **10**, 35 (1951).
[9] H. M. Rosenstock, Ph.D. thesis, University of Utah (1952).

Expansion of Electronic Wave Functions of Molecules in Terms of "United-Atom" Wave Functions

TIEN CHI CHEN*
Department of Physics, Duke University, Durham, North Carolina
(Received August 31, 1955)

THE united-atom concept has often been used qualitatively in discussions of electronic energy levels and spectra, particularly of diatomic molecules. Morse and Stueckelberg[1] and recently Matsen[2] have calculated energy levels of H_2^+ by the united-atom treatment. Brown and Matsen[3] have suggested using united-atom orbitals as bond orbitals in conjugated systems. An attempt is being made here to expand electronic wave functions of polyelectronic molecules in terms of generalized "united-atom" wave functions in systematic energy level calculations.

Introducing "central" potentials $\phi_i=\phi(r_{ic})$ which are functions of distances from a fixed center, we can rewrite the molecular Hamiltonian ($H\Psi=E\Psi$) in two ways, differing in the location of electron repulsion terms:

$$H=H^0+H'=H^{00}+H'',$$
$$H^0=\Sigma(-\tfrac{1}{2}\nabla_i^2+\phi_i)+\Sigma'1/2r_{ij},$$
$$H'=\Sigma(-\phi_i-\Sigma Z_\alpha/r_{i\alpha})=\Sigma h_i',$$
$$H^{00}=H^0-\Sigma'1/2r_{ij},\quad H''=H'+\Sigma'1/2r_{ij}.$$

Solutions of the "unperturbed" problems

$$H^0\Psi^0=E^0\Psi^0,\quad H^{00}\Psi^{00}=E^{00}\Psi^{00}$$

must form normalizable orthogonal sets, and the true solution Ψ can be expanded in terms of either, and, in principle, can be as accurate as we like. Consideration of labor, however, will limit the expansion to a few terms only, and also the application to simple or highly symmetrical molecules.

In general the ϕ_i's may or may not be the united-atom potentials. Their choice is dictated by the rapidity of convergence and the ease of the ensuing calculation. The most convenient choices are Coulomb and Hooke's law potentials; the corresponding Ψ^{00}'s are then, respectively, hydrogenic and Hermite functions.

In the expansion in terms of Ψ^{00}'s, there exist in the secular determinant only three types of integrals: kinetic energy, nuclear attraction, and one-center electron repulsion integrals. Their evaluation (at least for hydrogenic or Hermite functions) is relatively uncomplicated. Problems of polycentric integrals naturally do not arise.

The alternate expansion, in terms of Ψ^0, is superior in several respects. For well-chosen Coulomb potentials the E⁰'s are just atomic (or ionic) term values where the electron repulsions are already minimized. Excellent tables[4] are available, enabling detailed calculations in restricted cases, including that in which the ϕ_i's are the true united-atom potentials. This semiempirical method is expected to converge faster than the corresponding *ab initio* calculation with the same ϕ_i's.[5] The true Ψ^0's are, of course, unknown, but adequate approximations can be had in terms of, for example, Hartree-Fock, Morse-Young-Haurwitz[6] and even nodeless Slater orbitals. Only one type of integral, the nuclear attraction integrals, needs to be evaluated here. An added feature is that, since the electron repulsion terms are already incorporated in H^0, it is unnecessary to write antisymmetric determinantal wave functions, i.e., products of orbitals obeying naively the exclusion principle will do.

The choice of ϕ_i, however, is limited in the semiempirical method because of existent data. For instance, the best choice for H_2 is not the united-atom (He) potential, but that of the H^- ion; yet of the latter we have little knowledge beyond the ground state. The semiempirical method is most fruitful for problems of electronic spectra, where the absolute location of the ground state is unimportant. Otherwise, a more extensive table of ionization potentials would be required than is available.

Nuclear attraction integrals up to $(a|3d\delta 3d\delta)$ are being evaluated with Slater orbitals of nonidentical exponents for 31 nuclear separations to 8 digit accuracy. The results will soon be published with applications.[7]

The writer wishes to thank Professor Hertha Sponer for her interest and encouragement.

* Supported by Duke University Research Council.

[1] P. M. Morse and E. C. G. Stueckelberg, Phys. Rev. **33**, 932 (1929).
[2] F. A. Matsen, J. Chem. Phys. **21**, 928 (1953).
[3] R. D. Brown and F. A. Matsen, J. Chem. Phys. **21**, 1298 (1953).
[4] *Atomic Energy Levels* compiled by Mrs. C. Moore (National Bureau of Standards, Washington, D. C.), two volumes in print.
[5] This is analogous to the method of "atoms in molecules" of W. Moffitt [Proc. Roy. Soc. (London) **A210**, 245 (1951)] but used in a different context.
[6] Morse, Young, and Haurwitz, Phys. Rev. **48**, 948 (1935).
[7] After the completion of the first draft of the present note, the writer learned that Dr. R. K. Nesbet has programmed the MIT Whirlwind computer to evaluate all free atom one-center integrals involving Slater orbitals, and Dr. L. C. Allen and Dr. R. K. Nesbet together have independently developed an *ab initio* one-center method which is, however, different in emphasis from ours. See Quarterly Progress Report, Solid-State and Molecular Theory Group, MIT. July 15, 1955, pp. 27–29. The writer is indebted to Dr. Robert K. Nesbet for advance information.

Concentration Dependence of Solvent Shift in the C—H (and C—D) Stretching Frequencies of Chloroform and Pentachloroethane

RICHARD B. BERNSTEIN AND MILTON TAMRES
Department of Chemistry, University of Michigan, Ann Arbor, Michigan
(Received September 12, 1955)

STRONG interaction of chloroform (and chloroform-*d*) with oxygenated solvents, e.g., ether and acetone, and basic solvents, e.g., pyridine and triethylamine, are known[1,2] to give rise to large changes in the intensity of the C—H (and C—D) stretching band in the infrared. In some cases a new band, attributed to the hydrogen-bonded species, appears at a slightly lower frequency with an increased half-width and intensity.

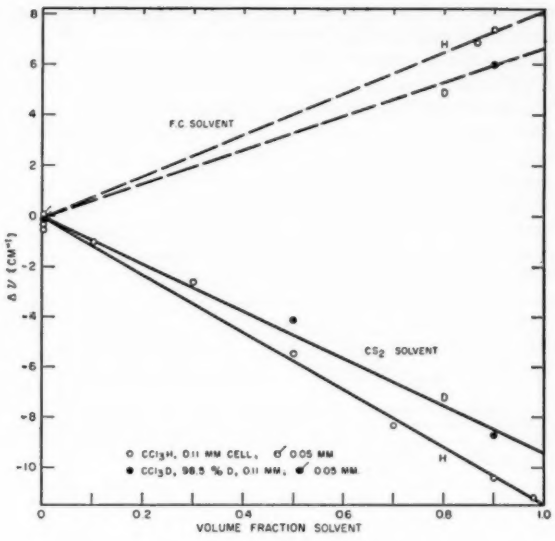

FIG. 1.

Small negative shifts in the C—H frequency are commonly noted even with "inert" solvents such as CS_2 and CCl_4 [where ΔH(soln) is small and positive]. Reported here is the dependence of the frequency shift upon concentration and type of solvent for CCl_3H, CCl_3D, C_2Cl_5H, and C_2Cl_5D.

Figure 1 shows the shift, $\Delta\nu$ (cm^{-1}), as a function of the volume fraction of *solvent* for solutions of chloroform and chloroform-*d* in carbon disulfide and in a fluorochemical (type 0–75 of Minnesota Mining and Manufacturing Company[3]). Figure 2 shows similar plots for pentachloroethane and pentachloroethane-*d* in the same solvents. The data were obtained using a Perkin-Elmer Model 21 Infrared Spectrophotometer with a CaF_2 prism. Positions of the absorption maxima were reproducible to ± 1 cm^{-1} in the 3000 cm^{-1} (C—H) region and somewhat better near 2250 cm^{-1} (C—D).

The shift in the C—H (and C—D) frequency in CS_2 appears to vary linearly with concentration. The low solubility of the compounds in the fluorochemical limited the range of concentration that could be investigated. Similar observations on these solute molecules and on trichloroethylene in CS_2 and in CCl_4 were made using a NaCl prism, but with lower precision. The shifts for trichloroethylene appear to be smaller than those for the other two

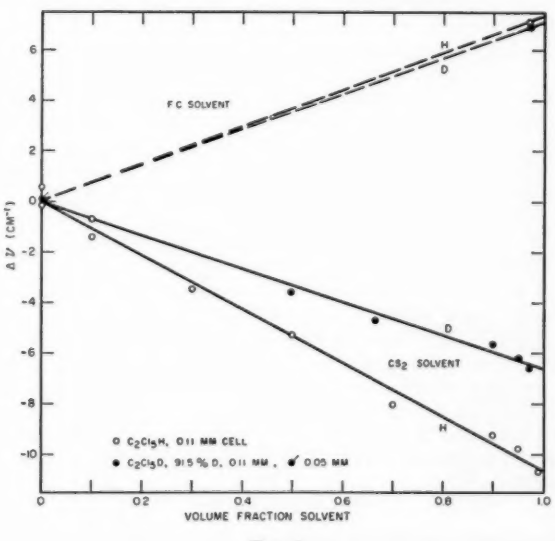

FIG. 2.

compounds, and the frequency shifts for all three compounds in CCl_4 are very slightly negative (*ca* 2 cm^{-1}).

The half-widths of the C−H band in CCl_3H and the C−D band in CCl_3D were 18±1 cm^{-1} and 10±1 cm^{-1}, respectively (in agreement with reference 1), and showed no apparent variation with concentration of CS_2. In the case of C_2Cl_5H and C_2Cl_5D the average values of the half-widths were 22 cm^{-1} and 12 cm^{-1}, respectively, although some variation with concentration was observed (decreased width with increased CS_2 concentration).

Further studies of spectral shifts, integrated intensities, and heats of mixing for these systems are in progress.

The authors acknowledge the assistance of J. C. Angus and T. J. Houser; the cooperation of Dr. G. B. B. M. Sutherland and Dr. D. L. Wood with regard to the use of the CaF_2 prism; and the financial support of the U. S. Atomic Energy Commission, and the H. H. Rackham Fund of the University of Michigan.

[1] Lord, Nolin, and Stidham, J. Am. Chem. Soc. **77**, 1365 (1955).
[2] C. M. Huggins and G. C. Pimentel, J. Chem. Phys. **23**, 896 (1955).
[3] Stated to be a completely fluorinated cyclic ether with the empirical formula $C_8F_{16}O$.

Fluorescence and Average Lifetime of Excited OH($^2\Sigma^+$) in Flames*

H. P. Broida and Tucker Carrington†
National Bureau of Standards, Washington 25, D. C.
Received August 19, 1955

SPECTROSCOPIC studies show a nonequilibrium population of rotational levels of $^2\Sigma^+$ OH molecules in certain flames[1] and discharges.[2] Such results have been assumed to indicate a persistence of the initial rotational distribution produced in the process in which the electronically excited OH molecules are originally formed. It has been implicitly assumed that the OH remains in the excited state for the normal radiative lifetime of the electronic transition, 6×10^{-7} sec,[3] undergoing at atmospheric pressure about 1000 collisions before radiating. Persistence of rotation through so many collisions is surprising. If a radiationless transition, such as quenching by collisions, is important in removing excited OH molecules, the average lifetime of the state is decreased, and hence the molecules whose emission is observed will have undergone fewer collisions before radiating. This would make observed nonequilibrium distributions of rotational states less significant in implying long relaxation times, and more significant in terms of initial distributions. This letter reports measurement of fluorescence of OH in an atmospheric-pressure flame. Interpreting the result on the basis of quenching collisions indicates that the electronic energy of OH in the flame is removed by each collision.

The experimental arrangement is shown in Fig. 1. Most of the work was done in the outer cone of an oxy-acetylene flame burning on a commercial welding torch of port diameter 3.5 mm. Typical flow rates (cc/sec) were argon 15, oxygen 3.1, acetylene 1.5. In this flame, just above the inner cone, absorption of the strong $Q_1 7$ and $Q_2 2,3$ lines of the 0,0 band is about 25%. An $f/10$ grating-monochromator with photoelectric detection[4] was used with a slit width giving a resolution of 0.25 A.

The measured fluorescence was about one part in 10^7 of the light incident on the flame. The fluorescence signal-to-noise ratio was 5. Scattering of light from the discharge into the monochromator and thermal emission from the flame were signals of the order of magnitude of the fluorescence. The possibility that the observed fluorescence is scattering from the flame was ruled out by the fact that no signal was found when the flame was illuminated with the 3131 A doublet of mercury.

To calculate the importance of quenching, the ratio of the observed fluorescence, I, to that in the absence of quenching, I_0, is needed,

$$I/I_0=A/(A+Z),$$

where Z is the number of quenching collisions suffered per sec by one OH molecule, and A is the electronic transition probability for the free molecule. I_0 was estimated as the intensity absorbed by the flame, reduced by the factor 1/1600 corresponding to the $f/10$ aperture of the monochromator. The intensity incident on the flame is taken to be the intensity observed in the monochromator when the discharge is in the flame position, times a factor of $100\,[(F/1:F/10)^2]$. In this way we measure $I/I_0=8\times10^{-4}$. Thus, the number of quenching collisions during the radiative lifetime of the free molecule is $Z/A=I_0/I=1.3\times10^3$. At one atmosphere the number of collisions suffered by one molecule‡ is 1.6×10^9 per second, or 1×10^3 in the normal radiative lifetime. Hence 1.3/1.0 of each kinetic theory collision leads to quenching, and the average lifetime of excited OH in the flame is of the order of 6×10^{-10} second.

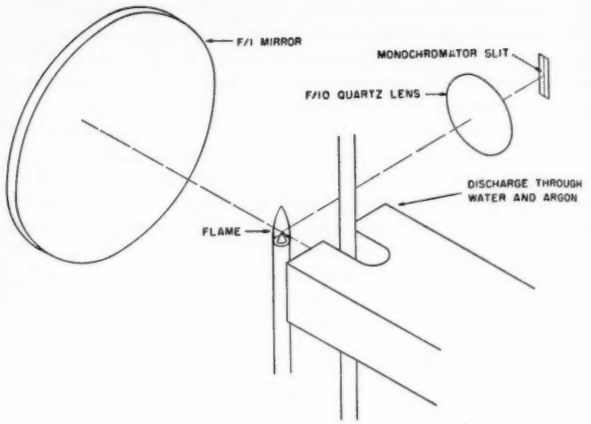

FIG. 1. Schematic diagram of apparatus. Various diaphragms and shields reduced scattered light.

* This research was supported by the United States Air Force through the Air Research and Development Command.
† Department of the Army, Aberdeen Proving Ground, Maryland.
[1] A. G. Gaydon and H. G. Wolfhard, Proc. Roy. Soc. (London) **A194**, 169 (1948); W. R. Kane and H. P. Broida, J. Chem. Phys. **21**, 347 (1953).
[2] O. Oldenberg, Phys. Rev. **46**, 210 (1934); H. P. Broida and W. R. Kane, Phys. Rev. **89**, 1053 (1953).
[3] J. R. Dwyer and O. Oldenberg, J. Chem. Phys. **12**, 351 (1944); O. Oldenberg and F. F. Rieke, J. Chem. Phys. **7**, 485 (1939).
[4] W. G. Fastie, J. Opt. Soc. Am. **42**, 641 (1952).
‡ By using a mean diameter of 2.7 A, a reduced mass of 12, and $T=2000°K$.

Microwave Spectrum and Planarity of Formamide*

R. J. Kurland†‡
Mallinckrodt Chemical Laboratory, Harvard University, Cambridge 38, Massachusetts
(Received August 26, 1955)

THIS letter is a preliminary report of results from the microwave spectrum of formamide which show the molecule to be planar. This planarity is in accord with the resonance representation of the nitrogen-carbon-oxygen linkage in amides and polypeptides given by Pauling[1]:

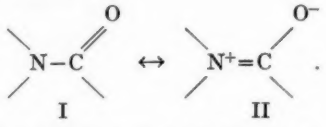

I II

The sample used was vacuum distilled from Mathieson and Bell (99% pure) formamide; the fraction taken had a boiling point of 76.3°C at about two mm Hg pressure. The principal impurity removed by the distillation was methanol and the principal impurity remaining was ammonia (present only in small concentration, judging from the intensity of NH_3 lines observed). The spectrum was studied in the frequency range 14 kmc to 33 kmc, using a

TABLE I. Microwave spectrum of formamide.

Transition $J_{K-1,\,K1} \rightarrow J'_{K-1',\,K1'}$	$F \rightarrow F'$[a]	Centrifugal distortion corr.	Calculated freq. (mc)	Observed freq. (mc)
$0_{00} \rightarrow 1_{01}$	1→2		21 207.42	21 207.43
	1→1	0.00	21 208.01	21 207.96
	1→0		21 206.54	21 206.56
$2_{02} \rightarrow 1_{11}$	3→2		18 956.34	
	2→1	0.00	18 956.21	18 956.28
	1→0		18 955.93	
$3_{13} \rightarrow 4_{04}$	4→5	not	26 924.98	
	3→4	calculated	26 924.28	26 924.05
	2→3		26 925.27	
$4_{14} \rightarrow 4_{13}$	5→5		15 392.63	15 392.71
	4→4	−1.37 mc	15 390.83	15 390.80
	3→3		15 393.10	15 392.88
$5_{15} \rightarrow 5_{14}$	6→6		23 082.26	23 082.26
	5→5	−3.09 mc	23 080.06	23 080.06
	4→4		23 081.89	23 081.86
$6_{16} \rightarrow 6_{15}$	7→7		32 297.87	32 298.19
	5→5	−6.05 mc	32 298.18	
	6→6		32 296.02	32 296.18
$7_{16} \rightarrow 6_{25}$	8→7	not	16 956.25	
	7→6	calculated	16 956.53	16 960.96
	6→5		16 956.21	

[a] Only the relatively intense hyperfine components were considered—i.e., for $\Delta J=1$, the $\Delta F=1$; for $\Delta J=-1$, $\Delta F=-1$; and for $\Delta J=0$, $\Delta F=0$ transitions. Note that for the less intense transitions involving "*b*-type" selection rules ($\mu_b^2/\mu_a^2 \sim 1/20$) the quadrupole hyperfine structure was not resolved.

typical square wave Stark modulation spectrograph and frequency standard monitored by WWV, details of which are described elsewhere.[2,3]

Rotational transitions were assigned to seven of the lines observed (Table I) and were confirmed by studies of the Stark effect. Quadrupole hyperfine structure was observed at low sample pressures for the more intense lines; this hyperfine structure was resolved for the $0_{00}-1_{01}$ transition and partially resolved for the *Q*-branch transitions. Rotational constants were calculated from the frequencies of the $0_{00}-1_{01}$, $2_{02}-1_{11}$, $4_{14}-4_{13}$, and $5_{15}-5_{14}$ transitions, corrections for quadrupole coupling and centrifugal distortion effects being made. The centrifugal distortion corrections were taken to be negligible for the $0_{00}-1_{01}$ and $2_{02}-1_{11}$ transitions and proportional to $[J(J+1)]^2$ for the *Q*-branch transitions.[4] The frequencies observed for the $6_{16}-6_{15}$ transition were predicted to within a small error using these rotational constants and this choice of centrifugal distortion correction. Frequencies calculated for the other transitions agree reasonably well with those observed, considering that no centrifugal distortion corrections were made for these.

Moments of inertia calculated from the above rotational constants (Table II are $I_a=6.952$, $I_b=44.448$ and $I_c=51.407$ a.m.u. A^2.) The defect, $\Delta=I_c-(I_a+I_b)$, from the planarity relationship, $I_c=I_b+I_a$, is only 0.007 a.m.u. A^2 and therefore readily attributable to the usual inertial defect arising from zero-point vibrations.[5]

It is hoped that work being undertaken on the isotopically substituted species D_2NCHO and DHNCHO will enable the structural parameters of the molecule to be determined; these are to be submitted, along with values for the quadrupole coupling constants and dipole moment components, in a future report.

TABLE II. Rotational constants and moments of inertia of formamide.

$\left(a-\frac{b+c}{2}\right)=62\,112.5\pm0.3$ mc

$\frac{b+c}{2}=10\,603.76\pm0.03$ mc

$\delta=0.0250981\pm1.0\times10^{-7}$

$I_a=6.952$ a.m.u. A^2

$I_b=44.448$ a.m.u. A^2

$I_c=51.407$ a.m.u. A^2

$\Delta=I_c-(I_b+I_a)=0.007$ a.m.u. A^2

The author wishes to thank Professor E. Bright Wilson, Jr., for helpful advice given in many discussions and to acknowledge gratefully the financial support tendered by the Office of Naval Research and the General Electric Company.

* The research reported in this paper was made possible in part by support extended Harvard University by the Office of Naval Research under ONR Contract N5ori-76, Task Order V.

† General Electric Industrial Fellow, 1954–1955.

‡ Present address: National Bureau of Standards, Washington 25, D. C.

[1] L. Pauling, *The Nature of the Chemical Bond* (Cornell University Press, Ithaca, 1948), second edition, p. 133.

[2] McAfee, Hughes, and Wilson, Rev. Sci. Instr. **20**, 821 (1949).

[3] J. H. Goldstein, Ph.D. thesis, Harvard University (1949).

[4] This form for the centrifugal distortion correction may be justified by inspecting expressions given by Lawrance and Strandberg for centrifugal distortion frequency shifts in transitions between members of asymmetry doublets and noting that formamide is a nearly prolate rotor. Phys. Rev. **83**, 363 (1951).

[5] B. T. Darling and D. M. Dennison, Phys. Rev. **57**, 128 (1940).

Effect of Probe Size on Ion Concentration Measurements in Flames*

I. R. KING AND H. F. CALCOTE
Experiment Incorporated, Richmond 2, Virginia
(Received August 22, 1955)

IN a recent article[1] a technique for measuring the ion concentration as a function of distance through a flame front by means of Langmuir probes was described and preliminary results reported. At that time it was pointed out that when known concentrations of salts were introduced into a flame, the measured ion concentration was lower than the theoretical value by a factor of some 200 to 400, depending upon the salt used. This was attributed to the cooling effect of the probe; that is, the probe cooled the gas in its immediate vicinity and thus lowered the amount of thermal ionization in this region.

However, a more detailed investigation has shown that the measured value of positive-ion concentration, N_+, is dependent on the size of the measuring probe—the larger the probe, the lower the measured value of ion concentration. This means the measured value of ion concentration must be corrected for probe size in order to obtain a true value in the undisturbed plasma. The amount of this correction can be shown[2] to depend on the size of the probe and the length of the mean free path:

$$N_+(\text{corrected}) = (r/l)N_+(\text{exptl.}), \qquad (1)$$

where r is the radius of the probe and l is the mean free path.

In an attempt to verify this correction several approaches were used. Table I shows the effect of probe size on ion-concentration measurements. All measurements were made in the same Meker burner flame under identical conditions except for probe size. The second column shows the indicated values measured with the probe while the third column shows the experimental values after being corrected for probe size. A glance at column three shows that the correction r/l must be reasonable since in a given flame the ion concentration at a point should be the same regardless of the size of the measuring probe.

TABLE I. Effect of probe size on positive-ion-concentration (N_+) measurements. Propane-air flame at equivalence ratio of 0.92 with platinum probe.

Probe diameter cm	N_+(expt.) ions/cm^3	N_+(corrected) ions/cm^3
0.063	4.68×10^6	3.76×10^9
0.051	6.85	4.26
0.032	8.6	3.44
0.020	16.5	4.08
0.014	23.0	4.02

TABLE II. Calculation of mean free path of alkali metal ions. Propane-air flame at an equivalence ratio of 0.92.

$$1=\tau\frac{N_+(\text{exptl.})}{N_+(\text{theory})}$$

N_+(ions/cc)

Salt	Theory	Exptl.	Calculated mean free path
LiCl	1.5×10^{11}	2.1×10^{8}	4.5×10^{-5} cm
	4.7	4.2	2.9
NaCl	0.90	3.7	13
	2.8	9.6	11
	9.0	32	11
KCl	7.4	16	7.0
	23	49	6.7
RbCl	11	34	9.5
	36	130	12
CsCl	24	72	9.4
	77	240	10

For salts added to a Meker burner flame the measured and theoretical ion concentrations as well as the probe size are known; thus the mean free path of salt ions in the gas may be calculated from Eq. (1).

The results of such calculations are shown in Table II. The calculated mean free paths are reasonable, thus lending additional support to the correction. We now believe that the discrepancy in ion concentration with salts added to the flame is caused by probe size effects and not cooling.

In other tests of the thermal ionization of salts in flames the mean free path has been varied by replacing nitrogen in the air with helium and introducing salts into low-pressure flames. The results are consistent with the postulated correction. A fuller account of this work will be submitted for future publication.

* This research was conducted under the auspices of Project Squid, jointly sponsored by the Office of Naval Research, Office of Scientific Research (Air Force), and Office of Ordnance Research (Army), under contract N6-ori-105, T.O. III, NR-098-038.

[1] H. F. Calcote and I. R. King, "Studies of ionization in flames by means of Langmuir probes," Fifth Symposium (International) on Combustion (to be published).

[2] Bohm, Burhop, and Massey, *The Characteristics of Electrical Discharges in Magnetic Fields* (McGraw-Hill Book Company, Inc., New York, 1949), Chap. 2.

Dielectric Absorption of Triethylamine Solutions

MANSEL DAVIES AND A. H. PRICE
The Edward Davies Chemical Laboratories, University College of Wales, Aberystwyth, Wales
(Received September 1, 1955)

WE have reported what appeared to be an unusually interesting example of a "resonance" type dielectric absorption, found for triethylamine in Nujol (medicinal paraffin) solutions.[1] The type of the absorption appeared to be established (i) by the conformity of the tanδ−log(frequency) curves to the equations of Fröhlich and of Van Vleck and Weisskopf for an absorption arising from a characteristic internal molecular frequency which can (and did in our case) assume a distinctly non-Debye contour; (ii) by the concentration variation of the frequency of maximum absorption, and (iii) by the agreement with the relation, $t\times\text{conc}=\text{const}$, where $t=1/2\pi\cdot\Delta\nu$ and $\Delta\nu$ is the half-width of the absorption curve.

Further study of this and other related systems has now shown that the absorption is not of the supposed resonance type. The reason for the earlier practical deduction is of general interest. Tetrachlorethylene shows no measurable absorption (i.e., tanδ $<0.05\times10^{-3}$) up to $f=100$ Mc/sec. Measurements of its mixtures with Nujol show that the small loss usually found in the latter with a maximum near $f=50$ Mc/sec, tan$\delta=1.01\pm0.05\times10^{-3}$ varies both in magnitude and in peak position with the changing viscosity of the Nujol-tetrachlorethylene mixtures. When the correction for the (small) Nujol contribution to the triethylamine solution absorptions is made in terms of its value at the same viscosity with tetrachlorethylene, the marked distortion of the triethylamine curve from the Debye type is lost, and the other anomalies are removed. The absorptions of the triethylamine then fit the normal relations for a rigid dipole molecule in this medium: e.g., for 0.47 M triethylamine in Nujol at 20°C: η (solution) = 81 centipoise and $\tau=25\pm5\times10^{-10}$ sec.

[1] J. phys. radium **15**, 307 (1954).

Infrared Absorption Spectrum of *N*-Dimethyl-Aminodiborane between 15 and 40 Microns

JAMES E. STEWART
National Bureau of Standards, Washington 25, D. C.
(Received August 23, 1955)

THE infrared and Raman spectra of *N*-dimethylaminodiborane have been studied by Mann.[1] Recently Mann[2] revised his earlier assignments on the basis of some bands observed by this author in the KBr spectral region. Breene[3] used the experimental data from Mann's first paper and a slightly different assignment in a normal coordinate treatment. The spectrum has now been extended through the CsBr region, permitting further modification of the assignment.

Spectra were obtained with a Perkin-Elmer Model 12-B spectrometer equipped with a KBr prism and a Perkin-Elmer Model 21 spectrophotometer equipped with a CsBr prism. Stray radiation in the latter instrument was reduced to two percent or less between 15 and 38μ with LiF and CaF_2 reststrahlen filters. The CsBr spectrum is shown in Fig. 1 and frequencies and assignments are tabulated in Table I.

The groups of bands near 600 cm^{-1} and 420 cm^{-1} have been discussed by Mann; however, more efficient water vapor compensation and higher resolution with the CsBr prism have revealed the latter group to have the appearance of a single Type B band with a weak, probably double Q branch (separation about 4 cm^{-1}) and P and R branches separated by about 16 cm^{-1}. This band is now assigned to the NMe_2 rocking vibration ν_{41} (b_2). The weak band at 396 cm^{-1} must be the NMe_2 deformation $\nu_{13}(a_1)$ corresponding to the line at 399 cm^{-1} in the Raman spectrum. It must be added that Breene's treatment makes the assignment of 396 cm^{-1} to ν_{41} slightly preferable and that Mann's depolarization measurements on 399 cm^{-1} do not show it to be polarized.

No infrared band was found at 325 cm^{-1} which Mann assumed for the bridge hydrogen bending mode $\nu_{42}(b_2)$. But a band at 379 cm^{-1} can be assigned to this vibration. The corresponding band in the infrared spectrum of diborane is at 368 cm^{-1}. The Raman line at 325 cm^{-1} is now available for assignment to NMe_2 twisting $\nu_{20}(a_2)$. The two bands at 261 and 269 cm^{-1} can be assigned, respectively, to methyl rotation $\nu_{31}(b_1)$ and NMe_2 bending $\nu_{30}(b_1)$, to $\nu_{30}+\nu_i-\nu_i$ and ν_{30}, or to Q and R branches of ν_{30}. The third alternative is unlikely because of the occurrence of ν_{30} at 279 cm^{-1} in the Raman spectrum (269 cm^{-1} anti-Stoke's line).

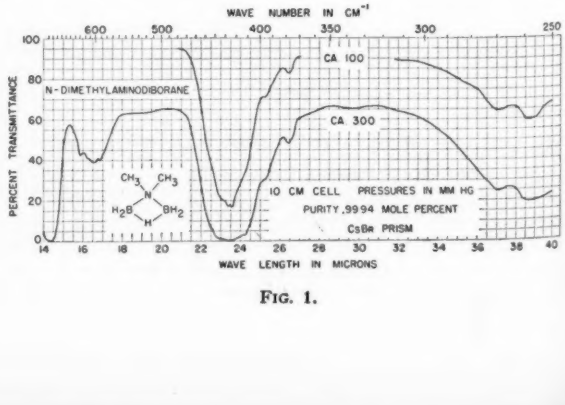

FIG. 1.

The entropy of *N*-dimethylaminodiborane at 271.60°K was calculated for this modified assignment using Mann's values of moments of inertia, etc. The entropy of translation, rotation, and free internal rotation is 75.66 erg-deg^{-1}-mole^{-1}. The total entropy determined calorimetrically by Furukawa *et al.*[4] is 72.25±0.14 erg-deg^{-1}-mole^{-1}. A barrier to internal rotation of 3.7 kcal/mole is necessary for agreement. A methyl torsional oscillator with a sinusoidal potential of amplitude 3.7 kcal/mole has a fundamental frequency of about 250 cm^{-1}, in support of the assignment of 260 and 236 cm^{-1} to methyl torsion oscillations.

TABLE I. Infrared spectrum of *N*-dimethylaminodiborane (KBr prism: 635–596 cm^{-1}, CsBr prism: 432–261 cm^{-1}).

Frequency (cm^{-1})	Assignment
635 w	236+396 =632 (A_1)
616 w	236+379 =615 (B_2)
611 w	1011 −396 =615 (A_1)[a]
596 w	269+325 =594 (B_2)
432 m	$\nu_{41}(b_2)R$
427 m	$\nu_{41}(b_2)Q$
424 m	$\nu_{41}(b_2)Q$
416 m	$\nu_{41}(b_2)P$
396 W	$\nu_{13}(a_1)$
379 w	$\nu_{42}(b_2)$
269 w	$\nu_{30}(b_1)$
261 w	$\nu_{21}(b_1)$; $\nu_{30}-\nu_5+\nu_5$

[a] 1011+396 =1407 (A_1) has been observed at 1414 cm^{-1} in the NaCl prism spectrum.

[1] D. E. Mann, J. Chem. Phys. **22**, 70 (1954).
[2] D. E. Mann, J. Chem. Phys. **22**, 762 (1954).
[3] R. G. Breene, Jr., J. Chem. Phys. **23**, 97 (1955).
[4] Furukawa, McCoskey, Reilly, and Harman, J. Research Natl. Bur. Standards (September, 1955).

Effect of V_2O_5 on Nickel-Zinc Ferrite Formation

D. M. GRIMES, L. THOMASSEN, C. F. JEFFERSON, AND N. C. KOTHARY*
Engineering Research Institute, University of Michigan, Ann Arbor, Michigan
(Received September 7, 1955)

IT is well known that certain minor components greatly alter the rate of a solid state reaction. We have found that the addition of V_2O_5 has such an effect upon ferrite formation from a mixture of NiO, ZnO, and Fe_2O_3. For a fixed firing time the vanadium acts to decrease the necessary firing temperature.

Similar effects have been sought unsuccessfully (at least in degree) using Li_2CO_3, KCl, BeO, $FeCl_2$, B_2O_3, As_2O_3, Sb_2O_3, P_2O_5, $K_2Cr_2O_7$, CrO_3, and MoO_3.

The measured temperature decrease is dependent upon the percent of V_2O_5 added and the characterizing criteria. 0.75 mole percent V_2O_5 decreases this temperature as much as 400°C for $Ni_{0.4}Zn_{0.6}Fe_2O_4$.

The following data were taken on material fired four hours. The average size of the oxide particles used were[1]

Fe_2O_3	0.26 micron
NiO	0.64 micron
ZnO	0.58 micron.

The Fe_2O_3 was a calcinated ferric sulfate.

We consider five methods of determining reaction completeness. (1) *Color.* Ferrites not containing vanadium shade gradually from a red at 1000°C to a bluish at around 1200°. Those containing the vanadium went suddenly from red to a dark black between 800 and 850°. (2) *Grain Size.* The mean grain size of the cores containing vanadium and fired at 950° is approximately the same as that for cores without vanadium fired at 1350° (see Fig. 1). (3) *Density.*

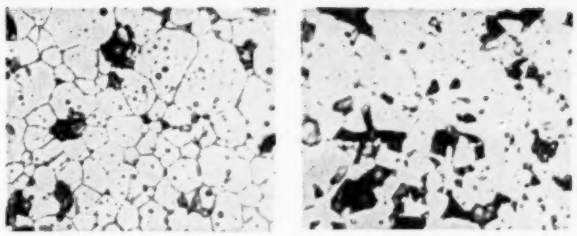

(a) (b)

FIG. 1. Comparative photomicrographs of a Ni-Zn ferrite fired at 1350°C and a Ni-Zn ferrite containing V_2O_5 fired at 950°C. (a) Specimen A-112 (250×). Plain Ni-Zn ferrite core, fired for four hours at 1350°C. (b) Specimen B-2018–1 (250×). Nickel-zinc ferrite core containing V_2O_5 and fired for four hours at 950°C.

The density of the material not containing vanadium went from slightly greater than the green density at 1050° to about 0.95 the x-ray density when fired at 1250°. The material containing vanadium had a density very nearly equal to the green density but slightly less at 800°, and were approximately 0.95 of the x-ray density when fired at 950°C. (4) X-ray diffraction photographs of the material fired at 850°C containing V_2O_5 showed sharp lines in the back reflection region. To obtain the same line sharpness, the material not containing vanadium must be fired at a temperature several hundred degrees higher. (5) *Magnetic Properties.* Figure 2 shows comparative measurements of the permeability and Q or inverse loss tangent, for a vanadium containing material and for material not containing vanadium.

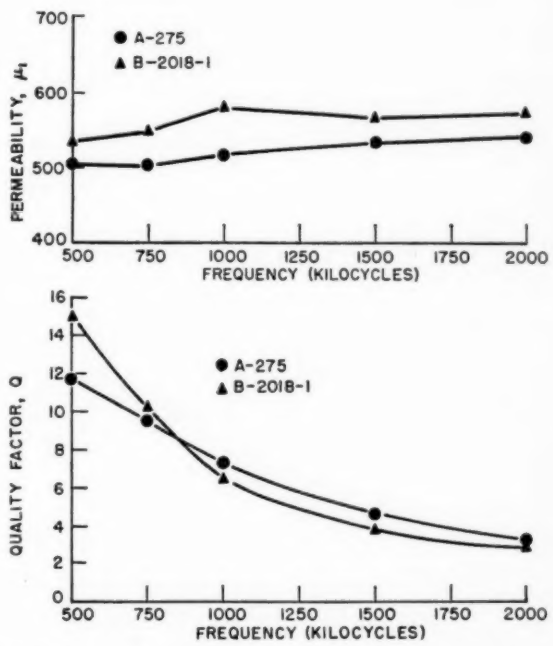

FIG. 2. Comparative measurements of μ and Q *vs* frequency for cores A-275 and B-2018–1. A-275 Ni-Zn ferrite core fired at 1250°C for four hours. B-2018–1 Ni-Zn ferrite core containing vanadium, fired at 950°C for four hours.

A more thorough study of this phenomenon is being made.

* This work was done by the Engineering Research Institute of the University of Michigan under the sponsorship of the U. S. Army Signal Corps.
[1] These data were obtained by the Carboloy Corporation, Detroit, using an electron microscope.

Erratum: Some Theorems Concerning the Mutual Polarizabilities of Atoms and Bonds in Conjugated Molecules

[J. Chem. Phys. 23, 1 (1955)]

H. H. JAFFÉ
Department of Chemistry, University of Cincinnati, Cincinnati, Ohio

EQUATION (9) should read[1]:

$$\pi_{rs,tu}=4\sum_{j<k<0}\sum(c_{jr}c_{ks}-c_{js}c_{kr})(c_{jt}c_{ku}-c_{ju}c_{kt})/(\epsilon_j+\epsilon_k).$$

[1] C. A. Coulson and H. C. Longuet-Higgins, Proc. Roy. Soc. (London) **A192**, 16 (1947).

Erratum: Vacuum Photolysis of Silver Bromide and Silver Chloride

[J. Chem. Phys. 23, 882 (1955)]

GEORGE W. LUCKEY
Research Laboratories, Eastman Kodak Company, Rochester 4, New York

THE cuts for Figs. 1 and 2 were transposed. Figure 1 should be Fig. 2 and Fig. 2 should be Fig. 1.

Absorption Bands of CCl_4 in the Far Infrared Region*

HIROSHI YOSHINAGA
Department of Physics, The Ohio State University, Columbus 10, Ohio

(Received September 1, 1955)

MANY measurements of the far infrared bands of CCl_4 in the liquid phase have been reported by other investigators including Schaefer and Kern[1] and Barchewitz and Parodi.[2] Some of the data do not agree well with corresponding Raman data.[3] These discrepancies are eliminated on the basis of data reported here.

TABLE I. Absorption bands of CCl_4 in the liquid state.

Observed value	Assignment	Raman shift
(cm^{-1})		(cm^{-1})
627.4	$2\nu_4$	628.0
567.6		
531.8	$\nu_2+\nu_4$	531.9
477.4	$\nu_1+\nu_4-\nu_4$	476.5
448.4	$\nu_3-\nu_4$	448.0
327.8		
309.9	ν_4	314.0
218.0	ν_2	217.9
144.	$\nu_1-\nu_4$	145.

The absorption bands of CCl_4 in the liquid state have been remeasured in the region from 660 to 100 cm^{-1} with the far infrared spectrograph in this laboratory.[4] Figure 1 shows the absorption curves for 1.5, 3.0, and 6.5 mm thicknesses of liquid, and Table I gives the frequencies and assignments of absorption maxima observed.

It is not clear whether the 327.8 and 309.9 cm^{-1} absorptions are separate bands or are components of the same band, but the wavelength of the weighted mean coincides with the Raman shift of 314.0 cm^{-1} which has been assigned to the ν_4 band. If the $(\nu_1+\nu_4)$ and ν_3 bands are assigned to absorptions at 790.5 and 762.0 cm^{-1}, then the 477.4 and 448.4 cm^{-1} far infrared absorptions correspond to the Raman shifts of 476.5 and 448.0 cm^{-1}, that is $(\nu_1+\nu_4-\nu_4)$ and $(\nu_3-\nu_4)$, respectively. The 531.8 cm^{-1} band agrees well with the Raman shift of 531.9 cm^{-1}, that is $\nu_2+\nu_4$. The 567.6 cm^{-1} band is located between the $(\nu_3-\nu_2)$ and $(\nu_1+\nu_4-\nu_2)$ bands which occur at 544.1 and 572.6 cm^{-1}, respectively. The weak absorption at 144 cm^{-1} corresponds to the Raman shift at 145 cm^{-1}, assigned to $\nu_1-\nu_4$.

The author wishes to acknowledge suggestions given by Professor Robert A. Oetjen and Professor Ely E. Bell.

* Construction and maintenance of the far infrared spectrograph used in this investigation was supported in part by Wright Air Development Center through a contract with The Ohio State University Research Foundation.

[1] C. Schaefer and R. Kern, Z. Physik **78**, 609 (1932).
[2] P. Barchewitz and M. Parodi, J. phys. radium **10**, 143 (1939).
[3] G. Herzberg, *Molecular Spectra and Molecular Structure II* (D. Van Nostrand Company, Inc., New York, 1949).
[4] Oetjen, Haynie, Ward, Hansler, Schauwecker, and Bell, J. Opt. Soc. Am. **42**, 559 (1952).

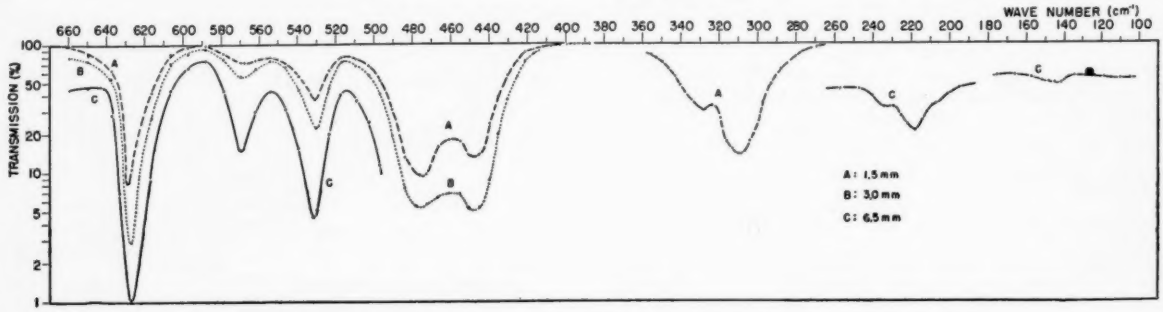

FIG. 1. Absorption bands of liquid CCl_4. Thicknesses of absorption cells: 1.5, 3.0, and 6.5 mm.

Contents

Letters to the Editor:

Thermoluminescence Induced by Ionizing Radiations. . . . John L. Weeks, and Farrington Daniels 2187

Spectroscopic Studies of Some Aromatic Amines with a Heteroatom in the Side-Chain . . . . . A. I. Kiss and B. R. Muth 2187

Spectroscopic Studies of Aromatic Sulfonic Acids and Their Derivatives . . . A. I. Kiss and B. R. Muth 2189

X-Ray Crystallographic Study of Phase Transformation of Boric Acid during Thermal Dehydration . . . . . D. R. Dasgupta and B. K. Banerjee 2189

Study of Phase Transformation of Orthoboric Acid by X-Ray Diffraction Method . . . . . D. R. Dasgupta and B. K. Banerjee 2190

Internal Rotation in Methyl-Trifluorosilane Molecule . . . . . David R. Lide, Jr., and Daniel Kivelson 2191

Infrared Spectrum of Plutonium Hexafluoride . . . . . N. J. Hawkins, H. C. Mattraw, and W. W. Sabol 2191

Infrared Spectra of NpF_6 and PuF_6 . . . . . John G. Malm, Leonard Weinstock, and Howard H. Claassen 2192

Multiple Thio-Radicals in Sulfuric Acid Solution . . . . . John E. Wertz and James L. Vivo 2193

Re-Examination of Two Free Radicals . . . . . John E. Wertz, C. F. Hiskey, and James L. Vivo 2194

Successive Excitation by Low-Energy Electrons: General Principles . . . . . Milton Burton and John L. Magee 2194

Successive Excitation by Low-Energy Electrons: Application to Electric Discharge in Methane . . . . . Milton Burton and John L. Magee 2195

Examination of the Isotope Effect in the Condensation of o-Benzoylbenzoic Acid-Carboxyl-C^{14} to Anthraquinone-β-C^{14} . . . . . Gus A. Popp 2196

Quenching of Biacetyl Fluorescence in Solution . . . . . Hans L. J. Bäckström and Kjell Sandros 2197

Note on the Absorption Spectra of the Benzoyl Radical . . . . . Jiro Higuchi 2197

Reversible Flash Bleaching of Chlorophyll . . . . . Edwin W. Abrahamson and Henry Linschitz 2198

Homogeneity Condition in Thermodynamics . . . . . Henry A. Bent 2199

Entropy Requirements of the Hammett Relationship . . . . . John E. Leffler 2199

Metastable Ions in Mass Spectra . . . . . H. M. Rosenstock, A. L. Wahrhaftig, and H. Eyring 2200

Expansion of Electronic Wave Functions of Molecules in Terms of "United-Atom" Wave Functions . . . . . Tsan Chi Chen 2200

Concentration Dependence of Solvent Shift in the C—H (and C—D) Stretching Frequencies of Chloroform and Pentachloroethane . . . . . Richard B. Bernstein and Milton Tamres 2201

Fluorescence and Average Lifetime of Excited $CH(^2\Sigma^+)$ in Flames . . . . . H. P. Broida and Tucker Carrington 2202

Microwave Spectrum and Planarity of Formamide . . . . . R. J. Kurland 2202

Effect of Probe Size on Ion Concentration Measurements in Plasmas . . . . . I. R. King and H. F. Calcote 2203

Dielectric Absorption of Triethylamine Hydrogen Chloride . . . . . Mansel Davies and A. H. Price 2204

Infrared Absorption Spectrum of N-Dimethylaminodiborane between 15 and 40 Microns . . . . . James E. Stewart 2204

Effect of V_2O_5 on Nickel-Zinc Ferrite Properties . . . . . D. M. Grimes, T. Thompson, C. F. Jefferson, and N. C. Kothary 2205

Erratum: Some Theorems Concerning Bond and Polarizabilities of Atoms and Bonds in Conjugated Molecules . . . . . H. H. Jaffé 2206

Erratum: Vacuum Photolysis of Silver Bromide and Silver Chloride . . . George W. Luckey 2206

Absorption Bands of CCl_4 in the Far Infrared Region . . . . . Hiroshi Yoshinaga 2206